THE

INTERNATIONAL SERIES

OF

MONOGRAPHS ON PHYSICS

THE INTERNATIONAL SERIES OF MONOGRAPHS ON PHYSICS

GENERAL EDITORS

Already Published

THE THEORY OF ELECTRIC AND MAGNETIC SUSCEPTIBILITIES. By J. H. VAN VLECK. 1932. Royal 8vo, pp. 396.

THE THEORY OF ATOMIC COLLISIONS. By N. F. MOTT and H. S. W. MASSEY. 1933. Royal 8vo, pp. 300.

RELATIVITY, THERMODYNAMICS, AND COSMOLOGY. By R. C. TOLMAN. 1934. Royal 8vo, pp. 518.

ELECTROLYTES. By HANS FALKENHAGEN. Translated by R. P. BELL. 1934. Royal 8vo, pp. 364.

CHEMICAL KINETICS AND CHAIN REACTIONS. By N. SEMENOFF. 1935. Royal 8vo, pp. 492.

RELATIVITY, GRAVITATION, AND WORLD-STRUCTURE. By E. A. MILNE. 1935. Royal 8vo, pp. 378.

THE QUANTUM THEORY OF RADIATION. By W. HEITLER. *Second Edition*. 1944. Royal 8vo, pp. 264.

THEORETICAL ASTROPHYSICS: ATOMIC THEORY AND THE ANALYSIS OF STELLAR ATMOSPHERES AND ENVELOPES. By S. ROSSELAND. 1936. Royal 8vo, pp. 376.

THE THEORY OF THE PROPERTIES OF METALS AND ALLOYS. By N. F. MOTT and H. JONES. 1936. Royal 8vo, pp. 340.

ECLIPSES OF THE SUN AND MOON. By SIR FRANK DYSON and R. V. d. R. WOOLLEY. 1937. Royal 8vo, pp. 168.

THE PRINCIPLES OF STATISTICAL MECHANICS. By R. C. TOLMAN. 1938. Royal 8vo, pp. 682.

THE ULTRACENTRIFUGE. By THE SVEDBERG and KAI O. PEDERSEN. 1940. Royal 8vo, pp. 488.

ELECTRONIC PROCESSES IN IONIC CRYSTALS. By N. F. MOTT and R. W. GURNEY. 1940. Royal 8vo, pp. 275.

GEOMAGNETISM. By S. CHAPMAN and J. BARTELS. 1940. Royal 8vo, 2 vols., pp. 1076.

THE SEPARATION OF GASES. By M. RUHEMANN. *Second Impression*. 1945. Royal 8vo, pp. 298.

KINETIC THEORY OF LIQUIDS. By J. FRENKEL. 1946. Royal 8vo, pp. 500.

THE PRINCIPLES OF QUANTUM MECHANICS. By P. A. M. DIRAC. *Third Edition*. 1947. Royal 8vo, pp. 324.

COSMIC RAYS

BY

L. JÁNOSSY

OXFORD
AT THE CLARENDON PRESS
1948

Oxford University Press, Amen House, London E.C. 4

EDINBURGH GLASGOW NEW YORK TORONTO MELBOURNE
WELLINGTON BOMBAY CALCUTTA MADRAS CAPE TOWN

Geoffrey Cumberlege, Publisher to the University

PRINTED IN GREAT BRITAIN
AT THE UNIVERSITY PRESS, OXFORD
BY CHARLES BATEY
PRINTER TO THE UNIVERSITY

PREFACE

THIS book was written in an attempt to present a critical and at the same time a more or less complete survey of the complex subject of cosmic rays. I have dealt with both experimental and theoretical aspects and though I have gone into considerable detail I have tried to avoid intricacies. As an example, the classical and semi-classical theories of collisions are discussed in Chapter III, while the exact quantum treatment of the problem, with its complicated mathematical details, is omitted. In Chapter II I have given an account of experimental methods leaving out purely technical detail. This presentation, it is hoped, will be of use especially to the research worker.

Chapters I–IV give a general background of our knowledge of cosmic-ray phenomena; the later chapters are accounts of more specialized subjects: meson decay, cascade theory, geomagnetic effects, and meson formation.

The greater part of this book was written during the last years of the war. Cosmic-ray research was greatly slowed down during this period and so it became possible to survey the whole of the subject without getting utterly out of date. Nevertheless it was impossible to make all chapters equally up to date, and certain inconsistencies have crept into the presentation due to changes of view during the process of writing. I am asking the reader's indulgence on this point and also on occasional incompleteness caused by the difficulty of obtaining up-to-date literature.

I shall highly appreciate criticism and comments, particularly concerning details, and hope to make use of them at a later date.

Apart from the difficulties of collecting up-to-date material, I found it also impossible to acquire expert knowledge on all of the very different branches of cosmic-ray theory and experiment. It is a great pleasure to acknowledge the help I received to overcome some of these difficulties.

I owe a debt of gratitude to the late Professor E. J. Williams for elucidating in detail the impact-parameter method and for clarifying many obscure points.

I am indebted to Professor P. M. S. Blackett and to Drs. J. G. Wilson and G. D. Rochester for many comments and suggestions. In particular the section on cloud-chamber technique is largely due to Dr. Wilson. Further I am indebted to Drs. Powell and Occhialini for contributing to Appendix III.

The photographs in Plates 1–6 are reproduced from original photographic prints, for the loan of which I have much pleasure in thanking Professors Anderson, Auger, Blackett, Johnson, and Williams, and also Drs. Daudin, Hazen, Rochester, Wilson, Powell, and Occhialini. I am also indebted to authors and editors for permission to reproduce a large number of figures.

I want to express my gratitude to the late Professor Sir Ralph Fowler and to Professor N. F. Mott for the trouble they have taken to improve the manuscript. Finally, I am greatly indebted to the Clarendon Press for the excellent execution and the great trouble they have taken with a difficult manuscript.

L. J.

Dublin, 1947

CONTENTS

PLATES

I

HISTORICAL INTRODUCTION

A. Discovery of Cosmic Radiation

1. The ground was prepared for the discovery of cosmic radiation by the investigations of electrical conductivity of gases. C. T. R. Wilson (1900, 1) and Elster and Geitel (1900) independently observed that an electroscope in a vessel at earth potential gradually lost its charge even if very carefully insulated. It was shown that the loss of charge was due to gaseous ions.

An ion current can only be maintained if the ions, which are swept away by the electric field, are constantly replaced by new ones. The assumption that the ions are produced by some internal mechanism as, for example, by thermal agitation, was rejected as improbable, and it was concluded that the ionization must be due to some outside agency such as X-rays or γ-rays.

C. T. R. Wilson (1900) tentatively suggested that the ionizing agency might be an extremely penetrating radiation of extra-terrestrial origin. Observations made to test this hypothesis proved at that time inconclusive, and the hypothesis of the extra-terrestrial origin, though now and then discussed (e.g. Richardson (1906)), was dropped for the following ten years.

2. Later investigations showed that the ionization in a closed vessel is due to a 'penetrating radiation' which emanates partly from the walls of the vessel and partly from outside. That part of the radiation comes from outside was established by Rutherford and Cook (1903) and by McLennan and Burton (1902–3) by showing that the rate of ionization in a closed vessel decreases when the vessel is surrounded by a sufficiently thick layer of material.

3. A large number of investigations on the conductivity of gases and its cause followed. Wulf (1909) and Gockel (1909), as a result of the analysis of their own results and those of others, came to the conclusion that the whole of the penetrating radiation can be accounted for in terms of the γ-rays emitted by the radioactive substances present near the surface of the earth.

This conclusion was not accepted by Pacini (1912), who observed simultaneous variations of the rate of ionization on mountains, over a lake, and over the sea. Pacini concluded that a certain part of the

ionization must be due to sources other than the radioactivity of the earth or the air.

The observations of Simpson and Wright (1911) showed a considerable rate of ionization over the sea. This also could not be accounted for by radioactivity, as sea-water contains only a negligible amount of radioactive contamination. It was also noticed that the ionization in a closed vessel changed with the barometric pressure.

4. In spite of these difficulties physicists were reluctant to give up the hypothesis of a terrestrial origin of the penetrating radiation. Wulf (1910) measured the rate of ionization on the top of the Eiffel Tower in Paris (300 m. above ground). He expected to find at the top of the tower a much smaller ionization than on the ground, because of the absorption in air of the γ-rays emanating from the ground. The rate of ionization showed, however, too small a decrease to confirm the hypothesis of a terrestrial origin.

Similarly Gockel (1910, 11), ascending in a balloon up to 4,000 m. above sea-level, found that the ionization did not decrease with height as expected on the hypothesis of a terrestrial origin. Gockel's results were somewhat uncertain as he used an ionization vessel in which the pressure varied with the outside pressure and no correction was made for this factor.

5. The extra-terrestrial origin of at least part of the radiation causing the observed ionization was established during the next few years. In a number of balloon flights up to 5,000 m. above sea-level Hess (1912, 13) succeeded in showing that the ionization, after passing through a minimum, increases considerably with height. Hess concluded that the increase of the ionization with height must be due to a radiation coming from above, and he thought that this radiation was of extra-terrestrial origin.

The results of Hess were later confirmed by Kolhörster (1914–19) in a number of flights up to 9,200 m. above sea-level. An increase of the ionization up to ten times that at sea-level was found. The absorption coefficient of the radiation was estimated to be 10^{-5} per cm. of air at N.T.P. This value caused great surprise as it was eight times smaller than the absorption coefficient of air for the most penetrating γ-rays known at the time.

The ionization–height curve was extrapolated from the heights where the ionization was certainly caused by cosmic radiation alone down to sea-level. It was estimated that the cosmic rays coming from above were responsible for the production of 1 to 2 ion pairs per c.c. per sec.

of the ionization near the ground, while most of the ionization, which amounted to 6 to 10 ion pairs per c.c. per sec., had to be attributed to the radioactivity of the ground. The ionization over the sea is mainly due to cosmic rays.

After the publication of the first results by Hess and Kolhörster a violent controversy as to the existence of an extra-terrestrial radiation or cosmic radiation resulted, in which Millikan and his co-workers (1923, '4), Hoffmann (1925), Behounek (1926) took part. The original results were, however, maintained by Hess (1926) to be correct; they were fully confirmed somewhat later and the existence of cosmic radiation has been fully accepted since about 1926.

B. The Penetrating Power of Cosmic Rays

Absorption in Lead

6. The large penetrating power of cosmic rays is the feature which distinguished cosmic rays from other kinds of radiation known at the time of their discovery. Therefore many investigators concentrated on measuring the absorption coefficient of cosmic radiation in attempts to confirm the evidence obtained from the height-altitude measurements.

Observations of this kind carried out by Hoffmann (1925) and also by Behounek (1926) did not seem at first to support the assumption of the existence of a radiation more penetrating than γ-rays. These observations were carried out with ionization chambers shielded with absorbers of lead. The rate of ionization in the chamber was measured as a function of the thickness of lead surrounding the chamber; and the decrease of ionization obtained for the first 10 cm. was found to be of the same order as expected for γ-rays.

The reason why these observations did not at first reveal the existence of cosmic rays was discovered later. Firstly, the lead absorption curve of cosmic rays is strongly influenced by the air-lead transition effect. Owing to secondary effects the rate of ionization under lead is less than that under an equivalent amount of air, and therefore the total cosmic ray intensity drops sharply when a recorder is shielded with an absorber a few centimetres thick. This sharp drop was confused with the absorption of the radioactive rays from the surroundings.

Secondly, the cosmic radiation hardens while passing through absorbers. Therefore the radiation after having penetrated 10 cm. of lead is much less weakened by further absorbers than one is led to expect from the absorption in air. The small rate of absorption under absorbers exceeding 10 cm. of lead was at first overlooked, and the ionization

observed under more than 10 cm. of lead was taken to be due to the residual ionization of the chamber.

The absorption of cosmic rays in lead was observed by Hoffmann (1926, 7), a year after the unsuccessful experiments described. It was also observed by Steinke (1927, 8), by Myssowsky and Tuwim (1928), and later by many others.

The complicated transition effects taking place between air and a dense absorber and also between two absorbers of different atomic number were discovered by Hoffmann (1926). More detailed measurements were carried out later by Steinke (1927) and Schindler (1931).

Kolhörster (1923) determined the absorption coefficient of cosmic radiation in the ice of a glacier on the Jungfrau Joch. Myssowsky and Tuwim (1925) observed the absorption under the water of Lake Onega near Leningrad. Millikan and Cameron (1928, 31) measured the change in the intensity of the radiation in mountain lakes down to depths of 18 m.

All these determinations gave an absorption coefficient between 1 and 3×10^{-3} cm.^{2} per gram. These values were thus in good agreement with the original value derived from the height-ionization data.

Barometer Effect

7. Myssowsky and Tuwim (1928) found that the cosmic-ray intensity varies with atmospheric pressure. This effect was interpreted as being due to the absorption of cosmic rays in air. It was shown that the order of magnitude of the effect can be accounted for by assuming an absorption coefficient of the same order as found by other experiments. It was pointed out by Myssowsky and Tuwim that the barometer effect was probably first observed by Simpson and Wright (1911) before the discovery of cosmic rays. No interpretation of the effect could be given at the time.

The barometer effect was later studied by many observers; a summary of the early literature is given by Corlin (1934).

Directional Distribution

8. Information about the absorption of cosmic rays in air was obtained indirectly by measuring the directional distribution of the cosmic-ray intensity. It was found that the cosmic-ray intensity is larger in the vertical direction than in inclined directions. Observations of this kind were first reported by Gockel (1915) and were later confirmed by many other authors. Quantitative measurements of the directional distribution were carried out later with counters. The experiments of Medicus

(1932), Bernardini (1932), and those of Johnson (1933 *a*) showed that the intensity in inclined directions is nearly proportional to $\cos^2\vartheta$, where ϑ is the angle of inclination to the vertical.

The observed directional distribution can be accounted for at least qualitatively on the assumption that inclined rays have to pass through larger amounts of air to reach sea-level than rays coming down vertically. This interpretation of the directional distribution, first suggested by Myssowsky and Tuwim (1926), has to be somewhat modified, as will be seen in § 47.

Absorption under Ground

9. The rate of ionization was also measured under ground in mines and under great thicknesses of water. The original object of many of these measurements was to shield an ionization chamber completely from cosmic rays in order to determine the zero current of the chamber; but these experiments turned out to be most interesting, as they led to the discovery of cosmic rays much more penetrating than the radiation above sea-level. The measurements of Regener (1930), Millikan and Cameron (1931), Corlin (1934), Kolhörster (1934), Barnóthy and Forro (1937–9), Nishina and Ishii (1937), Ehmert (1937), V. C. Wilson (1937–8), Clay and Gemert (1939), and others revealed the presence of cosmic rays at very great depths. The more recent measurements were carried out with counters and not with ionization chambers. The greatest depth at which cosmic rays have been observed is about 1,400 m. water-equivalent and there is every reason to believe that cosmic rays penetrate to much greater depths.

Spectrum

Discrete components?

10. Many attempts were made to express the radiation in terms of discrete components each having an exponential absorption. This procedure proves to be most unsatisfactory owing to the large number of components required. In fact it was found that the absorption coefficient decreases continuously with depth. The absorption curve was decomposed by Eckart (1934) into a continuous spectrum of exponential components; such a spectrum has, however, no physical significance as was realized later.

Power spectrum

11. A physically significant interpretation of the absorption curve was found later. Follet and Crawshaw (1936) measured the intensity

distribution under 60 m. of water-equivalent. They found that the directional-distribution obeys under ground a cosine-squared law similar to that found near sea-level (§ 8). If the directional distribution is to be explained in terms of absorption, the intensity in a direction inclined at ϑ to the vertical has to be assumed to be proportional to

$$I(\theta \sec \vartheta), \tag{1}$$

where $I(\theta')$ is the vertical intensity under an absorbing equivalent θ'. The observed cosine-squared distribution can thus be understood by assuming

$$I(\theta') \sim \theta'^{-2}. \tag{2}$$

Follet and Crawshaw (1936) pointed out that the directional distribution should remain the same at any depth, provided the absorption function is of the type

$$I(\theta') \sim \theta'^{-z}, \tag{3}$$

where the exponent z is independent of depth.

Measurements of the absorption curve by Ehmert (1937) and others (compare § 9) showed that the absorption curve can in fact be represented by (3). The exponent z is smaller than two near sea-level and increases slightly with increasing depth.

It was pointed out by Blackett (1937*b*) and Clay, Gemert, and Clay (1938) that this absorption function can be understood in terms of an inhomogeneous radiation having a differential range spectrum of the type

$$\mathfrak{S}(R)\,dR \sim \frac{dR}{R^3}. \tag{4}$$

Comparing (4) with the spectrum of high-energy particles as found by Blackett (§ 16) it is inferred that the range of the particles is roughly proportional to their energy, i.e.

$$R \sim w.$$

C. The Nature of Cosmic Rays

1. *Charge and Energy*

'Ultra γ-rays'

12. In the period after the discovery of cosmic rays it was generally assumed that cosmic rays are very penetrating γ-rays. This assumption appeared natural as γ-rays were the most penetrating rays known.

Later investigations revealed, however, that cosmic rays consist largely of charged particles. It was first shown that the radiation near sea-level consists of ionizing particles and somewhat later it was realized

a. Diffused track
(photograph, W. E. Hazen)

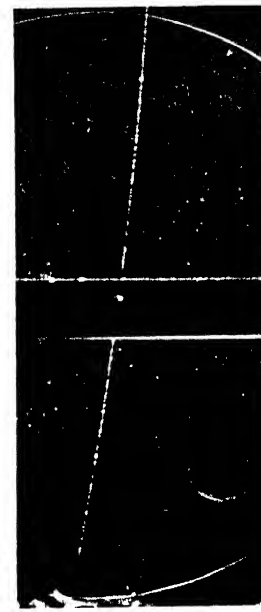

b. Penetrating particle
(J. G. Wilson)

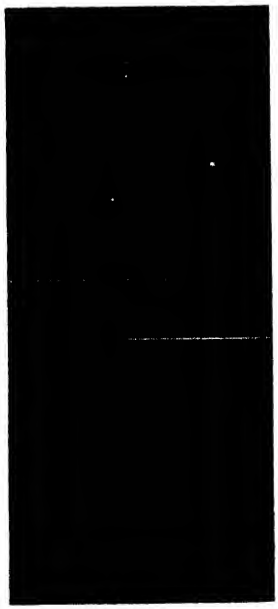

c. Meson and secondary electron
in a magnetic field (J. G. Wilson)

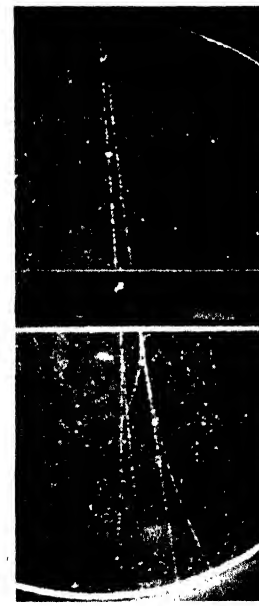

d. Electron shower (J. G. Wilson)

PLATE 2

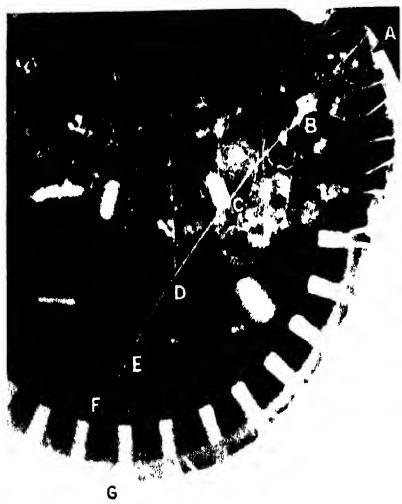

a. Decaying meson (E. J. Williams and Roberts, 1940)

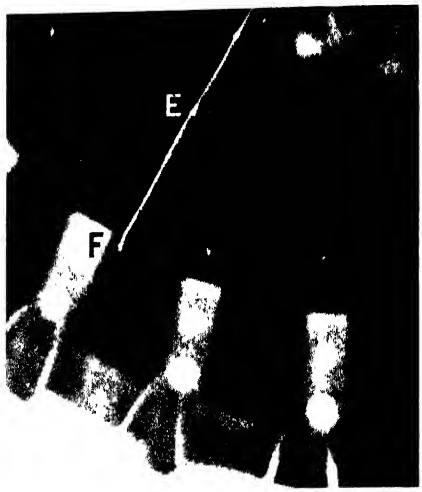

b. End of the track of decaying meson, enlarged from Fig. *a*

c. Decaying meson (T. H. Johnson)

d. Slow meson (Neddermeyer and Anderson, 1942)

that at least part of the primary rays themselves must be ionizing. These investigations will be described in the following paragraphs.

At the time when the cosmic rays were assumed to be γ-rays the name 'ultra γ-rays' was suggested. Later this was modified to 'ultra rays' ('Ultrastrahlen'). This name can still be found in the literature.

(*a*) *Coincidence Experiment*

13. Bothe and Kolhörster (1929) observed that cosmic rays are capable of producing coincident discharges in two Geiger-Müller counters placed close above each other. Such coincidences were interpreted as being due to the passage of single ionizing particles through both counters. It was concluded from the analysis of the experiments that the cosmic rays at sea-level consist mainly of ionizing particles.

The experiments of Bothe and Kolhörster were extended by Rossi (1931 *a*) and others. It was eventually shown that the ionizing particles themselves constitute the penetrating part of the cosmic-ray beam and that these particles are not the secondaries of a more penetrating non-ionizing radiation.

Rossi (1933, 4 *c*) showed that single cosmic-ray particles are capable of penetrating 1 m. of lead. Compare also Street, Woodward, and Stevenson (1935). The energy loss due to ionization by a singly charged particle in 1 m. Pb is 1,000 MEV., therefore these experiments established the occurrence of particles with at least this energy.

(*b*) *Cloud Chamber*

14. Direct evidence for the existence of fast ionizing particles was obtained by Skobelzyn (1927) in the course of γ-ray investigations with a cloud chamber in a strong magnetic field. During an investigation in 1927 he observed the track of a fast particle which was not noticeably deflected by the magnetic field. From the straightness of the track it was concluded that the particle must have possessed a momentum exceeding 20 MEV./*c*. This track must have been due to a cosmic ray passing through the chamber, although at the time it was believed that the track might be a 'run-away electron', that is, an electron accelerated in the field of a thunder cloud (C. T. R. Wilson, 1925).

Two years later Skobelzyn (1929) found 32 straight tracks on 613 photographs. Each of these tracks was due to a particle with momentum exceeding 15 MEV./*c*. These tracks were recognized as cosmic rays. It was shown that their rate was of the right order of magnitude to account for the rate of ionization of the total cosmic-ray beam. Some of Skobelzyn's

photographs had two or three simultaneous cosmic-ray tracks. These photographs are examples of cosmic-ray showers (cp. § 18).

(c) *The Momentum Spectrum*

15. After Skobelzyn's discovery many cloud-chamber investigations into the properties of cosmic-ray particles were carried out.

Cloud-chamber photographs of cosmic rays were taken in magnetic fields much stronger than that used by Skobelzyn. It was found that most of the cosmic-ray particles could be deflected.

16. The first rough determination of the momentum spectrum was carried out by Kunze (1932, 3 *a*, *b*). A solenoid was used which gave a magnetic field of 18,000 gauss. About 90 particles were observed. Momenta up to 3,000 MEV./*c* were measured.

More efficient magnets with iron cores were used by other observers. The momentum spectrum was determined by Anderson and Neddermeyer (1934) up to 6,000 MEV./*c* and in great detail up to about 20,000 MEV./*c* by Blackett and Brode (1936), Blackett (1937 *a*); in this latter investigation more than 800 tracks were measured.

The low-momentum end of the spectrum was measured with a randomly operated chamber by Williams (1939 *b*). It was also measured by Hughes (1940), Wilson (1946), and by Jones (1939).

Other measurements of the momentum spectrum were carried out by Herzog and Scherrer (1935) (at the Jungfrau Joch), Leprince-Ringuet, and Crussard (1937).†

The measurements revealed the following features. The numbers of positively and negatively charged particles were roughly equal with a slight excess of positive particles.

Apart from small irregularities the high-momentum part of the spectrum obeyed a power law, namely the number of particles with momenta between p and $p+dp$ is given by

$$\mathfrak{S}(p)\,dp \sim p^{-(z+1)}\,dp.$$

The average momentum of the particles was about 3,000 MEV./*c*.

17. In the literature the result of curvature measurement is often referred to as an 'energy spectrum'. It must be pointed out, however, that the curvature of a particle in a magnetic field can only be used to deter-

† The loss of momentum of cosmic-ray particles when traversing a metal plate placed in the chamber was also investigated. The difference of curvature of the track above and below the plate gives directly the amount of momentum lost in the traversal. Measurements of this kind have been carried out by Anderson (1933 *a*), Anderson and Neddermeyer (1937), Crussard and Leprince-Ringuet (1937 *a*, *b*), Blackett and Wilson (1937), J. G. Wilson (1938, 9), and by Ehrenfest (1938 *a*, *b*).

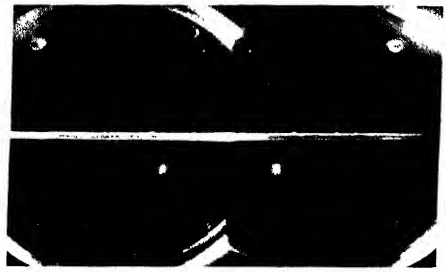

a. Electron pair produced by photon in the gas of the chamber (Anderson)

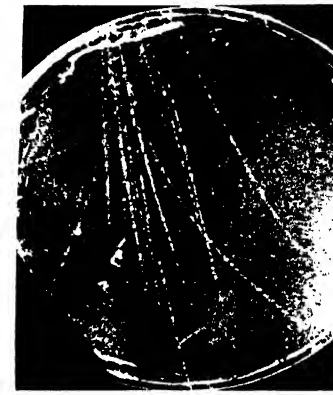

b. Shower (P. M. S. Blackett and G. P. S. Occhialini)

e. Knock-on shower (?) (T. H. Johnson)

d. **Cascade shower produced by electron (Anderson)**

f. Cascade shower (Anderson)

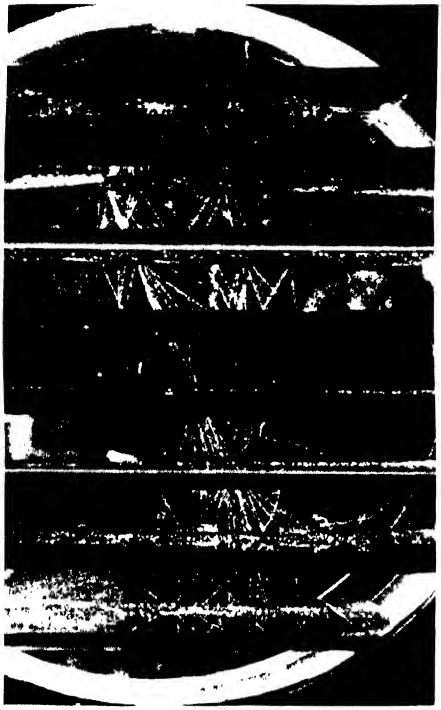

c. Cascade shower passing through eight metal plates (Hazen)

h. Extensive air shower (Wilson and Lovell)

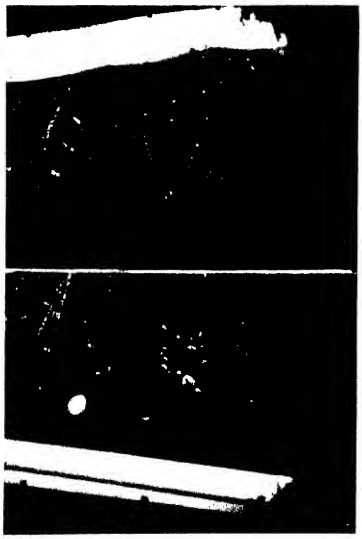

g. Shower (Fussel)

PLATE 4

a. Penetrating shower (Rochester)

d. Penetrating shower (Auger and Daudin)

b. Penetrating shower (Rochester)

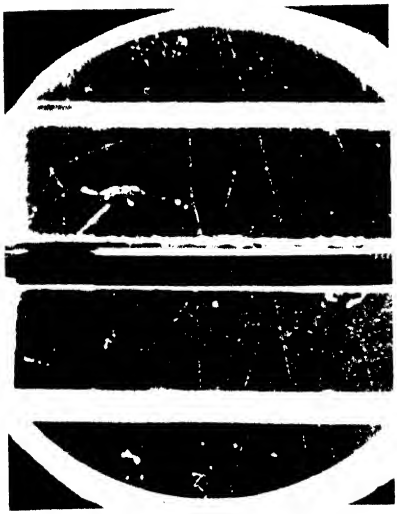

c. Penetrating shower (T. H. Johnson)

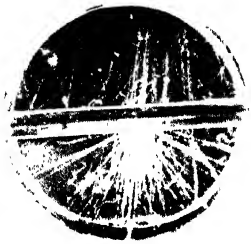

g. Complicated penetrating shower (Rochester)

e. Explosion (Blackett)

f. Penetrating shower (W. E. Hazen)

mine the momentum of the particle. The energy can only be derived from the momentum if the rest-mass is known. For fast particles, that is, for particles with momentum $p \gg mc$ (when m is the rest-mass), the energy is nearly proportional to the momentum, that is

$$cp \simeq w. \tag{5}$$

In the high-velocity region it is therefore not essential to distinguish between energy and momentum. At the time when the spectrum was measured it was assumed that the particles were electrons and therefore the relation (5) seemed to be well satisfied for practically all particles. Later it was found that cosmic rays contain particles of different mass. Thus to find the exact value of the energy of a cosmic-ray particle it is necessary to know both curvature and mass.

It seems therefore more suitable to interpret curvatures in terms of momentum as this interpretation is exact and independent of mass.

2. *Showers*

(*a*) *Observations of Anderson and of Blackett and Occhialini*

18. Skobelzyn (1929) observed that cosmic rays occur in groups. On twenty photographs containing cosmic-ray tracks Skobelzyn found three photographs containing two particles and one photograph containing three particles.

Complex showers of particles were later found by many other observers. Anderson (1933), Blackett and Occhialini (1933), Herzog and Scherrer (1935), Anderson and Neddermeyer (1936), Ehrenfest and Auger (1936), Stevenson and Street (1936), and many others.

19. The cloud-chamber technique was greatly improved by Blackett and Occhialini (1932, 3) who succeeded in triggering the expansion of the chamber by a set of Geiger-Müller counters whenever cosmic rays passed through the chamber. With this technique most of the photographs obtained show tracks of cosmic-ray particles. Besides, the counter-controlled chamber is suitable for selecting showers.

Controlling the chamber by the coincidences of two Geiger counters, one above and one below the chamber, the following results were obtained.

1. About 80 per cent. of the photographs contained single particles while the rest showed more or less complex showers.

2. Both the single particles and the shower particles were found to contain positively and negatively charged particles in equal numbers.

3. Shower particles were found to have a strong tendency to produce

secondary showers. This was shown clearly by placing a horizontal lead plate across the chamber; shower particles falling on the plate frequently give rise to secondary showers in the plate.

4. Secondary showers were also observed emerging out of the bottom of the plate without an ionizing particle entering the plate from above. Such showers must be attributed to non-ionizing links contained in the showers.

5. Some of the showers were found to contain heavily ionizing particles moving in random directions. Such particles may be attributed to nuclear disintegrations. A clear case of a nuclear disintegration obtained by Blackett is shown in Plate 3.

20. The above features of shower photographs were also found by many other workers. In particular all the above features can be found on photographs obtained by Anderson (1936) at Pike's Peak, 4,300 m. above sea-level. Anderson used in his experiments a randomly operated chamber. Such a chamber is quite efficient at high altitudes owing to the large increase of the cosmic-ray intensity with height.

Anderson also obtained direct evidence for non-ionizing links—he obtained photographs showing the production of pairs of particles in the gas. As will be seen later, this process represents the production of an electron pair in the gas of the chamber by a photon.

(*b*) *Rossi's Arrangement*

21. The occurrence of showers of cosmic-ray particles was established independently of the cloud-chamber evidence by Rossi (1933). Rossi observed coincidences between three GM-counters placed in a triangle. The counters were so placed that no coincidence could be caused by a single particle. The coincidences were due to showers, that is, to groups of simultaneous particles.

Rossi found that the rate of coincidences in a triangular coincidence arrangement increases when a thin lead absorber is placed close above the counters. Varying the thickness of absorber above the counters it was found that the coincidence rate increases up to a thickness of about 1·5 cm. of lead. For larger thicknesses of lead above the counters the coincidence rate decreases again and the rate reaches an almost constant value for thicknesses larger than 5–8 cm. of lead.

This transition effect was observed later by many other observers, e.g. by Sawyer (1933–5), Fünfer (1933), Gilbert (1934), Woodward (1936), Stearns (1936).

The transition effect is known as the Rossi transition.

22. A number of observers have reported the occurrence of a second smaller maximum under a thickness of about 17 cm. of lead. Other observers have found no second maximum. The available experimental evidence is not in favour of the existence of a second maximum (see § 403, Ch. VI).

(*c*) *Bursts* (*Hoffmann Stösse*)

23. A phenomenon closely connected with showers was discovered by Hoffmann (1927) (cf. Hoffmann and Pforte, 1930); see also Hoffmann and Lindholm (1928). It was found that the ionization current in an ionization chamber shows occasional discontinuities. These discontinuities were attributed by Hoffmann to the simultaneous passage of a large number of particles through the chamber. This phenomenon, called 'Stösse' or 'bursts', was investigated in great detail by many workers.

Montgomery and Montgomery (1935 *b*) found that the size-frequency distribution of bursts follows a simple power law, and that this distribution can be extrapolated smoothly to include the showers observed by coincidence methods. The connexion between showers and bursts was also demonstrated by Ehrenberg (1936).

24. Bursts show transition effects similar to those of showers, except that the maxima are found at somewhat larger thicknesses than for showers observed with counter arrangements. Transition effects for bursts were obtained by Young and Street (1934–7), Nie (1936), Boggild (1937), Boggild and Karkov (1937), Carmichael and Chou (1939), Chou (1943).

3. *Hard and Soft Components*

25. Absorption measurements of the cosmic-ray intensity in lead showed that the intensity is reduced by about 30 per cent. in the first 10 cm. of lead. Half of the beam capable of penetrating 10 cm. of lead can also penetrate 1 m. of lead: Rossi (1933), Street, Woodward, and Stevenson (1935). These results suggested that the cosmic-ray beam consisted of a penetrating and a soft component.

Absorption measurements were also carried out in various materials. It was found that the penetrating component is absorbed proportional to mass. This was indicated by measurements of Steinke and Tielsch (1933), Street, Woodward, and Stevenson (1935), and others. The latter authors find that the absorption is more nearly proportional to the electron density than to the mass density.

The soft component was found to be absorbed more strongly in heavy elements than in light elements. The absorption was found to be proportional to Z^2 per atom (i.e. Z^2/A per gram) by Rossi and Alocco (1935), Auger and Rosenberg (1935 *b*, *c*), and others.

The hypothesis of two independent components was much emphasized by Auger and his co-workers (1935 *a*, *b*) (Auger, Leprince-Ringuet, Rosenberg (1935)); in support absorption measurements were carried out at various heights above sea-level, at sea-level, and under ground.

26. The hypothesis of the two components was fully confirmed later. It is known now that the soft component consists of electrons as already suggested by Auger and others. The penetrating component consists of mesons, a new kind of particle (see § 28). It was found, however, that the soft component is not entirely independent of the hard component.

Clay, Gemert, and Clay (1939), V. C. Wilson (1939), and others observed that the soft component persists down to great depths below sea-level; the relative intensity of the soft component increases with depth. The intensity of the primary soft component should be negligible under ground and therefore the soft component observed there is secondary.

Soft Component and Showers

27. It was noticed variously that the intensity of showers is proportional to the intensity of the soft component (Woodward (1936), Auger (1935 *a*), and others). E. Regener and Ehmert (1939) found that the shower intensity is strictly proportional to the total intensity at large heights (10–16 km. above sea-level). As at those heights the soft component is preponderant, Regener's results show that the shower intensity is proportional to the intensity of the soft component at great heights.

The observations described so far refer to small showers. Large showers or bursts increase with height much more rapidly than the soft component. This was shown by Montgomery and Montgomery (1935 *a*) and others.

The shower intensity was also observed under ground by a number of observers, e.g. Follet and Crawshaw (1936), Clay and Clay (1935), Ehmert (1937), Barnóthy and Forro (1937), V. C. Wilson (1939), and others.

It was found that the shower intensity under ground is roughly proportional to the soft component.

D. Cosmic-ray Particles

1. *Positron and Meson*

28. The ionizing cosmic-ray particles are found to contain positive and negative electrons, mesons, and protons.

Both the positive electron and the meson were discovered in the course of cloud-chamber studies of cosmic rays.

1. The positive electron was found by Anderson (1932, 3 *a*, *b*). The evidence brought forward by Anderson was much supported and enlarged by Blackett and Occhialini (1933). Apart from many photographs showing positive electrons the latter authors have shown that the positive electron can be identified with the 'hole' of Dirac's relativistic theory of the electron.

2. The meson is a particle with a mass μ intermediate between that of the electron and that of the proton. Approximately we have

$$\mu = 200 m_e. \tag{6}$$

A meson has either a positive or a negative elementary charge. Further, the meson is unstable, it decays spontaneously, emitting an electron and probably a neutrino.

The meson and its property of instability was predicted by Yukawa (1935) theoretically. It was discovered experimentally by Anderson. Photographs indicating the occurrence of mesons were obtained by various authors. In fact a photograph showing the track of a meson was published by Kunze (1933 *b*) before Yukawa's theory. No notice of this photograph was taken.

A convincing photograph of a meson was published by Williams and Pickup (1938). The first clear case of a particle with mass intermediate between electron and proton was published by Neddermeyer and Anderson (1938) and is shown in Plate 2.

Photographic evidence for the instability of the meson was first obtained by Williams and Roberts (1940). Compare Plate 2.

2. *The Analysis of Cosmic-ray Particles*

(*a*) *Ionization and Mass*

29. The nature of the various types of cosmic-ray particles was established mainly by the analysis of cloud-chamber photographs. We give a survey of the development of this problem.

Examining the track of a particle in the cloud chamber one can determine the density of ionization and the magnetic curvature of the track. The magnetic curvature is proportional to the momentum p.

The rate of ionization of a charged particle is proportional to

$$(Ze/v)^2 f(p), \tag{7}$$

where v and p are velocity and momentum of the particle. Ze is the charge of the particle. $f(p)$ is a slowly varying function of the momentum p. $f(p)$ increases roughly as $\log p$ when $p \gg mc$. For not too high values of p the function $f(p)$ can be regarded as a constant.

According to (7) the ionization density decreases with increasing velocity v, and reaches a limiting value for high velocities $v \sim c$. We see that all fast singly charged particles show the same ionization density irrespective of mass.

30. Most cosmic-ray particles show an ionization density comparable with that of fast β-particles. It is concluded therefore that most cosmic-ray particles are singly charged and are fast.

A few tracks show ionization exceeding that of β-particles. Such tracks are due to slow particles. 'Slow' means a velocity appreciably smaller than c. A particle with velocity $\frac{1}{2}c$ or less may be termed slow.

Fast particles carrying multiple charges would also show heavy ionization. It is, however, very unlikely that multiply-charged heavy particles occur at all among cosmic rays except as low-energy particles from nuclear explosions.

31. The mass of a slow particle can be determined when both velocity and momentum are known. The velocity can be determined from the density of ionization while the momentum can be determined from the curvature.

In case of *fast* particles with velocity $v \sim c$ the mass cannot be determined from the curvature. It can be shown, however, that the rest-mass of the particle must be less than p/c. Thus we have

$$m < p/c. \tag{8}$$

(*b*) *Electrons*

32. Fast cosmic-ray particles with a curvature corresponding to a momentum of the order of 10 MEV./c are observed frequently, especially among shower particles. From the relation (8) it is seen that such tracks are due to particles with small mass; such tracks are assumed to be electron tracks.

The positron

33. Anderson (1932, 3) found particles with positive curvature and low momentum; he showed that these particles had to be interpreted as positively charged electrons. Experimental material supporting the

evidence for the occurrence of positive electrons was put forward by Blackett and Occhialini (1933).

34. The sign of charge of a particle moving in a magnetic field can only be determined if the direction of motion is known. There are a number of methods which can be used to ascertain the direction of motion of a particle.

Among other methods we mention the following. A particle traversing an absorber is losing energy and therefore its curvature is smaller before entering than after leaving the plate.

One of the first photographs which was taken by Anderson as evidence for the positive electron showed the following features. A particle with a curvature corresponding to 63 MEV. was seen to enter a lead plate 0·6 cm. thick. The track emerged with a curvature corresponding to 23 MEV. The particle showed positive charge and an ionization density suggesting electronic mass.

The mass of the positron was later shown to be exactly equal to that of the negative electron by Thibaud (1933 *a*).

Properties of the positron

35. From curvature measurements it was inferred that most of the shower particles are positive or negative electrons. Blackett and Occhialini suggested as a possible source for these electrons that they are created in pairs together with negative electrons by photons. It was suggested that a photon with energy exceeding

$$2m_e c^2 \simeq 1 \text{ MEV.}$$

can be absorbed in the neighbourhood of a nucleus giving rise to a pair of electrons.

This suggestion was later confirmed experimentally by Chadwick, Blackett, and Occhialini (1933), by Anderson (1933 *b*), and by Curie and Joliot (1933). It was shown that electron pairs can be produced by the γ-rays emitted by ThC″ (2·6 MEV.).

Dirac's relativistic theory of the electron

36. The experimental discovery of the positive electron threw new light on the Dirac theory of the electron.

Before the discovery of the positive electron one of the most serious difficulties of Dirac's theory was the prediction of the existence of states of negative energy apart from the ordinary states of positive energy. This difficulty was realized to be fundamental, as it seemed impossible to exclude transitions between states of positive and negative energy

by some minor modification of the theory. Moreover the negative energy states were found to play as essential a part as intermediate states in processes where Dirac's theory led to agreement with experiment.

Dirac's interpretation of the states of negative energy was as follows. Electrons occupying states of negative energy cannot be observed directly, but once an electron is lifted from a state of negative energy into a state of positive energy the empty state of negative energy or 'hole' becomes observable and it behaves as a particle with positive charge.

Dirac thought that the empty states of negative energy have to be identified with protons. It was shown by Weyl that these empty states must be assumed to appear as particles of electronic mass.

Identification of positron

After its discovery the positive electron was identified by Blackett and Occhialini with Dirac's hole.

37. It was pointed out that the creation of an electron pair can be regarded as the lifting of an electron from a state of negative energy into a state of positive energy by a photon of energy exceeding $2m_e c^2$. Further, according to Blackett and Occhialini the falling of a (negative) electron into an empty hole would appear as the collision of a positive electron with a negative electron, resulting in the annihilation of both. The liberated energy was assumed to be emitted in form of two quanta. This later process was confirmed experimentally by Thibaud (1933 *b*). The anomalous absorption of γ-rays observed for energies above 1 MEV. can also be interpreted in terms of the creation and subsequent annihilation of electron pairs (Blackett and Occhialini (1933), Curie and Joliot (1933)).

Bethe-Heitler theory

38. Bethe and Heitler (1934) derived both the cross-sections for the production of electron pairs by photons and the cross-section for the emission of photons by electrons in inelastic collisions with atomic nuclei.

Both cross-sections are of the same order of magnitude, and lead to the following conclusions:

1. The rate of loss of energy, of an electron due to the emission of energetic photons increases rapidly with energy and therefore the range of energetic electrons increases only slightly with increasing primary

energy. The cross-section for pair production by photons is so large that high-energy photons are absorbed almost exclusively by this process. The range of energetic photons is of the same order as that of energetic electrons.

2. Both cross-sections, that for pair production and that for emission of quanta, are proportional to Z^2. Thus electrons or photons are absorbed much more strongly in heavy elements than in light elements.

Cascade showers

39. An energetic electron or photon falling on an absorber is quickly absorbed but it starts a complex secondary process and the descendants of the primary may penetrate much farther than the primary.

A primary electron will be stopped after having emitted one or more photons with energies comparable with its own. The secondary photons will be absorbed, giving rise to pairs of electrons, and some of these electrons will have energies comparable with those of the photons. These electrons will produce new photons and the process will go on until comparatively low-energy photons and electrons are produced.

The idea that the absorption of energetic electrons or photons leads to cascades of this sort was put forward simultaneously by Bhabba and Heitler (1937) and by Carlson and Oppenheimer (1937). These authors pointed out that most cosmic-ray showers can be interpreted in terms of such cascades.

40. It was further shown that the intensity distribution of cosmic rays in the higher atmosphere could be accounted for by assuming primary electrons incident on the top of the atmosphere; the variation of the cosmic-ray intensity with geomagnetic latitude could also be accounted for in terms of the cascade theory on the assumption that low-energy particles are cut off by the magnetic field of the earth (Heitler, 1937*b*; Nordheim, 1938).

(c) *Penetrating Particles*

Two hypotheses

41. The cascade theory was thus found to be capable of accounting for the properties of the soft component. To account for the hard component the following two alternative hypotheses were put forward (the second hypothesis was found ultimately to be the correct one):

1. The hard component consists of electrons. To account for the great penetrating power of the hard component it must be assumed in this case that the Bethe-Heitler theory breaks down for sufficiently high

energies and that the rate of loss of very high-energy electrons is much smaller than predicted by the theory.

Alternatively:

2. The Bethe-Heitler theory is valid up to the highest energies but the penetrating particles are not electrons. In this second case it must be assumed that the penetrating particles have a rest-mass exceeding that of the electron as the rate of radiative loss is inversely proportional to the square of the rest-mass.

Fallacy of the breakdown hypothesis

42. Hypothesis 1 seemed to be favoured by measurements of the rate of loss of momentum of particles crossing metal plates (Anderson and Neddermeyer (1937); Blackett and Wilson (1937)). It appeared that particles with low momentum were losing energy in accordance with the calculated loss for electrons, while particles with higher momentum were found to lose much less energy than expected for electrons from the Bethe-Heitler theory (1934).

These experimental results were explained later. It was established eventually that hypothesis 1 is inaccurate and that the high-momentum particles are mesons while the low-momentum particles are electrons. The apparent change of behaviour at about 200 MEV./c is due to the fact that most electrons have momenta less than 200 MEV./c while most mesons have momenta above this limit. These two limits are quite independent of each other and it seems purely accidental that the two spectra have only a small overlap.

43. The electron and meson spectra do actually overlap. A small number of electrons with momentum above 200 MEV./c and also mesons below 200 MEV./c have been found. Before the experimental discovery of the meson Anderson showed that the cosmic-ray particles can be divided into two groups—the first group containing 'shower-producing particles', the second group containing penetrating particles. The energy loss of the first group of particles was found to be of the order to be expected for electrons.

44. The breakdown hypothesis 1 was (wrongly) accepted for some time, because theoretical reasons were put forward to the effect that the Bethe-Heitler theory might become invalid for energies above $137 m_e c^2$. These theoretical arguments were, however, fallacious. It was shown by Williams (1934 *a*, *b*, *c*) by means of semi-classical considerations that the Bethe-Heitler (1934) theory must be valid for high energies if valid for low energies.

Protons

45. Before the experimental discovery of the meson the alternative to the breakdown hypothesis was taken to be the hypothesis that the penetrating cosmic-ray particles are protons.

The proton hypothesis met with immediate difficulties. Firstly, it would have implied the assumption of negative protons, while no direct evidence for the occurrence of negative protons has ever been found.

46. The main difficulty of the proton hypothesis was, however, that protons with momentum less than say 1,000 MEV./c are slow and ionize more thickly than fast particles. The analysis of Brode, McPherson, and Starr (1936) and of Blackett (1937 *a*) showed that the number of heavily ionized tracks is too small to be compatible with the proton hypothesis. Blackett found that among 150 tracks corresponding to particles with momentum less than 600 MEV./c only three positive ones showed any sign of more than average ionization density.

From these observations it was concluded that the number of fast protons cannot exceed about 10 per cent. of the number of fast particles. It is not unlikely that the actual number of fast protons is even very much smaller.

Mesons

47. The penetrating particles found among cosmic rays were eventually shown to be mainly mesons. The meson has a rest-mass of about 200 times that of the electron, therefore mesons with momentum less than about 100 MEV./c ionize more heavily than electrons of the same momentum. Mesons with momentum of the order of 50 MEV./c can be therefore distinguished clearly from electrons on account of their heavier ionization; they can also be distinguished from protons as protons of this momentum ionize extremely heavily. Besides a proton of 50 MEV./c has a remaining range of only 2 cm. of air while a meson of this energy has a remaining range of several metres of air at N.T.P.

48. The first clear case of a meson track was obtained by Neddermeyer and Anderson (1938)† (see Plate 2). A somewhat heavily ionizing track is seen to enter a lead plate. It emerges as a thickly ionized track ending in the gas. From the curvature of the track, its ionization, and its range below the plate it can be shown that the track must be due to a particle with a mass intermediate between electron and proton.

Slow mesons are very rare. This is due to the fact that the remaining

† A track of a slow meson was actually published by Kunze (1933 *a*) [p. 10, Fig. 5]; no notice of this photograph seems to have been taken.

range of a meson once it has become slow is very short. The small number of slow mesons observed is therefore in no contradiction with the fact that most fast cosmic-ray particles are mesons.

3. *The Meson*

(*a*) *Yukawa's Theory*

49. The meson was predicted theoretically by Yukawa (1935) long before its experimental discovery. Yukawa introduced the meson as a hypothetical particle responsible for the short range forces between nucleons (i.e. proton or neutron).

Yukawa predicted that this particle should have a mass $300m_e$ with positive or negative elementary charge and he suggested that such particles might be found among cosmic rays.

To account for the radioactive β-decay Yukawa assumed the hypothetical particle to be unstable and to decay after a half-life of $0{\cdot}25.10^{-6}$ sec. into an electron and a neutrino.

The predictions of Yukawa have been fulfilled with a surprising accuracy and there seems little doubt that the meson discovered among cosmic rays is identical with Yukawa's particle.

We may note that the cosmic-ray meson has been found to be unstable.

(*b*) *The Instability of the Meson*

50. The cosmic-ray meson has been shown experimentally to be unstable, having a half-life of about 2.10^{-6} sec. This value is somewhat longer than that predicted by Yukawa.

Photographic evidence

Direct evidence for the instability of the meson was first obtained by E. J. Williams and Roberts (1940) on a cloud-chamber photograph. The photograph is reproduced on Plate 2, and it will be shown later that this photograph must be interpreted as showing a slow meson entering the gas of the chamber, coming to rest, and emitting a fast electron.

More photographs of this kind were obtained by Williams and Evans (1940) and by Johnson and Shutt (1942) in high-pressure cloud chambers. The high pressure is used to increase the probability of mesons being brought to rest inside the gas of the chamber.

Absorption anomaly

51. Indirect evidence for the instability of mesons could be deduced from experimental results which were obtained before the experimental discovery of the meson.

Follet and Crawshaw (1936) compared the vertical intensity of cosmic

rays under 60 m. water-equivalent below ground with the intensity near sea-level in inclined directions. They found that the absorption in air appeared to be stronger than the absorption in the ground. A similar anomaly was observed by Ehmert (1937).

Auger and his co-workers (Auger, Ehrenfest, Fréon, and Fournier (1937), also Fréon (1942, 4)) observed very pronounced anomalies in the absorption of cosmic rays in air. It was found that the absorption of the atmosphere in directions inclined to the vertical was markedly stronger than the absorption in mass-equivalent layers traversed in the vertical directions.

52. The anomalies were interpreted by Kulenkampff (1938) in terms of the decay of the meson. A meson beam passing through an absorber of small density is more weakened than it would be after passing through a dense absorber of the same mass. The passage through the absorber with the smaller density takes a longer time than the passage through the dense absorber and therefore the fraction of the beam lost through decay is larger during the passage through the less dense absorber.

The theory of the absorption anomaly was treated in some detail by Euler and Heisenberg (1938) and also by Rossi (1939).

The absorption anomaly was observed more directly by comparing the absorption of mesons in air with the corresponding absorption in dense materials. Such experiments were carried out by Rossi, Hilberry, and Hoag (1940), Neher and Stever (1940), Alichanov (1942), and others. The observations lead to a reasonable half-life of the meson.

Temperature effect

53. It was pointed out by Blackett (1938*b*) that the temperature effect observed by Hess, Graziadei, and Steinmaurer (1935), Barnóthy and Forró (1936), Compton and Turner (1937), Clay and Bruins (1939), Beardsley (1940), and in great detail by Duperier (1944*a*, *b*), and others can be accounted for in terms of the instability of the meson. If the temperature of the atmosphere increases without change of pressure then the mass of air expands and the time of travel of the mesons through the atmosphere is increased. Thus an increase of the temperature should be accompanied by a decrease of the meson intensity.

Direct measurement of the mean life of mesons

54. The mean life of mesons was also observed directly. The experimental arrangement permitted the direct measurement of the time interval between the instant a meson was brought to rest inside an absorber and the emission of a decay electron by the meson.

Experiments of this type were attempted but unsuccessfully by Montgomery, Ramsey, and Cowie (1939). After improvements in the experimental method such experiments were carried out by Rasetti (1941), Maze (1941), Auger, Maze, and Chaminade (1942), Chaminade, Fréon, and Maze (1944), Rossi and Neresen (1942–3). The latter investigators obtained for the half-life of the meson $2{\cdot}1 \pm 0{\cdot}1 \,.\, 10^{-6}$ sec. This result is probably the most accurate value of the lifetime of the meson.

The relativistic time contraction

55. It is interesting to compare the value obtained for the half-life of the meson by direct measurement with the values obtained from the absorption anomaly.

According to the theory of relativity it is necessary to distinguish between the proper life of a meson, that is, the life as it appears to an observer travelling with the meson, and the apparent life found by an observer on the earth having a large velocity relative to the meson. Owing to the relativistic time contraction the apparent life of a meson is much longer than the proper life. To compare the determinations of the life of the meson from absorption and from direct measurement it is necessary to convert apparent life of the fast meson into the proper time. When the conversion is carried out the results of the two determinations are found to be in good agreement.

We note, incidentally, that the agreement between the two determinations of the life of the meson yields a direct confirmation of the relativistic time contraction in a region where this contraction is not a small effect but gives rise to a factor of the order of ten.

E. Geomagnetic Effects

56. The researches so far described give evidence as to the nature and composition of cosmic rays at various points of observation. No direct information about the nature of the primary cosmic rays falling on the earth from outside can thus be obtained. The only certain conclusion is that the penetrating component, consisting of mesons, must be of secondary origin because of the instability of mesons.

Direct information as to the nature of primaries can be obtained by observing the effects of the earth's magnetic field upon cosmic radiation.

1. *Störmer's Theory*

57. Electrically charged particles are deflected in the magnetic field of the earth when approaching from outside. The orbits of electrically charged particles in the field of a magnetic dipole were studied in great

detail by Störmer. A summary of Störmer's early results is given by Störmer (1930). The theory was further developed by Lemaître and Vallarta (1933); see for a summary Vallarta (1938). It was found that particles of any momentum can approach the poles of the earth while only particles of sufficiently high momentum can approach the earth at lower latitudes or at the equator. The minimum momentum for a singly charged particle capable of reaching the equator in a vertical direction is found to be 15,000 MEV./c and only particles of momentum exceeding 60,000 MEV./c can approach the earth from any direction.

The total intensity of cosmic rays is therefore expected to decrease with decreasing geomagnetic latitude, provided the primaries are electrically charged, and provided at least some of the primaries have sufficiently small momentum.

2. *Observations*

(*a*) *Latitude Effect*

Low altitudes

58. The magnetic latitude effect was first observed by Clay (1930) in the course of a voyage between Genoa and Bangkok. Clay's results were not generally accepted at first because of a number of previous negative results.

The effect observed by Clay was later fully confirmed. The latitude effect was observed by Compton and his co-workers (Compton (1933)), Bowen, Millikan, and Neher (1934), J. Clay (1934), and many others. Literature has been collected by Miehlnickel (1938).

A particularly detailed survey was organized by A. H. Compton (1933). Seventeen physicists equipped with large ionization chambers of similar design measured the cosmic-ray intensity in sixty-nine stations distributed over the whole world. The combined observations of these observers showed very clearly the dependence of cosmic-ray intensity upon geomagnetic latitude.

The latitude effect can be expressed by the relative change of intensity between geomagnetic equator and pole. This change is given by

$$r = (I_{90} - I_0)/I_{90}.$$

It was found that $r \sim 0{\cdot}1$ for sea-level. The effect increases with height and at 4,360 m. altitude (corresponding to a pressure of 45 cm. of Hg) $r \sim 0{\cdot}33$.

The survey organized by Millikan led to much the same result.

High altitudes

59. Millikan and his co-workers measured the latitude effect up to very great heights (2 cm. Hg pressure). (A summary is given by Millikan, Neher, and Pickering (1943).) The latitude effect increases considerably with height and at a height corresponding to 3 cm. of Hg pressure is about 80 per cent.

The latitude effect extends only up to geomagnetic latitudes of about $\pm 50°$. For higher geomagnetic latitudes the intensity remains constant. This latitude cut-off was revealed by Compton's survey (1933). Such a cut-off was also found by Clay, van Hooft, and Clay (1935) and Cosyns (1936*a*) at great heights when collecting measurements carried out in balloon flights over the continent of Europe. The cosmic-ray intensity remains constant from 50° to the magnetic poles, as was shown by Carmichael and Dymond (1939). A number of balloon flights were carried out from stations at high geomagnetic latitudes, including one near the magnetic pole. It was found that the height-intensity curves thus obtained were in agreement with that obtained by Pfotzer (1936) over Germany.

(*b*) *Longitude Effect*

60. On a voyage on which the geomagnetic equator was crossed several times Clay, Alphen, and Hooft (1934) found that the cosmic-ray intensity depends also on geomagnetic longitude. This effect was observed independently by Millikan and Neher (1935, 6). Along the geomagnetic equator the maximum of the intensity is found in South America and the minimum near the Philippines. The effect can be accounted for in terms of the asymmetric position of the equivalent magnetic dipole (Vallarta, 1935).

(*c*) *Asymmetries*

61. The magnetic field of the earth also causes an asymmetry of the intensity distribution round the vertical. A comparatively large asymmetry between east and west is to be expected and a smaller asymmetry between the intensities from the south and north. Apart from these asymmetries one is led to expect that the intensity distribution round the vertical shows a fine structure (Schremp, 1938).

An indication for an east–west asymmetry was found by Rossi (1931*b*). The east–west asymmetry was observed first by Johnson and Street (1933) and Johnson (1933*a*, *b*, 4, 5*b*) and also by Rossi (1934) and Clay (1935*a*, *b*). The observations show an excess of the intensity from the

west over that from the east. This excess indicates an excess of positively charged particles in the primary beam.

The north–south asymmetry was observed by Johnson (1935*a*), Clay (1935*a*, *b*), and Rossi (1934*a*). On the northern hemisphere an excess from the south above the intensity from the north was found. An extensive survey of asymmetries is due to Johnson (1935*b*).

3. *Interpretation of the Geomagnetic Effects*

Theories of Störmer and of Lemaître and Vallarta

62. Störmer's theory of the motion of charged particles in the magnetic field of a dipole was originally developed to account for the aurora borealis. The theory was applied to cosmic rays by Störmer (1930–8), Lemaître and Vallarta (1933, 5, 6), Fermi and Rossi (1933), Rossi (1934*b*), and Swann (1933). A comprehensive summary of the theory is given by Vallarta (1938).

The problem of the intensity distribution was much simplified when it was shown by general dynamical reasoning that the effect of the magnetic field on an isotropically distributed primary radiation was merely to cut out particles of a given momentum in certain directions. The problem of the intensity distribution reduced therefore to that of the determination of forbidden directions as functions of geomagnetic coordinates and momentum.

The determination of forbidden directions was much complicated by the shadow effect of the solid earth. The theory of the forbidden cones was treated in great detail by Vallarta and his co-workers, e.g. Lemaître, Vallarta, and Bouckaert (1935), Schremp (1938), and others.

63. The observed geomagnetic effects were shown to be capable of interpretation in terms of the theory of the magnetic deflexion. The comparison between theory and observation could not be carried out strictly as (1) the spectrum of the primaries was not known, (2) the details of the secondary processes were not known.

Conclusions

64. The following may now be stated:

1. The latitude effect in the upper atmosphere is probably caused by incident electrons with a spectral distribution roughly obeying a power law, and there is some evidence that the spectrum is banded.

2. The latitude effect near sea-level is probably due to primaries different from those producing the effects at high altitudes. It was suggested by Johnson (1938*c*, *d*, 9*a*, *b*) and later by others that the primaries responsible for the low-altitude effects are protons.

3. The cut-off of the magnetic effects near 50° is accounted for most easily by assuming that the primary spectrum is cut off at the low end by some other agency than the earth's field and it does not contain primaries with momentum less than 3,000 MEV./c. Such a cut-off of the spectrum could be accounted for by the magnetic field of the sun as was suggested by Jánossy (1937) and later by Vallarta (1937 *b*) and Epstein (1938). The hypothesis was discussed in some detail by Vallarta and Godart (1939).

Primary energies

65. In interpreting the geomagnetic effects the following interesting feature has to be accounted for. Only primaries with momentum exceeding 15,000 MEV./c can approach the earth vertically at all latitudes. (Only particles with momentum larger than 60,000 MEV./c can approach the earth freely from all directions at all latitudes.) The latitude effect at sea-level is only 10 per cent. It must be concluded therefore that 90 per cent. of the particles reaching sea-level are due to latitude insensitive primaries, thus the primaries responsible for 90 per cent. of the intensity at sea-level must have momenta larger than 15,000 MEV./c.

The average momentum of the mesons at sea-level is of the order of 3,000 MEV./c, while a meson passing through the atmosphere is expected to lose 2,000 MEV./c. Therefore the mesons must have started with an average momentum of 5,000 MEV./c. This momentum is much smaller than the average momentum of the primaries as deduced from the latitude effect.

The margin between the momentum of the primaries and the secondary mesons can be best accounted for by assuming that each primary splits up its energy and gives rise to several mesons while passing through the atmosphere.

This interpretation of the latitude effect was put forward by Nordheim (1938) and by Bowen, Millikan, and Neher (1937). As a result of this consideration it was realized even before the discovery of the meson that the penetrating component must be of secondary origin. That the penetrating component must indeed be secondary became quite clear as soon as it was established that the penetrating component consists of mesons and that the mesons are unstable.

F. The Origin of the Meson

66. Since the mesons are unstable they must originate inside the atmosphere. As the meson component shows a magnetic latitude effect

it is also clear that the mesons are the secondaries of a primary radiation coming from outer space. It was pointed out by Johnson (1938*d*, *e*, 9*a*, *b*) and later elaborated by others that the most likely primaries giving rise to the meson components are protons.

The most important objective of present cosmic-ray research seems to be to determine the process by which mesons are produced.

Height of Production

67. The mesons must be created at very high altitudes. It was shown by Euler and Heisenberg (1938) that the absorption anomalies can be accounted for on the assumption that they are formed in a region about 16 km. above sea-level.

A more sensitive test of the height of origin of the mesons is obtained from the analysis of the temperature effect. It was shown by Duperier (1940, 4*b*) that the temperature effect is best accounted for on the assumption that mesons have originated at a height of 16 km. or even higher.

Penetrating Showers

68. Though it is clear from the evidence given in the last paragraph that the bulk of the mesons are produced at very great heights a few mesons are also produced near sea-level. Various observers have obtained photographs containing groups of penetrating particles (Fussel (1938), Braddick and Hensby (1939), Herzog and Bostick (1940), Powell (1940, 1), Jánossy and co-workers (1941), Wollan (1941), Bostick (1942), Hazen (1943, 4), Bose and co-workers (1944), Rochester (1944, 6), Dandin (1944)). Such photographs are most easily interpreted in terms of the production of mesons near the cloud chamber.

Wataghin and his co-workers (1940) observed showers penetrating 17 cm. of lead. Independently Jánossy and Ingleby (1940) observed showers penetrating 50 cm. of lead. These showers must also be interpreted as groups of mesons produced near the recorder.

Transition effects of such penetrating showers were observed by Jánossy (1941) and Jánossy and Rochester (1944*a*). These effects show that the cross-section for the production of mesons is of the order of magnitude of the size of atomic nuclei (compare also Regener (1943*b*)).

Stars

69. A phenomenon which may be connected with the production of mesons was first observed by Blau and Wambacher (1937*a*, *b*). It was found that suitably prepared photographic plates exposed for a long

time to cosmic rays at high altitudes show 'stars' after development. Each star consisted of a number of tracks left by particles which emanated from a common centre. The ranges of these particles were often much longer than expected for radioactive α-particles. It was concluded that stars are disintegrations of nuclei caused by cosmic rays. Only slow particles give rise to a sufficient density of ionization to be observable in an emulsion. The question whether or not stars contain fast particles cannot therefore be decided. Cloud-chamber photographs by Hazen (1943, 4*a*), however, show explosions which seem to be intermediate between penetrating showers and 'stars'. It is therefore likely that the two phenomena are closely connected. The first cloud-chamber photograph of a 'star' originating in the gas of a cloud chamber was obtained by Blackett in 1933 (compare E. J. Williams, 1934*a*).

Theory of Hamilton, Heitler, and Peng

70. The details of the process of meson formation are still somewhat uncertain. A theory of the production of mesons in terms of the collisions between fast nucleons has been given recently by Heitler and Peng (1943) and Hamilton and Peng (1943). The theory is capable of accounting for much of the experimental material connected with the hard component as was shown by Hamilton, Heitler, and Peng (1943), Heitler and Walsh (1945), Jánossy (1943).

G. Extensive Air Showers (*A*-Showers)

71. Auger and his co-workers discovered in 1938 large showers covering many hundreds of square metres (Auger and Maze (1938), Auger, Maze, and Grivet-Meyer (1938)). Auger, Maze, and Robley observed showers with counters separated up to 300 m. Similar observations were reported by Kolhörster and his co-workers (1938). These showers were investigated by many observers and they are believed to be large cascade showers started by energetic primaries and developing through the atmosphere.

Some of the showers had an extremely high particle density and it was estimated from cloud-chamber photographs that the total energy must have exceeded 10^7 MEV.

The theory of extensive air showers in terms of the cascade process was given by Euler and Wergeland (1940) and modified by many others (see Ch. VIII). While there is some discrepancy in the treatment of the phenomenon by different authors it is clear that it is necessary to assume

primaries with energies of the order of 10^{10} MEV. in order to account for the phenomenon.

72. Auger (1938) has noticed that some extensive air showers have a surprisingly high penetrating power. It was later observed by Wataghin (1940) and also by Jánossy (1941) and Cocconi (1942) that some of the penetrating showers are connected with extensive air showers.

II

EXPERIMENTAL TECHNIQUE

73. The development of experimental technique has played a decisive role in cosmic-ray investigation. It was a long time before physicists could convince themselves of the mere existence of cosmic rays. Thanks to the development of a suitable technique the existence of the cosmic rays can now be demonstrated as a matter of routine, and minute details of the properties of the radiation can be investigated successfully.

In this chapter we give a detailed description of the various experimental techniques which are employed for the investigation of cosmic rays.

The chapter is intended to serve a double purpose. Firstly, we shall describe experimental methods so as to facilitate the understanding of the significance of the experiments. In particular we shall discuss in some detail the significance of the counter-controlled cloud chamber and some aspects of the anticoincidence method.

Secondly, we shall attempt to give sufficient technical detail to be of use to the research worker. For convenience of the reader we shall mark with an asterisk the paragraphs which are exclusively of technical interest.

A. The Ionization Chamber

1. *Total Intensity*

74. Most of the early investigations were carried out with the ionization chamber. Ionization chambers are still used for continuous recording of the cosmic-ray intensity and for the investigation of large showers and bursts. For other investigations the ionization chamber has been superseded by other instruments.

A schematic drawing of an ionization chamber is given in Fig. 1. The chamber usually consists of a cylindrical metal container and a central collecting rod. It is desirable that the wall of the container should be as thin as possible in order to avoid effects caused by the material of the wall. The chamber is filled with gas at as high pressure as practicable in order to increase the sensitivity. A compromise between these two requirements has to be found according to the actual experiment for which the chamber is intended. It is not unusual to find chambers with walls about 3 mm. steel.

A recording electrometer is connected to the central collecting elec-

trode. Great precautions have to be taken in insulating the collecting rod and the electrometer from the other parts of the apparatus. To facilitate the insulation the electrometer is sometimes placed inside the chamber. This arrangement, used by Hoffmann (1926, 7*b*) and by

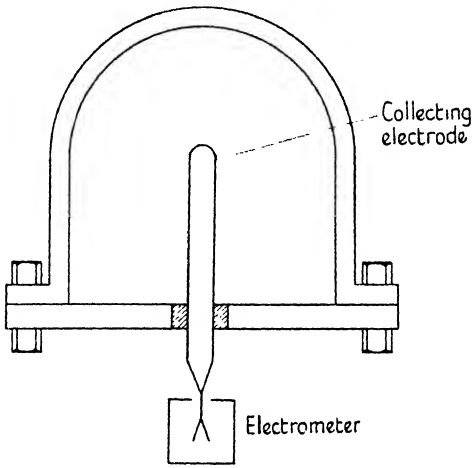

FIG. 1. The ionization chamber.

Kolhörster (1926), has the further advantage that the capacity of the central system can be kept very small. The position of the electrometer is read through a window by a small microscope.

Most ionization chambers are used with an electrometer placed outside the chamber. A guard ring kept approximately at the average potential of the electrometer is placed round the lead connecting the central electrode with the electrometer.

75.* The rate of ionization produced in the gas can be measured in two different ways. In the first method the vessel is kept at earth potential and the rate of discharge of the electrometer from some initial potential is observed. In the second method the vessel is kept at a high potential and the rate of charging of the electrometer is observed. Using the latter method great care has to be taken to keep the potential of the walls of the chamber constant, as a change of the voltage of the walls induces charges on the electrometer.

To reduce background ionization, a grid near the wall of the chamber is sometimes introduced and the ionization current between the grid and the central electrode is measured (Hoffmann (1927*b*)). The grid is kept at such a potential that the ions produced by α-particles from radioactive contamination of the wall are prevented from reaching the central

electrode. The distance between the grid and wall must of course exceed the range of radioactive α-particles in the gas of the chamber.

If all the ions of one sign produced in a chamber of volume $\mathscr{V}$ are collected by the central electrode, then the ionization current observed can be written as

$$i = epr\mathscr{V}, \tag{1}$$

e being the elementary charge, p the pressure in the chamber in atmospheres, r the number of ions produced per c.c. per sec. The rate of change of potential in volts per second is

$$\frac{d\Phi}{dt} = 300epr\mathscr{V}/C, \tag{2}$$

where C is the capacity of the central system.

The actual rate of change of potential is smaller than that given by (2), as ions are lost by recombination. The loss of ions due to recombination is large for small voltages but becomes small for voltages exceeding the saturation voltage. Care must be taken therefore that the potential difference between the electrodes should never fall below the saturation voltage.

The rate of recombination also depends on the pressure and on temperature, see e.g. Compton, Wollan, and Bennett (1934). More ions are lost at high pressures and low temperatures than at low pressures and high temperatures. Therefore the ionization current increases less than proportionally with the pressure. The effect of pressure recombination is smallest for the monatomic gases; high-pressure chambers are therefore most effective when filled with a noble gas. It was found, however, that even small contaminations increase the recombination considerably; the use of a rather pure noble gas is therefore recommended. (Compare Fig. 2.)

76.* As an example consider a chamber at atmospheric pressure. Let $p = 1$, $\mathscr{V} = 5{,}000$ c.c., and $C = 1$ cm. The ionization due to cosmic rays at sea-level is of the order of

$$r_c = 2 \text{ ions per c.c. and per sec. in air of 1 atmosphere.}$$

The total ionization is, however, of the order of $r = 10$ ions per c.c. per sec. because of the radioactivity.

We obtain from (2)

$$\frac{d\Phi}{dt} = 7{\cdot}2 \times 10^{-3} \text{ volt per sec.}$$

Thus the electrometer will change its potential by about 25 volts per

hour and saturation can be safely maintained if the electrometer is brought back to its initial position about once an hour.

Chambers with larger volumes and pressures up to 100 atmospheres are sometimes used. The dimensions of the apparatus designed by Steinke (see Corlin (1934)) for precision recording were $\mathscr{V} = 22{,}600$ c.c., $p = 10$ atm., and $C = 14{\cdot}25$ cm. For this apparatus one finds

$$\frac{d\Phi}{dt} = 0{\cdot}022 \text{ volt per sec.}$$

The voltage change of the electrometer is compensated by inducing at half-minute intervals constant amounts of charge on the electrometer needle. In this way only the difference between the induced charge and the charge due to the ionization current is recorded. The position of the needle is photographed hourly, and after the photograph has been taken the needle is earthed, and the arrangement is reset for the next hour.

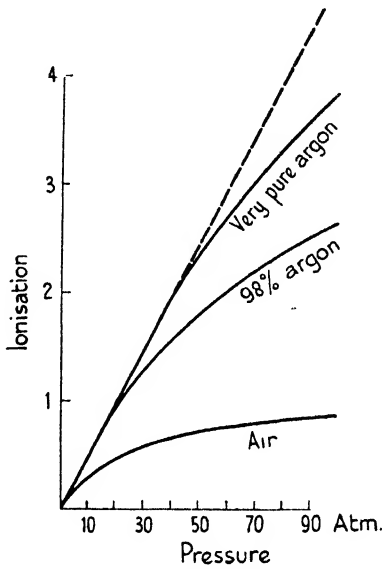

FIG. 2. Pressure ionization curves.

The charge is compensated at intervals in order to keep the needle at almost constant potential all the time. This is important since, even in the region of saturation, changes in the current with changing voltage cannot be excluded. Besides by keeping the electrometer needle always near earth potential the strain on the insulation can be reduced.

77.* Standard ionization chambers were designed by Kolhörster (1926), Hoffmann (1926), Hoffmann and Lindholm (1928), Steinke (1928, 29), Millikan and Cameron (1928, 31), and others. A most elaborate instrument, the Compton meter, was designed by Compton, Wollan, and Bennett (1934). As many models of this type are used for continuous recording of cosmic rays we give a description of the instrument (Fig. 3).

The ionization is measured in a spherical steel bomb filled with pure argon at 50 atm. pressure. The ionization current is compensated by the current of a small auxiliary chamber which is exposed to the radiation of a source of metallic uranium. By varying the distance between the uranium source and the small chamber the compensating current can be adjusted so as to be very nearly equal to the average ionization current

in the main chamber. The electrometer deflexion is recorded continuously by a moving film. The dimensions of the two chambers are so chosen that a small change in the voltage supply causes opposite charges to be induced on to the collecting electrodes of the two chambers and therefore such a change has no effect on the electrometer deflexion.

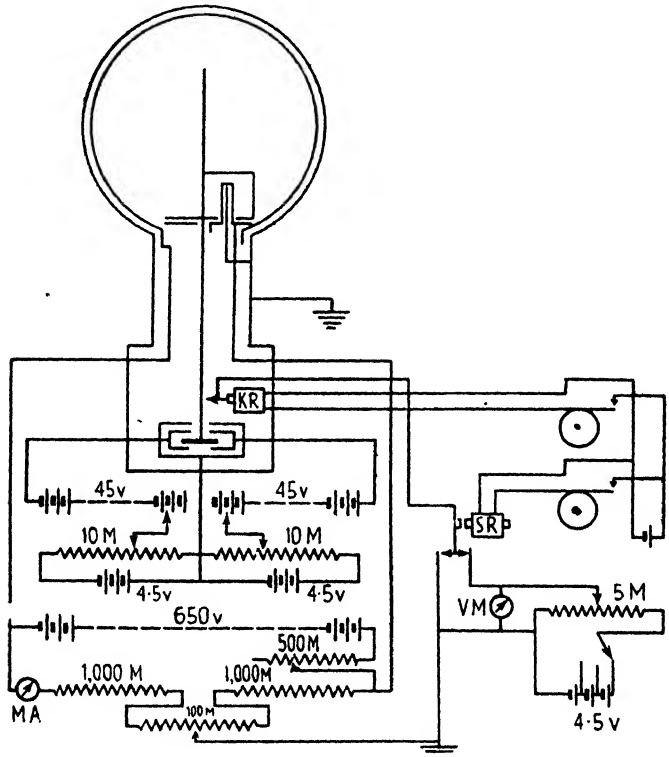

FIG. 3. The Compton meter.

The standard Compton meter is covered with lead shot equivalent to 10·7 cm. of solid lead. Continuous recording of the cosmic-ray intensity with such meters is carried on at a number of stations (see Forbush, 1939).

2. *Bursts*

78. The bursts described in § 23 are observed conveniently with ionization chambers. Hoffmann and Lindholm (1928) and in greater detail Hoffmann and Pforte (1930) observed sudden jumps of an electrometer string which were caused by bursts of ionization released suddenly.

A typical circuit which can be used to record bursts is reproduced in Fig. 4. The collecting electrode of the chamber is connected through a

condenser to the grid of the input valve. The plate of the input stage operates a linear amplifier of several stages; the output of the amplifier may be connected to the deflector plates of an oscillograph or to some mechanical recorder. Using an oscillograph one can brighten the beam

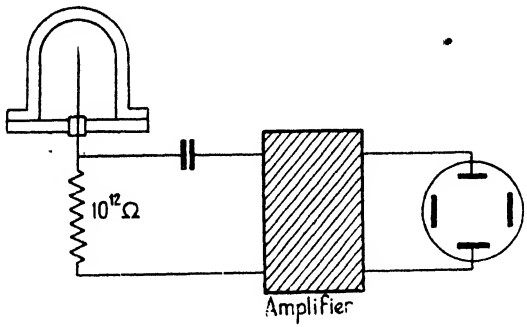

FIG. 4. Recording of bursts.

for a short time after each burst and thus record the beam only while it is deflected.

The size of the pulse caused by a burst can be estimated as follows. Consider a chamber filled at 70 atm. pressure, the combined capacity of collecting electrode coupling unit and grid of the input stage being 10 cm. and the average path length of a particle through the chamber 15 cm. Assuming that a particle gives rise to 50 ions per cm. per atmosphere the voltage pulse due to the passage of a single particle is found as

$$70 \times 50 \times 15 \times 300e/10 = 10^{-3} \text{ volt.}$$

The collecting time of the ions produced by a burst is of the order of $\frac{1}{10}$ of a second. The time constant CR of the input must be large compared with this time. The input capacity can hardly be reduced to less than 10 cm., thus the leak resistance R must be at least of the order of 10^{12} ohm. Only a valve with a well insulated grid is therefore suitable for the input stage. An electrometer valve can be used but most H.F. pentodes with the grid terminal on the top are satisfactory and amplify more than electrometer valves.

79. Pulses of a few millivolts can be amplified easily and therefore it would not be difficult to design an amplifier which records even the smallest bursts. A lower limit for the burst size which can be recorded is imposed by the statistical fluctuation of the incident rays. An accidental crowding in time of independent particles cannot be distinguished from a real burst. We estimate the smallest burst size which can be

distinguished from a background fluctuation as follows. If the time of collection of the ionization caused by a burst is t, while the average rate of particles passing the chamber is $\mathfrak{r}$, then the average number of particles crossing the chamber simultaneously with a burst is $N = \mathfrak{r}.t$. From the figures given in § 643, Ch. X, it can be inferred that fluctuations up to five times the standard fluctuation cannot be completely excluded. Thus it cannot be excluded that owing to statistical fluctuation during a period of the length t the number of independent particles crossing the chamber is anything up to

$$N_0 = N + 5\sqrt{N}. \qquad (3)$$

Thus only pulses corresponding to more than $N_0 - N$ particles can be attributed to bursts. With $t = \frac{1}{5}$ sec., $\mathfrak{r} = 20$ particles per sec., we have $N = 4$, and the smallest burst which can be recognized must contain $N_0 - N = 10$ particles.

Another limiting factor is the fluctuations due to highly ionizing α-particles. The effect of α-particles can be eliminated, however, by a grid. In high-pressure chambers the range of α-particles is so small that they do not cause a serious disturbance and no grid is needed.

B. Geiger-Müller Counters

1. *Properties of the Counter*

(*a*) *Description*

80. The Geiger-Müller counter (1928–9) is an improved version of the original point counter of Geiger (1924) (see also Hess and Lawson (1916)). It consists of a cylindrical cathode and a thin concentric wire as anode (Fig. 5). The counter is filled with a gas at a pressure of about $\frac{1}{5}$ of an atmosphere. A voltage of the order of 1,000 volts is applied between the electrodes. If one or more ions are produced inside the counter by some ionizing agency, these ions are accelerated by the field and an electric discharge results. The discharge is quenched shortly after its onset, and the resulting electric pulse is recorded either by a sensitive electroscope attached to the anode of the counter or by a valve and a mechanical recorder.

The counting action of a counter sets in when the potential difference between the electrodes exceeds the starting potential. The counting efficiency of a counter increases with increasing potential up to voltages 50–100 volts above starting potential. For higher 'over-voltages', i.e. in the region of the plateau, the counting rate is almost independent of voltage. The plateau of a good counter extends over a few hundred volts.

For higher voltages the counter starts 'racing' or a continuous discharge sets in (see for details Cosyns and de Bruyn (1934) and Werner (1934)). Counters are used with voltages inside the range of the plateau, as for this voltage range the counter is most efficient and its counting rate is only slightly affected by variations of the high-tension supply.

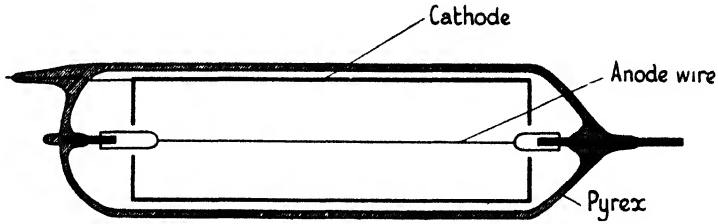

FIG. 5. Geiger-Müller counter.

81. The potential usefulness of the Geiger-Müller counter for cosmic-ray research was realized immediately after its invention. Its practical application was, however, handicapped by the great instability of the early counters.

The properties of Geiger-Müller counters were investigated in great detail by Cosyns and de Bruyn (1934) and by Cosyns (1936*b*). Cosyns succeeded in constructing highly reliable counters. The counters were filled with pure hydrogen and no organic substances were used so as to avoid slow changes of properties due to the instability of organic compounds.

82. Counter technique was greatly simplified by the discovery by Trost (1935, 7) that counters filled with a mixture of an organic vapour (e.g. ethyl alcohol) and a permanent gas show excellent properties. The alcohol counter is a perfectly reliable instrument and can be used for precision work.

(*b*) *The Discharge Mechanism of the GM Counter*

83. The discharge mechanism of the GM counter was studied in detail and explained by Cosyns (1936*b*).

Similar investigations, apparently without knowledge of Cosyns's work, were carried out by C. D. and D. D. Montgomery (1940), Ramsey (1940), Stever (1942), and others. The role of the organic vapour in the discharge of counters has been investigated by Korff and Present (1944).

The discharge in a counter is initiated by the production of at least one positive ion and a free electron. The electron is accelerated towards the anode by the electric field. In the immediate vicinity of the anode

the acceleration is so great that the electron ionizes by collision and thus liberates more electrons. The secondary electrons produce further ionization and an electric discharge results. The condition for the onset of a discharge is roughly that the potential drop along a mean free path of an electron in the vicinity of the anode should exceed the ionization potential of the gas molecules.

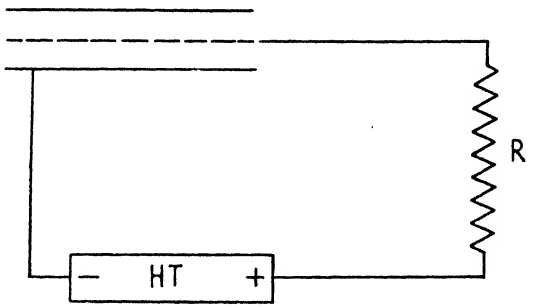

FIG. 6. External quenching of counter discharge.

According to the experiments of Werner (1934) the actual condition for counting action to set in is that the potential drop along seventy mean free paths exceeds 400 V.

84. The discharge proceeds in the following way.

In the region round the anode, where the potential gradient is sufficiently large, positive and negative ions are produced and secondary electrons are set free. The negative charge is absorbed by the anode and the positive ions having a small mobility remain, giving rise to an increasing amount of space-charge. The space-charge weakens the field until secondary ionization ceases and the discharge comes to an end.

For a short period t_d the ions remain in the vicinity of the anode. This period lasts for 10^{-4} to 10^{-3} seconds and during this time the counter remains insensitive to ionizing particles.

The positive ions are eventually driven off and neutralized at the cathode. While the positive ions are dispersing, the field in the vicinity of the anode increases in strength; it reaches its full strength as soon as all ions have disappeared. There is a period t_r for which the field, though not fully recovered, is already strong enough to make the counter sensitive. This period is of the same order as the dead time and is usually called the recovery time.

The dead time and recovery time were discovered by Cosyns (1936*b*). They were also investigated independently by Stever (1942) and by others.

After dispersal of the positive ions the discharge does not necessarily come to an end. The positive ions have a tendency to emit secondary electrons on impact with the cathode. These electrons give rise to secondary discharges. There are two ways of preventing secondary discharges.

(c) *Quenching of the Counter Discharge*

External quenching

85. A large leak resistance R is used (Fig. 6). The current flowing during a discharge produces a voltage drop across the resistance R. If the resistance is sufficiently high, then this potential drop reduces the

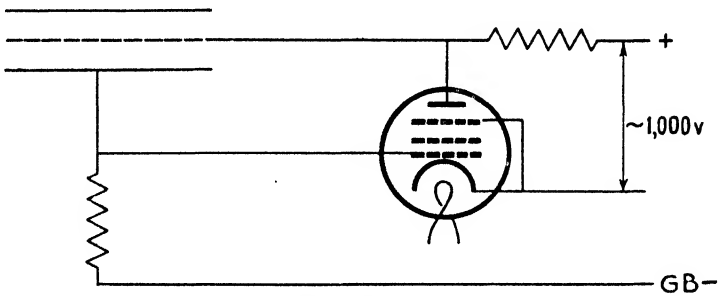

FIG. 7. Neher-Harper circuit.

potential between the counter electrodes to a value below the starting potential of the counter and thus cuts off all further discharges.

How large a resistance R is required to cut off the discharge depends on the characteristic of the discharge—in particular of the nature of the gas. Cosyns found that comparatively low resistances can be used with pure hydrogen or with a mixture of hydrogen and a rare gas.

Resistances of the order of 10^{10} to 10^{11} ohm were frequently used. Hydrogen counters, however, can be used with resistances as low as 10^{9} ohm. It is of advantage to use non-ohmic resistances. Cosyns recommends the use of a very hard photocell illuminated by a small lamp: the illumination can be varied in order to adjust the saturation current through the cell.

The great advantage of the hydrogen counter in comparison with the alcohol counter is its greater stability; in particular the hydrogen counter is independent of temperature while alcohol counters deteriorate when used at low temperatures.

The alcohol counter, however, has the advantage of short recovery time and is also easy to manufacture.

Instead of relying on the quenching of the discharge by means of an external resistance Neher and Harper (1936) use a pentode which cuts off the H.T. of the counter soon after the discharge has set in. The circuit diagram is given in Fig. 7.

Getting (1938) used a multivibrator circuit for cutting off the H.T. after onset of a discharge.

A discussion of the Neher-Harper circuit is given by Maze (1941).

Internal quenching

86. The discharge in counters containing alcohol vapour is quenched internally—Trost (1935–7). It seems that in the presence of alcohol vapour no secondary electrons are emitted after the initial discharge has been stopped by the space-charge. As the quenching of the discharge is independent of the leakage resistance, this resistance can be small and the time constant of the counter output can be made short.

The function of the organic vapour in quenching the discharge was investigated by Korff and Present (1944) and was found as follows:

1. The organic vapour molecules being very heavy are helping to set up the positive space-charge round the anode.
2. The organic vapour molecules absorb photons and thus prevent the discharge from spreading away from the anode.
3. The organic vapour molecules prevent the emission of secondaries from the cathode after the impact of the positive ions.

Spread of discharge

87. It was shown by Brode (quoted by Stever (1942)), Ramsey (1942), Wilkening and Kane (1942), and Stever (1942) that counter discharges spread quickly along the counter wire. The amount of charge liberated in a fast counter discharge is proportional to the length of the wire, and therefore it must be assumed that the discharge takes place uniformly along the wire. The spreading of the counter discharge was demonstrated as follows. The cathode of a counter was split in the middle (Fig. 8). The anode was kept at a constant potential and pulses were registered from both halves of the cylinder. It was found that pulses always occurred simultaneously on both halves of the cylinder, showing that discharges started in either half of the counter spread to the other half. It was further shown that a small bead placed on the counter wire was sufficient to stop the spreading of the discharge. It was concluded therefore that the spread takes place in the region immediately surrounding the wire. The spread is probably due to photons.

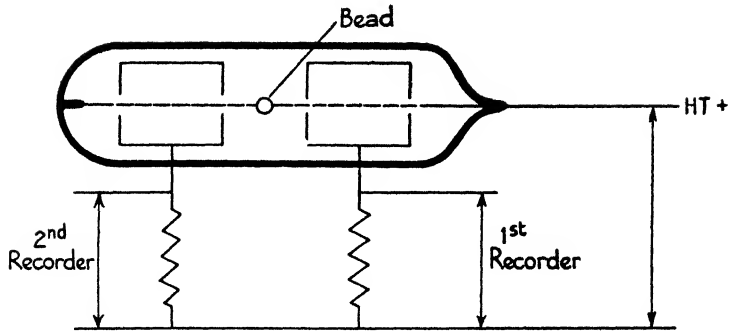

FIG. 8. Investigation of the spread of discharge along the counter wire.

(*d*) *Efficiency of Counters*

88. (i) The efficiency f_0 of a counter is defined as the probability that a discharge is initiated by a particle crossing the sensitive volume. The quantity $1-f_0$ may be called the lack of efficiency. The efficiency of a counter will be found smaller than unity for two reasons. A particle may pass through a counter without giving rise to any ions. This may happen either because the path of the particle through the counter is shorter than the mean free path for an ionizing collision or because of fluctuations. The efficiency determined by this process increases with the pressure inside the counter (Cosyns, 1934). Danforth and Ramsey (1936) measured the efficiency of a counter as a function of the pressure and used the results to determine the density of primary ions along the path of cosmic-ray particles. More refined experiments of this type were carried out by Cosyns (1937, 42).

(ii) Particles passing through a counter during the dead time following a discharge will cause no new discharge, while particles passing through the counter during the recovery time will give rise to pulses smaller than usual. A counter is therefore inefficient for a time t after each discharge given by

$$t = t_d + \alpha t_r,$$

where α has a value between 0 and 1 depending on the minimum size of pulse required to set off the recorder. The efficiency determined by the above process is found to be

$$f_0 = 1 - rt,$$

where r is the rate of discharges registered. For $r \sim 5$ per sec. and $t = 2.10^{-4}$ sec. one finds $f_0 = 99{\cdot}9$ per cent. This is of the same order as the values observed by various observers for fast counters.

(iii) For a slow counter some inefficiency arises due to the fact that for some time after each discharge the counter voltage owing to the external resistance is reduced to a value below starting potential.

The recovery time of a slow counter is of the order of $\frac{1}{100}$ sec. The lack of efficiency of slow counters is therefore much greater.

(iv) It was shown by Rose and Ramsey (1941) that in counters containing some electro-negative gas molecules all electrons liberated by the primary passing through the counter may be captured and the discharge may be delayed or even prevented.

The most serious source of inefficiency is the dead time of the counter after discharge. To shorten the dead time of a counter Simpson (1945) applies a strong negative pulse on the counter wire after discharge and before it has time to disperse the positive ion cloud is absorbed through the counter wire. It is found that the dead time of a counter can be shortened in this way.

2. *The Recording of Counter Discharges*

(*a*) *Single Pulses*

Slow counting rates

89. A simple recorder for counter discharges is shown in Fig. 9 (*a*) and (*b*).

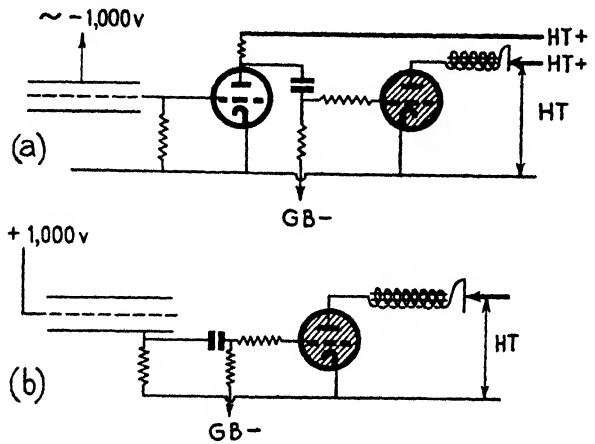

FIG. 9. Recording of counter discharges.

In the circuit of Fig. 9 (*a*) the negative pulse arising on the anode of the counter is fed to the input of a triode or pentode. The reversed and amplified pulse is fed from the input valve to the grid of a gas-filled relay which controls the mechanical recorder. The mechanical recorder

may be of the type used by the G.P.O. to record telephone calls or the high-speed 'Cenco' counter (compare Neher (1939)).

The discharge in the gas-filled relay initiated by the counter discharge can be cut off by a switch in the anode circuit of the relay operated by the mechanical recorder. Difficulties arise sometimes due to the electric disturbance caused by this switch. Circuits for the electric quenching of the discharge of the relay have been given, e.g. by Pickering (1938).

Instead of reversing the counter pulses by an extra stage the gas-filled relay can be operated directly from the counter as shown in Fig. 9 (*b*), where the pulse is taken from the cathode instead of the anode (e.g. Curren and Petrzilka (1939)). The circuit shown in Fig. 9 (*a*) is, however, usually preferred as the amplification obtained by the input stage makes the working of the arrangement more stable.

Counting of fast rates

90. A loss of counts is incurred because the mechanical recorder is unable to record a pulse while resetting. The resetting time $t = 1/M$, where M is the maximum counting rate of the counter. Recording random input pulses, the relation between the recorded rate r and the true rate r_0 is

$$\mathrm{r}_0 = \frac{\mathrm{r}M}{M-\mathrm{r}}. \tag{4}$$

If $\mathrm{r} \ll M$, that is, if the correction is small, eq. (4) can be used safely; the correction becomes uncertain when r approaches M. One can sometimes avoid large correction by using high-speed recorders. For a G.P.O. counter $M \sim 25$ per sec. The Cenco counter can be adjusted so as to give $M = 1{,}000$ per sec.

Alternatively the output rate can be reduced in a constant ratio by using an electric scaling device. The simplest scaling device uses a condenser which stores a constant amount of charge for each input pulse. A gas discharge tube is connected across the condenser, and after a certain number of pulses the discharge tube strikes and discharges the condenser. A large scaling ratio can be obtained in this way but this type of circuit has not been found to be very stable.

Some authors make use of an integrating circuit which allows to read the average counting rate at any instant. A circuit used by Cosyns and de Bruyn (1934) is shown in Fig. 10. The amplifier operates a delicate relay A. For each pulse the relay charges a small condenser C_1. The condenser is discharged into the larger condenser C_2, which is bridged by a resistance R. The voltage across the resistance R adjusts itself to

such a value that the current through R becomes equal to the average rate of charge supplied from C_1 to C_2. Thus the voltage across R is a direct measure of the counting rate. This voltage can be measured with an electrometer.

Similar circuits are described by other authors.

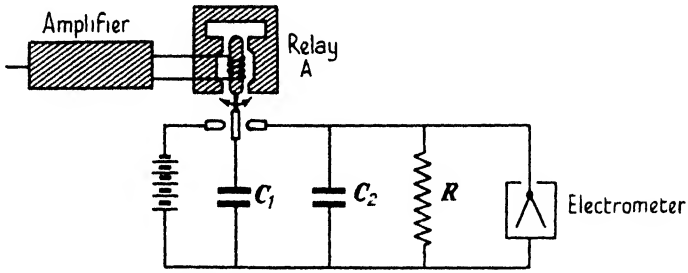

FIG. 10. Integrating circuit (Cosyns and de Bruyn).

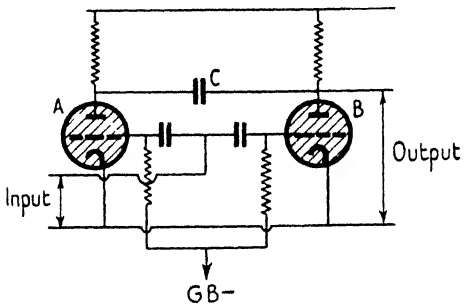

FIG. 11. Wynn-Williams scale-of-two.

91.* A reliable scaling circuit has been devised by Wynn-Williams (1931). This circuit consists of a number of similar scale-of-two units in series, thus giving a scaling ratio of 2^n when n units are used. The Wynn-Williams unit consists of two gas-filled relays in parallel as shown in Fig. 11. The two gas-filled relays are symmetrically arranged and usually one of them is discharging while the other is in the non-conducting state. Assume relay A (Fig. 11) has been struck. A positive input pulse applied to the grids of the two relays will strike a discharge in B but will not affect the discharge in A. The resulting sudden drop of potential on the anode of B is fed to the anode of A through the condenser C, quenching the discharge of A. Thus a positive input pulse causes the discharge to 'jump' from the one relay to the other. Negative input pulses have no effect, as a discharging relay cannot be controlled by the grid. The output of the scale-of-two is taken from the plate of

one of the relays, say B. Positive input pulses give rise alternately to positive and negative output pulses. The output is fed either to another scale-of-two unit or to the grid of a gas-filled relay. In both cases only the positive output pulses and therefore only every other input pulse will be effective.

The Wynn-Williams circuit has been improved by W. B. Lewis (1934).

92.* Scaling circuits have also been devised using hard valves only (see Neher (1939) for a summary). As an example we describe an

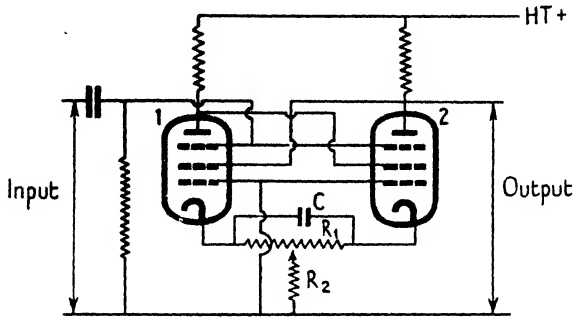

FIG. 12. Scale-of-two (Frisch).

unpublished circuit due to Frisch. The circuit diagram is shown in Fig. 12. It consists of two pentodes. The screen-grid of the pentode 1 is connected to the plate of the pentode 2 and the plate of the pentode 1 is connected to the screen-grid of the pentode 2. As the circuit is symmetrical with respect to the two pentodes a state is possible in which both pentodes carry equal anode and screen currents. For a suitable choice of circuit components, however, this state is unstable, and the stable states are those in which the one pentode carries considerably larger current than the other. The input pulses are applied simultaneously to the suppressor grids of the two pentodes. Positive input pulses will increase for their duration the difference between the anode currents of the pentodes without producing a lasting effect. A negative pulse on the other hand will cut off both anode currents and after the passing of the negative pulse the excess of anode current will have to establish itself in one of the two pentodes. If the state of the circuit were perfectly symmetrical after the currents have been cut off, the excess current could establish itself at random in one of the pentodes. An asymmetry, however, is introduced by the 'memory circuit' consisting of the condenser C and the resistances R_1, R_2. The discharge of the condenser C through R_1 gives rise to a negative bias to the pentode

which previously carried the excess current. Because of this bias the excess current builds up in the other pentode. Thus the excess current is switched over from one pentode to the other by negative input pulses. Alternative positive and negative output pulses are obtained from one of the plates.

(*b*) *Coincidence Counting*

The Rossi circuit

93. Simultaneous discharges of a number of counters are called coincidences. A coincidence between n counters can be caused either

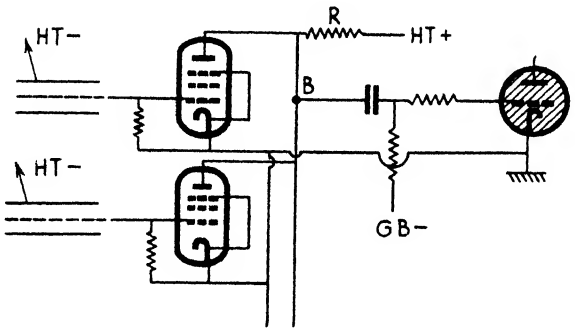

Fig. 13. The Rossi circuit.

by one particle passing through the counters or by a number of simultaneous particles discharging the counters individually.

Coincidences are usually recorded by a circuit due to Rossi (1930) (Fig. 13). Each counter is connected to the grid of a pentode. The plates of the pentodes are connected together, and they are fed through the common load resistance R. The value of the resistance R is large compared with the impedance of the pentodes; values between 0·2 and 1 MΩ are usual. Most of the voltage drop takes place across R and the plates are kept at a voltage amounting to a small fraction of the applied voltage Φ. The total current does not change much if the anode currents in some of the pentodes are cut off by negative pulses applied to the grids as long as at least one pentode remains conducting. The voltage at the point B where all the anode leads meet will therefore not change appreciably when some of the pentodes receive negative pulses. If, however, all the pentodes receive negative pulses simultaneously, the anode current will be cut off completely, and a large voltage pulse at the point B results. A gas-filled relay coupled to the point B can be made to respond to the large coincidence pulses but not to the smaller

pulses due to discharges not involving all the counters. As the difference in size between the two types of pulse is large it is easy to discriminate between them.

Resolving time

94. Any arrangement recording coincidences is bound to record both genuine and also accidental coincidences, i.e. coincidences caused by

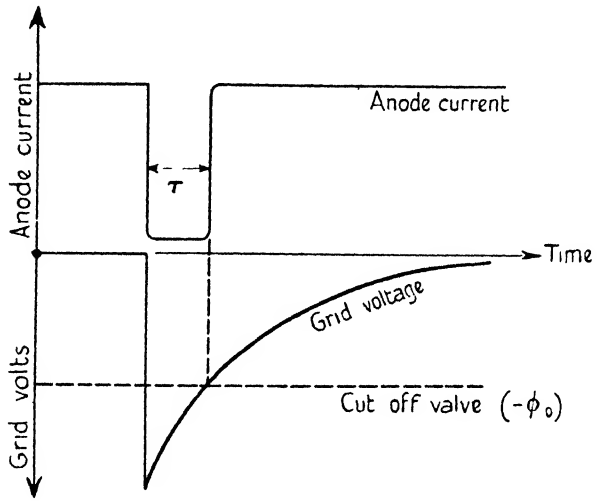

FIG. 14. Grid voltage and anode current variation caused by counter discharge.

independent particles arriving at too short an interval to be resolved by the arrangement. The resolving time of the Rossi circuit depends on the values of the components and is estimated as follows.

The voltage pulse on the grid of one of the pentodes is shown schematically in Fig. 14. The voltage drops rapidly to some negative value $-\Phi$ and rises again exponentially to the original value. The anode current of the pentode is cut off rather suddenly when the grid approaches the value $-\Phi_0$. The change of anode current with time is also shown in Fig. 14. The anode current pulse is nearly square. One finds easily that the width of the anode pulse is approximately

$$\tau = \frac{\log(\Phi/\Phi_0)}{CR}, \tag{5}$$

where R is the resistance of grid to earth, C is the sum of the capacities of counter wire and grid. With $C = 2.10^{-5}\,\mu\text{F}$, $R = 0{\cdot}1\,\text{M}\Omega$, τ is found to be of the order of a few micro-seconds. Shorter resolving times cannot be obtained with the ordinary Rossi circuit because of the finite break-

down time of the counter voltage which is itself of the order of a micro-second. Resolving times down to one micro-second can, however, be obtained by inserting one or more amplifying stages between the counter and the input of the Rossi circuit. The amplifying stages are used to 'sharpen' the pulse obtained from the counter (compare e.g. Maze, 1941).

A coincidence circuit with a resolving time better than 10^{-7} sec. has been described by Brandt and Scherrer (1943). The disadvantage of too high resolving power circuits is that they lead to loss of genuine coincidences. The time of travel of electrons through the counter is not much less than 10^{-7} sec. and therefore random delays of this order are to be expected betwen the passage of the particle and the onset of the discharge, hence genuine coincidences are sometimes separated so much that they are not recorded by a high resolving amplifier.

Rossi and Nereson (1942) find delays up to a fraction of a micro-second in ordinary alcohol argon counters. According to Brandt and Scherrer (1943) half of the pulses are delayed up to 3.10^{-8} sec.

Accidental coincidences

95. Consider n counters, the rates of pulses registered by the counters being $N_1, N_2, \ldots, N_n$. An accidental n-fold coincidence takes place when each of the counters registers a pulse inside an interval τ, where τ is the resolving time of the recorder. The rate of accidental coincidences due to n-fold overlappings can be shown to be

$$A_n = nN_1 N_2 \ldots N_n \tau^{n-1} + \text{terms of higher order in } \tau. \qquad (6)$$

Compare e.g. Eckart and Shonka (1938); for terms of higher order Schrödinger (1944*b*) and Jánossy (1944*a*).† Under practical conditions $N\tau \ll 1$ and therefore the terms of higher order are usually negligible.

In particular for $n = 2$ one finds

$$A_2 = 2N_1 N_2 \tau + \ldots = N_1 e^{-N_1\tau} + N_2 e^{-N_2\tau} - (N_1 + N_2) e^{-(N_1+N_2)\tau}. \qquad (7)$$

When evaluating the rate of accidental coincidences in an n-fold arrangement, $n > 2$, one finds that this rate consists of a number of terms. Accidental coincidences will arise when a genuine $(n-1)$-fold coincidence overlaps with a single pulse in the nth counter. The rate of such coincidences is given by

$$2(\mathscr{C}^{(1)}_{n-1} N_1 + \mathscr{C}^{(2)}_{n-1} N_2 + \ldots + \mathscr{C}^{(n)}_{n-1} N_n)\tau + \text{terms of higher order,}$$

† The exact expression is

$$A_n = \left(\sum_{i=1}^{n} \frac{N_i e^{-N_i\tau}}{1 - e^{-N_i\tau}}\right)(1 - e^{-N_1\tau})(1 - e^{-N_2\tau}) \ldots (1 - e^{-N_n\tau}).$$

where $\mathscr{C}_{n-1}^{(i)}$ is the rate of genuine $(n-1)$-fold coincidences which are not accompanied by the discharge of the ith counter. Accidental coincidences arise further from the overlap of genuine $(n-2)$-fold coincidences with two single pulses and so on. The contributions thus obtained are of the order of $\tau, \tau^2, \ldots$, and so on. It is useless, however, to add the various contributions unless the 'terms of higher order' (eq. (6)) are included in every contribution.

In many practical cases it is sufficient to neglect all but the term in τ.

Determination of the resolving time

96. The simplest method of determining the resolving time τ of an arrangement is to record coincidences of two distant counters. If the distance is sufficiently large, the rate of genuine coincidences can be assumed to be small and most of the coincidences recorded can be taken to be accidental. From the observed rate of accidental coincidences τ can be determined by means of (7). This method is, however, reliable only if the resolving time of the arrangement is long, that is, of the order of 100 μsec. or more. For shorter resolving times the accidental rate may be of the same order as the rate of coincidences due to extensive air showers even for distances between the counters of the order of a few metres.

A short resolving time can be determined, however, by exposing one or both of the separated counters to a radioactive source. By comparing the increase of coincidences accompanying the increased single rates the resolving time of the arrangement can be determined.

The resolving time of an arrangement can also be determined directly either by applying artificial pulses with known time interval to the inputs (compare Getting (1937)), or by counting genuine coincidences and delaying electrically the input pulses to one input. The time of delay sufficient to decrease the coincidence rate noticeably is equal to τ.

Modifications of the Rossi circuit

97. For a large number of experiments it is useful to modify the Rossi circuit. Take as an example the recording of showers by means of n counters placed in a horizontal plane. Coincidences between some of these counters will be caused by particles moving in a nearly horizontal direction and by showers of particles. Showers are expected to discharge some of the counters, and the set can be made very sensitive to showers if it is arranged that coincidences between any two counters are recorded.

A very simple circuit can be employed for the recording of any twofold

coincidence between three counters. The diagram is shown in Fig. 15. Each of the three counters is connected to two out of three pentodes so that there is one pentode corresponding to each counter to which it is not connected. It is seen easily that discharges of any two of the counters affect all three pentodes. Thus if the pentodes are used with

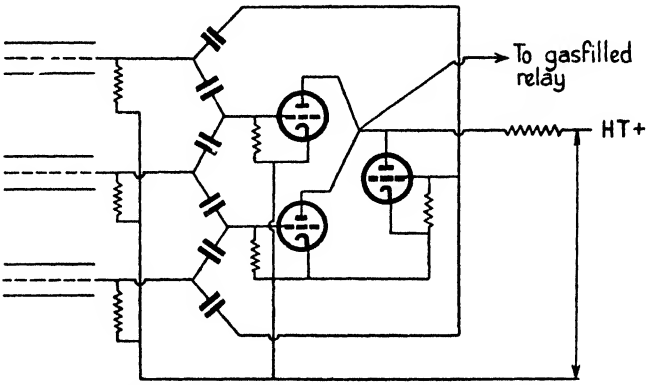

FIG. 15. Counting of twofold coincidences between three counters.

a common load in an ordinary Rossi circuit then large output pulses are obtained whenever at least two counters discharge.

The above method can be used with advantage in many other cases. Before designing more complicated amplifiers to select coincidences of a specified type one should find out whether the selection can be obtained more simply by cross connexions as described above.

Anticoincidences

98. It is often desirable to ascertain whether some counters of a given arrangement are *not* discharged while the others take part in a coincidence. Coincidences of this type are usually called anticoincidences. An anticoincidence 1, 2, $-A$ for instance means a coincidence between the counters 1 and 2 which is not accompanied by the discharge of the counter A.

The following method is often suggested for the recording of anticoincidences (compare e.g. Strong, *Laboratory Technique*). The negative counter pulses are fed to pentodes in the usual way, but the impulse of the anticoincidence counter is reversed and the anode current of the pentode corresponding to the anticoincidence counter is cut off by negative bias (Fig. 16). Usually therefore the pentodes in the coincidence stages carry current while that of the anticoincidence stage does not carry current.

A large voltage pulse at the junction of the plates is obtained therefore when all the coincidence pentodes receive negative pulses, as in this case the anode current is cut off completely for the duration of the pulse. If, however, the coincidence is accompanied by the discharge of the anti-coincidence stage, then the anticoincidence pentode becomes conducting

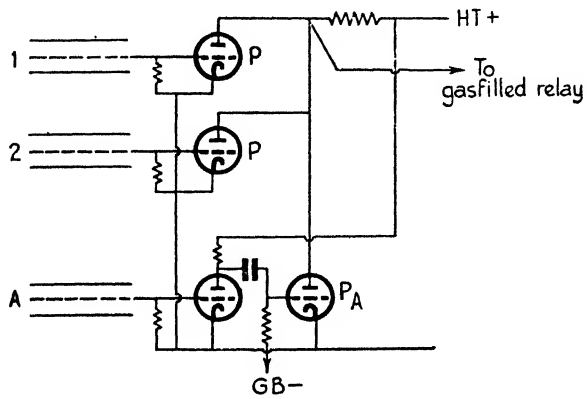

FIG. 16. Anticoincidence amplifier.

for the duration of the pulse and the current through the anticoincidence pentode suppresses the voltage pulse and no coincidence is registered.

This circuit cannot be recommended, however, if a very strict selection of anticoincidences is required.

99. No anticoincidence circuit can discriminate absolutely between coincidences and anticoincidences. It is, however, possible to make the discrimination safe in one direction: i.e. a discriminator can be made so as to reject *all* coincidences, but it cannot be avoided that such a discriminator would also reject occasionally some anticoincidences. The opposite extreme would be a discriminator which passes *all* anti-coincidences but occasionally passes also some coincidences.

The intermediate type would be a discriminator which is subject to both kinds of errors: occasional passing of coincidences and occasional rejecting of anticoincidences, the two errors compensating each other on average.

Which of the three types of discriminators is preferable has to be decided with a view to the experimental requirements. For many applications, especially for the investigation of non-ionizing radiation, the first type of requirement is needed. In such experiments (see §§ 288, 296) a few anticoincidences may be missed, but it is of importance that no coincidences should be recorded for anticoincidences.

100.* A circuit which is safe in rejecting all coincidences was designed by Rossi and co-workers (1940). The circuit is shown in Fig. 17. Its function is briefly as follows.

The coincidence pulses are fed to the grid of a gas-filled relay T_1 while the anticoincidence pulses are fed to the grid of a second gas-filled relay

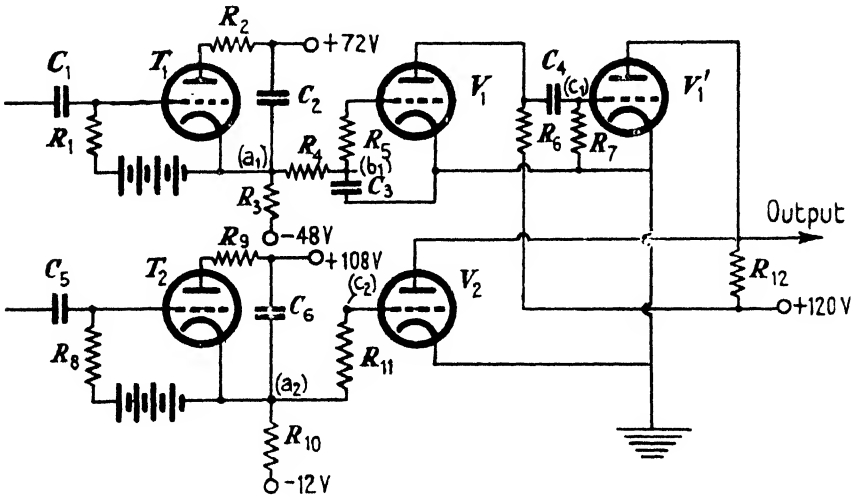

Fig. 17. Anticoincidence amplifier.

T_2. The pulses initiate arcs in the gas-filled relays; by a suitable RC circuit these arcs are quenched and the relays reset after about 100 μsec. The coincidence pulse is delayed and shortened by a pentode V_1 and fed to a second pentode V_1'. The anticoincidence pulse is fed directly to a pentode V_2. The pentodes V_1' and V_2 operate in a way similar to the pentodes P and P_A in Fig. 16. Thus the pentode V_2 is biased so as to carry no current in the passive state while V_1' carries full current in the passive state.

An anticoincidence cuts off the current in V_1' and does not affect V_2, thus such a pulse gives rise to a large rise of potential in the output, and thus sets off the recording relay.

A coincidence which is not an anticoincidence operates both pentodes V_1' and V_2. But owing to the shaping of the coincidence pulse in the stage V_1 the current in V_1' is cut off *after* the current in V_2 has come on, and the current in V_1' starts again *before* the pentode V_2 has gone back to its passive state. Thus the action of the two pentodes overlap and no coincidence is recorded even should the anticoincidence counter discharge be slightly delayed due to some accidental process as discussed in § 88.

We note that the slow recovery of the relays T_1 and T_2, far from being a disadvantage, is in fact an essential feature of the circuit.

During the recovery time of T_2 the amplifier is effectively blocked. This time, however, coincides with the dead time of at least one of the anticoincidence counters. But during the dead time of any of the anticoincidence counters the anticoincidence system is not fully effective

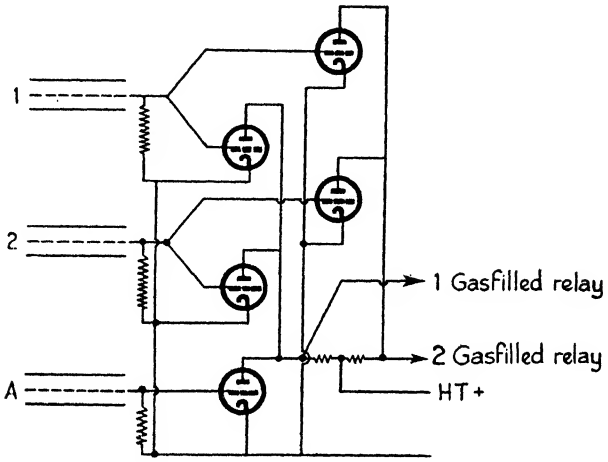

FIG. 18 (*a*). Anticoincidence amplifier.

and thus safe discrimination is not possible during such a period. Thus the relay T_2 blocks the amplifier during such periods in which safe discrimination between coincidences and anticoincidences is impossible.

During the recovery time of T_2 some genuine anticoincidences are also suppressed. This loss of anticoincidences cannot be avoided if it is essential to have strict discrimination.

101.* If no extreme discrimination is needed simple methods can be used. For instance, anticoincidences $1, 2, -A$ can be recorded as follows.

We record simultaneously coincidences $1, 2$ and coincidences $1, 2, A$. The difference between the counts obtained is equal to the number of anticoincidences. It is, however, important that the two types of coincidences are observed simultaneously.

These coincidences can be recorded by different methods, but we shall describe two of them—Fig. 18 (*a*) and (*b*).

Two pentodes (Fig. 18 (*a*)) are controlled by each of the coincidence counters 1, 2, while a fifth pentode is controlled by the anticoincidence counter A. Two pentodes, one from each coincidence counter, are connected in one Rossi circuit while the remaining three pentodes are

connected in an independent Rossi circuit. Whenever the twofold circuit responds without the threefold we have an anticoincidence.

The second method is as follows:

Each counter is connected to a separate pentode (Fig. 18 (*b*)). The coincidence pentodes are fed through a common load resistance R_1 while the anticoincidence pentode is also fed through the same resistance but

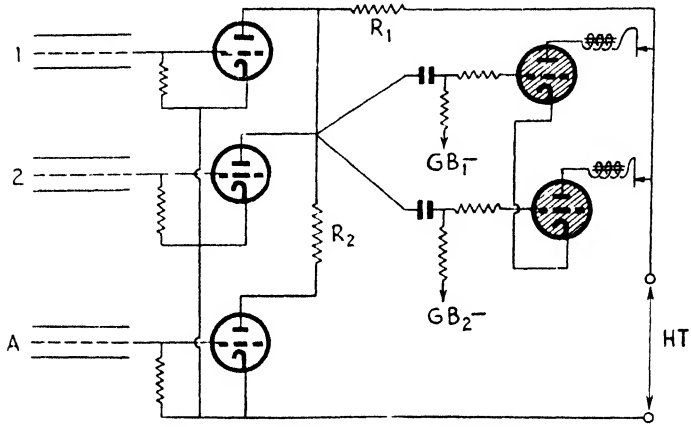

FIG. 18 (*b*) Anticoincidence amplifier.

through an additional resistance R_2. Pulses at the junction of the anode leads caused by counter discharges are of different sizes.

1. In case of a coincidence between all of the three counters the currents in all pentodes are cut off and a very large pulse results.
2. In case of a coincidence 1, 2 not accompanied by A the coincidence pentodes are cut off; the size of the resulting pulse is, however, reduced due to the current flowing through the resistance R_2 and the last pentode.
3. In case of coincidences not involving all the coincidence pentodes only very small pulses are obtained due to the current flowing through the unaffected coincidence pentode.

The pulses are fed to the grids of two gas-filled relays, and by means of suitable bias these relays discriminate between the very large pulses corresponding to coincidences 1, 2, A and the large pulses corresponding to coincidences 1, 2, without A.

Self-recording counters

102.* It is often useful, particularly for recording showers, to have the following arrangement. A number of counters S each control a neon lamp. Whenever a second set of master counters records a coincidence

the neon lamps record which of the counters S has been discharged simultaneously with the coincidence.

Circuits serving this purpose have been given by Johnson and Stevenson (1933), Jánossy and Ingleby (1942). A large set containing over a hundred neon lamps has been constructed by V. H. Regener (1943).

Regener's† circuit is shown in Fig. 19. It works as follows. Neon bulbs $s_1, s_2 \ldots$ are controlled by the counters $S_1, S_2 \ldots$ in the following way.

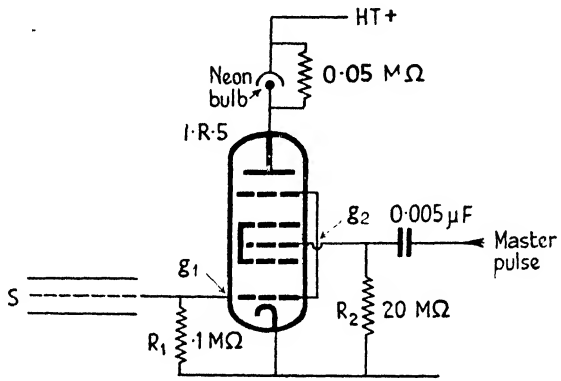

FIG. 19. Self-recording unit (Regener).

The neon lamps s are usually on. A master pulse extinguishes for a short time all the bulbs s except those which correspond to counters S taking part in the coincidence.

The bulbs s are covered by a shutter. The shutter opens shortly after each master pulse M and while the shutter is open all the neon lamps which have not been extinguished by the master pulse are recorded photographically.

The grids g_1 and g_2 of the hexode are earthed through the resistances R_1 and R_2; the neon bulb is inserted into the anode circuit and the bulb is on in the quiescent state. The neon lamp is by-passed by a 0·05 MΩ resistance. For each master pulse a positive pulse is applied to the grid g_2. The positive pulse draws grid current and after the pulse a negative charge is left on the grid g_2. This charge leaks away slowly through the large resistance R_2 and the anode current is blocked for a considerable time after the master pulse. The bulb is extinguished for the period where the anode current is cut off.

The counter S is coupled directly to the grid g_1. The negative pulses

† I am indebted to Dr. V. Regener for communicating the details of his circuit.

coming from the counter S cut off the anode current for short periods: these periods are too short to affect the neon lamps noticeably. If, however, the master pulse comes simultaneously with the pulse of the counter S, then the master pulse cannot draw grid current as the current is cut off by the first grid g_1 and therefore the anode current comes on again after the passing of the pulses. The bulb s will therefore be lit while the shutter opens provided the hexode has received simultaneous pulses M and S.

The above circuit may appear at first sight to be unnecessarily complicated. It might seem simpler to have the neon lamps extinct in the quiescent state and flashing only while recording. It is found, however, that neon lamps which have not been flashed for a long time do not strike readily and therefore special precautions are necessary when neon lamps are to be flashed in long intervals. Regener's method is of great advantage as the neon lamps are kept on all the time.

Delayed coincidences

103. For the direct measurement of the mean life of the meson it is necessary to record the time interval between a coincidence caused by an incident meson and the subsequent emission of the decay electron. Circuits of this type have been described by Maze (1941), Rasetti (1941), Auger, Maze, and Chaminade (1942), and by Rossi and Nereson (1942).

C. The Cloud Chamber†

104. The cloud chamber was invented by C. T. R. Wilson (1911) in the course of experiments on the formation of artificial clouds. It is now a research tool with a scope far greater than its application to cosmic-ray phenomena.

1. *Technique of the Cloud Chamber*

(*a*) *The Operation of the Cloud Chamber*

Expansion ratio

105. Wilson studied cloud formation initiated by adiabatic expansion in a vessel. A cloud can be formed when a volume of gas, saturated with water vapour, is expanded adiabatically. The adiabatic expansion causes the gas to cool and to become supersaturated; in the presence of condensation nuclei droplets may be formed round these nuclei.

An important characteristic of the expansion is the *expansion ratio*, that is the ratio of the volume before and after the expansion.

† Section C is largely due to Dr. J. G. Wilson.

At small expansion ratios condensation takes place round dust particles. This kind of cloud formation is usually undesirable and it can be got rid of by expanding the gas several times in succession. The droplets forming round the dust particles contained in the gas fall in form of a fine rain to the bottom of the chamber carrying the dust particles away.

106. Once the dust particles have been removed no condensation of water vapour takes place unless the expansion ratio exceeds 1·25. For expansion ratios exceeding 1·25 condensation takes place on negative ions. Condensation of water on positive ions starts for ratios exceeding 1·31. At a very slightly greater expansion ratio other nuclei of condensation become effective in numbers which increase rapidly as the expansion ratio is increased.

For the investigation of tracks of fast particles one utilizes the ions which are formed along the path of the particle. In order to obtain satisfactory cloud tracks one has to adjust conditions so as to obtain drops on all ions produced by the fast particles accompanied by as small a number of background drops as practicable.

Background

107. Background condensation is caused by a number of processes. An important source of background is the formation of droplets at expansion ratios exceeding that necessary for the condensation of positive ions. This last form of condensation takes place on uncharged molecules or small molecular aggregates, and the expansion ratio of onset is extremely sensitive to the contamination of the chamber by molecules or aggregates, upon which condensation takes place more readily than in an uncontaminated chamber. Since the difference of expansion ratio between that appropriate to ion condensation and that for the background condensation is small, scrupulous care is required in practice to avoid the introduction into the chamber of materials with a tendency to increase background. Aluminium is usually considered to be unsatisfactory material from this point of view, and its use in contact with the interior parts of the chamber is as a rule avoided; knowledge of contamination background is, however, still largely empirical.

108. After a normal expansion into the region of ion condensation it is found that a certain number of nuclei persist in the chamber for a considerable time. They are probably formed by the incomplete evaporation of some of the droplets to small equilibrium size. For these nuclei condensation takes place with an ease comparable to that for small dust

particles. A succession of track expansions will quickly lead to an unacceptable concentration of this additional background condensation and it is therefore necessary to remove these nuclei after using expansions into the ion condensation region.

This can be done by means of normal expansions to an expansion ratio less than the ion limit.

Mechanically it is more convenient to remove the nuclei formed after a normal expansion by a smoothed slow expansion to the full expansion ratio. In such a slow expansion the normal gas heating from the chamber wall does not permit the full supersaturation to be reached: the effect of the slow expansion is therefore equivalent to a fast expansion to a lower expansion ratio.

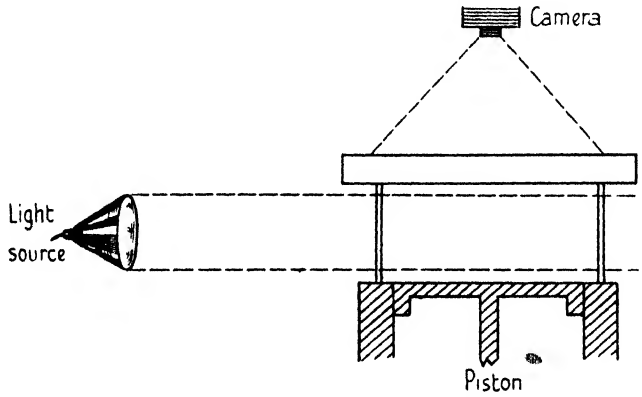

FIG. 20. Scheme of cloud chamber.

(*b*) *Construction of Chambers*

(*Compare Blackett* (1927), *Auger* (1926))

109. The basic features of a cloud chamber for the photography of tracks is illustrated in Fig. 20. The chamber has a transparent window of good optical quality facing the camera. The cylindrical wall is also transparent, the illumination entering through this wall. The expansion is made by moving the piston mechanically through a determined distance.

Since the expansion ratio of the chamber requires frequent adjustment, it is necessary to furnish means to adjust continuously the stroke of the piston.

As a rule the piston is made to move between stops, of which one set is adjustable from outside the chamber.

110. The chamber is operated either at will of the observer or by a

trigger system such as the counter control (see § 123). In either case the photograph of tracks is taken a fraction of a second after the expansion has been made. This may be done with a normal photographic shutter, but it is frequently profitable to place the apparatus lamp in a passive state chamber and camera in a dark enclosure and flash the light source in order to take the photograph. So much light is needed that the heating effect of a continuously running lamp would give rise to an appreciable disturbance of the chamber.

111. An electrostatic field within the chamber sweeps ions out of the gaseous volume very shortly after their formation. The ions formed within a small fraction of a second before expansion, or during the period after the expansion for which sufficient supersaturation persists, stand out conspicuously, and give droplets very close to their points of formation. The track of a fast ionizing particle therefore appears as a line of droplets, the number of drops corresponding to the number of ions formed.

Limits of expansion ratio

112. The expansion ratio for a particular condensation phenomenon (for example that for condensation on ions of a given sign) is defined as the ratio of volume of chamber after the expansion to volume of the chamber before the expansion, the expansion being assumed to be sufficiently rapid to make conditions adiabatic.

Practical interest is confined to the ion condensation limits of various vapours for which ion condensation takes place at an appreciably lower ratio than the background condensation (Przibram (1906), Laby (1908)). There is a different limiting ratio for condensation on negative and positive ions; water appears to be unique in condensing preferably on negative ions.

113. The numerical value of the expansion ratio is a function of gas and vapour. As regards the gas, the expansion ratio is determined to give a certain drop of temperature, $d\theta$; hence for adiabatic change

$$d\theta/\theta = (\gamma-1)d\mathscr{V}/\mathscr{V}.$$

Monatomic gases ($\gamma = \frac{5}{3}$) therefore require smaller expansion ratios than diatomic gases ($\gamma = \frac{7}{5}$), and usually argon is used when the distortion attending expansion is to be reduced to a minimum.

Since the condensing vapour is as a rule polyatomic, and is present to a constant vapour pressure, the expansion ratio is a function of the total pressure; in very high pressure chambers (Johnson, Benedetti, and Shutt (1943)) the effective γ is almost that of the permanent gas and the

expansion ratio correspondingly low, while at low pressures γ is reduced towards that of the vapour and a higher expansion ratio is required.

Vapours requiring a smaller expansion ratio than pure water are known, and in particular ethyl and propyl alcohols and their aqueous mixtures have been studied. In these mixtures the expansion ratio for ion condensation varies continuously with composition, and there is a mixture of minimum expansion ratio (Flood (1934)).

114. Combinations of gas and vapour with low expansion ratios are of practical importance when precision measurements are to be made on tracks of particles which traverse the chamber before expansion. The distortion of such a track at expansion is ideally a simple strain in one dimension, but this clearly fails to describe the motion in the neighbourhood of the chamber walls and of absorbing plates within the chamber. Deviations from the simple motion are reduced to a minimum by reducing the whole of the motion as far as possible. The monatomic gases with water alcohol mixtures are generally preferred for use in counter-controlled expansion chambers.

Spreading of the negative ions due to slow transition from free electrons to heavy negative ions has been reported when a pure monatomic gas was used. A small proportion of oxygen is frequently added therefore to minimize such spreading.

Sensitive time

115. When a cloud chamber is expanded to a degree slightly greater than the minimum required to permit condensation on ions, the sensitive time of the chamber is the interval between the time when minimum supersaturation is first attained and that at which it is last present as the whole of the gas of the chamber heats up.

A considerable sensitive time is of value in some cosmic-ray applications, but it must be emphasized that the sensitive time is not the distortion-free time, and applications involving precise measurements require the selection of tracks over an extremely short range of time.

116. In the absence of heavy condensation, and assuming the initial supersaturation to be attained instantly, Williams (1939*a*) showed that after expansion the gas near the chamber wall is heated by conduction and that the gas remote from the walls is then compressed adiabatically. This central mass of gas therefore all becomes insensitive for track formation at the same time. Williams gives the expression

$$t = 0{\cdot}77 \frac{\rho s}{\kappa(\gamma-1)^2} (\mathscr{V}/\mathscr{S})^2(\delta r/r)^2 \qquad (8)$$

for the sensitive time t, where $\mathscr{V}$ is the volume and $\mathscr{S}$ the total surface area of the chamber, κ is the thermal conductivity of the gas, s is the specific heat, r is the expansion ratio, and $r-\delta r$ the smallest ratio for ion condensation. This relation applies only in a chamber sufficiently large to have a region for which conductive heating is inappreciable in the time t. The sensitive time is further limited by condensation, which simultaneously leads to depletion of vapour in the body of the chamber and the release of heat of condensation.

The sensitive time may be artificially extended by the method described by Beardon (1935) in which the fall of supersaturation is counteracted by a continued slow expansion.

Resolving time

117. The interpretation of observations either with counter systems or with the cloud chamber must frequently be based on the assumption that particles are contemporary and are thus associated in origin. The resolving time, the minimum interval between events for which the existence in difference of time can be established, is therefore an important constant either of counter arrays or of cloud-chamber arrangement.

The cloud chamber is very much inferior to counter systems in its ability to distinguish events of small separation in time. In any photograph sharp tracks are formed on the trajectories of all particles entering the chamber between establishment of critical supersaturation and either the time of photography or the end of sufficient supersaturation, whichever is the earlier. Particles entering during this period cannot therefore be distinguished as to their time of entry.

118. Operating a chamber by counter control (see § 123), the triggering particles enter the chamber before the expansion, and the extent of the ion diffusion before expansion provides a measure of the age of individual tracks.

Blackett (1934) has shown that X, the 90 per cent. breadth of the track image (i.e. the breadth containing 90 per cent. of the drop images), is given by

$$X = 4{\cdot}68\sqrt{(\mathscr{D}t)}, \tag{9}$$

where $\mathscr{D}$ is the diffusion coefficient of the ions and t is the time from the passage of the particle to drop formation.

Only particles with a track breadth X corresponding to the time t can be regarded as simultaneous with the particles which have triggered the control system. Therefore in a counter-controlled photograph only the tracks with the breadth X as given by (9) can be regarded as

contemporary. If the photographic technique does not enable us to distinguish tracks of breadth X' from those of the breadth X, with

$$fX < X' < X/f \quad (f < 1), \tag{10}$$

then the tracks formed during an interval

$$T = t(f^{-2} - f^2) \tag{11}$$

appear to be of the same breadth.

Under good conditions, f may be as great as 0·7, and in a chamber designed for rapid controlled operation t may be less than 0·01 sec., then T will be of the order of 0·01 sec.; no great improvement on this figure seems likely.

In a slow chamber of the porous diaphragm type and with less critical technique, T may very easily become as great as 0·03 sec.

Illumination

119. The drops formed in an expansion grow to nearly full size in a time of the order of 10^{-3} sec. The amount of light scattered by a drop increases with the size of the drop, thus photography should not take place earlier than about $\frac{1}{1000}$th of a second after the onset of drop formation.

Unless photography is delayed to make use of the prolonged sensitivity of the chamber, speedy photography is of advantage (see § 125). To obtain the optimum timing of the photograph provision is made for varying the time interval between the expansion and flash or shutter movement. The time interval is reduced until the intensity of the image starts to decrease.

120. Webb (1935) has shown experimentally that drops scatter only a very small amount of light at right angles. Unfortunately, for practical reasons one has to use for the photography of tracks light which is scattered nearly at right angles to the illuminating beam (see Fig. 20). Very strong sources of illumination are therefore required. It is therefore necessary to control the light beam very accurately so as to prevent those parts of the structure of the chamber to be illuminated which are in the view of the camera.

Light sources which have been used with success include the condenser discharge through mercury vapour at atmospheric pressure (C. T. R. Wilson), transformer discharge through a similar lamp (Blackett), flashing of a preheated carbon arc (Anderson), and for work not demanding rapid illumination, the overload flashing of tungsten filament lamps with or without preheating.

All of these sources are likely to be superseded by the condenser

discharge in rare gas mixtures at about atmospheric pressure between suitable electrodes. Lamps of this type have been developed recently with oustanding success and they appear to be exceptionally promising sources for chamber illumination (Hazen).

(c) *The Design of Cosmic-ray Chambers*

Constant pressure change and constant volume change

121. All chambers which are used in cosmic-ray research are based either on the constant volume-change apparatus of C. T. R. Wilson (1911) or on the constant pressure-change apparatus also due to Wilson (1933).

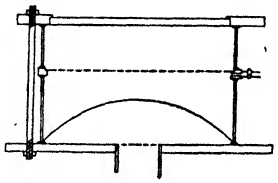

FIG. 21. Constant pressure-change apparatus (C. T. R. Wilson).

The latter does not seem to offer any significant advantage and is for many purposes inferior to the constant volume-change apparatus. The disadvantages of the constant pressure-change apparatus are that it is difficult to make provision for an expansion ratio to remain constant without further attention for a long period of time. Further, the expansion is by nature slow in its later stages and therefore it does not lead to most rapid condensation on pre-expansion tracks.

The use of a flow-controlling partition (see Fig. 21), first described in the pressure-change chamber, however, has frequently been applied to volume-defined chambers. Originally intended to control gas flow, the partition of velvet supported on a perforated metal plate has proved attractive as a photographic background.

When the greatest accuracy of gas flow is required, the function of this partition as a flow regulator is open to criticism, and for work of high precision, where minimum distortion of gas flow is essential, it has not been used.

Requirements of the cosmic-ray chamber

122. The particular characteristics of the cosmic-ray chamber design arise from the following necessities.

1. The chamber has to be used in a vertical plane and therefore the liquid seal used in earlier chambers has to be replaced by some other means.
2. The chamber geometry may have to conform with the geometry of field coils or may have to fit into the gap of an electromagnet.
3. The expansion must be produced *after* the passage of the particle.

The first two of these requirements are sufficiently demonstrated by reference to Figs. 22 and 23: the first shows the design used by Blackett and Occhialini (1933) within a large solenoid. The second shows the chamber designed by Blackett for use in a large electromagnet, where

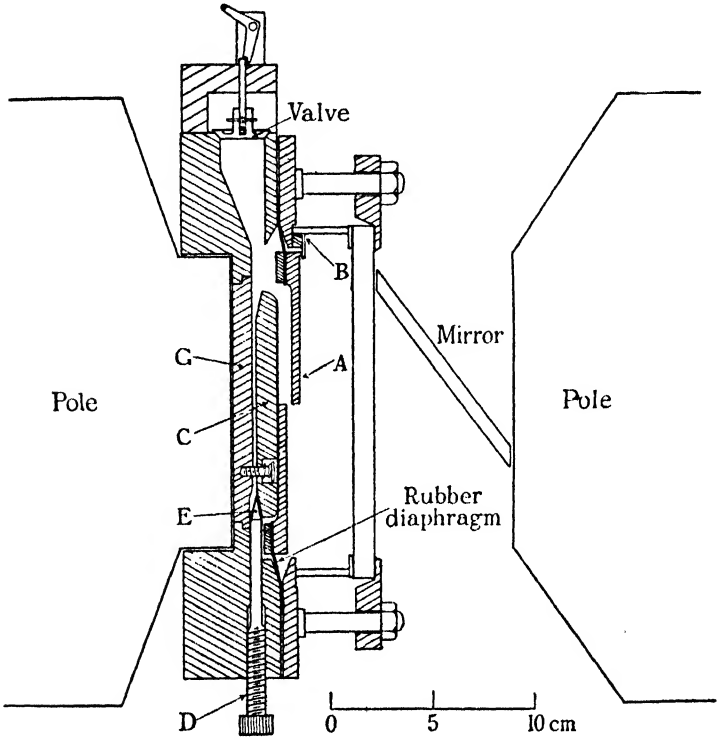

FIG. 22. Cloud chamber, adapted for use between the pole pieces of an electromagnet (Blackett, 1934).

it is essential to allow the air gap of the magnet to be reduced as far as possible.

2. *Counter Control*

123. Blackett and Occhialini (1933) succeeded in triggering a cloud chamber by means of a counter telescope covering the chamber. In this way particles traversing the chamber could be photographed efficiently.

The alternative method to counter control is to make expansions at random and to minimize the time for resetting and cleaning of the chamber. Using random expansions it is difficult to make the chamber sensitive to incoming particles for more than $\frac{1}{1000}$th to $\frac{1}{200}$th of the total time of operation.

Using random expansions the relative efficiency of a chamber can be increased by using large volume and long sensitive time. The particular advantage of the random expansion is that the chamber shows no bias on

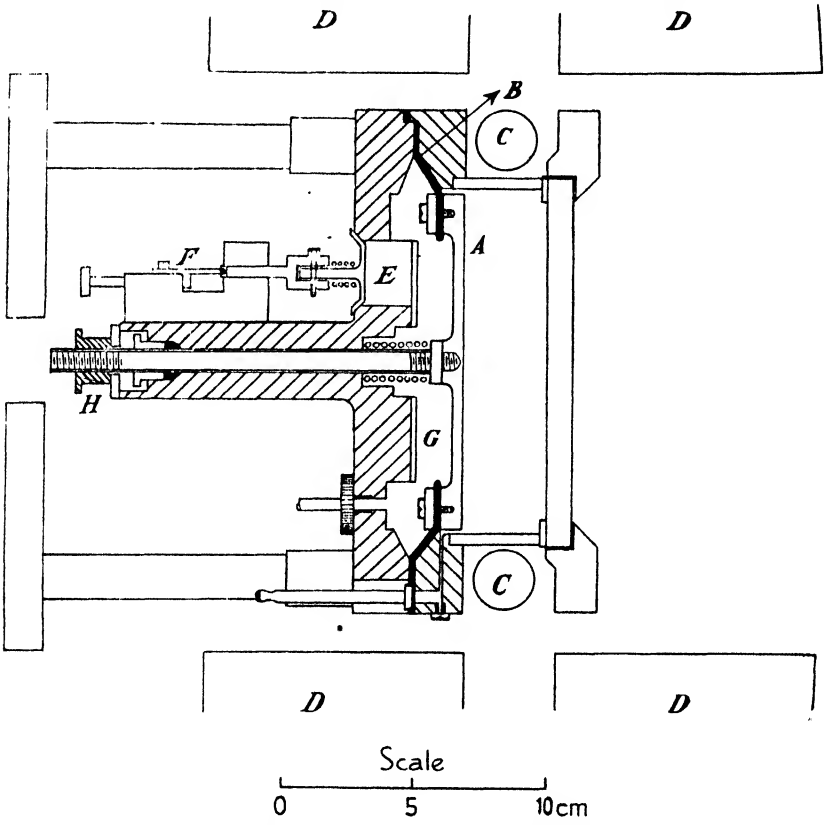

FIG. 23. Layout of cloud-chamber mechanism (Blackett).

the observed sample of particles, while a chamber with counter control necessarily introduces a bias connected with the geometry of the counters.

Large chambers with long sensitive time are, however, unsuitable when precision measurements on the tracks are required. Therefore for precision work counter-controlled chambers are largely used.

More recently, chambers have been operated by more discriminating counter arrays; such systems are described below (e.g. Chap. IX).

(*a*) *Technique of the Counter Control*

124. The technique of counter control has been fully discussed by Blackett (1934). It is shown that a track containing N_0 ions per cm.

will diffuse in a time t so that the projected distribution of ions will be given by

$$\rho(x) = N_0(4\pi\mathscr{D}t)^{-\frac{1}{2}}e^{-x^2/4\mathscr{D}t}, \tag{12}$$

where $\rho(x)$ is the density of ion images at a distance x from the line of formation, and $\mathscr{D}$ is the diffusion coefficient of the ions. The 90 per cent. breadth, X, of the track is given by

$$X = 4{\cdot}68\sqrt{(\mathscr{D}t)}. \tag{13}$$

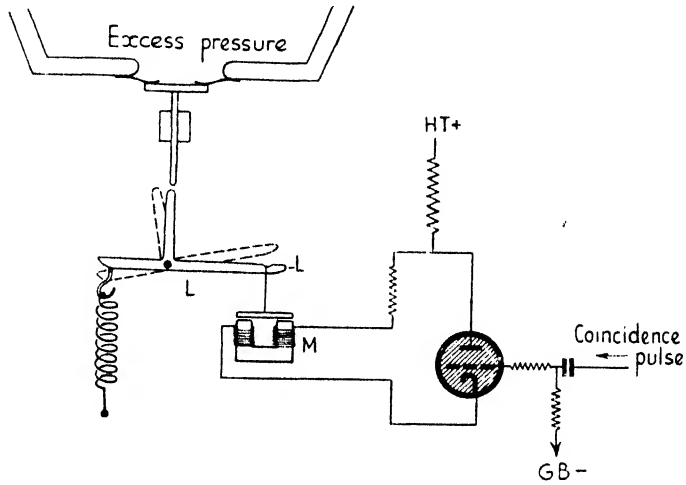

FIG. 24. Operation of the expansion.

For air at N.T.P. for both positive and negative ions $\mathscr{D}$ is 0·034 cm.²/sec., and hence

$$X = 0{\cdot}86\sqrt{t}. \tag{14}$$

This result sets the time scale on which the counter control of cloud chamber must be based. If X is to be less than 1 mm., t must be less than $\frac{1}{70}$th of a second.

This rapid operation is as a rule obtained by releasing pressure behind a piston held forward by excess air pressure, following the mechanism (Fig. 24) developed by Blackett and Occhialini. A mechanism in which the piston is held and released directly has been used with success by Anderson.

125. When it is required to count drops along a track image in order to determine the density of primary ionization by the fast particle, expansion is delayed so that the ions are sufficiently separated by diffusion for the resulting drops to be distinguished. The electric sweeping field will be maintained during the expansion delay in order to separate positive and negative ions into two columns. In water vapour, for example, substantially complete condensation on positive

ions establishes that complete condensation on negative ions has taken place. This technique was applied by Corson and Brode (1938), Sen Gupta (1940, 3), and by Hazen (1944*c*); a photograph of Hazen is shown on Plate 1.

(*b*) *Some Aspects of Counter Control*

126. Using counter control the number of significant photographs can be increased considerably. At the same time, however, some bias is necessarily introduced and a set of counter-controlled photographs cannot in general be taken as a random sample. The bias is particularly disturbing if photographs are taken with the view of determining statistically some properties of the cosmic-ray beam.

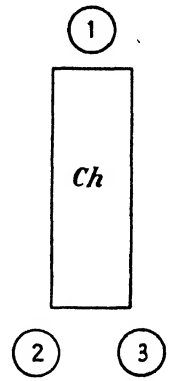

FIG. 25. Chamber controlled by triple-coincidence arrangement.

Consider as an example the determination of the momentum spectrum. Because of scattering of low-energy particles a counter-controlled chamber has always a bias towards high-momentum particles. It is therefore essential for the determination of the low-momentum part of the spectrum to use a random chamber which is free of bias.

For higher-momentum values the bias becomes negligible and therefore the higher-momentum regions can be measured with a controlled chamber which has a much greater efficiency than the random chamber.

127. Counter control was used very successfully to obtain photographs of showers. Using, for example, a chamber controlled by the three counters of a triangular arrangement we expect a high proportion of the photographs to contain showers, as the coincidence arrangement responds to showers only.

128. It must be pointed out, however, that the absolute rate of shower photographs is in general not increased but decreased by a selective control. The main advantage of the control is therefore that unwanted photographs are not taken. Take as an example the arrangement shown in Fig. 25 which is selective for showers. Connecting the two lower counters 2, 3 in parallel instead of having them in coincidence we can reduce the bias in favour of showers. Each shower, however, which is capable of setting off the arrangement when controlled by the more selective triple coincidences is also capable of setting off the arrangement when controlled by double coincidences. Besides, there are showers which set off only one of the counters 2, 3. Therefore the

absolute rate of shower photographs is, if anything, smaller with the triple-coincidence control than with the double-coincidence control.

Rare phenomena

129. The above argument must not be carried too far. There are cases where the more rigid control *increases* the absolute rate of the photographs of some rare types.

Take as an example a search for slow mesons. It will be seen later (§ 277) that the rate of slow mesons traversing a chamber of average dimensions is less than 1 per hour. The rate of single particles is of the order of 2,000 per hour.

Because of the resetting time of a chamber not more than about twenty successful photographs per hour can be taken. Thus working the chamber at its maximum speed one cannot take photographs of more than 20 particles out of every 2,000. The yield is therefore only about 1 per cent. of all particles and if the chamber is controlled by single particles one cannot expect to take photographs of more than 1 per cent. of the slow particles traversing the chamber.

Using a bias in favour of slow mesons the rate of photographs of slow mesons can thus be increased. In the most favourable case one can photograph all slow mesons entering the chamber, in this case the selective control increases the yield by a factor 100.

Similar considerations show that by using a suitable control it should be possible to increase the yield of photographs showing meson decay.

Selection has been used with advantage to obtain photographs of penetrating showers.

130. A suitable counter control can also give information about processes seen on photographs which could not be obtained from the photograph alone.

An anticoincidence control, for instance, can reveal that showers seen inside the chamber are produced by non-ionizing primaries outside the chamber.

Controlling a chamber by a set of counters spread out over a large area one obtains photographs of parts of extensive air showers. Such photographs cannot always be recognized as showing parts of extensive air showers except for the counter control (compare Ch. IX).

3. *The Cloud Chamber in a Magnetic Field*

131. Measurements of track curvature when cloud-chamber photographs are taken in a magnetic field are of the first importance since

they can be used to determine the momentum and sign of the particle. The technique of curvature measurement on trajectories only slightly deviated in the field has up to now been confined to the province of cosmic-ray measurements; this method will therefore be treated in some detail.

Curvature measurement

132. The radius of curvature $\mathfrak{R}$ of the track of a particle of momentum P MEV./c in a magnetic field of H gauss is given by

$$\mathfrak{R} = \tfrac{1}{3}P/(10^{-4}H). \tag{15}$$

Hence the maximum deviation, d, of a length l of track from a straight line is

$$d = l^2/8\mathfrak{R} = \frac{3}{8}\frac{10^{-4}Hl^2}{P}. \tag{16}$$

For $H = 10^4$ gauss, $l = 30$ cm., and bearing in mind that the width of the track is of the order of 0·1 cm., we expect to measure momenta of 1,000 MEV./c readily, while momenta of 10,000 MEV./c should just be recognizable. The method described by Anderson (1933*b*), and very widely followed, using a travelling microscope with micrometer eyepiece set at right angles to the main motion, gives a performance of about this standard.

133. The actual measurement of curvature may readily be carried out to a much higher precision by a method due to Blackett (1937*a*) and improved by Ehrenfest.† This is a null method in which the track image is reprojected through an achromatic prism, placed normal to the axis of the projection lens, on a magnesium-oxide coated screen which is viewed at grazing angle. The prism introduces a curvature, r, into the image of a straight line which is given by

$$\mathrm{r} = \mathrm{r}_0 \sin\vartheta,$$

where ϑ is the angle between the line and the principal plane of the prism. To measure the curvature of the curved track the value of ϑ is determined which produces a straight image, straightness being judged by visual inspection of the projected image at a grazing angle.

The probable error of curvature measurement (referring to the actual curvature on the photographic plate) with an instrument of this type was found by Blackett to be 0·016 m.$^{-1}$, corresponding to a radius of curvature on 2·5 cm. of the image of 60 m.!

This device cannot be used for the measurement of curvatures greater than about $0{\cdot}7\mathrm{r}_0$ and hence this high accuracy of measurement is not

† Unpublished.

available for low-momentum particles. The model of greatest range yet used (J. G. Wilson, 1939) allowed of measurement up to a curvature of 10 m.$^{-1}$ on the photographic plate, corresponding with $H = 10^4$ gauss and a photographic magnification of 0·1 to a particle momentum $p = 300$ MEV./c.

Limitation of momentum measurement

Distortions

134. Disturbances and distortions render measurements of actual momenta very much less accurate than the mere measurement of curvature.

The following are some of the most important sources of error of the momentum determination, apart from the error of measurement of curvature.

1. There are a number of factors which tend to displace the track before photography. Such effects are:

(*a*) Convection currents in motion in the chamber before expansion.

(*b*) Turbulent motion and vortices produced at the expansion.

(*c*) Convection currents developing after expansion from the temperature difference between the chamber wall and the adiabatically cooled gas.

(*d*) Distortion arising from non-axial movement of the piston. The non-axial movement of the piston may be modified by eddy currents due to the magnetic field.

(*e*) Fall of the droplets relative to the surrounding gas according to Stokes's law.

All these distortions, except (*d*), develop after the expansion and therefore they can be reduced by speedy photography.

2. Distortions arise from faults of the photographic technique. We have to be careful to avoid the following distortions.

(*a*) Distortion by the front plate of the chamber and by the photographic lenses.

(*b*) Distortion due to change of size and shape of the film at development.

3. A serious limitation of the accuracy of momentum measurement arises from the scattering of the primary particle in the gas.

135. Of the features listed in the last section 1 (*b*) was tentatively identified by Blackett with electrical winds from hairs and dust charged by motion, this trouble is not always encountered.

The effect of 1 (*a*) is particularly marked in cloud chambers containing

metal plates, for the plates have little metallic connexion with external parts and hence are adjusted to temperature changes of the remainder of the apparatus almost entirely by convection. Careful control of temperature throughout the chamber and its immediate surroundings greatly reduces this source of distortion (Blackett and Wilson, 1937).

The optical distortion 2 (*a*) can largely be eliminated by special adjustment of the lens in manufacture. It may also be corrected for in detail from a map of corrections based on photographs of straight wires in different parts of the chamber (Blackett and Brode, 1936).

No systematic investigation of 2 (*b*) seems yet to have been carried out, but for high-precision work glass plates have been preferred in spite of handling difficulties.

The distortion due to non-axial movement of the piston, if not due to the magnetic field, can be mapped out in a way similar to that used for the distortions due to photography, except that the distortions due to movement of piston are determined from the images of tracks in zero field and not from the images of straight wires.

The part of the distortion 1 (*d*) caused by eddy currents in the piston cannot be observed directly. The effect of such distortions on *change* of *curvature* of particles passing through a plate placed in the chamber can be investigated (compare J. G. Wilson, 1938).

Scattering

136. The spurious curvature arising from Coulomb scattering has been treated by Williams (1940*a*). It is shown that the probable error of the measure of the momentum of a fast particle arising from scattering can be expressed in terms of the ratio r/r_s, where r is the radius of curvature due to deflexion in the magnetic field and r_s is the mean curvature due to scattering. r_s/r is given by

$$r_s/r = 0{\cdot}20\frac{H\beta l^{\frac{1}{2}}}{\bar{\alpha}Zq^{\frac{1}{2}}};$$

l is the track length, q is the potential number of nuclei per c.c. divided by Avogadro's number, and

$$\bar{\alpha} = 3{\cdot}69+0{\cdot}28\log_{10} Z^{\frac{1}{2}}Dl/A\beta^2.$$

For fast particles in air at N.T.P. and for $l = 10$ cm.

$$r/r_s = 40/H,$$

and thus for the normal momentum measurements in high magnetic fields this correction is not of importance. For slower mesons, however, the effect is of importance. Take as an example the meson measured

by Williams and Pickup (1938). We have $l = 20$ cm., $H = 2{,}300$ gauss, $v/c = 0{\cdot}4$, $q = 1$, and $r/r_s = \frac{1}{40}$.

For the very end of a meson track the scattering is still more important. For the last 5 cm. of track we have

$$r/r_s = 500/H.$$

It must be borne in mind that this is the spurious curvature for mean scattering of the particle, and the probability of larger scattering is appreciable. A spurious curvature up to one-third of the average cannot be excluded (see Ch. X).

The limitations of very high pressure chambers, even in the higher magnetic fields, from this cause do not need to be stressed.

137. Apart from actual distortion of the image, the measured curvature of a track may be influenced by undue weight given to dense groups of ions, from ionization by low-energy secondaries, which may be centred appreciably off the line of trajectory. These groups may be ignored in either method of curvature measurement provided that the photographic exposure has been sufficient to record clearly the normal single drops of primary ionization. This source of error is a direct consequence of faulty photographic technique.

A maximum detectable momentum of 10,000 MEV./c has been obtained by Wilson (1938, 9) using a length of track of about 10 cm.; corresponding to a central deflexion of the track from straightness of $\frac{1}{20}$th mm. It is unlikely that any significant improvement in precision can be made by further attention to detail. It is probable that greater precision must now be sought in the use of larger equipment and stronger magnetic fields.

Maximum detectable momentum

138. When all possible sources of curvature error have been eliminated, the residual random errors of curvature may be expressed either directly or in terms of the 'maximum detectable momentum'—that momentum which would give curvature equal to the probable curvature due to residual random distortion. In a single compartment chamber this quantity can be measured only in zero magnetic field. Blackett obtained a maximum detectable momentum in this way of 20,000 MEV./c.

In a chamber separated into two halves by a metal plate, it is possible to make a comparable determination of maximum detectable momentum in the full magnetic field (Wilson, 1938). Values so obtained have shown excellent agreement with those measured in zero field. We have

stressed the very numerous sources from which distortion of track images may arise; in many cases distortion is encountered without external indication that error has been introduced. It is important that all possible measurements which can serve as cross-checks of internal consistency of a set of track photographs should be investigated.

D. Proportional Counters

139. Proportional counters are based on a process intermediate between those utilized in the ionization chamber and in the GM-counter. In the ionization chamber the ions produced by a primary are collected and the resulting charge is measured. In the GM-counter the primary ions are sufficiently accelerated to initiate a gas discharge and the amount of charge liberated by the discharge is independent of the number of primary ions.

The proportional counter is a GM-counter worked under starting potential but with a sufficiently high voltage to secure secondary ionization. Thus in the proportional counter each primary ion gives rise to a fixed number of secondary ions without, however, initiating a discharge. The amount of charge liberated is proportional to the primary ionization and can be taken as a measure of it. A description of the use of Geiger's point counter as a proportional counter was given by Geiger and Klemperer (1928).

140. Proportional counters can be used in cosmic-ray work for detecting the tracks of slow particles giving rise to more than average ionization or else to detect narrow showers. The main application of proportional counters has been in the investigation of slow neutrons.

The Neutron Counter

Fünfer (1938) has used proportional counters with a deposit of metallic boron on the inner surface of the counter. Neutrons passing through the wall can produce disintegrations according to either of the following reactions:

$$B^{10}+N = Li^{7}+\alpha,$$

$$B^{10}+N = Be^{10}+P.$$

The process giving rise to α-particles is assumed to be more frequent. The α-particles (or protons) emerging from the wall can be detected by their large ionization.

A somewhat different arrangement has been used by Montgomery and Montgomery (1939) and Korff (1939). In these investigations the

counter is filled with BF_3. Thus neutrons are recorded by means of α-particles produced in the gas.

Though the two methods of detecting slow neutrons are very similar, the following features may be noted. Fünfer's method has a larger absolute efficiency as a large fraction of the neutrons will be absorbed in the boron wall. The limit to the efficiency is given by the range of α-particles in the metallic boron. The disadvantage of this method is that the pulses obtained differ widely since the remaining ranges of α-particles in the gas depend on the depth of their formation; moreover, because of the complicated geometry it is not easy to calculate the intensity of the neutron beam from the number of observed disintegrations.

E. Photographic Plate Method

141. Densely ionizing particles leave distinct tracks in photographic plates. Such tracks appear as a sequence of blackened grains.

Blau and Wambacher (1937*a*, *b*) exposed photographic plates to cosmic rays by leaving them for four months at the top of Hafelekar, 2,300 m. above sea-level. The photographic plates showed tracks of particles with ranges too long to be accounted for by radioactive particles. Using Ilford half-tone plates the number of tracks was estimated at between 120 and 270 per cm.^{2} (emulsion 70 μ thick). Only tracks which had ranges exceeding an equivalent of 10 cm. of air were counted. Thus tracks which might be of radioactive origin were excluded.

By an ingenious method it was shown that the tracks were not due to α-particles but were probably due to protons.

142. Blau and Wambacher (1937*a*, *b*) and others (e.g. Schopper and Schopper (1939), Rumbaugh and Locher (1936), Heitler, Powell, and Fertel (1939), Bose and Choudhuri (1942)) have also found 'stars' on photographic plates, that is groups of tracks starting at one point. These stars are most likely nuclear disintegrations caused by cosmic rays.

143. Information about the primaries giving rise to stars has been obtained by counting the rate of stars at various heights. The rate of stars has been found to increase rapidly with height, showing that the primaries are strongly absorbed in air. Experiments have also been carried out by various observers with plates covered by dense absorbers.

It is generally assumed that most of the stars are produced by neutrons.

III

THEORY OF FAST COLLISIONS

A. Introduction

144. The theory of collisions between elementary particles and atoms was developed in attempts to account for the behaviour of radioactive rays. The formulae obtained for energy loss, ionization, scattering, etc., of radioactive rays were later applied to cosmic rays. This application met a twofold difficulty. Firstly, the cosmic rays have energies much exceeding those of radioactive particles and therefore it was not clear whether one was justified in extrapolating the formulae from the radioactive region where they were known to be valid to the region of the cosmic-ray energies. Secondly, for a long time the nature of cosmic-ray particles was unknown.

As the result of long series of researches both difficulties have been overcome. The cosmic rays contain, like radioactive radiations, electrons, photons, protons, and neutrons; apart from these particles cosmic rays contain also mesons.

It has been established that the relativistic quantum theory of the collisions of fast electrons and energetic photons is certainly valid in the region of cosmic-ray energies. There are, however, good reasons to believe that the interaction of fast neutrons and protons is very much stronger than it would appear from the theory based on electromagnetic interaction alone. It is believed that nucleons apart from the electromagnetic field they produce give rise also to another field which is termed the *meson field*. The meson field is assumed to be responsible for the short range forces between nucleons and therefore the meson field is assumed to be the agency keeping the atomic nuclei together.

In collisions two nucleons will interact by means of their electromagnetic fields as well as through their meson fields. It seems that the interaction through the meson field is much stronger than the electromagnetic interaction; hence the energy loss of fast nucleons when traversing matter is assumed to be mainly determined by the meson interaction which results in the emission of mesons.

145. It should be pointed out that the validity of the quantum theory when dealing with the energy loss of fast electrons or energetic photons must be regarded as firmly established. It can be shown from elementary

principles that the radiation formulae governing these losses must be assumed to be valid for high energies provided they are found to be valid for radioactive energies (Williams (1934*a*, *b*, 1936)). The validity of the formulae in the region of radioactive energies has been well established by experiment.

Apart from these theoretical considerations there is much experimental evidence supporting the validity of the radiation formulae in the region of cosmic-ray energies.

146. The theory of the interaction of nucleons through the meson field is on a much weaker basis. The assumption that nucleons are giving rise to the meson field is inferred from Yukawa's (1935) theory of the nuclear forces and β-activity. This theory led to the surprisingly accurate prediction of the properties of the meson and must be taken very seriously.

The application of the theory of the meson field to collision processes meets with great difficulties as divergent integrals appear in the theory. Definite results can therefore only be obtained by some cutting-out process which eliminates the divergencies.

The most successful attempt to get rid of divergency was made by Heitler (1941) and also by A. H. Wilson (1941); it was shown that by considering radiation damping it is possible to give an unambiguous method of dealing with the divergent terms.

The experimental evidence for the meson field interaction is rather indirect, though a large number of phenomena can be accounted for in terms of the meson theory. The strongest argument in favour of the meson field is of course the experimentally well-established occurrence of the mesons and the fact that these mesons being unstable must have been emitted in some collision process.

In the present chapter we give a short account of the theory of collision processes but we shall confine ourselves mainly to electromagnetic interactions, that is, to the processes where the validity of the theory can be regarded as well established. A brief account of some aspects of the meson theory will be given in section E of this chapter.

B. Summary of the Theory of Relativity

Lorentz Transformation

Coordinates and Time

147. An event taking place at the time t at a point with the Cartesian coordinates x, y, z with respect to a coordinate system K will appear to

have happened at the time t' at a point with coordinates x', y', z' when observed from a coordinate system K', where

$$\left.\begin{aligned} x' &= (x-vt)B, \\ y' &= y, \\ z' &= z, \\ t' &= \left(t-\frac{v}{c^2}x\right)B, \end{aligned}\right\} \tag{1}$$

and

$$B = \frac{1}{\sqrt{(1-v^2/c^2)}}; \tag{2}$$

v is the constant velocity of the system K' with respect to K. This velocity is assumed to be parallel to the x-axis, and at the time $t = t' = 0$ the origins of the two systems are supposed to coincide.

From the transformation (1) the following effects have been derived. Firstly, the length of a rod which is at rest in the system K appears contracted in a system K' in which the rod is in relative motion. The projection parallel to the velocity vector is contracted by a factor B, while the component perpendicular to the motion remains unaffected. Secondly, a clock moving with a velocity v towards the observer appears to lose time in the ratio $1 : B$. The two effects are complementary and are referred to as Lorentz's length contraction and time contraction.

We find from (1)

$$x^2+y^2+z^2-c^2t^2 = x'^2+y'^2+z'^2-c^2t'^2. \tag{3}$$

Momentum and Energy

148. The momentum of a particle with rest-mass m_0 when moving with a velocity $\mathbf{v}$ is given by

$$\mathbf{p} = m\mathbf{v}, \tag{4}$$

with

$$m = Bm_0; \tag{5}$$

m is called the relativistic mass.

According to Einstein's principle of the equivalence of mass and energy, the energy of a particle can be written as

$$w = mc^2 = Bm_0c^2. \tag{6}$$

For a particle at rest we have

$$w_0 = m_0c^2; \tag{7}$$

w_0 is the rest-energy of the particle. The kinetic energy w_k of a particle is defined as the excess of the energy w over the rest-energy w_0. We have

$$w_k = w-w_0 = (B-1)m_0c^2. \tag{8}$$

Developing B in powers of v/c we have

$$w_k = m_0 v^2/2 + \text{terms of higher order in } v/c. \tag{9}$$

We see, that for $v \ll c$ the kinetic energy w_k defined by (8) is very nearly equal to the kinetic energy of non-relativistic mechanics.

149. The components of momentum and the energy of a particle transform similarly to coordinates and time. Consider a particle with momentum p and energy w when referred to a system of reference K. The values of the momentum and energy as referred to a system K' in relative motion is obtained as

$$p'_x = B\left(p_x - \frac{v}{c^2}w\right), \qquad p'_y = p_y, \qquad p'_z = p_z, \qquad w' = B(w - vp_x). \tag{10}$$

With the help of (2) and (10) we obtain the following relation between momentum and energy of a particle

$$w = c\sqrt{(p^2 + m_0^2 c^2)}. \tag{11}$$

Another relation is obtained from (4) and (6). We have

$$cp/w = v/c. \tag{12}$$

Considering particles of very high velocity, that is particles with

$$v \sim c \quad \text{and} \quad B \gg 1, \tag{13}$$

we find $$w = pc + m_0^2 c^3/2p + \text{higher order terms} \approx pc. \tag{14}$$

The above approximation will be referred to as the *extreme relativistic approximation.*

The Electromagnetic Field

150. The electromagnetic field can be expressed either by the components of **E** and **H**, the electric magnetic field strengths, or by the components of the vector potential **A** together with the scalar potential Φ. The connexion between field strengths and potentials is given by the following Lorentz invariant equations:

$$\mathbf{E} = -\frac{1}{c}\frac{\partial \mathbf{A}}{\partial t} - \operatorname{grad}\Phi, \qquad \mathbf{H} = \operatorname{curl}\mathbf{A}. \tag{15}$$

The components of the potentials transform as the components of the momentum and the energy. The field strengths are transformed from the system K to the system K' by the following equations:

$$E'_x = E_x, \qquad E'_y = \left(E_y - \frac{v}{c}H_z\right)B, \qquad E'_z = \left(E_z + \frac{v}{c}H_y\right)B;$$

$$H'_x = H_x, \qquad H'_y = \left(H_y + \frac{v}{c}E_z\right)B, \qquad H'_z = \left(H_z - \frac{v}{c}E_y\right)B. \tag{16}$$

It is seen that the components in the direction of motion remain unaffected while the components perpendicular to the direction of motion are increased by a factor B. Besides, the electric field gives rise to a magnetic component, while the magnetic field gives rise to an electric component. The induced components are proportional to vB/c. Thus for transformations corresponding to small velocities the induced components will be small; for transformations between systems moving with velocities of the order of c the induced components will be of the same order of magnitude as the transformed transverse components.

Applications

151. Two applications of the equations (16) will be discussed:

Static field of moving charge

1. The field of a uniformly moving charge e can be determined by transforming the Coulomb field in the rest-system into the system of the observer. The Coulomb field can be written as

$$\mathbf{E} = e\mathbf{r}/r^3, \qquad \mathbf{H} = 0,$$

with

$$\mathbf{r} = (x, y, z). \tag{17}$$

The field of a charge moving with the velocity v is obtained by transforming (15) into a system K moving with velocity $-v$ with respect to the rest-system of the charge. It can be seen, with the help of (14), (15), and (1), that

$$E'_x = \frac{e\xi}{R'^3}, \qquad E'_y = B\frac{ey'}{R'^3}, \qquad E'_z = B\frac{ez'}{R'^3};$$

$$H'_x = 0, \qquad H'_y = \frac{v}{c}E'_z, \qquad H'_z = -\frac{v}{c}E'_y, \tag{18}$$

where

$$\xi = B(x'+vt'), \qquad R'^2 = \xi^2+y'^2+z'^2.$$

The interpretation of (18) is as follows. The field of the charge moves as a solid body together with the charge. The moving field differs from a stationary field in the following ways:

(1) The length dimensions of the field are contracted in the ratio $1 : B$.
(2) The transverse component of the field strength is increased by a factor B. Due to (1) and (2) the electric field strength remains radial.
(3) The electric field of the moving charge is accompanied by a magnetic field.

It can be seen from (18) that the total electric flow through a surface

enclosing the moving charge is equal to $4\pi c$, that is equal to the flow of the charge when at rest. It follows therefore from Gauss's theorem that

$$e' = e. \tag{19}$$

Thus the value of an electric charge is not affected by the Lorentz transformation.

Doppler effect and aberration

152. 2. We consider the electromagnetic radiation emitted by a moving source. Consider a source moving with the velocity v along the x-axis of the system K. This source is at rest in the system K'.

A sufficiently small section of the radiation at a large distance from the source can be approximated by a plane wave. It is therefore sufficient to consider the transformation of an electromagnetic plane wave from the system K' to the system K.

We consider a plane wave moving at an angle ϑ' to the x'-axis in the system K', having a wavelength λ' and an intensity A'^2. Transforming the field of this wave according to (18) we find that the field in K represents also a plane wave moving at an angle ϑ to the x-axis with

$$\cos\vartheta = \frac{\cos\vartheta' + v/c}{1 + (v/c)\cos\vartheta'}. \tag{20}$$

The wavelength of the wave in K is given by

$$\lambda = \lambda' B\left(1 - \frac{v}{c}\cos\vartheta\right). \tag{21}$$

The intensity in the system K is found as

$$A^2 = A'^2 \Big/ \left(1 - \frac{v}{c}\cos\vartheta\right)^2 B^2. \tag{22}$$

Eq. (20) represents the aberration, while (21) and (22) represent the Doppler effect.

We are interested in the extreme relativistic case where $B \gg 1$. We have

$$v/c \sim 1 - \frac{1}{2B^2}.$$

Further $$\vartheta \sim 2\tan^2(\vartheta'/2)/B^2.$$

The above equation is only valid provided

$$B \gg \tan(\vartheta'/2).$$

We see that almost all directions of emission in K' appear in K as crowded together into a narrow cone round the forward direction.

We find, for instance, that all the directions which have a forward component in K' ($\vartheta' < \frac{1}{2}\pi$) appear in K inside a cone with the solid angle

$$\Omega = 2\pi\left\{1 - \sqrt{\left(1 - \frac{1}{B^2}\right)}\right\} \approx \frac{\pi}{B^2}. \tag{23}$$

The radiation emitted in the forward direction appears in K with shortened wavelength. We have

$$\lambda_{\vartheta=0} = \lambda' B\left(1 - \frac{v}{c}\right) = \lambda' \sqrt{\frac{1-v/c}{1+v/c}} \sim \lambda'/2B. \tag{24}$$

On the surface of the cone (23) the wavelength is unaffected, while the wavelength in the backward direction is

$$\lambda_{\vartheta=\pi} = \lambda' \sqrt{\frac{1+v/c}{1-v/c}} \sim 2B\lambda'. \tag{25}$$

Thus the wavelength, as seen in K, is increased in almost all directions.

The *intensity* of the radiation is increased in the forward direction by a factor $\sim 4B^2$ while in the backward direction it is reduced to approximately $1/4B^2$ of the original intensity.

The difference between forward and backward intensities appears to be due to the interaction of the electric and the magnetic vectors. Both the field of the waves moving in the forward direction and the field of the waves moving in the backward direction are transverse to the direction of motion of K' and therefore the transformed components contain the factor B. But the electric field in K is the sum of two contributions, namely the transformed electric component and the electric component set up in K by the magnetic component in K'. These two contributions are in phase when considering waves moving forward but are out of phase for the waves moving backwards. The difference in the backward and forward intensities is therefore due to the interference between the fields set up by the electric and magnetic components of the original field.

Consider a light source resting in K' and emitting the same intensity A'^2 uniformly in all directions. The rate of energy emitted is thus $4\pi A'^2$.

The rate of energy emitted as observed from K can be calculated with help of (22). We find

$$\int A^2 \, d\Omega = 4\pi A'^2. \tag{26}$$

Thus the rate of energy flow remains the same.

The total energy emitted in a flash of a given duration t' is, however, larger when measured in K than when measured in the rest-system.

Owing to the time contraction the duration of the flash appears in K as

$$t = Bt'$$

and therefore the energy flow as seen in K persists B times longer than it persists in the rest-system. The total energy emitted as measured in K is therefore

$$W = BW', \tag{27}$$

where W' is the energy emitted in the rest-system.

C. Application of Conservation Laws to Collisions

1. *Elastic Collisions*

(a) *Exact Treatment of Relativistic Collision*

153. Collisions between two particles in which energy and momentum are conserved may be called elastic. Consider two free particles, one having a rest-mass M_0, momentum $\mathbf{P}$, and energy $W = c\sqrt{(P^2+M_0^2c^2)}$, the second having a mass m_0, momentum $\mathbf{p}$, and energy w. In an elastic collision the total energies and momenta of the particles will be conserved. We have thus

$$\begin{aligned} \mathbf{P}+\mathbf{p} &= \mathbf{P}'+\mathbf{p}', \\ W+w &= W'+w', \end{aligned} \tag{28}$$

where primes indicate the values after the collision. The equations (28) have been solved and discussed by Jüttner (1914). It is convenient to refer the collision to the rest-system of one of the colliding particles. Thus we assume that

$$\mathbf{P} = 0, \qquad W = M_0c^2. \tag{29}$$

The results obtained with this special initial condition can be generalized by a Lorentz transformation.

By means of a simple calculation we obtain from (28) and (29), with help of (11),

$$\left.\begin{aligned} p' &= p\frac{(m_0^2c^2+M_0w)\cos\vartheta+(w+M_0c^2)\sqrt{(M_0^2-m_0^2\sin^2\vartheta)}}{(w/c+M_0c)^2-p^2\cos^2\vartheta}, \\ w' &= \frac{(w+M_0c^2)(m_0^2c^2+M_0w)+c^2p^2\cos\vartheta\sqrt{(M_0^2-m_0^2\sin^2\vartheta)}}{(w/c+M_0c)^2-p^2\cos^2\vartheta}, \\ P'^2 &= p^2+p'^2-2pp'\cos\vartheta, \end{aligned}\right\} \tag{30}$$

where ϑ is the angle of scattering, that is the angle between $\mathbf{p}$ and $\mathbf{p}'$ (see Fig. 26). Alternatively energies and momenta can be expressed in

terms of α, the angle of recoil, that is the angle between the vectors $\mathbf{p}$ and $\mathbf{P}'$. With this change eq. (31) is obtained:

$$\left.\begin{aligned} P' &= p\frac{2M_0(w+M_0c^2)\cos\alpha}{(w/c+M_0c)^2-p^2\cos^2\alpha}, \\ W' &= M_0c^2+\frac{2p^2\cos^2\alpha M_0c^2}{(w/c+M_0c)^2-p^2\cos^2\alpha}, \\ p'^2 &= p^2+P'^2-2pP'\cos\alpha. \end{aligned}\right\} \tag{31}$$

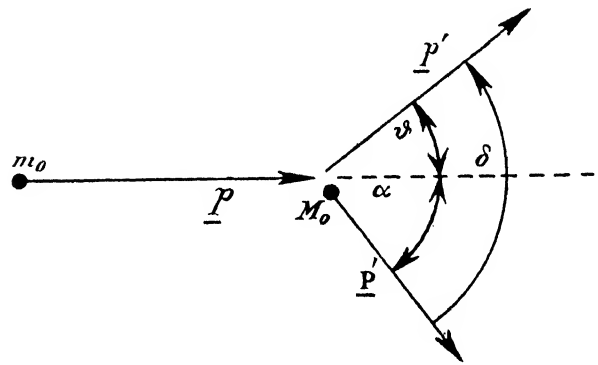

FIG. 26. Elastic collision.

The momentum of the colliding particle can also be determined from angle of recoil and recoil momentum: one finds

$$p = P'\frac{(W'+M_0c^2)M_0\cos\alpha+\sqrt{\{m_0^2(W'+M_0c^2)\cos^2\alpha-(M_0^2-m_0^2)c^2\}}}{(W'/c+M_0c)^2\cos^2\alpha-P'^2}. \tag{32}$$

Finally, it is useful to express α, the angle of recoil, in terms of the energy transferred in the collision. We find

$$\cos\alpha = \frac{w+M_0c^2}{pc}\sqrt{\frac{W'-M_0c^2}{W'+M_0c^2}}. \tag{33}$$

The corresponding expression for ϑ is rather elaborate and will be omitted.

Finally, we can express the mass m_0 of the colliding particle in terms of p', P', M_0, and the angle

$$\delta = \vartheta+\alpha. \tag{34}$$

δ is the angle between the directions of the two particles after collision. We find, with help of (23), as the result of a short calculation

$$m_0^2 = (p'/c)^2\left\{\left(\frac{cP'\cos\delta}{W'-M_0c^2}+\frac{M_0c}{p'}\right)^2-1\right\}. \tag{35}$$

The above relation was pointed out by Gorodetzky (1942) (see also Leprince-Ringuet and Gorodetzky (1941)), and it was shown to be of use for the determination of the mass of a colliding particle based on data obtained from a secondary electron (see Ch. IV, § 275).

(*b*) *Extreme Relativistic Approximation*

154. For most applications it will be sufficient to use the 'extreme relativistic' approximations of the collision formulae. These approximations are obtained by neglecting quantities of the order of $m_0 c/p$. We find

$$\left.\begin{aligned} p' \sim w'/c \sim p\,\frac{(p+M_0c)c\sqrt{(M_0^2-m_0^2\sin^2\vartheta)}+M_0cp\cos\vartheta}{(2p+M_0c)M_0c+p^2\sin^2\vartheta}, \\ P' \sim p\,\frac{2M_0c(p+M_0c)\cos\alpha}{(2p+M_0c)M_0c+p^2\sin^2\alpha}, \\ W'-M_0c^2 \sim cp\,\frac{2M_0c(p+M_0c)\cos\alpha}{(2p+M_0c)M_0c+p^2\sin^2\alpha}. \end{aligned}\right\} \quad (36)$$

In eq. (36) terms of the order of $M_0 c/p$ have been maintained. These terms are of importance in collisions between a light fast particle and a heavy particle provided the rest-energy of the heavier particle is not negligible compared with the kinetic energy of the lighter particle.

(*c*) *Discussion of the Collision Formulae*

Angle of scattering

155. According to (30) a heavy particle colliding with a lighter or equal particle can only be scattered through an angle $\vartheta \leqslant \vartheta_m$, with

$$\sin\vartheta_m = M_0/m_0. \quad (37)$$

A particle colliding with a heavier one can be scattered through any angle.

Angle of recoil

156. It follows from eq. (33) that the angle of recoil tends towards $\frac{1}{2}\pi$ for collisions where the energy transfer is small compared with the rest-energy of the recoiling particle. All slow secondaries of a sufficiently fast particle will be ejected nearly at right angles. Slow secondaries at right angles to a fast primary are frequently seen on cloud-chamber photographs.

Transfer of energy

157. No energy is transferred in a collision for which $\vartheta = 0$. The maximum possible energy is transferred in a head-on collision with $\alpha = 0$. The maximum transferable energy W_m is therefore found from eq. (31) as

$$W_m = (W' - M_0 c^2)_{\max} = \frac{2p^2 M_0 c^2}{m_0^2 c^2 + M_0(2w + M_0 c^2)}. \tag{38}$$

This formula can, however, only be applied to the collisions of two unlike particles. In the case of the collision of two like particles it is impossible to distinguish between the scattered and the recoiling particle. In this case one defines the particle which comes out of the collision with more energy to be the scattered particle. The energy transfer cannot therefore exceed half the primary energy and thus for like particles we obtain

$$W_m = (w - m_0 c^2)/2. \tag{39}$$

In the extreme relativistic approximation

$$W_m = \begin{cases} w & \text{unlike particles} \\ w/2 & \text{like particles} \end{cases} \quad (w \gg m_0 c^2, M_0 c^2). \tag{40}$$

The above approximate formula for unlike particles is only valid if $w \gg m_0^2 c^2/M_0$. In the case of incident heavy particles colliding with lighter particles the above limit may be very high. Eq. (40) applied to protons colliding with electrons is only correct for $w \gg 10^6$ MEV. and in the case of mesons colliding with electrons it is correct for $w \gg 10^4$ MEV. For the intermediate region, that is for $m_0 c^2 \ll w \ll m_0^2 c^2/M_0$, we have, approximately,

$$W_m = 2(p/m_0 c)^2 M_0 c^2. \tag{41}$$

158. Regarding the dependence of the energy transfer on the angle of scattering two cases have to be distinguished:

(i) The energy of the incident particle is large compared with both its own rest-energy and the rest-energy of the knocked-on particle. In this case the transfer of energy is of the same order as the primary energy except when the angle of scattering is of the order of $\sqrt{(2M_0 c^2/w)}$ or less. The momentum loss as a function of ϑ, the angle of scattering, is shown in Figs. 27, 28.

(ii) A light particle collides with a much heavier one. The energy of the light particle is much larger than its own rest-energy but does not exceed the order of the rest-energy of the recoiling particle. In this case the transferred energy changes uniformly with angle of scattering as

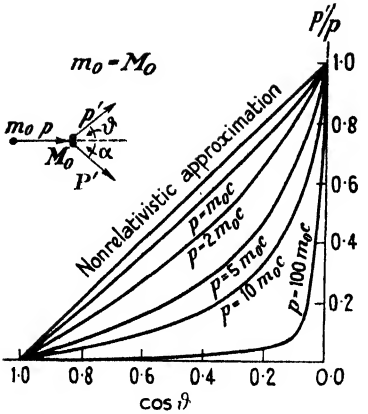

a. Transfer of momentum in a collision between equal particles.

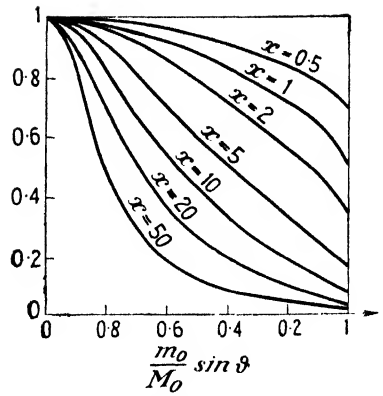

b. Transfer of momentum from a heavy to a light particle. $x = M_0 p/m_0^2 c$.

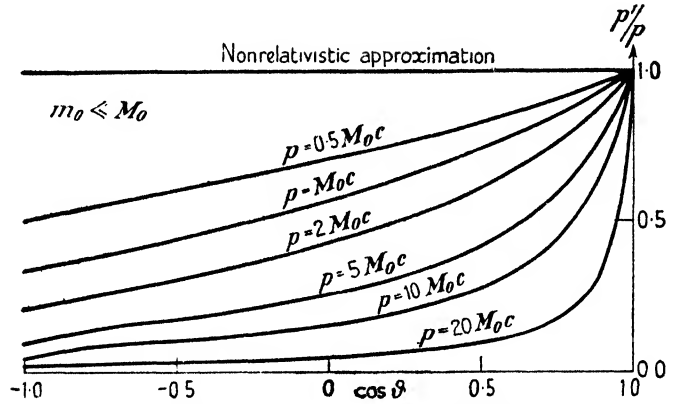

c. Transfer of momentum from a light to a heavy particle.

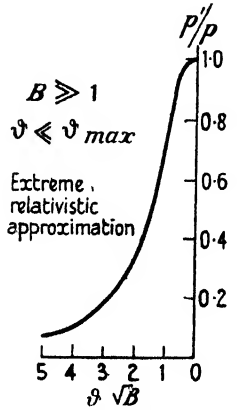

d. Transfer of momentum in the extreme relativistic case. $B = p/M_0 c$.

FIG. 27.

seen in Fig. 28. An example is the collision of an electron of say 10^3 MEV. with a proton.

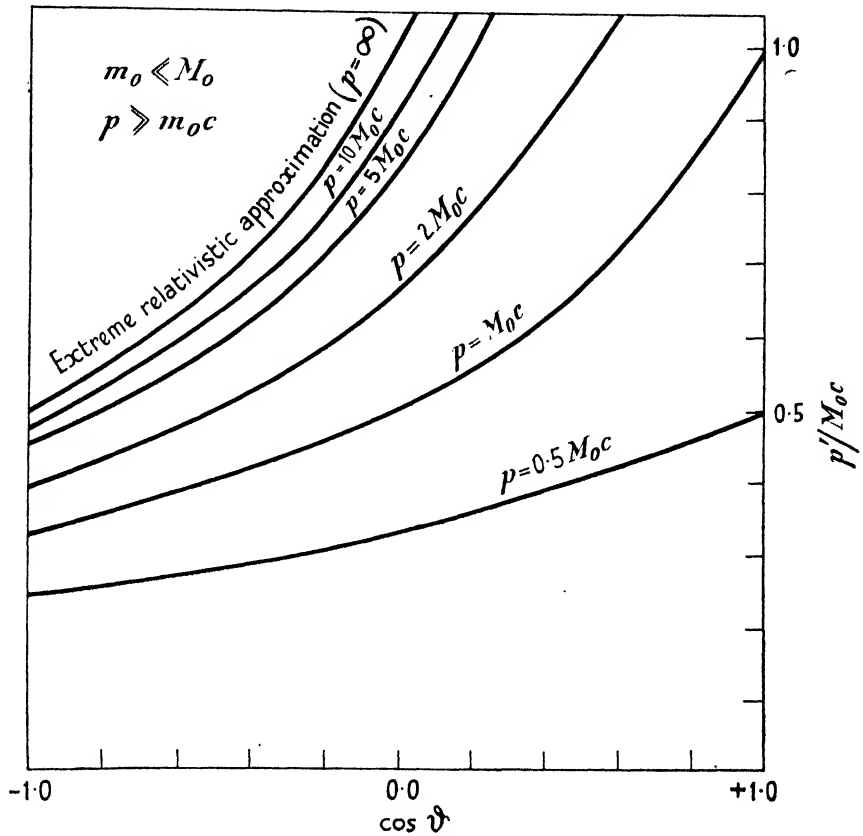

FIG. 28. Transfer of momentum from a light particle to a heavy particle for large angles of scattering.

Compton effect

159. A photon can be regarded as a particle with zero rest-mass and $w = pc = h\nu$. Introducing $m_0 = 0$ we obtain from (30) and (31)

$$\left.\begin{aligned} \nu' &= \frac{(1+M_0c^2/h\nu)(1+\cos\vartheta)M_0c^2/h}{(2+M_0c^2/h\nu)M_0c^2/h\nu+\sin^2\vartheta}, \\ P' &= \frac{2M_0c(1+M_0c^2/h\nu)\cos\alpha}{(2+M_0c^2/h\nu)M_0c^2/h\nu+\sin^2\alpha}. \end{aligned}\right\} \tag{42}$$

2. *Inelastic Collisions*

160. There are collision processes which can only occur in the presence of a third particle which suffers a recoil in the collision. Processes

of this kind are essentially inelastic although the recoil-energy may often be small compared with the total transfer of energy in the collision.

Pair production

Consider a process in which a photon is absorbed giving rise to a number of particles with momentum $P_1, P_2, \ldots$ and energies $W_1, W_2, \ldots$. The conservation laws require

$$h\nu/c = |\mathbf{P}_1+\mathbf{P}_2+\ldots|. \tag{43}$$

For particles with non-zero rest-mass $P < W/c$ and therefore

$$|\mathbf{P}_1+\mathbf{P}_2+\ldots| \leqslant |\mathbf{P}_1|+|\mathbf{P}_2|+\ldots < W_1/c+W_2/c+\ldots. \tag{44}$$

Comparing (43) and (44) we see that energy and momentum cannot be both conserved in this process. If the energy is conserved an excess of momentum remains. Thus the creation of particles with finite rest-mass by photons is only possible in the presence of heavy particles capable of taking the excess momentum in the form of a recoil particle.

D. Fast Collisions

161. In order to obtain information about the relative probabilities of collisions we have to consider the forces acting between the colliding particles.

As the quantum theory of collisions is dealt with elsewhere (e.g. Heitler, *Quantum Theory of Radiation*, Oxford, 1944; Mott and Massey, *The Theory of Atomic Collisions*, Oxford, 1933) we restrict ourselves to a very brief sketch of the quantal treatment; we shall, however, give an account of the very instructive classical theory of collisions based on the work of Bohr (1913, 15), Weizsäcker (1934), and Williams (1933*a*, 4*a*, 6).

1. *Classical Theory*

(*a*) *Impact Parameter Method*

The impact parameter

162. Consider two particles, one of mass m, charge ze, and momentum $\mathbf{p}$, and the other of mass M, charge $Z_1 e$, initially at rest.

The distance a of closest approach between the particles will denote the impact parameter. If the impact parameter is sufficiently large, the orbit of the moving particle can be taken in first approximation to be a straight line and the change of velocity can be neglected. The force acting upon the stationary particle perpendicular to the direction of motion at a time t is

$$F_x = Z_1 ze^2 Ba/(a^2+B^2v^2t^2)^{\frac{3}{2}}, \tag{45}$$

$$B = \frac{1}{\sqrt{(1-v^2/c^2)}},$$

where it is assumed that the nearest approach takes place at $t = 0$. v is the velocity of the colliding particle. The recoil suffered by the stationary particle is given by the time integral of the force. We find

$$P'_x = \int F_x \, dt = 2Z_1 ze^2/va. \tag{46}$$

The momentum transferred in the longitudinal direction can be treated similarly. It is seen, however, that the longitudinal component of P' vanishes if treated in the same approximation as before. We shall assume therefore in the following

$$P'_{\text{long}} = 0, \qquad P'_x = P'.$$

163. The momentum transferred in a collision is limited by the conservation laws and therefore (46) is clearly inaccurate for too small impact parameters. This inaccuracy arises from having neglected the motion of the recoiling particle and also from having neglected the reaction of the collision upon the colliding particle. A more accurate treatment of the collision, according to Bohr (1915), gives for the recoil momentum

$$P' = \frac{2Z_1 ze^2}{v\sqrt{(a^2+b^2)}}, \tag{46 a}$$

with

$$b = \frac{Z_1 ze^2(M+m)}{Mmv^2 B}. \tag{46 b}$$

The loss for $a = 0$ is therefore

$$P'_{\max} = \frac{2Mp}{M+m} \tag{46 c}$$

as is expected.

In most considerations it is sufficient to use the approximate formula (46).

Differential cross-section

Momentum transfer

164. The impact parameter a can be expressed in terms of the momentum transferred. We find from (46)

$$a = 2Z_1 ze^2/vP'. \tag{47}$$

The above expression defines the distance at which the momentum transfer is equal to P'.

Consider an absorber of thickness $\mathfrak{z}$ containing N stationary particles per c.c. A particle traversing the absorber will suffer on the average $d\mathcal{N}$ collisions at distances between a and $a+da$ from any of the stationary particles, where

$$d\mathcal{N} = N\mathfrak{z}2\pi a \, da. \tag{48}$$

From (47) and (48) we find that the average number of collisions leading to transfers between P' and $P'+dP'$ is given by

$$d\mathcal{N} = N_3 8\pi Z_1^2 z^2 e^4/v^2 \frac{dP'}{P'^3}. \tag{49}$$

We divide (49) by N_3 and obtain the average number of collisions per scattering particle

$$\chi(P')\,dP' = 8\pi Z_1^2 z^2 e^4/v^2 \frac{dP'}{P'^3}. \tag{50}$$

$\chi(P')\,dP'$ is the differential cross-section. It has the dimensions of an area and it can be regarded as the effective area per scattering centre in which the specified collision takes place.

Scattering

165. The angle of scattering, if small, is given by

$$\vartheta = P'/p \tag{51}$$

and the differential cross-section for an angle of scattering in the interval ϑ, $d\vartheta$ is found from (50) and (51):

$$\chi(\vartheta)\,d\vartheta = 8\pi Z_1^2 z^2 e^4/p^2 v^2 \frac{d\vartheta}{\vartheta^3}. \tag{52}$$

Sometimes it is useful to consider the projection ϑ' of the angle of scattering on to a plane parallel to the initial direction of the particle. As the result of a simple geometrical consideration we find for the differential cross-section in terms of the projected angle

$$\chi(\vartheta')\,d\vartheta' = \tfrac{1}{2}\chi(\vartheta)\,d\vartheta. \tag{53}$$

Energy transfer

166. The differential cross-section for the loss of energy is obtained from (50) by expressing the momentum in terms of energy. With the help of (11) we find

$$\chi(W')\,dW' = 8\pi Z_1^2 z^2 e^4/v^2 c^2 \frac{W'\,dW'}{P'^4}. \tag{54}$$

In the non-relativistic case we have

$$W' \sim Mc^2, \qquad P' \sim (2MW'_k)^{\frac{1}{2}},$$

and $dW'_k = dW'$, where W_k is the kinetic energy. We find thus

$$\chi(W'_k)\,dW'_k \approx 2\pi Z_1^2 z^2 e^4/Mv^2 \frac{dW'_k}{W'^2_k}. \tag{54 a}$$

In the extreme relativistic case we have instead

$$\chi(W')\,dW' \approx 8\pi Z_1^2 z^2 e^4 \frac{dW'}{W'^3_k}. \tag{54 b}$$

Rate of energy loss

167. The rate of loss of energy of a fast particle traversing matter is obtained by averaging over the effects of independent collisions. It is seen from (54 a) that the loss of energy is inversely proportional to the mass of the stationary particle; in collisions with atoms most energy is therefore lost to atomic electrons and the loss of energy due to collisions with nuclei can be neglected.

We restrict ourselves, therefore, to electronic collisions and put

$$Z_1 = 1, \qquad M = m_e. \tag{55}$$

By averaging over collisions leading to various amounts of energy transfer we obtain with the help of (54 a) for the average rate of loss of energy

$$-\frac{dW}{d\mathfrak{z}} = N \int W' \chi(W')\, dW' = \frac{2\pi N z^2 e^4}{m_e v^2} \log \frac{W_{\max}}{W_{\min}}, \tag{56}$$

where $W_{\max}$ is the maximum transferable energy. The expression (56) is based on the non-relativistic cross-section (54 a). If $W_{\max} \gg m_e c^2$, this is not justified and the cross-section as given by (54) should be used. It is seen, however, that for relativistic energies the cross-section decreases with $1/W'^3$ and therefore the contribution to the total loss arising from energetic collisions is negligible. The total loss is found in this case to be approximately

$$-\frac{dW}{d\mathfrak{z}} = \frac{2\pi N z^2 e^4}{m_e v^2} \log \frac{m_e c^2}{W_{\min}}. \tag{56 a}$$

168. The expression (56) was obtained by Thomson and also by Whiddington (see Bohr (1913)). The expression (56) diverges however if $W_{\min}$ approaches zero. The theory as presented is therefore not consistent.

Effect of binding forces

The divergence of the expression (56) is due to the distant collisions, and it must be assumed therefore that the transfer of momentum (or energy) for distant collisions is less than expected from (46).

In earlier attempts it was postulated that the momentum transferred in collisions is given correctly by (46) up to distances of the order of the atomic radius, and that for larger distances the loss is smaller than predicted by (46). Such a postulate is unsatisfactory (compare § 180), and it leads also to results incompatible with observations.

The problem of energy loss of fast particles was eventually solved by Bohr (1913, 15). Bohr realized that it was not permissible to treat the

atomic electrons as free electrons; he showed that the momentum transfer especially in distant collisions is strongly affected by the binding force between the electron and atom.

Bohr assumes the electrons to be bound by harmonic forces to the atoms; the energy transferred to the bound electron is approximately the same as that transferred to free electrons provided the time of collision is short compared with the natural period of the electron. In slow collisions, the energy transfer is much reduced by the binding force.

Time of collision

169. The time of collision is the time during which the interaction between the colliding particles is relatively strong. According to (46) the Coulomb field is relatively strong for a period $2a/Bv$, and we may put therefore for the time of collision

$$t_{\text{coll}} = 2a/Bv. \tag{57}$$

We may write therefore

$$2a_{\max}/Bv = 1/\bar{\nu},$$

where $\bar{\nu}$ is the average atomic frequency and $a_{\max}$ the collision parameter for which the time of collision is equal to the period of free oscillation. We have therefore

$$a_{\max} = Bv/2\bar{\nu}. \tag{58}$$

The effect of binding forces can be introduced schematically by assuming that collisions at distances less than $a_{\max}$ are not affected by the binding while no energy is transferred for collisions at distances exceeding $a_{\max}$.

The energy transferred at the distance $a = a_{\max}$ is obtained from (46), (58), and (56). We have

$$W'_{\min} = \frac{P'^2_{\min}}{2m_e} = 8z^2e^4\bar{\nu}^2/B^2v^4m_e. \tag{59}$$

Introducing $W_{\min}$ from (59) into (56) we have for the rate of loss

$$-\frac{dW}{d\mathfrak{z}} = -N\frac{2\pi e^4z^2}{mv^2}\log\frac{B^2v^4m_e^2c^2}{8z^2e^4\bar{\nu}^2} = -N\frac{4\pi e^4z^2}{mv^2}\log\frac{Bv^2m_ec}{\sqrt{8}ze^2\bar{\nu}}. \tag{60}$$

It was pointed out by Bohr (1913, 15) that in the case of bound electrons the momentum transferred into the longitudinal direction must not be neglected. Including longitudinal terms Bohr obtained

$$-\frac{dW}{d\mathfrak{z}} = \frac{4\pi Nz^2e^4}{mv^2}\left\{\log(\ldots)+\log B-\frac{v^2}{2c^2}\right\}. \tag{61}$$

Bohr's expression under the log differs slightly from that given in (60).

Distant collisions

170. It is interesting to note the actual magnitude of $a_{\max}$ (see Williams, 1933). The order of magnitude of $\bar{\nu}$ can be assumed to be

$$\bar{\nu} \sim Zm_e c^2/137^2 h$$

and therefore

$$a_{\max} = 137 a_0 B/Z,$$

where $a_0 = 137^2 r_0$ is the Bohr radius of the H-atom. For air we have approximately

$$a_{\max} = B.10^{-7} \text{ cm.}$$

Thus for $B = 10^7$ we have $a_{\max} = 1$ cm. and for sufficiently energetic primaries $a_{\max}$ can be of the order of metres. If the primaries are electrons, then $B = 10^7$ corresponds to 10^{13} eV. primaries. Energies of this order and much greater energies are expected to occur in extensive air showers. Thus sufficiently energetic particles may lose energy in collisions at distances up to centimetres or even metres.

Classical energy loss formula

171. The number of electrons contained in a cubic centimetre of an absorber can be written as

$$N = L(Z/A)k, \tag{62}$$

where A is the atomic weight of the absorber and Z the atomic number. L is Avogadro's number and k the density. We may express the thickness of absorber in grams per cm.^{2} instead of centimetres. We introduce therefore

$$\theta = \mathfrak{z}k. \tag{63}$$

Introducing numerical values we have further

$$4\pi L r_0^2 m_e c^2 = 0{\cdot}3 \text{ MEV. per (gram/cm.}^2) \tag{64}$$

and

$$\frac{dW}{d\theta} = 0{\cdot}3 \frac{(Z/A)}{(v/c)^2} \left\{ \log \frac{Bv^2 m_e c}{\sqrt{8}\, ze^2 \bar{\nu}} + \log B - \frac{v^2}{2c^2} \right\}$$

$$\text{MEV. cm.}^2 \text{ per (gram/cm.}^2). \tag{65}$$

We note the following features of the energy loss formula (65).

1. The rate of loss of energy is nearly proportional to $1/v^2$. Thus slow particles lose much more energy than fast ones. The rate of loss decreases with primary energy, reaches a minimum, and increases logarithmically with the energy for higher energies.

The density of ionization produced by fast particles is proportional to the rate of energy loss and therefore the ionization density of particles is high for slow particles, reaches a minimum for a velocity near c, and increases with the logarithm of the energy for high-energy particles.

2. The atomic number of the absorber appears outside the logarithm only in the combination Z/A. This ratio does not change greatly with atomic number and therefore the rate of loss is roughly mass proportional. The expression under the logarithm depends, however, on Z as the electrons are bound more strongly in heavy elements than in light ones: therefore the rate of loss of energy expressed on a mass scale decreases somewhat with increasing Z.

3. The rate of loss is proportional to z^2; thus the loss of multiply charged particles greatly exceeds that of singly charged ones. In particular α-particles lose about four times as much energy as electrons or protons of the same velocity.

Secondaries

172. In collisions where an electron receives an energy exceeding the ionization energy the electron is ejected from the atom and appears as a secondary.

The cross-section for the production of secondaries with energies in the interval W', dW' is obtained from (54 a) as

$$\chi(W')\,dW' = 2\pi z^2 r_0^2 \left(\frac{c}{v}\right)^2 \frac{m_e c^2\,dW'}{W'^2}. \tag{66}$$

The equation (66) is in agreement with the corresponding equation obtained from quantum theory provided W' is much larger than the ionization energy and much smaller than the maximum transferable energy.

The cross-section for the production of high-energy secondaries is also influenced by the interactions of spins and magnetic moments of the colliding particles.

Scattering

Multiple scattering and large-angle scattering

173. A particle traversing an absorber suffers a large number of collisions and the change of direction of the particle is due to the resultant effect of the single collisions.

The distribution of the angles of scatter suffered in the individual collisions is given by (52). We see that the number of deflexions of a given size increases very rapidly with decreasing size; collisions leading to small angles of deviation are therefore predominant.

The individual angles of scatter have independent azimuth and therefore they compensate each other to a large extent. The total deflexion increases on average with the square root of the number of collisions.

Occasionally a particle suffers a close collision in which it is deflected by a comparatively large angle. The effect of such a collision can be much larger than the cumulative effect of the frequent distant collisions, and the two processes can be treated separately.

174. We call *multiple scattering* the scattering due to the cumulative effect of many small-angle deflexions. This scattering has to be distinguished from the *large-angle scattering* due to a single close collision.

Distribution of angles of scattering

The difference between multiple scattering and large-angle scattering becomes apparent from the distribution of the total angles of scattering of similar particles traversing the same absorber.

The particles traversing an absorber can be divided into two groups: (1) Particles which have passed through the absorber without having encountered any close collisions. (2) Particles which did encounter one or more close collisions.

The angles of total scattering of the first group are distributed according to a Gaussian law; this can be shown exactly, but it is plausible when remembering the random azimuth of the individual collisions. The angles of deviation of the second group will follow closely the distribution (52) as most of these particles will have suffered one collision only, and this collision is expected to give a predominant contribution to the total angle.

Thus the distribution of the angles of scattering is given for small angles by a Gaussian, but for large angles the distribution tails off according to a law of the form

$$d\vartheta/\vartheta^3. \tag{67}$$

Scattering angles lying in the region where the Gaussian distribution is predominant may be ascribed to multiple scattering, while the larger angles in the region where the distribution obeys (67) may be ascribed to large-angle scattering.

The region where the two distributions intersect is called the region of plural scattering. Particles in this region are expected to have suffered a small number of collisions at intermediate distances.

175. *Limiting impact parameter.* There is no sharp division between large-angle scattering and multiple scattering. It is useful to introduce a limiting impact parameter a_1 so that a particle traversing an absorber of thickness ζ suffers on average one collision at a distance less than a_1. Thus we put

$$N\zeta\pi a_1^2 = 1$$

or
$$a_1 = \frac{1}{\sqrt{(\pi N \mathfrak{z})}} \tag{68}$$
corresponding to an angle
$$\vartheta_1 = \frac{2Z_1 ze^2}{vp\sqrt{(\pi N \mathfrak{z})}} \tag{68a}$$
(Williams (1939*c*)). We consider collisions at distances less than a_1 as close collisions giving rise to large-angle scattering and collisions at distances larger than a_1 as distant collisions contributing to multiple scattering.

The expression (68) for a_1 depends on the thickness $\mathfrak{z}$ of the absorber. This is justified, as a collision which is rare in a thin absorber may not be rare in a much thicker absorber. The distinction between what is taken as a rare large-angle collision and what is taken to be a 'frequent' small collision depends necessarily on the thickness of the absorber.

Averaging over collisions

The theory of scattering of fast particles crossing absorbers was developed largely by Williams (1939*c*). We reproduce parts of the theory which will be of importance in connexion with cosmic-ray observations.

176. We proceed to average over the individual collisions encountered by a fast particle traversing an absorber. We are interested mainly in the angle of scatter and the linear displacement resulting from a large number of independent collisions. We shall always assume that the energy loss of the scattered particle on its way through the absorber is negligible, and therefore we shall assume the velocity of the particle to be constant through the absorber. The problem of the scattering of electrons in thick absorbers will be treated in some detail in Ch. VIII.

The differential scattering cross-section according to (52) is proportional to Z_1^2. Hence the scattering due to nuclei is usually much more important than the electronic scattering and we shall not consider the electronic scattering.

In the following we shall assume therefore
$$Z_1 = Z \quad \text{and} \quad m = AM_P. \tag{69}$$

177. The mean square angular deflexion and the mean square displacement can be determined as follows.

Consider a particle traversing an absorber $\mathfrak{z}$ cm. thick. Assume collisions to take place at the depths $\mathfrak{z}_1, \mathfrak{z}_2, \ldots$, resulting in deflexions $\vartheta_1, \vartheta_2, \ldots$; the azimuth of the orbit will change after each collision, and the subsequent azimuths are assumed to be $\phi_1, \phi_2, \ldots$.

The projected angle of deflexion at the depth $\mathfrak{z}$ is given by

$$\vartheta' = \vartheta_1 \cos\phi_1 + \vartheta_2 \cos\phi_2 + \ldots, \tag{70}$$

while the projection of the linear displacement can be written as

$$x = (\mathfrak{z} - \mathfrak{z}_1)\vartheta_1 \cos\phi_1 + (\mathfrak{z} - \mathfrak{z}_2)\vartheta_2 \cos\phi_2 + \ldots. \tag{71}$$

178. We have to average over the parameters of the single collisions. The azimuths can be taken to be independent and therefore we may assume for the average values

$$\langle \cos\phi_i \cos\phi_k \rangle = \begin{cases} 0 & i \neq k, \\ \frac{1}{2} & i = k. \end{cases} \tag{72}$$

Further, as we neglect the change of energy of the particle while passing through the absorber, we may assume that the values of $\mathfrak{z}_i$ are independent of each other and are distributed at random. We assume therefore

$$\langle (\mathfrak{z} - \mathfrak{z}_i)^2 \rangle = \frac{1}{\mathfrak{z}} \int_0^{\mathfrak{z}} (\mathfrak{z} - \mathfrak{z}_i)^2 \, d\mathfrak{z}_i = \tfrac{1}{3}\mathfrak{z}^2. \tag{73}$$

Introducing (72) into (70) we find

$$\langle \vartheta'^2 \rangle = \frac{3n}{2} \bar{\vartheta}^2, \tag{74}$$

where n is the average number of collisions per cm. absorber and $\bar{\vartheta}^2$ is the mean square angle of scattering in *one* collision. We have

$$n = (N/Z) \int \chi(\vartheta) \, d\vartheta, \qquad \bar{\vartheta}^2 = \int \vartheta^2 \chi(\vartheta) \, d\vartheta \Big/ \int \chi(\vartheta) \, d\vartheta, \tag{75}$$

and, finally,

$$\langle \vartheta'^2 \rangle = \frac{N\mathfrak{z}}{2Z} \int \vartheta^2 \chi(\vartheta) \, d\vartheta. \tag{76}$$

Similarly we obtain for the mean-square displacement, with help of (71), (72), (73), and (75),

$$\langle x^2 \rangle = \frac{N\mathfrak{z}^3}{3Z} \int \vartheta^2 \chi(\vartheta) \, d\vartheta. \tag{77}$$

The expressions (76) and (77) refer to the projection of the angle of scatter and the projection of the linear displacement. The mean-square values of the actual angle and the full displacement are twice those of their projections and thus we have

$$\langle \vartheta^2 \rangle = \frac{N\mathfrak{z}}{Z} \int \vartheta^2 \chi(\vartheta) \, d\vartheta \tag{78}$$

and

$$\langle r^2 \rangle = \frac{2N\mathfrak{z}^3}{3Z} \int \vartheta^2 \chi(\vartheta) \, d\vartheta \tag{79}$$

179. It remains to determine the numerical value for the integral

$$\int \vartheta^2 \chi(\vartheta)\, d\vartheta.$$

Inserting the cross-section from (52) we obtain

$$\int \vartheta^2 \chi(\vartheta)\, d\vartheta = \frac{8\pi Z^2 z^2 e^4}{v^2 p^2} \log \frac{\vartheta_{\max}}{\vartheta_{\min}}. \tag{80}$$

It is seen that the integral (80) diverges due to the contributions of the small angles and thus it diverges due to the contributions of the distant collisions. It must be concluded therefore that the contribution of the distant collisions is reduced by some process.

Screening

180. The analogous difficulty in case of the energy loss was overcome by considering the effect of the binding forces between electrons and atoms. As, however, scattering is mainly due to nuclear collisions, and the nuclei can be regarded as practically free, the divergency in the expression for the scattering cannot be overcome by introducing the effect of binding forces.

Nuclear scattering at large distance is, however, reduced by the electrostatic shielding of the nucleus by its electrons.

The electrostatic shielding reduces the scattering of distant particles but it does not reduce the loss of energy. It was seen in § 170 that sufficiently energetic primaries are capable of losing energy to atoms very far from their path. Thus a primary travelling at a distance such that the fields of the electrons and the nuclei compensate each other almost completely is still capable of transferring energy to the atom.

The physical reason why screening reduces scattering much more than the energy transfer is as follows. A fast particle passing an atom transfers a certain amount of momentum to each electron and also to the nucleus. The angle of scattering is, however, determined by the transverse component of the total recoil. Due to the opposite sign of charge the electrons recoil in the opposite direction to the nucleus, and if the fast particle passes at a sufficient distance, the transverse components of the recoiling electrons cancel the transverse component of the nuclear recoil and thus no scattering results. The total energy transferred is equal to

$$\sum_{i=1}^{Z} \frac{p_i^2}{2m_e} + \frac{p_{\text{nucleus}}^2}{2M_A}.$$

The energy transferred to any of the electrons or to the nucleus is

positive, and is not affected by the presence of the other particles except for the small effect of binding forces.

In other words, a particle passing an atom suffers $Z+1$ collisions with the constituents of the atom and loses energy to every one of them. The $Z+1$ angles of scattering, however, tend to compensate each other and therefore the scattering is reduced strongly by shielding.

181. The scattering of a fast particle at increasing distances is reduced gradually due to shielding. Schematically we may assume, however, that in collisions up to a distance $a = 2r_{sc}$ the effect of shielding is negligible, while for distances larger than $2r_{sc}$ no scattering takes place. We may put

$$r_{sc} = a_0 Z^{-\frac{1}{3}}, \qquad a_0 = 137^2 r_0 \tag{81}$$

(a_0 is the Bohr radius of the H-atom) and thus obtain from (46) and (54)

$$\vartheta_{min} = Zze^2/vpr_{sc} = \frac{Z^{\frac{1}{3}}zm_e c^2}{137^2 vp} \quad \text{(classical)}. \tag{82}$$

Finite nucleus (see Williams (1939c))

182. The value of ϑ_{max} depends on circumstances. If no more stringent limitation of the angle of scattering is imposed we may put (compare (68 a))

$$\vartheta_{max} = \vartheta_1. \tag{83}$$

183. It was pointed out by Williams (1939c) that in case of fast particles an upper limit for ϑ is imposed by the finite size of the nucleus. The nucleus can be taken as a sphere with radius

$$r_Z = Z^{\frac{1}{3}} r_0. \tag{84}$$

The Coulomb field inside this sphere is much weaker than that of a point charge and therefore the angles of deflexion for collisions with

$$a < r_Z$$

are smaller than expected for a point nucleus. In a schematic treatment one can neglect all collisions at distances less than r_Z. One finds thus for the maximum angle of deflexion

$$\vartheta_{max} = 2Zze^2/vpr_Z = \frac{2Z^{\frac{1}{3}}zm_e c^2}{vp}. \tag{85}$$

For fast particles ϑ_{max} as obtained from (85) is small. With $v \sim c$, we have

$$\vartheta_{max} = 2Z^{\frac{1}{3}}z(m_e/mB) \quad \text{(classical, finite nucleus)}. \tag{86}$$

It will be seen that the value for ϑ_{max} obtained from quantum theory (§ 192) is 137 times larger, but even this larger value is fairly small and

thus no large-angle scattering of fast particles due to Coulomb interaction is to be expected.

Large-angle deflexions of fast mesons have, however, been observed. Such observations give direct evidence for the existence of non-Coulomb forces between nucleus and mesons (compare Ch. IV, § 319, and also § 193).

184. Introducing (52) into (85) and (82), we find with the help of (78) and (79)

$$\left.\begin{aligned} \langle \vartheta^2 \rangle &= \frac{16\pi Z z^2 r_0^2 N_3}{(p/m_e c)^2} \log 137 Z^{-\frac{1}{3}}, \\ \langle r^2 \rangle &= \frac{32\pi Z z^2 r_0^2 N_3}{3(p/m_e c)^2} \log 137 Z^{-\frac{1}{3}}. \end{aligned}\right\} \tag{87}$$

It will be seen later that (87) is confirmed by the quantal treatment.

(*b*) *Limitation of Classical Theory of Elastic Collisions*

185. It remains to point out the limitation of the classical treatment of elastic collisions (compare Williams (1940*a*)).

All considerations were based on eq. (46) which gives the momentum transferred in a collision with impact parameter a.

In an exact treatment of the collision the wave properties of the particles have to be considered. The position and momentum of a particle represented by a wave packet are uncertain by amounts given by the uncertainty relation of Heisenberg:

$$\Delta p \Delta x \sim h. \tag{88}$$

The classical treatment of a collision is only valid if the transverse extension of the wave packet representing the moving particle is small compared with the impact parameter a. Thus we have the following condition:

$$\Delta x \ll 2a. \tag{89}$$

At the same time it is necessary that the transverse component of the recoil momentum should be small compared with the uncertainty of the momentum in this direction. Therefore with the help of (46) we obtain the second condition

$$\Delta p \ll 2P'_x = 4Z_1 z e^2/va. \tag{90}$$

From (88), (89), and (90) the following condition is obtained,

$$8Z_1 z e^2/v \gg \Delta p \Delta x \sim 2\pi\hbar,$$

and therefore we find that the classical treatment is only valid provided

$$\frac{Z_1 z}{137(v/c)} \gg \tfrac{1}{4}\pi \sim 1. \tag{91}$$

The condition (91) is, however, only fulfilled for slow particles and large values of Z_1. For fast cosmic-ray particles the condition (91) is not satisfied and therefore the classical treatment cannot be relied upon.

186. In spite of the condition (91), which is not satisfied for fast particles, the formulae obtained from the classical treatment lead to qualitatively correct results. It is found that the classical expressions for energy loss or scattering are only in error under the logarithm while the factor outside the logarithm is obtained correctly. The reason for this partial agreement between classical treatment and quantal treatment is due to the analytical accident that in the case of a Coulomb interaction the two treatments lead to the same expression for the differential cross-section.

The difference between the two treatments becomes, therefore, only apparent when collision parameters appear explicitly; the collision parameters occur, however, always under the logarithm and therefore do not affect the results considerably.

2. *Quantal Treatment of Elastic Collisions*

(*a*) *Elastic Collisions*

187. We give the following very brief treatment of the quantum theory of elastic collisions. The non-relativistic treatment of this problem was given by Wentzel (1927) and by Gordon (1928); the relativistic treatment of the problem according to Dirac's theory was carried out by Mott (1932). The loss of energy of fast particles was treated by Möller (1932), Bethe (1932), Williams (1932), Bloch (1933).

Transition probabilities

188. Consider an atomic system the stationary states of which are represented by wave functions

$$\Psi_1, \quad \Psi_2, \quad \ldots. \tag{92}$$

A perturbation switched on at a time $t = 0$ may cause transitions of the system from one to another of its stationary states. It can be shown that the probability of a transition from state 1 to state 2 due to a perturbation Π is given by

$$T_{12} = \frac{1}{\hbar^2}\left|\int_0^t \Pi_{12}\, dt\right|^2, \tag{93}$$

with

$$\Pi_{12} = \int \Psi_1 \Pi \Psi_2^* \, d\tau^*, \tag{94}$$

where the integration denoted by $d\tau^*$ has to be carried out over all

coordinates; the time integration (93) has to be carried out over the time of the perturbation. Π_{12} will be referred to as the matrix element of the transition.

In case of a time-independent perturbation it is useful to introduce a transition probability per unit time. We assume the final state to lie in a continuum; the transition probability per unit time is then given by

$$t_{12} = \frac{1}{\hbar}|\Pi_{12}|^2 \frac{dN}{dW}, \tag{95}$$

where dN is the number of stationary states in the vicinity dW of the final state. The expression (95) for t_{12} refers to transitions in which the total energy of the system is conserved (compare e.g. Dirac, *Quantum Mechanics*, Oxford, 1935, p. 173).

It is often convenient to replace transition probabilities by effective cross-section. We find

$$\Phi_{12} = t_{12}\frac{k}{v}, \tag{96}$$

where k is the density of incident particles and v is their velocity.

The above approximate treatment is referred to as the Born approximation.

The Rutherford formula

Matrix element

189. Consider two free particles of mass m and M and initial momentum $\mathbf{p}$ and $\mathbf{P}$. To a first approximation we consider the particles as free and introduce the Coulomb force as a perturbation causing transitions.

The initial state of the system is described by the following wave function:

$$\Psi_1 = \frac{1}{\Lambda^3}\exp\left\{\frac{i}{\hbar}[\mathbf{PR} - Wt + \mathbf{pr} - wt]\right\}. \tag{97}$$

This wave function corresponds to the non-relativistic approximation and is normalized to represent one particle of each kind per volume Λ^3. It is further assumed that the particles are different.

Consider the transition into a final state 2 with the wave function

$$\Psi_2 = \frac{1}{\Lambda^3}\exp\left\{\frac{i}{\hbar}[\mathbf{P'R} - W't + \mathbf{p'r} - w't]\right\}. \tag{98}$$

Take the one particle to be a nucleus of charge Ze surrounded by Z electrons. Due to the shielding effect of the electrons the Coulomb field

of the nucleus dies out exponentially at large distances and we may put for the interaction energy

$$\Pi(\mathbf{r},\mathbf{R}) = \frac{zZe^2}{s}\exp(-s/2r_{sc}), \tag{99}$$

where

$$\mathbf{s} = \mathbf{R}-\mathbf{r} \quad (s = |\mathbf{s}|). \tag{100}$$

The matrix of transition from the initial to final state is obtained with the help of (94), (97), and (98)

$$\Pi_{12} = zZe^2 \int\int \frac{\exp(-s/r_{sc})}{s} \Psi_1 \Psi_2^* \, d\mathbf{r}d\mathbf{R}. \tag{101}$$

Both $\mathbf{R}$ and $\mathbf{r}$ have to be integrated over the volume Λ^3.

Centre of gravity system

190. It is convenient to introduce new variables, namely

$$\mathbf{s} \text{ and } \mathbf{S} = (M\mathbf{R}+m\mathbf{r})/(M+m). \tag{102}$$

$\mathbf{S}$ is the position vector of the centre of gravity. We find

$$d\mathbf{r}d\mathbf{R} = d\mathbf{s}d\mathbf{S}, \tag{103}$$

where we write $d\mathbf{r}$, etc., for the differential volume element, thus

$$d\mathbf{r} \equiv dr_x dr_y dr_z, \quad \text{etc.}$$

The integral (101), expressed in terms of the variables $d\mathbf{s}$ and $d\mathbf{S}$ can be written as follows (note $w-w'+W-W' = 0$):

$$\Pi_{12} = \frac{1}{\Lambda^3}\int \exp\left\{\frac{i}{\hbar}[\mathbf{p}-\mathbf{p}'+\mathbf{P}-\mathbf{P}']\mathbf{S}\right\} d\mathbf{S} \, \frac{1}{\Lambda^3}\int \frac{\exp\{(i/\hbar)\mathbf{q}\mathbf{s}-s/2r_{sc}\}}{s} \, d\mathbf{s},$$

with

$$\mathbf{q} = \left[\frac{m}{M}(\mathbf{P}-\mathbf{P}')-(\mathbf{p}-\mathbf{p}')\right]\Big/\left(1+\frac{m}{M}\right). \tag{104}$$

The integral into $d\mathbf{S}$ is equal to one provided

$$\mathbf{p}+\mathbf{P} = \mathbf{p}'+\mathbf{P}' \tag{105}$$

and vanishes otherwise.

Eq. (105) expresses the conservation of momentum and thus we see that transition can only take place in accordance with the conservation of momentum.

With the help of (104) and (105) we find

$$\mathbf{q} = \mathbf{P}-\mathbf{P}', \tag{106}$$

thus $\mathbf{q}$ is the amount of momentum transferred in the collision. The remaining integration in (104) can be carried out analytically. We find with the help of (94)

$$\Pi_{12} = \frac{4\pi z Ze^2}{(q/\hbar)^2+(1/2r_{sc})^2}. \tag{107}$$

In order to find the actual collision cross-section we have to determine the density dN/dW of final states. It is convenient to consider the collision in the centre of gravity system. In this system we have

$$\mathbf{p}' = -\mathbf{P}'. \tag{108}$$

The number of stationary states in which the momentum of the scattered particle is found in the interval p', dp' and moving in a direction inside a solid angle Ω is found to be

$$dN = \frac{\Lambda^3 p'^2\, dp' d\Omega}{(2\pi\hbar)^3}. \tag{109}$$

The energy in the centre of gravity system is

$$W = \frac{p'^2}{2}\left(\frac{1}{M}+\frac{1}{m}\right),$$

and therefore we have, remembering that $k = 1/\Lambda^3$,

$$\frac{k}{v}\frac{dN}{dW} = \frac{m^2 d\Omega}{(2\pi\hbar)^3(1+m/M)}. \tag{110}$$

Inserting (107) and (110) into (96) we obtain for the cross-section in the centre of gravity system

$$\chi_0(q)\, d\Omega = \frac{4Z^2z^2e^4m^2\, d\Omega}{(q^2+\hbar^2/4r_{sc}^2)^2}\,\frac{1}{1+m/M}. \tag{111}$$

Transformation into rest-system

191. We note that $v\chi(q)\, d\Omega$ has the same value for any system of reference and thus the cross-section in the rest-system of the scatterer becomes

$$\chi(q)\, d\Omega = \frac{4Z^2z^2e^4m^2\, d\Omega}{(q^2+\hbar^2/4r_{sc}^2)^2}. \tag{112}$$

The cross-section (112) may also be expressed in terms of ϑ, the angle of scattering. For small scattering angles we have

$$p \sim p' \quad \text{and} \quad q \sim Zp\sin\tfrac{1}{2}\vartheta \tag{113}$$

besides $$d\Omega = 2\pi\sin\vartheta\, d\vartheta.$$

And thus we have

$$\chi(\vartheta)\, d\vartheta = \frac{8\pi Z^2z^2e^4\sin\vartheta\, d\vartheta}{v^2p^2[4\sin^2\tfrac{1}{2}\vartheta+(\hbar/2pr_{sc})^2]^2}. \tag{114}$$

Putting further $\sin\vartheta \sim \vartheta$ and neglecting $\hbar/2pr_{sc}$ compared with ϑ we find finally

$$\chi(\vartheta)\, d\vartheta = \frac{8\pi Z^2z^2e^4}{v^2p^2}\frac{d\vartheta}{\vartheta^3}. \tag{115}$$

Comparison with the classical result

192. It is seen that the cross-section (115) obtained from quantal treatment is identical with the cross-section (52) obtained from the classical treatment. A notable difference between the two treatments appears in the limitation for small angles. It is seen from the fuller expression (114) that for small angles $\vartheta < \vartheta_{\min}$ the scattering cross-section increases much less than $d\vartheta/\vartheta^3$ with decreasing angle. The difference becomes apparent for angles smaller than

$$\vartheta_{\min} = \hbar/2pr_{sc}. \tag{116}$$

The classical value for $\vartheta_{\min}$ is $137v/c$ times smaller (see § 181).

Finite nucleus

193. The large-angle scattering of fast particles is limited by the finite size of the nucleus. The Coulomb field inside the nucleus is much smaller than that of a point charge. Schematically the field can be represented by

$$\frac{Ze}{R}\left(e^{-R/2r_{sc}} - e^{-R/2r_z}\right) \tag{117}$$

(Williams, 1939*c*). Inserting (117) into (94) we see that the matrix element can be split into two similar contributions and we have

$$H_{12} = 4\pi Zze^2\left\{\frac{1}{q^2+(\hbar/2r_{sc})^2} - \frac{1}{q^2+(\hbar/2r_z)^2}\right\}. \tag{118}$$

The cross-section can be derived from this new matrix element exactly as before and we obtain

$$\chi(\vartheta)\,d\vartheta = \frac{8\pi Z^2z^2e^4}{p^2v^2}\left\{\frac{1}{\vartheta^2+\vartheta_{\min}^2} - \frac{1}{\vartheta^2+\vartheta_{\max}^2}\right\}^2 \vartheta\,d\vartheta, \tag{119}$$

with
$$\vartheta_{\min} = \hbar/2pr_{sc}, \qquad \vartheta_{\max} = \hbar/2pr_z. \tag{120}$$

For angles in the region
$$\vartheta \ll \vartheta_{\max} \tag{121}$$

the second term in the curly bracket is small compared with the first term and therefore the cross-section is only slightly affected by the finite size of the nucleus.

For angles
$$\vartheta \gg \vartheta_{\max}$$

the two terms in the curly bracket tend to cancel each other and therefore the probability of scattering through angles much larger than $\vartheta_{\max}$ is negligibly small.

In Fig. 29 we have reproduced from Williams (1939*c*) the cross-section for scattering through various angles. Curve A refers to scattering by

Coulomb interaction only, while curve C gives the scattering by the short-range forces between the nucleus and the scattered particle. It is seen that for a pure Coulomb interaction scattering through large angles is unimportant.

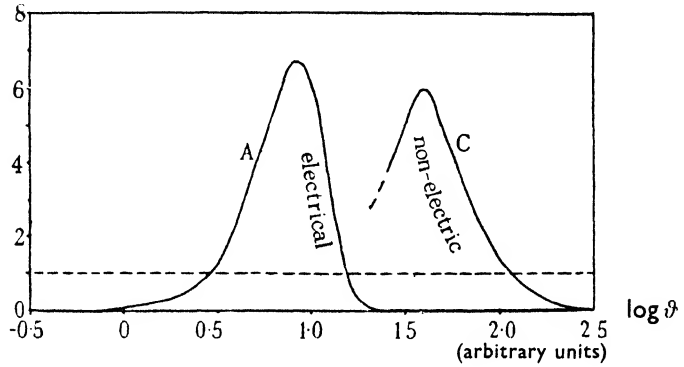

FIG. 29. Showing scattering by 1 cm. lead plate due to 'non-electrical' and electrical forces respectively. From E. J. Williams, *Proc. Roy. Soc.* A, **169**, 553.

(*b*) *Inelastic Collisions*

194. The energy transferred in an inelastic collision is equal to the energy of excitation or ionization of the atom. This energy is large compared with the energy which can be transferred in an elastic collision and therefore the energy loss of charged particles traversing an absorber is mainly due to the inelastic collisions.

The rate of loss of energy can be worked out by evaluating the matrix elements and by averaging over the various collisions. A different method which corresponds much more closely to the classical treatment of the problem is due to Williams (1933*a*). In this method the collision between primary and atom is treated as a time-dependent perturbation, the field of the primary particle sweeping over the atom being regarded as the perturbation.

The probability of a transition being induced by the disturbing field of the passing particle is given by (93). The integration has to be carried out over the duration of the encounter.

Collision with a hydrogen atom

195. We consider the collision of an H-atom with a charged particle passing at a large distance a. If a is much larger than the dimension of the atom then it can be assumed that the disturbing field is constant at any instant over the region occupied by the atom.

The perturbation energy can thus be written as

$$\Pi(t) = xF_x, \tag{122}$$

where x is the coordinate of the electron parallel to the field, F_x is the force defined in (45). With (122) and (93) we obtain for the transition probability

$$T_{12} = \left(|x_{12}|^2/\hbar^2\right)\left|\int F_x e^{-it(W_1-W_2)/\hbar}\,dt\right|^2, \tag{123}$$

where

$$x_{12} = \int \psi_1(\mathbf{r}_1) x \psi_2^*(\mathbf{r}_1)\,d\mathbf{r}_1;$$

$$\psi_1(\mathbf{r}_1)e^{-iW_1t/\hbar}, \qquad \psi_2(\mathbf{r}_1)e^{-iW_2t/\hbar}$$

are the wave functions representing ground state and excited state of the atom.

If the time of collision is short compared with the time of oscillation,

$$t_{\text{coll}} \ll \hbar/(W_1 - W_2), \tag{123a}$$

then the exponential in the time interval can be taken as constant and thus we have

$$\int F_x e^{-it(W_1-W_2)/\hbar}\,dt \sim \int F_x\,dt = P'_{\text{cl}}, \tag{124}$$

where P'_{cl} is the momentum transferred according to classical theory to one of the atomic electrons.

The total energy transferred to the atom according to classical theory is

$$W'_{\text{cl}} = \frac{P'^2_{\text{cl}}}{2m_e}. \tag{125}$$

We proceed to compare the energy loss obtained from classical theory with that obtained from quantum theory.

The transition probability according to quantum theory can be written with the help of (123), 124), and (125)

$$T_{12} = W'_{\text{cl}}\frac{2m_e}{\hbar^2}|x_{12}|^2. \tag{126}$$

The average energy transferred is obtained by averaging over all types of transitions. We have

$$\overline{W} = W'_{\text{cl}}\frac{2m_e}{\hbar^2}\sum_k |x_{1k}|^2(W_k - W_1), \tag{127}$$

where the sum has to be extended over all stationary states of the atom including the continuum. It was shown by Bethe (1932) that

$$\sum |x_{1k}|^2(W_k - W_1) = \hbar^2/2m_e.$$

And thus one finds

$$\overline{W} = W_{\text{cl}}. \tag{128}$$

Thus the average energy lost by a fast particle in collisions at large distances is given correctly by the classical theory; the actual amounts lost in individual collisions are, however, much larger than predicted by the classical theory. A fast particle passing an atom at a large distance will usually pass without interacting, while in rare cases a strong interaction leading to excitation or ionization will take place.

We note that the above derivation becomes invalid for slow collisions where (123a) is not fulfilled. It can thus be shown that inelastic collisions with atoms at distances larger than $a_{\max}$ (54a) are improbable.

3. *Radiative Collisions*

Treatment as two-body collision

196. Charged particles involved in close collisions suffer sudden acceleration and thus emit electromagnetic radiation. According to the classical theory the rate of energy emitted is given by

$$\frac{dW}{dt} = \frac{2e^2}{3c^3}\left(\frac{d^2\mathbf{r}}{dt^2}\right)^2. \tag{129}$$

Radiative collisions cause a much greater loss of energy for fast particles than the inelastic collisions.

The theory of radiative collisions using Born's method was given by Bethe and Heitler (1934). The radiative collisions can also be treated by the impact parameter method (Williams (1933*a*) and Weizsäcker (1934)). In the following we sketch the latter method of approach.

Energy loss in rest-system of colliding particle

197. Consider an electron with velocity $v \sim c$ flying past a nucleus of charge Ze. We proceed to calculate in terms of the classical theory the radiation emitted by the electron.

It is convenient to consider the collision in the rest-system of the electron and to transform eventually the results thus obtained from the rest-system of the electron to the rest-system of the nucleus.

In the rest-system of the electron the nucleus is flying past the electron; the Coulomb field of the nucleus acting upon the electron is given by (45).

The electron is accelerated and the rate of energy thus emitted is obtained from (129) and (45) on setting

$$Z_1 = Z, \qquad z = 1, \qquad m = m_e. \tag{130}$$

We find thus

$$\frac{dW_0}{dt} = \frac{2e^2}{3c^3}\left\{\frac{Ze^2Ba}{m_e(a^2+B^2v^2t^2)^{\frac{3}{2}}}\right\}^2. \tag{131}$$

The total energy emitted is obtained by integrating over the time of collision,

$$W_0 = \int \frac{dW_0}{dt} dt = \tfrac{1}{4}\pi \left(\frac{Zr_0}{a}\right)^3 B m_e c^2 \quad (v \sim c). \tag{132}$$

Transformation into rest-system of nucleus

198. We have to transform the energy into the rest-system of the nucleus.

In the rest-system of the electron the radiation is distributed as that of a radiating dipole. No radiation being emitted in the transverse direction, the maximum of the intensity is emitted in the plane perpendicular to a. We assume, however, for simplicity that the radiation is distributed isotropically round the electron.

Transforming into the rest-system of the nucleus we find from (27) that the total energy emitted in the system of the nucleus will be

$$W \simeq W_0 B. \tag{133}$$

The probability for a collision at a distance between a and $a+da$ from the nucleus is $2\pi a\, da$ and therefore the average energy loss per collision is obtained as

$$-\frac{dW}{d\mathfrak{z}} = N \int W 2\pi a\, da = \frac{\pi^2}{2} N Z^2 \frac{W^2}{m_e c^2} r_0^2 \left(\frac{r_0}{a_{\min}}\right). \tag{134}$$

The rate of loss of energy thus diverges due to the contribution of the close collisions.

Limitation of the method

199. The divergency of the expression (134) can be shown to be caused by the breakdown of the classical theory for close collisions. The limitation of the classical theory can be best shown in the rest-system of the electron.

The wave-packet representing the electron must be smaller than the width of the Coulomb field passing over the electron. The field has a width of the order of $2a/B$ and thus we have the condition

$$2a/B \gg \Delta x. \tag{135}$$

The uncertainty of the momentum of the electron must be small as compared with $m_e c$. We have therefore

$$m_e c \gg \Delta p. \tag{136}$$

With the help of (83) we have thus the condition

$$2a/B . m_e c \gg 2\pi\hbar$$

or

$$a \gg 137\pi r_0 B = a_{\min}. \tag{137}$$

Introducing the above value for $a_{\min}$ into (134) we have

$$-\frac{dW}{d\zeta} = \frac{\pi}{2}\frac{Z^2}{137}NWr_0^2. \tag{138}$$

(138) represents, however, a lower limit only, as collisions at distances less than $a_{\min}$, though not accessible to classical treatment, still contribute to the energy loss.

Treatment as scattering of light

200. The collisions at distances less than $a_{\min}$ can still be treated classically as follows.

The field of the fast-moving nucleus in the rest-system of the electron is almost identical with the field of an electromagnetic wave. The difference between the field of an electromagnetic wave and that of the moving nucleus is confined to discrepancies of the order of $1/B$; thus:

1. The field of the nucleus is almost exactly transverse. Because of the Lorentz contraction of the field the ratio of the longitudinal and transverse components is $1/B$.
2. The field moves almost with the velocity of light. The difference between v and c can be expressed as
$$1-\frac{v}{c} \sim \frac{1}{2B^2}.$$
3. The electric field is accompanied by an induced magnetic field. The electric and magnetic components are perpendicular and they differ only by amounts of the order of $1/2B^2$.

Equivalent spectrum

201. The passing field can be resolved into Fourier components and therefore the collision can be considered as the scattering of the monochromatic components by the electron.

The field strength $E(t)$ due to the passing nucleus consists of a short light pulse. The intensity in the spectral region ν, $d\nu$ is given by

$$dI(\nu) \sim d\nu\left(\int_{-\infty}^{+\infty} E(t)\cos\nu t\, dt\right)^2. \tag{139}$$

Considering small frequencies ν, the cosine term can be regarded as a slowly varying function, and we have approximately

$$\int E(t)\cos\nu t\, dt \sim \int E(t)\, dt.$$

For frequencies large compared with the period of the collision the function $E(t)$ can be taken to vary only slowly as compared with the

cosine term and thus the value of the integral is small. Schematically the spectrum (139) can be represented as follows:

$$\frac{dI(\nu)}{d\nu}\begin{cases} = \text{const.} & \text{for } \nu \ll \dfrac{2}{t_{\text{coll}}}, \\ = 0 & \text{for } \nu \gg \dfrac{2}{t_{\text{coll}}}. \end{cases} \tag{140}$$

202. According to the classical theory the cross-section for the scattering of radiation of any frequency by a free electron is given by the Thomson formula

$$\Phi_{\text{scattering}} = 8\pi r_0^2/3.$$

The energy scattered by the electron can thus be worked out and after transformation into the rest-system of the nucleus the energy loss of the electron is obtained. The total rate of loss thus obtained is of course the same as that obtained in the previous treatment.

Scattering of equivalent radiation field

203. The scattering of light by free electrons has been treated by Klein and Nishina (1929) using Dirac's relativistic quantum theory of the electron. It is found that the classical cross-section is valid only for small frequencies. For frequencies exceeding $\nu_e = m_e c^2/\hbar$, the scattering cross-section becomes much smaller than the Thomson cross-section.

This breakdown of the classical theory can be understood in general terms. The interaction of light with an electron can be treated classically as long as the wavelength λ of the light is large compared with the wave-packet representing the electron. Assuming that the uncertainty of the momentum of the electron is smaller than $m_e c$, this gives

$$\lambda m_e c \gg 2\pi\hbar$$

and thus

$$\nu = \frac{2\pi c}{\lambda} \ll m_e c^2/\hbar.$$

204. Thus the large frequencies contribute comparatively little to the total scattering. We can assume schematically that classical theory holds up to frequencies ν_e, but that no scattering takes place for higher frequencies.

At distance $a > a_{\min}/\pi$ (compare (137)) the time of collision is longer than $2/\nu_e$ and thus the spectrum (140) does not contain frequencies above ν_e. For these collisions the classical treatment is justified.

The limitation of the classical theory becomes important for smaller

distances. From (57) and (140) it is seen easily that for collisions at distances $a < a_{\min}/\pi$ only a fraction

$$\pi a/a_{\min}$$

of the spectrum contains low frequencies and therefore the classical expression for energy transfer must be reduced by this factor. Thus excluding frequencies larger than ν_c we have to replace (133) by

$$W_0 = \begin{cases} \frac{\pi Z^2}{4}\left(\frac{r_0}{a}\right)^3 B m_e c^2 & (a > a_{\min}/\pi), \\ \frac{\pi Z^2}{4}\left(\frac{r_0}{a}\right)^2\left(\frac{\pi r_0}{a_{\min}}\right) B m_e c^2 & (a < a_{\min}/\pi). \end{cases} \tag{141}$$

Inserting the value for $a_{\min}$ from (137) we can integrate over collisions at different distances and we obtain

$$-\frac{dW}{d\mathfrak{z}} = N\int W_0' 2\pi a\, da = \frac{\pi^2}{2}\frac{Z^2 r_0^2}{137} N\{\log(a_{\min}/a_1)+1\}, \tag{142}$$

where a_1 is the smallest distance for which the modified classical picture holds. As the wave-packet representing the particle is rather larger than $h/m_e c$ we may put

$$a_e = h/m_e c = 2a_{\min}/B,$$

and thus with the help of (137) and (142) we obtain

$$-\frac{dW}{d\mathfrak{z}} = \frac{\pi^2}{2} N \frac{Z^2 r_0^2}{137}\left\{\log\frac{W}{2\pi m_e c^2}+1\right\}. \tag{143}$$

Effect of screening

We have so far neglected the effect of screening due to the atomic electrons. For energies larger than

$$W > W_1 = \pi 137 m_e c^2 Z^{-\frac{1}{3}}$$

we find $a_{\min}/\pi = r_{sc}$, and thus for energies larger than W_1 many of the collisions take place outside the screen of the atomic electrons and are therefore ineffective.

The shielding of the electrons can be taken care of in a rough way by assuming that collisions at distances less than r_{sc} are not affected by screening while collisions outside r_{sc} lead to no energy transfer at all.

With these simplified assumptions we find

$$-\frac{dW}{d\mathfrak{z}} \simeq \frac{\pi^2}{2} N \frac{Z^2 r_0^2}{137}\log(192 Z^{-\frac{1}{3}}) \quad \left(\frac{e}{2}137 = 192\right). \tag{144}$$

205. The treatment of the collision radiation as given in the preceding section is due to Williams (1934*a*) and to Weizsäcker (1934).

Making use of the exact Klein-Nishina formula these authors also obtain expressions in good agreement with the results obtained by Bethe and Heitler from Born's method.

Discussion of radiation formulae

206. The following features of the radiation formulae should be noted.

1. The rate of loss of energy is proportional to the energy of the primary. The range of energetic electrons therefore increases only slightly with increasing energy.

2. The loss of energy for electrons is proportional to r_0^2 and therefore is proportional to $1/m_e^2$. It is seen therefore that the radiation loss for particles heavier than electrons is much smaller than the corresponding loss for electrons.

3. The rate of loss is proportional to Z^2. Therefore the radiation loss is much more important in heavy elements than in light elements.

4. The collisions take place at large distances as compared with the nuclear radius and therefore no effects due to the finite size of the nucleus should be expected. This is true irrespective of the energy of the incident electrons.

5. The possibility of a breakdown of the radiation formulae for high energies has been much discussed. It is seen, however, from the treatment of the collision in the rest-system of the electron that the theory of the radiative collisions is based on the scattering of quanta with energies less than $m_e c^2$. The high energies which appear in the system of the observer are only introduced later by the Lorentz transformation. It is therefore unlikely that the radiation formulae should become invalid even for very high energies.

E. Meson Theory

207. The meson theory was created by Yukawa (1935) (see also Yukawa and co-workers, 1937, 8) in an attempt to account for the forces acting between nucleons in atomic nuclei and to account for the β-activity. Yukawa's theory is an improved form of the theories of Heisenberg and Fermi. These older theories regard the nuclear forces as exchange forces due to the exchange of electron neutrino pairs. Yukawa postulated the existence of a new particle which is responsible for the short range forces. The meson, discovered among cosmic rays, has all the properties predicted by Yukawa for his hypothetical particle and it is now generally assumed that the meson is identical with Yukawa's particle.

After the experimental discovery of the meson the further problem arose of accounting for the properties of the free cosmic-ray mesons in terms of the meson theory.

No fully satisfactory formulation of the meson theory has been found. A formulation of the meson theory due to Möller and Rosenfeld (1940) seems to give a satisfactory account of nuclear phenomena. This formulation of the meson theory was adapted by Heitler and Peng (1944) to the treatment of the collisions between fast nucleons; cosmic-ray phenomena can be accounted for qualitatively on these lines.

In the following we give a short account of the important features of the meson theory.

1. *Yukawa's Hypothesis*

208. The short range forces between nucleons can be accounted for according to Yukawa (1935) by assuming that the nucleons are sources of a field somewhat similar to the electromagnetic field, called the 'meson field'. The nucleons have to be assumed to carry a 'meson charge' which gives rise to the field. Meson charge and meson field are analogous to quantities appearing in the electromagnetic theory.

To account for the strong spin dependence of the nuclear forces it is assumed that the meson charge consists of two parts.

1. A scalar meson charge, analogous to the ordinary electric charge.
2. A dipole charge having the direction of the spin of the nucleon and corresponding to magnetic dipole moment in the electromagnetic theory.

2. *The Meson Field*

(*a*) *General Properties*

The static field

209. A static electric field can be derived from a potential which obeys the Laplace-Poisson equation

$$\nabla^2\Phi = -4\pi\rho. \tag{145}$$

The field of a point charge is obtained by assuming $\rho = \delta(\mathbf{r})$, where $\delta(\mathbf{r})$ is the three-dimensional Dirac function. The corresponding solution of (145) is the Coulomb potential

$$\Phi = e/r.$$

The meson field is supposed to be derived from a meson potential $\bar{\phi}$,† obeying the following equation in free space:

$$\nabla^2\bar{\phi} = \mathfrak{k}^2\bar{\phi}, \tag{146}$$

† A bar ($\bar{}$) will be used to signify quantities referring to the meson field.

where $1/\mathfrak{k}$ has the dimension of a length. The solution of (146) corresponding to the field of a point charge is found as

$$\bar{\phi} = (1/r)\exp(-\mathfrak{k}r). \tag{147}$$

It is seen that the meson potential decreases exponentially with distance. The forces due to the meson field are therefore short range forces with a range of the order of $1/\mathfrak{k}$. The forces between nucleons are known to have ranges of the order of $r_0 = e^2/m_e c^2$ and therefore in order to account for the nuclear forces in terms of the meson field it is necessary to assume

$$1/\mathfrak{k} \simeq e^2/m_e c^2. \tag{148}$$

Meson waves

210. Electromagnetic waves in free space obey the following wave equation:

$$\begin{aligned} \nabla^2\Phi - \frac{1}{c^2}\frac{\partial^2\Phi}{\partial t^2} &= 0, \\ \nabla^2\mathbf{A} - \frac{1}{c^2}\frac{\partial^2\mathbf{A}}{\partial t^2} &= 0. \end{aligned} \tag{149}$$

One form of the wave equation of the meson field can be written as:—

$$\begin{aligned} \nabla^2\bar{\phi} - \frac{1}{c^2}\frac{\partial^2\bar{\phi}}{\partial t^2} &= \mathfrak{k}^2\bar{\phi}, \\ \nabla^2\overline{\mathbf{A}} - \frac{1}{c^2}\frac{\partial^2\overline{\mathbf{A}}}{\partial t^2} &= \mathfrak{k}^2\overline{\mathbf{A}}, \end{aligned} \tag{150}$$

where $\overline{\mathbf{A}}$ is the vector potential of the meson field. The meson field strength $\mathbf{E}$ and $\mathbf{H}$ can be derived from the potentials $\bar{\phi}$ and $\overline{\mathbf{A}}$ by the equations analogous to (15), which are valid for the electromagnetic case.

The general solution of (149) can be represented as a superposition of plane waves. Similarly the solution of the meson wave equation can be taken as a superposition of plane waves. To obtain a plane wave travelling in the x-direction we look for a solution depending only on x and t. Further we restrict ourselves to monochromatic waves with frequency ν and assume

$$\bar{\phi}(x,t) = \bar{\phi}_0(x)\exp(-i\nu t). \tag{151}$$

Introducing (151) into (150) we find the following equation for the amplitude $\bar{\phi}_0(x)$:

$$\frac{d^2\bar{\phi}_0}{dx^2} = \left(-\frac{\nu^2}{c^2} + \mathfrak{k}^2\right)\bar{\phi}_0, \tag{152}$$

and therefore the plane wave solution can be written as follows:

$$\bar{\phi}(x,t) = \text{const.} \times \exp i\left\{x\sqrt{\left(\frac{\nu^2}{c^2} - \mathfrak{k}^2\right)} - \nu t\right\}. \tag{153}$$

211. The solution (153) representing a plane wave of the meson field differs appreciably from a plane wave in the electromagnetic field. The main differences are as follows:

1. We state without proof that the meson wave, when expressed in terms of the field strength, has both longitudinal and transverse components. The longitudinal component is proportional to $\mathfrak{k}$ and disappears in the limiting case of $\mathfrak{k} \to 0$.
2. The phase velocity v_p of meson waves is larger than c. We find from (153)

$$v_p = \frac{\nu}{\sqrt{(\nu^2/c^2 - \mathfrak{k}^2)}} = \frac{c}{\sqrt{(1 - \mathfrak{k}^2 c^2/\nu^2)}}. \tag{154}$$

The meson

212. According to quantum theory the electromagnetic field can be resolved into quanta with energy

$$W = \hbar\nu$$

and momentum

$$P = \hbar/\lambda \quad (\lambda = \text{wavelength}/2\pi).$$

The corresponding treatment of the meson field leads to the following expressions:

$$W = \hbar\nu, \qquad P = \hbar\sqrt{\left(\frac{\nu^2}{c^2} - \mathfrak{k}^2\right)}, \tag{155}$$

where W and P are the energy and momentum of the quantum associated with the meson field. The velocity of the quantum is obtained from (12) as

$$v = \frac{cP}{W} = c\sqrt{\left(1 - \frac{\mathfrak{k}^2}{c^2\nu^2}\right)} = \frac{c^2}{v_p};$$

this velocity represents also the *group velocity* of a meson wave-packet. From the relation (6) we have

$$\mu = \sqrt{(W^2/c^4 - P^2/c^2)} = \frac{\hbar\mathfrak{k}}{c}, \tag{156}$$

where μ is the mass of the quantum. The quanta of the meson field are assumed to be the mesons and thus μ is the meson mass.

Comparing (156) and (148) we find

$$\mu = \frac{\hbar c}{e^2} m_e = 137 m_e. \tag{157}$$

The above estimation refers to the order of magnitude only. A more detailed treatment leads to a somewhat larger value of μ.

The observed value of the meson mass (see § 274) is about

$$\mu = 180 m_e,$$

in agreement with the prediction of the theory. There are, however, some indications for a meson of mass $\mu' \sim 1000 m_e$ (Leprince-Ringuet and Lhéritier, 1944).

(*b*) *Nuclear Forces*

Electric charge of the meson

213. Yukawa (1935) postulated that the mesons carry unit electric charges, either positive or negative.

The electric charge carried by the mesons can be expressed in terms of the meson field. Expressions have been given which represent the electric charge density and the electric current density associated with a meson field.

In analogy with the emission and absorption of electromagnetic radiation by an electric charge it must be assumed that nucleons are capable of emitting or absorbing mesons. To safeguard the conservation of charge it must be assumed that a proton can only emit a positive meson, changing thereby into a neutron, and that a neutron can only emit a negative meson, changing after emission into a proton.

Processes in which a proton emits a meson which is absorbed by another neutron give rise to exchange forces between the nucleons very similar to the exchange forces between atoms due to the exchange of electrons. It is believed that the internuclear forces are due to meson exchange.

Neutretto

214. Exchange forces as described in the preceding paragraph are expected to act only between unlike nucleons. Two protons or two neutrons are clearly incapable of the exchange of a charged meson. It was shown by Fröhlich, Heitler, and Kemmer (1938) that forces between like particles arise due to higher-order exchanges in which two mesons are exchanged simultaneously.

An essentially different approach is to postulate the existence of neutral mesons or 'neutrettos' (Arley and Heitler (1938)).

Kemmer (1938*b*) has given a formulation of the meson theory in which positive, negative, and neutral mesons are introduced and which leads to exchange forces between nucleons independent of their electric charge.

215. Kemmer's (1938*b*) formulation is made attractive by its great simplicity. It must be pointed out, however, that there is no experimental evidence available to indicate the occurrence of neutral mesons.† On the other hand no experimental evidence against the occurrence of neutral mesons has been brought forward.

The spin of the meson

216. It was shown by Kemmer (1938*a*) that there are four different possibilities for the formulation of the equations of the meson field.

In its simplest form the meson field has only a scalar potential obeying the first equation of (150). The 'meson field strength' is then defined by

$$\mathbf{F} = -\text{grad}\,\bar{\phi}, \qquad G = -\frac{\partial \bar{\phi}}{\partial t}. \tag{158}$$

It is readily seen that plane waves in this case are longitudinal and therefore the waves show no polarization. This case corresponds to mesons with spin zero.

The meson field originally suggested by Yukawa (1935) was actually the scalar field. The scalar field leads, however, to a wrong spin dependence of the nuclear forces: Assuming the scalar field, the force between a proton and a neutron is obtained to be attractive in the ^1S-state and repulsive in the ^3S-state. The deuteron is found experimentally to have a spin 1 and therefore the ground-state of the deuteron must be in first approximation a ^3S-state, in contradiction to the prediction of the scalar theory.

A better agreement with observation is obtained when the meson field of the vector type is assumed (Fröhlich, Heitler, and Kemmer (1938)). The vector field is that described in § 210. The state of polarization of the field is connected with the spin of the meson, the vector meson with three states of polarization has spin 1.

217. The actual value of the meson spin, though not known at present, should be accessible to experiment. The cross-section for the production of high-energy electron secondaries by fast mesons traversing matter depends strongly on the value of the spin of the meson. The spin of the meson could in principle be deduced from the number of high-energy secondaries produced by the meson component. The experimental evidence derived from cosmic-ray data will be discussed in

† Certain experiments are often quoted in the literature as evidence for the existence of neutral mesons. It will be shown in §§ 286, 294 that these results are quite inconclusive.

Chapter VI. In our opinion no conclusions can be drawn from the experimental evidence obtained so far.

218. Apart from the two types of fields discussed in § 216 two more possibilities giving rise to fields with similar properties can be envisaged. These fields may be denoted in accordance with their covariance properties as 'pseudo-scalar field' and 'pseudo-vector field'.

(*c*) *β-Decay*

Instability of the meson

219. To account for the β-activity Yukawa (1935) assumed the meson to be unstable against spontaneous decay into an electron and a neutrino. The mean life of the meson was assumed by Yukawa (1935) to be about $0{\cdot}25\times10^{-6}$ sec. It was pointed out later by Nordheim (1939*a*) that the life of the meson must be assumed to be shorter than predicted by Yukawa in order to account for the β-decay satisfactorily.

The experimentally observed mean life of the meson is longer than that predicted by Yukawa, namely

$$\ell_0 = 2{\cdot}1\times10^{-6} \text{ sec.}$$

(see § 345, Ch. V). There is therefore a serious discrepancy between observed and predicted lifetime.

In spite of the discrepancy between observed and predicted life of the meson the features of the observed particle are so similar to those of the predicted particle that the similarity cannot be regarded as accidental and one is tempted to overcome the difficulty by some modification of the theory.

It was suggested by Nordheim (1939*a*) that the decay of the meson might be a transition forbidden in first approximation. Due to the strong perturbations inside a nucleus the transition may take place more easily and therefore the life of the meson inside the nucleus could conceivably be shorter than the life of a free meson.

Theory of Møller and Rosenfeld

220. A different suggestion was put forward by Møller and Rosenfeld (1940). These authors assume the existence of two different types of mesons: the ordinary (pseudo-scalar) meson and a vector meson with a mean life of only 10^{-8} sec. Experimental evidence as to the existence of such mesons has to be awaited.

221. The following interesting order of magnitude relation between the observed half-life of the meson and other universal constants was observed by Blackett (1939).

One finds $$c\ell_0 = R_0(e/w), \qquad (159)$$

where $R_0 = e^2/\mu c^2$ and $w = \sqrt{G}\,\mu$ is the 'gravitational charge' of the meson. G is the gravitational constant.

The relation (159) is only qualitatively correct. As the order of magnitude of ℓ_0 cannot be expressed simply in terms of universal constants without the gravitational constant the above relation can be taken as strong evidence for a connexion between meson decay and gravitation.

The neutrino

222. It is well known that some β-active nuclei emit a continuous spectrum of β-particles, though the nuclei change their energy by a definite amount in the process of decay. It must be assumed therefore that only a variable fraction of the total energy liberated in the β-disintegration is taken up by the emitted β-particle.

Bohr suggests that the energy may not be conserved in the β-decay process. Pauli has pointed out that the missing energy could be taken up by an uncharged particle of small mass. Such a particle is expected to interact only slightly with matter and it might escape detection.

Pauli's idea was later elaborated by Fermi. The particle is now known as a neutrino and is supposed to safeguard the conservation of energy.

Experiments have also been carried out recently showing that the neutrino not only accounts for missing energy but gives rise to a recoil, thus the neutrino possesses momentum (Halpern and Crane (1939), Allen (1942)).

Further, the neutrino must be assumed to have a spin $\hbar/2$, to safeguard the conservation of angular momentum in the process of β-decay.

Thus there is indirect evidence for the neutrino having energy, momentum, and spin. The interaction of the neutrino with matter is so weak that no positive effects of the neutrino could be observed.

223. According to Yukawa's (1935) theory the decay of a meson is the most fundamental case of β-disintegration. It is clear that a particle in free space cannot disintegrate by the emission of a single particle, as in such a process the momentum cannot be conserved. In accordance with the theory of β-decay it is therefore assumed that the meson decays into an electron and a neutrino; the two decay products being emitted in opposite directions.

3. *Observational Evidence for the Meson Theory*

(*a*) *The Deuteron*

224. A crucial test of any formulation of the meson theory is whether the formulation leads to correct predictions of the properties of the deuteron.

The following relevant facts about the deuteron are known experimentally:

1. The ground state of the deuteron is a triplet state, probably ^3S.
2. Scattering experiments indicate the existence of a ^1S-state with roughly half the potential energy of the ground state.
3. According to the observations of Kellogg, Rabi, Ramsey, and Zacharias (1940) the deuteron possesses a quadripole moment. The moment is parallel to the spin and its magnitude is $Q = 2{\cdot}73 \times 10^{-27}$ cm.^{2} Thus the nucleus behaves as a prolate spheroid spinning about its major axis.

225. Each of the four possible meson fields described in the previous section contains two arbitrary parameters f and g corresponding to the meson charge and the meson magnetic moment of the nucleons.

It was found by Fröhlich, Heitler, and Kemmer (1938) that the requirements (1) and (2) can both be fulfilled by a suitable choice of the constants f and g provided the vector meson field is used.

However, the vector meson field gives rise to a dipole interaction between the nucleons leading to a force proportional to $1/r^3$. It is well known that stationary states cannot exist for such a high singularity and therefore no reliance can be based upon this treatment.

226. Bethe (1940) has investigated how far it is possible to eliminate the singularity by a 'cutting-off' process. It was found that it would be necessary to cut out the meson field up to distances of the same order as the radius of the deuteron to make the cutting off effective. This procedure appears quite unsatisfactory.

If only neutral mesons are assumed then a more satisfactory 'cutting-off' radius can be obtained. But as observations give evidence only for charged mesons, it appears unsatisfactory to formulate a theory of the nuclear forces based on neutral mesons only.

227. A way of eliminating the singularities was proposed by Møller and Rosenfeld (1940). It was shown that by choosing a suitable superposition of two meson fields it was possible to obtain an interaction free from dipole singularities.

In particular, by choosing the superposition of the pseudo-scalar field

with the vector-meson field it was possible to obtain a force between nucleons free from the dipole term and which at the same time satisfied all the three requirements given above regarding the deuteron.

228. According to this formulation of the meson theory the mesons have to be regarded as a mixture of two types, namely 'pseudo-scalar' mesons and 'vector' mesons. The former have spin zero while the latter have spin one. It is further suggested that the 'pseudo-scalar mesons' are the ordinary mesons observed in the penetrating component of cosmic rays while the vector mesons are supposed to have a mean life of only about 10^{-8} sec. and these mesons are supposed to be mainly responsible for the radioactive β-decay.

The theory of Møller and Rosenfeld (1940) represents at the time being the most satisfactory formulation of the meson theory. We note, however, that this theory requires the assumption of the occurrence of the short-lived 'transverse' meson, and besides it makes a definite assumption about the spin of the ordinary meson.

There is no experimental evidence available in support of the existence of the transverse meson, though no evidence against the existence of such a particle has been brought forward. No conclusive evidence as to the value of the meson spin has been obtained.

More experimental results must therefore be awaited before definite conclusions about the validity of the Møller-Rosenfeld theory can be made.

(*b*) *Collisions*

Scattering

229. The simplest collision process involving mesons is the scattering of mesons by nucleons. This process is analogous to the scattering of light by an electric charge, and therefore the classical treatment of the problem of scattering of meson waves necessarily leads to a scattering cross-section analogous to the Thomson cross-section for light.

The scattering cross-section obtained from the classical treatment is according to Bhabha (1938*b*)

$$\sim \left(\frac{f^2}{\mu c^2}\right)^2, \tag{160}$$

where f is the meson charge of the scattering nucleon. We note that the cross-section contains the meson mass and not the nucleon mass M. The reason for this can be understood by comparing the process of the scattering of meson waves with that of the scattering of electromagnetic waves in more detail.

A light wave falling on an electric charge makes the charge vibrate with an amplitude inversely proportional to the mass of the charge, resulting in emission of light by the vibrating charge inversely proportional to the square of the mass.

A meson wave falling on a nucleon produces two effects: (1) the nucleon as a whole vibrates with an amplitude inversely proportional to M; (2) the wave induces transitions between proton and neutron states accompanied by the emission and reabsorption of a meson. This second process may be compared with the polarization of the nucleon by the meson wave. The inertia in this process arises from the mass of the virtual meson and thus the cross-section is proportional to $1/\mu^2$. The second process is, of course, far more important than the first.

230. The cross-section (160) is of the same order as that obtained from the quantal treatment for low-energy mesons. According to this treatment the cross-section for scattering increases rapidly with the incident energy. The cross-section (160) is, however, clearly incompatible with observation.

We may write instead of (160)

$$\left(\frac{f^2}{\hbar c}\right)^2\left(\frac{\hbar}{\mu c}\right)^2. \tag{161}$$

$f^2/\hbar c$ is a number which plays a role in meson theory comparable with Sommerfeld's fine structure constant $e^2/\hbar c$ for the electromagnetic field. It is estimated that $f^2/\hbar c$ is of the order of unity. The cross-section (161) is therefore according to (148), (156) of the order of

$$\sim (\hbar/\mu c)^2 \sim (e^2/m_e c^2)^2 \sim 10^{-25} \text{ cm.}^2 \tag{162}$$

231. Because of the short range of the meson force most collisions should result in large-angle collisions. Thus the mean free path of a meson before being scattered through a large angle should be, according to (162),

$$\mathscr{R} \sim 20 \text{ gram/cm.}^2 \tag{163}$$

It will be seen that this value is quite incompatible with observation. The observed rate of large-angle scattering corresponds to a cross-section very much smaller than (162).

232. Various other collision processes have been treated by Born's approximation. Most of these cross-sections are too large to be compatible with observation; we have collected in Table 1 a few results.

TABLE 1

Cross-sections for processes involving mesons calculated without radiation damping

Process	*Cross-section*	*Author*
Scattering of meson by nucleon	$\Phi_{\text{scattering}} \sim 10^{-27}\,\text{cm.}^2 \dfrac{p^4}{\mu^2 w^2}$	Heitler (1938), Bhabha (1938 *b*), A. H. Wilson (1940), Ma (1942), and others.
Scattering of a photon by a meson.	$\dfrac{5\pi}{18}\left(\dfrac{e^2}{\mu c^2}\right)\dfrac{\hbar\nu}{\mu c^2}$	Smowolnisky (1940).
Absorption of meson emitting a photon, or emission of meson by photon: $h\nu + P \rightleftarrows N + \mu^+$, $h\nu + N \rightleftarrows P + \mu^-$.	$\sim 10^{-26}$ cm.^{2} for primary energy μc^2, decreasing with primary energy.	Massey and Corben (1939 *a*, *b*).
Emission of meson pair by photon.†	$\int_0^w d\Phi = \dfrac{25}{149}\dfrac{Z^2e^2}{\hbar c}\left(\dfrac{e^2}{\mu c^2}\right)^2 \dfrac{w}{\mu c^2}$	Booth and Wilson (1940).
Emission of photon† by meson.	$\int_0^{h\nu} w'\,d\Phi = \dfrac{5}{9}\dfrac{Z^2e^2}{\hbar c}\left(\dfrac{e^2}{\mu c^2}\right)^2 \dfrac{h\nu}{\mu c^2}$	Booth and Wilson (1940).
Scattering of meson by Coulomb field. Production of secondary electron by meson.	See §§ 240, 241.	

† In Coulomb field of nucleus.

Besides, the cross-sections thus obtained are increasing with energy; this is also difficult to reconcile with observational evidence.

It is thus seen that the meson theory in its simple formulation leads to results incompatible with observation.

An attempt was made (Heitler and Ma (1940), Bhabha (1940 *b*, 1)) to overcome the difficulties of the meson theory by postulating that proton and neutron are the lowest states of energy of the nucleon and assuming the existence of higher excited states corresponding to charges $-e, 2e, \ldots$ and to spin values $\frac{3}{2}, \ldots$.

This theory leads to the *strong coupling theory*; it gives smaller cross-sections for some of the collisions, but it has been largely abandoned because of its great internal difficulties.

233. The difficulties have been removed in a different way. It was pointed out by Bhabha (1940 *a*) that the radiation damping in the classical meson theory plays an important part. Radiation damping

was introduced into the quantal treatment of the meson field by Heitler (1941) and by A. H. Wilson (1941).

The treatment of the radiation damping is rendered difficult because diverging terms appear in the theory. A method was suggested according to which the diverging terms can be neglected in an unambiguous way.

234. The various cross-sections obtained by the treatment including radiation damping have reasonable values. A very satisfactory feature of the cross-sections thus obtained is that they decrease for large energies with increasing energy.

Some of the cross-sections thus obtained are given in the following table:

TABLE 2

Cross-sections involving mesons calculated with radiation damping

Process	*Cross-section*	*Author*
Scattering by nucleon.	$4\pi\left(\frac{\hbar}{\mu c}\right)^2 \frac{f^2}{g^2+3f^2}\left(\frac{\mu c^2}{w}\right)^2$ assuming charged mesons only.	Wilson (1941), Heitler and Peng (1942).
	$4\pi\left(\frac{\hbar}{\mu c}\right)^2\left(\frac{\mu c^2}{w}\right)^2$ assuming the symmetrical theory including neutrettos (§ 174).	
Emission of x (pseudo-scalar) meson by light quanta.	$\frac{\sqrt{2}\,\pi^2 f'^2}{f}\left(\frac{\hbar}{\mu c}\right)^2\left(\frac{\mu c^2}{w}\right)^2$.	Hamilton and Peng (1944).

All cross-sections for $w \gg \mu c^2/f$.

Low-energy interaction is discussed by Hamilton and Peng (1944), Heitler and Peng (1944).

Emission of mesons by nucleons

235. The collision between two nucleons can be treated by analogy with the radiative collisions between two electrically charged particles.

Consider a fast nucleon flying past a stationary nucleon. The meson field of the fast nucleon is comparable with the field of meson waves. In particular the meson field can be resolved into Fourier components, each component corresponding to a monochromatic meson beam. Thus the field of the nucleus can be represented by an equivalent meson spectrum.

The meson waves passing over the stationary nucleus are scattered

and the scattered waves appear to the observer as mesons emitted in the collision.

236. The emission of mesons in collisions between fast nucleons was treated in the above way by Heitler and Peng (1944), Heitler (1945).

The results obtained were shown to agree reasonably with experiments in a number of papers (Hamilton, Heitler, and Peng (1943), Heitler and Walsh (1945), Jánossy (1943)). This problem will be discussed in Chapter IX.

F. Summary of Theoretical Expressions

1. *Elastic and Inelastic Collisions*

(a) *Charged Particles*

Energy loss

237. *Charged particles* lose energy due to inelastic collisions. Most of this energy is spent in ionizing atoms. Some energy is also lost by exciting atoms.

The rate of energy loss is given by the Bloch (1933) formula for a particle of charge ze, mass m. We have

$$-\frac{dW}{d\theta} = \frac{2\pi N Z z^2 \Phi_0 m_e c^2}{(v/c)^2}\left\{\log\frac{B m_e v^2 W_{\max}}{I^2 Z^2} + \frac{1}{B^2} + \Psi\left(\frac{z}{137 v/c}\right)\right\}, \quad (164)$$

$\Psi(x) = 0{\cdot}577 + \log x + \ldots =$ real part of $(ix)!$ (electrons),

$N =$ number of atoms per gram,

$\Phi_0 = \left(\frac{e^2}{m_e c^2}\right)^2$,

$I = 13{\cdot}5$ eV.,

$W_{\max} =$ maximum transferable energy.

238. For fairly fast particles we shall use sometimes the following approximation (compare Rossi and Greisen (1941)):

$$-\frac{dW}{d\theta} = \frac{\mathscr{A}}{(v/c)^2}, \quad (165)$$

with

$$\mathscr{A} = 0{\cdot}153\frac{Z}{A} \times \left\{\begin{array}{l} \left\{20{\cdot}2 + 3\log\frac{p}{m_e c} - 2\log Z\right\} \quad \text{(electrons)} \\ \left\{20{\cdot}5 + 4\log\frac{p}{m_e c} - 2\log Z\right\} \quad \text{(protons, mesons).} \end{array}\right\} \quad (166)$$

Unit: MEV. per (gram/cm.^{2}).

Neglecting the terms $\log(p/m_e c)$, $\mathscr{A}$ can be regarded as constant; introducing

$$W_k = mc^2(B-1) \quad \text{and} \quad (v/c)^2 = 1 - \frac{1}{B^2} \quad (167)$$

eq. (165) can be integrated. We find for the range of a particle with initial energy W_k

$$\mathscr{R}(W_k) = \frac{W_k^2}{\mathscr{A}(W_k+mc^2)}. \tag{168}$$

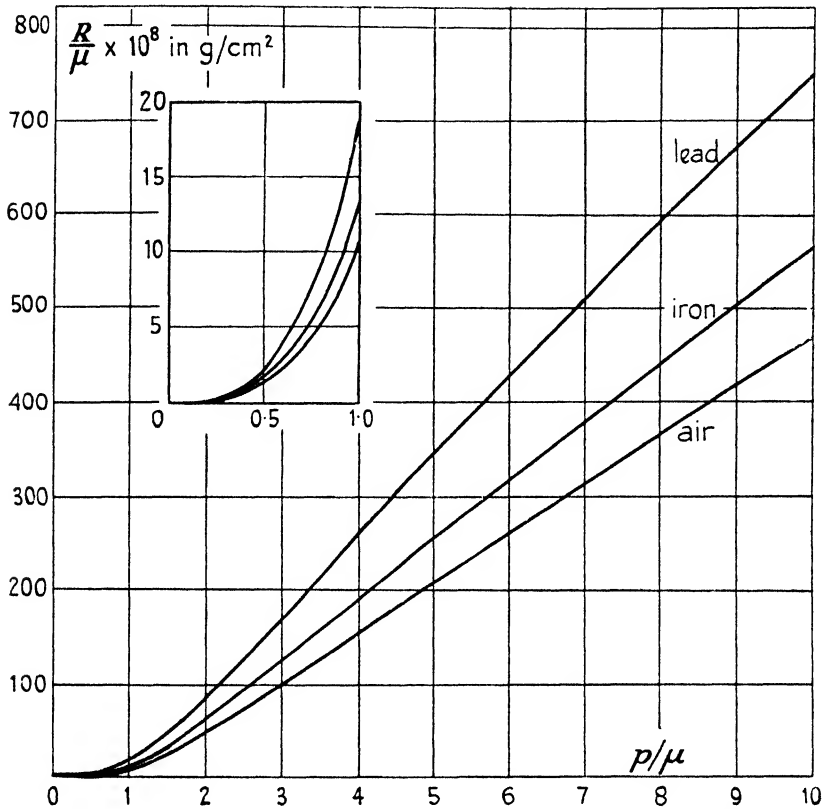

FIG. 30 *a*. Range of mesons or protons in air, iron, and lead. (From Rossi and Greisen, *Rev. Mod. Phys.* **13**, Fig. 3.)

The following two approximations are useful:

(1) non-relativistic case

$$\mathscr{R}(W_k) \sim \frac{W_k^2}{\mathscr{A}mc^2} \sim \frac{p^4}{4\mathscr{A}m^3c^2}; \tag{169}$$

(2) extreme relativistic case

$$\mathscr{R}(W_k) \sim \frac{1}{\mathscr{A}}(W_k-mc^2). \tag{170}$$

The exact range momentum relation is reproduced in Figs. 30 *a*, *b*, *c* for air, iron, and lead. The graphs are taken from Rossi and Greisen (1941).

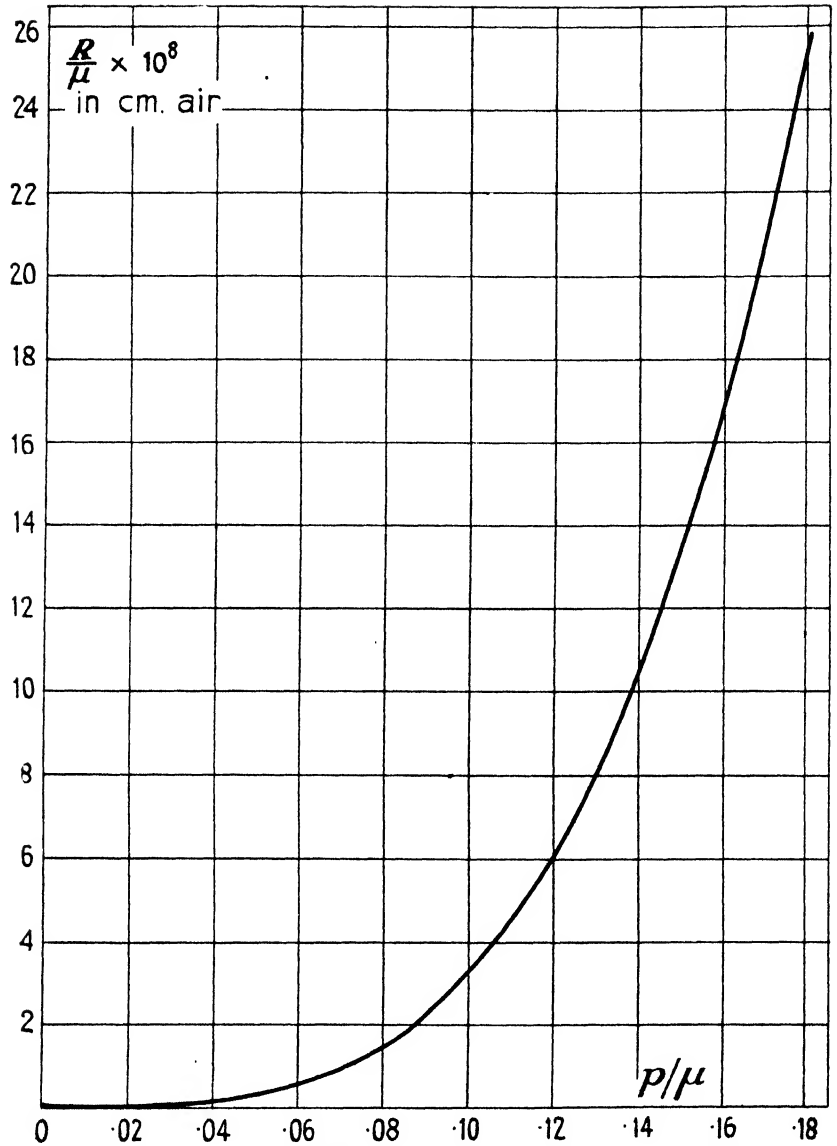

FIG. 30 *b*. Range of low-energy mesons in air (Livingstone and Bethe).

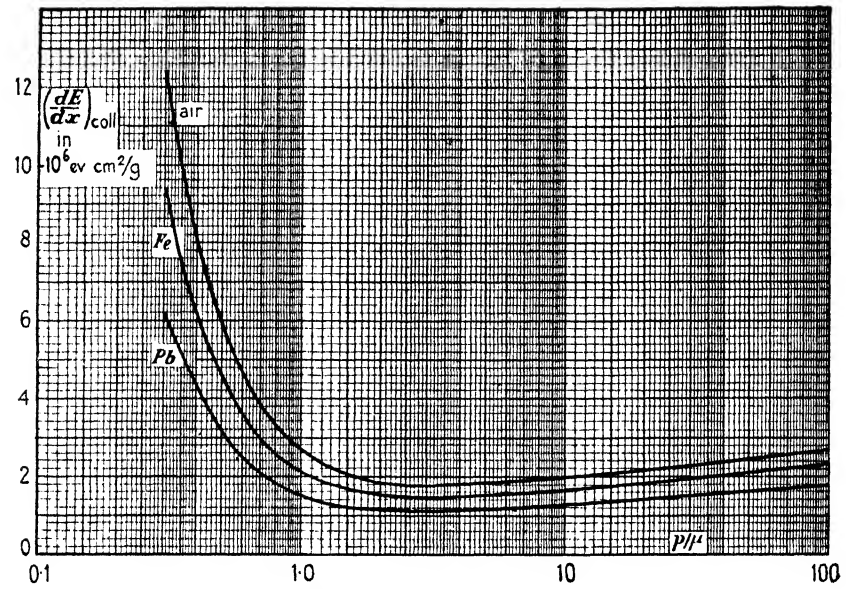

FIG. 30 c. Total collision loss of mesons in air, iron, and lead.
(Rossi and Greisen, Fig. 2.)

Rate of ionization

239. The rate of ionization of charged particles is nearly proportional to the rate of energy loss due to inelastic collisions. The average amount of energy expended per ion is 32 volts. Thus the rate of ionization can be taken roughly as

$$I(w) = -\frac{1}{32\,ev}\frac{dw}{d\theta}. \tag{171}$$

The rate of primary ionization is according to Bethe (1933) given by

$$I_p = \frac{2\pi N Z \Phi_0}{A(v/c)^2}\frac{a}{I_0}\left\{\log\frac{2m_e v^2 B^2}{I_0} + b - \frac{v^2}{c^2}\right\}, \tag{172}$$

where a and b depend on the absorbing material and I_0 is the excitation potential of the outer shell. For hydrogen an exact treatment is possible and one has

$$I_0 = 13{\cdot}5 \text{ eV.}, \qquad a = 0{\cdot}285, \qquad b = 3{\cdot}04. \tag{173}$$

Production of secondaries

240. The cross-section for the production of a secondary electron with an energy in the interval w', dw' by a primary of energy w is given approximately by

$$\chi(w, w')\,dw' = 2\pi\Phi_0\frac{m_e c^2}{(v/c)^2}\frac{dw'}{w_k'^2}. \tag{174}$$

The equation (174) is not valid for secondaries of the order of the ionization potentials of the atoms; it is also invalid for secondaries with energies near the energy of the primary.

For close collisions where the amount of energy transferred is comparable with the primary energy it is important to consider spin interaction and also interaction of the magnetic moments of the colliding particles.

The cross-section for the production of secondaries by an electron is obtained as (Møller (1932))—w_k kinetic energy:—

$$\chi(w,w')\,dw' = \frac{2\pi\Phi_0}{(v/c)^2}\left\{\frac{w_k}{w'_k(w-w')}-\frac{1}{w_k}\right\}^2 m_e c^2\,dw'_k. \tag{175}$$

The cross-section for the production of secondaries by positive electrons is given by (Bhabha, 1938*a*)

$$\chi(w,w')\,dw' = \frac{2\pi\Phi_0}{(v/c)^2}\left\{1-2\frac{w'_k}{w_k}+3\left(\frac{w'_k}{w_k}\right)^2-2\left(\frac{w'_k}{w_k}\right)^3+\left(\frac{w'_k}{w_k}\right)^4\right\}\frac{m_e c^2\,dw'_k}{w'^2_k}. \tag{176}$$

The cross-section for the production of secondaries by mesons depends on the assumptions regarding spin and magnetic moment. In the following we give the cross-sections computed for various assumptions.

Neglecting m_e/μ against unity one finds for meson spin 0, magnetic moment 0 (Bhabha, 1938*a*)

$$\chi(w,w')\,dw' = \frac{2\pi\Phi_0}{(v/c)^2}\frac{m_e c^2\,dw'}{w'^2_k}\left(1-\frac{v^2}{c^2}\frac{w'_k}{w_{k\max}}\right); \tag{177}$$

spin $\frac{1}{2}$, magnetic moment $e\hbar/2\mu c$ (Massey and Corben, 1939*b*; Bhabha, 1938*a*)

$$= \frac{2\pi\Phi_0}{(v/c)^2}\frac{m_e c^2\,dw'}{w'^2_k}\left[1-\frac{v^2}{c^2}\frac{w'_k}{w_{k\max}}+\frac{1}{2}\left(\frac{w'_k}{w}\right)^2\right]; \tag{178}$$

spin 1, magnetic moment $e\hbar/2\mu c$ (Massey and Corben, 1939*b*; Oppenheimer, Snyder, and Serber, 1940)

$$= \frac{2\pi\Phi_0}{(v/c)^2}\frac{m_e c^2\,dw'}{w'^2_k}\left[\left(1-\frac{v^2}{c^2}\frac{w'_k}{w_{k\max}}\right)\left(1+\frac{1}{3}\frac{w'_k}{w_c}\right)+\frac{1}{3}\frac{w'^2_k}{w^2}\left(1+\frac{1}{2}\frac{w'_k}{w_c}\right)\right]. \tag{179}$$

$$w_c = \mu c^2\frac{\mu}{m_e} \sim 2\times 10^4\ \text{MEV}.$$

Scattering

241. The differential cross-section for a particle of momentum p to be scattered through an angle $\vartheta \gg \vartheta_{\min}$ by a nucleus of charge Ze is given as follows:

Particle of spin 0 (Williams, 1939*c*):

$$\chi(\vartheta)\,d\Omega = \frac{Z^2\Phi_0(m_e c)^2}{4p^2(v/c)^2}\frac{d\Omega}{\sin^4\frac{1}{2}\vartheta}. \tag{180}$$

Particle spin $\frac{1}{2}\hbar$ (Mott, 1929)

$$= \frac{Z^2\Phi_0(m_e c)^2}{4p^2(v/c)^2}\left(1-\frac{v^2}{c^2}\sin^2\tfrac{1}{2}\vartheta\right)\frac{d\Omega}{\sin^4\frac{1}{2}\vartheta}. \tag{181}$$

Particle spin $\hbar$ (Massey and Corben, 1939)

$$= \frac{Z^2\Phi_0(m_e c)^2}{4p^2(v/c)^2}\left(1+\frac{1}{6}\frac{p^2v^2}{m^2c^4}\sin^2\vartheta\right)\frac{d\Omega}{\sin^4\frac{1}{2}\vartheta}. \tag{182}$$

For small deflexions these cross-sections reduce to (180).

242. The cross-sections are calculated for scattering by a point nucleus. If the finite size of the nucleus is taken into account the cross-section (180) has to be replaced by (Williams (1939*c*))

$$\chi(\vartheta)\,d\Omega = \frac{4Z^2\Phi_0(m_e c)^2}{p^2(v/c)^2}d\Omega\left(\frac{1}{\vartheta^2+\vartheta_{\min}^2}-\frac{1}{\vartheta^2+\vartheta_{\max}^2}\right)^2, \tag{183}$$

where it is assumed that $\sin\vartheta \sim \vartheta$, and

$$\vartheta_{\min} = \frac{m_e c}{137p}Z^{\frac{1}{3}}, \qquad \vartheta_{\max} = \frac{241 m_e c}{p}. \tag{184}$$

It is seen that scattering through angles $\vartheta > \vartheta_{\max}$ is very rare.

The cross-sections for the large-angle scattering of mesons due to short-range interaction is given in § 234.

It is seen that the number of secondaries with energies comparable to the primary energy depends strongly on the value of the meson spin. Such high-energy secondaries are found to be much more frequent for spin h than for spin $\frac{1}{2}h$ or zero.

243. The mean-square angle of scattering for fast electrons or mesons in an absorber $\mathfrak{z}$ cm. thick is given by

$$\langle\vartheta^2\rangle = \frac{8\pi N\mathfrak{z}}{A}\frac{Z^2\Phi_0(m_e c)^2}{p^2(v/c)^2}\log(181Z^{-\frac{1}{3}}). \tag{185}$$

The mean-square linear displacement after traversing an absorber of thickness $\mathfrak{z}$ is given by

$$\langle r^2\rangle = \frac{8\pi N\mathfrak{z}^3}{3A}\frac{Z^2\Phi_0(m_e c)^2}{p^2(v/c)^2}\log(181Z^{-\frac{1}{3}}). \tag{186}$$

(*b*) *Absorption of Photons*

244. Low-energy photons are mainly absorbed by the photo-electric effect. The cross-section for this effect is given by

$$\Phi_{\mathrm{PE}} = \begin{cases} \dfrac{32\sqrt{2}\pi}{3.137^4}Z^5\Phi_0\left(\dfrac{m_e c^2}{w}\right)^{\frac{7}{2}} & (w \ll m_e c^2), \\ \dfrac{4\pi}{137^4}Z^5\Phi_0\dfrac{m_e c^2}{w} & (w \gg m_e c^2). \end{cases} \tag{187}$$

The photo-electric effect is, however, unimportant for cosmic-ray photons. More important is the scattering of photons by electrons. The cross-section for scattering is given by the Klein-Nishina (1929) formula.

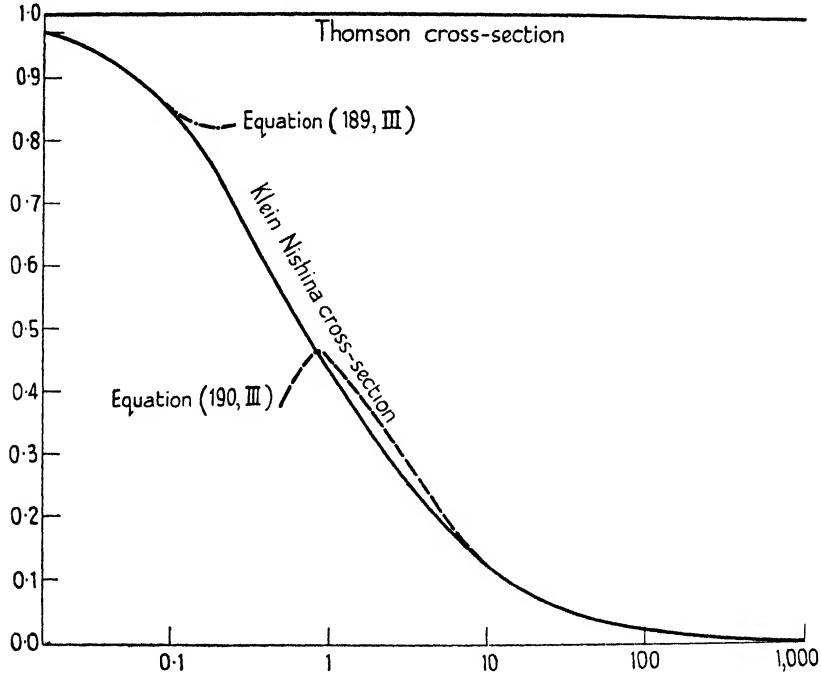

FIG. 31. Klein-Nishina cross-section.

The total scattering cross-section is given by (Klein and Nishina, 1929)

$$\Phi_{KN} = 2\pi\Phi_0\left\{\frac{1+\gamma}{\gamma^3}\left[\frac{2\gamma(1+\gamma)}{1+2\gamma} - \log(1+2\gamma)\right] + \frac{1}{2\gamma}\log(1+2\gamma) - \frac{1+3\gamma}{(1+2\gamma)^2}\right\},$$

with

$$\gamma = \frac{w}{m_e c^2}. \tag{188}$$

For low energies this cross-section tends to the limit of the classical Thomson cross-section, namely

$$\Phi_{KN} \approx \frac{8\pi}{3}\Phi_0\left\{1 - \frac{2w}{m_e c^2} + \frac{26}{5}\left(\frac{w}{m_e c^2}\right)^2 + \ldots\right\} \quad (w \ll m_e c^2). \tag{189}$$

For high energies we have in good approximation

$$\Phi_{KN} \approx \pi\Phi_0 \frac{m_e c^2}{w}\left(\log\frac{2w}{m_e c^2} + \frac{1}{2}\right) \quad (w \gg m_e c^2). \tag{190}$$

We note that for high energies the Klein-Nishina cross-section is much smaller than the corresponding classical cross-section. In Fig. 31 we have plotted Φ_{KN} as function of γ. We have also plotted as broken lines the approximations (189) and (190).

2. *Radiative collisions*

Electrons

245. Fast electrons lose energy due to the emission of light quanta. The rate of loss is different for high and low energies because of the effects of the screening of the nuclear field by atomic electrons.

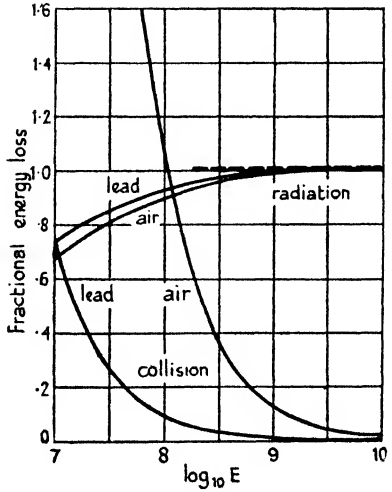

FIG. 32. Fractional energy loss of radiation for electrons per radiation length for air and lead. (Rossi and Greisen, Fig. 9.)

The rate of loss is given as follows (Bethe and Heitler (1934)):

$$-\frac{dw}{d\theta} = N\int w'\Phi_{\text{rad}}(w,w')\,dw'$$

$$= \frac{4NZ^2}{137}\Phi_0 x\begin{cases}\left\{\log\dfrac{2w}{m_e c^2}-\dfrac{1}{12}\right\} & \text{(screening neglected),}\\[2ex] \left\{\log 183Z^{-\frac{1}{3}}+\dfrac{1}{18}\right\} & \text{(complete screening,}\\ & \text{i.e. } w \gg 137m_e c^2 Z^{-\frac{1}{3}}).\end{cases} \tag{191}$$

The rate of loss of electrons in lead and air calculated from the combined effects of ionization and collision radiation is given in Fig. 32.

It should be remembered that the loss due to collision radiation takes

place in large but infrequent steps. The actual loss is therefore subject to large fluctuations.

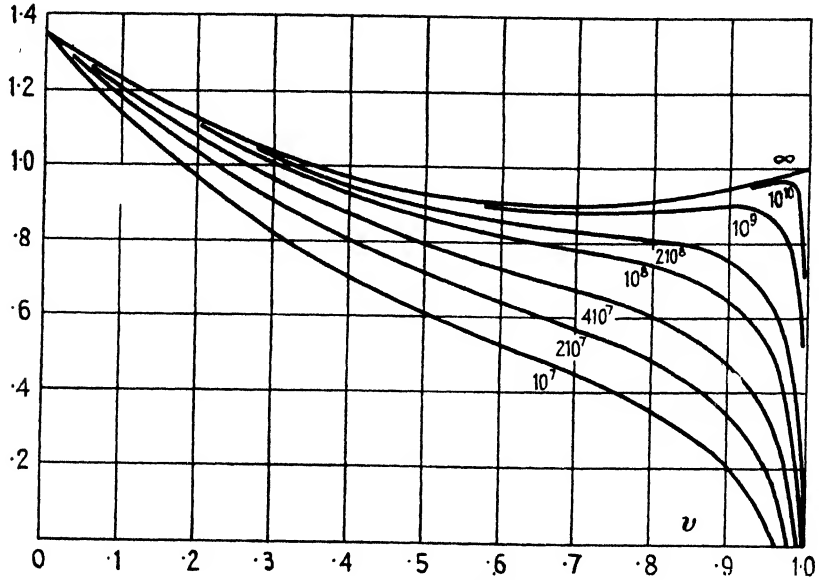

FIG. 33. Differential radiation probability per radiation length of air for electrons of various energies. (The numbers attached to the curves indicate the energy of the electrons in eV.) (Rossi and Greisen, Fig. 6.)

The cross-section for an electron of energy w to emit a photon with energy in the interval between w' and $w'+dw'$ is as follows:

$$\Phi_{\text{rad}}(w,w') = \bar{\Phi}\,\mathfrak{H}(w,w')\frac{w'\,dw'}{w^2}\log 183Z^{-\frac{1}{3}},$$

$$\bar{\Phi} = \frac{4Z^2}{137}\left(\frac{e^2}{m_e c^2}\right) = 2{\cdot}3Z^2.10^{-27}\ \text{cm.}^2, \tag{192}$$

$$\bar{\Phi}\log 183Z^{-\frac{1}{3}} = (12-1{\cdot}76\log_{10}Z)Z^2.10^{-27}\ \text{cm.}^2,$$

$$N\bar{\Phi}\log 183Z^{-\frac{1}{3}} = \frac{Z^2}{A}(0{\cdot}72-0{\cdot}106\log_{10}Z).10^{-2}\ \text{cm.}^2/\text{g}.$$

with†

$$\mathfrak{H}(w,w') = 1-(\tfrac{4}{3}+\alpha)\left(\frac{w}{w'}-\frac{w^2}{w'^2}\right),$$

$$\alpha = \frac{1}{9\log 183Z^{-\frac{1}{3}}} = \begin{cases} 0{\cdot}021 & \text{(H)},\\ 0{\cdot}026 & \text{(O)},\\ 0{\cdot}030 & \text{(Pb)}. \end{cases} \tag{193}$$

† Compare Fig. 33.

The value of $\mathfrak{H}(w, w')$ is valid for complete screening, i.e. if

$$\frac{w(w-w')}{w' m_e c^2} \gg 137 Z^{-\frac{1}{3}}. \tag{194}$$

The form of $\mathfrak{H}(w, w')$ in the case of partial screening may be obtained from the original paper of Bethe and Heitler (1934).

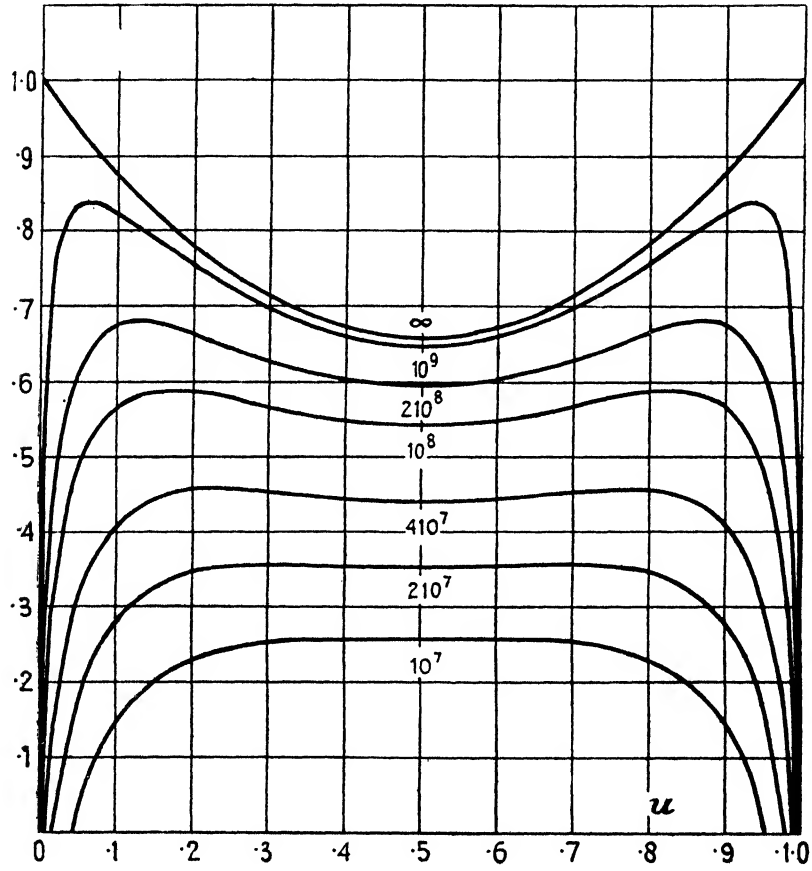

FIG. 34. Differential probability of pair production per cascade unit of air for photons of various energies. (The numbers attached indicate the energy of the primary photons in eV.) (Rossi and Greisen, Fig. 10.)

Photons

246. High-energy photons are largely absorbed by production of electron pairs. The cross-section of a photon producing a pair containing one electron with energy in the interval w', dw' is given by (compare also Fig. 34)

$$\Phi_{\text{pair}}(w, w')\, dw' = \overline{\Phi} R(w', w) \frac{dw'}{w} \log 183 Z^{-\frac{1}{3}}. \tag{195}$$

The total cross-section for the production of a pair by a photon of energy w is as follows:

$$\int_0^w \Phi_{\text{pair}}(w, w')\, dw' = \Phi_{\text{pair}} = \begin{cases} \bar{\Phi}\left[\frac{7}{9}\log\frac{2w}{m_e c^2} - \frac{109}{54}\right] & \text{(no screening)} \\ \Phi\left[\frac{7}{9}\log 183 Z^{-\frac{1}{3}} - \frac{1}{54}\right] & \text{(complete screening; } w \gtrsim 137 m_e c^2 Z^{-\frac{1}{3}}\text{).} \end{cases} \tag{196}$$

Mesons

247. The energy loss of fast mesons is mainly due to ionization. The rate of loss is given by the Bloch (1933) formula (compare E. J. Williams, 1938).

A beam of mesons is also diminished due to spontaneous decay. This process will be dealt with in Chapter V.

Radiative loss of mesons has a small probability only, as such a loss is inversely proportional to the square of the rest-mass. The radiation cross-section for mesons is therefore expected to be $(m_e/\mu)^2$ times that for electrons given in (191).

According to the meson theory without radiation damping the radiation cross-section increases with primary energy. Booth and Wilson (1940) find

$$\Phi_{\substack{\text{rad} \\ \text{meson}}}(w')\, dw' = \frac{1}{12}\frac{Z^2}{137}\left(\frac{e^2}{\mu c^2}\right)^2 \frac{w}{\mu c^2}\left(2 - 2\frac{w'}{w} + 7\frac{w'^2}{w^2}\right) dw'. \tag{197}$$

Taking, however, radiation damping into account the cross-section decreases with energy; compare Hamilton and Peng (1944).

Protons

248. Radiative loss is for protons even smaller than that for mesons. The energy loss of protons is therefore mainly due to ionization as far as electromagnetic forces are concerned.

According to the meson theory both protons and neutrons lose energy in collisions resulting in the emission of mesons. For fast nucleons the loss due to this process is believed to be much larger than that due to ionization loss.

G. Absorption Functions

1. *Straggling of Energy Loss*

The range of a particle is given by the average absorber thickness in which the particle is brought to rest. A mono-energetic beam of particles is, however, not stopped sharply at a given thickness of absorber. Due

to fluctuation of energy loss the actual ranges of the individual particles are distributed round the average value.

Catastrophic Absorption

249. If the absorption of a beam is due to collisions, each of which removes one primary particle completely, we speak of catastrophic absorption. An example of this kind of process is the absorption of photons by pair production. Assume the cross-section for a catastrophic collision to be Ψ and the number of centres per gram of absorber to be L. The probability of a collision along a path $d\theta$ is then $L\Psi\, d\theta$ (θ is the path expressed in grams per cm.^{2}) and the change of intensity dc along $d\theta$ is

$$dc = -(cL\Psi)\, d\theta, \tag{198}$$

whence $$c = c_0 \exp(-\mathfrak{a}\theta), \qquad \mathfrak{a} = L\Psi.$$

The absorption is exponential. We call the reciprocal absorption coefficient $1/\mathfrak{a}$ the mean range.

250. It is interesting to consider cases where the primaries are removed by a fixed number of collisions. Putting again $\mathfrak{a} = L\Psi$ we find that the average number of collisions a primary suffers in a path h would be $\mathfrak{a}\theta$, if the primaries could survive any number of collisions. The probability that a primary suffers exactly $n-1$ collisions when traversing θ is, according to Appendix I,

$$\exp(-\mathfrak{a}\theta)\frac{(\mathfrak{a}\theta)^{n-1}}{(n-1)!}. \tag{199}$$

And the probability that the primary suffers its nth collision in the interval θ, $\theta+d\theta$ is therefore

$$\exp(-\mathfrak{a}\theta)\frac{(\mathfrak{a}\theta)^{n-1}}{(n-1)!}\mathfrak{a}\, d\theta. \tag{200}$$

If primaries are removed by the nth collision, then the rate of primaries removed at h is

$$c_0 - c(\theta) = c_0 \int_0^\theta \exp(-\mathfrak{a}\theta)\frac{(\mathfrak{a}\theta)^{n-1}}{(n-1)!}\mathfrak{a}\, d\theta, \tag{201}$$

where c_0 is the rate of incident particles.

We find for $n = 2$

$$c(\theta) = c_0(1+\mathfrak{a}\theta)\exp(-\mathfrak{a}\theta). \tag{202}$$

Similar expressions are found for higher values of n. The cases $n = 1$, 5, 10, and 20, are shown in Fig. 35. It is seen that with increasing n the

absorption function approaches a step function. For very large values of n the particles have an almost sharp range

$$\mathscr{R} = n/\mathfrak{a}. \tag{203}$$

That $c(h)$ approaches a step function can also be seen from (201). According to Appendix I the integrand of the right-hand expression

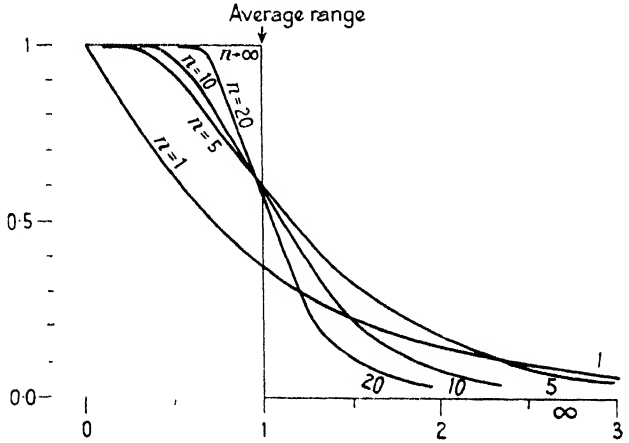

FIG. 35. Absorption functions.

(201) can be approximated by a Gaussian distribution having a sharp maximum near $\theta = n/\mathfrak{a}$. The width of the Gaussian distribution is of the order of

$$\delta R = \pm\sqrt{n}/\mathfrak{a}. \tag{204}$$

$2\delta R$ can therefore be regarded as the mean straggling.

Range Absorption

251. Primaries are absorbed according to range if the number of collisions required to stop a primary is large, so that the straggling can be neglected. Range absorption is expected, e.g. for particles losing energy mainly by ionization, as the ionization loss is built up of a large number of very small losses. A certain amount of fluctuation is, however, expected due to occasional large losses. A detailed investigation shows, however, that the straggling of the range of ionizing particles which results from the occasional emission of energetic secondaries is small (Landau (1944)).

2. *The Gross Transformation*

252. The absorption functions dealt with so far were all derived for a parallel beam of rays. Such absorption functions can be applied, for

instance, if the intensity of the radiation is measured with a vertical coincidence arrangement under varying thickness of absorber.

Cosmic-ray intensity is, however, often measured by means of an ionization chamber. An ionization chamber is equally sensitive for rays coming from any direction and therefore we measure with the ionization chamber the radiation intensity integrated over all directions of incidence.

The problem arises as to the relation of the intensities measured by an ionization chamber and by a vertical coincidence arrangement.

This problem was solved by Gross (1933) (compare also Williams, 1933 *b*) for cases where the following assumptions hold:

(1) It is assumed that the radiation incident on the top of the atmosphere is distributed isotropically;

(2) that the primary particles traverse the atmosphere without being appreciably scattered, or if the primaries produce secondaries these continue in the direction of the primary;

(3) that the intensity $c(\mathbf{r})$ at any depth below the top of the atmosphere is a function of the mass which the particles had to traverse when travelling in the direction $\mathbf{r}$.

253. Consider a point A below the top of the atmosphere so that the mass equivalent of the atmosphere above A is θ gram per cm.^{2} Denote the vertical intensity at A by $c(0,\theta)$. The intensity in a direction inclined by ϑ towards the vertical is according to the assumptions (1)–(3)

$$c(\vartheta,\theta) = c(0,\theta/\cos\vartheta). \tag{205}$$

We find therefore for the total intensity $C(\theta)$

$$C(\theta) = 2\pi \int_0^{\frac{1}{2}\pi} c(0,\theta/\cos\vartheta)\sin\vartheta\, d\vartheta. \tag{206}$$

Introducing as a new variable $x = \theta/\cos\vartheta$ under the integral one obtains, after dividing by θ and differentiating with regard to θ,

$$c(0,\theta) = \frac{1}{2\pi}\left(C(\theta) - \theta\frac{dC(\theta)}{d\theta}\right). \tag{207}$$

Equation (207) is the Gross transformation; it is very useful for the comparison of absorption curves obtained by means of the ionization chamber with absorption curves obtained with counters. The Gross transformation was generalized by Jánossy (1936).

254. We note two of the properties of the transformation (207):

1. Differentiating with regard to θ we find

$$\frac{dc(0,\theta)}{d\theta} = -\frac{1}{2\pi}\theta\frac{d^2C(\theta)}{d\theta^2}. \tag{208}$$

It is seen therefore that maxima of the vertical intensity $c(0,\theta)$ coincide with inflexions of the intensity $C(\theta)$.

2. Introducing $C(\theta) = 1/\theta^{\gamma}$ we find

$$c(0,\theta) = \frac{\gamma+1}{2\pi}\frac{1}{\theta^{\gamma}} = \frac{\gamma+1}{2\pi}C(\theta). \tag{209}$$

Thus if the intensity $C(\theta)$ changes according to a power law the vertical intensity is proportional to the total intensity.

IV

NATURE OF COSMIC RAYS AT SEA-LEVEL AND UNDER GROUND

255. The cosmic-ray beam near sea-level contains the following kinds of charged particles:

(1) positive and negative electrons;

(2) positive and negative mesons;

(3) protons.

Non-ionizing agencies have also been identified, namely:

(4) photons;

(5) neutrons.

It has been further suggested on theoretical grounds that cosmic rays contain

(6) neutrinos;

(7) neutrettos.

There is some evidence for the existence of neutrinos but little for neutrettos.

In this chapter we shall describe the experimental evidence showing the existence of the particles (1)–(5).

We shall disregard the historical development of the subject. A short description of the history is found in the Introduction.

A. Ionizing Cosmic-ray Particles

1. *Velocity and Charge*

Ionization of Fast Particles

256. The cloud-chamber tracks of cosmic rays can be classified roughly into two groups according to the density of ionization. Most of the observed tracks are thin, i.e. showing a low density of ionization, but we find thick tracks, i.e. tracks showing high density of ionization.

It was shown in § 125, Ch. II, that the individual ions giving rise to the track can be located if the expansion is made a short time after the passage of the particle so that the ions have time to diffuse before condensation takes place. With the technique of delayed expansions the rate of ionization of individual cosmic-ray particles can be measured.

257. The density of ionization produced by a particle of velocity v and charge $Z_1 e$ is given by

$$\mathscr{I}(w) = \frac{Z_1^2}{(v/c)^2} J(w), \tag{1}$$

where $J(w)$ is a function which increases logarithmically with energy and has nearly the same value for all types of particles (§ 238).

Due to the logarithmic increase of $J(w)$ the ionization density $\mathscr{I}(w)$ reaches a minimum for a certain velocity. The minimum is found to occur for

$$v = 0{\cdot}96c \text{ air}, \qquad v = 0{\cdot}95c \text{ argon},$$

corresponding to

$$B = 3{\cdot}6 \text{ air}, \qquad B = 3{\cdot}3 \text{ argon}.$$

The ionization minima are therefore as follows:

	Electron	*Meson*	*Proton*
P_{minimum}	2	420	4,500 MEV./c

For fast particles, $v \sim c$, with single charge $Z_1 = 1$, we have

$$\mathscr{I}(w) \simeq J(w). \tag{2}$$

As $J(w)$ varies only slowly with energy we find that the ionization density for a fast singly-charged particle is nearly independent of both the type of the particle and the actual value of its energy.

In the following table we give calculated values of the rate of ionization of fast particles in air of N.T.P.:

TABLE 1

$B =$	1·4	2	5	10	100	1,000
$J(w) =$	64·8	43·2	43·8	46·7	57·2	75·0

$B = (1-v^2/c^2)^{-1/2}$.

It is seen that the ionization up to reasonable values of B is of the order of 50 ion pairs per cm. This is of the same order as the ionization density observed for thin cosmic-ray tracks.

It must be concluded, therefore, that the majority of the tracks are due to cosmic-ray particles with single charges and with velocities $v \sim c$.

Positive and Negative Particles

258. The sign of the charge of cosmic-ray particles can be determined from the curvature of the tracks in a magnetic field provided the direction of the particles is known.

In order to determine the relative numbers of positive and negative particles appearing in the cosmic-ray beam we can assume that all the particles are moving downwards.

259. Experiments carried out by Leprince-Ringuet and Crussard (1937), Leprince-Ringuet, Nageotte, and Lhéritier (1941), Blackett (1937*a*), Jones (1939), and Hughes (1940) show that the numbers of positive and negative particles are roughly equal, but that the positively charged particles are slightly in excess.

The following figures are taken from Jones (1939).

TABLE 2

Positive excess of meson component

Range in MEV.	*Number of positively charged particles*	*Number of negatively charged particles*
200–2,700	274	208
2,700–5,700	106	81

260. For the determination of the charge of an individual particle it is not always safe to assume that the particle is travelling downwards. The direction of the particle can be sometimes determined by one of the following methods:

1. The direction of the particle can be determined if it happens to produce an energetic secondary, as such secondaries are always projected in the forward direction.

2. If the particle passes through an absorber which is placed inside the chamber it is sometimes possible to observe the difference in curvature of the parts above and below the absorber.

3. If the particle itself is the secondary of another particle it must be assumed to move away from its primary.

2. *Mass*

(*a*) *Electrons*

Determination of upper limit of mass by ionization

261. The rest-mass of a particle can be determined from the values of velocity and momentum (or energy). We have

$$m = p/Bv. \tag{3}$$

The momentum can be determined from the curvature of the track in a magnetic field while the velocity can be determined, at least in principle, from the density of ionization.

For fast particles, however, the density of ionization is practically independent of the velocity, while the expression (3) is very sensitive

to the exact value of the velocity. Therefore eq. (3) can only be used to determine the mass of a slow particle.

262. Though (3) is unsuitable for determining the rest-mass of a fast particle it can always be used to give an upper limit for the value of the mass of the particle.

Assuming for the moment that the function $J(w)$ is constant and equal to J_0 we find from (1) for the density of ionization of a particle of momentum p and rest-mass m

$$\mathcal{J}(p) = (c/v)^2 J_0 = J_0\{1 + (mc/p)^2\}. \tag{4}$$

Observing a thinly ionized track with a magnetic curvature corresponding to a momentum p, we can conclude that the track is due to a particle of mass

$$m \ll p/c.$$

In particular, if we are sure that the observed ionization is not greater than twice the minimum ionization J_0, then we conclude from (4) that

$$m \leqslant p/c.$$

Anderson (1932, 3) and also Blackett and Occhialini (1933) observed thinly ionized tracks of particles with momentum of about 10 MEV./c. These particles cannot be assumed to have masses much greater than electrons. It was concluded that such tracks are due to fast electrons.

263. Anderson first reported photographs showing pairs of oppositely charged particles of low momentum (see Plate 3) starting from the same point. These observations led to the discovery of the positive electron.

Evidence obtained from radiative collisions

264. Only electrons of comparatively small momentum can be identified by the procedure described above. Electrons of higher energy can, however, be recognized by their large tendency to emit collision radiation.

It is seen from § 245, Ch. III, that an electron passing through a lead plate 0·5 cm. thick suffers on the average one radiative collision. Therefore it is expected that electrons should lose a large fraction of their energy when passing through a comparatively thin lead absorber.

Observations of Anderson and Neddermeyer (1937), Blackett and Wilson (1937), Ehrenfest and Crussard (1938*a*, *b*) show that some cosmic-ray particles lose as large energies as expected for electrons from the theory of radiative collisions; these particles must be assumed to be electrons.

265. If an electron passes through a thick absorber it will lose most of its energy in the form of photons. The photons in their turn will be absorbed by the emission of pairs of electrons and the process goes on as a cascade. Thus an energetic electron falling on a lead plate, say 2 cm. thick, is expected to produce a group of electrons emerging from the bottom of the plate.

This process is frequently observed—we reproduce a typical case in Plate 3 *b*, Fig. *f*. The development of a cascade initiated by an electron is also seen very clearly in Plate 3 *b*, Fig. *c*. This photograph, due to Hazen (1944*a*), shows a chamber subdivided by seven thin lead plates. It is seen that the number of secondary electrons increases after the passage through each of the plates.

The analysis of photographs of the type shown in Plate 3 *b* leads to a fair agreement with the radiation theory as will be shown in Chapter VI.

266. Most cosmic-ray particles with momenta below 200 MEV./*c* lose energy at a high rate and are therefore electrons.

Electrons with energies much greater than 200 MEV./*c* have also been identified; such high-energy electrons are, however, comparatively rare.

Most cosmic-ray particles with momenta above 200 MEV./*c* lose only very little energy when passing through metal plates. The reason for this is that most of the particles above 200 MEV./*c* are not electrons but mesons (see § 273).

The reason why mesons are mainly found above 200 MEV./*c* will be given in § 277, while the reason why most electrons have momenta below 200 MEV./*c* will become apparent in Chapter VI. The limits are quite independent of each other and it is quite accidental that the two spectra do not overlap to any appreciable extent.

(*b*) *Protons*

Fast protons

267. Protons with momenta exceeding 1,000 MEV./*c* are fast and therefore they give rise to thin tracks similar to those of fast electrons. The minimum ionization is found at 4,000 MEV./*c*. Protons with this momentum ionize, however, only half as much as electrons with the same momentum. Electrons of this momentum ionize heavily because of the logarithmic increase of ionization with energy.

Most of the cosmic-ray tracks in the region of 2,000 MEV./*c* show an ionization density of the same order as expected near the minimum of

the ionization curve. The observed ionization density is definitely smaller than expected for electrons of such high momenta. This was taken as evidence that cosmic rays of high momentum are not electrons (Williams, 1932*b*, 4*b*).

Slow protons

268. The tracks of protons with momentum less than 500 MEV./*c* can be recognized clearly as they are sufficiently slow to ionize more heavily than electrons of the same momenta.

The observed rate of slow protons is of the order of 0·2 per cent. of all cosmic ray particles at sea-level. Compare Blackett (1937*a*), Brode, McPherson, and Starr (1936), Anderson and Neddermeyer (1934).

Estimation of the proton component

269. To estimate the total number of protons in the cosmic-ray beam it is necessary to make assumptions regarding their origin.

Some of the slow protons are due to fast protons which have been slowed down. Since, however, the tracks of slow protons are distributed in almost random directions it must be assumed that only few of them represent the ends of primary proton paths, which would be concentrated round the vertical.

270. We derive an upper limit for the number of primary protons by assuming that all the slow protons observed at sea-level represent the ends of the ranges of primary protons.

To obtain such an upper limit it is necessary to know the rate of energy loss of protons as function of the energy. The loss of energy is due to a number of processes.

1. Ionization. The rate of loss is given in eqs. (168–70), Ch. III.

2. Radiative collisions. The cross-section for radiative collisions is inversely proportional to the square of the rest-mass of the particle and therefore (see § 206) the contribution of radiative collisions to the rate of energy loss is negligibly small.

3. According to the meson theory fast protons are expected to emit mesons in collisions with atomic nuclei. The rate of loss of energy for fast protons is expected to be very large. According to the calculation of Heitler and Peng (1944) and Heitler (1945) this loss is at least 100 times greater than the loss due to ionization.

The experimental evidence for the loss of energy of fast protons by the emission of mesons is indirect. Therefore we estimate the upper limit for the number of primary protons first under the assumption that

no energy is lost due to meson production; we shall show how the conclusions regarding the numbers of protons have to be modified if meson production is introduced into the argument.

271. Denote the range of a proton of momentum p by $\mathscr{R}(p)$. The protons in the momentum interval $p, p+dp$ then have ranges between $\mathscr{R}$ and $\mathscr{R}+d\mathscr{R}$, with

$$d\mathscr{R} = \left(\frac{d\mathscr{R}}{dp}\right)_p dp, \tag{5}$$

and therefore the number of protons in the interval p, dp at sea-level is

$$\mathfrak{S}(p,\theta)\, dp = \mathfrak{S}(p,\theta)\frac{d\mathscr{R}}{(d\mathscr{R}/dp)_p}, \tag{6}$$

where $\mathfrak{S}(p,\theta)$ is the differential spectrum at sea-level. θ is taken to be the mass equivalent of the atmosphere. Both θ and $\mathscr{R}$ are assumed to be in grams per cm.^{2} The particles arriving with a remaining range $\mathscr{R}$ at sea-level must have started on the top of the atmosphere with a range

$$\theta+\mathscr{R}(p) = \mathscr{R}(p'), \tag{7}$$

where p' is the momentum of the particle when incident on the top of the atmosphere.

Differentiating (7) we find with the help of (5) and (6)

$$\mathfrak{S}(p,\theta) = \mathfrak{S}(p',0)\frac{(d\mathscr{R}/dp)_p}{(d\mathscr{R}/dp)_{p'}}. \tag{8}$$

Using the approximate expression (169, Ch. III) with $m = M_P$ we find

$$\frac{d\mathscr{R}}{dp} \simeq \begin{cases} \dfrac{1}{\mathscr{A}} & (p > M_P c), \\ \dfrac{1}{\mathscr{A}}\left(\dfrac{p}{M_P c}\right)^3 & (p < M_P c), \end{cases} \tag{9}$$

with $\mathscr{A} \sim$ const.

We see from (8) and (9) that owing to the decrease of $d\mathscr{R}/dp$ with momentum the spectrum appears decreased in intensity in the region of small momentum. Because of this effect slow particles are relatively rare. The actual ratio between slow and fast particles depends somewhat on the incident spectrum. To estimate this ratio we assume the incident spectrum to be given by (see e.g. § 310)

$$\mathfrak{S}(p,0) = A/p^{z+1}, \tag{10}$$

where z is a constant between 2 and 3. Write p_0 for the momentum

required to penetrate the atmosphere. The total number of particles $\mathfrak{T}(\theta)$ reaching sea-level is then according to (10)

$$\mathfrak{T}(\theta) = \int_{p_0}^{\infty} \mathfrak{S}(p, 0)\, dp = \frac{p_0}{z}\mathfrak{S}(p_0, 0). \tag{11}$$

p_0 is of the order of 2,000 MEV./c if only ionization loss is taken into account.

From (8) and (9) we find

$$\mathfrak{S}(p, \theta) = \mathfrak{S}(p', \theta)\left(\frac{p}{cM_P}\right)^3, \tag{12}$$

where p' is the initial momentum required for a particle to arrive with a momentum p near sea-level. Considering a narrow range only, we may put approximately

$$p' \sim p_0.$$

Integrating over (12) we find

$$\mathfrak{T}(p, \theta) = \int_0^p \mathfrak{S}(p, \theta)\, dp = \frac{M_P c}{4}\mathfrak{S}(p_0, 0)\left(\frac{p}{cM_P}\right)^4$$

and therefore

$$\mathfrak{T}(p, \theta)/\mathfrak{T}(\theta) = \frac{z}{4}\frac{M_P c}{p_0}\left(\frac{p}{M_P c}\right)^4. \tag{13}$$

Particles with momentum $p < M_P c/2$ will give rise to dense tracks and therefore the relative number of dense tracks is estimated as

$$\mathfrak{T}(M_P c/2, \theta) = \frac{z}{128} \approx \frac{1}{50}. \tag{14}$$

The last value is obtained for $z+1 = 2{\cdot}5$ and $p_0 \sim 2M_P c$.

According to § 268 at sea-level only two tracks due to slow protons are found per 1,000 incident particles. Therefore according to (14) not more than 10 per cent. of the fast particles can be assumed to be protons.

272. If it is assumed that fast protons lose energy by meson production at a rate 100 times larger than by ionization we obtain with the help of (8) an upper limit the value of which is 100 times smaller, i.e.

$$10 \text{ per cent.}/100 = 0{\cdot}1 \text{ per cent.}$$

Further, according to the meson theory, protons change into neutrons when emitting a positive meson and neutrons change back into protons when emitting a negative meson. Therefore at sea-level about half of the original protons have become neutrons and thus the actual upper

limit for the number of fast protons is only half of the value given above.

Remembering further that the upper limit is certainly too high, as many of the slow protons observed cannot in fact be due to primary protons, the number of fast protons is probably only of the order of a few per 10,000 particles. This estimation is in good agreement with conclusions based upon the observation of penetrating showers (see Ch. IX).

(*c*) *Mesons*

273. Most of the cosmic-ray particles with momenta exceeding 200 MEV./*c* are too penetrating to be electrons and most of the penetrating particles between 200 and 600 MEV./*c* ionize too little for protons. It was further shown in the previous paragraph that only a small fraction of the particles with momenta exceeding 600 MEV./*c* can be assumed to consist of protons. It is seen therefore that most of the particles with moments exceeding 200 MEV./*c* are neither protons nor electrons.

These particles must have a mass larger than electrons or they could not be penetrating. On the other hand the particles must have smaller masses than protons or otherwise they would give rise to thick tracks in the region between 200 and 600 MEV./*c*. It is therefore plausible to assume that most of the penetrating particles observed are mesons.

Mass of mesons

274. An upper limit for the meson mass can be obtained from the observation of thin tracks of penetrating particles with momenta less than 600 MEV./*c*. The actual mass of the meson can be deduced only from the tracks of slow mesons.

The first track, which must clearly be attributed to a particle of mass intermediate between electron and proton, was obtained by Neddermeyer and Anderson (1938). The photograph is reproduced in Plate 2 (*d*).

The rest-mass of a meson can be determined if any two of the three quantities W_k, P, v are known.

The rest-mass is given by the following equations in terms of these quantities

$$\mu = \frac{p}{vB} = \frac{p^2 - w_k^2/c^2}{2w_k} = \frac{w_k}{(B-1)c^2}. \qquad (15)$$

Alternatively, the mass of a meson can be determined from eq. (35), Ch. III, when it is giving rise to an electron secondary. The mass is expressed as a function of the momenta of electron and meson after the

collision and the angle between the scattered meson and the recoiling electron.

The momentum of the meson can be determined from curvature of its track in a magnetic field.

The kinetic energy W_k or the velocity v can only be determined with sufficient accuracy from the track of a slow particle.

If the track of the slow particle happens to end in the gas of the chamber, then the energy of the particle can be determined directly from the total ionization, assuming that the average energy per ion is 32 volts.

If the ionization is too dense for the ions to be counted, the energy can be determined from the theoretical energy range relation (see Fig. 30, § 239).

275. The experimental value of the mass of the meson must be based at present on the combination of isolated results by various observers using different techniques. It is therefore difficult to assess the relative weights to be assigned to the available determinations and we here only indicate the broad status of the methods which have been used.

We distinguish two main types of determination. Direct methods may be based either on the classical experiments used for electrons, in which magnetic and electrostatic deflexions are compared, or on close collisions with electrons, the collision being assumed elastic. The first method involves severe experimental difficulties and has not yet been applied (compare Gorodetzky (1942, 3)). The second, used by Leprince-Ringuet and Gorodetzky (1941) and by Hughes (1941), must rank as the method with the soundest theoretical basis. However, because of the scarcity of particles in the appropriate range of energy, the method depends on the occurrence of a rare event and extensive results are hardly to be expected.

Indirect methods are based on the relation between momentum, rate of ionization, and energy loss in the region where the velocity is appreciably less than c. These methods are based on principles which, while less fundamental than those described above, are used under conditions which we have strong reasons to regard as reliable.

276. The relative reliability of individual determinations is affected in all cases by the spurious curvature of cloud tracks due to Coulomb scattering which has been discussed by Williams (1940*a*). We have considered this error elsewhere (§ 136, Ch. II). We emphasize that Williams's figures refer to the average spurious scattering and that the probability of a spurious curvature several times as great is appreciable.

This effect in particular increases the uncertainty of determinations based on momentum measured in low magnetic fields and when $v \ll c$. Notably, methods using the last few centimetres of tracks stopping in the gas of a cloud chamber are strongly affected by scattering.

In Table 3 we have tabulated results in an order which indicates the broad reliability of the method used. We include only results for which the observer claims a probable error of not more than 30 mass units, more extensive references are given by Wheeler and Ladenburg (1941).

It must be noted that uncertainty of measurement does not lead to a symmetrical distribution of the errors. The scatter in general is much more tolerant of an increase of mass than of a decrease.

TABLE 3

Mass of the meson

Method	*Observer*	*Mass in units of m_e*
Elastic collision	Leprince-Ringuet and Gorodetzky (1941)	240 ± 20
	Hughes (1941)	180 ± 25
Momentum loss in plate	Nishina and others (1939)	180 ± 20
	Wilson, J. G. (1939)	170 ± 20
Momentum and ionization	Williams, E. J., and Pickup (1938)	160 ± 30
	Nielsen and Powell (1943)	210 ± 20
		180 ± 20
		190 ± 15
		145 ± 30

A meson of mass $\sim 1000 m_e$ has been reported by Leprince-Ringuet and Lhéritier (1944).

Rate of slow mesons

277. We show in the following that the small number of slow meson tracks observed is no obstacle to the assumption that most of the tracks of fast particles are those of fast mesons.

Assuming that all the slow mesons observed are due to fast mesons which have come to the end of their range we can apply the considerations of § 271 to estimate the ratio of fast and slow mesons.

We assume that mesons are slowed down mainly by ionization. We obtain from (13) when replacing the proton mass M_P by the meson mass μ for the fraction of mesons with momentum less than $\mu c/2 \sim 50$ MEV./c

$$\mathfrak{T}_{\text{meson}}(\mu c/2, \theta)/\mathfrak{T}_{\text{meson}}(\theta) \sim \frac{1}{500}. \tag{16}$$

This estimation gives, however, a too high value for two reasons: (1) a considerable number of the mesons will decay, (2) there is evidence that some of the mesons are captured by nuclei. Taking these two effects into consideration we estimate the fraction of slow mesons to be of the order of 1/2000. Though no exact statistics are available, this ratio seems to be compatible with the rate of slow mesons observed on cloud-chamber photographs.

It is interesting to note the absolute rate at which slow mesons cross a cloud chamber of usual dimensions. Consider a chamber of 30 cm. diameter and a few centimetres depth. The rate at which particles cross this chamber is of the order 1,000 per hour and therefore a slow meson will traverse the chamber about once per two hours. Many photographs of slow mesons could thus be obtained with a triggering arrangement setting off the chamber whenever a slow meson is crossing its sensitive volume. We shall come back to this question in Ch. V, § 337.

3. *Experimental Test of Momentum Ionization Relation*

278. Many of the arguments brought forward in the previous section are based on the theoretical relation between ionization density and momentum.

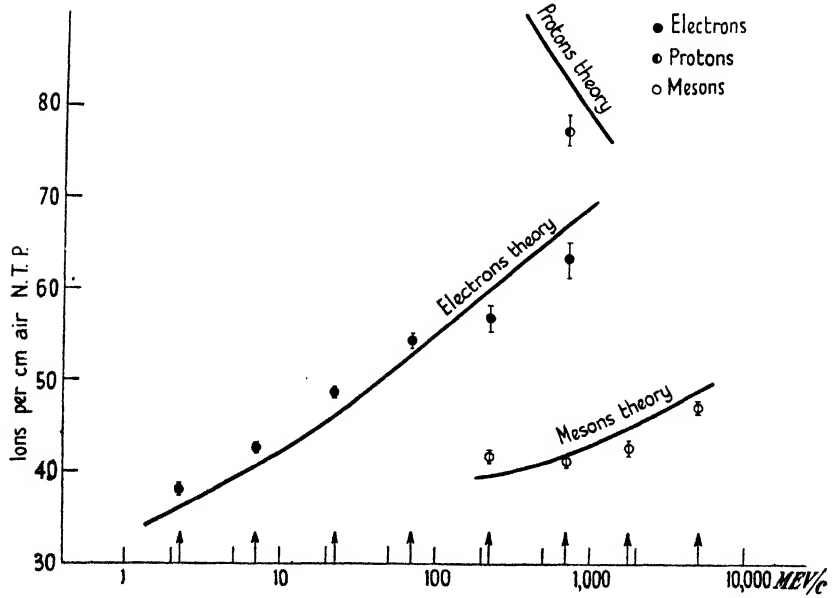

FIG. 36. Rate of ionization as function of momentum (R. L. Sen Gupta).

The density of ionization of cosmic-ray tracks has been measured by various observers.

The numbers of secondaries with sufficient energy to ionize themselves can be found by counting the small blobs along the tracks of cosmic rays. The blobs are caused by secondaries of short range.

The actual number of ions per cm. of track can be counted by using delayed expansions permitting the ions to diffuse before the drops are formed.

Using this technique Corson and Brode (1938) and Sen Gupta (1940, 3) have measured the ionization density as a function of momentum. It is found that the cosmic-ray tracks can be separated into three groups corresponding to electrons, mesons, and protons. The momentum ionization curves are in good agreement with the theory, both for small velocities and above the minimum of ionization. In Fig. 36 we have reproduced the results of Sen Gupta. The logarithmic increase of the rate of ionization with momentum can be seen clearly.

B. Non-Ionizing Components

1. *Experiment of Bothe and Kolhörster*

279. Most cosmic rays near sea-level are ionizing particles. These particles constitute the main cosmic-ray beam and they are not the secondaries of a more penetrating non-ionizing radiation as was supposed for a long time after the discovery of cosmic rays.

It was shown by Bothe and Kolhörster (1929) that two GM-counters placed close above one another show coincident discharges too frequently to be accidental. These coincidences were attributed to single rays passing through both counters. From the geometry of the arrangement it was shown that rays passing through both counters have a high probability of discharging both. Thus it was found that the efficiency of counters is high for counting of cosmic-ray particles; the efficiency of counters for recording non-ionizing rays must be small. Therefore the cosmic-ray particles must be ionizing.

280. Coincidences between two GM-counters show only that cosmic-ray particles have sufficient energy to penetrate the walls of the counters. These particles could still be secondaries of energetic non-ionizing rays. Skobelzyn (1927, 9) observed fast ionizing particles and assumed tentatively that these particles were the Compton electrons due to energetic γ-rays.

In order to show that the ionizing particles have long ranges for themselves coincidence experiments were carried out with counters separated by thick absorbers. The coincidences thus obtained must be due to particles of long range.

281. Bothe and Kolhörster (1929) observed coincidences between two counters separated by 8 cm. of gold. More elaborate experiments were carried out by Rossi (1933), Street, Woodward, and Stevenson (1935), and others. Rossi found that about half of the particles which are

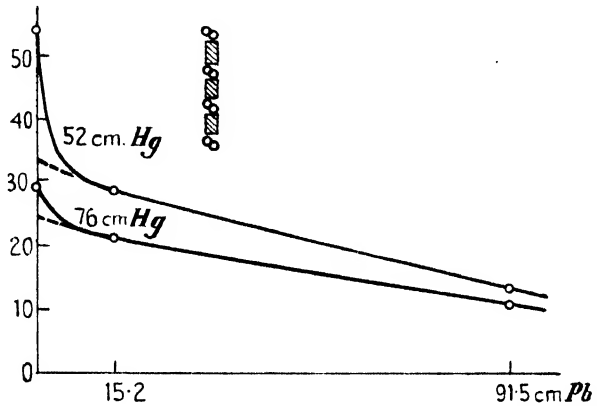

FIG. 37. Absorption curve (from *Kernphysik*, p. 98).

capable of penetrating 10 cm. of lead are also capable of penetrating 1 m. of lead (Fig. 37). One metre of lead has a mass equivalent exceeding that of the whole atmosphere. Thus it is seen that about 40 per cent. of the cosmic-ray particles near sea-level have remanent ranges sufficient to penetrate the whole of the atmosphere. This result strongly suggests that the observed particles themselves constitute the penetrating part of cosmic rays and are not the secondaries of some more penetrating rays.

282. In the experiments of Street, Woodward, and Stevenson (1935) particular care was taken to show that the particles penetrating the lead absorber were single particles travelling in a vertical direction. The counter arrangement is shown in Fig. 38. Fourfold coincidences 1, 2, 3, 4 were observed. The absorber was distributed equally into the three gaps between the counters. A non-ionizing ray only gives rise to such a coincidence by producing four ionizing secondaries in the correct places and the chance of this happening must be assumed to be negligible. Thus the coincidences must have been due to single ionizing particles.

Further, six counters in anticoincidence were placed near to the coincidence counters. These counters were not in line with the coincidence counters and could not be discharged by a single particle passing through the coincidence counters 1 to 4. Therefore the six anticoincidence counters did not affect coincidences 1, 2, 3, 4 due to single particles. The anticoincidence counters would, however, cut out coincidences due to showers coming from the side.

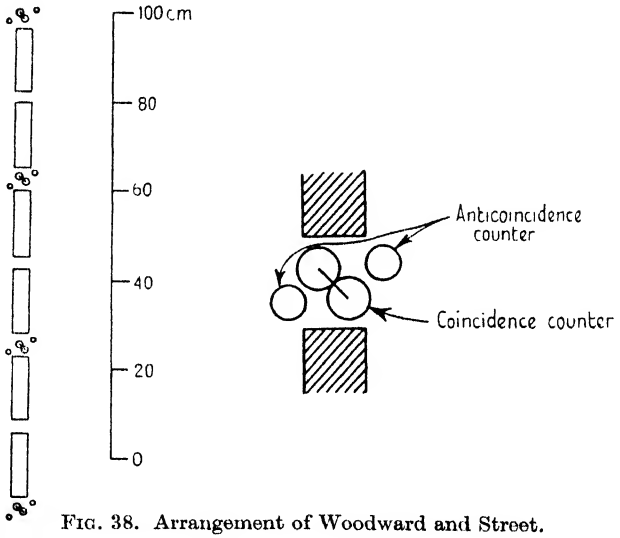

FIG. 38. Arrangement of Woodward and Street.

283. The existence of particles at sea-level with remaining ranges much greater than the thickness of the atmosphere are also shown by the measurement of the momentum of particles in the cloud chamber. It was found that about half of the penetrating particles observed in a cloud chamber had momenta exceeding 2,000 MEV./*c*. If the energy loss of the penetrating particles was assumed to be mainly determined by ionization then the initial momentum for a penetrating particle for traversing the atmosphere was about 2,000 MEV./*c*. The comparison between momentum spectrum and absorption curves will be discussed in more detail in § 311.

2. *Search for Non-Ionizing Components*

284. The observations described so far show that a considerable part of cosmic rays consists of ionizing particles.

The ionizing particles are, however, accompanied by some non-ionizing rays.

Direct evidence for photons was obtained by Anderson, who obtained photographs of electron pairs initiated in the gas of the chamber (see Plate 3 (*a*)).

Showers initiated by non-ionizing particles were also observed. An interesting example is a shower containing many particles emerging from the bottom of a lead plate with no particle entering the top of the plate (Stevenson and Street (1936)).

(*a*) *Coincidence Experiments*

Secondaries of non-ionizing particles

285. More detailed investigations of non-ionizing rays have been carried out using counter methods.

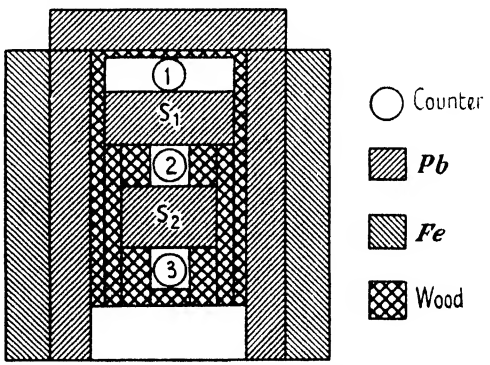

FIG. 39. Rossi's arrangement.

The following experiment was carried out by Rossi (1931 *a*) in an attempt to find non-ionizing primaries.

An absorber 30 cm. thick (Fig. 39) was placed alternatively above and between the counters of a coincidence arrangement. Non-ionizing primaries giving rise to ionizing secondaries in the absorber might contribute to the coincidence rate when the absorber is above the counter arrangement, while no contribution due to such secondaries could be expected with the absorber between the counters. Non-ionizing primaries should therefore produce an increase of the coincidence rate when the absorber is moved from between the counters to above the counters.

In the actual experiment a small increase of this kind was observed. This increase was, however, not attributed by Rossi to non-ionizing secondaries. A small change of the counting rate is to be expected in

any case due to scattering in the absorber and to showers. Experiments to be described later show that the increase found by Rossi was indeed due to such effects.

286. Experiments of the type carried out by Rossi were later repeated by other observers. Some of the large positive effects found in the later experiments (e.g. Maass (1936)) are certainly due to scattering and showers.

Carefully designed experiments of this type were carried out by Schein, Wollan, and Groetzinger (1940) in the stratosphere, showing that at high altitudes a considerable number of ionizing rays are produced by non-ionizing secondaries. As the effects reported by these authors are of the order of 100 per cent. they must be attributed to non-ionizing primaries rather than to showers or scattering. These experiments will be discussed in greater detail in Chapter IX.

Showers produced by non-ionizing particles

287. The question was also discussed whether showers are produced by ionizing or non-ionizing agents. The arrangements used were mostly

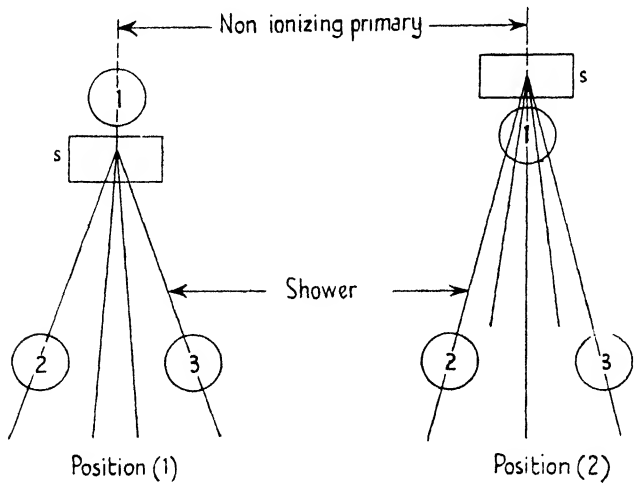

FIG. 40. Production of showers.

of the type shown in Fig. 40. The lower set of counters can only be discharged by showers. The absorber s was placed alternatively above and below the top counter 1. Showers produced in s by non-ionizing radiation can only discharge all counters 1 to 3 if the absorber s is above the top counter. If s is placed below the counter 1 then fourfold coincidences can only be expected due to showers coming from the air

or else from showers produced by an ionizing particle in s; in the latter case the counter 1 is discharged by the particle giving rise to the shower. This experiment has been carried out by various observers using slightly different arrangements. The results were quite contradictory. The reason for this ambiguity is that by moving the absorber s the whole geometry of the arrangement is affected; some showers emerging from s may discharge the counters when s is in one position but not if s is in the other position. Thus the actual interpretation of the coincidence rates as obtained with an arrangement as shown in Fig. 40 is rather complicated and the results do not permit conclusions as to the nature of the primary radiation.

(*b*) *The Anticoincidence Method*

288. The main difficulty of the coincidence experiments described in the previous section arises from the circumstance that the counting rates for an absorber s in two different positions have to be compared. It is clear that the arrangements shown in Fig. 39 and Fig. 40 are both more sensitive to non-ionizing rays when the absorber s is in the higher position; but it is difficult to assess how much the background rate is affected by moving the absorber s. Therefore one cannot decide how much an observed change of the counting rate is due to non-ionizing primaries and how much it is due to the changing background. The following arrangement due to Rossi is free from this ambiguity.

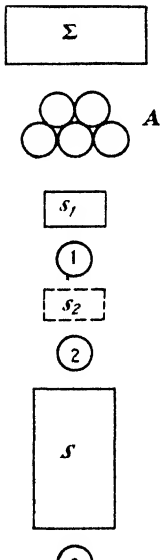

FIG. 41. Anticoincidence arrangement.

Genuine and spurious anticoincidences

289. The arrangement is an anticoincidence set as shown schematically in Fig. 41. Coincidences between the counters 1, 2, and 3 not accompanied by the discharge of any of the counters A are recorded. An absorber s is placed between the top counter of the coincidence arrangement and the anticoincidence counters. The anticoincidence counters must cover rather more than the solid angle subtended by the coincidence arrangement.

Anticoincidences recorded with such an arrangement are in the main due to the following processes:

1. Anticoincidences will be caused by non-ionizing rays falling on s and giving rise to ionizing secondaries which discharge the counters 1,

2, and 3. In the following discussion we shall be interested mainly in anticoincidences due to this process and therefore we shall call them genuine anticoincidences. Anticoincidences caused by other processes given below will be called spurious ones.

2. Spurious anticoincidences will result if a particle coming from above crosses all counters but happens not to discharge the anticoincidence counters because of inefficiency. This type of spurious anticoincidence can be much reduced by using double or multiple layers of anticoincidence counters.

3. Particles coming from the side may be scattered in s and thus discharge the coincidence counters without passing through the anticoincidence. Alternatively a shower coming from the side may discharge the coincidence counters but not the anticoincidence counters. Spurious anticoincidences of these types can be avoided by covering the coincidence system with anticoincidence counters from all sides except from below. (No anticoincidence counters should be placed below as such counters would cut out genuine anticoincidences as well.)

4. Particles coming from below which are absorbed in s give rise also to spurious anticoincidences. This effect seems to be negligible in practice.

Test for genuine anticoincidences

290. In order to detect non-ionizing rays with an arrangement of the type shown in Fig. 41 one has to investigate what fraction of the anticoincidences is genuine in the sense explained above. This can be done by placing absorbers Σ above the anticoincidence counters. The absorber Σ absorbs non-ionizing rays and therefore is expected to reduce the rate of genuine anticoincidences. At the same time Σ has only little effect on the rate of spurious anticoincidences. It is seen that only the type (2) (§ 289) of spurious anticoincidences can be affected by absorbers above the anticoincidence counters. The rate of spurious anticoincidences of type (2) is a constant fraction of the coincidences 1, 2, 3, and therefore the spurious anticoincidence rate cannot be expected to decrease more rapidly due to the absorber than the rate of threefold coincidences 1, 2, 3. If the observed decrease of the anticoincidence rate is noticeably greater than that of the coincidence rate, one must then assume that the decrease is due to the decrease of the rate of genuine anticoincidences.

291. The rate of genuine anticoincidences decreases due to the absorber Σ as some of the non-ionizing rays are absorbed when traversing

Σ. The term 'absorption' is not used in its usual sense. A non-ionizing ray appears as absorbed in connexion with anticoincidences when it loses its ability to give rise to an anticoincidence. This happens either when the ray is stopped in a collision, or when it gives rise to one or more ionizing secondaries which accompany the primary non-ionizing ray when traversing the anticoincidence counters.

The rate of genuine anticoincidences plotted against thickness θ of the absorber Σ can be regarded as the absorption curve of the incident non-ionizing radiation. This curve does not necessarily represent the true absorption curve but represents the relative probability of non-ionizing rays traversing various thicknesses of absorber without suffering a collision. If the incident radiation is homogeneous and the mean free path before a collision in which secondaries are given rise to is $\mathfrak{m}$, then the fraction of primaries not having suffered a collision in a thickness θ is $\exp(-\theta/\mathfrak{m})$ and

$$\text{rate of anticoincidences} = \mathscr{C}_A \exp(-\theta/\mathfrak{m}). \tag{17}$$

(i) Photons

292. Experiments with the arrangement shown in Fig. 42 were carried out by Jánossy and Rossi (1940). The rate of anticoincidences

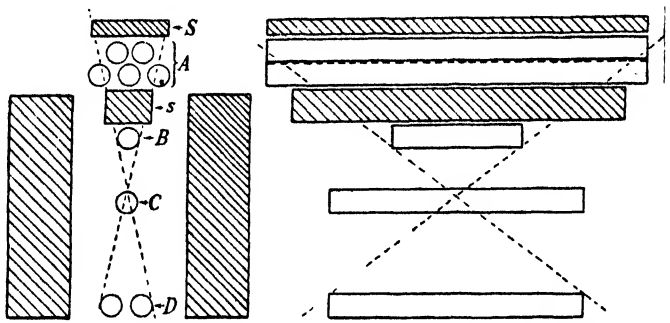

FIG. 42. The experimental arrangement. (Jánossy and Rossi, *Proc. Roy. Soc.* A, **175** (1940), 89, Fig. 1.)

was found to decrease markedly up to a thickness of 5 cm. of lead. The rate of genuine anticoincidences as a function of the thickness θ is shown in Fig. 43 in a logarithmic plot (assuming the anticoincidence rate with $\theta = 5$ cm. to be spurious). It is seen that the mean free path of the non-ionizing radiation is about 1 cm. of lead. This result is interpreted most easily in terms of energetic photons according to the theory of Bethe and Heitler (see dotted lines).

The production of showers by photons was studied by similar arrangements. Experiments of this kind were carried out by Jánossy and Rossi (1940), by Nereson (1942), and by Trumpy (1943). The results of Trumpy are shown in Fig. 44.

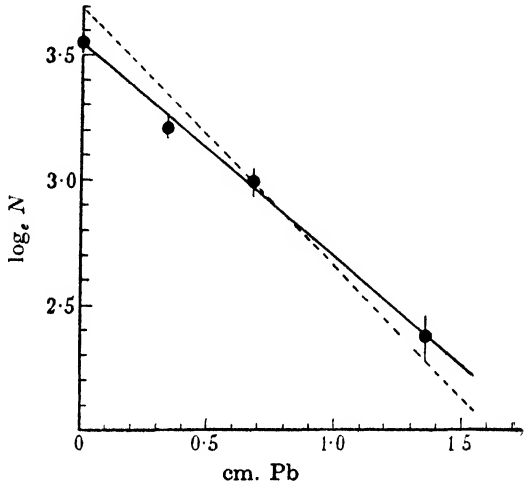

FIG. 43. The absorption curve of cosmic-ray photons.
s = 0, 35 cm. Pb. ϕ observed, ---- calculated.
(Jánossy and Rossi, op. cit., p. 97, Fig. 3.)

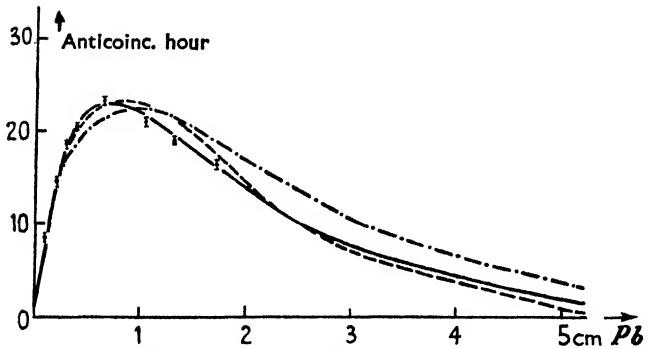

FIG. 44. Photon-initiated showers observed (Trumpy), calculated (Arley).
(N. Arley, *Stochastic Processes*.)

It can be concluded that the cosmic radiation near sea-level contains a photon component; the intensity of this component is estimated to exceed 10 per cent. near sea-level. Further it can be concluded that the Bethe-Heitler theory agrees with experiment, at any rate for energies of the order of 10^8 eV. (We shall see later that there is indirect evidence for the validity of this theory up to very high energies.)

293. Rossi and his co-workers (Rossi, Jánossy, Rochester, and Bound (1940)) have also shown that the rate of genuine anticoincidences decreases very much if absorbers amounting to 10 cm. of lead are placed between the coincidence counters. This experimental result further supports the interpretation of the experiments described in § 292 in terms of photons producing electron pairs. The range in lead of the electrons produced by the photons is expected to be small and only electrons exceeding 10^{10} eV. have an appreciable chance of penetrating an absorber of 10 cm. of lead. Thus the 10 cm. of lead placed between the coincidence counters prevents the electrons produced by the photons from discharging the lowest counter of the coincidence arrangement and therefore the rate of genuine anticoincidence is strongly reduced by 10 cm. Pb absorber.

It can be concluded that photons produce only rarely, if at all, mesons.

294. Incidentally it was found that the rate of coincidences 1, 2, 3 obtained with the arrangement Fig. 42 is larger when the absorber s is in the position s_1 above the counter 1 than the rate obtained when the absorber s is put below the counter 1 in position s_2. This effect might have been interpreted as being due to ionizing secondaries produced in s by non-ionizing radiation (compare § 286). Such an interpretation is, however, incorrect as the anticoincidence rate 1, 2, 3, $-A$ was found to be almost unaffected by the position of s. The difference in the coincidence rates arising from the change of position of s is therefore not connected with non-ionizing primaries.

(ii) Penetrating non-ionizing rays

295. In a search for non-ionizing rays with a mean free path exceeding that of photons Rossi and Regener (1940) have carried out anticoincidence experiments at Mt. Evans (4,300 m. above sea-level). An arrangement somewhat similar to that shown in Fig. 42 was used and it was found that the rate of anticoincidences decreased noticeably when an absorber Σ above the anticoincidence counters was increased from 2·5 to 10 cm. of lead. This effect shows clearly the occurrence of non-ionizing rays with a mean free path exceeding that of photons. The absorber s_1 consisted of 5 cm. of lead while an absorber S 10 cm. thick was also placed between the counters. It is seen therefore that the ionizing secondaries produced by the penetrating non-ionizing rays are themselves more penetrating than electrons.

The effect has probably to be interpreted in terms of mesons produced by neutrons.

296. Penetrating non-ionizing rays were also found by Jánossy and Rochester (1943*a*) near sea-level. The experimental arrangement is based on the same principles as those described above. The intensity of the penetrating non-ionizing rays at sea-level was found, however, to be very small and therefore extreme precautions had to be taken in order to reduce the background of spurious anticoincidences to less than

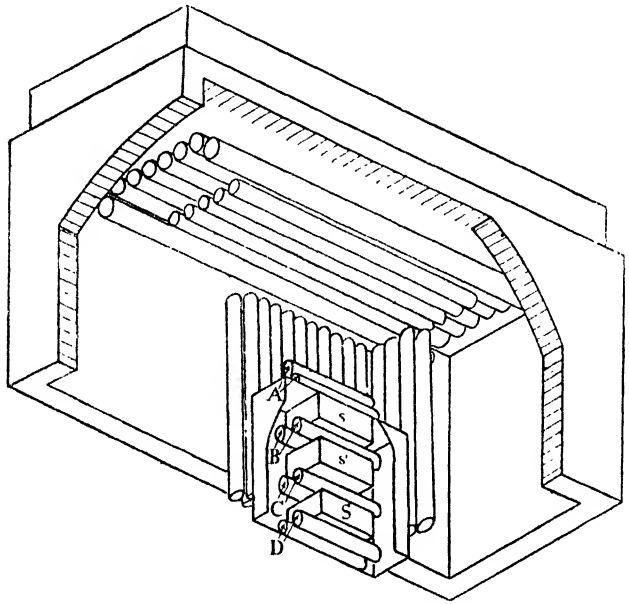

FIG. 45. Experimental layout of Jánossy and Rochester (1942) (seen from below). (Jánossy and Rochester, *Proc. Roy. Soc.* A, **181**, 401, Fig. 3.)

the rate of genuine anticoincidences. The coincidence arrangement was therefore surrounded by an anticoincidence set consisting of 76 counters in parallel and the rate of spurious anticoincidences could be reduced to less than one per 3,000 coincidences.

Evidence was obtained with this arrangement (Fig. 45) for a weak non-ionizing component with a mean free path of about 10 cm. of lead. The intensity of the component was estimated to be one non-ionizing ray per 700 ionizing particles. It is likely that the non-ionizing rays observed at sea-level and at Mt. Evans are parts of the same component of cosmic rays.

Other Non-Ionizing Rays

(*a*) *Slow Neutrons*

297. We shall give in Chapter IX arguments to the effect that the penetrating non-ionizing radiation described in the previous section

consists of fast neutrons. This interpretation is supported by the fact that the occurrence of slow neutrons in the cosmic-ray beam can be shown directly.

298. Slow neutrons have been investigated by means of boron counters (Fünfer (1938), Montgomery (1939)).

The experimental results are collected in Fig. 46. It is seen that the neutron intensity increases very strongly with height.

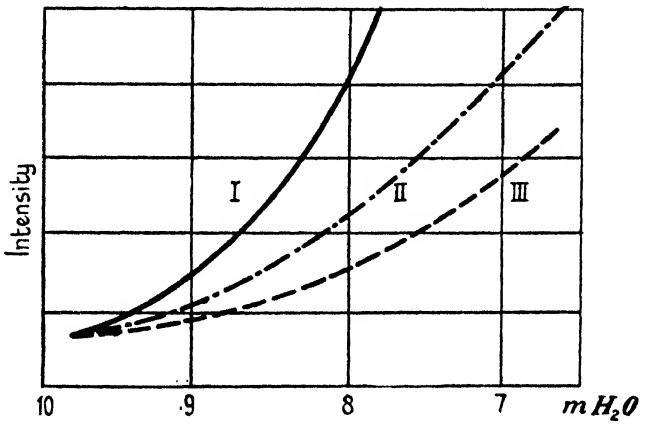

FIG. 46. Height and intensity distribution of cosmic-ray neutrons (Fünfer).
I. Neutrons. II. Shower intensity. III. Cosmic-ray intensity.

A summary of the experimental results for slow cosmic-ray neutrons has been given by Bethe, Korff, and Placek (1940). In this paper a detailed discussion of the experiments and their interpretations can also be found. According to Bethe the absorption of these neutrons is due mainly to elastic scattering and therefore the intensity distribution in the atmosphere is given by a diffusion equation. The actual distribution is approximated by a Gaussian with its maximum near the height with 7 cm. Hg pressure. No experiments have been carried out at sufficient height to confirm the decrease of intensity predicted by Bethe.

(*b*) *Neutrinos*

299. There are good reasons to believe that a large number of neutrinos are produced by cosmic rays (compare § 222). No direct experimental evidence for the existence of a neutrino component is available. The difficulties in establishing a neutrino component are not purely experimental. As no clear theoretical predictions have been made as to what processes would be initiated by neutrinos it is impossible

at the moment to know for certain what are the best experiments to carry out to prove their existence.

(c) *Neutrettos*

300. As was seen in Chapter III there are theoretical grounds for assuming the existence of neutral mesons or neutrettos. Various properties of the neutretto can be predicted. One finds, for example, a finite cross-section for the transformation of a neutretto into a charged meson and for the reverse process (Heitler and Peng (1944)). Such processes, if they occur, could be detected. No extensive search for neutrettos has been carried out. Preliminary experiments of Lovell (1939) failed to detect such a particle.

301. The theory of Möller and Rosenfeld (1940) predicts also the occurrence of charged and neutral vector mesons. These mesons are expected to have a mass comparable with that of the other mesons but they should have a mean life of the order of 10^{-8} sec. only.

No experimental evidence either for or against the occurrence of such mesons has been brought forward.

C. Cosmic Rays Under Ground

1. *Absorption Function*

302. The cosmic-ray intensity was measured under ground in mines and under water both with ionization chambers and with coincidence counters.

The counter measurements have a great advantage over ionization-chamber measurements. The zero current in an ionization chamber cannot be determined accurately and therefore only the difference of the intensities at various depths can be established with an ionization chamber.

The zero effect of a coincidence arrangement is due to accidental coincidences and it is always possible to reduce the rate of accidental coincidences to a small fraction of the observed effect.

With an ionization chamber the intensity integrated over all directions of incidence is measured. On the other hand with a counter arrangement the intensity can be measured in the vertical direction. The absorption curves obtained with a counter arrangement and with an ionization chamber cannot in general be compared directly.

The two absorption curves can, however, be transformed into each other by using the Gross transformation described in § 252.

303. The depth ionization curve was investigated by a large number of observers. It was found that the ionization still decreases under 500 m. water equivalent. Most elaborate measurements were carried out by Regener and his collaborators. An ionization chamber together with a complete photographic recording arrangement was enclosed in a water-tight tank and submerged to various depths down to 230 m. in Lake Constance.

In the course of these measurements it was discovered that dry batteries were radioactive and that therefore the batteries used in the recorder disturbed the measurements. After having eliminated this difficulty a very satisfactory depth-ionization curve was obtained (compare Weischedel (1936)).

304. Coincidence experiments under ground were carried out by a large number of observers. Ehmert (1937) submerged a full automatic coincidence arrangement down to 240 m. in Lake Constance. Clay and Van Gemert measured the coincidence rate with an apparatus which they submerged to 440 m. under the North Sea. Observations were carried out in mines. Clay and Gemert (1939) measured down to 1,380 m. water equivalent, Barnóthy and Forró (1937) down to 980 m., V. C. Wilson (1937, 8) down to 1,420 m. The absorption curves can all be represented by a power law, the exponent increasing only slightly with depth. Some of the results are summarized in the following:

Absorption function according to Ehmert:

	Exponent
$13 < \theta < 43$	$-1{\cdot}56$
$45 < \theta < 243$	$-1{\cdot}78$

According to V. C. Wilson (1938*a*, *b*):

$20 < \theta < 250$	$-1{\cdot}77$
$250 < \theta < 1{,}420$	$-2{\cdot}52$

According to Clay and Gemert (1939):

$60 < \theta < 300$	$-1{\cdot}93$
$300 < \theta < 1{,}380$	$-2{\cdot}95$

The agreement between Ehmert and Wilson is very good. The single point given by Barnóthy and Forró (1937) at about 1,000 m. agrees also with Wilson's results. The absorption found by Clay and Gemert seems to be slightly greater than that found by the other observers. The results of V. C. Wilson are shown in Fig. 47.

The inconsistencies may be at least partly due to different arrangements; thus, for example, the absorption curve may be affected by the solid angle subtended by the arrangement.

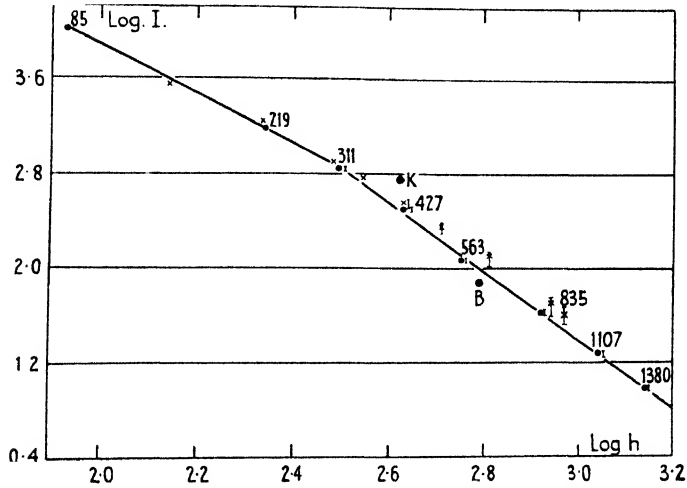

FIG. 47. Comparisons of decrease of cosmic-ray intensity in rock by various observers: • Clay and Gemert, × Wilson, • K Kolhörster, • B Barnóthy and Forró. (Clay and Gemert, *Physica*, **6**, 509, Fig. 7.)

2. *Nature of Rays Under Ground*

(*a*) *Cloud-chamber Evidence*

305. There is good reason to believe that cosmic rays under ground have much the same composition as cosmic rays at sea-level.

Cloud-chamber photographs of particles under ground were taken by Braddick and Hensby (1939), by Wilson and Hughes (1943), and by Hazen (1944*b*) at 30 m. of water equivalent. The tracks obtained under ground have the same appearance as those obtained at sea-level.

(*b*) *Coincidence Experiments*

306. Various authors, however, suggested that the radiation under ground differs essentially in composition from the radiation near sea-level.

1. It was suggested that the radiation under ground consists of relatively soft particles produced by more penetrating primaries.
2. It was also suggested that the radiation at depths greater than 300 m. water equivalent consists mainly of showers.

We describe in what follows experiments which disprove the above assumptions.

Absorbers of lead were placed between the counters of a vertical

coincidence arrangement, and thus the absorption of the rays in lead was measured (V. C. Wilson (1939); compare also Clay and Gemert (1939)); call this absorption curve, curve B.

The absorption curve can also be determined by measuring the cosmic-ray intensity at successive depths. The absorption curve obtained by this second method may be called curve A.

The curve B shows a decrease of the order of 10 per cent. for the first

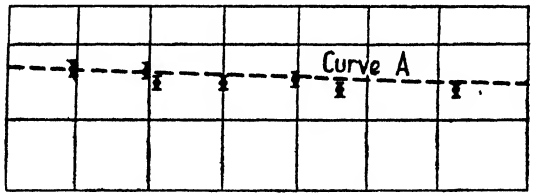

FIG. 48. Absorption curve in lead (curve A); (⊕) observed points under 71 m. H_2O equivalent (curve B). (Hughes and Wilson, 1943.)

7 cm. of lead. This decrease is due to a transition effect. For larger thicknesses of lead the curve B shows a very small absorption. The absorption in lead as found from curve B corresponds exactly to the corresponding part of curve A if mass-proportional absorption is assumed (see Fig. 48).

307. The similarity of curve A and curve B can be understood immediately if it is assumed that the cosmic rays consist of ionizing particles only. In this case the two arrangements measure the same effect.

The curves A and B would be expected to differ if the ionizing particles were the secondaries to a more penetrating non-ionizing radiation. For in this case the curve B would represent the absorption of the soft secondaries, while the curve A would represent the absorption curve of the more penetrating primaries. It is clear that the experimental evidence does not support such an assumption.

308. It has also been shown conclusively that the radiation under ground consists of single particles and not of showers.

Thus V. C. Wilson (1939) observed the rate of fivefold coincidences with a set of five counters placed in a plane. It was found that the rate was essentially the same as the corresponding rates for lower multiplicities. It is seen therefore that the cosmic rays below ground are still sufficiently ionizing to set off counters with a high efficiency.

It was found further that the rate of fivefold coincidences was reduced considerably when the counters were shifted out of line. It must be assumed therefore that the coincidences under ground are mainly due to single particles and not to showers.

The most penetrating particles are, according to theory, the mesons. If the cosmic rays at 1,000 m. water equivalent are mesons, it must be assumed that they have started with momenta exceeding 2.10^5 MEV./c. This value is, however, only a lower limit for the primary energies as no doubt many of the particles have not come to the ends of their ranges.

Further, the possibility cannot be excluded that very energetic mesons lose energy other than by ionization. If this is the case, initial momenta exceeding 2.10^5 MEV./c have to be assumed.

D. Momentum Spectrum

1. *The Spectrum*

309. The momentum spectrum of cosmic rays has been measured by many observers (see § 15). The most significant data obtained so far have been collected by Wilson (1946). The following table is reproduced from Wilson's paper.

Table 4

The meson spectrum above 1,000 *MEV./c*

Range	*Author*		
	Blackett (1937)	*Jones* (1939)	*Wilson* (1946)
Number of tracks with momentum < 1,000 MEV./c	620	802	301
	Number of particles for a total of 1,000 *in the range* 1,000–10,000 *MEV./c*		
1,000–2,000	383	393	367
2,000–3,000	219	243	223
3,000–6,000	280	258	288
6,000–10,000	118	106	122
10,000–20,000	86	(289)	102
20,000	80		82

Table 5

The meson spectrum below 1,000 *MEV./c* (*Wilson* (1946))

Range of momenta in MEV./c	*Number of particles for a total of* 1,000 *in the range* 1,000–10,000 *MEV./c*
500–1,000	238
300–500	76
200–300	35
100–200	18
30 (Williams (1939*b*))	2 in a band of about 30 MEV./c

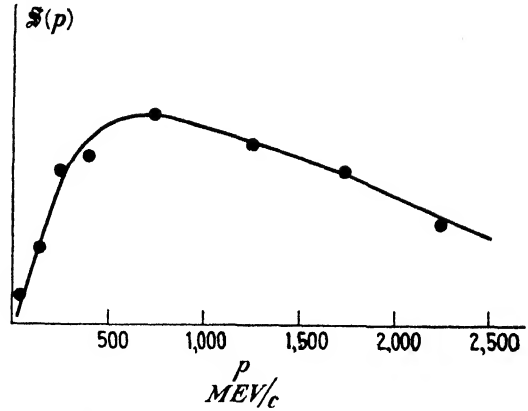

FIG. 49. Meson spectrum (collected by J. G. Wilson).

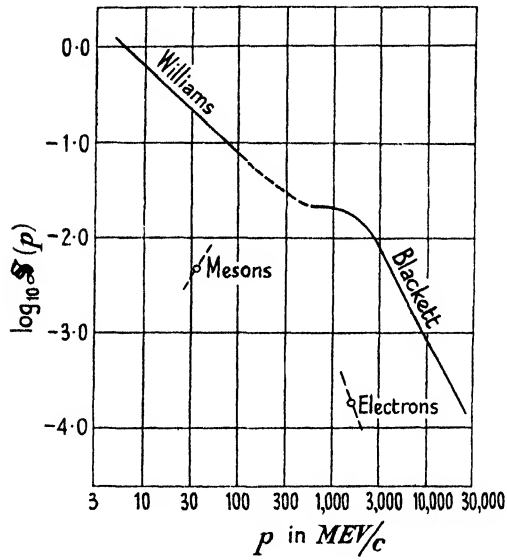

FIG. 50. Differential momentum spectrum of cosmic rays at sea-level according to E. J. Williams, 1939.

In Fig. 49 the meson spectrum has been plotted.

In Fig. 50 we have reproduced the electron and meson spectra according to Williams (1939 *b*).

2. *Interpretation of Observed Spectrum*

310. The momentum spectrum as obtained by Blackett (1937 *a*, *b*) shows an irregularity round 2,000 MEV./*c*. It was pointed out by

Blackett that this irregularity occurs in the region of $2M_P c^2$ and may be connected with some process involving protons.

(a) *Analytic Expressions*

The high-energy part of the spectrum can on the whole be well represented by a power function such as

$$\mathfrak{S}(p) \sim p^{-(z+1)}, \tag{18}$$

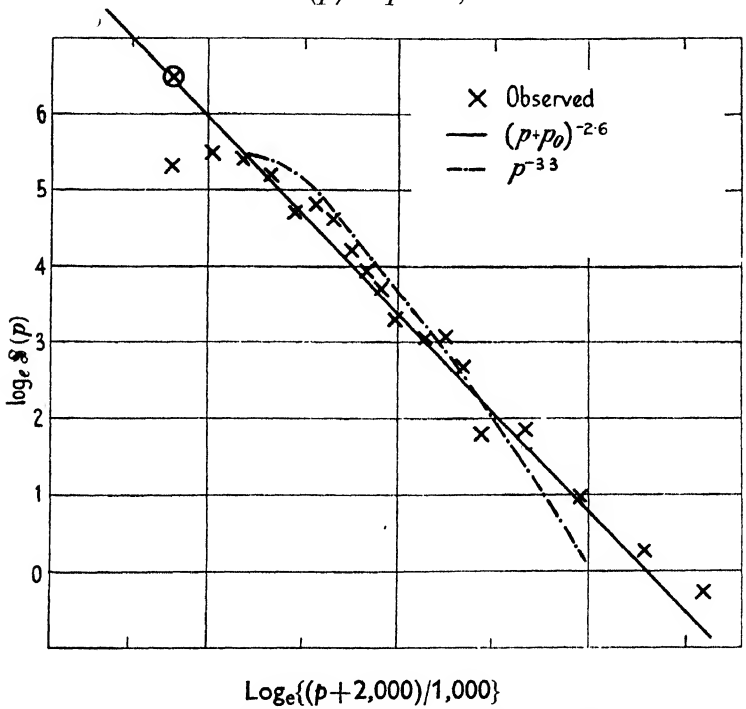

FIG. 51. Momentum spectrum (Blackett, 1936).

with $z \sim 1$. The spectrum may be regarded to be significant up to say 10^{10} eV.

It may be noted that for high momenta the spectrum must tail off more rapidly than $1/p^2$ as otherwise the total momentum would be infinite.

For our purpose it is more relevant to represent the differential spectrum by

$$\mathfrak{S}(p) \sim (p+p_0)^{-(z+1)} \tag{19}$$

and the integral spectrum by

$$\mathfrak{T}(p) \sim (p+p_0)^{-z}. \tag{20}$$

We have plotted in Fig. 51 Blackett's data in a double logarithmic plot.

Assuming $p_0 = 2{,}000$ MEV./c; we see that the whole of the spectrum can be fitted fairly satisfactorily by (20) with $z = 1{\cdot}6$. For later application we work out the following average values:

$$\langle p \rangle = \frac{\int_0^\infty p\,\mathfrak{S}(p)\,dp}{\int_0^\infty \mathfrak{S}(p)\,dp} = \frac{p_0}{z-1} \approx 3{,}500 \text{ MEV./}c \tag{21}$$

and similarly $$\left\langle \frac{1}{p+p_0} \right\rangle = \frac{1}{p_0}\frac{z}{z+1} = \frac{1}{3{,}300 \text{ MEV./}c}. \tag{22}$$

(b) Range Momentum Relation

311. There is a simple connexion between an absorption curve and the energy spectrum of the particles. Assume an absorption process in which fluctuations are negligible. The range $\mathscr{R}$ of a particle is a monotonic function of momentum. We have

$$\mathscr{R} = \mathscr{R}(p). \tag{23}$$

Reversing the above equation we obtain

$$p = p(\mathscr{R}).$$

Introducing the last expression into the momentum spectrum we find the number of particles with ranges exceeding a given value $\mathscr{R}$. All particles with ranges

$$\mathscr{R} > \theta$$

are capable of penetrating to a depth exceeding θ, and thus the intensity at a depth θ is equal to the number of particles with ranges exceeding θ. We have therefore

$$\mathscr{C}(\theta) = \mathfrak{T}\{p(\theta)\}, \tag{24}$$

where $\mathscr{C}$ is the depth intensity function and $\mathfrak{T}$ the integral spectrum.

312. For moderate depths the absorption function is given by

$$\mathscr{C}(\theta) = \mathscr{C}(0)\left(\frac{\theta_0}{\theta+\theta_0}\right)^{1\cdot6} \quad (\theta_0 = 1{,}000 \text{ grams per cm.}^2 \text{ (equivalent of atmosphere)}). \tag{25}$$

Comparing this with the analytic expression (20) obtained for the momentum spectrum we find

$$\theta = p\frac{\theta_0}{p_0}$$

and therefore $$\frac{dp}{d\theta} = \frac{p_0}{\theta_0} \sim 2 \text{ MEV./}c \text{ cm.}^2 \text{ per gram.}$$

The above rate of loss is in good agreement with the loss expected for mesons due to ionization in light elements. It can be concluded therefore that the meson spectrum together with the absorption curve for small depths favour the assumption that mesons are mainly absorbed by ionization loss.

A similar conclusion can be drawn from the comparison of the absorption curve in lead and the spectrum. About 50 per cent. of the penetrating component is capable of penetrating 1 m. of lead. From the spectrum (20) we find that 50 per cent. of the mesons have energies exceeding 1,100 MEV./c. From the theoretical momentum range relation reproduced in Fig. 30b we find that the range of 1,100 MEV./c mesons is just about 1 m. of lead.

313. The question whether or not high-energy mesons lose energy by processes other than ionization could be decided experimentally by measuring the meson spectrum up to momenta of the order of 10^5 MEV./c. If the energy loss of these fast mesons is mainly due to ionization, then the exponent of the momentum spectrum should show the same increase as is observed for the exponent of the absorption function.

A further point which could be tested experimentally is as follows. If the mesons lose energy by ionization only, then the momentum spectrum at a depth θ should be given by

$$\mathfrak{S}(p) \sim \frac{1}{\{p+p(\theta)\}^{z+1}},$$

with

$$p(\theta) = 2{,}000 \text{ MEV.} \frac{\theta}{\theta_0}.$$

The average meson energy should therefore increase with depth. We should expect

$$\langle p \rangle_\theta = 2{,}000 \text{ MEV.} \frac{\theta}{\theta_0} \frac{1}{z-1}. \qquad (25\,a)$$

Because of the increase of $\langle p \rangle_\theta$ with θ, meson tracks obtained in a cloud chamber deep under ground should show a markedly higher ionization density than the tracks at sea-level. The only relevant experiments of this type are due to Hazen (1944b). It was found that tracks obtained under 30 m. of water equivalent do not show the expected increase in density. More experiments of this type, especially at greater depths, would be desirable.

3. *Momentum Loss in Absorbing Plates*

314. Direct measurement of the loss of momentum of cosmic-ray particles traversing metal plates can be carried out in two ways. Either

a single cloud chamber with a metal plate placed into the middle of the chamber is used; the momentum loss can be determined from the difference of magnetic curvature in the two halves of the chamber. Or alternatively the curvature of a particle can be measured in two chambers separated by an absorber (see § 16).

315. In particular Anderson and Neddermeyer (1937) could show that cosmic-ray particles can be divided into two types according to their behaviour when crossing metal plates. The two types of particles are now known to be electrons and mesons.

The electrons are predominant in the region below 200 MEV./c; they lose large amounts of energy and the energy loss is subject to great fluctuations. It was shown by Anderson and Neddermeyer (1937) and by Blackett (1938a) that the distribution of energy loss of electrons is in accordance with the theory of radiative collisions.

316. Precise measurements of the momentum loss of mesons have been carried out by Ehrenfest (1938a, b) using a gold plate 9 cm. thick and by J. G. Wilson (1939) using a 2-cm. gold plate.

The following figures are taken from J. G. Wilson (1939).

TABLE 6

Momentum loss of mesons per cm. of lead in MEV/c.

Momentum range	200–400	400–700
Observed loss	$12{\cdot}1 \pm 2{\cdot}0$	$14{\cdot}3 \pm 3{\cdot}6$
Calculated loss for $\mu = 200m_e$	13·2	14·0

It is clear that the momentum loss of the particles observed in the above work can be fully accounted for in terms of ionization.

317. The accuracy of momentum-loss measurement decreases rapidly with increasing momentum, and the experimental results for momenta higher than those given in Table 6 must be regarded as tentative.

Wilson (1939) observed a small number of particles in the momentum range of 1,000–2,000 MEV./c which suffered large losses but were not electrons; with one exception these particles were of positive sign. Wilson considered tentatively the particles entering the plate to be protons; judging from ionization density at least some of the outgoing particles were mesons. The process may possibly be interpreted in terms of protons losing large amounts of energy due to the emission of mesons.

Ehrenfest (1938) did not find any anomaly in the absorption in the region round 2,000 MEV./c. Ehrenfest, however, observed under a lead screen 16 cm. thick. Because of their large rate of loss protons cannot

be expected to be able to traverse such an absorber (compare Ch. IX); therefore the results of Ehrenfest and of Wilson do not appear to be contradictory.

4. *Scattering*

(*a*) *Multiple Scattering*

318. The scattering of mesons when passing through metal plates has been investigated by several workers. The early measurements of Blackett and Wilson (1938), in which mesons and electrons were not separated, showed that the major effect was due to Coulomb forces. The following features were observed: (1) the root mean square of the angle of scattering is inversely proportional to the momentum; (2) the angles of scattering of one momentum are distributed according to a Gaussian. The measurements were extended up to momenta of 2,000 MEV./*c*.

The results of J. G. Wilson (1940) and of Code (1941) are collected in the following Table 7. $\langle\overline{\vartheta^2}\rangle$ is the projected angle of scattering. According to eq. (185), § 243, the product $p^2\langle\overline{\vartheta^2}\rangle$ is independent of momentum. Table 7 gives the theoretical average value of $p\sqrt{\langle\overline{\vartheta^2}\rangle}$ for various observers; in the last column this value is compared with the observed values.

TABLE 7

Observer	*Scattering plate*	$p\sqrt{\langle\overline{\vartheta^2}\rangle}$ *(theoretical)*	*Ratio of observed and calculated values*
J. G. Wilson (1940)	1 cm. Pb	0·91	$1{\cdot}01\pm0{\cdot}06$
	0·3 cm. Pb	0·48	$1{\cdot}00\pm0{\cdot}13$
	2 cm. Cu	0·73	$0{\cdot}98\pm0{\cdot}10$
	2 cm. Au	1·75	$1{\cdot}06\pm0{\cdot}05$
Code (1941)	3·8 cm. W	2·20	0·98

The agreement between observed and calculated values is excellent. The agreement would not be as good if the observation were compared with the scattering calculated for a point nucleus.

(*b*) *Large-angle Scattering*

319. A few cases of large-angle scattering were found, for which the product $p\vartheta$ is far too large to be reconciled with the Gaussian distribution arising from Coulomb scattering. The more recent observations of J. G. Wilson (1940), Code (1941), and Shutt (1942) were directed to separating these examples of large-angle scattering from the main Coulomb group.

The occurrence of large-angle scattering is of great interest as it must be attributed almost entirely to short-range interaction. The observed cross-section for large-angle scattering can be used as sensitive test for the correct formulation of meson theory (see §§ 193 and 231).

Wilson (1940) and Code (1941) both used the direct method in their search for large-angle scattering. They both measured the product $p\vartheta$ for individual particles and showed the occurrence of deviations from a normal Gaussian distribution.

Shutt (1942), however, avoided the necessity of measuring the momentum of individual particles, using the following method. A chamber is used containing two plates, one 1 cm. thick, the other 5 cm. thick. The distribution of angles of scattering in the two plates is compared and the occurrence of large-angle scattering is deduced statistically.

320. The results of the above authors are in general agreement, collected by Shutt (1942) they are as follows:

TABLE 8

Observer	*Cross-section of large-angle scattering per nucleon in* 10^{-28} *cm.*^{2}
Wilson (1940)	4·0
Code (1941)	5·7
Shutt (1942)	6·5

The observed cross-section for large-angle scattering is somewhat smaller than that calculated by Heitler and Peng (1944) using the symmetrical meson theory of Möller and Rosenfeld (1940). The cross-section obtained from the 'charged' theory is in better agreement. Cross-sections obtained from the meson theory not including radiation damping are of the order of 10^{-26} cm.^{2} and thus are far too large to be compatible with the observational results (see § 231).

V

THE INSTABILITY OF THE MESON

A. Mathematical Relations

Before discussing the facts connected with the meson decay we give a few mathematical relations which are needed for the interpretation of the effects connected with meson decay.

1. *Mean Range of Mesons*

(a) *Mesons traversing Free Space*

321. Mesons are assumed to decay spontaneously and therefore the probability of a meson decaying during any time interval dt is the same, and this probability is independent of the previous history of the meson.

Consider N mesons at the time $t = 0$. The average number of mesons still intact at a time t is denoted by $N(t)$; the number of mesons decaying in the interval t, $t+dt$ is

$$-dN(t) = N(t)\, dt/\ell_0. \tag{1}$$

Integrating equation (1) we find

$$N(t) = Ne^{-t/t_0}. \tag{2}$$

From (2) we see that ℓ_0 is the mean life of the meson.

322. To obtain the mean range of a fast meson one has to distinguish clearly between apparent life and proper life. The half-life of a meson is equal to ℓ_0 in the rest-system of the meson. Due to relativistic time contraction a meson with a velocity v appears to have a half-life

$$\ell_0' = \ell_0 B \tag{3}$$

(compare § 147). The mean range of a meson with a velocity v is therefore

$$\mathscr{R}^*(v) = v\ell_0' = v\ell_0' B, \tag{4}$$

and with the help of eqs. (4, 5), Ch. III,

$$\mathscr{R}^*(v) = \frac{\ell_0}{\mu} P, \tag{5}$$

where μ and P are rest-mass and momentum of the meson. The range $\mathscr{R}^*$ of a meson increases therefore more rapidly than its velocity.

The following remark may be useful. In the system of reference where the meson is moving, the apparent life of the meson is prolonged due to time contraction, and therefore the meson can cover a range $\mathscr{R}^*$ which could not be covered during the time ℓ_0. In the rest-system of

the meson, however, the time available for the meson is only equal to τ_0, but the range which was found to be equal to $\mathscr{R}^*$ in the system where the meson was moving appears contracted by a factor $1/B$ in the rest-system, and therefore the meson has to live only for the time the contracted range $\mathscr{R}^*/B$ is moving past.

(b) *Mesons traversing an Absorber*

323. In the following we calculate the mean range of a meson passing through an absorber (compare e.g. Euler and Heisenberg (1938)).

Consider mesons with momentum P entering an absorber. Due to absorption the mesons reaching a depth $\mathfrak{z}$ will have a momentum

$$P(\mathfrak{z}) < P.$$

Denote the average number of mesons reaching $\mathfrak{z}$ by $\mathscr{N}(\mathfrak{z})$. The average number decaying in the interval $\mathfrak{z}$, $d\mathfrak{z}$ is obtained with the help of (1) and (3):

$$-d\mathscr{N} = \mathscr{N}(\mathfrak{z})\frac{\mu}{\tau_0}\frac{d\mathfrak{z}}{P(\mathfrak{z})}. \tag{6}$$

Integrating over $\mathfrak{z}$ we find

$$\mathscr{N}(\mathfrak{z}) = \mathscr{N}(0)\exp\left[-\frac{\mu}{\tau_0}\int_0^{\mathfrak{z}}\frac{d\mathfrak{z}}{P(\mathfrak{z})}\right]. \tag{7}$$

The following special cases are of importance.

(i) Mesons traversing a homogeneous absorber

324. For fast mesons, i.e. for $P \gg \mu c$, we may assume

$$dP/d\mathfrak{z} = \text{const.} = \mu c/a, \quad \text{say,} \tag{8}$$

and therefore

$$P(\mathfrak{z}) = P_0 - \frac{\mathfrak{z}}{\mathfrak{z}_1}(P_0 - P_1), \tag{9}$$

where P_0 is the momentum of the incident mesons and P_1 is the momentum of the mesons which have reached a depth $\mathfrak{z} = \mathfrak{z}_1$. Introducing (8) into (7) we find

$$\mathscr{N}(\mathfrak{z}_1) = \mathscr{N}(0)\left(\frac{P_0}{P_1}\right)^{-\mu\mathfrak{z}_1/\tau_0(P_0-P_1)}. \tag{10}$$

(ii) Mesons nearing the end of their range

325. We may use the approximate range momentum relation (169, Ch. III); we find with help of (8)

$$\mathscr{R}(p) \sim \tfrac{1}{4}(P/\mu c)^4 . a, \tag{11}$$

and with help of (7) we find

$$\mathscr{N}(\mathfrak{z}) = \mathscr{N}(0)\exp\left(-\frac{a}{3c\tau_0}\frac{P(0)^3 - P(\mathfrak{z})^3}{(\mu c)^3}\right). \tag{12}$$

The fraction of mesons with initial momentum μc which decay only after being brought to rest is therefore

$$\mathcal{N}(P=0)/\mathcal{N}(P=\mu c) = \exp\left(-\frac{a}{3c\ell_0}\right). \tag{13}$$

In the case of air at N.T.P. we have approximately

$$\frac{dP}{d\mathfrak{z}} = 2{\cdot}5\times10^{-3}\ \text{MEV./cm.}, \qquad a = 4\times10^4\ \text{cm.};$$

further $\qquad c\ell_0 = 6{\cdot}3\times10^4$ cm. (see § 342),

and therefore $\qquad \mathcal{N}(P=0)/\mathcal{N}(P=\mu c) = 0{\cdot}81. \tag{14}$

Thus most slow mesons moving in air at N.T.P. will be brought to rest before decaying. The numerical values of course represent only the correct orders of magnitude. Using the correct momentum range relation given in Fig. 30, $\mathcal{N}(\mathfrak{z})$ can be evaluated by numerical integration. The result of this integration carried out for air at N.T.P. is shown in Fig. 52. For convenience both ordinary and logarithmic plots are shown.

(iii) Mesons traversing the free atmosphere

326. The change in air density with height has to be taken into account. For simplicity we assume the density distribution to be exponential. Thus we assume

$$\theta(\mathfrak{z}) = \theta_0 e^{-\mathfrak{z}/\mathfrak{z}_0}, \tag{15}$$

where $\mathfrak{z}_0$ is the height of the homogeneous atmosphere. $\theta(\mathfrak{z})$ is the absorption equivalent of the atmosphere at the height $\mathfrak{z}$. θ_0 is the absorption equivalent of the whole atmosphere.

Fast mesons arriving at sea-level with a momentum P_1 must be supposed to have had a momentum

$$P(\mathfrak{z}) = P_1+\mu c\frac{\mathfrak{z}_0}{a}(1-e^{-\mathfrak{z}/\mathfrak{z}_0}) \tag{16}$$

at the height $\mathfrak{z}$. Denoting the loss of momentum throughout the whole of the atmosphere by

$$P_A = \frac{\mu c\mathfrak{z}_0}{a}, \tag{17}$$

we find from (7), (16), and (17)

$$\mathcal{N}(0) = \mathcal{N}(\mathfrak{z})\left(\frac{P_A}{P_1}\frac{P(\mathfrak{z})}{P_A+P_1-P(\mathfrak{z})}\right)^{-(\mathfrak{z}_0/c\ell_0)\{\mu c/(P_1+P_A)\}}. \tag{18}$$

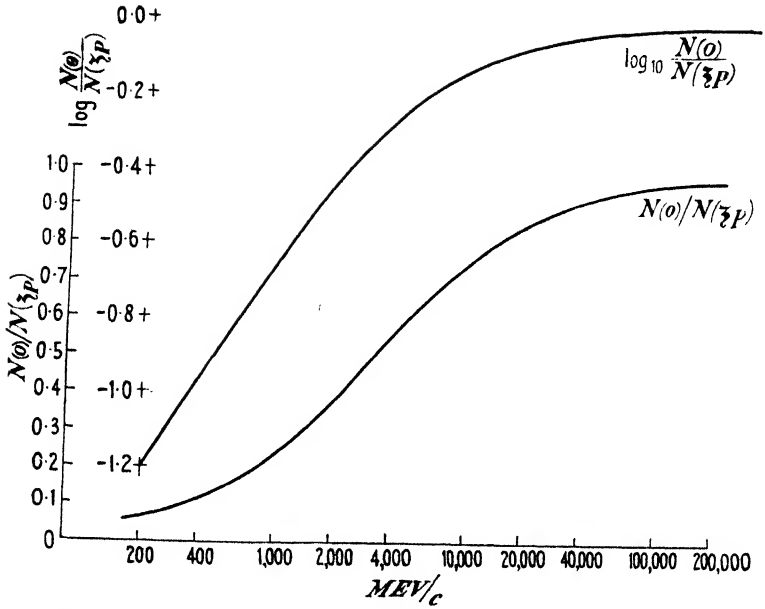

FIG. 52 *a*. Decay probability of mesons traversing the atmosphere.

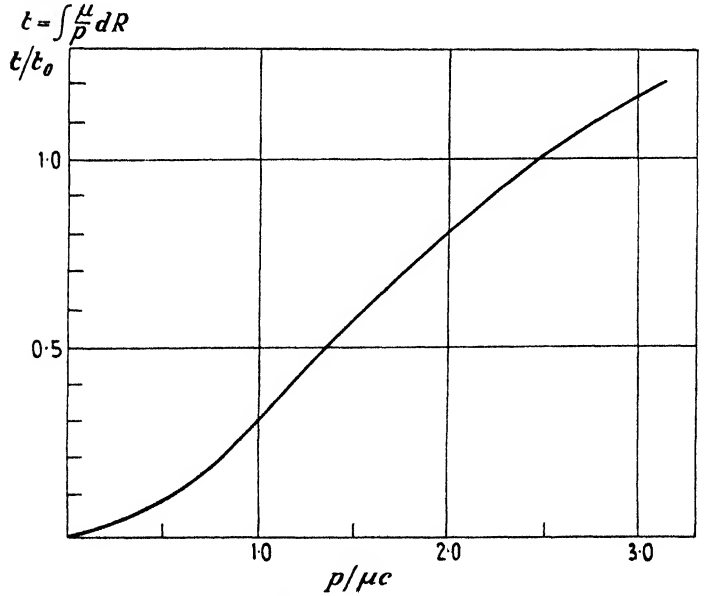

FIG. 52 *b*. Decay probability of mesons near end of range.

327. As the mesons are unstable they must be assumed to be the secondaries of stable primary particles. Assume that the mean range of the primaries before giving rise to mesons is θ_P. According to (15) the mean height of production of the mesons can be taken to be

$$\mathfrak{z}_P = \mathfrak{z}_0 \log(\theta_0/\theta_P). \tag{19}$$

Introducing this into (18) we find

$$\mathcal{N}(0)/\mathcal{N}(\mathfrak{z}_P) = \left\{\frac{\theta_0}{\theta_P}\left(1+\frac{P_A}{P_1}\right)-\frac{P_A}{P_1}\right\}^{-(\mathfrak{z}_0/ct_0)\{\mu c/(P_1+P_A)\}}. \tag{20}$$

The above equation gives the fraction of mesons which but for the decay would have reached sea-level with a momentum P_1.

Equation (20) has been derived on the assumption that all vertical mesons are produced at the same height $\mathfrak{z}_P$. This assumption is not strictly correct; it must be assumed that the mesons are produced by their primaries over an extended range.

Some numerical values of the decay probability as given in (20) are collected in the following table (see also Fig. 52).

TABLE 1

Decay probabilities according to (20) *with* $P_A = 2{,}000$ *MEV./c*, $\theta_0/\theta_P = 10$

$$\frac{\mathfrak{z}_0}{ct_0}\frac{\mu c}{P_A} = 0{\cdot}66.$$

P_1 MEV./c =	200	400	1,000	2,000	4,000	10,000	20,000	40,000	100,000	200,000
$-\log_{10}\frac{\mathcal{N}(0)}{\mathcal{N}(\mathfrak{z}_P)}$ =	1·200	0·956	0·637	0·422	0·256	0·118	0·062	0·032	0·013	0·007

The probability of decay of mesons arriving with small velocities can be obtained in two steps. One can work out first the probability of decay of the meson down to a level where its momentum is of the order of μc. For the rest of its range the variation of the air density can be neglected and the probability of decay can be worked out using the graph Fig. 52 or with the approximate expression (12).

(iv) Mesons traversing the atmosphere in inclined directions

328. At any given point in the atmosphere the probability of decay of mesons incident at an angle ϑ to the vertical is greater than for those incident in the vertical direction owing to the larger path travelled if both are taken to have started at the same height $\mathfrak{z}$. The decay

probabilities for mesons moving in inclined directions can be found from (18) by replacing $\mathfrak{z}_0$, P_A, and θ_0 by:

$$\left.\begin{aligned} \mathfrak{z}_0' &= \mathfrak{z}_0/\cos\vartheta, \\ P_A' &= P_A/\cos\vartheta, \\ \theta_0' &= \theta_0/\cos\vartheta. \end{aligned}\right\} \tag{21}$$

One must be careful in evaluating the height $\mathfrak{z}_P'$ where the mesons which are inclined at an angle ϑ are produced. Assume that the mesons are emitted in the direction of their primaries. The primaries will have traversed an absorber equivalent θ_P at a point lying at a depth $\theta_P \cos\vartheta$ below the top of the atmosphere. The inclined mesons can therefore be assumed to originate at a height (compare Blackett (1938*b*), Fréon (1942, 4))

$$\mathfrak{z}_P' = \mathfrak{z}_0 \log\left(\frac{\theta_0}{\theta_P \cos\vartheta}\right). \tag{22}$$

The decay probability for inclined mesons is therefore found with the help of (18) and (21) as

$$\mathcal{N}'(0)/\mathcal{N}'(\mathfrak{z}_P') = \left\{\frac{\theta_0}{\theta_P \cos\vartheta}\left(1+\frac{P_A}{P_1\cos\vartheta}\right)+\frac{P_A}{P_1\cos\vartheta}\right\}^{-(\mathfrak{z}_0/c t_0)(\mu c/(P_1\cos\vartheta + P_A))}. \tag{23}$$

2. *The Decay Electron*

(*a*) *Momentum*

329. The meson is supposed to decay into an electron and a neutrino. In the rest-system of the meson the electron and neutrino must have equal but opposite moments. From the conservation of the energy we find for the absolute value of the momentum of the electron

$$P_d = \frac{\mu c}{2}\left(1-\frac{m_c^2}{\mu^2}\right) \approx \frac{\mu c}{2}, \tag{24}$$

assuming the rest-mass of the neutrino to be zero.

In the rest-system of the meson the electron must be assumed to be emitted in random direction. Thus we assume the probability of the electron being emitted into the solid angle $d\Omega$ to be $d\Omega/4\pi$.

Considering the components, one finds for the probability that the x-component of P is in an interval P_x, dP_x

$$d\mathcal{P} = dP_x/2P_d. \tag{25}$$

330. The momentum of the decay electron of a moving meson is obtained by a Lorentz transformation. Let us consider a new system of reference in which the meson is moving in the direction of the

positive x-axis. We denote the momentum of the meson in the new system by P_μ and its energy by W_μ.

The x-component of the momentum of the decay electron in the new system is obtained with the help of eqs. (4), (5), (10), Ch. III, and (24) as follows:

$$P'_{d,x} = (P_{d,x} W_\mu + W_d P_\mu)/\mu c^2, \tag{26}$$

where $W_d = \sqrt{(c^2 P_d^2 + m_e^2 c^4)}$ is the energy of the decay electron in the original system of reference. It is seen from (26) that the component of the momentum of the decay electron is inside the interval $P_{\min}$, $P_{\max}$ with

$$\begin{aligned} P_{\min} &= (-P_d W_\mu + W_d P_\mu)/\mu c^2, \\ P_{\max} &= (P_d W_\mu + W_d P_\mu)/\mu c^2. \end{aligned} \tag{27}$$

The probability of finding $P'_{d,x}$ in an interval dP' which is inside the interval $P_{\min}$, $P_{\max}$ is independent of $P'_{d,x}$ and it is according to (25) and (26)

$$d\mathscr{P}' = dP'/(P_{\max} - P_{\min}). \tag{28}$$

Assuming as a first approximation

$$P_d \approx W_d/c \approx \mu c/2, \tag{29}$$

(27) can be simplified and it reduces to

$$P_{\min} = -\frac{\mu^2 c^2}{2(W_\mu/c + P_\mu)}, \qquad P_{\max} = \frac{W_\mu/c + P_\mu}{2}. \tag{30}$$

It is seen that for high meson velocities

$$P_{\min} \sim 0 \quad \text{and} \quad P_{\max} \sim P_\mu. \tag{31}$$

Thus for high velocities decay electrons will be emitted mainly in the forward direction uniformly distributed between zero and P.

For very high energies the expression (30) for $P_{\min}$ becomes invalid, as for such energies (29) gives an insufficient approximation of $W_\mu/c - P_\mu$. Neglecting nothing, we find from (24) and (27)

$$P_{\min} = -\frac{\mu^2 c^2}{2(W_\mu/c + P_\mu)} + \frac{m_e^2}{2\mu^2}(W_\mu/c + P_\mu). \tag{32}$$

The second term in (32) becomes predominant for

$$P_\mu > \frac{\mu^2 c}{2m_e} \sim 10^4 \text{ MEV./}c.$$

It can be shown easily that for $P_\mu = \mu^2 c/2m_e$ the velocity of the meson is equal to the velocity of the decay electron in the rest-system of the meson. It is therefore clear that for larger momentum the decay electron is always projected forward.

(b) *Angle of Emission*

331. The angle ϑ_d between the direction of motion of the meson and that of the decay electron can be determined as follows. We have

$$\tan\vartheta_d = P'_{d,y}/P'_{d,x}, \tag{33}$$

where the y-axis is chosen in the direction of the normal component of P_d. The components of the momentum perpendicular to the direction of motion are not affected by the Lorentz transformation and therefore we have

$$P'_{d,y} = P_{d,y} = \sqrt{(P_d^2 - P_{d,x}^2)}. \tag{34}$$

We find with the help of (26)

$$\tan\vartheta_d = \frac{\mu c^2\sqrt{(P_d^2 - P_{d,x}^2)}}{P_{d,x}W_\mu + W_d P_\mu}. \tag{35}$$

We introduce

$$P_{d,x} = P_d(1-2\mathscr{P}). \tag{36}$$

Comparing (36) with (25) we see that $\mathscr{P}$ is the probability that the electron has a momentum exceeding $P_{d,x}$ in the forward direction when measured in the rest-system of the meson; $\mathscr{P}$ is at the same time the probability that the electron has a momentum exceeding $P'_{d,x}$ in the forward direction when measured in the system where the meson is moving.

Neglecting $P_{\min}$ as compared with P_μ we find from (35) and (36)

$$\tan\vartheta_d = \frac{\mu c^2}{W_\mu}\sqrt{\frac{\mathscr{P}}{1-\mathscr{P}}}, \quad \text{or} \quad \mathscr{P} = \frac{\tan^2\vartheta_d}{(\mu c^2/W_\mu)^2 + \tan^2\vartheta_d}. \tag{37}$$

As the angle ϑ_d decreases monotonically with increasing $P_{d,x}$ we conclude that $\mathscr{P}$ is the probability that the electron is emitted at an angle smaller than ϑ_d.

Inserting $\mathscr{P} = \frac{1}{2}$ into (37) we find

$$\tan\vartheta_d = \frac{\mu c^2}{W_\mu} \quad \text{for} \quad \mathscr{P} = \tfrac{1}{2},$$

thus half of the decay electrons are emitted inside a cone with the opening angle $2\vartheta_d = 2\mu c^2/W_\mu$. This result bears some analogy to the distribution of light emitted by a fast-moving source dealt with in § 152. The probability of an emission at an angle exceeding 45° is found to be about $(\mu c^2/W_\mu)^2$.

Thus the decay electrons of a fast meson are concentrated into the forward direction. This effect is very similar to the Doppler effect as discussed in § 152. The difference between the Doppler effect and the emission of decay electrons is that there is always a finite Doppler intensity backwards, while a sufficiently fast meson emits in the forward

direction only. Physically the difference is due to the finite rest-mass of the electron. Decay electrons can only be projected backwards if the velocity of the meson is smaller than that of the electron. In the case of the photon emission the velocity of the photon always exceeds that of the emitting particle and therefore the photon may move forward or backward.

B. Experimental

1. *Direct Evidence*

(*a*) *Photographs of Meson Decay*

Discussion of photograph of Williams and Roberts

332. Direct evidence for the decay of the meson was obtained with the cloud chamber. The first photograph showing a decaying meson was obtained by Williams and Roberts (1940). The photograph is reproduced in Plate 2. A similar photograph was obtained by Williams and Evans (1940), Johnson and Shutt (1942), and by Shutt, Benedetti, and Johnson (1942). We discuss the details of the photograph of Williams and Roberts in the following.

The thick track stretching from A to F is that of the incident meson. From the end of the meson track a thin track FG emerges. The thin track is assumed to be the track of the decay electron.

333. The meson track is much thicker than the track of the decay electron and is also much thicker than the tracks of a number of electron tracks seen on the same photograph; thus it is the track of a slow particle.

The photograph is taken in a magnetic field of 1,180 gauss. The curvature of the meson track between A and C is about 70 cm. and therefore the momentum of the particle at the point B is estimated as

$$P_B = 300.70.1{,}180.10^{-6}\ \text{MEV}./c$$
$$= 25\ \text{MEV}./c.$$

Assuming that the particle has come to the end of its range in F, the remaining range is BF and is equal to 41 cm. air N.T.P. From the momentum range one finds that the mass of the particle giving rise to the track AF must be

$$\mu = (250 \pm 70) m_e.$$

Thus the incident particle must be a meson.

We note that the track AF is very different from the track of an electron or a proton. An electron track of the same density would have

been curled into a small spiral, while a proton track showing the initial curvature AC would be expected to have a remaining range only one-tenth of the observed range BF. Thus the track must be due to a particle of intermediate mass.

334. The momentum of the decay electron is expected to be 50 MEV./c, and to have a curvature of 140 cm. As unfortunately only a very short section of the electron track is visible on the photograph the curvature of the electron track could not be measured. The short electron track obtained appears straight, in agreement with what one expects.

335. Though the photograph, Plate 2, shows all the features one would expect for a photograph showing a decay process it is useful to refute a number of alternative interpretations of the photograph.

1. One might try to assume that the process seen in Plate 2 does not represent a decaying meson but a fast particle coming from G, being scattered through a large angle at F, losing hereby most of its energy.

This interpretation cannot be correct, however, for several reasons. In case of a large-angle scattering of a fast particle a recoil particle should appear, while on the photograph there is no indication of a recoil particle.

Besides, there can be no doubt about the direction of motion of the slow particle. The slow particle moves downwards from A to F and not in the opposite direction for the following reasons. A δ-track is emitted from the point E moving initially downwards in the direction of the meson. Further, the number of δ-tracks emitted increases along the meson track when going downwards. This is to be expected as a result of the slowing down of the meson. Finally, the end of the meson track near F shows a large-angle deflexion. Such deflexions are to be expected near the ends of slow tracks.

The large-angle deflexion near the end of the track gives also evidence that the meson has come to rest somewhere near F before decay.

2. The direction of motion of the slow track being known, the slow and the fast tracks cannot be interpreted as an electron pair due to a photon absorbed in A.

3. The possibility that the two tracks are independent could not be ruled out altogether. One might for instance assume that the slow track ends in A, and by accident a fast photo or Compton electron is produced by a photon at the same point. The probability for such a process is, however, so small that such a coincidence need not be considered seriously.

Estimated rate of decay photographs

336. There seems to be no reason to doubt the interpretation of the photograph shown in Plate 2 as the track of a decaying meson. It would be desirable, however, to obtain more photographs of this kind. The rate of photographs obtainable showing decaying mesons is small under most practical conditions as shown by the following calculation.

In estimating the rate of occurrence of photographs showing decaying mesons, two types have to be considered.

1. A meson is brought to rest in the gas of the chamber and decays afterwards.

The rate of mesons under an absorber of θ grams per cm.^{2} at sea-level is according to § 312

$$\mathcal{N}(\theta) = \mathcal{N}(0)(\theta+\theta_0)^{-1\cdot6}.\theta_0^{1\cdot6}, \tag{38}$$

with $\theta_0 = 1{,}000$ grams per cm.^{2} the absorbing equivalent of the atmosphere.

The fraction of mesons stopped in an absorber of thickness $d\theta$ is

$$\frac{d\mathcal{N}}{\mathcal{N}(0)} = 1\cdot6\frac{d\theta}{\theta_0}. \tag{39}$$

Considering a chamber filled with air of atmospheric pressure having a diameter of about 30 cm. we can put

$$d\theta = 0\cdot04 \text{ gram per cm.}^2,$$

where $d\theta$ is the absorbing equivalent of the air in the chamber. We find from (39) for the fraction of mesons being brought to rest in the gas of the chamber

$$d\mathcal{N}/\mathcal{N}(0) = 6.10^{-5}. \tag{40}$$

Thus taking photographs of mesons traversing the chamber one expects one meson stopped in the gas for every 13,000 photographs.

337. We shall see later that only about every second slow meson decays and therefore the rate of photographs showing decaying mesons is only half of that estimated for mesons stopped in the gas.

The rate of mesons stopped in the gas is of course proportional to the pressure inside the chamber. A better yield can therefore be obtained using a high-pressure chamber. A chamber filled with 100 atm. of air is described by Johnson, Benedetti, and Shutt (1943).

The rate of decaying mesons to be expected in a chamber is small. Assuming that 1,000 particles per hour are crossing the chamber one expects one meson to decay inside the chamber in every 13 hours. The decay electron could be used to trigger the chamber (compare § 277), and

thus it should be possible to obtain several decay photographs per day with a chamber operated at ordinary pressure.

2. A meson might decay inside the chamber without having been brought to rest. The probability of a meson decaying along a path $\mathfrak{z}$ is according to (6)

$$\mathscr{P} = \frac{\mathfrak{z}}{c\ell_0}\frac{\mu c}{P}. \tag{41}$$

For a chamber of 30 cm. diameter we thus obtain

$$\mathscr{P} \sim \frac{1}{2{,}000}\frac{\mu c}{P}. \tag{42}$$

The above expression is only valid if the loss of momentum in the gas can be neglected compared to P. For very slow mesons the probability of a meson decaying in the chamber does not increase with decreasing momentum as one might expect from (42). The rate of mesons with momentum inside an interval dp was shown to be proportional to $1/(d\mathscr{R}/dp)$ (compare (8), Ch. IV). Using the approximation (9), Ch. IV, we find therefore for slow mesons

$$d\mathscr{N}/\mathscr{N} = \frac{1}{2{,}000}\frac{P^2}{(\mu c)^2} \quad (P \lesssim \mu c); \tag{43}$$

the relative number of mesons with momentum $0 < P < \mu c$ decaying in the chamber is

$$\frac{1}{2{,}000}.$$

Thus, apart from mesons actually brought to rest, momenta in the region of $\sim \mu c$ are most favourable for the observation of decaying mesons.

338. A fast meson decaying in the gas of the chamber may be difficult to recognize. If the angle of the emission is small, the process cannot be distinguished from a meson being scattered in an elastic collision. Therefore the process can only be recognized as decay if the decay electron is emitted at a large angle to the direction of the meson.

The probability that the decay electron is emitted at a large angle is of the order of $(\mu c/P)^2$. Assuming for the differential spectrum

$$\mathfrak{S}(p) = \mathfrak{S}(0)(p+2{,}000)^{-2\cdot6},$$

we obtain for the fraction of mesons with momentum $p > 2\mu c$ which decay in the chamber and emit electrons at large angles

$$\mathscr{N}_d = \frac{\int_{2\mu c}^{\infty} \mathscr{P}(\mu c/P)^2 \mathfrak{S}(p)\, dp}{\int_{2\mu c}^{\infty} \mathfrak{S}(p)\, dp} \simeq 1/50{,}000.$$

This process is therefore very rare. It is seen therefore that photographs of decaying mesons are expected most frequently of mesons which have been brought to rest in the chamber.

(*b*) *The Neutrino*

339. No direct evidence for the emission of the neutrino in the decay can be obtained from cloud-chamber photographs. Valuable indirect information could be obtained, however, by taking photographs of decaying mesons in a magnetic field which is sufficiently strong to permit the measurement of the momentum of the decay electron.

340. The conception of the neutrino was originally introduced by Fermi in order to safeguard the conservation of momentum, energy, and angular momentum in the process of β-disintegration. The cross-sections derived for the interaction of neutrinos with matter are, however, so small that the probability of observing a neutrino interacting with matter seems to be negligible.

It is very unsatisfactory to have to assume the occurrence of such a particle which has no observable properties: it was therefore suggested by Bohr that it might be preferable to assume the breakdown of the conservation laws instead of assuming the existence of a neutrino.

341. The point of view accepted by many physicists is that the assumption of the existence of the neutrino should be made subject to the outcome of the following kind of experiment.

After the emission of a β-particle by a β-active nucleus a certain amount of energy is 'missing'; this energy may be attributed to the neutrino. At the same time it is expected that the momentum of the system consisting of β-particle and nucleus alone is not conserved during the decay; the 'missing' momentum may be attributed to the neutrino. It is argued that it is reasonable to attribute the missing momentum and the missing energy to one particle if these quantities obey the energy momentum relation (6, Ch. III) in each individual case observed.

Experiments of this kind have been carried out recently by Halpern and Crane (1939) using radio chlorine (Cl^{38}) and improved by Allen (1942) with Be^{7}. The experimental results obtained favour the existence of the neutrino.

342. The meson decay can on this view be taken as the simplest form of β-decay. Observations of the decay electrons should therefore give clear evidence of the existence of the neutrino. The conservation laws require that all decay electrons have the momentum $\mu c/2$ in the rest-

system of the meson. If this could be established experimentally it could be taken as clear evidence in favour of the neutrino.

The alternative possibility would be that decay electrons show a continuous energy spectrum just as in the case of ordinary β-decay. Such a behaviour would have to be interpreted by assuming the breakdown of the conservation laws.

343. It may be noted that, assuming the existence of the neutrino, the decay momentum of the electron could be used to determine the meson mass μ accurately, by means of eq. (24).

(c) *Direct Measurement of the Half-life of the Meson*

344. The half-life of mesons can be measured directly in the following way. An absorber is placed between two sets of counters, Fig. 53. Particles entering the absorber from above are recorded by the top set of counters. The lower counters are made sensitive by an electric arrangement for a short period after the discharge of any of the top counters. The lower counters are made to register only pulses which occur at a time more than t_1 sec. but less than t_2 sec. after any pulse of the top counters. Such pulses may occur when a meson discharges the top counters and is afterwards brought to rest inside the absorber and decays after a time t with $t_1 < t < t_2$.

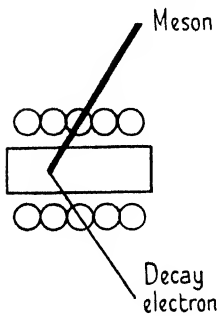

FIG. 53. Arrangement for measuring the half-life of the meson.

Experiments of this kind have been carried out by Montgomery, Ramsey, and Cowie (1939), but they were indecisive. The main difficulty with the arrangement as shown in Fig. 53 is the large background. There are a very large number of discharges of the top counters not due to mesons stopping in the absorber. Thus only a minute fraction of the master pulses of the top counters can be expected to be accompanied by delayed pulses due to decay taking place inside the absorber. Accidentally delayed pulses due to any cause are therefore very important and tend to mask a real effect.

345. An improved arrangement to measure the meson life was used by Maze (1941), by Rasetti (1941), by Auger, Maze, and Chaminade (1942), by Rossi and Nereson (1942, 3). The arrangement is shown in Fig. 54 and works as follows. The absorber S is placed below a coincidence arrangement I–II. A set of anticoincidence counters A is placed below S. Anticoincidences I, II—A are caused mainly by particles coming from above and stopping in S. To reduce the effect of showers

the top counters are surrounded by lead and a lead block 10 cm. thick is placed between the coincidence counters. Due to this selection the anticoincidences are mainly due to mesons stopping in S.

The sides of the absorber S are covered with a counter battery. The counter battery is made sensitive immediately after each anti-coincidence. If any of the counters a are discharged shortly after the coincidence pulse, then the pulse is recorded and the time delay between

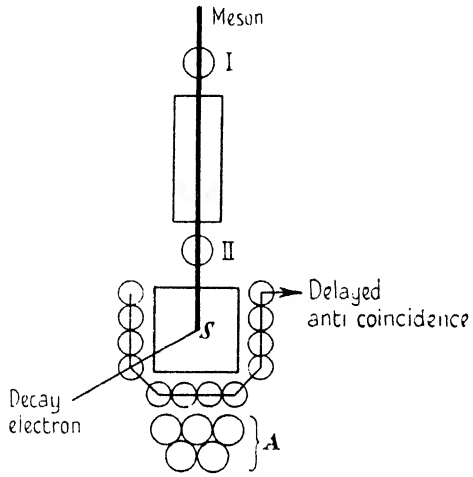

FIG. 54. Improved arrangement for measuring the half-life of the meson.

the anticoincidence and the pulse of the counter a is also recorded. Such delayed pulses are mainly due to mesons stopping in S and emitting a decay electron afterwards. The registered time delay can be regarded as the time spent by the meson in the absorber before it decayed.

As a result of extensive measurements it was found that the rate of delayed pulses corresponding to delays greater than t is given by

$$\mathscr{C}\ (>t) \sim e^{-t/t_0}, \tag{44}$$

with

$$t_0 = \begin{cases} 2{\cdot}2 \pm 0{\cdot}2 & \text{Chaminade, Fréon, and Maze (1944),} \\ 2{\cdot}15 \pm 0{\cdot}1\ \mu\text{sec.} & \text{Rossi and Nereson (1943),} \\ 1{\cdot}5 \pm 0{\cdot}4 & \text{Rasetti (1941).} \end{cases} \tag{45}$$

The numerical value obtained by Maze and by Rossi may be the more accurate ones; Rossi calibrated his arrangement with a quartz-oscillator of known frequency.

From equation (44) it is seen that mesons decay at random times.

346. Comparing the rate of anticoincidences with the rate of delayed pulses, it can be determined roughly what fraction of those mesons which are stopping in the absorber is emitting decay electrons.

Rasetti (1941), and also Rossi and Nereson (1943), came to the conclusion that only about half of the mesons emit electrons. It was suggested as a possible explanation that negative mesons may be liable to be captured by nuclei before decaying, so that only the decay electrons of positive mesons will be observed.

The experiments of Conversi, Pancini, Picciani (1945), in which the mesons are deflected by a magnetic field before decaying, confirm the above suggestion.

347. We note that according to Heitler and Peng (1944) slow mesons may transform into neutral mesons in collisions with nuclei. The possibility of a meson being absorbed by a nucleon emitting a photon of energy μc^2 must also be considered (Ferretti). These processes may remove a fraction of the slow mesons. (A charged meson changing into a neutral meson would give rise to an anticoincidence but not to a delayed pulse; a neutral meson changing into a charged meson while passing through S would not be noticed at all.)

348. The above experiments have no bearing on the question whether mesons with a half-life much less than 2 μsec. occur (see § 220). Decay electrons emitted after a time much less than 2 μsec. would not have been resolved by the arrangement and thus would not have been recorded at all.

2. *Indirect Evidence for the Instability of Mesons*

349. The absorption of a beam of fast mesons is mainly due to two processes. Firstly, ordinary absorption: that is, mesons are slowed down due to elastic collisions. Secondly, mesons are removed from the beam due to the spontaneous decay. The ordinary absorption is nearly mass-proportional, while the decay is quite independent of the material. The two effects together give rise to the so-called absorption anomaly. This is that the mass absorption of a beam appears to be greater in air than in a dense medium. All measurements of the half-life of fast mesons are connected with observations of the absorption anomaly.

(*a*) *Observation of the Absorption Anomaly*

(i) Directional distribution

350. The absorption anomaly was observed by Follet and Crawshaw (1936); they found that the vertical intensity at a depth θ under ground

is larger than the intensity at sea-level inclined at ϑ to the vertical, where

$$(\theta + \theta_0)\cos\vartheta = \theta_0. \tag{46}$$

If the absorption of the cosmic rays in various materials was proportional to mass, the two intensities would be equal.

The absorption anomaly was also observed by Auger, Ehrenfest, Fréon, and Fournier (1937) in a series of counter experiments. The intensity of cosmic rays at various heights and in various directions was measured. If the cosmic-ray particles were stable, as they were supposed to be at that time, the cosmic-ray intensity in any direction and at any height above sea-level should be a function of $\theta \sec\vartheta$, where ϑ is the angle of incidence and θ is the absorption equivalent of the atmosphere above the observer. In particular, the vertical intensity observed at A should be equal to the intensity in a direction inclined by ϑ to the vertical at a point B, provided

$$\theta_A = \theta_B \sec\vartheta, \tag{47}$$

where θ_A, θ_B are the absorption equivalents of the atmosphere above the points A and B. The observations of Auger and co-workers showed that these two intensities were in fact very different, the vertical intensities at the lower stations being considerably larger than the corresponding inclined intensities at the higher stations.

351. The anomalies were interpreted in terms of the instability of the meson by Kulenkamff (1938). Considering mesons of momentum P_1 arriving vertically at A and those at an angle ϑ at B the ratio of the intensities is found with help of (20) and (23).

To get an idea of the magnitude of the anomaly, the following numerical values may be considered. At the Jungfrau Joch (3,400 m. above sea-level) we have $\theta_B = 600$ grams/cm.^{2} Comparing with sea-level observations we have

$$\cos\vartheta = \frac{\theta_B}{\theta_0} = 0{\cdot}6$$

and $\vartheta = 53°$. Thus the intensity inclined at 53° on the Jungfrau can be compared with the vertical intensity at sea-level. Assume $P_A = 2.10^9$ eV. and as a rough average $P_1 = 10^9$ eV. Assuming further $\theta_P = \theta_0/10$, which means that the mesons are produced at a height of about 16 km., we find

$$\mathcal{N}(\theta_B, \vartheta)/\mathcal{N}(\theta_0, 0) \sim \tfrac{1}{2}. \tag{48}$$

Auger and his co-workers found for this ratio 0·6; thus the calculated value is of the right order of magnitude. A better agreement could not be expected in view of the very schematic treatment.

(ii) The temperature effect

352. A negative correlation between temperature and cosmic-ray intensity has been found. This effect can be accounted for according to Blackett (1938*b*) in terms of the instability of the meson. Consider a change of the atmospheric temperature by $\delta\Theta$. If this change is not accompanied by a change of pressure then it can be assumed to cause an expansion of the atmosphere, and the height of the homogeneous atmosphere can be assumed to change by

$$\delta\lambda_0 = \lambda_0 \frac{\delta\Theta}{\Theta}. \tag{49}$$

The corresponding change of the rate of mesons with momentum P_1 arriving vertically at sea-level is obtained from (20) and (49):

$$\frac{\delta\mathcal{N}}{\mathcal{N}} = -\frac{\lambda_0}{c\ell_0}\frac{\mu c}{P_1+P_A} \times \log\left\{\frac{\theta_0}{\theta_P}\left(1+\frac{P_A}{P_1}\right)-\frac{P_A}{P_1}\right\}\frac{\delta\Theta}{\Theta}. \tag{50}$$

To obtain the temperature coefficient we have to average $\delta\mathcal{N}/\mathcal{N}$ over the momentum spectrum. We may put in good approximation

$$\left\langle \frac{\log\{(\theta_0/\theta_P)(1+P_A/P_1)-P_A/P_1\}}{P_A+P_1} \right\rangle = \left\langle \frac{1}{P_A+P_1} \right\rangle \log\left\{\frac{\theta_0}{\theta_P}\left(1+\frac{P_A}{\langle P_1\rangle}\right)-\frac{P_A}{\langle P_1\rangle}\right\}. \tag{51}$$

Introducing into (51) the numerical values given in eqs. (21), Ch. IV, and (22), Ch. IV, and assuming $P_A = 2{,}000$, $\theta_0/\theta_P = 10$, $\Theta = 300$, we obtain for the temperature coefficient

$$\Gamma_{\mathcal{N}\Theta} \equiv \left\langle \frac{100}{\mathcal{N}}\frac{\partial\mathcal{N}}{\partial\Theta} \right\rangle = -0{\cdot}35 \text{ per cent. per deg. K.} \tag{52}$$

This value is slightly larger than that found by Compton and Turner (1937) from the seasonal variation of cosmic-ray intensity, namely

$$\Gamma_{\mathcal{N}\Theta} = -0{\cdot}18 \pm 0{\cdot}011 \text{ per cent. per deg. K.}$$

The agreement between the data is as good as could be expected from the schematic treatment of the effect.

(iii) Barometer effect

353. Closely connected with the temperature effect is the barometer effect. An increase of the air pressure by db cm. Hg corresponds to an increase of the absorption equivalent of the atmosphere by

$$d\theta = db.13{\cdot}6. \tag{53}$$

Apart from the effects due to instability, the change in pressure causes

therefore a change in intensity. The barometer coefficient due to this process can be obtained with help of eq. (25), Ch. IV, as

$$\Gamma^{(1)}_{\mathcal{N}b} = \frac{100}{\mathcal{N}}\left(\frac{\partial \mathcal{N}}{\partial b}\right)_{\mathfrak{z}=\text{const.}} = -100\frac{1{\cdot}6}{b} = -2{\cdot}1 \text{ per cent. per cm. Hg.} \tag{54}$$

The increase of pressure is accompanied by an increase of $\mathfrak{z}_0$; we have

$$d\mathfrak{z}_0 = \mathfrak{z}_0 \frac{db}{b}. \tag{55}$$

Neglecting changes in P_A and θ_0 under the logarithm we find for the regression coefficient of this second effect, with the help of (20), (50), and (51),

$$\Gamma^{(2)}_{\mathcal{N}b} = \frac{(\cdot)}{b}\Gamma_{\mathcal{N}\Theta} = -1{\cdot}4 \text{ per cent. per cm. Hg.} \tag{56}$$

Adding the two effects we find

$$\Gamma_{\mathcal{N}b} = \Gamma^{(1)}_{\mathcal{N}b} + \Gamma^{(2)}_{\mathcal{N}b} = -3{\cdot}5 \text{ per cent. per cm. Hg.}$$

The above value for the barometer coefficient is somewhat larger than the value obtained from observations with the ionization chamber but it agrees well with the counter observations of Duperier (1944*a*), namely

$$\Gamma_{\mathcal{N}b} = -3{\cdot}45 \text{ per cent. per cm. Hg (Duperier).}$$

(iv) Effects of temperature and pressure distribution

354. The main weakness of the preceding treatments of the temperature effect and of the barometer effect is that the atmosphere is assumed to have uniform temperature distribution. In reality the temperature of the atmosphere changes with height and a change of pressure or temperature near sea-level may be accompanied by a complicated change of the temperature distribution.

The height of formation of mesons is given by

$$\mathfrak{z} = \mathfrak{z}_0 \int_{\theta_P}^{\theta_0} \frac{\Theta(\theta)}{\Theta_0}\frac{d\theta}{\theta}, \tag{57}$$

where $\Theta(\theta)$ is the temperature at a level corresponding to a pressure $b = \theta/13{\cdot}6$. The values of $\Theta(\theta)$ can be obtained from meteorological records and thus $\mathfrak{z}$ can be evaluated for the periods of observation. Comparing records obtained during periods of equal pressure but different temperature distributions one expects a good correlation between $\mathfrak{z}$ as obtained from (57) and the observed intensities.

A correlation of this kind was carried out by various observers.

Duperier (1944*b*) carried out the correlation with various assumptions as to the value of θ_P. The correlation coefficients thus obtained are as follows:

TABLE 2

θ_P gm./cm.^{2}	*Height in km.*	$\gamma_{\mathcal{N}_3}$
100	16·1	−0·67
153	13·5	−0·54
255	10·3	−0·32
510	5·5	−0·30

The correlation improves with decreasing θ_P; the best correlation is found for $\theta_P = 100$ grams per cm.^{2}, the smallest value used.

These results show that most mesons are produced by primaries with a mean range of the order of or smaller than 100 grams per cm.^{2}

355. It seems to be possible to account for both the barometer effect and the temperature effect on the lines described above. Many details are, however, still obscure and much more experimental material will be needed.

The barometer and temperature effects may in future prove to be very useful to meteorology as the variations of cosmic radiation may be found to be a useful indicator of the temperature and pressure distribution of the atmosphere.

The main difficulty for the meteorological application seems to be that the cosmic-ray intensity shows occasional variations due to causes which cannot be traced. Variations occur in connexion with magnetic storms. There are cases where the correlation of the magnetic intensity with the cosmic-ray intensity is very pronounced. The detailed connexion is, however, very obscure. Large magnetic disturbances may be accompanied by large or small changes of intensity and cases of large changes of intensity during slight magnetic disturbances have also been observed.

(*b*) *Measurement of the Ratio* μ/t_0

356. The observation of the absorption anomaly permits the experimental determination of the ratio μ/t_0. As t_0 can be measured directly, the anomalies can be used to determine the rest-mass μ.

The effects described in §§ 350–5 were analysed by Euler and Heisenberg (1938) and it was found that they can be interpreted by assuming

$$t_0 = 2{\cdot}7.10^{-6} \text{ sec.} \quad \text{for} \quad \mu = 80 \text{ MEV.}/c^2.$$

(The value of μ was of course assumed to be known from cloud-chamber evidence.)

These effects are, however, not very suitable for the exact determination of the ratio μ/ℓ_0, as their interpretation depends upon $_3P$, the height of formation of the mesons, and also on the air distribution over the observer. Experiments which permit a simpler interpretation have been carried out by Rossi, Hilbery, Hoag (1940), and by Neher and Stever (1940), and others.

Anomaly under controlled conditions

357. In these experiments it is attempted to compare the absorption of a well-defined cosmic-ray beam in air with the absorption of a similar beam in a dense material. The absorption in the dense material can be chiefly attributed to the stopping down of mesons in the absorber. In air the absorption is due to both the stopping down of particles and the decay of mesons. The difference between the absorption in a dense absorber and an equivalent amount of air gives the effect due to decay alone.

358. A difficulty arises, as according to Fermi (1939) the rate of loss of particles in a gaseous state may differ from the rate of loss in the same element when in the solid state, the reason for the difference being the polarization of the crystal lattice by the passing particle. Calculation showed, however, that the effect of polarization is small and it cannot be responsible for more than a small fraction of the observed anomalies.

Average decay probability of the mesons in the hard component

359. The actual experimental procedure of Rossi, Hilbery, and Hoag (1940) is as follows.

The vertical meson intensity was measured with a coincidence arrangement at various heights above sea-level; and thus an absorption curve of the meson intensity in air was obtained. At each elevation the absorption of the cosmic-ray beam was measured in carbon by placing absorbers of carbon on top of the coincidence arrangement.

The experimental results thus obtained are shown in Fig. 55. The full curve represents the height-intensity curve obtained without carbon absorber. The dotted lines branching off the main curve show the absorption of the cosmic rays in carbon at the various stations. The difference between the dotted and full curves is due to decay.

360. If all mesons had the same momentum p, then the fraction of mesons decaying in a layer $d\theta$ of air would be

$$\frac{d\theta}{k}\frac{\mu}{\ell_0}\frac{1}{p}, \tag{58}$$

where k is the density of air.

The rate of absorption due to decay is obtained by averaging over the spectrum. We find

$$\frac{1}{\mathscr{C}}\left(\frac{\partial \mathscr{C}}{\partial \theta}\right)_{\text{decay}} = -\frac{1}{k}\frac{\mu}{t_0}\left\langle\frac{1}{p}\right\rangle.$$

And therefore

$$\frac{\mu}{t_0} = \frac{k}{\langle 1/p\rangle}\left\{\frac{1}{\mathscr{C}}\left(\frac{\partial \mathscr{C}}{\partial \theta}\right)_{\text{dense material}} - \frac{1}{\mathscr{C}}\left(\frac{\partial \mathscr{C}}{\partial \theta}\right)_{\text{air}}\right\}.$$

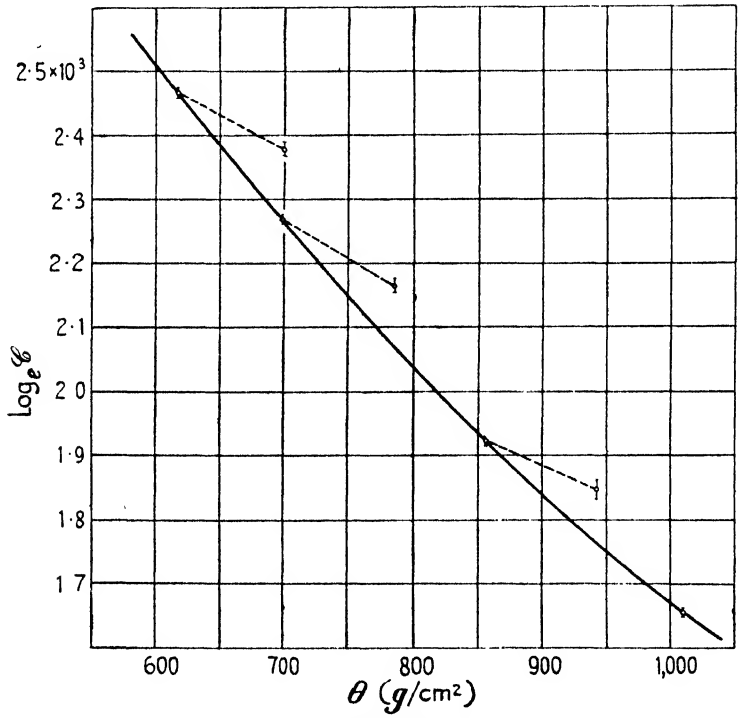

FIG. 55. Intensity of hard component as function of atmospheric depths. From Rossi and others, *Phys. Rev.* **57**, 466.

The numerical results of Rossi, Hilbery, and Hoag (1940) are collected in the following table.

TABLE 3

Depth interval	$-\frac{1}{\mathscr{C}}\left(\frac{\partial \mathscr{C}}{\partial \theta}\right)_{\text{air}}$ 10^{-3} *cm.²/gm.*	$-\frac{1}{\mathscr{C}}\left(\frac{\partial \mathscr{C}}{\partial \theta}\right)_{\text{carbon}}$ 10^{-3} *cm.²/gm.*	$ct_0' = \frac{ct_0}{\langle \mu c/p\rangle}$ 18° C.
616–700	2·42	1·08	$9{\cdot}4 \pm 0{\cdot}9$
699–786	2·295	1·16	$9{\cdot}9 \pm 1{\cdot}2$
857–944	1·824	0·84	$9{\cdot}5 \pm 1{\cdot}7$
1,010	1·47	0·59	$9{\cdot}4 \pm 1{\cdot}6$

$\times 10^5$ cm.

Assuming $1/\langle 1/p\rangle = 1{,}300$ MEV./c, the value obtained from Blackett's spectrum near sea-level, one finds

$$\tau_0' = 2.10^{-6} \text{ sec.} \quad \text{for} \quad \mu c^2 = 100 \text{ MEV.}$$

This value is in good agreement with the directly observed values of μ and τ_0'. The main uncertainty of the method lies in the fact that the energy spectrum has only been measured at sea-level. One would expect $\langle 1/p\rangle$ to change with height. The good agreement between the values of $c\tau_0'$ obtained at different heights seems to indicate that the value of $\langle 1/p\rangle$ does not in fact change very much.

Decay probability as function of momentum

361. The uncertainty due to the energy spectrum can be eliminated by using an arrangement due to Rossi and Hall (1941); see also Rossi,

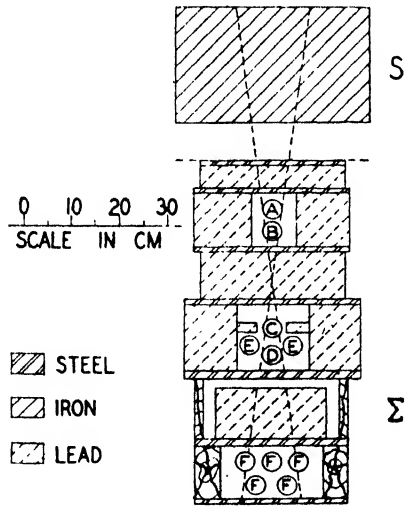

FIG. 56. Experimental arrangement of Rossi and Hall.
From Rossi and others, *Phys. Rev.* **59**, 224.

Greisen, Stearns, Froman, Koontz (1942) (this article gives also full list of references to the literature). This arrangement enables one at the same time to measure the dependence of the apparent lifetime τ_0' on p; it is described in the following.

The coincidence arrangement 1, 2, 3 is replaced by an anticoincidence arrangement A, B, C, D—F (Fig. 56). The anticoincidence counters F are placed below the coincidence system and are separated by some absorber. Anticoincidences are caused by particles which have a sufficient range to cause coincidences A, B, C, D but have too short a range to

penetrate the additional absorber Σ placed between the coincidence and anticoincidence counters. Thus anticoincidences are caused by particles inside a defined range interval and therefore by particles inside a defined momentum interval $p_1 < p < p_2$.

The rate of mesons with momentum between p_1 and p_2 is measured under the following two conditions.

1. At a height ζ' with no absorber Σ above the arrangement (Fig. 57).

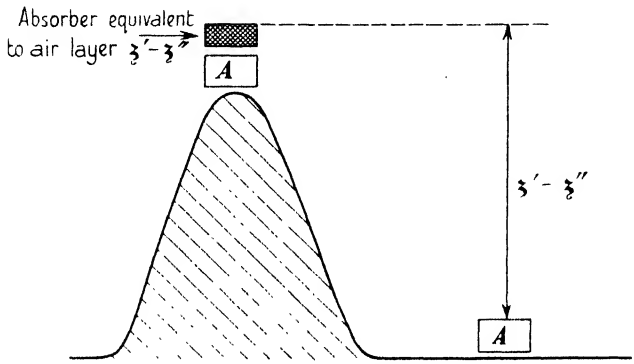

FIG. 57. Scheme of the experiment of Rossi and Hall.

2. At a larger height ζ'' with an absorber Σ above the arrangement having an absorbing effect equal to the layer of air between the two heights. Without decay the two intensities would be equal; the ratio of the intensities can be used to determine the apparent lifetime of mesons in the interval p_1 to p_2.

The dense absorber compensating for the air was of iron. The Bloch formula (§ 237, eq. (164), Ch. III) was used for the comparison of the air and iron absorption equivalents. According to the Bloch formula one finds that 147 grams per cm.^{2} of air is equivalent to 200 grams per cm.^{2} of iron.

In this way Rossi and Hall (1942) found the following values for the mean ranges of mesons:

TABLE 4

Momentum	$10^{-5}c\ell'_0$ = *mean range in* 10^5 *cm.*
Group of mesons round 500 MEV./*c*	4·5±0·6
Mesons with momentum exceeding 580 MEV./*c*	13·3±0·9

It is seen from the above data that the mean life of mesons increases with increasing momentum.

362. The ratio for ℓ_0/μ is obtained from Table 4 as follows:

$$\frac{\ell_0}{\mu} \cdot \frac{100 \text{ MEV.}/c^2}{10^{-6} \text{ sec.}} = 3 \pm 0{\cdot}4.$$

Using the observed value for ℓ_0 we find

$$\mu = (140 \pm 20) m_e.$$

The above value is lower than that observed in the cloud chamber. The discrepancy cannot be taken seriously because of the large experimental errors involved.

We note, however, that the above determination of μ has been carried out assuming that all mesons have the same mass and the same decay constant. Neither of the two assumptions is certain.

It would be most desirable to have more experimental information regarding the absorption anomaly.

363. Ageno and others (1941) have carried out decay observations at high altitudes. These authors find that the average life of the mesons appears to decrease with altitude.

These observations, if further confirmed, may indicate the occurrence of short-lived mesons at high altitudes.

(*c*) *The Relativistic Time Contraction*

364. The observation of the absorption anomaly is of great interest as this anomaly depends not on the proper life ℓ_0 of the meson but upon its apparent life ℓ_0' given in (3).

The proper lifetime ℓ_0 of the meson can be measured directly as was shown in § 345. The analysis of the absorption anomalies can be used for determining ℓ_0'. The comparison of the two measurements can be used therefore to check the relativistic relation (3) experimentally. This is noteworthy as this method permits us for the first time to test experimentally the relativistic time contraction in a region where this contraction does not give rise to a small effect but gives rise to a factor exceeding ten.

365. The relation (3) is confirmed at least roughly by the measurements of Rossi and Hall (1941) and in more detail by Rossi and others (1942), see § 361.

It can be seen, however, that an assumption to the effect that ℓ_0 is not contracted would lead to serious contradiction with observations. Indeed, if no time contraction took place the range of fast mesons would be

$$v\ell_0 \sim c\ell_0 \sim 600 \text{ m}.$$

This value is completely incompatible with the results described in previous paragraphs.

VI

SOFT COMPONENT

366. THE soft component of cosmic rays consists of electrons and photons. In the present chapter we shall deal with the theory of the passage of fast electrons and photons through matter; we shall follow the ideas of Bhabha and Heitler (1937) and of Carlson and Oppenheimer (1937). In the later parts of this chapter it will be shown that most of the observational results concerning behaviour of the soft component can be accounted for in terms of electrons and photons.

The origin of the soft component is, however, only partly understood. The soft component at high altitudes is probably mainly due to primary electrons incident on the top of the atmosphere. The existence of primary electrons is, however, not altogether certain; the arguments in favour of the existence of primary electrons will be dealt with in Chapters VII and VIII.

The soft component at medium heights is at least partly secondary to the meson component. The main processes responsible for the secondary soft component are the emission of decay electrons and the production of electron secondaries. In heavy elements the emission of *bremsstrahlung* by mesons is of importance for the production of energetic cascades.

A. CASCADE THEORY

1. *Statement of the Problem*

367. Fast electrons traversing matter lose energy mainly in inelastic collisions and in radiative collisions. The first process gives rise to ionization along the path of the electron while the second process results in the emission of photons.

The rate of loss of energy due to ionization increases only slowly with increasing energy of the primary; the relative rate of loss of energy

$$(dW/d\theta)_{\text{collision}}/W \approx \frac{\text{const.}}{W}$$

decreases with energy.

The rate of loss in radiative collisions is roughly proportional to the primary energy of the electron. Therefore the relative rate of loss is about constant; thus we have

$$(dW/d\theta)_{\text{radiation}}/W \sim \text{const.}$$

Hence the higher the energy of an electron, the larger amounts of energy

it is likely to lose in its first few collisions. The range of energetic electrons is therefore severely limited by radiation and it can be shown that the range of electrons increases only slightly with increasing primary energy.

Energetic photons traversing an absorber are likely to be absorbed while giving rise to pairs of electrons. The order of magnitude of the cross-section for pair production is independent of the energy of the photon provided the energy exceeds say 10 MEV. Therefore the range of photons, like the range of energetic electrons, does not increase with increasing primary energy.

Considering the cross-sections for pair production and for radiative collisions as given in §§ 245, 246, we find the following values for the mean ranges of electrons and photons:

TABLE 1

	Mean range in cm.	
	Lead	*Aluminium*
Electrons . .	0·5	10
Photons . . .	0·7	14

368. An electron falling on an absorber is soon slowed down, its energy being transferred to a small number of energetic photons. An energetic photon when absorbed giving rise to an electron pair produces at least one energetic electron, as at least one of the electrons of the pair must have an energy of the same order as the energy of the photon.

Thus electrons when absorbed give rise to energetic photons and the photons in their turn give rise to energetic electrons. The process goes on and the primary energy is distributed to a growing number of electrons and photons. The process comes eventually to an end due to the loss of energy by ionization.

The above process is called an electron cascade. It was first pointed out and investigated by Bhabha and Heitler (1937) and by Carlson and Oppenheimer (1937) (Fig. 58).

369. In the first part of this chapter we shall reproduce the mathematical treatment of the cascade process. Thus we shall deal with the question as to the numbers of photons and electrons produced in a given absorber by a primary electron or photon.

We note that this problem is essentially a statistical problem. The laws of collisions are probability laws and therefore the exact number of secondaries produced by a given electron varies.

In the following treatment of the problem we shall determine the *average* number of secondaries produced by a primary of given energy; further we shall quote some results as to the scatter of the actual numbers round the average.

The mathematically very difficult stochastic problem of determining how the actual numbers of shower particles are distributed round the average number has not been solved so far.

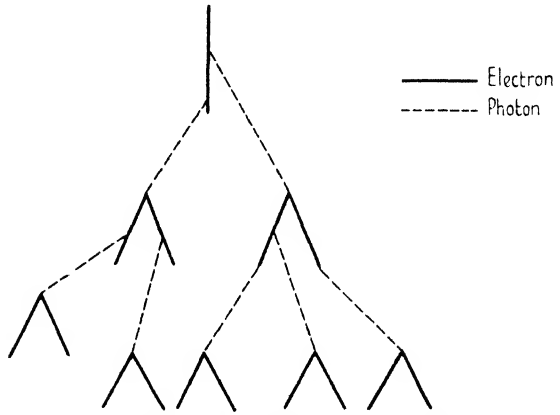

FIG. 58. Schematic representation of cascade shower.

We shall follow a procedure given by Landau and Rumer (1938) and elaborated by Snyder (1938), Serber (1938), Iwanenko and Sokolow (1938), Tam and Belenky (1939), Schönberg (1940), Rossi and Greisen (1941), Bhabha and Chakrabarty (1943).

2. *The Diffusion Problem*

(*a*) *Preliminaries*

Units of length and energy

370. The cross-sections for radiative collisions and for the production of electron pairs by photons are both proportional to

$$\frac{4Z^2}{137}r_0^2\log_e(183Z^{-\frac{1}{3}}), \qquad r_0 = \frac{e^2}{m_e c^2}.$$

It is therefore useful to introduce as the unit of length in an absorber

$$\Delta = \left(\frac{4NZ^2}{137}r_0^2\log_e(183Z^{-\frac{1}{3}})\right)^{-1}, \tag{1}$$

where N is the number of atoms per unit volume.

It is convenient to introduce an energy W_c equal to the energy lost due to ionization by a fast particle along one cascade unit.

We have thus $$W_c = -\left(\frac{dW}{d\theta}\right)_{\text{collision}, W=W_c}. \tag{2}$$

We note that the rates of loss due to ionization and due to radiation are about equal for an electron of energy W_c.

For energies below W_c the loss due to ionization is more important than that due to radiation, above W_c the energy loss due to radiation becomes predominant.

371. In the following we shall write ζ for a thickness expressed in cascade units and we shall write w for an energy when expressed in units of W_c. Thus we have

$$\zeta = \theta/\Delta, \qquad w = W/W_c. \tag{3}$$

The rate of loss of energy due to ionization expressed in cascade units is nearly unity:

$$o = -\left(\frac{dw}{d\zeta}\right)_{\text{coll.}} \sim 1 \quad \text{(compare (2))}. \tag{4}$$

The critical energy W_c and the cascade unit Δ have the following numerical values:†

Substance:	Air	H_2O	Al	Fe	Pb
W_c	103·0	114·6	55·56	25·88	6·927 MEV.
Δ	34·200	43·4	9·80	1·84	0·525 cm.
	44·2	43·4	26·5	14·4	5·83 gm./cm.^{2}

372. The probabilities for radiative collisions are independent of material, if expressed in cascade units, provided full screening can be assumed (compare § 245). The latter condition is fulfilled for the collision of an electron energy W, producing a photon energy W' provided we have

$$\frac{W(W-W')}{W'm_ec^2} \gg 137Z^{-\frac{1}{3}}. \tag{5}$$

For light elements the condition (5) affects mainly particles with energies below W_c, while for heavier elements collisions involving energies appreciably above W_c are still affected (see Fig. 59).

For mathematical convenience we shall disregard the condition (5). This will cause errors in the calculated numbers of low-energy particles, the errors being more serious in the case of heavy elements than in the case of lighter elements.

† Arley (1938) gives a slightly different definition, see § 390, eq. (79).

We shall thus base further calculations on the following probabilities.

Let
$$\mathfrak{H}(w, w') = 1-(\tfrac{4}{3}+\alpha_0)\left(\frac{w}{w'}-\frac{w^2}{w'^2}\right) \tag{6}$$

with
$$\alpha_0 = \frac{1}{9\log 183 Z^{-\frac{1}{3}}}. \tag{6a}$$

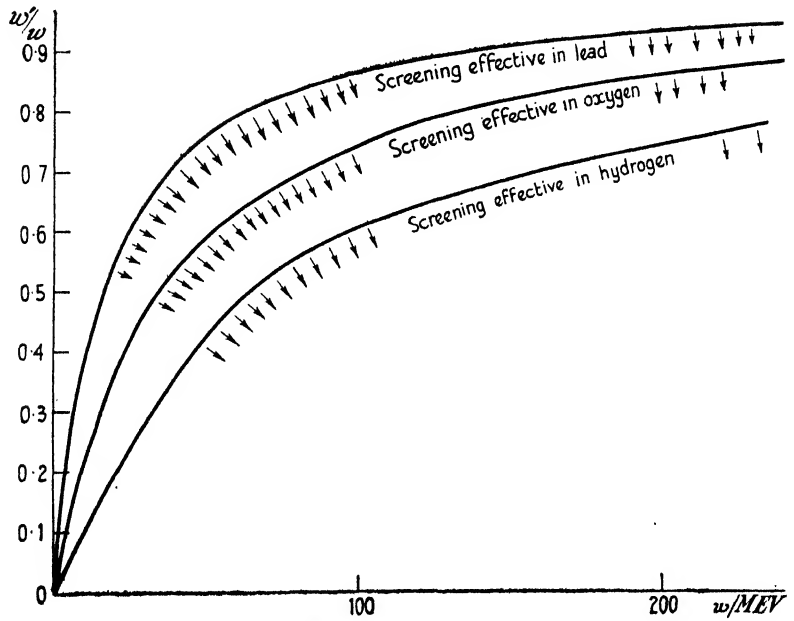

FIG. 59. Energy regions affected by screening.

The quantity α_0 depends slightly on Z. As α_0 represents a small correction only we shall disregard the dependence of α_0 upon Z and assume as an average value

$$\alpha_0 = 0{\cdot}0246. \tag{6b}$$

1. The probability of an electron of energy w emitting a photon with energy in the interval w', dw' along the path $d\zeta$ is given by

$$\mathfrak{H}(w, w')\frac{w'\,dw'}{w^2}d\zeta. \tag{7}$$

2. The probability of a photon of energy w giving rise to a pair along a distance $d\zeta$ is given by

$$\mathfrak{H}(w', w)\frac{dw'}{w}d\zeta; \tag{8}$$

it is assumed that the energy of the positive electron is in the interval

w', dw'. The probability for the production of a pair in which the negative electron is in the interval w', dw' is also given by (8).

(*b*) *Diffusion Equation*

Derivation of the diffusion equation

373. Denote by $\mathfrak{q}(w,\zeta)\,dw$ the number of electrons (positive and negative) with energies in the interval w, dw at a depth ζ. Denote similarly the number of photons at the same depth and in the same energy interval by $\mathfrak{p}(w,\zeta)\,dw$. The number of electrons and photons changes when going from the depth ζ to the depth $\zeta+d\zeta$ due to the following processes.

1. The number of electrons is increased due to pairs produced by photons. The probability of a photon of energy w' giving rise to an electron in the interval w, dw is obtained from (8) as

$$2\mathfrak{H}(w,w')\frac{dw}{w'}d\zeta;$$

the factor 2 takes care of the contributions of electrons of both signs. The total number of electrons in the interval w, dw thus produced is obtained by integrating over the photon spectrum. We find

$$dq_1 = 2\,d\zeta dw\int_w^\infty \mathfrak{p}(w',\zeta)\mathfrak{H}(w,w')\frac{dw'}{w'}. \tag{9}$$

2. Electrons with energies in w, dw emitting quanta are lost out of the interval. The change due to this process is given by

$$dq_2 = -\mathfrak{q}(w,\zeta)\,dwd\zeta\int_0^w \mathfrak{H}(w,w')\frac{w'\,dw'}{w^2}. \tag{10}$$

3. Electrons with energy w' may lose $w'-w$ by emission of a quantum and thus contribute to the interval w, dw the following amount:

$$dq_3 = dwd\zeta\int_w^\infty \mathfrak{q}(w',\zeta)\mathfrak{H}(w,w'-w)\frac{(w'-w)\,dw'}{w'^2}. \tag{11}$$

4. The energy of each electron changes by $o\,\delta\zeta$ due to collision loss, giving rise to a change

$$dq_4 = o\,dwd\zeta\frac{\partial\mathfrak{q}(w,\zeta)}{\partial w}, \qquad o = -\left(\frac{\partial w}{\partial\zeta}\right)_{\text{coll.}} \sim 1. \tag{12}$$

5. The number of quanta is increased due to the emission of quanta of energy w, dw by electrons of higher energies. This gives rise to

$$dp_1 = dw d\zeta \int_w^\infty q(w', \zeta) \mathfrak{H}(w', w) \frac{w\, dw'}{w'^2}. \tag{13}$$

6. Finally, quanta are lost out of the interval as they give rise to pairs. We find for the last contribution

$$dp_2 = -p(w, \zeta)\, dw d\zeta \int_0^w \mathfrak{H}(w', w) \frac{dw'}{w}. \tag{14}$$

Taking the contributions of the various processes together we find the following diffusion equations for q and p:

$$\begin{aligned}
\frac{\partial q(w, \zeta)}{\partial \zeta} &= \int_w^\infty q(w', \zeta) \mathfrak{H}(w', w'-w) \frac{(w'-w)\, dw'}{w'^2} + \\
&+ 2 \int_w^\infty p(w', \zeta) \mathfrak{H}(w, w') \frac{dw'}{w'} - q(w, \zeta) \int_0^w \mathfrak{H}(w, w') \frac{w'\, dw'}{w^2} + o \frac{\partial q(w, \zeta)}{\partial w}, \\
\frac{\partial p(w, \zeta)}{\partial \zeta} &= \int_w^\infty q(w', \zeta) \mathfrak{H}(w', w) \frac{w\, dw'}{w'^2} - p(w, \zeta) \int_0^w \mathfrak{H}(w', w) \frac{dw'}{w}.
\end{aligned} \tag{15}$$

We shall first give a solution of the system (15) neglecting the term

$$o \frac{\partial q(w, \zeta)}{\partial w}$$

which takes care of ionization loss. We shall denote the solution of the approximate equation (i.e. $o \sim 0$) without the ionization term with a suffix 0. Thus we shall write

$$q_0(w, \zeta), \qquad p_0(w, \zeta)$$

for the approximate solutions of (15).

Laplace transform of the diffusion equation

374. It was noticed by Landau and Rumer (1938) and others that the equations (15) can be simplified by introducing the Laplace transforms† of the functions q and p.

† For Laplace transformation and the Mellin transform compare e.g. Carslaw and Jaeger, *Operational Methods*, Oxford, 1941.

We thus introduce

$$\mathfrak{L}_{\mathfrak{q}}(\mathfrak{y},\zeta)=\int_0^\infty w^{\mathfrak{y}-1}\mathfrak{q}(w,\zeta)\,dw;\qquad \mathfrak{L}_{\mathfrak{p}}(\mathfrak{y},\zeta)=\int_0^\infty w^{\mathfrak{y}-1}\mathfrak{p}(w,\zeta)\,dw, \quad (16)$$

where $\mathfrak{y}$ is an arbitrary parameter. The functions $\mathfrak{q}$ and $\mathfrak{p}$ can be determined from their Laplace transforms $\mathfrak{L}_{\mathfrak{q}}$ and $\mathfrak{L}_{\mathfrak{p}}$ by means of the Mellin transformation†

$$\left.\begin{aligned}\mathfrak{q}(w,\zeta)&=\frac{1}{2\pi i}\int_{\mathfrak{y}_0-i\infty}^{\mathfrak{y}_0+i\infty} w^{-\mathfrak{y}}\mathfrak{L}_{\mathfrak{p}}(\mathfrak{y},\zeta)\,d\mathfrak{y},\\ \mathfrak{p}(w,\zeta)&=\frac{1}{2\pi i}\int_{\mathfrak{y}_0-i\infty}^{\mathfrak{y}_0+i\infty} w^{-\mathfrak{y}}\mathfrak{L}_{\mathfrak{p}}(\mathfrak{y},\zeta)\,d\mathfrak{y},\end{aligned}\right\} \quad (17)$$

where $\mathfrak{y}_0$ has to be chosen so that for values of $\mathfrak{y}$ with the real part of $\mathfrak{y} > \mathfrak{y}_0$ $\mathfrak{L}_{\mathfrak{q}}$ and $\mathfrak{L}_{\mathfrak{p}}$ are analytic. The path of integration has to be chosen to the right of the imaginary axis and to the right of all singularities of the integrands.

375. In order to introduce the Laplace transforms $\mathfrak{L}_{\mathfrak{q}}$ and $\mathfrak{L}_{\mathfrak{p}}$ into (15), we multiply the equations by $w^{\mathfrak{y}-1}$ and integrate from 0 to infinity. We find for instance for the first term of the first equation (15) with help of (6)

$$\int_0^\infty w^{\mathfrak{y}-1}\,dw\int_w^\infty \mathfrak{q}(w',\zeta)\mathfrak{H}(w',w'-w)\frac{w'-w}{w'^2}\,dw'$$
$$=\left\{\frac{1}{\mathfrak{y}}-\frac{1}{\mathfrak{y}+1}+(1+\tfrac{4}{3}\alpha_0)\int_0^1\frac{\epsilon^{\mathfrak{y}}}{1-\epsilon}\,d\epsilon\right\}\mathfrak{L}_{\mathfrak{q}}(\mathfrak{y},\zeta);$$

all other terms, except that due to ionization loss, can be treated similarly. The ionization term can be transformed, integrating by parts:

$$\int_0^\infty w^{\mathfrak{y}-1}\frac{\partial\mathfrak{q}(w,\zeta)}{\partial w}\,dw=[w^{\mathfrak{y}-1}\mathfrak{q}(w,\zeta)]_0^\infty-(\mathfrak{y}-1)\int_0^\infty w^{\mathfrak{y}-2}\mathfrak{q}(w,\zeta)\,dw. \quad (18)$$

The expression in the square brackets vanishes for the upper limit if we exclude the presence of particles of infinite energy. It vanishes for the lower limit also provided the real part of $\mathfrak{y}$ is greater than 1, and provided $\mathfrak{q}(w,\zeta)$, $w\to 0$, is finite. The latter will be shown to be correct farther down.

† See note †, p. 208.

Thus with the help of (15) and (16) we obtain the following differential equations

$$\frac{\partial \mathscr{L}_q(\mathfrak{y},\zeta)}{\partial \zeta} = -\mathfrak{A}(\mathfrak{y})\mathscr{L}_q(\mathfrak{y},\zeta)+\mathfrak{B}(\mathfrak{y})\mathscr{L}_p(\mathfrak{y},\zeta)-(\mathfrak{y}-1)\mathscr{L}_q(\mathfrak{y}-1,\zeta)\,.\,o,$$
$$\frac{\partial \mathscr{L}_p(\mathfrak{y},\zeta)}{\partial \zeta} = \mathfrak{C}(\mathfrak{y})\mathscr{L}_q(\mathfrak{y},\zeta)-\mathfrak{D}\mathscr{L}_p(\mathfrak{y},\zeta); \tag{19}$$

the following abbreviations have been used

$$\mathfrak{A}(\mathfrak{y}) = \int_0^1 \left\{\epsilon-(\tfrac{4}{3}+\alpha_0)\left(1-\frac{1}{\epsilon}\right)\right\}\{1-(1-\epsilon)^{\mathfrak{y}-1}\}\,d\epsilon$$
$$= (\tfrac{4}{3}+\alpha_0)\{\Psi(\mathfrak{y})-\Psi(1)\}+\tfrac{1}{2}-\frac{1}{\mathfrak{y}(\mathfrak{y}+1)}; \qquad \Psi(\mathfrak{y}) = \frac{d}{d\mathfrak{y}}\log(\mathfrak{y}!),$$
$$\mathfrak{B}(\mathfrak{y}) = 2\int_0^1 \{1-(\tfrac{4}{3}+\alpha_0)(\epsilon-\epsilon^2)\}e^{\mathfrak{y}-1}\,d\epsilon = 2\left\{\frac{1}{\mathfrak{y}}-(\tfrac{4}{3}+\alpha_0)\frac{1}{(\mathfrak{y}+1)(\mathfrak{y}+2)}\right\},$$
$$\mathfrak{C}(\mathfrak{y}) = \int_0^1 \left\{1-(\tfrac{4}{3}+\alpha_0)\left(\frac{1}{\epsilon}-\frac{1}{\epsilon^2}\right)\right\}\epsilon^{\mathfrak{y}}\,d\epsilon = \frac{1}{\mathfrak{y}+1}+(\tfrac{4}{3}+\alpha_0)\frac{1}{\mathfrak{y}(\mathfrak{y}-1)},$$
$$\mathfrak{D} = \int_0^1 \{1-(\tfrac{4}{3}+\alpha_0)(\epsilon-\epsilon^2)\}\,d\epsilon = \tfrac{7}{9}-\tfrac{1}{6}\alpha_0. \tag{20}$$

Differentiating the first of the equations (19) with respect to ζ and eliminating the terms containing $\mathscr{L}_p$ with help of the old equation one obtains the following differential equation:

$$\frac{\partial^2 \mathscr{L}_q}{\partial \zeta^2}+\{\mathfrak{A}(\mathfrak{y})+\mathfrak{D}\}\frac{\partial \mathscr{L}_q}{\partial \zeta}+\{\mathfrak{A}(\mathfrak{y})\mathfrak{D}-\mathfrak{B}(\mathfrak{y})\mathfrak{C}(\mathfrak{y})\}\mathscr{L}_q$$
$$= o(\mathfrak{y}-1)\left(\mathfrak{D}+\frac{\partial}{\partial \zeta}\right)\mathscr{L}_q(\mathfrak{y}-1,\zeta), \tag{21}$$

containing only $\mathscr{L}_q$ and its derivatives.

376. The Laplace transforms for $\mathfrak{y} = 1, 2$ have simple physical significance. From (16) it is seen that

$$\mathscr{L}_q(1,\zeta), \qquad \mathscr{L}_p(1,\zeta)$$

are the numbers of particles and photons at a depth ζ, while

$$\mathscr{L}_q(2,\zeta), \qquad \mathscr{L}_p(2,\zeta)$$

are equal to the total energies carried by electrons and by photons.

From (20) we find

$$\mathfrak{A}(2) = \mathfrak{C}(2), \qquad \mathfrak{B}(2) = \mathfrak{D}. \tag{22}$$

Adding the equations (19) with the help of the equations (22) we find

$$\frac{\partial}{\partial\zeta}\{\mathscr{L}_q(2,\zeta)+\mathscr{L}_p(2,\zeta)\} = -\,o\,\mathscr{L}_q(1,\zeta). \tag{23}$$

This equation shows that the energy in the cascade is conserved. The left-hand side gives the rate of decrease of the total energy of particles and photons. The right-hand expression represents the rate of loss due to ionization.

3. *Formal Solution of the Diffusion Equations neglecting Ionization*

(*a*) *Solution of the Transformed Equation*

General solution

377. In the following we shall give the solutions of the transformed diffusion equations (19) neglecting ionization. Thus we shall solve the equations

$$\begin{aligned}\frac{\partial\mathscr{L}_{q_0}(\eta,\zeta)}{\partial\zeta} &= -\mathfrak{A}(\eta)\mathscr{L}_{q_0}(\eta,\zeta)+\mathfrak{B}(\eta)\mathscr{L}_{p_0}(\eta,\zeta),\\ \frac{\partial\mathscr{L}_{p_0}(\eta,\zeta)}{\partial\zeta} &= \mathfrak{C}(\eta)\mathscr{L}_{q_0}(\eta,\zeta)-\mathfrak{D}\mathscr{L}_{p_0}(\eta,\zeta).\end{aligned} \tag{24}$$

Equations (24) are a system of linear and homogeneous differential equations with constant coefficients of the first order; therefore their solutions can be represented as the linear combination of two exponentials

$$e^{-\alpha_1(\eta)\zeta}, \qquad e^{-\alpha_2(\eta)\zeta}.$$

α_1 and α_2 are the roots of the following quadratic equation

$$\begin{vmatrix} -\mathfrak{A}(\eta)+\alpha(\eta) & \mathfrak{B}(\eta) \\ \mathfrak{C}(\eta) & -\mathfrak{D}+\alpha(\eta) \end{vmatrix} = 0. \tag{25}$$

We shall write for the solutions of (25)

$$\begin{aligned}\alpha_1(\eta) &= \tfrac{1}{2}\{\mathfrak{A}(\eta)+\mathfrak{D}\}-\tfrac{1}{2}\sqrt[+]{[\{\mathfrak{A}(\eta)-\mathfrak{D}\}^2+4\mathfrak{B}(\eta)\mathfrak{C}(\eta)]},\\ \alpha_2(\eta) &= \tfrac{1}{2}\{\mathfrak{A}(\eta)+\mathfrak{D}\}+\tfrac{1}{2}\sqrt[+]{[\{\mathfrak{A}(\eta)-\mathfrak{D}\}^2+4\mathfrak{B}(\eta)\mathfrak{C}(\eta)]}.\end{aligned} \tag{26}$$

Note that for any positive value of η

$$\alpha_1 < \alpha_2. \tag{27}$$

The solution of (24) can be written in the following form

$$\begin{aligned}\mathscr{L}_{q_0}(\eta,\zeta) &= w_0^{\eta-1}\{\mathfrak{M}_q(\eta)e^{-\alpha_1\zeta}+\mathfrak{N}_q(\eta)e^{-\alpha_2\zeta}\},\\ \mathscr{L}_{p_0}(\eta,\zeta) &= w_0^{\eta-1}\{\mathfrak{M}_p(\eta)e^{-\alpha_1\zeta}+\mathfrak{N}_p(\eta)e^{-\alpha_2\zeta}\},\end{aligned} \tag{28}$$

where $\mathfrak{M}_q(\eta)$,... are four coefficients depending on the two constants of integration. w_0 is an arbitrary energy. The factor $w_0^{\nu-1}$ has been introduced into (28) in order to make the coefficients $\mathfrak{M}_q(\eta)$,... pure numbers.

378. Only two of the four coefficients $\mathfrak{M}_q(\eta)$,... are independent. With the help of (24), (26), and (28) the following relations between the coefficients can be obtained

$$\begin{aligned}(\mathfrak{D}-a_2)\mathfrak{M}_q+\mathfrak{B}\mathfrak{M}_p &= 0,\\ (\mathfrak{D}-a_1)\mathfrak{N}_q+\mathfrak{B}\mathfrak{N}_p &= 0.\end{aligned} \tag{29}$$

We can add to these equations two initial conditions. Inserting $\zeta = 0$ into (28) we find

$$\begin{aligned}\mathfrak{M}_q+\mathfrak{N}_q &= \mathscr{L}_{q_0}(\eta,0)w_0^{-\nu_0+1},\\ \mathfrak{M}_p+\mathfrak{N}_p &= \mathscr{L}_{p_0}(\eta,0)w_0^{-\nu_0+1}.\end{aligned} \tag{30}$$

Expressions for the coefficients $\mathfrak{M}$ and $\mathfrak{N}$ obtained from (29) and (30) are collected in the following table. The first line gives the solutions for $\mathscr{L}_{p_0}(\eta,0) = 0$, i.e. for incident electrons, while the second line refers to $\mathscr{L}_{q_0}(\eta,0) = 0$, i.e. to incident photons.

TABLE 2

	Coefficients referring to:				
	Electrons		*Photons*		
Primaries	$\mathfrak{M}_q$	$\mathfrak{N}_q$	$\mathfrak{M}_p$	$\mathfrak{N}_p$	
Electrons	$\mathfrak{D}-a_1$	$a_2-\mathfrak{D}$	$\mathfrak{C}$	$-\mathfrak{C}$	$\times\dfrac{\mathscr{L}_{q_0}(\eta,0)w_0^{-\nu+1}}{a_2-a_1}$
Photons	$\mathfrak{B}$	$-\mathfrak{B}$	$a_2-\mathfrak{D}$	$\mathfrak{D}-a_1$	$\times\dfrac{\mathscr{L}_{p_0}(\eta,0)w_0^{-\nu+1}}{a_2-a_1}$

Numerical values of the various quantities and their derivatives have been given by Rossi and Greisen (1941) and also Bhabha and Chakrabarty (1943). Newly evaluated tables are given in Appendix II.†

Initial conditions

379. The initial condition for one primary electron of energy w_0 is as follows:

$$q(w,0) = \delta(w-w_0), \qquad p(w,0) = 0. \tag{31}$$

We find therefore from (16)

$$w_0^{-\nu+1}\mathscr{L}_{q_0}(\eta,0) = 1, \qquad \mathscr{L}_{p_0}(\eta,0) = 0. \tag{32}$$

† I am indebted to Mr. Howlett for having evaluated the tables.

Similarly for a cascade started by a photon of energy w_0 we have

$$\mathscr{L}_{q_0}(\mathfrak{y}, 0) = 0, \qquad w_0^{-\mathfrak{y}+1}\mathscr{L}_{p_0}(\mathfrak{y}, 0) = 1. \tag{33}$$

In order to calculate the absorption function of electrons or photons in the atmosphere it is necessary to consider a primary spectrum rather than primaries of definite energy. The value for $\mathscr{L}$ corresponding to an incident spectrum can be obtained by integration over the incident spectrum. We may consider an incident spectrum of the type

$$\Xi^{(z)}(w_1)\,dw_1 = \begin{cases} (1/z)(w_1/w_0)^{-z-1}\,dw_1/w_0 & (w_1 \geq w_0), \\ 0 & (w_1 < w_0). \end{cases} \tag{34}$$

Integrating (32) over this spectrum we obtain

$$w_0^{-\mathfrak{y}+1}\mathscr{L}_{q_0}(\mathfrak{y}, 0) = \frac{z}{z+1-\mathfrak{y}}. \tag{35}$$

The integration into w_0 is only legitimate if

$$\mathrm{Rl}(\mathfrak{y}) < z+1. \tag{36}$$

(*b*) *Mellin Transforms*

Expressions for various spectra

The actual solution of (15) for a given initial condition is obtained with help of (17), (24).

We find

$$q_0(w, \zeta) = \frac{1}{2\pi i w_0}\int_{\mathfrak{y}_0-i\infty}^{\mathfrak{y}_0+i\infty}\left(\frac{w_0}{w}\right)^{\mathfrak{y}}\{\mathfrak{M}_q(\mathfrak{y})e^{-\mathfrak{a}_1\zeta} + \mathfrak{N}_q(\mathfrak{y})e^{-\mathfrak{a}_2\zeta}\}\,d\mathfrak{y}. \tag{37}$$

Inserting from Table 2 we find for the case of a cascade due to a primary electron of energy w_0

$$\begin{aligned} q_0(w, \zeta) &= \frac{1}{2\pi i w_0}\int_{\mathfrak{y}_0-i\infty}^{\mathfrak{y}_0+i\infty}\left(\frac{w_0}{w}\right)^{\mathfrak{y}}\left\{\frac{\mathfrak{D}-\mathfrak{a}_1}{\mathfrak{a}_2-\mathfrak{a}_1}e^{-\mathfrak{a}_1\zeta} + \frac{\mathfrak{a}_2-\mathfrak{D}}{\mathfrak{a}_2-\mathfrak{a}_1}e^{-\mathfrak{a}_2\zeta}\right\}d\mathfrak{y}, \\ p_0(w, \zeta) &= \frac{1}{2\pi i w_0}\int_{\mathfrak{y}_0-i\infty}^{\mathfrak{y}_0+i\infty}\left(\frac{w_0}{w}\right)^{\mathfrak{y}}\frac{\mathfrak{C}}{\mathfrak{a}_2-\mathfrak{a}_1}\{e^{-\mathfrak{a}_1\zeta} - e^{-\mathfrak{a}_2\zeta}\}\,d\mathfrak{y}. \end{aligned} \tag{38}$$

Similar expressions can be found easily for other initial conditions.

380. Before giving the methods of evaluating the complex integrals encountered, we derive expressions for a number of physically significant quantities (compare Rossi and Greisen, 1941).

1. *Integral spectra.* The integral spectra of the particles and of photons can be defined as

$$\mathfrak{Q}_0(w,\zeta) = \int_w^\infty \mathfrak{q}_0(w',\zeta)\,dw', \qquad \mathfrak{P}_0(w,\zeta) = \int_w^\infty \mathfrak{p}_0(w',\zeta)\,dw'. \tag{39}$$

Inserting (37) into (39) and interchanging the order of the integrations we find that the expressions for the integral spectra are obtained from (37) by replacing $\mathfrak{M}$ and $\mathfrak{N}$ by

$$\overline{\mathfrak{M}} = \frac{\mathfrak{M}}{\eta-1}w, \qquad \overline{\mathfrak{N}} = \frac{\mathfrak{N}}{\eta-1}w. \tag{40}$$

2. Similar expressions are obtained for the flow of energy carried by the electrons or the photons with energies exceeding w. The energy flow can be defined by

$$\mathfrak{W}^{(e)}(w,\zeta) = \int_w^\infty w'\mathfrak{q}_0(w',\zeta)\,dw', \qquad \mathfrak{W}^{(p)}(w,\zeta) = \int_w^\infty w'\mathfrak{p}_0(w',\zeta)\,dw', \tag{41}$$

and the expressions for the flow are obtained from (37) by replacing $\mathfrak{M}$ and $\mathfrak{N}$ by

$$\overline{\overline{\mathfrak{M}}}(\eta) = \frac{\mathfrak{M}(\eta)}{\eta-2}w^2, \qquad \overline{\overline{\mathfrak{N}}}(\eta) = \frac{\mathfrak{N}}{\eta-2}w^2. \tag{42}$$

Average values with respect to depth

381. Further quantities can be derived from the Laplace integrals with respect to ζ† of $\mathfrak{q}$, $\mathfrak{Q}$, $\mathfrak{W}$, etc. We have, for instance,

$$\mathscr{L}^{(\zeta)}_{\mathfrak{q}_0}(\lambda,w) = \int_0^\infty e^{-\lambda\zeta}\mathfrak{q}_0(w,\zeta)\,d\zeta. \tag{43}$$

Inserting (37) into (43) and interchanging the order of the integrations we find

$$\mathscr{L}^{(\zeta)}_{\mathfrak{q}_0}(\lambda,w) = \frac{1}{2\pi i w_0}\int_{\eta_0-i\infty}^{\eta_0+i\infty}\left(\frac{w_0}{w}\right)^{\eta}\left\{\frac{\mathfrak{M}_{\mathfrak{q}}(\eta)}{a_1(\eta)+\lambda}+\frac{\mathfrak{N}_{\mathfrak{q}}(\eta)}{a_2(\eta)+\lambda}\right\}d\eta. \tag{44}$$

The corresponding expressions for the $\mathfrak{Q}_0$ or $\mathfrak{W}_0$ are obtained by replacing $\mathfrak{M}$ and $\mathfrak{N}$ by $\overline{\mathfrak{M}}$ and $\overline{\mathfrak{N}}$ or by $\overline{\overline{\mathfrak{M}}}$ and $\overline{\overline{\mathfrak{N}}}$.

From the Laplace integral of $\mathfrak{Q}_0$ we derive the following physically significant quantities (compare Rossi and Greisen, 1941).

1. The total length of electron track due to electrons with energy $> w$ is found as

$$\mathfrak{Z}^{(e)} = \int_0^\infty \mathfrak{Q}_0(w,\zeta)\,d\zeta = \mathscr{L}^{(\zeta)}_{\mathfrak{q}_0}(0,w). \tag{45}$$

† The Laplace transformation can be carried out in respect of either w or ζ. In the latter case we shall use an index ζ.

2. The centre of gravity of the shower particles with energy $> w$ can be defined as

$$\langle\zeta\rangle^{(e)} = \frac{1}{\mathfrak{Z}^{(e)}} \int_0^\infty \mathfrak{Q}_0(w, \zeta)\zeta \, d\zeta \tag{46}$$

and is expressed in terms of the Laplace integral as

$$\langle\zeta\rangle^{(e)} = -\left(\frac{\partial \log \mathscr{L}_{q_0}^{(\zeta)}(\lambda, w)}{\partial\lambda}\right)_{\lambda=0}. \tag{47}$$

3. The mean longitudinal spread of a shower particle with energies $> w$ can be defined as

$$\tau^2 = \langle(\zeta - \langle\zeta\rangle^{(e)})^2\rangle^{(e)} = \langle\zeta^2\rangle^{(e)} - \langle\zeta\rangle^{(e)^2}. \tag{48}$$

And we find

$$\tau^2 = \left(\frac{\partial^2 \log \mathscr{L}_{q_0}^{(\zeta)}(\lambda, w)}{\partial\lambda^2}\right)_{\lambda=0}. \tag{49}$$

4. *Numerical Evaluation of the Integrals*

The following methods can be used to evaluate numerically the integrals occurring in the last section.

(a) *The Method of Residua*

(i) Cauchy's theorem

382. The integrals occurring in the Mellin transform have to be taken along lines parallel to the imaginary axis. Thus the integrals have the form

$$\frac{1}{2\pi i} \int_{\vartheta_0 - i\infty}^{\vartheta_0 + i\infty} f(\mathfrak{y}) \, d\mathfrak{y}. \tag{50}$$

The integral (50) may be regarded as a limiting value

$$\lim_{R=\infty}\left(\frac{1}{2\pi i} \int_{\vartheta_0 - iR}^{\vartheta_0 + iR} f(\mathfrak{y}) \, d\mathfrak{y}\right). \tag{51}$$

If the function $f(\mathfrak{y})$ is single-valued and if it tends sufficiently to zero to the right of the line of integration for $|\mathfrak{y}| \to \infty$, the integral (51) can also be taken as the limiting value of

$$\frac{1}{2\pi i} \oint f(\mathfrak{y}) \, d\mathfrak{y}, \tag{52}$$

where the integration has to be carried out along the line $ABCDA$ (Fig. 60); note that the integral along the arc CDA tends to zero with increasing radius of the arc. If the function $f(\mathfrak{y})$ tends towards zero on

the left instead of the right of the line ABC then the integration may be carried out along the line $ABCD'A$. The integral over a function along a closed line in the complex plane is zero provided the function is regular inside the region surrounded by the line. If the function $f(\mathfrak{y})$ has poles but no other singularities in the region surrounded by the line of integration then the integral can be expressed in terms of residua in the following way

$$\frac{1}{2\pi i}\oint f(\mathfrak{y})\,d\mathfrak{y} = \pm \sum R_i, \tag{53}$$

where the + sign has to be chosen if the line of integration is anti-

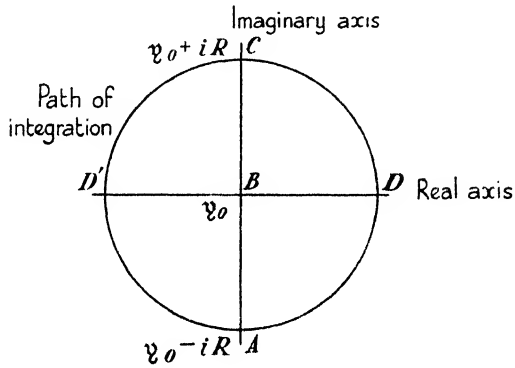

FIG. 60. Path of integration

clockwise ($ABCD'A$) and the — sign has to be taken for the integration in the clockwise direction ($ABCDA$).

Each R_i corresponds to a singularity $\mathfrak{y}_i$ inside the path of integration and is equal to the coefficient $c^{(i)}_{-1}$ in the series

$$f(\mathfrak{y}) = \sum_{\nu} c_\nu^{(i)}(\mathfrak{y}-\mathfrak{y}_i)^\nu.$$

(ii) Applications

383. To illustrate the method of residua we determine $\mathfrak{q}(w,\zeta)$ for $w > w_0$. We have

$$\mathfrak{q}_0(w,\zeta) = \frac{1}{2\pi i w_0}\int_{\mathfrak{y}_0-i\infty}^{\mathfrak{y}_0+i\infty}\left(\frac{w_0}{w}\right)^{\mathfrak{y}}\mathfrak{R}_0(\mathfrak{y},\zeta)\,d\mathfrak{y} \tag{54}$$

with
$$\mathfrak{R}_0(\mathfrak{y},\zeta) = \{\mathfrak{M}_\mathfrak{q}(\mathfrak{y})e^{-a_1\zeta} + \mathfrak{N}_\mathfrak{q}(\mathfrak{y})e^{-a_2\zeta}\}. \tag{55}$$

The singularities of the function $\mathfrak{R}$ are to the left of the line of integration as can be seen from the definition of $\mathfrak{y}_0$. For $w > w_0$ the integrand tends to zero for $\mathrm{Rl}(\mathfrak{y}) \to \infty$ and therefore the value of the integral

can be expressed by (53). As there are no singularities for real $(\eta) > \eta_0$ the integral vanishes and we find

$$q_0(w, \zeta) = 0 \quad (w > w_0),$$

as must be expected.

Absorption of a power spectrum

384. An interesting result is obtained when evaluating the numbers of electrons or photons with energies $w > w_1$ produced by an incident spectrum of the type (34).

The integrand in this case shows a singularity at $\eta = z+1$ (compare (35)). η_0 has to be chosen so that

$$\eta_0 < z+1 \quad \text{(compare (36))}.$$

We have therefore one singularity at the right of the path of integration. We obtain with the help of (53)

$$\left.\begin{aligned} q_E(w, \zeta) &= \left(\frac{w_1}{w}\right)^{z+1}\{\mathfrak{M}_q(z+1)e^{-a_1(z+1)\zeta} + \mathfrak{N}_q(z+1)e^{-a_2(z+1)\zeta}\} \\ p_E(w, \zeta) &= \left(\frac{w_1}{w}\right)^{z+1}\{\mathfrak{M}_p(z+1)e^{-a_1(z+1)\zeta} + \mathfrak{N}_p(z+1)e^{-a_2(z+1)\zeta}\} \end{aligned}\right\} \quad (w > w_1). \quad (56)$$

The expression in the curly brackets does not depend upon the energy w; it is seen therefore that an incident power spectrum produces a spectrum of the same type at any depth. The total intensity changes as the superposition of two exponentials. Introducing from Table 2 the values for the coefficients $\mathfrak{M}$ and $\mathfrak{N}$ we find that the number of electrons given by (56) declines monotonically from $\zeta = 0$ onwards. The number of photons, which is initially zero, increases up to a maximum and declines exponentially for larger depth.

For large values of ζ it is sufficient to consider the a_1 terms only. Taking for the exponent of the incident spectrum $z = 1{\cdot}8$ we find for the absorption coefficient from Table 2, Appendix II,

$$a_1(2{\cdot}8) = \begin{cases} 0{\cdot}469 \text{ cascade units}^{-1}, \\ 1/90 \text{ (grams per cm.}^2 \text{ air)}. \end{cases}$$

385. For $w \ll w_0$ the Laplace transform (43) can be evaluated by the residuum method (compare Nordheim and Hebb (1939), Rossi and Greisen (1941)). Examining the expressions (20) one finds that the singularities of the integrand of (37) are confined to the points

$$\eta = 1, 0, -1, \ldots . \quad (57)$$

The residuum method gives therefore a power series in powers of

w/w_0 for the integral. This series, however, converges very slowly and is not suitable for numerical evaluation.

The integrand of (43) has an additional singularity for

$$\mathfrak{y} = \mathfrak{y}(\lambda) \quad \text{with} \quad \mathfrak{a}_1\{\mathfrak{y}(\lambda)\} = -\lambda.$$

In particular for $\lambda = 0$, we have

$$\mathfrak{a}_1(2) = 0 \tag{57 a}$$

and therefore

$$\mathfrak{y}(0) = 2 \tag{57 b}$$

(compare (22) and (26)) and therefore the integrand of (43) can be developed round $\mathfrak{y} = 2$ as

$$\text{integrand} = \left(\frac{w_0}{w}\right)^{\mathfrak{y}} \frac{\mathfrak{M}(\mathfrak{y})}{\mathfrak{a}_1'(2)(\mathfrak{y}-2)}.$$

For $w \ll w_0$ the singularity at $\mathfrak{y} = 2$ gives the most important contribution to the integral. We find thus, with help of (43) and (51),

$$\mathfrak{Z} = \mathscr{L}^{(\zeta)}(0, w) \approx \frac{w_0}{w^2} \frac{\mathfrak{M}(2)}{\mathfrak{a}_1'(2)} = 0{\cdot}437 \frac{w_0}{w^2}. \tag{58}$$

Using a similar procedure we obtain further

$$\langle\zeta\rangle = -\left(\frac{\partial \log \mathscr{L}^{(\zeta)}(\lambda, w)}{\partial\lambda}\right)_{\lambda=0} \approx \frac{\log(w_0/w) + \{\log \mathfrak{M}(2)\}'}{\mathfrak{a}_1'(2)} - \frac{\mathfrak{a}_1''(2)}{\mathfrak{a}_1'^2(2)}, \tag{59}$$

$$\tau^2 = \left(\frac{\partial^2 \log \mathscr{L}^{(\zeta)}(\lambda, w)}{\partial\lambda^2}\right)_{\lambda=0} \approx \frac{\mathfrak{a}_1''(2)}{\mathfrak{a}_1'^3(2)} \log\frac{w_0}{w} + \frac{\{\log \mathfrak{M}(2)\}''}{\mathfrak{a}_1'^2(2)} - \\ - \frac{\mathfrak{a}_1''(2)\{\log \mathfrak{M}(2)\}'}{\mathfrak{a}_1'^3(2)} - \frac{\mathfrak{a}_1'''(2)}{\mathfrak{a}_1'^3(2)} + 2\left(\frac{\mathfrak{a}_1''(2)}{\mathfrak{a}'^2(2)}\right)^2, \tag{60}$$

dashes (′) signifying differentiation with respect to $\mathfrak{y}$.

Introducing numerical values from Tables 2, 3 of Appendix II into (58), (59) and (60) the following table is obtained:

TABLE 3

	Primary				
	Electron producing:		*Photon producing:*		
	Electrons	*Photons*	*Electrons*	*Photons*	*Spectrum*
$\mathfrak{Z} = \begin{Bmatrix} w_0/w^2 \\ w_0/w \end{Bmatrix} \times$	0·437	0·572	0·437	0·572	differential integral
$\langle\zeta\rangle = 1{\cdot}01 \log(w_0/w) +$	1·04 0·03	1·20 0·19	1·85 0·84	2·02 1·01	differential integral
$\tau^2 = 1{\cdot}61 \log(w_0/w) +$	0·06 −0·61	1·14 0·47	1·24 0·57	2·32 1·65	differential integral

(b) Saddle-point Method

(i) The method

386. Consider the integral

$$\int_{-\infty}^{\infty} e^{-\Xi(\mathfrak{y})}\, d\mathfrak{y}. \tag{61}$$

If the function $\Xi(\mathfrak{y})$ has a sharp minimum at $\mathfrak{y} = \bar{\mathfrak{y}}_0$ and increases rapidly to both sides, the main contribution to the integral can be assumed to arise from the region round $\bar{\mathfrak{y}}_0$. We may put

$$\Xi(\mathfrak{y}) = \Xi(\mathfrak{y}_0) + \tfrac{1}{2}(\mathfrak{y}_0 - \bar{\mathfrak{y}}_0)^2\, \Xi''(\mathfrak{y}_0) + \ldots. \tag{62}$$

Neglecting the higher power terms in $\mathfrak{y} - \bar{\mathfrak{y}}_0$ we have therefore

$$\int_{-\infty}^{+\infty} e^{-\Xi(\mathfrak{y})}\, d\mathfrak{y} \approx e^{-\Xi(\mathfrak{y}_0)} \int_{-\infty}^{+\infty} e^{-\frac{1}{2}\mathfrak{y}^2 \Xi''(\mathfrak{y}_0)}\, d\mathfrak{y} = e^{-\Xi(\mathfrak{y}_0)} \sqrt{\frac{2\pi}{\Xi''(\bar{\mathfrak{y}}_0)}}. \tag{63}$$

The integrals (37), (38), etc., have to be taken along a line parallel to the imaginary axis. The intersection of the path of integration with the real axis is at a point $\mathfrak{y}_0$, and the value of $\mathfrak{y}_0$ must be sufficiently large but otherwise it can be chosen arbitrarily. The integral

$$\frac{1}{2\pi i} \int_{\mathfrak{y}_0 - i\infty}^{\mathfrak{y}_0 + i\infty} e^{-\Xi(\mathfrak{y})}\, d\mathfrak{y} \tag{64}$$

can thus be evaluated by choosing $\mathfrak{y}_0$ so as to make $\Xi(\mathfrak{y}_0)$ a maximum on the real axis. We have then

$$\Xi'(\mathfrak{y}_0) = 0, \qquad \Xi''(\mathfrak{y}_0) < 0, \tag{65}$$

and according to (63),

$$\frac{1}{2\pi i} \int_{\mathfrak{y}_0 - i\infty}^{\mathfrak{y}_0 + i\infty} e^{-\Xi(\mathfrak{y})}\, d\mathfrak{y} \approx \frac{e^{-\Xi(\mathfrak{y}_0)}}{\sqrt{\{-2\pi \Xi''(\bar{\mathfrak{y}}_0)\}}}. \tag{66}$$

(ii) Application of the saddle-point method

Evaluation of spectra

387. The integrand of the integrals in (37) and (38) has a pronounced minimum on the real axis. The integration can therefore be carried out along a line parallel to the imaginary axis intersecting the real axis at this minimum.

We may write

$$\Xi(\mathfrak{y}) = \mathfrak{y} \log\left(\frac{w_0}{w}\right) + \log\{\mathfrak{M}(\mathfrak{y}) e^{-a_1 \zeta} + \mathfrak{N}(\mathfrak{y}) e^{-a_2 \zeta}\} \tag{67}$$

and we obtain the following equation for η_0, the coordinate of the saddle point,

$$\Xi'(\eta_0) = \log\frac{w_0}{w} + \frac{\{\mathfrak{M}'(\eta_0) - \mathfrak{M}(\eta_0)a_1'\zeta\}e^{-a_1\zeta} + \{\mathfrak{N}'(\eta_0) - \mathfrak{N}(\eta_0)a_2'\zeta\}e^{-a_2\zeta}}{\mathfrak{M}(\eta_0)e^{-a_1\zeta} + \mathfrak{N}(\eta_0)e^{-a_2\zeta}}. \tag{68}$$

Large thicknesses. For given w_0/w and ζ the value of η_0 can be determined from (68). It is found that provided

$$\left.\begin{aligned} &\zeta \gg 1, \\ &e^{-a_1\zeta} \gg e^{-a_2\zeta} \quad \text{for} \quad \eta = \eta_0 \end{aligned}\right\} \tag{69}$$

and therefore the second exponential can be neglected. Dropping the second exponential, (67) reduces to the following much simpler equation

$$\Xi(\eta) = \eta\log\left(\frac{w_0}{w}\right) - a_1\zeta + \log\mathfrak{M}(\eta), \tag{67 a}$$

and

$$\Xi'(\eta_0) = \log\left(\frac{w_0}{w}\right) - a_1'\zeta + \{\log\mathfrak{M}(\eta)\}'_{\eta=\eta_0} = 0, \tag{68 a}$$

$$\Xi''(\eta_0) = -\{\log\mathfrak{M}(\eta_0)\}''a_1''(\eta)\zeta. \tag{70}$$

These equations can be used for determining η_0 as a function of w and ζ. It is much more convenient, however, to regard (70) as a parametric representation of ζ. In this way we obtain

$$(\mathfrak{q}) = \frac{\mathfrak{M}(\eta_0)(w_0/w)^{\eta_0}e^{-a_1(\eta_0)\zeta}}{\sqrt{\{-2\pi\Xi''(\eta_0)\}}} \tag{71}$$

with

$$\zeta = \frac{1}{a_1'(\eta_0)}\left[\log\frac{w_0}{w} + \{\log\mathfrak{M}(\eta_0)\}'\right] \tag{72}$$

and

$$\Xi''(\eta_0) = a_1''(\eta_0)\zeta - \{\log\mathfrak{M}(\eta_0)\}''. \tag{73}$$

η_0 is taken as an independent parameter. $(\mathfrak{q})$ stands for any of the quantities $\mathfrak{q}_0$, $\mathfrak{p}_0$, $\mathfrak{Q}_0$, $\mathfrak{P}_0$, etc. $\mathfrak{M}$ can be obtained with help of Table 2, § 378, and eq. (40) or (42). Values of the functions $\mathfrak{M}$ and their first and second logarithmic derivatives are collected in Tables 2 and 3 of Appendix II.

388. *The cascade maximum.* For applications of the theory it is important to determine the position of the maximum of the functions with respect to ζ.

Thus we put

$$\frac{\partial(\mathfrak{q})}{\partial\zeta} = 0 \quad \text{for} \quad \zeta = \zeta_{\max}. \tag{74}$$

Differentiating (71) with respect to ζ and neglecting terms proportional to $\partial\eta/\partial\zeta$ we find

$$a_1(\eta_0) = 0 \quad \text{for} \quad \zeta(\eta_0) = \zeta_{\max}, \tag{75}$$

and therefore we see with help of (57 a) that the maximum is obtained for

$$\eta_0 = 2. \tag{76}$$

With the help of (72) and Table 2, Appendix II, we find

$$\zeta_{\max} = 1{\cdot}01\{\log_e(w_0/w) \mid A\}. \tag{77}$$

Numerical values for A are collected in the table below.

TABLE 4

	Cascade started by:	
Maximum of	*Electron*	*Photon*
Electrons . .	−1·55	−0·75
Photons . .	−1·38	−1·64

The above values for A refer to the maximum of the integral spectrum. The corresponding values for the differential spectrum are obtained by replacing A by $A+1$.

The numbers of particles or photons at the maximum can be obtained from (71) and (72). We find

$$N_{\max} = \begin{cases} \dfrac{0{\cdot}137(w_0/w)}{\sqrt{\{\log_e(w_0/w)+B\}}} & \text{(numbers of electrons} > w), \\ \dfrac{0{\cdot}180(w_0/w)}{\sqrt{\{\log_e(w_0/w)+B\}}} & \text{(numbers of photons} > w). \end{cases} \tag{78}$$

The values of B are as follows:

TABLE 5

	Primary	
Number of	*Electron*	*Photon*
Electrons . .	−1·33	−0·59
Photons . .	−0·64	−0·79

389. *Small thicknesses.* The saddle-point method can be also applied to determine the numbers of electrons or photons for small thicknesses. For small thicknesses, however, one is not justified in neglecting the second exponential and one has to use the full expression (67) for $\Xi(\mathfrak{y})$

In case of the *integral* spectra we obtain saddle points right down to $\zeta = 0$ (Jánossy and Tzu (1946)). In fact we have for $\zeta = 0$

$$\Xi(\mathfrak{y}) = (\mathfrak{y}-1)\log\frac{w_0}{w} - \log(\mathfrak{y}-1), \qquad \frac{1}{\mathfrak{y}_0-1} = \log\frac{w_0}{w},$$

and therefore $$\mathfrak{Q}(w, \zeta = 0) \approx \frac{e}{\sqrt{(2\pi)}} = 1{\cdot}08.$$

The correct value is of course 1. Thus one may expect the values for $\mathfrak{Q}$ to be in error by about 10 per cent. for small thicknesses.

5. *Solution of the Diffusion Equation considering Ionization Loss*

(*a*) *Arley's Approximation*

390. We deal in the following with the solutions of the diffusion equation when the ionization term is not neglected.

A rough approximation of this problem was obtained by Arley (1938). In his work Arley assumes that the ionization loss can be neglected for particles with energies above the critical energy w_c, while the loss due to radiative collisions can be neglected for particles with energies below the critical energy.

In Arley's calculation the critical energy is defined as

$$W_c' = \frac{160\nu m_e c^2}{Z} \quad \text{and} \quad \Delta' = \log_e 2W_c' \Big/ \left(\frac{dW}{d\theta}\right)_{\text{coll.}}, \tag{79}$$

where W_c is the energy defined in (3). Some of the numerical values obtained by Arley are collected in Table 9 of Appendix II.

(*b*) *Exact Solutions of Diffusion Equations*

391. Attempts were made to expand the exact solution of (15) in a series of powers of o. It is suggested, however, by Bhabha and Chakrabarty (1943) that the series of the type

$$\mathfrak{Q} = \mathfrak{Q}_0 + o\mathfrak{Q}_1 + \ldots \tag{80}$$

obtained in a formal way is *divergent*. The series (80) is not even an asymptotic representation of the solution of (15)†.

The ionization term is dealt with by Tamm and Belenky (1939) by introducing the Laplace transform of (24) with respect to ζ. The resulting equation admits a formal solution containing the parameter η and another parameter introduced by the second Laplace transformation. The actual solutions are obtained by means of a double Mellin transformation, that is transformations with respect to both parameters.

392. According to Bhabha and Chakrabarty (1943) the exact solution of (15) is assumed to have the form

$$\mathfrak{Q}(w, \zeta) = \frac{1}{2\pi i} \int_{\eta_0 - i\infty}^{\eta_0 + i\infty} \left\{\frac{w_0}{w + g(\eta, \zeta)}\right\}^n f(\eta, \zeta)\, d\eta, \tag{81}$$

where the functions f and g have to be chosen suitably.

† Bhabha's method was criticized recently by Belenky (1947).

In particular if one were to assume

$$g(\mathfrak{y}, \zeta) = 0$$

and

$$f(\mathfrak{y}, \zeta) = \mathfrak{R}_0(\mathfrak{y}, \zeta)$$

(compare eq. (55)), the integral (81) would reduce to the solution neglecting ionization loss.

393. Inserting (81) into the equation (15) and imposing suitable boundary conditions the functions f and g can be determined. The expressions thus obtained are complicated and we summarize only the result of the procedure.

1. The function $f(\mathfrak{y}, \zeta)$ can be expanded in a power series of the type

$$f(\mathfrak{y}, \zeta) = \mathfrak{R}_0(\mathfrak{y}, \zeta) + \frac{1}{w_0^2} \mathfrak{R}_2(\mathfrak{y}, \zeta) + \ldots . \tag{82}$$

Introducing (82) into (81) and integrating term by term, the solution appears as a series. It was shown that this series converges rapidly and that for most purposes the first term alone gives a sufficient approximation. The function g is given by a complicated expression. A few numerical values, computed by Bhabha and Chakrabarty (1943) are collected in Table 7 of Appendix II.

For small values of ζ we have approximately

$$g(\mathfrak{y}, \zeta) \sim \zeta \tag{83}$$

while for large values of ζ, g becomes independent of ζ and has a limiting value of the order of 1.

The function $g(\mathfrak{y}, \zeta)$ has a simple physical significance.

Comparing equation (81) with (37) we see that the solution considering ionization loss differs from the solution neglecting ionization mainly in that the energy w in the approximate solution has to be replaced by

$$w + g(\mathfrak{y}_0, \zeta) \tag{84}$$

to give the solution with ionization loss. Thus to a first approximation the effect of ionization is to shift the spectrum downwards by an amount $g(\mathfrak{y}_0, \zeta)$.

For $\zeta \gg 1$ we have $g(\mathfrak{y}, \zeta) \sim 1$, thus

$$\mathfrak{Q}(w, \zeta) \sim \mathfrak{Q}_0(w+1, \zeta). \tag{84a}$$

6. *Fluctuations*

394. For the interpretation of experimental findings it is of importance to consider the fluctuation of the actual numbers of particles round the average number.

In their original treatment Bhabha and Heitler (1937) assumed that the particles at a given depth fluctuate as if they were independent. Thus it is assumed that the probability of finding $\mathfrak{Q}^*$ particles while the average is $\mathfrak{Q}$ is given by the Poisson formula

$$\mathfrak{F}(\mathfrak{Q}^*, \mathfrak{Q}) = e^{-\mathfrak{Q}} \frac{\mathfrak{Q}^{\mathfrak{Q}^*}}{\mathfrak{Q}^*!}. \tag{85}$$

395. The fluctuation problem was dealt with in more detail by Furry (1937). Furry worked out the exact distribution function for an idealized cascade process. The idealized cascade process is, however, very different from the actual process and Furry's fluctuation formula is probably only justified for small thicknesses (compare Euler and Heisenberg, 1938).

The mean square deviations of the numbers of particles were calculated by Nordsieck, Lamb, and Uhlenbeck (1940) and by Scott and Uhlenbeck (1942) for the exact cascade process. The numerical results thus obtained show that the fluctuations are somewhat larger than expected from the Poisson law but that the fluctuations are very much smaller than expected from the Furry model.

396. The fluctuation problem was also treated by Arley (1943). In this paper it is suggested that the distribution function has a form intermediate between the Poisson distribution and the distribution given by Furry (1937). It is assumed that the actual distribution has some similarity to the Pólya distribution, a distribution which is used successfully in connexion with biological problems.

The Poisson distribution is probably applicable to showers under great thicknesses of absorbers. In the first stages of a shower, however, the fluctuations must obey a law very different from the Poisson law as can be shown by the following consideration.

Consider a high-energy electron falling on a comparatively thin absorber. The average number of particles produced by the electron is called N. According to the Poisson law, fluctuations greater than say $4N^{\frac{1}{2}}$ are very unlikely. If $N^{\frac{1}{2}} \gg 1$, then the probability that the shower contains one particle only becomes negligibly small.

In actual fact, however, a primary may occasionally traverse an absorber without any collision and thus give rise to no secondary particle at all. We expect on an average about one collision per cascade unit and therefore the probability of a primary traversing an absorber of thickness ζ without encounter is of the order of $e^{-\zeta}$.

Thus for small thicknesses the probability of an electron giving rise

to a small shower only, remains considerable, in spite of high energy; and the distribution must be expected to extend noticeably into the region of small showers.

Some of the figures obtained by Arley (1943) are collected in Appendix II, Table 10.

B. Investigation of the Soft Component

In the section below we give an account of experimental findings related to the soft component.

1. *Intensity of the Soft Component*

Soft and hard components

397. Photographs of cosmic rays passing through metal plates show clearly that the cosmic rays consist of two groups of particles:

(1) Penetrating particles.

(2) Electrons.

Electrons passing through metal plates lose much energy and give rise to small showers. The photograph *d* reproduced in Plate 1 shows a clear example of a cascade shower initiated by a single particle.

398. The cosmic-ray beam can also be shown to have two components by means of absorption experiments. It is found that the intensity decreases rapidly with absorber thickness up to about 10 cm. of lead. For larger thicknesses the intensity decreases only slightly with increasing thickness of absorber (see Fig. 37, Ch. IV). This is because the absorbable soft component causes the first rapid drop.

The intensity of the hard component is extrapolated to zero thickness. The difference between the extrapolated hard component and the total intensity can be taken as the intensity of the soft component. Near sea-level the soft component is about 30 per cent. of the total intensity.

Height-intensity distribution

399. At very great heights the intensity of the soft component is much greater than that of the hard component. Therefore in the upper part of the atmosphere the total intensity as measured with ionization chambers or coincidences can be taken as a fairly accurate measure of the intensity of the soft component.

In Fig. 61 we have plotted the total vertical intensity as measured by Pfotzer (1936); we have also plotted the intensity of the hard component as observed by Schein, Jesse, and Wollan (1941) with a coincidence arrangement (see Ch. IX). The broken lines are extrapolated.

It is seen that the intensity of the soft component increases rapidly up to a height of about 80 grams per cm.^{2} below the top of the atmosphere. At this height the intensity reaches a maximum and for greater heights the intensity of the soft component decreases again.

We note that the penetrating component does not show a maximum

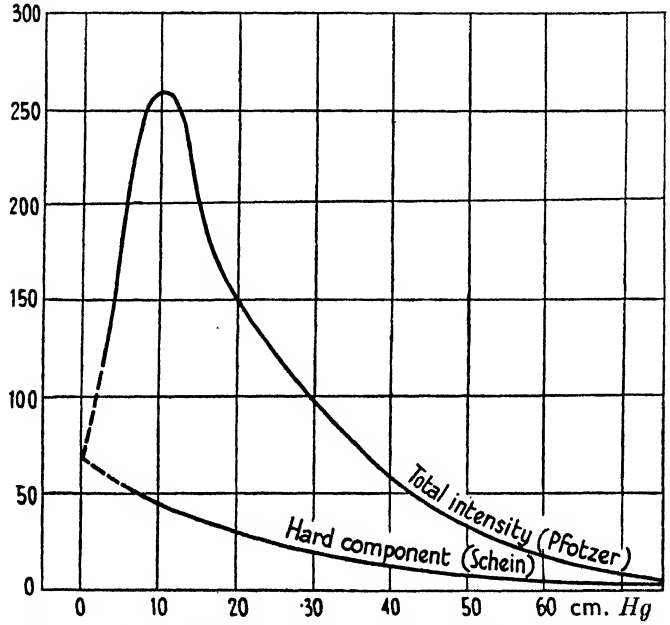

FIG. 61. Height-intensity curves of hard and soft components.

but increases up to the greatest heights observed; it is difficult to estimate the ratio of the two components near the top of the atmosphere.

The measurements thus reported were carried out at geomagnetic latitudes greater than 50°. The results obtained at other latitudes will be discussed in Chapter VII.

Soft component under ground

400. The intensity of the soft component in relation to the hard component was measured under ground by various observers.

The relative soft intensity decreases for the first few metres of water-equivalent under ground. The minimum of the relative soft intensity is of the order of 5 per cent. according to Auger (1935*a*), Auger and Rosenberg (1935*a*, 6), and Bernardini and co-workers (1940). For larger depths the relative soft intensity increases again, its value at greater depth being of the order of 30 per cent. (see V. C. Wilson (1937, 8, 9), Clay and Gemert (1939), and others).

From the rate of absorption of the soft component in lead or in air it is clear that the primary soft component cannot penetrate with appreciable intensity to great depths under ground. To account for the presence of the soft component under ground it is therefore necessary to assume that the soft component under ground is secondary to the hard component.

2. *Showers*

(*a*) *Size Distribution*

401. Small showers can be best observed with the cloud chamber. Counting the numbers of particles in individual showers their size distribution can be obtained.

Larger showers are most conveniently observed by means of an ionization chamber. A shower crossing an ionization chamber will give a rise to a 'burst' of ionization. The size of the burst is a measure of the number of particles contained in the shower.

The size distribution of showers was thus investigated by several authors. Montgomery and Montgomery (1935 *b*) find the following size distribution for showers observed under a thin layer of lead:

$$S(N) \sim A/N^{z+1}, \tag{86}$$

where $z \sim 2{\cdot}3$, A is a constant, $S(N)$ is the rate of showers containing N particles.

For showers containing 50–1,000 particles the distribution (86) was established by means of a burst chamber, while the distribution of smaller showers was obtained from the analysis of cloud-chamber photographs. The results of Montgomery are shown in Fig. 62. The distribution is given in a double logarithmic plot. The straight line in Fig. 62 represents the distribution (86) while the observed frequencies are shown by a step line.

(*b*) *Shower Coincidences*

402. Showers can also be observed by counter arrangements. The prototype of a shower arrangement is the triangular arrangement used by Rossi (1933) which is shown in Fig. 63. It is seen that threefold coincidence between the counters can only be caused by groups of two or more particles.

Five counters arranged in the corners of a regular pentagon were also used. This arrangement needs at least three particles to be set off.

The interpretation of counter observations is more difficult than that

of results obtained with either cloud chamber or ionization chamber. It must be emphasized that a shower arrangement is only rarely set off by the minimum number of particles required. Most coincidences

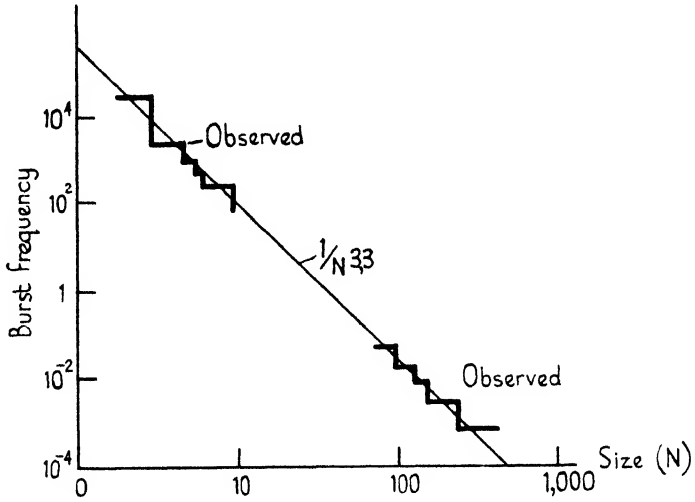

FIG. 62. Size–frequency distribution of bursts (Montgomery and Montgomery, *Phys. Rev.* **48**, 786 (1935)).

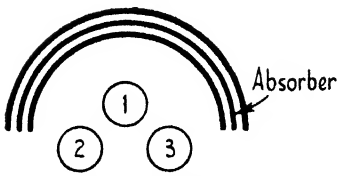

FIG. 63. Counter arrangement for the observation of showers.

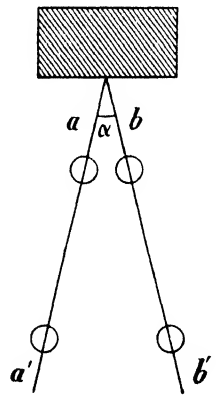

FIG. 64. Counter arrangement.

of a shower arrangement are due to showers containing many particles (see §§ 444–7). It is therefore a fallacy to connect the number of particles in a shower with the number of counters employed in coincidence. Neither is there a simple connexion between the position of shower counters and the angular divergence of a shower.

The counter arrangement shown in Fig. 64 is by no means particularly

sensitive to showers with the opening angle α, the angle between the planes aa' and bb'.

Transition effect

403. Rossi (1933) found that the rate of coincidences observed by a shower arrangement is strongly affected when an absorber is placed close above it.

The rate of coincidences plotted against the thickness of absorber increases first, reaches a maximum, and decreases for larger thicknesses.

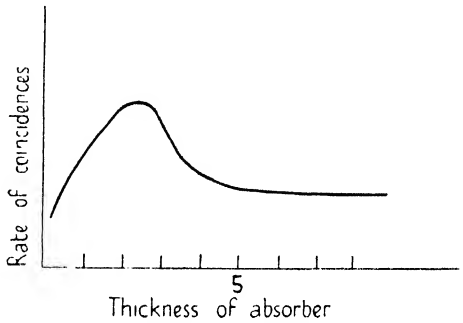

FIG. 65. Rossi transition curve.

The maximum for lead is reached near 2 cm. The shower rate decreases again when the absorber is increased from 2 to 5 cm. of lead. For larger thicknesses no further decrease is observed.

The rate of coincidences plotted against the thickness of lead is shown in Fig. 65. This curve is usually referred to as the 'Rossi curve' and the effect is called the 'Rossi transition'.

The rate of shower coincidences increases also when absorbers are placed closely below the arrangement. This effect is probably due to the scattering back of slow secondaries.

Various observers have also found a small second maximum at thicknesses of about 17 cm. of lead. The experimental evidence with regard to this 'second maximum' is very contradictory and it seems safe to assume that no such second maximum exists; at any rate no second maximum exceeding 1–2 per cent. of the intensity of the tail (compare Altman, Walker, Hess (1940) and George, Jánossy, and McCaig (1942)).

The tail of the Rossi curve

404. It can be seen readily that the Rossi curve results from the superposition of two different effects. The long tail of the Rossi curve

suggests the presence of penetrating particles. The showers observed under thick absorbers of lead could be interpreted either as penetrating showers produced by soft primaries or as soft showers produced by penetrating primaries. The first maximum with its steep rise and fall must, however, be interpreted in terms of soft particles only.

It will be seen later that the first maximum can be interpreted in terms of electron cascades while the tail is mainly due to soft showers (cascades) produced by penetrating particles. A small number of penetrating showers produced by less penetrating primaries are also present.

405. The fact that the Rossi curve represents two superposed effects was shown convincingly by the experiments of Schwegler (1935). The

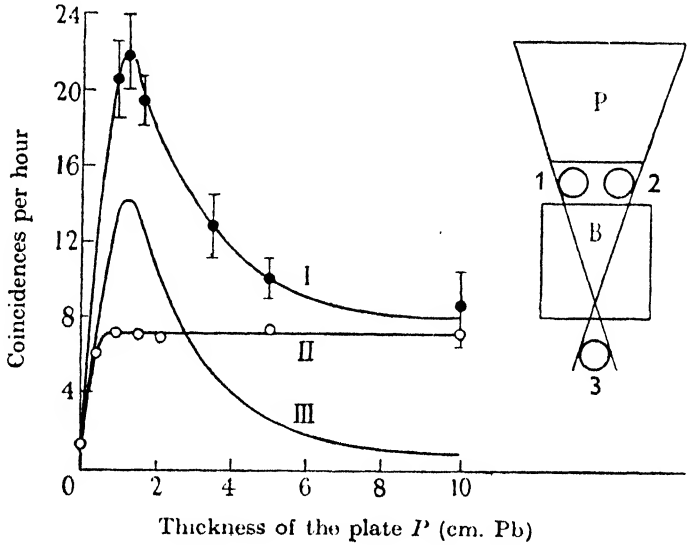

Fig. 66. The experimental arrangement of Schwegler and his results. From N. Arley, *Stochastic Processes*, p. 181.

experimental layout is shown in Fig. 66. Threefold coincidences are recorded between the counters 1, 2, 3. The Rossi transition in an absorber P close above the counters is observed (1) with a 10-cm. thick lead block B between the counters and (2) without any absorber between the counters. The transition effects thus obtained are also shown in Fig. 66.

The arrangement (1), with the lead block B between the counters, responds only to showers containing at least one penetrating particle capable of traversing the lead B. Showers of this type are seen to show a saturation effect without a maximum (curve II, Fig. 66).

The difference between the rates observed with and without the lead can be attributed to showers not containing any penetrating particles. The difference curve (III) which represents these soft showers is seen to show a pronounced maximum and to tail off rapidly for larger thicknesses.

(c) Properties of Shower Particles

First slope of transition curve

406. The first slope of the shower transition curve has a simple significance; this slope is proportional to the cross-section for the produc-

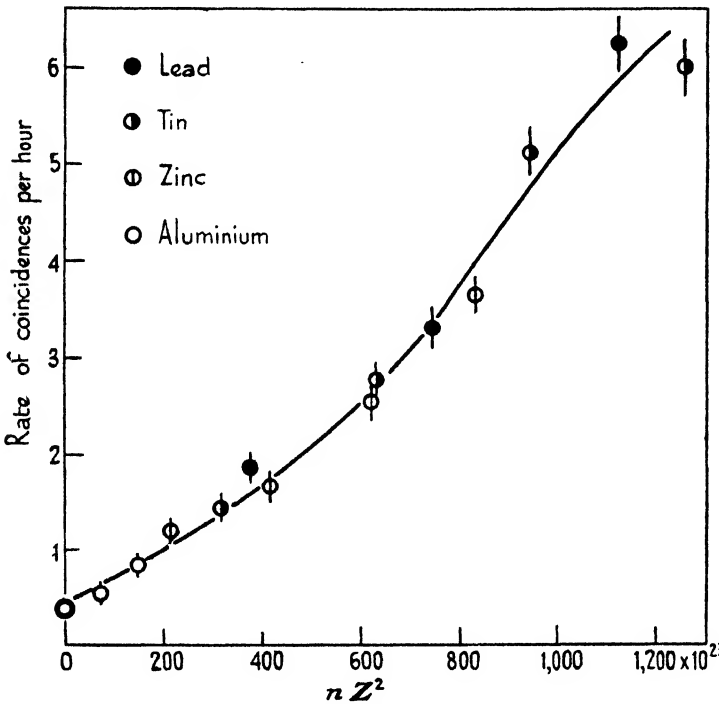

FIG. 67. The initial part of transition curves for lead ●, tin ◑, zinc ⊕, aluminium ○. From Hu Chien Shan, *Proc. Roy. Soc.* A, **158**, 588.

tion of showers by the primaries. Comparing the slopes obtained for various materials above the counter arrangement, the dependence of the cross-section upon the atomic number Z of the shower-producing material can be determined.

Measurements of this kind were carried out by Morgan and Nielsen (1936) and also by Hu (1937) and Hu and co-workers (1937). The results of Hu and co-workers are reproduced in Fig. 67. It is seen that the

cross-section for shower production is very nearly proportional to Z^2 per atom.

The measurements of Morgan and Nielsen (1936) were carried out with triangular arrangements and those of Hu by a coincidence arrangement consisting of five counters placed on the corners of a regular pentagon.

The range of shower particles

407. The range of shower particles can be measured directly by an arrangement of the type shown in Fig. 68. Showers are recorded by the

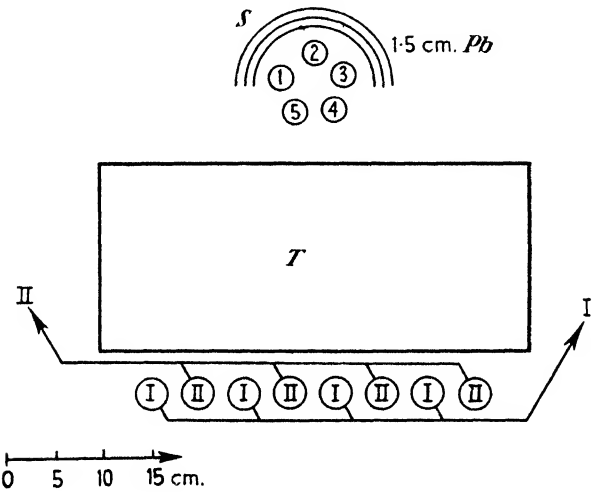

Fig. 68. The penetrating power of shower particles (arrangement). *Proc. Camb. Soc.* **34**, 614 (1938).

coincidences of the counters 1, 2, 3, 4, 5, I, II. Absorbers are placed between the top counters 1, 2, 3, 4, 5 and the bottom counters I, II. In the presence of the absorber T only showers which can penetrate the absorber T are capable of producing coincidences and therefore the rate of coincidences as function of the thickness of T can be taken as the absorption curve of the shower particles.

Experiments of this kind have been carried out by a large number of observers (Nielsen (1938), Schmeiser and Bothe, Hu (1937), Jánossy (1938)). In spite of very different arrangements the various results agree fairly well. The results of some authors are collected in Fig. 69. It is seen that most of the shower particles are absorbed in 5–7 cm. of lead though there are a few showers which penetrate as much as 10 cm. of lead.

Absorption measurements were also carried out in different materials. It was found that the first part of the absorption curve is nearly mass proportional while for larger thicknesses a small but significant difference between light and heavy absorbers appears; the absorption curve for light materials shows an extended tail (Fig. 69).

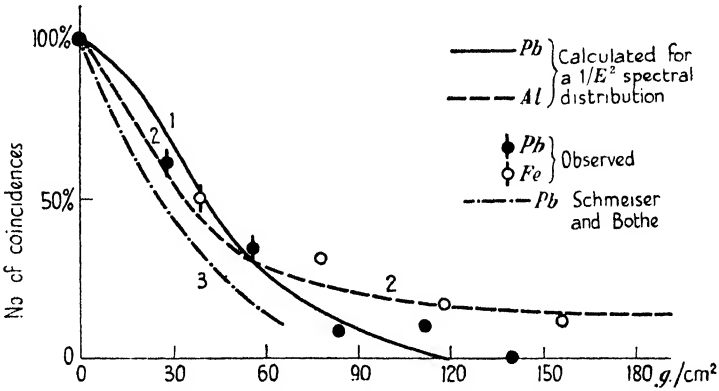

Fig. 69. Absorption curve of shower particles. *Proc. Camb. Soc.* **34**, 614 (1938).

408. By placing various thicknesses of material and various kinds of material above the top counters it is possible to investigate showers from different materials and produced in various thicknesses. Measurements of Schmeiser and Bothe (1937) show that the absorption curve of showers produced under about 1·5 cm. of lead have the same absorption curve as those produced under 17 cm. of lead. This result shows clearly that the showers produced under thick absorbers are soft showers of the same type as those produced under thin absorbers. It can be concluded therefore that showers observed in the tail of the Rossi curve are mainly soft showers produced by penetrating particles and they are not penetrating showers produced by soft primaries (compare § 404).

409. Comparing the absorption curves of showers from the air and those from lead it is found that the lead showers are slightly less penetrating than those from air. Similarly it was observed by various authors that showers from light elements are slightly more penetrating than those from heavier elements (compare e.g. J. Clay (1936)).

3. *Connexion between Showers and the Soft Component*

410. The absorption curve for shower particles is very similar to the absorption curve of the soft component (see Fig. 69). It is therefore

plausible to assume that the soft component consists of shower particles. This assumption is supported by the fact that the shower intensity observed both above and below sea-level is proportional to the intensity of the soft component.

411. The Rossi transition curve was measured at various elevations above sea-level. In Fig. 70 we reproduce the measurements of Woodward (1936). It is seen that the Rossi curves show the same shape at

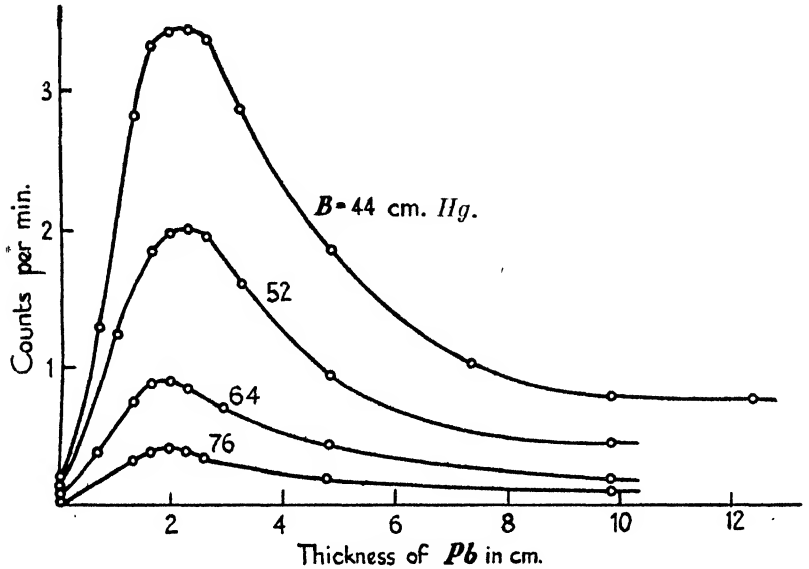

FIG. 70. Shower production curves at Mt. Evans 4,300 m., Echo Lake 3,250 m., Denver 1,620 m., Cambridge, U.S.A. 60 m. (Woodward). From *Journ. Franklin Inst.* **226**, 611.

all altitudes and the curves obtained at various altitudes can be converted into each other by multiplication with constant factors.

Because of this similarity the Rossi curves obtained at different heights can be taken conveniently as a measure of the shower intensity at the corresponding heights. It is seen from Woodward's (1936) data that the shower intensity at 4,300 m. above sea-level is 8·5 times larger than the intensity at sea-level. The soft component increases from sea-level to this height by a factor 7·9 according to Woodward. Thus the shower intensity appears proportional to the intensity of the soft component.

We note that the intensity of the tail of the transition curve increases with height at the same rate as the intensity of the maximum. This is a surprising result, as the first part of the transition effect must be

assumed to be a process different from that responsible for the tail of the transition curve (compare §§ 404, 405).

412. A most convincing proof of the connexion between shower intensity and soft component was given by the observations of Regener and Ehmert (1939). An automatic recording arrangement was sent up in a balloon and reached heights corresponding to 7 cm. Hg pressure. The arrangement consisted of a fourfold coincidence arrangement with four horizontal counters placed at the corners of a quadrangle. A 1-cm. thick lead plate was placed close above the counters to increase the rate of showers.

The rate of showers as obtained with this arrangement is plotted against the mass of the atmosphere above the arrangement. 6·5 cm. Hg is added to the actual pressure to correct for the mass of the lead absorber (Fig. 71). It was noticed by Regener that the height-intensity curve thus obtained for the shower intensity can be fitted exactly to the intensity distribution of the soft component. The two intensity distributions would not fit satisfactorily without the correction of 6·5 cm. Hg for the lead plate. This correction can be justified when assuming that lead and air have to be compared on a Z^2 scale (cascade units).

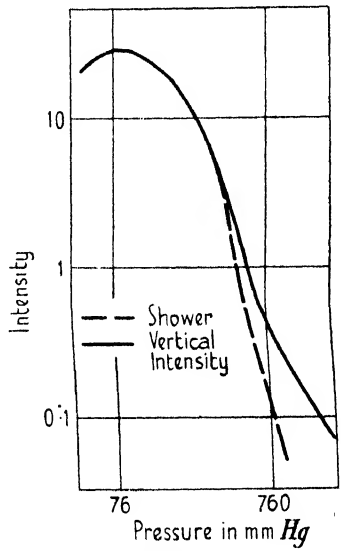

FIG. 71. Height-intensity distribution of showers and of soft component (Regener).

413. The shower intensity below ground was also measured. Ehmert (1937) used an automatic coincidence arrangement which was submerged into the Lake Constance. Similarly Clay used an arrangement which was submerged into the North Sea down to 250 m. below the sea-level. Measurements in deep mines were carried out by V. C. Wilson down to 1,000 m. H_2O. The measurements of these authors and of many others show that the shower intensity decreases at a rate slightly smaller than the vertical intensity. Ehmert (1937), for instance, finds for the shower intensity at a depth θ below the top of the atmosphere ($10 < \theta < 243$ m. H_2O)

$$S(\theta) \sim \theta^{-1\cdot40}. \tag{87}$$

Comparing these results with § 304 we see that the shower intensity obeys a power law like the vertical intensity.

The results of V. C. Wilson (1938) are shown in Fig. 72. It is seen

that the shower intensity decreases slightly less with increasing depth than the vertical intensity.

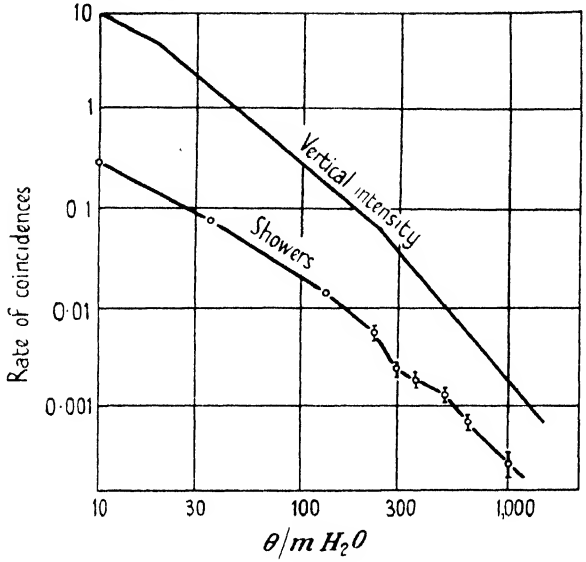

FIG. 72. Vertical intensity and showers under ground (V. C. Wilson).

C. INTERPRETATION OF THE SOFT COMPONENT IN TERMS OF ELECTRONS AND PHOTONS

414. In the present section we shall discuss how far the observational material relating to the soft component can be accounted for in terms electrons and photons.

We shall discuss the following main subjects:

1. We shall show that, assuming a suitable primary spectrum of electrons, the atmospheric transition curve of the soft component (Pfotzer (1936) curve) can be accounted for. We shall restrict ourselves to the consideration of high latitudes where there are no geomagnetic effects to be expected. The change of the transition curve with latitude will be discussed in Chapter VII.

2. We shall give an estimate as to the absolute intensity of the primary soft component and determine the spectra arising from the primary electrons at various depths below the top of the atmosphere. It will be seen that the observed soft intensity cannot be accounted for near sea-level and at moderate heights above sea-level in terms of primary cascades alone.

3. To account for the soft component at depth beyond the reach of

the primary soft component it must be assumed that the hard component gives rise to a secondary soft component. Two processes contributing to this secondary soft component will be considered: (1) the emission of decay electrons; (2) the production of electron secondaries.

4. We shall analyse shower and burst phenomena. It will be seen that a satisfactory picture can be obtained of both the size distribution and the absolute frequencies of bursts.

5. We shall give a short account of the analysis of bursts under ground. This problem is connected with the question as to the value of the spin of the meson.

1. *The Atmospheric Transition*

(*a*) *Incident Spectrum*

415. The height-intensity curve of the soft component can be accounted for in terms of incident electrons provided a suitable primary spectrum is assumed.

One might be tempted to assume an incident power spectrum of the type

$$\mathfrak{S}(w) \sim w^{-(z+1)}. \tag{88}$$

However, using the eq. (88) we obtain with the help of (84a) and (56) for the number of electrons at a depth ζ

$$\mathfrak{Q}(0,\zeta) \sim \mathfrak{M}(z+1)e^{-a_1(z+1)\zeta} + \mathfrak{N}(z+1)e^{-a_2(z+1)\zeta}. \tag{89}$$

It can be seen easily that the expression (89) shows no maximum inside the atmosphere.

416. The observed intensity of the soft component has a maximum at a depth of about 8·5 cm. Hg (compare § 399 and Fig. 62), which corresponds to a depth of

$$\zeta = 3 \tag{90}$$

expressed in cascade units. This maximum cannot be accounted for in terms of the spectrum (88) and therefore this spectrum cannot correspond to the actual incident spectrum.

A maximum of the intensity at about the right depth can be obtained, however, by cutting off the low-energy part of the spectrum (88). That is, by assuming a power spectrum for energies greater than w_1,

$$\mathfrak{S}(w) = \begin{cases} \dfrac{I_0 z}{w_1}\left(\dfrac{w_1}{w}\right)^{z+1} & (w > w_1), \\ 0 & (w < w_1), \end{cases} \tag{91}$$

with $z = 1{\cdot}6$ and $w_1 = 2{,}000$ MEV.

Assuming an incident spectrum given by (91) the number of particles as function of depth can be evaluated by the methods given in the beginning of this chapter. The height-intensity curve thus obtained, together with the observed intensity of the soft component is shown in Fig. 73 (*a*). There is a fair agreement between the two curves for not too large depths. For larger depths the calculated intensity is much smaller than the observed one. The calculated curve has also a too narrow maximum. In Fig. 73 (*b*) we have plotted the calculated spectrum for $z = 2{\cdot}0$; the latter curve falls off much more rapidly than the observed intensity.

417. The agreement between the calculated curve and the observation could be improved by modifying the incident spectrum. In fact, as was pointed out by Nordheim (1938), it is possible to obtain any absorption curve by a suitable choice of the incident spectrum. Compare also Heitler (1937 *b*). Agreement between calculation and observation is therefore no proof of the validity of the cascade theory. We shall, however, give reasons which make the assumption of a spectrum of the type (92) likely; it is therefore satisfactory that this spectrum can roughly account for the intensity distribution of the soft component at high altitudes.

(*b*) *Absolute Intensity*

418. The absolute intensity of the incident spectrum can be estimated according to E. Regener (1933) and according to Bowen, Millikan, and Neher (1937) in the following way.

The total influx of energy $\mathfrak{W}$ can be evaluated when assuming that all the energy incident to the atmosphere is eventually converted into ionization. The average energy required to produce one ion pair is 32 eV. and the total energy spent in ionization can be written as

$$\mathfrak{W} = 32 \text{ eV.} \int i(\theta)\, d\theta, \tag{92}$$

where $i(\theta)$ is the rate of ionization at the depth θ and the integration is to be carried out from the top of the atmosphere down to the greatest depths below sea-level.

We note that for two reasons the inflowing energy is in fact somewhat larger than (92): (1) A certain amount of energy is spent in the production of low-energy quanta and this energy is transformed into heat. This effect has been investigated theoretically by E. J. Williams (1940 *b*); it does not seem to be of great importance. (2) A certain fraction of the energy is transformed into neutrinos; it is very difficult to decide whether or not any of the energy given to neutrinos reappears in form

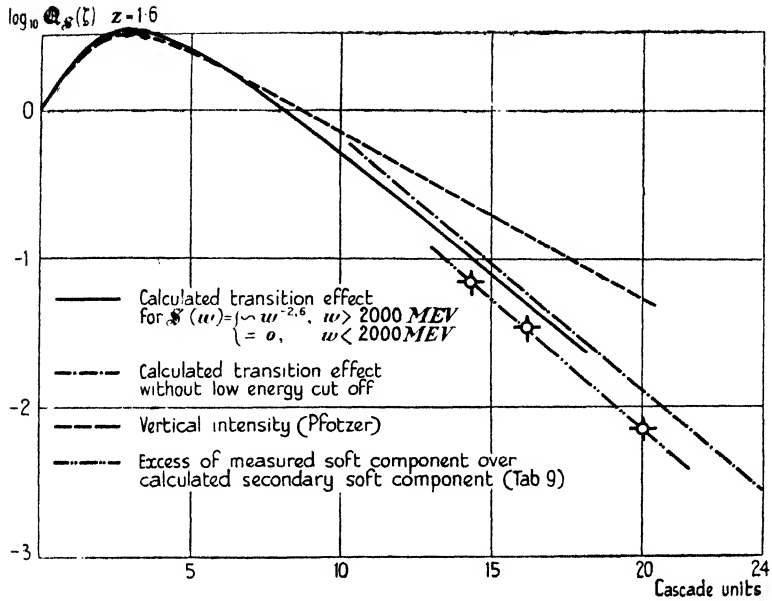

FIG. 73 (*a*). Calculated and observed height-intensity distribution of soft component ($z = 1{\cdot}6$).

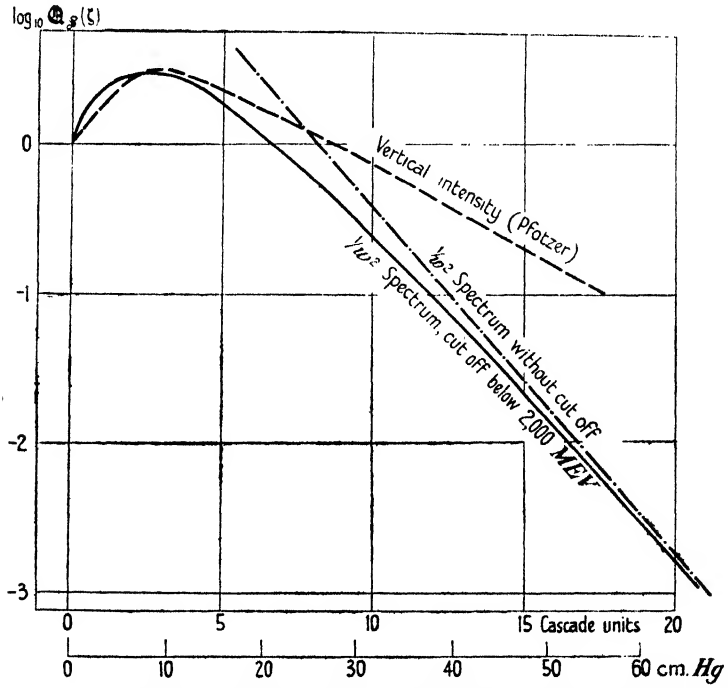

FIG. 73 (*b*). Calculated and observed height-intensity distribution of soft component ($z = 2$).

of ionization. This second effect might give rise to a factor up to 2 on the right-hand side of (92).

419. The energy flow $\mathfrak{W}$ represents the flow due to all primaries. Assuming two types of primaries, namely electrons and protons (see next chapter), we have

$$\mathfrak{W} = \mathfrak{W}_{\text{el.}} + \mathfrak{W}_{\text{protons}}. \tag{93}$$

There is no indication as to the relative values of $\mathfrak{W}_{\text{el.}}$ and of $\mathfrak{W}_{\text{protons}}$ though the two flows might be of comparable orders of magnitudes. Considering the various uncertainties we shall assume in the following as a first approximation

$$\mathfrak{W}_{\text{el.}} \sim \mathfrak{W}. \tag{94}$$

Using the observed height-ionization curves Millikan, Neher, and Pickering (1942) obtain

$$\mathfrak{W} = 1{\cdot}4 \times 10^5 \text{ MEV. per cm.}^2 \text{ per min.} \tag{95}$$

The above value is found for geomagnetic latitudes exceeding 50°. The flow for lower latitudes will be discussed in the next chapter.

The flow of energy can be expressed in terms of the spectrum $\mathfrak{S}(w)$ as follows:

$$\mathfrak{W} = \int_0^\infty w\mathfrak{S}(w)\, dw. \tag{96}$$

We have with help of (91)

$$\mathfrak{W} = 2\pi I_0 \frac{w_1 z}{z-1}. \tag{97}$$

The numerical value of I_0 can thus be determined from (95) and (97). The exact value depends on the choice for z. We find:

TABLE 6

Primary Intensity I_0

	$z = 1{\cdot}6$	1·8	2·0
I_0 in particles per cm.² per min. per unit solid angle	4·2	5·0	5·6

420. The total primary electron intensity can be worked out with help of Table 6 and the cascade theory. For sufficiently large values of ζ the effect of the cut-off of the primary spectrum at low energies can be neglected and we can assume the vertical intensity to be given by (89). The intensity in a direction inclined at ϑ to the vertical is therefore given by (we neglect the second exponential)

$$I(\zeta, \vartheta) \cong \mathfrak{M}_q(z+1)e^{-a_1(z+1)\zeta/\cos\vartheta}.$$

Integrating over all directions of incidence we find for the total intensity

$$\bar{I}(\zeta) = 2\pi \int_0^{\frac{1}{2}\pi} I(\zeta, \vartheta) \sin\vartheta \, d\vartheta. \tag{98}$$

And using the approximate relation

$$\int_0^{\frac{1}{2}\pi} e^{-a\zeta/\cos\vartheta} \sin\vartheta \, d\vartheta \sim \frac{e^{-a\zeta}}{a\zeta}, \tag{99}$$

we find

$$\bar{I}(\zeta) = 2\pi I_0 \left(\frac{w_1}{w_c}\right)^z \mathfrak{M}_q(z+1) \frac{e^{-a_1\zeta}}{a_1\zeta}. \tag{100}$$

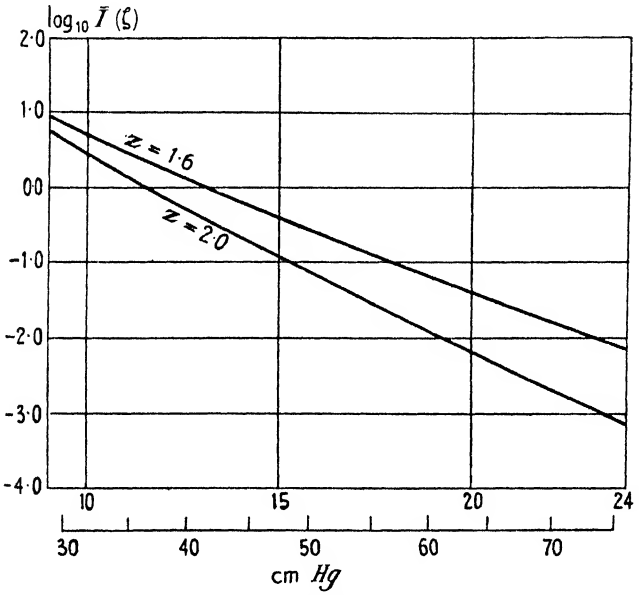

FIG. 74. Primary soft component at various depths calculated for $z = 1{\cdot}6$ and $2{\cdot}0$.

In Fig. 74 we have plotted $\log \bar{I}(\zeta)$ against ζ. We see from Fig. 74 that primary cascades cannot contribute more than a negligible amount to the soft component at sea-level. The contribution of primary cascades to the soft intensity at 4,300 m. is probably more important.

The spectral distribution of the descendants of a primary spectrum is the same at any depth and is given by

$$\mathfrak{S}(w) \sim \frac{w_c^z}{(w+w_c)^{z+1}} \tag{101}$$

(compare eq. (56)).

421. It is interesting to note which primary energies are responsible for

electrons near sea-level. From the graphs, Fig. 128, Appendix II, we find as an empirical relation

$$w_0/w \sim 6{\cdot}3 \exp(0{\cdot}276\zeta),$$

where w_0 is the energy of an electron which produces on the average one electron with energy greater than w under the absorber ζ.

We find the following numerical values:

TABLE 7

$\zeta =$	13·7	24·0
$w_0 =$	$2{\cdot}8.10^4$	$4{\cdot}7.10^5$ MEV.

w_0 is the primary energy which gives rise to one electron above the critical energy (100 MEV.) at the depth ζ.

From the above table we note incidentally that primaries below $w_1 = 2{,}000$ MEV. give rise only to very few electrons below $\zeta = 13$, say, and therefore we are justified in neglecting the cut-off below w_1 when evaluating the electron intensities for $\zeta > 13$ (compare also Figs. 73 (*a*) (*b*)).

2. *The Secondary Soft Component*

422. We see from Fig. 74 that the soft component observed at sea-level and at moderate heights cannot be accounted for in terms of primary cascades reaching sea-level, if the spectrum is given by (91). For the sake of completeness we note that the observed intensity distribution could be accounted for in terms of cascades provided a primary spectrum rather different from that given by (91) was assumed.

In fact, if we were to assume a spectrum with an exponent z decreasing with energy so that

$$z \to 1 \quad \text{for} \quad w \to \infty, \tag{102}$$

we would find that for large depths the effective value of the absorption coefficient α would approach zero and the intensity would approach asymptotically a constant value.

The spectrum $z = 1$ is, however, singular as it contains an infinite amount of energy. By choosing a spectrum which approaches this singular spectrum, one could account for an arbitrarily small absorption of the intensity.

It will be seen, however, in Chapter VIII that a primary spectrum with an exponent appreciably smaller than 1·5 is incompatible with observation of the extensive air showers.

Thus the soft component at low altitudes must be assumed to be of secondary origin.

(*a*) *Decay and Knock-on Electrons*

423. It was pointed out by Euler and Heisenberg (1938) that the soft component at sea-level can be accounted for in terms of the decay electrons of mesons.

The soft component under ground and under thick absorbers was interpreted by Bhabha (1938*a*) in terms of electron secondaries produced by mesons. Such secondaries are usually termed 'knock-on electrons'.

In the following section we shall evaluate the numbers of decay electrons and knock-on electrons to be expected at various heights above and below sea-level. It will be seen that only part of the soft component can be well accounted for by these two processes.

Calculation of the intensity of the secondary soft component

424. The magnitude of the soft intensity can be estimated by a procedure suggested by Williams (1940*b*) and later improved by Rossi and Greisen (1942) and by Rossi and Klapman (1942).

It is pointed out that all the energy lost by the mesons and transferred to electrons is eventually converted into ionization. Assuming therefore stationary conditions one is led to expect that the average rate of energy transfer from the soft component is equal to the average rate of energy converted into ionization by the accompanying soft component. We have therefore for stationary conditions

$$\frac{dw}{d\theta} = no, \tag{103}$$

where $dw/d\theta$ is the rate of energy transferred from the mesons to the soft component, n is the average number of secondary electrons, and o is the rate of loss of energy by ionization for the electrons.

The equation (103) does not hold exactly as no exact equilibrium between the two components can be assumed. Most electrons at a given height have their origin higher up in a layer where the meson intensity is somewhat larger.

Estimation of the intensity of decay electrons

425. The probability that a meson of momentum p decays along a path $d\theta$ giving rise to a decay electron of energy in the interval w', dw' is according to Ch. V, eqs. (6), (28), (31),

$$d\mathscr{P}(w') = \frac{dw'}{p^2}\frac{\mu}{c\ell_0}\frac{d\theta}{k}. \tag{104}$$

We assume $w' = p'c$ for the electron. The average energy of the decay electron is $cp/2$, as half of the energy of the meson is taken up by the electrons while the rest is taken up by the neutrinos. Therefore the average rate of energy converted from mesons into electrons is, according to (104),

$$\left(\frac{dw}{d\theta}\right)_{\text{decay}} = \frac{1}{2}\frac{\mu c^2}{c\ell_0}\frac{1}{k} \text{ per meson.} \tag{105}$$

We note that the expression (105) does not depend on the momentum of the meson emitting the electrons. The rate of energy converted into electrons is therefore

$$I(\zeta)\left(\frac{dw}{d\theta}\right)_{\text{decay}} = I(\zeta)\frac{\mu c^2}{c\ell_0}\frac{1}{k} = 0{\cdot}55\frac{I(\zeta)}{\zeta}, \tag{106}$$

where ζ is the thickness of the atmosphere above the observer in cascade units. $I(\zeta)$ is the meson intensity per cm.^{2}

Taking $\qquad o = 2{\cdot}1$ MEV. per gram per cm.^{2}

we find from (106), (103)

$$n = \frac{(dw/d\theta)_{\text{decay}}}{o} = 0{\cdot}26 \times \frac{24}{\zeta}. \tag{107}$$

426. The actual number of decay electrons observed is larger than given by (107) as most of the decay electrons are parts of cascades coming from higher above. Thus the actual intensity at sea-level depends on the number of mesons higher above and the decay probability higher above in a region of smaller pressure and larger decay rate. A detailed calculation carried out by Rossi and Greisen (1942) shows that the lack of equilibrium is taken care of when introducing into (107) both the intensity and the air density corresponding to a height $\zeta - 3$ instead of the height ζ.

The correct expression for the number of decay electrons per meson is therefore obtained as

$$n' = n\frac{I(\zeta-3)}{I(\zeta)}\frac{\zeta}{\zeta-3}. \tag{108}$$

Introducing numerical values we find:

TABLE 8

Height	$I_{\text{decay}}/I_{\text{meson}}$ *calculated*
259 (Chicago)	0·44
4,300	0·79

427. For sake of completeness we note that we have so far neglected the contribution of mesons which have been stopped completely and decay afterwards. The number of mesons brought to rest is equal to

$$\frac{dI}{d\zeta} \text{ per cascade unit;}$$

each meson at rest gives rise to a decay electron of energy

$$\mu c^2/2 \simeq w_c/2.$$

Hence the range of the decay electrons is $\frac{1}{2}$ cascade unit and the relative number of decay electrons thus produced is given by

$$n'' = \frac{1}{2I}\frac{dI}{d\zeta}.$$

This figure is somewhat uncertain as there is evidence to the effect that some of the slow mesons are captured by nuclei before decay. The above value of n'' is therefore an upper limit.

Intensity of knock-on electron component

428. The mesons also give rise to electron secondaries. The intensity of the soft component due to such knock-on electrons can be estimated in a way very similar to that due to the decay electrons.

The probability of a meson giving rise to a secondary with an energy in the interval w', dw' is according to eq. (177), Ch. III,

$$\mathscr{C}\frac{m_e c^2 dw'}{w'^2}\left(1 - \frac{w'}{w_m}\right); \tag{109}$$

w_m = maximum transferable energy.

This formula is approximately valid for all energies exceeding $m_e c^2$ provided the spin of the meson is taken to be 0 or $\frac{1}{2}$. (Should the spin of the meson be 1, the equation (109) has to be modified for energies w' exceeding 2.10^4 MEV.) The total energy transferred by a meson to electron secondaries with energies w,

$$w_I > a.m_e c^2 \quad (a \gg 1),$$

is obtained from (109) as

$$\frac{dw_I}{d\theta} = \mathscr{C} m_e c^2\left(\log\frac{w_m}{a m_e c^2} - 1\right). \tag{110}$$

For not too high meson energy, we may put

$$w_m = \frac{m_e c^2 p^2}{(\mu c)^2}, \tag{111}$$

where p is the momentum of the meson. Thus we obtain for the rate of energy spent in the production of secondaries

$$\frac{dw_I}{d\theta} = 0{\cdot}15\left(\log_e \frac{\langle p\rangle}{100\sqrt{a}} - 0{\cdot}5\right) \text{ MEV./gram per cm.}^2 \quad (p \text{ in MEV./}c), \tag{112}$$

where $\langle p\rangle$ is the average meson momentum.

We obtain for the average number of knock on electrons accompanying the mesons from (103)

$$n_{\text{knock-on}} = \frac{(dw_I/d\theta)}{o}. \tag{112 a}$$

Introducing

$a = 20$ (corresponding to electrons above 10 MEV.),

$\langle p\rangle = 3{,}500$ MEV. (compare Ch. IV, eq. (21)),

we find $n_{\text{knock-on}} = 0{\cdot}10$ (sea-level).

429. As most of the knock-on electrons have low energies the correction to $n_{\text{knock-on}}$ caused by the lack of equilibrium between electrons and mesons can be neglected.

Comparison with observations

Sea-level and above

430. The intensity of the secondary electron component at a depth ζ can be calculated from (108) and (112a). We proceed to compare these formulae with observations of Greisen (1942).

Greisen carried out measurements at various altitudes, corresponding to values of ζ between 13 and 24. He measured the absorbable part of the cosmic-ray intensity. Greisen measured that fraction of the total intensity which consists of particles with ranges less than

$$167 \text{ grams per cm.}^2$$

The main contribution to this absorbable part is due to electrons. In analysing Greisen's data we have to assume the following contributions to the absorbable intensity:

(1) Knock-on electrons as estimated in § 428.

(2) Decay electrons, estimated in §§ 425–6.

(3) Mesons with ranges less than 167 grams per cm.^{2}

The contribution (3) is of the order of

$$\left(\frac{dI}{d\theta}\right)_{\text{dense}} . 167 \text{ grams per cm.}^2$$

The values of $(dI/d\theta)_{\text{dense}}$ can be taken from the measurements of Rossi, Hilberry, and Hoag (1940) as reported in § 360, Ch. V.

Collecting all data the following table is obtained:

TABLE 9

Relative intensities

Altitudes		*Decay electrons*					
m	ζ	*Fast mesons*	*Slow mesons*	*Slow mesons*	*Knock-on electrons*	*Total calculated*	*Observed*
259	23·4	0·22	0·01	0·07	0·1	0·4	$0·50 \pm 0·02$
1616	19·9	0·31	0·01	0·09	0·1	0·5	$0·74 \pm 0·05$
3240	16·5	0·39	0·02	0·13	0·1	0·65	$1·20 \pm 0·05$
4300	14·3	0·47	0·06	0·27	0·1	0·9	$1·81 \pm 0·06$

It seems from the table above that the soft component *near sea-level* can be accounted for in terms of decay electrons and of knock-on electrons. The observed intensity of the soft component increases, however, much more rapidly than the calculated intensity. It seems, therefore, that the soft component at 4,000 m. above sea-level is only partly due to knock-on electrons and to decay electrons. The excess of the observed component over the calculated secondary soft component is probably due to the descendants of primary electrons. It is seen from Fig. 73 (*a*) that the gap between calculated and observed values shown in Table 9 is of the same order as the primary soft intensity produced by an incident electron spectrum with exponent 1·6.

Below ground

431. The calculation of § 428 of knock-on intensity is based on the approximation (111) for the maximum transferable energy. This approximation holds only for primary energies much smaller than

$$20{,}000 \text{ MEV}. \tag{113}$$

(compare § 157). The average energy of the mesons at sea-level and above is safely below this limit and therefore the use of the approximation (111) is justified for these regions.

The average meson energy is, however, expected to increase below ground (compare eq. (25 a), § 313). For depths of the order of 100 m. water equivalent or more the average meson energy will be above the limit (113) and therefore for these depths the maximum transferable energy may be approximated by

$$w_m \sim pc \tag{114}$$

instead of (111). For such depths we have for the relative intensity of the soft component

$$r_I = 0{\cdot}075\left(\log_e \frac{\langle p\rangle}{am_e c^2} - 1\right). \tag{115}$$

Inserting the value for $\langle p\rangle$, namely

$$\langle p\rangle = \frac{\theta}{\theta_0}\,\frac{2{,}000\ \text{MEV}./c}{z-1}, \tag{116}$$

from equation (21), Ch. IV, we find

$$r_I = 0{\cdot}32 + 0{\cdot}17\log(\theta/\theta_0) \quad \text{for} \quad \theta \geqslant 20\theta_0. \tag{117}$$

Inserting numerical values we find

TABLE 10

Depth in metres H_2O	$n_{\text{knock-on}}$
200	0·58
500	0·65
1,000	0·70

The values of Table 10 may be of the right order of magnitude, though no sufficiently accurate determinations of the relative intensity of the soft component at great depth are available.

(*b*) *Spectrum of the Secondary Soft Component*

432. We determine in the following the differential spectra

$$\mathfrak{S}^{(d)}(w,\zeta) \quad \text{and} \quad \mathfrak{S}^{(k)}(w,\zeta)$$

of electrons found at a depth ζ below the top of the atmosphere. The index (d) refers to 'decay' while the index (k) refers to 'knock-on'.

We shall write $\mathfrak{S}_m(w,\zeta)$ for the differential meson spectrum at the depth ζ and

$$I_m(\zeta) = \int_0^\infty \mathfrak{S}_m(w,\zeta)\,dw$$

for the total meson intensity.

We write for the probability that a meson of energy w' gives rise to an electron of energy in the interval w, dw

$$P(w',w)\,dw d\zeta.$$

The spectrum of electrons produced in a layer $d\zeta$ is then given by

$$\mathfrak{s}(w,\zeta)\,d\zeta = \int^\infty \mathfrak{S}_m(w',\zeta)P(w',w)\,dw'. \tag{118}$$

The electrons of the spectrum $s_{el.}$ produce cascades and the spectrum of electrons at a depth ζ arising from all layers above is given by

$$\mathfrak{S}(w,\zeta) = \int_0^\zeta \int_w^\infty s_{el.}(w',\zeta')q(w',w;\ \zeta-\zeta')\,dw'd\zeta'. \tag{119}$$

We have to evaluate the integral (119) for the cases of decay and of knock-on.

(i) High-energy region

Decay electrons

433. We approximate the meson spectrum by

$$\mathfrak{S}_m(w,\zeta) \simeq zAw^{-(z+1)}. \tag{120}$$

In this approximation we find from (118) and (104) for the differential decay electron spectrum, disregarding cascade multiplication,

$$s^{(d)}(w,\zeta)\,d\zeta = \frac{zA}{z+2}\frac{\mu c^2}{c\ell_0}\frac{\Delta d\zeta}{k(\zeta)}w^{-(z+2)}. \tag{121}$$

To obtain the actual spectrum at a depth ζ below the top of the atmosphere it is necessary to consider the cascade multiplication of the decay electrons.

434. We proceed to calculate the decay spectrum at a depth ζ below the top of the atmosphere arising from all decay electrons produced above. We have to insert (121) into (119).

We note that according to (121) the electrons produced in any layer $d\zeta$ form a power spectrum. According to (56) an incident power spectrum produces a similar spectrum at any depth below. Therefore the integration with respect to w' in (119) can be carried out analytically, and we find

$$\int_w^\infty s_{el.}(w',\zeta')q_0(w',w;\ \zeta-\zeta')\,dw'$$
$$= s_{el.}(w.\ \zeta')\left\{\frac{(\mathfrak{D}-a_1)e^{-a_1(\zeta-\zeta')}+(a_2-\mathfrak{D})e^{-a_2(\zeta-\zeta')}}{a_2-a_1}\right\}_{\mathfrak{y}=z+2}.$$

Introducing $\zeta'' = \zeta-\zeta'$ we have further

$$\mathfrak{S}^{(d)}(w,\zeta) = \frac{zA}{z+2}\frac{\mu c^2}{c\ell_0}\Delta\int_0^\zeta \frac{(\mathfrak{D}-a_1)e^{-a_1\zeta''}+(a_2-\mathfrak{D})e^{-a_2\zeta''}}{(a_2-a_1)k(\zeta-\zeta'')}\,d\zeta'',$$
$$\mathfrak{y} = z+2.$$

The density $k(\zeta-\zeta'')$ varies inversely with depth and we may put approximately

$$\frac{1}{k(\zeta-\zeta'')} = \frac{1}{k(\zeta)}\frac{\zeta}{\zeta-\zeta''} \sim \frac{1}{k(\zeta)}\left(1+\frac{\zeta''}{\zeta}\right). \tag{122}$$

Because of the rapid decrease of the exponentials the integration can be carried to infinity. We thus obtain

$$\mathfrak{S}^{(d)}(w') = \frac{\mathfrak{S}_m(w')}{(z+2)w'} \frac{\mu\Delta}{c\ell_0 k(\zeta)} \left\{ \frac{\mathfrak{D}}{a_1 a_2} + \frac{1}{\zeta} \left(\frac{(a_1+a_2)\mathfrak{D}}{a_1^2 a_2^2} - \frac{1}{a_1 a_2} \right) \right\}_{\mathfrak{p}=z+1}. \quad (123)$$

We may put $z = 2{\cdot}3$

(see Fig. 75). We find $$\frac{\mathfrak{S}^{(d)}(w')}{\mathfrak{S}_m(w')} = \frac{A_D(\zeta)}{w'}, \quad (124)$$

where $A_D(\zeta)$ has the following numerical values:

TABLE 11

Height	ζ	$A_D(\zeta)$
Sea-level	24·0	9·2 MEV.
4,300	13·7	17·0 MEV.

We see from (124) that the spectrum of decay electrons decreases more rapidly than that of the mesons.

In Fig. 75 we have plotted the calculated integral spectra for mesons, decay electrons, and electrons arising from primary cascades. The curves all refer to sea-level. The spectra for higher altitudes are similar, except that the primary electron spectrum becomes rapidly predominant with increasing height.

We note that at sea-level the decay spectrum is more important than the 'primary' spectrum up to moderately high energies. For very high energies the spectra cross and the 'primary' spectrum is predominant. For a primary spectrum with $z = 1{\cdot}6$ the two spectra become equal at 10^5 MEV.

Spectrum of knock-on electrons

435. The rate of knock-on electrons produced in a layer $d\theta$ with energies in the interval w', dw' is obtained from (177), Ch. III, with $v \sim c$, as

$$\mathfrak{s}_k(w', \zeta)\, d\theta = 0{\cdot}075 \frac{dw'}{w'^2} \int \left(1 - \frac{w'}{w_m}\right) \mathfrak{S}_m(p)\, dp d\theta, \quad (125)$$

where p' is the smallest momentum at which a meson can give rise to an electron of energy w'.

Confining ourselves to energies $w' \gg 2 \times 10^4$ MEV. we put

$$w' \sim cp'.$$

With help of (118) and (125) we obtain

$$\mathfrak{s}_k(w', \zeta) = \frac{\mathfrak{S}_m(w')}{z(z+1)w'} 0{\cdot}075. \quad (126)$$

The electron spectrum at a depth ζ is obtained by integrating over the cascades produced above. We obtain as the result of a short calculation

$$\mathfrak{S}^{(k)}(w') = \frac{\mathfrak{S}_m(w')}{w'} 0{\cdot}536 \quad (w' \text{ in MEV.}; \; w' \gg 20{,}000 \text{ MEV.}). \quad (127)$$

We see that the high-energy end of the knock-on spectrum is very

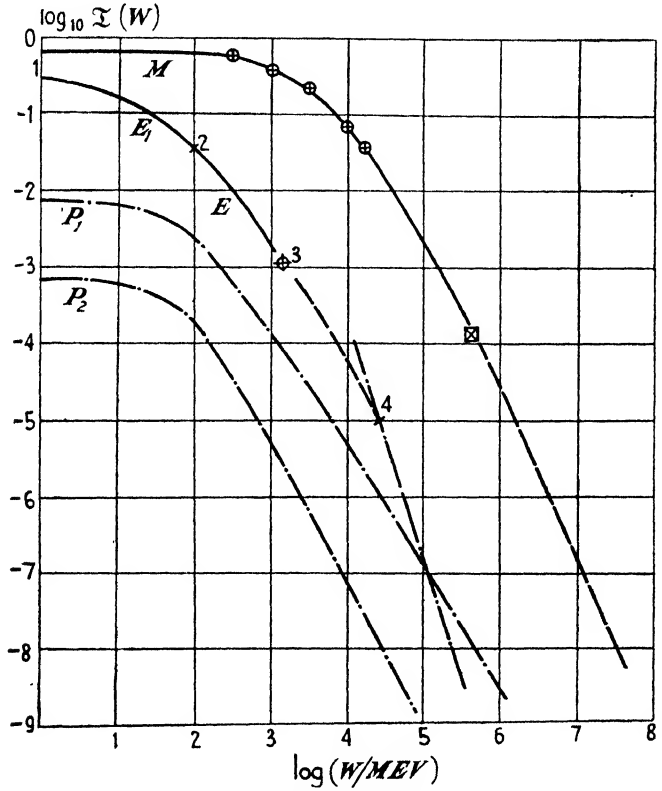

FIG. 75. Integral spectra (particles per sq. cm. per min.).

Curve M, meson spectrum:
- ⊕ observed points
- ⊠ calculated from intensity under 1,000 m. water equivalent
- ——— extrapolated ($z = 2{\cdot}3$)

Curve E, electron spectrum:
- between 1 and 2, obs. Williams (1939)
- 3, obs. Williams (1939)
- beyond 4, calc. from eq. (124)

Curve P_1, calculated spectrum of primary electrons ($z = 1{\cdot}6$)
Curve P_2, as above ($z = 2{\cdot}0$)

similar to that of the spectrum of the decay electrons; both spectra decrease in the same way.

We note that the knock-on spectrum is strongly modified if one

assumes that the mesons have a spin 1 and not 0. In this case we have to replace (125) by

$$s_k(w,\zeta) = 0{\cdot}075\frac{dw'}{w'^2}\int_{w'}^{\infty}\left[\left(1-\frac{w'}{w}\right)\left(1+\frac{1}{3}\frac{w'}{w_0}\right)+\frac{1}{3}\left(\frac{w'}{w}\right)^2\left(1+\frac{1}{2}\frac{w'}{w_0}\right)\right]\mathfrak{S}_m(w)\,dw, \tag{128}$$

where $w_0 = \mu^2c^2/m_e = 20{,}000$ MEV. (see (179), Ch. III). We obtain for the knock-on spectrum

$$\mathfrak{S}^{(k)}(w') = \mathfrak{S}_m(w')\left\{\frac{0{\cdot}726}{w'}+\frac{0{\cdot}485}{w_0}\right\}. \tag{129}$$

Due to the second term in the curly bracket the knock-on spectrum (129) tails off in the same way as the meson spectrum itself for energies $w' \gtrsim w_0$.

We shall discuss the evidence as to the high-energy region of the secondary electron spectrum in §§ 455 and following.

(ii) Low-energy regions

436. The exact spectrum of the low-energy electrons is difficult to estimate, but the following remarks are useful for the determination of the orders of magnitude.

1. *Decay.* The number of low-energy decay electrons is very small as can be shown easily. Low-energy electrons are, however, produced by the cascades due to high-energy electrons. The number of electrons below the critical energy in air may be assumed to be about half the total number of electrons. It is not unreasonable to assume that 5 to 10 per cent. of these have energies below 10 MEV. (compare §§ 392–3).

2. *Knock-on.* The number of knock-on electrons emitted with energies less than w_c is not negligible. Assuming that these electrons are mainly absorbed by ionization we may assume that the range of an electron energy $w < w_c$ is

$$\mathscr{R}(w) = w/w_c.\Delta. \tag{130}$$

The number of electrons with energies in the interval w', dw' is therefore given by

$$\mathfrak{S}^{(k)}(w')\,dw' = 0{\cdot}075\frac{dw'}{w'w_c}I_m = 0{\cdot}033I_m\frac{dw'}{w'}. \tag{131}$$

437. The observed number of electrons between 3 and 100 MEV. is, according to Williams (1939*b*),

$$\text{intensity of electrons } (3 < w' < 100) = 0{\cdot}25I_m, \tag{132}$$

while we find from (131)

$$\int_3^{100} \mathfrak{S}^{(k)}(w')\,dw' = 0{\cdot}033 I_m \log_e \tfrac{100}{3} = 0{\cdot}11 I_m; \tag{133}$$

adding to this number the number of slow electrons arising from decay we obtain a total in reasonable agreement with Williams's figure.

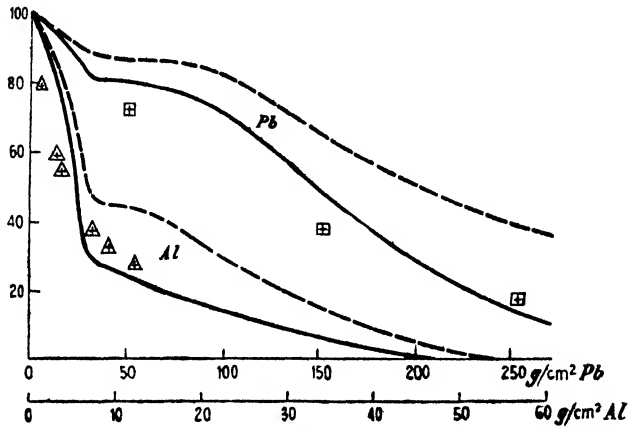

Fig. 76. Calculated absorption curves and observed points. From Arley, *Proc. Roy. Soc.* A, **168**, 537.

(c) *Absorption Curves*

438. The absorption of the soft component in lead and aluminium has been treated by Arley (1938) in terms of cascades. Arley determined the probability of an electron producing at least one electron emerging out of a given absorber.

We write for this probability

$$\mathscr{P}(w, \theta, N \geqslant 1),$$

where θ is the thickness of absorber, w the energy of the incident electron. The absorption function for the soft component is obtained by averaging this probability over the electron spectrum incident on the top of the absorber. One obtains

$$\mathscr{C}(\theta) = \int P(w, \theta, N \geqslant 1)\mathfrak{S}^{(\mathrm{el.})}(w)\,dw. \tag{134}$$

The integral (134), evaluated by Arley (1938), together with some observed points are shown in Fig. 76. The full and broken curves refer to two different assumptions as to the spectral distribution of the electrons.

While there is a qualitative agreement between theory and observation

there are too many uncertainties involved to make the comparison between calculation and observation of this absorption curve a significant test of the theory.

3. *Interpretation of Showers*

Showers are observed by means of:

1. Cloud chamber.
2. Burst chamber.
3. Counter arrangement.

(*a*) *Cloud-chamber Evidence*

439. Cloud-chamber photographs of showers make it likely that most of the showers are cascades. Typical photographs are shown in Plate 2. A few particles are seen to enter a lead plate. While traversing the lead plate the particles give rise to a great number of secondaries. The secondaries spread out fanwise.

The incident particles can be assumed to be electrons forming part of a cascade shower coming from above. These electrons give rise to separate cascades in the lead, and thus a larger number of particles emerge from the bottom of the plate.

According to the cascade theory a large fraction of the particles coming out of the lead must have energies of the order of the critical energy in lead, that is of the order of 7 MEV. The scattering of such low-energy electrons in lead is quite appreciable and therefore the low-energy particles are scattered almost uniformly into widely diverging directions.

Interesting photographs of cascades were also obtained by Hazen (1944*a*). A cloud chamber was used with seven horizontal lead plates. Primary electrons falling on the top plate give rise to cascade showers and the showers are seen to develop while passing through the plates.

440. A photograph of this type is shown in Plate 3. As the photographs were taken without a magnetic field the energies of the shower particles could not be determined. A comparison with the cascade theory can be carried out in the following way.

Assuming a shower to be a cascade the energy w of the primary can be determined from the observed number N of tracks seen on the photograph. From the energy determined in this way the number of particles at the *maximum* can be derived. It is found that the maximum number of particles thus estimated agrees roughly with the observed maximum number seen in the photographs.

The photographs of Hazen thus support the assumption that the showers are cascade showers. More experiments of this kind would be useful.

441. According to the cascade theory, cascade showers should contain positive and negative electrons in about equal numbers. This had already been observed in the early cloud-chamber investigations.

Cloud-chamber evidence is also forthcoming for the occurrence of photons in showers. The photographs *a* and *g*, Plate 3, give examples of showers containing photons.

442. The investigations with the burst chamber can be interpreted very simply; the burst sizes are proportional to the numbers of particles in the showers. Burst chambers are, however, only reliable when large showers are to be investigated.

The combined observations with cloud chamber and burst chamber show that the size distribution of showers obeys a power law within very wide limits (see § 401).

(*b*) *Counter Experiments*

443. Most shower observations have been carried out with counters. Unfortunately, however, results obtained with counter arrangements cannot be interpreted in a simple way. The interpretations are rendered difficult by the complicated geometrical aspects of shower recording sets. It will be therefore necessary to discuss some of the purely geometrical aspects of shower coincidences before giving the physical interpretations of the phenomena.

The geometry of counter arrangements

444. The most important question for the interpretation of counter results is the efficiency of a given counter system of recording a shower containing N particles.

Various authors assume that a shower arrangement which can be discharged by a minimum of n particles is most sensitive to showers containing about n particles. This assumption is completely fallacious as will be seen in the following.

445. The efficiency of a counter arrangement of recording showers of given sizes was measured directly by Montgomery and Montgomery (1935 *b*) in the following way.

A triangular counter set was placed immediately below a spherical burst chamber. A certain fraction of the bursts corresponding to N particles crossing the ionization chamber was found to give rise to

coincidences of the counter arrangement. The fraction of bursts accompanied by coincidences is plotted in Fig. 77 against N, the number of particles.

We note that only bursts containing many more than three particles are recorded efficiently by the triple coincidence system.

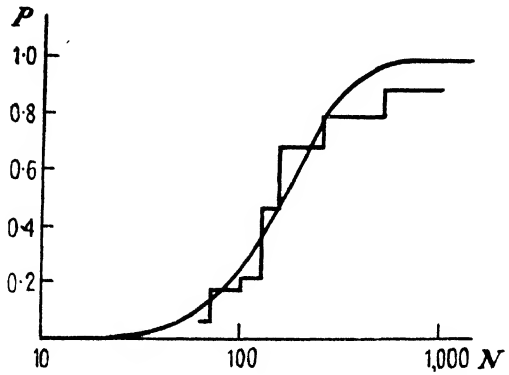

FIG. 77. Observed and calculated relation between bursts and shower coincidences (Montgomery and Montgomery, *Phys. Rev.* **48**, 786 (1935)).

446. The observations shown in Fig. 77 were interpreted by Montgomery in the following way.

Most of the showers recorded by chamber and counters can be assumed to originate from a 2·5-cm. thick lead absorber placed over the chamber. The solid angle subtended by the chamber as seen from a point in the absorber may be denoted Ω while the solid angle subtended by any of the counters is ω.

It is assumed that the probability that a shower particle after having passed through the chamber is also passing through a given counter is given by

$$p = \omega/\Omega. \tag{135}$$

For the actual arrangement of Montgomery it is found that

$$p = 0{\cdot}01. \tag{136}$$

Consider n counters placed below the chamber. The probability that out of N particles passing through the chamber, j_1 pass through the first counter, j_2 through the second counter, and so on, is given by

$$\mathscr{P}(j_1, j_2, \ldots) = \frac{N!\, p^{j_1+j_2+\ldots}(1-np)^{N-j_1-j_2-\ldots}}{j_1!\, j_2! \ldots (N-j_1-j_2-\ldots)!}. \tag{137}$$

An n-fold coincidence is registered whenever at least one particle passes through each of the counters. This probability is given by

$$\mathscr{P}_N = \sum \mathscr{P}(j_1 \geqslant 1, j_2 \geqslant 1, \ldots). \tag{138}$$

The summation in (138) can be carried out and as the result of a short calculation we obtain

$$\mathscr{P}_n = \sum_{j=0}^{n} \binom{n}{j} (-1)^j (1-jp)^j. \tag{139}$$

The expression (139) was found by Montgomery and is plotted in Fig. 77 for $p = 0{\cdot}01$, and for various p in Fig. 78. The agreement

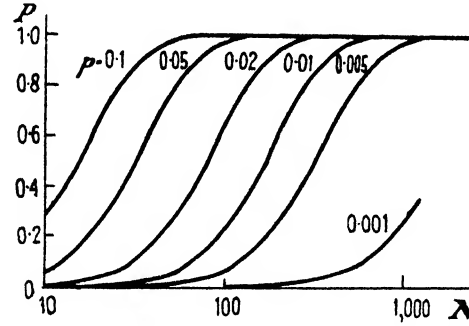

FIG. 78. *A priori* probabilities. (Montgomery, *Phys. Rev.* **48**, 786 (1935).)

between (139) and the observation is remarkably good when we remember that the expression (139) contains no adjustable parameter.

The total rate of coincidences is

$$\mathscr{C}_n = A \sum_{N=n}^{\infty} \mathscr{P}_N \frac{z}{N^{z+1}}. \tag{140}$$

It was found that (140) is in fair agreement with observation.

It is convenient to replace the distribution (139) by the following approximation: for $p \ll 1$ we may put

$$(1-jp)^N \sim \exp(-jpN),$$

and therefore we have instead of (139)

$$\mathscr{P}_N \approx \{1-\exp(-pN)\}^n. \tag{141}$$

447. It is interesting to estimate the size of showers which are mainly responsible for the observed coincidences.

Introducing (141) into (140) and replacing the sum by an integral we have

$$\mathscr{C}_n = A \int_{n-\frac{1}{2}}^{\infty} \frac{z\,dN}{N^{z+1}} (1-e^{-pN})^n. \tag{142}$$

Introducing a new variable

$$\log y = N, \tag{143}$$

we may write

$$\mathscr{C}_n = A \int \exp\{-zy + n \log(1 - e^{-pN})\}\, dy. \tag{144}$$

For $n > z$ the integrand has a strong maximum, and the integral can be evaluated by the saddle-point method. As the result of a simple calculation we find that the maximum is reached for $N = N_0$, with

$$N_0 = a/p, \tag{145}$$

where a is the solution of the following equation:

$$\frac{z}{n} = \frac{a}{e^a - 1}. \tag{146}$$

The value of the integral itself is obtained as

$$\mathscr{C}_n = \frac{A}{N_0^z} \gamma, \tag{147}$$

with

$$\gamma = \frac{\sqrt{(2\pi z)}(1 - e^{-a})^n}{\sqrt{\{(z/n)e^a - 1\}}}. \tag{148}$$

Introducing $n = 3$ and $z = 2{\cdot}3$ we find

$$a = 0{\cdot}5.$$

For the arrangement of Montgomery (1935*b*) we may put $p = 0{\cdot}01$ and thus we have

$$N_0 = 50. \tag{149}$$

The size distribution of showers and the cascade theory

In the following we shall interpret shower observations in terms of cascades. We shall make use in this section of the electron spectra derived further above. These spectra are given by eq. (101) for primary, eq. (124) for decay, eqs. (127), (129) for knock-on electrons.

(i) Showers due to decay electrons

448. The number $N(w)$ of particles produced by an electron of energy w falling on an absorber of thickness ζ is roughly given by

$$N \sim w^{\vartheta_0 - 1} \tag{150}$$

as can be seen from (70) and (71). The number of showers containing more than $N(w)$ particles is expected to be equal to the number of electrons with energies exceeding w. We assume the incident electron spectrum to be given by

$$\mathfrak{S}_{\text{el.}}(w) \sim w^{-(z+1)} \quad (z = 2{\cdot}6) \tag{151}$$

(compare (124)). The observed distribution (86) can thus be derived from the spectrum (151) provided the following equation is fulfilled:

$$2{\cdot}3/(\eta_0 - 1) = 2{\cdot}6; \tag{152}$$

and therefore

$$\eta_0 = 1{\cdot}8. \tag{153}$$

We have evaluated $N(w)$ for $\zeta = 3$ and $\zeta = 5$ with help of (70) and (71)

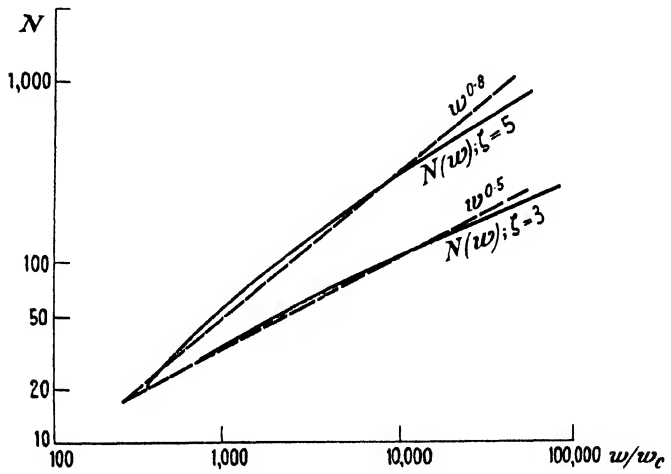

FIG. 79. Cascade figures for $\zeta = 3$ and $\zeta = 5$.

(Fig. 79). It is seen that for $\zeta = 5$, $N(w)$ is fairly well approximated by $w^{0{\cdot}8}$ (broken line) in the region from 20 to 1,000 particles.

We conclude therefore that the size distribution of bursts as observed by the Montgomerys (1935 *b*) can be accounted for in terms of cascade showers produced by decay electrons.

449. Further evidence for the interpretation of bursts in terms of cascade showers is obtained from the observations of Braddick (1939). Braddick used an ionization chamber under 1·5 cm. of lead. This absorber corresponds to

$$\zeta = 3.$$

We have plotted in Fig. 79 $N(w)$ for $\zeta = 3$. It is seen from the graph that we can put approximately

$$N(w) \sim w^{0{\cdot}5} \quad \text{for} \quad \zeta = 3$$

and therefore the burst distribution should be given by

$$\mathfrak{S}(N) \sim N^{-5{\cdot}2}.$$

The exponent observed by Braddick is 4·2 instead of 5·2, this is in qualitative agreement with the calculation. The actual cascade calculation

is of course not very accurate for such a small thickness. Comparing the results of Montgomery ($\zeta = 5$) with those of Braddick ($\zeta = 3$), it must be regarded as satisfactory that the observed value of the exponent z increases with decreasing thickness of absorber, just as expected from the theory of cascade showers.

450. The absolute rate of bursts can also be understood qualitatively. The rate of bursts at sea-level observed by Braddick (1939) was 4·6 per hour. The collecting area of the lead was 630 cm.^{2} Thus the rate of bursts per cm.^{2} per min. is

$$4{\cdot}6/(60\times 630) = 1{\cdot}2.10^{-4}. \tag{154}$$

The rate (154) is equal to that of decay electrons of

$$w = 6{,}000 \text{ MEV.} = 860 w_c \text{ (lead)}$$

as can be seen from Fig. 75. Further, we find from Fig. 79 that electrons of 6,000 MEV. give rise to showers of about 30 particles.

According to Braddick's calibration the smallest bursts recorded contained 40 particles.

We conclude that the observed rate of showers is in agreement with the calculated intensity of decay electrons.

(ii) Showers due to knock-on electrons

451. The electron spectrum at sea-level contains apart from decay electrons also knock-on electrons. Inspecting eqs. (124) and (127) we see that the number of knock-on electrons must be assumed to be small compared with the number of decay electrons. The actual number of knock-on electrons is correctly given by theory, as shown by J. G. Wilson (1938*a*) and in more detail by Seren (1942).

That showers above sea-level are due to both decay electrons and knock-on electrons is, however, supported by observations showing that the shower intensity shows a very pronounced 'absorption anomaly'.

It was found by Drigo (1935), Auger, Leprince-Ringuet, and Ehrenfest (1936*b*), Jánossy (1938*a*), and others that the rate of showers observed decreases strongly when layers of dense material are placed above the arrangement.

This anomaly is shown even more clearly by measurements due to Ehmert (1937) showing that for the first few metres under ground the rate of showers is absorbed much more strongly than the hard component. The absorption is interpreted as bein g due to the absorption of the decay electrons in the ground.

(iii) Primary electrons

452. *Height-intensity distribution of showers.* Considering the height-intensity distribution of showers one has to distinguish clearly two types of experiments.

1. Showers observed under thin lead 1–3 cm. thick.

2. Showers observed under thick screens of lead, say 10 cm. thick.

453. (1) Showers observed under thin layers of lead increase very strongly with height. The following figures have been collected by Euler and Heisenberg (1938).

TABLE 12

Increase of shower rate under thin absorbers

Size of shower	*Increase between sea-level and 45 cm. Hg pressure*	*Observer*
< 10	8·5	Woodward (1936)
10	10	Young and Street (1937)
20	17	
30	22	
40	26	Montgomery (1935*a*)

It is seen that the rate of showers increases more rapidly for larger showers than for smaller showers. This difference in the rates of increase was explained by Euler and Heisenberg (1938) as being due to the superposition of the decay spectrum and the primary spectrum of electrons.

The different rates of increase with height for showers of different sizes can be understood as follows.

Considering showers due to *decay* electrons only, we expect a small increase of shower rate with height. The increase of the decay-electron showers is mainly due to the increase of the decay rate with height due to the decrease of air density.

The showers due to *primary* electrons are expected to increase very rapidly with height. The increase is expected to be roughly exponential and the rate of increase is independent of shower size (see § 384).

The total shower rate is due to both decay showers and primary showers. At small energies, however, the decay spectrum is relatively more important than the primary spectrum. Therefore the rate of increase of the small showers will be nearly that of the increase of the decay spectrum. At large energies the primary spectrum becomes gradually more important than the decay spectrum. Therefore the rate

of increase of large showers is mainly determined by the (large) rate of increase of the primary spectrum.

The increase of the burst rates as observed for different shower sizes could not be accounted for in terms of decay electrons alone. This conclusion confirms that of Rossi and Greisen (1942) to the effect that the soft component increases with height more rapidly than the decay-electron component.

One expects therefore that with increasing shower size the primary showers become gradually predominant and the rate of increase with height increases gradually from that of the decay electrons to that of the primary electrons.

454. (2) Showers observed under sufficiently thick lead absorbers cannot be due either to decay electrons or to primary electrons. Such bursts must be assumed either to be due to knock-on electrons or to quanta emitted by mesons in radiative collisions. The rate of such bursts should be proportional to the intensity of the more energetic part of the meson spectrum and therefore the rate of such bursts is not expected to increase with increasing height.

The rate of bursts observed by Schein and Gill (1939) under 12 cm. of lead shows, however, a slight increase with height as can be seen from the following table.

TABLE 13

Relative burst frequency under 12 *cm. of lead*

(Schein and Gill, 1939)

Height	*Sea-level*	*2,285 m.*	*3,350 m.*
Relative frequency	1	2·0	3·6

The increase of burst frequency with height as shown in the above table may be due to the presence of a few energetic primary electrons, capable of penetrating 12 cm. of lead.

The spin of the meson

455. The rate of bursts observed under thick absorbers can be used to determine the number of energetic electrons produced by mesons. The number of secondary electrons of high energy depends strongly on the spin of the meson. From (127) and (129) it is seen that many more high-energy secondaries are to be expected from the meson if it has spin 1 than are to be expected from the meson with spin 0 or $\frac{1}{2}$. Detailed calculations of Christy and Kusaka (1941 *b*) show that the rate of bursts observed by Schein and Gill (1939) can be well accounted for by

assuming the meson to have spin 0 or $\frac{1}{2}$. The assumption of a spin 1 is shown to lead to a too large number of expected bursts (see Fig. 80).

As a spin $\frac{1}{2}$ is not very likely on general grounds it is most likely therefore that the meson has a spin 0. A different conclusion is reached by Chakrabarty (1942*a*).

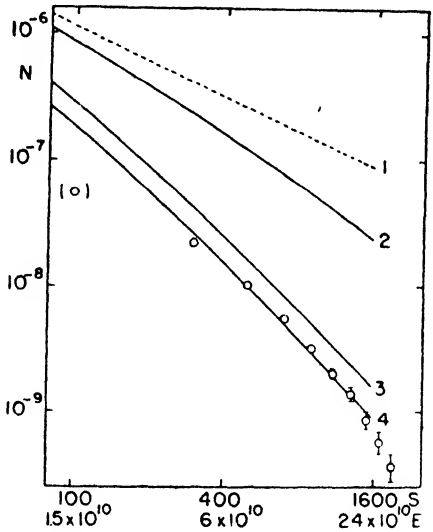

FIG. 80. Plot of burst frequency per sec. per cm.² against minimum burst size. Curves 1, 2 calculated for spin 1, curve 3 calculated for spin $\frac{1}{2}$, curve 4 calculated for spin 0. Christy and Kusaka, *Phys. Rev.* **59**, 414 (1941).

We note that according to Möller and Rosenfeld (1940) the spin of the 'ordinary' meson is 0, while that of the short-lived vector meson is 1 (see § 220, Ch. III).

The Rossi transition effect

Position of the maximum

456. The Rossi transition (see Fig. 65) can be accounted for in terms of cascade showers. Assume for simplicity that showers containing more than N_0 particles are always recorded by a given arrangement while showers with fewer particles are never recorded. According to § 447, for a typical arrangement, we may put N_0 of the order of 50.

The rate of showers under an absorber is therefore to be expected of the order of

$$\mathscr{C}(\zeta) = \mathfrak{T}_{\text{el.}}\{w(N_0, \zeta)\}, \tag{155}$$

where $w(N_0, \zeta)$ is the primary energy giving rise to N_0 particles under the thickness ζ. Plotting $w(N_0, \zeta)$ against ζ, for fixed N_0, we obtain a curve

with a flat minimum at ζ_0 (see Fig. 81). The transition curve itself is obtained from (155); we see that the maximum of the shower rate is found at $\zeta = \zeta_0$. At the thickness $\zeta = \zeta_0$ the largest possible part of the spectrum is capable of producing coincidences.

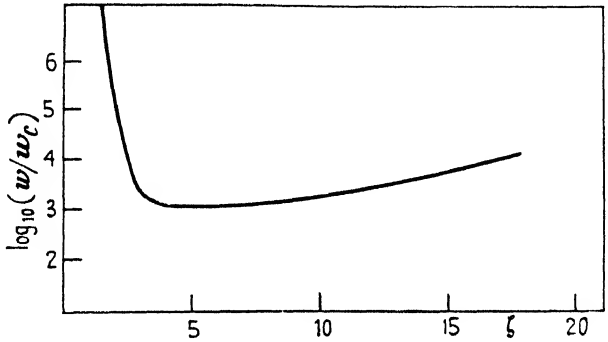

FIG. 81. The function $w(N_0, \zeta)$ for $N = 50$.

Assuming for instance $N_0 = 50$ (compare (149)) we find

$$w(\zeta_0) = 5{,}000 \text{ MEV. and } \zeta_0 = 4{\cdot}5 \text{ cascade units} = 2{\cdot}3 \text{ cm. Pb.} \quad (156)$$

The above value of ζ_0 is of the same order as the depth at which the Rossi maximum is observed.

First slope of the transition curve

457. The first slope of the transition curve is found to be roughly proportional to Z^2/A when comparing different elements (see § 406). Thus

$$\frac{d\mathscr{C}_n}{d\theta} \sim Z^2/A. \quad (157)$$

The above relation can be understood in the following way, provided we confine ourselves to very small thicknesses only:

We note that the energies responsible for most of the cascades are large compared with both the critical energy in air and the critical energy of the absorber. A high-energy electron traversing a thin layer of material gives rise only to few low-energy electrons and therefore the numbers of particles produced by high-energy primaries in thin layers of different elements are about the same per cascade unit, provided the thicknesses are sufficiently small.

Thus we expect $$\frac{d\mathscr{C}_n}{d\zeta} = \frac{d\mathscr{C}_n}{d\theta}\Delta(Z) \sim \text{const.}$$

and $$\Delta(Z) \sim A/Z^2.$$

We are led to the relation (157).

For larger thicknesses, the low-energy electrons become increasingly important. Therefore a cascade in a light element develops to a much smaller extent than a cascade of the same energy develops in a heavy element. It is therefore clear that the maximum rates of showers are smaller in light elements than they are in heavy elements. Transition curves in Fe and Pb observed by Morgan and Nielsen (1937) are shown in Fig. 82.

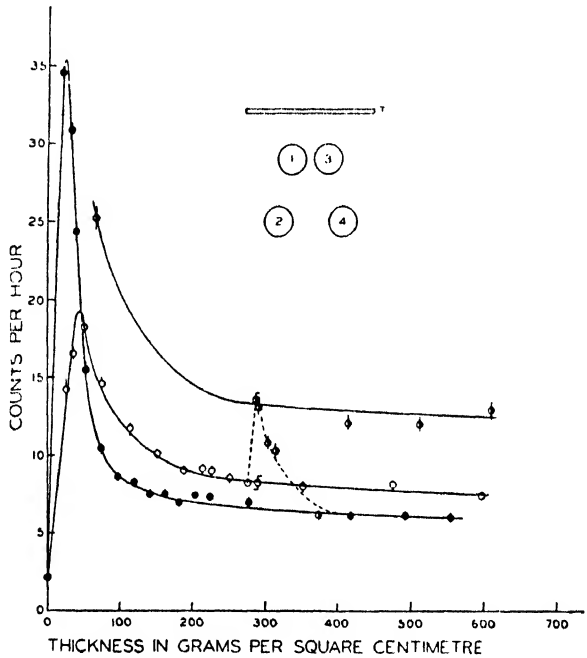

FIG. 82. Shower transition curves for lead ● and iron ○. From Morgan and Nielsen, *J. of Franklin Inst.* **226**, 617.

VII

GEOMAGNETIC EFFECTS

458. The cosmic-ray intensity is found to vary with geomagnetic coordinates. Near sea-level the intensity is about 10 per cent. smaller at the geomagnetic equator than at high latitudes. The latitude effect and other similar effects can be understood in terms of the deflexion of charged primary cosmic-ray particles in the magnetic field of the earth while far outside the earth's atmosphere.

In the first part of this chapter we give the theory of the motion of charged particles in the earth's field due to Störmer (see for references to earlier work Störmer (1930)), and further developed by Lemaître and Vallarta (1933) (see also Vallarta (1938)). In the second part we shall give the observations and their interpretations in terms of the theory of the motion of charged particles in the field of a magnetic dipole.

A. Theory of the Motion of Charged Particles in a Magnetic Field

1. *Equations of Motion*

459. The equation of motion of a charged particle in an electromagnetic field with components **E** and **H** can be written as

$$\frac{d}{dt}(m\dot{\mathbf{r}}) = e\left(\mathbf{E} + \frac{1}{c}\dot{\mathbf{r}} \wedge \mathbf{H}\right). \tag{1}$$

The left-hand side of (1) represents the rate of change of the relativistic momentum, while the right-hand side is equal to the Lorentz force. We have

$$m = m_0 B, \tag{2}$$

where m_0 is the rest-mass of the particle.

460. For later application we give the Hamiltonian form of the equation of motion.

The canonical coordinates and momenta of a charged particle can be shown to be (compare e.g. Heitler, *Quantum Theory of Radiation*, p. 15)

$$q_i = x, y, z \quad \text{and} \quad \pi_i = p_i + \frac{e}{c}A_i, \tag{3}$$

where A_i $(i = 1, 2, 3)$ are the components of the vector potential **A** at the position of the particle and p_i $(i = 1, 2, 3)$ are the components of the momentum of the particle.

The relativistic Hamilton function is given by

$$\mathscr{H} = c\sqrt{\left\{m_0^2c^2+\left(\boldsymbol{\pi}-\frac{e}{c}\mathbf{A}\right)^2\right\}}+e\Phi. \tag{4}$$

And the equations of motion are

$$\dot{q}_i = \frac{\partial\mathscr{H}}{\partial\pi_i}, \qquad \dot{\pi}_i = -\frac{\partial\mathscr{H}}{\partial q_i}. \tag{5}$$

The equations (3), (4), and (5) can be reduced to the original equation (1) with the help of the well-known relations

$$\mathbf{H} = \operatorname{curl}\mathbf{A}, \qquad \mathbf{E} = -\frac{1}{c}\frac{\partial\mathbf{A}}{\partial t}-\operatorname{grad}\Phi, \qquad \operatorname{div}\mathbf{A}+\frac{1}{c}\frac{\partial\Phi}{\partial t} = 0. \tag{6}$$

461. In a pure magnetic field $\mathbf{E} = 0$, and from (1)

$$m\dot{\mathbf{r}}\frac{d}{dt}(m\dot{\mathbf{r}}) = 0. \tag{7}$$

Therefore

$$|\mathbf{p}| = |m\dot{\mathbf{r}}| = \text{const.} \tag{8}$$

We note that the absolute value of the momentum is constant and therefore the relativistic mass itself is constant.

In case of a pure magnetic field we may write instead of (1)

$$\frac{d^2\mathbf{r}}{dt^2} = (e/mc)(\mathbf{r}\wedge\mathbf{H}), \tag{9}$$

where m is the constant relativistic mass of the particle.

(*a*) *Liouville's Theorem*

462. In the following we consider the motion of a large number of electrically charged particles. It will be assumed that the number of particles is sufficiently large so that the distribution of the particles can be described in terms of a density. It is also assumed that the particle density is sufficiently small so that the interaction between the particles can be neglected.

Write δN^* for the number of particles which have at the time t coordinates in the interval $\mathbf{r}$, $\delta\mathbf{r}$ ($\delta\mathbf{r} = \delta x\delta y\delta z$) and momenta in the interval $\boldsymbol{\pi}$, $\boldsymbol{\pi}+\delta\boldsymbol{\pi}$. The particle density round the point $\mathbf{r}$ and momentum $\boldsymbol{\pi}$ can thus be expressed as

$$D = \frac{\delta N^*}{\delta\mathscr{V}^*} \tag{10}$$

with

$$\delta\mathscr{V}^* = \delta x\delta y\delta z\delta\pi_x\,\delta\pi_y\,\delta\pi_z. \tag{11}$$

During a short time interval Δt the δN^* particles will move, and at the time $t+\Delta t$ they will occupy instead of the region $\delta\mathscr{V}^*$ the region

$$\delta\mathscr{V}^{*\prime} = \delta x'\delta y'\delta z'\delta\pi_x'\,\delta\pi_y'\,\delta\pi_z' \tag{12}$$

with

$$\delta x' = \delta x\left(1+\frac{\partial\dot{x}}{\partial x}\Delta t\right),\ldots, \text{ etc.}, \qquad \delta\pi_x' = \delta\pi_x\left(1+\frac{\partial\dot{\pi}_x}{\partial\pi_x}\Delta t\right),\ldots, \text{ etc.} \tag{13}$$

Neglecting higher powers of Δt we find with (11), (12), and (13)

$$\delta\mathscr{V}^{*\prime}-\delta\mathscr{V}^* = \Delta t\,\delta\mathscr{V}^*\left(\frac{\partial\dot{x}}{\partial x}+\frac{\partial\dot{y}}{\partial y}+\frac{\partial\dot{z}}{\partial z}+\frac{\partial\dot{\pi}_x}{\partial\pi_x}+\frac{\partial\dot{\pi}_y}{\partial\pi_y}+\frac{\partial\dot{\pi}_z}{\partial\pi_z}\right), \tag{14}$$

and therefore with the help of (5) and (10)

$$\frac{dD^*}{dt} = 0. \tag{15}$$

The above equation is known as Liouville's theorem.

463. For a constant electromagnetic field Liouville's theorem can be reformulated in the following way. Consider the particle density defined instead of (10) thus:

$$\bar{D}^* = \frac{\delta\bar{N}^*}{\delta\bar{\mathscr{V}}^*} \quad \text{with} \quad \delta\bar{\mathscr{V}}^* = \delta x\delta y\delta z\delta p_x\,\delta p_y\,\delta p_z. \tag{16}$$

$\delta\bar{N}^*$ is the number of particles in $\delta\bar{\mathscr{V}}^*$. We find with the help of (3) and (5)

$$\frac{d}{dt}(\bar{D}^*-D^*) = \frac{e}{m}D^*\operatorname{div}\mathbf{A}.$$

For a constant field $\operatorname{div}\mathbf{A} = 0$ (eq. (6)) and therefore

$$\frac{d\bar{D}^*}{dt} = 0. \tag{17}$$

464. We discuss the connexion between the density $\bar{D}^*$ and particle intensity.

The intensity i of the particles with momentum p at a point A in direction $\mathbf{n}$ can be written as

$$i = \frac{\delta N}{\delta S\delta\Omega\delta p\delta t}, \tag{18}$$

where δN is the number of particles with momentum in the interval δp crossing the area δS in the time δt moving inside the solid angle $\delta\Omega$. It is supposed that the solid angle $\delta\Omega$ is small, and that the particles move nearly at right angles to δS.

We write $$\delta N = \int\ldots\int \bar{D}^*\,dp_x dp_y dp_z dxdydz, \tag{19}$$

where the integrations have to be carried out over the region occupied by the δN particles at the time t. Introducing new variables we find easily

$$dxdydz = dS\frac{p\,dt}{m} \quad \text{and} \quad dp_x dp_y dp_z = p^2 dpd\Omega.$$

Thus $$\delta N = \int \ldots \int \bar{D}^* \frac{p^3}{m} dSdtdpd\Omega = (\bar{D}^*)_{\text{average}}\, \delta S \delta\Omega \delta p \delta t, \qquad (20)$$

where $(\bar{D}^*)_{\text{average}}$ is the average value of $\bar{D}^*$ taken over the region of integration. Dropping the average sign we see therefore

$$i = \frac{p^3}{m}\bar{D}^*;$$

as p and m are constants of the motion for a static magnetic field we find from (17)

$$\frac{di}{dt} = 0. \qquad (21)$$

The significance of (21) is that a group of particles starting from a volume element $\delta\mathscr{V}$ with momenta $\mathbf{p}$, $\delta\mathbf{p}$ give rise to a beam of *constant intensity* along their path.

(*b*) *Application of Liouville's Theorem to the Motion of Cosmic-ray Particles*

465. The theorem given in the last paragraph was applied to the distribution of the cosmic-ray intensity in the vicinity of the earth (Lemaître and Vallarta (1933, 5), Swann (1933), Fermi and Rossi (1933), Rossi (1934*b*)). Assume the cosmic-ray intensity i_∞ at a large distance from the earth to be isotropic. The particles reaching the vicinity of the earth can be traced back to infinity along beams of constant intensity, and therefore the intensity in any point and direction near the earth, which can be reached at all by particles coming from infinity, must be i_∞. As will be seen later there are directions which cannot be reached by particles coming from infinity. The intensity in directions which are accessible to particles of momentum p coming from infinity is the same as it would have been without the magnetic field.

The intensity distribution of the incident particles near the earth can thus be determined if it is known which directions of incidence are 'forbidden' by the magnetic field. The determination of the forbidden directions will be the main task of the following paragraphs.

466. It may be noted that the actual shapes of individual orbits will only be important in connexion with problems where the radiation intensity cannot be regarded as isotropic at infinity. Problems of this

kind may arise in attempts to localize the sources of cosmic rays in definite directions. An anisotropy at large distances is also assumed in the theory of Compton and Getting (1935), in which it is assumed that the radiation intensity is anisotropic inside our galaxy due to the Doppler effect and aberration caused by galactic rotation.

Anisotropy at large distance from the earth may also be caused by the permanent magnetic field of the sun (Jánossy (1937)).

2. *Orbits in the Field of a Magnetic Dipole*

(*a*) *The Dipole Field*

467. The field of a dipole with moment M which is parallel to the z-axis can be written

$$\mathbf{H} = -\text{grad}(\mathrm{M}z/r^3), \tag{22}$$

whence with the help of (9) we find

$$\frac{d^2\mathbf{r}}{dt^2} = -\frac{e\mathrm{M}}{mc}\left(\frac{d\mathbf{r}}{dt} \wedge \text{grad}(z/r^3)\right). \tag{23}$$

As the velocity of the particles is constant, we can introduce instead of the time the length of arc as the independent variable. We thus put

$$t = s/v. \tag{24}$$

Introducing (24) into (23), the momentum of the particles and the moment of the dipole occur only in the combination

$$\mathfrak{s}^2 = |e\mathrm{M}/cp|. \tag{25}$$

$\mathfrak{s}^2$ has the dimension of a length. It is convenient to introduce $\mathfrak{s}^2$ as the unit of length (Störmer) and thus to put

$$\mathfrak{s} = 1. \tag{26}$$

In this way the equations of motion written down in components are as follows (the positive z-axis has to be taken in the direction of $e\mathbf{M}$):

$$\left.\begin{aligned} x'' &= -\frac{1}{r^5}[3yzz' - (3z^2 - r^2)y'], \\ y'' &= -\frac{1}{r^5}[(3z^2 - r^2)x' - 3xzz'], \\ z'' &= -\frac{1}{r^5}[3xzy' - 3zyx'], \end{aligned}\right\} \tag{27}$$

where the dash represents differentiation with respect to s. In the above units the equations of motion (27) are freed from both p and M. We note, however, that the unit of length depends on these quantities.

The respective units of length have to be converted when comparing the orbits of particles with different momenta moving in the same field.

(b) Integration of the Equations of Motion

468. Introduce cylindrical coordinates defined by

$$\varpi^2 = r^2 - z^2 = x^2 + y^2, \qquad \phi = \tan^{-1}\frac{y}{x}. \tag{28}$$

The equations (27) can thus be separated into two independent systems. Multiplying the first of the equations (27) by $-y$, the second by x, and adding, a new equation is obtained, both sides of which have the forms of total differentials. Integrating this equation we obtain with the help of (28)

$$\varpi^2\phi' = 2\mathfrak{g} - \frac{\varpi^2}{r^3}. \tag{29}$$

The constant of integration $\mathfrak{g}$ is the angular momentum of the particle at infinity with respect to the dipole.

469. According to the definition of s

$$\varpi'^2 + \varpi^2\phi'^2 + z'^2 = 1 \tag{30}$$

and thus we obtain from (29) and (30)

$$\varpi'^2 + z'^2 = 1 - \left(\frac{2\mathfrak{g}}{\varpi} - \frac{\varpi}{r^3}\right)^2. \tag{31}$$

Putting

$$Q = 1 - \left(\frac{2\mathfrak{g}}{\varpi} - \frac{\varpi}{r^3}\right)^2 \tag{32}$$

we find with the help of (27), (29), and (32)

$$z'' = \frac{1}{2}\frac{\partial Q}{\partial z}. \tag{33}$$

Further, differentiating (30) with respect to s we obtain with the help of (31), (32), and (33) $\left(\text{note that } Q' = \frac{\partial Q}{\partial \varpi}\varpi' + \frac{\partial Q}{\partial z}z'\right)$

$$\varpi'' = \frac{1}{2}\frac{\partial Q}{\partial \varpi}. \tag{34}$$

470. The motion of the particle is defined by the equation (29) together with the equations (32), (33), (34). These equations are due to Störmer (see e.g. Störmer (1934)) and they permit the following simple interpretation.

The equation (29) describes the motion of the meridian plane containing

the particle; the equations (32), (33), (34) describe the motion of the particle in this moving meridian plane (Fig. 83).

The position of the particle in the meridian plane is defined by the rectangular coordinates ϖ and z. From (33), (34) it is seen that the motion is exactly the same as if the particle were moving under the influence of a potential $-Q/2$. From (31) and (32) it is clear that the velocity

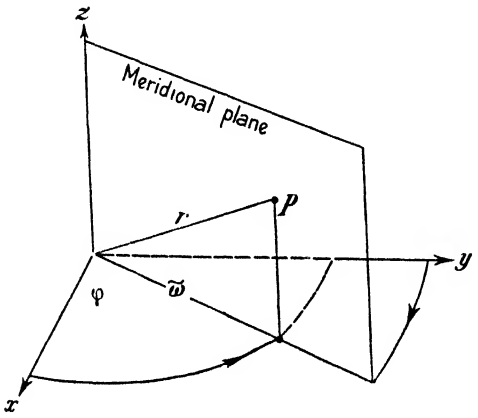

FIG. 83. Separation of the motion of a particle into two components.

of the particle is equal to unity when at infinity. (For simplicity the expression 'velocity' is used for derivatives with respect to s.)

Orbits in the equatorial plane

471. In the following we derive the orbits which lie entirely in the equatorial plane. For such orbits

$$z = z' = 0 \quad \text{and} \quad \varpi = r. \tag{35}$$

Introducing these values into (29) and (30)

$$\begin{aligned}\phi - \phi_0 &= \int \frac{(2g - 1/r)\,dr/r^2}{\sqrt{\{(1-1/r^2)(2g-1/r)^2\}}} \\ &= +\frac{1}{2}\sin^{-1}\left(\frac{2g}{r} - \frac{1}{r^2}\right) + \frac{g}{\sqrt{2}} F\left(\frac{\sqrt{(1+g^2)}}{\sqrt{2}}, \cos^{-1}\frac{g - 1/r}{\sqrt{(1+g^2)}}\right),\end{aligned} \tag{36}$$

with

$$r > \sqrt{(1+g^2)} - g,$$

where F is the elliptic integral of the first kind defined as

$$F(k, \phi) = \int_0^{\phi} \frac{d\psi}{\sqrt{(1 - k^2 \sin^2\psi)}}.$$

472. For
$$\mathfrak{g} = 1 \tag{37}$$
the expression (36) tends towards infinity for $r \to 1$. The corresponding orbit is a spiral which approaches the circle $r = 1$ asymptotically either from outside or from the inside. From (29) and (30) it can be seen that the equations of motion admit also the following singular solution
$$r = 1, \qquad \phi = s. \tag{38}$$
The solution (38) represents a periodic orbit. This periodic orbit is unstable, as the smallest disturbance would throw the particle out from this orbit into one of the two asymptotic orbits. The periodic orbit (38) is an example of an infinite number of periodic orbits.

The periodic orbits and the orbits asymptotic to periodic orbits have been investigated in great detail by Störmer, Lemaître (1934), and others (see for literature Vallarta (1938), Vallarta and Godart (1939)). They play an important role in connexion with the determination of forbidden directions.

(c) *Forbidden Directions*

Forbidden directions in the equatorial plane

A direction is called forbidden if no particles coming from infinity can approach along this direction. We proceed to determine forbidden directions in the equatorial plane.

473. Introduce the angle ω between the tangent to the circle round the dipole and the tangent of the orbit. The positive direction in the circle should be taken in the direction of the periodic orbit (38). We have thus
$$\cos\omega = r\phi', \qquad \sin\omega = -r' \tag{39}$$
and with help of (29),
$$\cos\omega = 2\mathfrak{g}/r - 1/r^2 \tag{40}$$
or
$$\mathfrak{g} = \frac{1+r^2\cos\omega}{2r}. \tag{41}$$

Orbits of particles moving in the equatorial plane can also be represented in the $(r, \mathfrak{g})$-plane. As $\mathfrak{g}$ is a constant of the motion, each orbit is represented there as a straight line parallel to the r-axis.

474. As $\cos\omega$ has necessarily a value between 1 and -1 only certain parts of the $(r, \mathfrak{g})$-plane are accessible to orbits. The boundaries of this region are found by inserting the extreme values for the cosine into (41). The equations of the boundary lines are as follows:
$$\left.\begin{aligned} &\text{(I)} \quad \mathfrak{g} = (1+r^2)/2r, \\ &\text{(II)} \quad \mathfrak{g} = (1-r^2)/2r. \end{aligned}\right\} \tag{42}$$
The equations (42) represent two hyperbolae in the $(r, \mathfrak{g})$-plane. These

hyperbolae are shown in Fig. 84 as curves I and II; the inaccessible region is shaded.

Orbits in the equatorial plane are represented by straight lines in the $(r, \mathfrak{g})$-plane. Examples of such orbits are drawn in Fig. 84 as point-dotted lines. Orbits coming from infinity are represented by the lines O_1, O_2, and O_3. These orbits approach according to their $\mathfrak{g}$-value either

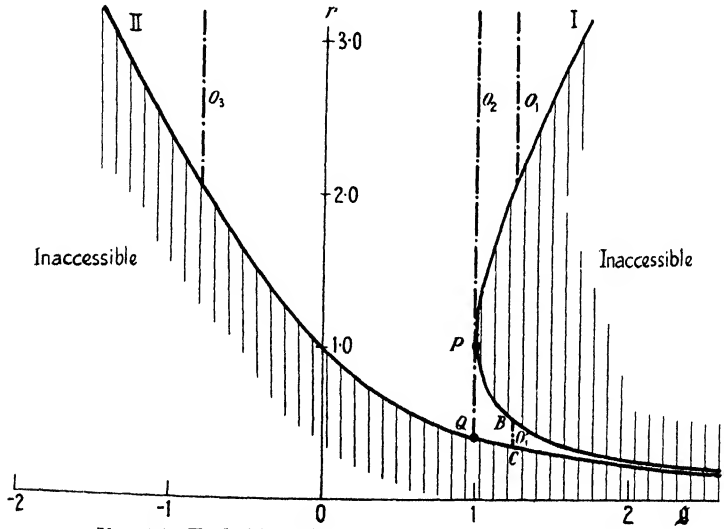

FIG. 84. Forbidden directions in the equatorial plane.

the boundary I or the boundary II. With the exception of the orbit $\mathfrak{g} = 1$ each orbit reaches the boundary and is turned back after contact. These orbits may be called unbounded orbits.

An example of a bounded orbit is the line O_1' in Fig. 84. This bounded orbit oscillates between the points B and C. The orbit $\mathfrak{g} = 1$ behaves in a singular manner. When moving towards P, this orbit approaches P asymptotically without ever reaching P. The unstable periodic orbit (eq. (38)) is represented by the point P alone.

475. Through a fixed point R there is only one orbit moving in a given direction. Thus if the orbit approaching R from a direction n is a bounded orbit, then the direction is forbidden; when the orbit approaching R in the direction n is unbounded the direction is allowed.† From Fig. 84 it is seen that in the equatorial plane all orbits with

$$\mathfrak{g} > 1, \qquad r < 1 \tag{43}$$

† For the sake of completeness we may mention the occurrence of half-bounded orbits. An example of such an orbit is the asymptotic orbit approaching from outside the periodic orbit. This orbit is bounded in one direction and unbounded in the opposite direction. We shall disregard in the following discussion such orbits.

are bounded. All unbounded orbits fulfil either or both of the following conditions

$$\mathfrak{g} < 1, \qquad r > 1. \tag{44}$$

Note further that all bounded orbits are inside the periodic orbit $r = 1$. Unbounded orbits cannot approach the dipole to a distance less than the distance corresponding to the point Q, Fig. 84, that is they cannot approach nearer than

$$r = \sqrt{2} - 1 = 0{\cdot}414. \tag{45}$$

Thus at distances exceeding 1 all directions are allowed, at distances smaller than 0·414 all directions are forbidden, between these two limits we have both allowed and forbidden directions.

476. The distances in the above paragraph are expressed in units defined by (25) and (26). Introducing ordinary units of length we may put

$$r' = \mathfrak{s}^2 r. \tag{46}$$

With the help of (25), (26) the results of the last paragraph can be expressed as follows.

A point at a distance r' (cm.) from the centre can be approached from any direction in the equatorial plane by particles with momentum exceeding

$$p_{\max} = \frac{e\mathrm{M}/c}{r'^2}. \tag{47}$$

A point at a distance r' (cm.) is forbidden for all directions in the equatorial plane for particles with momentum less than

$$p_{\min} = \frac{p_{\max}}{(\sqrt{2}+1)^2} = \frac{p_{\max}}{5{\cdot}84}. \tag{48}$$

Particles with momentum between $p_{\max}$ and $p_{\min}$ can approach the point r' from certain allowed directions only.

Introducing for r' the radius of the earth, for M the magnetic dipole moment of the earth as given in § 512, we find

$$\left.\begin{aligned} p_{\max} &= 59{,}300 \text{ MEV./}c, \\ p_{\min} &= 10{,}200 \text{ MEV./}c. \end{aligned}\right\} \tag{49}$$

477. It remains to determine the forbidden directions in the region

$$1 > r > 0{\cdot}414.$$

We see from (40) and (41) that a direction is forbidden provided

$$r < 1 \quad \text{and} \quad \frac{1+r^2\cos\omega}{2r} > 1. \tag{50}$$

The boundary between allowed and forbidden directions is obtained by replacing the $>$ sign by $=$ sign in (50). We thus find for the limiting direction (directions $\omega < \omega_l$ are forbidden)

$$\cos\omega_l = \frac{2}{r} - \frac{1}{r^2} \tag{51}$$

or

$$r = \frac{1}{1+\sqrt{(1-\cos\omega_l)}}. \tag{52}$$

Introducing ordinary units of length we find for $\omega_l = \frac{1}{2}\pi$

$$p_{\text{vert}} = p_{\max}/4 = 15{,}000 \text{ MEV./}c. \tag{53}$$

The numerical value refers to conditions on the earth. p_{vert} is the smallest momentum which can approach the equator in the vertical direction.

Forbidden directions in general

Störmer's cone

478. In this section the general problem of finding the forbidden directions of approach at any point A in the vicinity of the dipole is considered.

In view of the application to problems on the surface of the earth, introduce the coordinates r, λ, ϕ for the point A:

$$\cos\lambda = \varpi/r. \tag{54}$$

λ and ϕ are, of course, latitude and longitude with respect to the dipole. λ is taken to be positive on the hemisphere in the direction of $e\mathbf{M}$, ϕ is measured in the direction of the periodic orbit.

The direction of approach of a particle to the point A can be defined by the angles ω and η. The angle ω is the angle between the orbit and the circle λ, $r = \text{const.}$; its sign being defined in accordance with § 467. In the case of the earth ω is the angle between the orbit and the east–west direction for positive particles, and the direction between the orbit and the west–east direction for negative particles.

479. Measuring in units of ς it is found that

$$\cos\omega = \varpi\phi'. \tag{55}$$

η is the angle between the radius vector and the direction of the orbit. The sign of η will be so defined that $\eta = 0$ for an orbit approaching the dipole in the radial direction. Thus

$$\cos\eta = -r'. \tag{56}$$

The geometrical significance of the various angles is shown in Fig. 85.

With the help of (29), (54), and (55) we find

$$\cos\omega = \frac{2\mathfrak{g}}{r\cos\lambda} - \frac{\cos\lambda}{r^2}. \tag{57}$$

Thus the tangents of the orbits through a fixed point A belonging to the same value of $\mathfrak{g}$ generate a cone. The axis of the cone is tangent to the circle of longitude, the semi-vertical angle of the cone is ω.

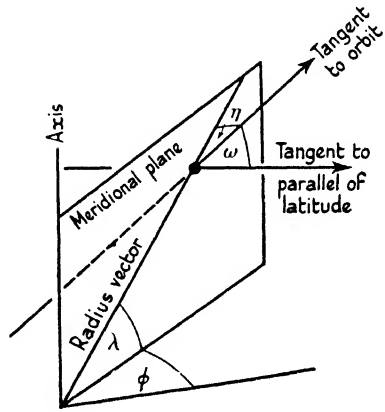

FIG. 85. The angles η, ω, λ, ϕ.

480. The motion of a particle can be split into two components (§§ 468–9): (1) the motion in the meridional plane $(r, z$-plane); (2) the rotation of this plane round the z-axis. The second motion can be determined from (29) provided the motion in the meridional plane is already known. We investigate the component of motion in the (r, z)-plane.

According to equations (31), (33), (34) the motion in the (r, z)-plane is equivalent to the motion of a particle of unit mass and zero energy in the field of a potential $-\frac{1}{2}Q$. The potential Q defined by (32) differs in so far from an ordinary potential as it contains $\mathfrak{g}$, a parameter of the motion.

481. It is clear, from (31), that the region

$$Q < 0 \tag{58}$$

of the (r, z)-plane is inaccessible to particles. The boundary of the accessible part is thus formed by the line $Q = 0$. It should be noted that the region defined by (58) depends on the value of $\mathfrak{g}$; therefore orbits corresponding to different $\mathfrak{g}$-values have access to different parts of the (r, z)-plane. As orbits can pass through any point of space, it is

concluded that any point of the (r,z)-plane must be accessible for orbits with a suitably chosen $\mathfrak{g}$.

482. To find forbidden regions and forbidden directions it is necessary to determine regions and directions which are approached by bounded orbits only. For this purpose it is useful to consider the boundary $Q = 0$ in some detail.

Introducing the coordinates r and λ into (32) the following equations are found for the boundary line†

$$r = \begin{cases} \dfrac{\sqrt{(\mathfrak{g}^2+\cos^3\lambda)}-\mathfrak{g}}{\cos\lambda} & \text{(any } \mathfrak{g}\text{)}, \\ \dfrac{\mathfrak{g}+\sqrt{(\mathfrak{g}^2-\cos^3\lambda)}}{\cos\lambda} \\ \dfrac{\mathfrak{g}-\sqrt{(\mathfrak{g}^2-\cos^3\lambda)}}{\cos\lambda} \end{cases} \quad (\mathfrak{g} > \cos^{\frac{3}{2}}\lambda). \tag{59}$$

The lines have been plotted for $\mathfrak{g} = 1{\cdot}001$, $0{\cdot}999$, $0{\cdot}8$, and $0{\cdot}3$ in Fig. 86. (The curves have been reproduced from Vallarta (1938).)

483. We note that for $\mathfrak{g} > 1$ the accessible part of the (r,z)-plane consists of two unconnected regions. The left-hand part of the region lies inside the space between the half-circle $r = 1$ and the z-axis. Orbits inside this region are necessarily bounded and therefore we conclude that

$$\text{points } r < 1 \text{ are forbidden for orbits } \mathfrak{g} > 1. \tag{60}$$

For $\mathfrak{g} < 1$ the two regions melt together, but as long as $\mathfrak{g} \sim 1$ the potential distribution consists of two valleys connected by a narrow path on the equator near $r = 1$.

We find further with help of (57) and (60) that directions are forbidden for which

$$\cos\omega > \frac{2}{r\cos\lambda} - \frac{\cos\lambda}{r^2} \quad (r < 1). \tag{61}$$

These forbidden directions lie inside a circular cone with an axis in the east–west direction and a semi-vertical angle ω_s which is obtained from (61) by replacing the $>$ sign by the equality sign. This cone is called the Störmer cone.

484. The intersection of the Störmer cone for $\lambda = 0$ with the equatorial plane gives exactly the boundary between allowed and forbidden

† For $\mathfrak{g} < \cos^{\frac{3}{2}}\lambda$ the radius vector intersects the boundary once, for $\mathfrak{g} > \cos^{\frac{3}{2}}\lambda$ there are three intersections (see also Fig. 86).

directions in this plane. It was tentatively suggested by Fermi and Rossi (1933) that all directions inside the Störmer cone are allowed.†

It will be seen later that this assumption gives a rough approximation of the facts.

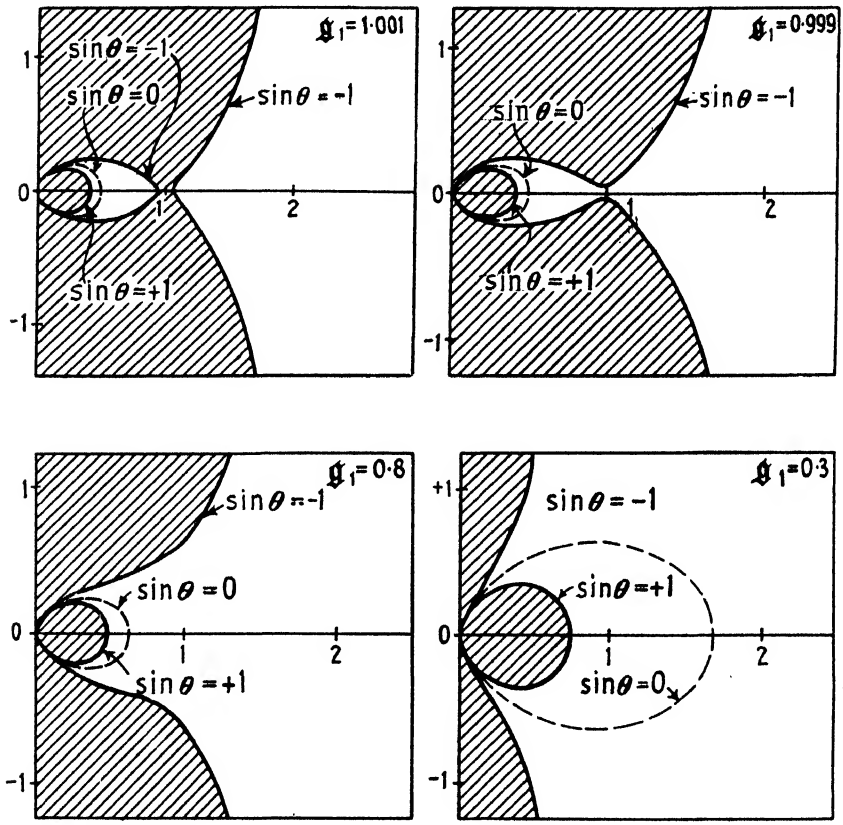

FIG. 86. Allowed and forbidden regions in r, λ. From Vallarta, 'Outline of the theory of the allowed cone'. *University of Toronto Studies*, Applied Math. Series No. 3, 21, 1938.

485. A better approximation is obtained by introducing a critical g-value, $\mathfrak{g}_c$ say, and assuming that all directions corresponding to directions with

$$\cos\omega < \cos\omega_s = \frac{2\mathfrak{g}_c}{r\cos\lambda} - \frac{\cos\lambda}{r^2} \quad (r < 1) \tag{62}$$

are forbidden while all other directions are allowed. This $\mathfrak{g}_c$ value has

† With the exception of a set of singular orbits, all directions inside the Störmer cone are allowed in the sense of being unbounded. The shadow effect of the solid earth however, introduces important modifications (see § 488).

to be assumed to depend on latitude; Lemaître and Vallarta (1933) find the following numerical values:

TABLE 1

λ	$\mathfrak{g}_c$
0°	1
10°	0·978
20°	0·911
30°	0·806
31° 40′	0·783

Limiting momenta and latitudes

486. From (62) it is seen that

$$r = \frac{\cos^2\lambda}{\sqrt{(\mathfrak{g}_c^2 - \cos\omega\cos^3\lambda)} + \mathfrak{g}_c}. \tag{63}$$

Introducing ordinary units of length we obtain with help of (47)

$$p(\lambda,\omega) = p_{\max}\frac{\cos^4\lambda}{\{\sqrt{(\mathfrak{g}_c^2 - \cos\omega\cos^3\lambda)} + \mathfrak{g}_c\}^2}. \tag{64}$$

$p(\lambda,\omega)$ is the smallest momentum which can reach the earth from outside at a latitude λ through an angle ω to the east–west direction.

487. The following special cases, obtained from (64), are of importance.

1. Particles with momenta

$$p > p(\lambda,0) = p_{\max}\frac{\cos^4\lambda}{\{\sqrt{(\mathfrak{g}_c^2 - \cos^3\lambda)} + \mathfrak{g}_c\}^2} \tag{65}$$

can approach the observer at latitude λ from all directions.

2. Particles with momenta

$$p < p(\lambda,\pi) = p_{\max}\frac{\cos^4\lambda}{\{\sqrt{(\mathfrak{g}_c^2 + \cos^3\lambda)} + \mathfrak{g}_c\}^2} \tag{66}$$

are forbidden in all directions at the latitude λ.

3. $$p_{\text{vert}}(\lambda) \equiv p(\lambda, \tfrac{1}{2}\pi) = \frac{p_{\text{vert}}}{\mathfrak{g}_c^2}\cos^4\lambda. \tag{67}$$

$p(\lambda,0)$, $p(\lambda,\pi)$, and $p(\lambda,\frac{1}{2}\pi)$ are plotted in Fig. 87 against λ. $\mathfrak{g}_c = 1$ is assumed. Equation (67) gives the limiting momentum incident in the vertical direction. As $\mathfrak{g}_c$ does not depend greatly on latitude (67) is often replaced by

$$p_{\text{vert}}(\lambda) \simeq p_{\text{vert}}(0)\cos^4\lambda. \tag{68}$$

Finally, with the help of (64) it is found that particles with momentum p are partly forbidden in a belt of latitude λ:

$$\lambda_1 > \lambda > \lambda_2, \tag{69}$$

with

$$\left.\begin{aligned} \cos\lambda_1 &= \frac{1+\sqrt{(1+8g_c/r^3)}}{2r^2}, \\ \cos\lambda_2 &= \frac{-1+\sqrt{(1+8g_c/r^3)}}{2r^2}, \\ p &= p_{\max} r^2. \end{aligned}\right\} \tag{70}$$

In the region round the pole above λ_1, p is allowed in all directions, while in the equatorial belt $\pm\lambda_2$, p is forbidden in all directions. These

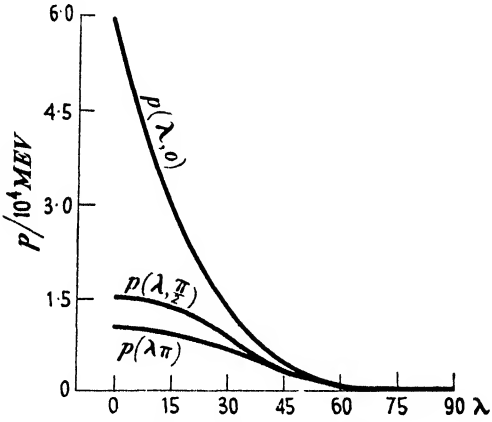

FIG. 87. Limiting momenta.

limiting latitudes occur, of course, only for appropriate values of the momentum.

Deviations from the Störmer cone

488. The results presented in the preceding section give a rough approximation of the magnitudes of the allowed cones. Such an approximation is sufficient for the analysis of many problems. Problems arise, however, which make a more accurate treatment necessary.

It was assumed in § 485 that directions are forbidden or allowed according to their g-value. This assumption implies automatically that the allowed cones are circular. The accurate treatment shows, however, that the allowed cones are not exactly circular and that the deviations give rise to an asymmetry of the intensities from south and north.

The asymmetry between north and south can be understood easily in terms of the shadow of the solid earth. Consider a point of observation at the surface; a charged particle leaving the observer in a direction perpendicular to the direction of the magnetic force is bent round. If the momentum of the particle is sufficiently small the particle is brought

back again. Therefore most directions of approach perpendicular to the field strength will be forbidden for low momenta. The direction parallel to the line of force is not forbidden as far as determined by the local

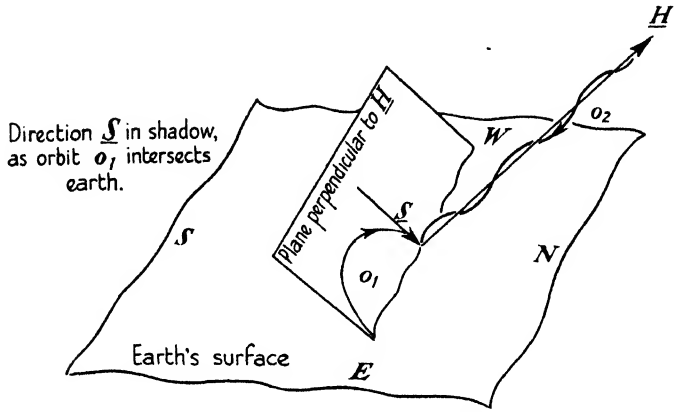

FIG. 88. The north–south asymmetry.

field only. As at the northern hemisphere the lines of force are inclined towards the south, we expect a shadow effect there which cuts out more of the northerly directions than of the southerly directions. The intensity from the south should therefore be greater than from the north on the northern hemisphere; a corresponding excess from the north is expected on the southern hemisphere (see Fig. 88).

A quantitative treatment of the north–south asymmetry was given by Lemaître, Vallarta, and Bouckaert (1935) and by Lemaître and Vallarta (1936*a*); it will be described later.

489. A detailed theory of the allowed cone is required to deal with the finer details of the geomagnetic effects of cosmic rays. Such a treatment was given by Lemaître and Vallarta (1936*a*) and others. In the following the main results are summarized.

A very brief outline of the actual theory will be given in §§ 490–9. An account of the theory of the allowed cone was given by Vallarta (1938) and the reader is referred to this paper for more detailed information.

3. *The Theory of the Allowed Cone*

(*a*) *Summary of Results*

490. From the preceding sections it is clear that the directions outside the Störmer cone (eq. (61)) are forbidden. It remains to investigate which directions inside the Störmer cone are allowed.

Vallarta has defined a *main cone* (see Fig. 89) which lies inside the Störmer cone, and all directions inside the main cone are allowed. Further, a region can be delimited which is called the simple shadow cone. All directions outside this cone are forbidden. Thus the Störmer

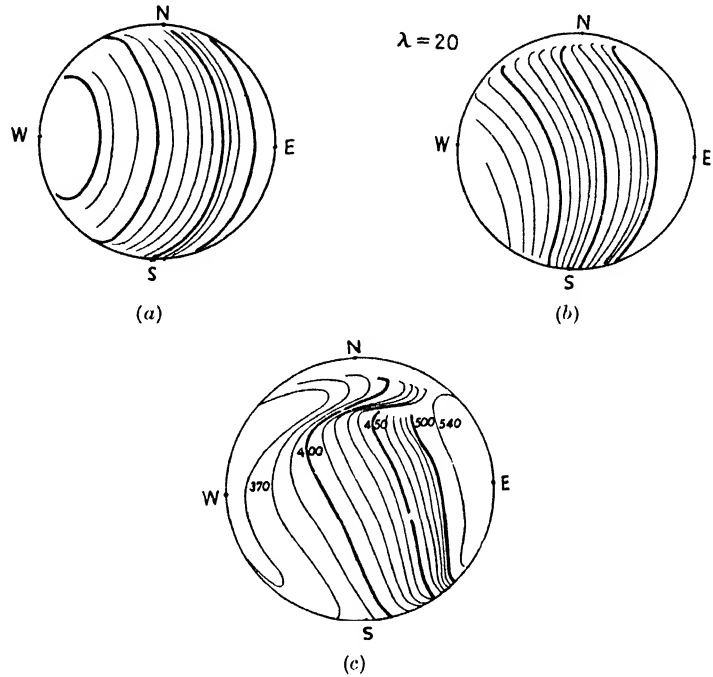

FIG. 89. From Vallarta, 'Outline of the theory of the allowed cone'. *University of Toronto Studies*, 1938.

(*a*) Main cone. $\lambda = 0°$, thick lines $r = 0{\cdot}45$, $0{\cdot}5$, $0{\cdot}6$ Störmer units.
(*b*) Main cone. $\lambda = 20°$, thick lines $r = 0{\cdot}45$, $0{\cdot}5$, $0{\cdot}6$ Störmer units.
(*c*) Main cone. $\lambda = 30°$, energy in milli-Störmer.

cone together with the simple shadow cone form an upper limit for the extent of the allowed cone. The main cone forms a lower limit.

Between the simple shadow cone and the main cone there is a region which is called the penumbra. The penumbra is a complex region containing an infinite number of allowed and forbidden subregions. Some of these subregions are of finite extension, others are infinitesimal.

The results of Vallarta and others are collected in Figs. 89, 90. Fig. 89 gives the extent of the main cone for various latitudes and energies. Fig. 90 gives the extent of the simple shadow cone. The penumbra has been studied in some detail and results can be found in a paper of Hunter (1939). For the equator there is no penumbra and the allowed cone coincides with the main cone. For high latitudes the penumbra

consist almost entirely of allowed regions and therefore at high latitudes the allowed cone is limited almost exactly by the simple shadow cone and the Störmer cone. The penumbra is most complex at intermediate latitudes.

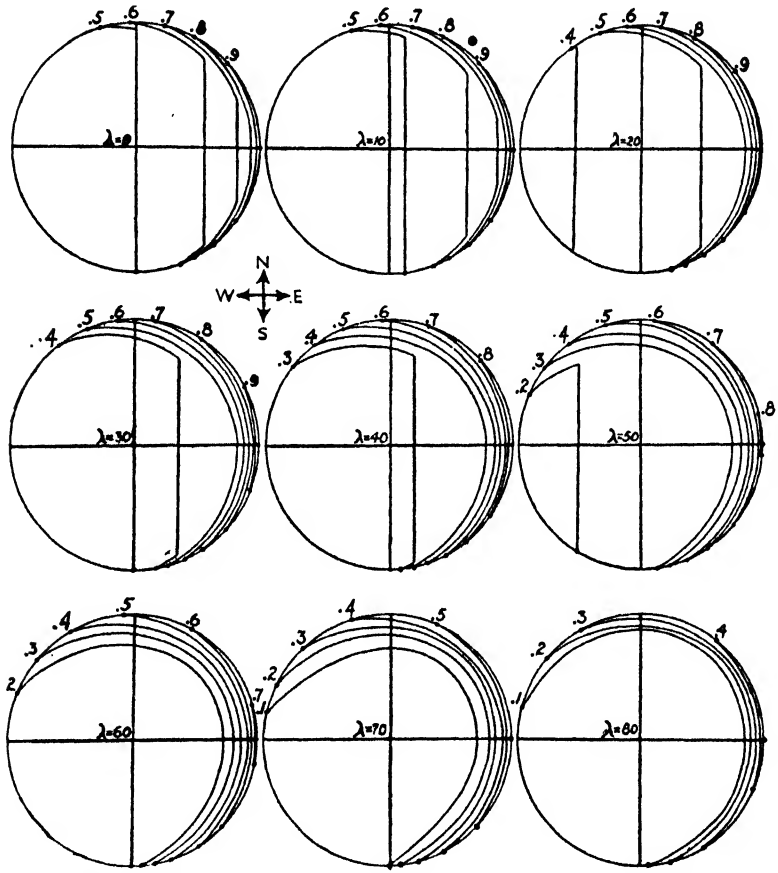

FIG. 90. Simple shadow cones. From Vallarta, 'Outline of the theory of the allowed cone'. *University of Toronto Studies*, 1938.

The following section, dealing with the details of the cones, is not essential for the understanding of other parts of this book and it may be omitted by the reader.

(*b*) *A Brief Outline of the Theory of the Allowed Cone*†

Bounded and unbounded orbits

491. A direction may be forbidden for two different reasons: (1) if the corresponding trajectory does not come from infinity, and (2) if the

† For details see Vallarta (1938).

trajectory passing through it intersects the solid earth before arriving at the point of observation (see Fig. 91). In the second case the direction is said to lie in the shadow of the earth.

The problem of determining the allowed cone without the effects of the solid earth has been treated satisfactorily. It has been shown that there are no bounded orbits for

$$g < 0{\cdot}78856. \qquad (71)$$

It is conjectured by Schremp (1938) that the set of bounded orbits with

$$1 > g > 0{\cdot}78856 \qquad (72)$$

is of zero measure. Whether or not this conjecture proves correct it appears likely that the bounded orbits inside the Störmer cone give a negligible contribution to the intensity. It can be concluded that neglecting the shadow effect of the solid earth, the allowed cone is practically bounded by the Störmer cone.

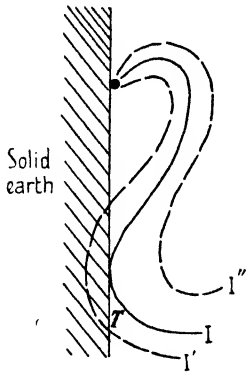

FIG. 91. Orbits forming the boundary of the simple shadow cone.

Shadow effects

492. Considerable difficulties arise when the effects of the solid earth are included in the consideration of the allowed cone. The difficulties are connected with the fact that the equations of motion cannot be solved analytically.

The trajectories can be evaluated by numerical integration. Störmer and his co-workers have evaluated a large number of trajectories in a period extending over more than thirty years.

A quicker way of obtaining trajectories has been made possible by the invention of the Bush differential analyser. Lemaître and Vallarta have evaluated more than 1,000 trajectories using the differential analyser.

493. The boundary of the allowed cone could be found, at least in principle, by evaluating orbits with all possible initial conditions. After having evaluated a sufficiently large number of single trajectories through a given point the trajectories corresponding to allowed orbits can be taken together as the directions of the allowed cone. Such a procedure is, however, extremely tedious and, because of many discontinuities, very small intervals have to be taken in order to obtain reliable information.

Störmer, Lemaître, Vallarta, and many collaborators have studied the

properties of large numbers of trajectories with the view of finding the boundaries systematically.

494. For the actual analysis two families of periodic orbits are of great importance. For a certain range of g-values there is a periodic orbit near the pass which connects the two parts of the meridian plane (§ 482). This orbit is symmetrical to the equator, reaches on both sides of the equator the line $Q = 0$, and, in common with all orbits reaching this line, it is self-reversing.

These orbits are farther from the dipole than any other periodic orbit for the same value of g; they are called the outer periodic orbits. Besides the outer periodic orbit there exists another self-reversing orbit, called the inner periodic orbit. There are an infinite number of periodic orbits between these two principal periodic orbits, but as shown by Störmer, all periodic orbits lie between the two principal periodic orbits.

The projections of the outer periodic orbit have been calculated in detail by Lemaître and Vallarta according to a procedure due to Lemaître (1934) (compare also Godart (1938)). They are shown in Vallarta's paper.

For $g = 1$ the outer periodic orbit is the circular orbit discussed in § 472. Its projection in the meridian plane appears as a point. For $g = 0{\cdot}78856$ the outer and the inner periodic orbits coincide. For still smaller values of g no periodic orbits exist.

Re-entrant and non-re-entrant orbits

495. Examining the equivalent potential Q as shown in Fig. 86 it is clear that orbits can be classified broadly into two types. Take as an example for the one type a particle with $g > 1$ approaching from infinity. The Q force is repulsive in the whole of the accessible part of the meridian plane; the particle approaches from infinity with steadily decreasing velocity. The velocity reaches a minimum at the point of nearest approach and the particle leaves again for infinity. Orbits of this type, computed by Störmer, are shown in Fig. 92 (*a*). It is clear that orbits of this simple kind can enter the surface of the earth only once and therefore such orbits form part of the allowed cone.

The simple type of orbit described above may also occur for $g < 1$. For these g values, however, the potential hole to the left of the pass (Fig. 86) is open and some orbits enter the potential hole and carry out complicated oscillations inside the hole (Fig. 92 (*b*), (*c*)). An orbit which enters the hole may intersect the surface of the earth several times and thus enter the surface of the earth in several consecutive points (see

Fig. 91). An actual particle is stopped at the first contact with the earth surface and therefore all the subsequent entries must correspond to directions blocked by the solid earth.

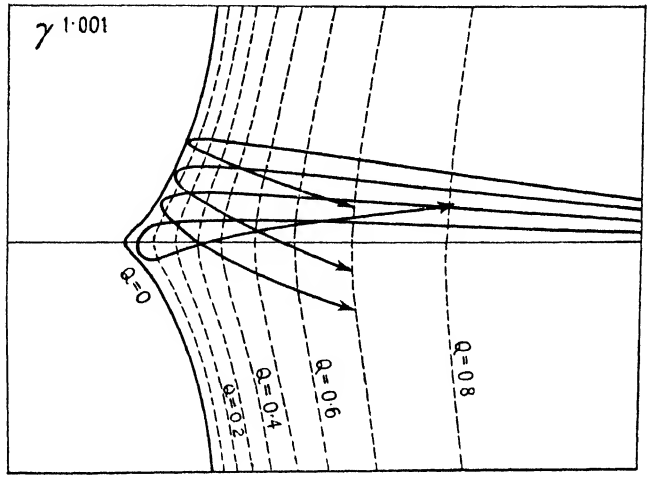

FIG. 92(*a*). Orbits in the (*r*, *z*)-plane. From Störmer, *Astr. Norv.* **1**, Plate IX_2.

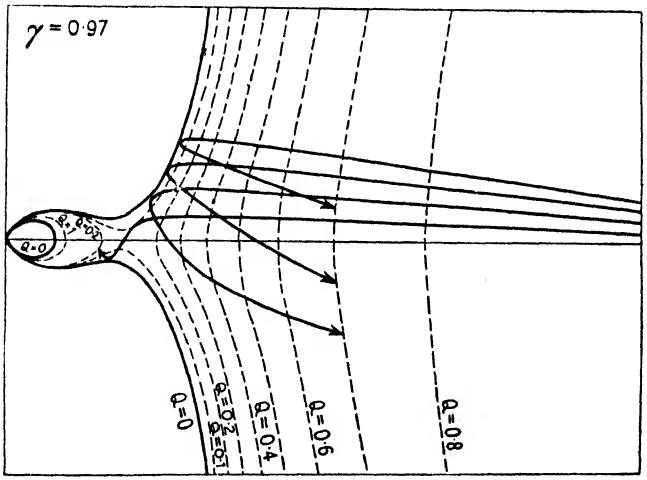

FIG. 92(*b*). Orbits in the (*r*, *z*)-plane. From Störmer, ibid., Plate IX_1.

We see therefore that directions accessible to the simple kind of orbit are always allowed, while those accessible to oscillating orbits may or may not be allowed.

496. To make the qualitative distinction between the two types of orbits more precise Lemaître and Vallarta introduced the following definitions.

A section of an orbit is called *re-entrant* if it contains the points between two consecutive relative maxima of Q. An orbit is called *re-entrant* or *non-re-entrant* according to whether it contains re-entrant sections.

The simple type of orbit considered before is non-re-entrant as its velocity has no maximum. The non-re-entrant orbits reach the earth

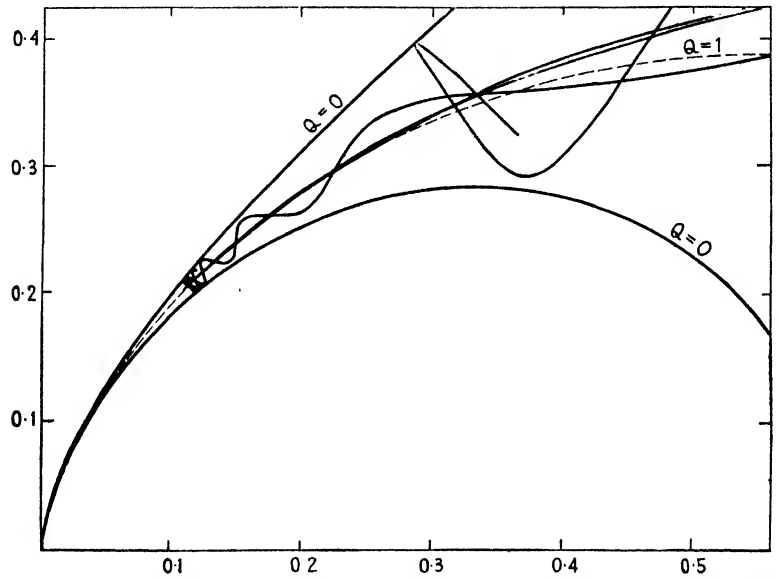

FIG. 92(c). Orbits in the (r, z)-plane. From Störmer, *Astr. Norv.* **1**, Plate X_2.

surface freely. The tangents of all orbits which are non-re-entrant in the past define a cone in every point of space. This cone is called the *main cone* and it is necessarily part of the allowed cone.

497. The main cone (§ 490) forms for all energies and for all latitudes the most important part of the allowed cone. The boundary of the main cone can be determined as follows.

When changing a non-re-entrant orbit continuously into a re-entrant orbit it is found that the transition orbit is an orbit asymptotic to the outer periodic orbit. Therefore the boundary between re-entrant and non-re-entrant orbits is formed by the orbits asymptotic to the outer periodic orbit. Thus the main cone is bounded by the orbits asymptotic to the outer periodic orbits.

These asymptotic orbits were determined by Lemaître and Vallarta and thus the main cone was found for a number of latitudes and energies (see Fig. 89).

Penumbra

498. Directions which are reached by re-entrant orbits may or may not be forbidden. The investigation of such orbits yields the penumbral bands.

A connected region of the penumbra termed the 'F-region' can be shown to be completely dark.

499. Besides the penumbra, a region which is termed the simple shadow cone can be shown to exist. Consider an orbit I of the type shown in Fig. 91 (full line). The orbit is clearly a boundary between the two kinds of orbits I', I'' shown by broken lines. The I' orbit is blocked by the earth in the point T and therefore is unable to reach the point where I and I'' intersect the earth's surface. The full-drawn orbit I is clearly a boundary between the two types of orbits. Orbits to the I'-side of the orbit I are certainly blocked before reaching this point.

It can be shown that orbits of the kind I occur only up to latitudes λ, with

$$\cos\lambda = r^2, \qquad \mathfrak{g} = r^3,$$

where r is the energy in Störmer units.

These orbits form the boundary of the simple shadow cone (see Fig. 90).

B. Observation of the Geomagnetic Effects

500. At least part of the primaries of cosmic rays are electrically charged and are therefore deflected by the magnetic field of the earth while far outside the earth's atmosphere.

The effects produced by the magnetic deflexion of the primaries may be termed geomagnetic effects.

The possibility of geomagnetic effects was foreseen before such effects were actually observed. The first attempts to find geomagnetic effects failed partly because of experimental inaccuracy and partly because intensity changes were looked for at high latitudes.

501. The following geomagnetic effects have been observed.

1. Change of intensity with both geomagnetic latitude and longitude. These effects are referred to as the latitude effect and the longitude effect.

2. Asymmetries. The intensity of cosmic rays is found to depend not only on the inclination between the direction of incidence and the vertical but also to some extent on the azimuth.

The most pronounced asymmetries are the east–west asymmetry and the north–south asymmetry. Apart from these main asymmetries the cosmic-ray intensity reveals a complicated fine structure.

502. The first observations of the latitude effect with positive results were obtained by Clay (1930) on a voyage between Amsterdam and Bangkok and back. It was found that the intensity at low latitudes was smaller than that at Amsterdam.

1. *Effects at Sea-level and Low Altitudes*

(*a*) *Latitude Effect*

503. Clay's results were later confirmed by many other observers. Some results due to Compton (1933) are shown in Fig. 93. It is seen that the rate of ionization at sea-level increases between the geomagnetic equator and the geomagnetic latitudes 50° by about 10 per cent.

At higher altitudes the latitude effect is more pronounced, as the following data (from Compton) show.

TABLE 2

Height above sea-level (*m.*)	*Average pressure* (*cm.* Hg)	*Effect* (%)
0	76	14
2,000	60	22
4,360	45	33

504. Compton (1933) also showed that the observed effect was, in fact, connected with the magnetic field of the earth. For this purpose he plotted the results (1) against geographical latitude, (2) against magnetic latitude,† (3) against geomagnetic latitude. It was found that the observed points could be most satisfactorily represented when using geomagnetic latitude. The scatter of the points round a smoothed curve increases very much if the points are plotted against geographic latitude instead of the geomagnetic latitude. Thus it was inferred that the observed intensities are a function of the geomagnetic latitude.

† Magnetic latitude is the latitude defined by the direction of the magnetic intensity at the point of observation. Geomagnetic coordinates are those defined with respect to the position of the equivalent magnetic dipole.

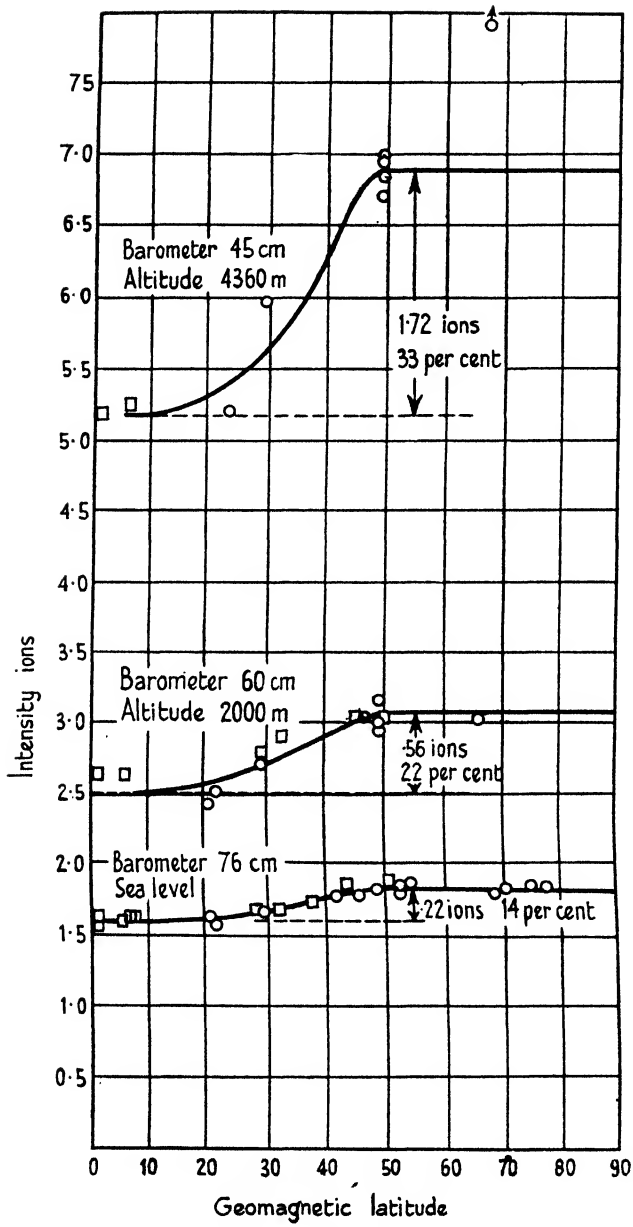

FIG. 93. The latitude effect at different altitudes (A. H. Compton). From Corlin, 'Cosmic Ultra Radiation', *Annals of the Observatory, Lund*, No. 4.

(*b*) *Longitude Effect*

505. On a voyage where they crossed the geomagnetic equator several times Clay, Alphen, and Hooft (1934) observed that the cosmic-ray intensity depends not only upon the geomagnetic latitude but also on the geomagnetic longitude. This was also observed independently by Millikan and Neher (1935, 6).

It was found that the cosmic-ray intensity has a maximum near Peru and a minimum near the Philippines. The difference between the intensities is about 7 per cent. The minimum coincides with the closest approach to the magnetic centre of the earth, that is the nearest approach to the centre of the equivalent magnetic dipole.

(*c*) *Asymmetry Effects*

506. The effect of the magnetic field of the earth can also be detected at a single point of observation, as an asymmetry in the directional distribution of the incident radiation.

It was found by Rossi (1934*a*) in Eritrea, and by Johnson and Street (1933) and Johnson (1934) at many different places, that the cosmic-ray intensity inclined at an angle η to the west from the vertical is larger than the corresponding intensity of the radiation inclined by η to the east from the vertical.

The east–west asymmetry was found to depend on altitude, latitude, and angle of inclination. Some of the observations are collected in Table 5, § 537.

507. An asymmetry between north and south was also observed (Johnson (1935*a*, *b*)). The intensity was found to be larger from the south than from the corresponding direction inclined to the north from the vertical for observations on the northern hemisphere.

Following up a suggestion of Schremp (1938), Ribner (1939) and Cooper (1940) observed the intensity at a constant zenith angle η as a function of azimuth. These observations reveal a complicated pattern. It was suggested that the results could be interpreted in terms of the magnetic penumbra.

2. *Geomagnetic Effects at High Altitudes*

(*a*) *Latitude Effect*

508. The cosmic-ray intensity has been measured up to considerable heights with instruments carried in aeroplanes and balloons. The

intensity at great heights shows a considerable variation with latitude between the equator and about 50° magnetic latitude. Height-intensity curves for a number of latitudes have been obtained by Bowen, Millikan, and Neher (1934, 7, 8) and by others. Some of the results of Millikan's school are shown in Figs. 94, 95.

Height-intensity curves were also obtained using either single counters or coincidence arrangements by Neher and Pickering (1942), and at high latitude by Pfotzer (1936).

At latitudes below 50° the latitude effect increases very rapidly with altitude. At 7 km. height (50 cm. Hg pressure) for instance, the intensity above the equator is roughly one-half of that at high latitudes.

509. The intensity at latitudes exceeding $\sim 50°$ is independent of latitude up to the greatest heights observed. The independence of the intensity upon latitude for latitudes above 50° may be called the latitude cut-off. The latitude cut-off was shown by Compton's (1933) survey up to 4,000 m. above sea-level. Collecting high-altitude data obtained in a balloon which was drifting over the European continent Cosyns (1936*a*) found that the intensity shows a sharp knee near 49° for various altitudes.

The latitude cut-off was finally ascertained for the northern hemisphere by the observations of Carmichael and Dymond (1939). Balloon flights with a counter telescope were made at various latitudes up to the geomagnetic latitude of 88°. At 88° N. a height corresponding to 5 cm. Hg pressure was reached. The height-intensity curves are, inside the experimental error, identical with those obtained by Pfotzer at magnetic latitude 49°.

The height-ionization curve was also measured by Carmichael and Dymond up to the geomagnetic latitude 85° and up to height corresponding to 1·4 cm. Hg pressure. The height-ionization curve at this high latitude is identical with the curves obtained by Millikan and co-workers at 55° N. and 60° N. A small difference between 50° and 55° N. for high altitudes seems to occur (see Fig. 96).

(*b*) *The Longitude Effect and Asymmetries*

510. Aeroplane flights were carried out by Neher and Pickering (1942) both above the Philippines and above Peru to study the longitude effect at high altitudes. The flights reached only a height of 7 km. The result of the measurements was entirely negative and no difference between the intensities at high altitudes was observed. The

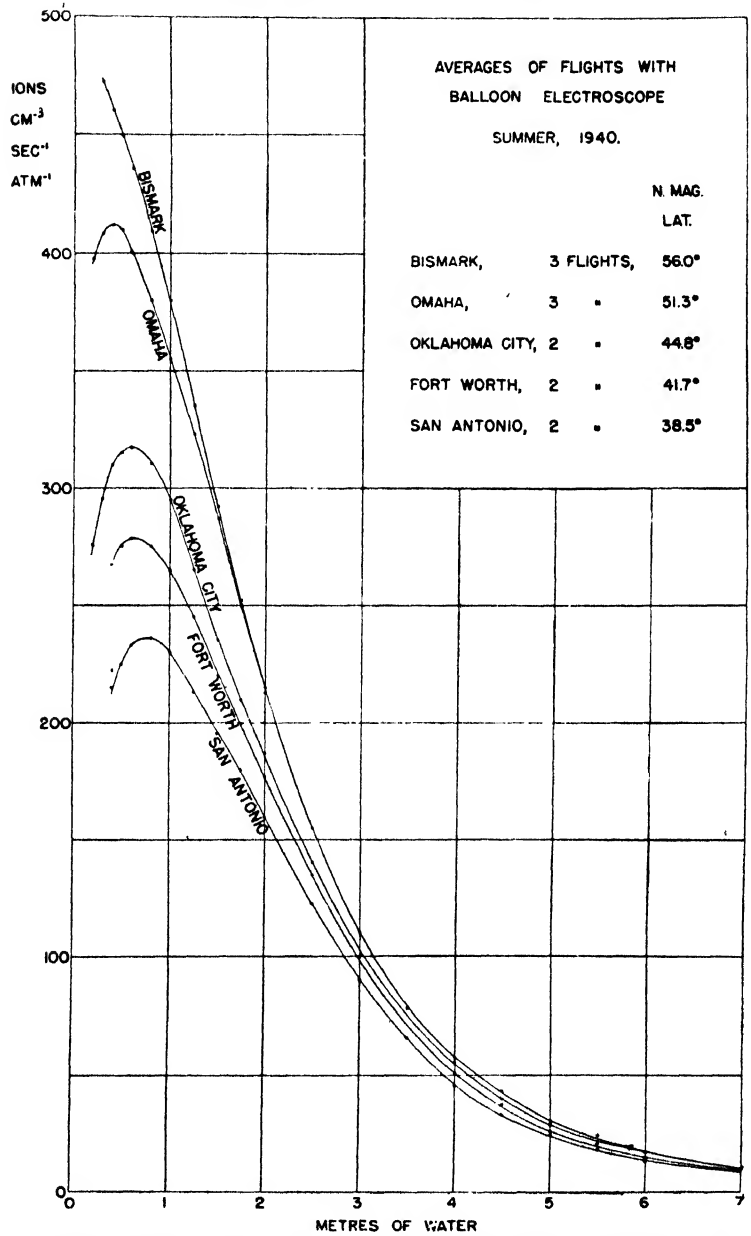

FIG. 94. Height-intensity curves of Millikan and co-workers. *Phys. Rev.* **61**, 299 (1944).

measurements were not of high accuracy and thus a difference between the intensities amounting to 5 per cent. must be regarded as compatible with the measurements. It must be concluded from these observations

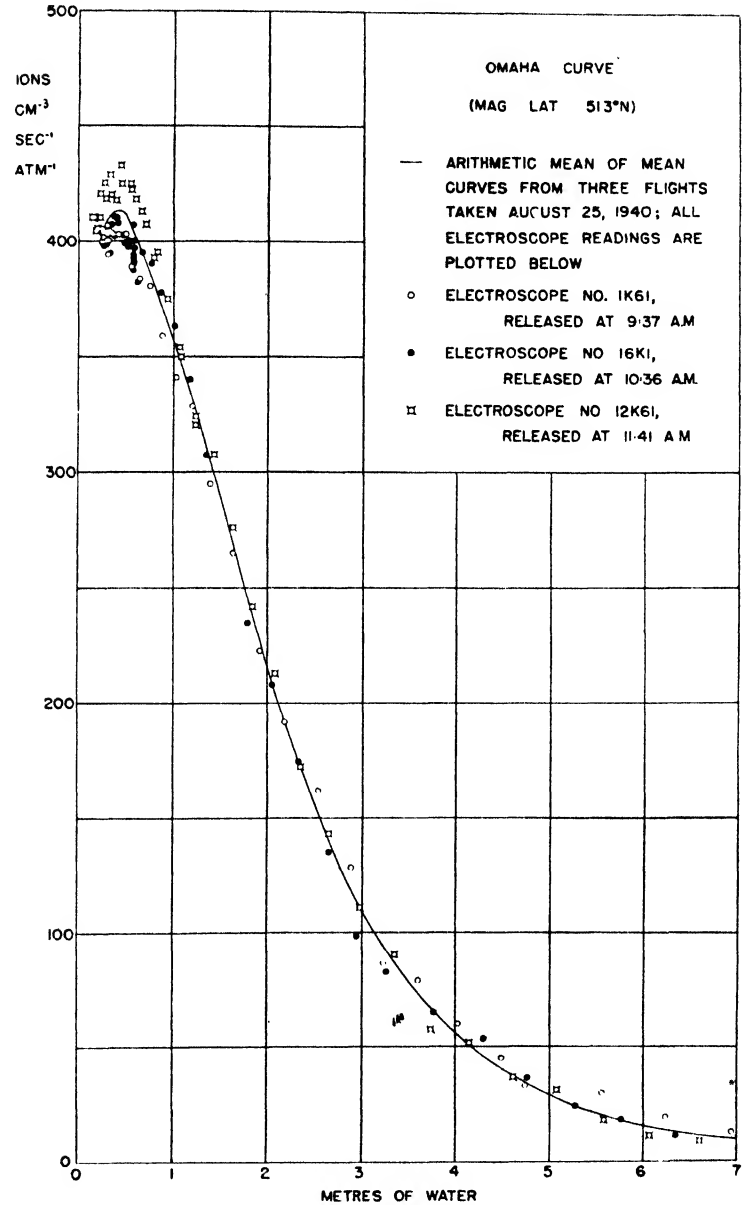

FIG. 95. Height-intensity curve with experimental points (Millikan and co-workers). *Phys. Rev.* **61**, 297 (1944).

that the longitude effect does not increase with height, or at any rate not more rapidly than the vertical intensity itself.

511. The only attempt to observe the east–west asymmetry at high

altitudes was carried out by Johnson and Barry (1939). An automatic coincidence recorder was flown in a balloon to heights corresponding to pressures less than 10 cm. Hg. Ascents were made above the Panama Canal zone at a geomagnetic latitude of 20° N. The recorder consisted

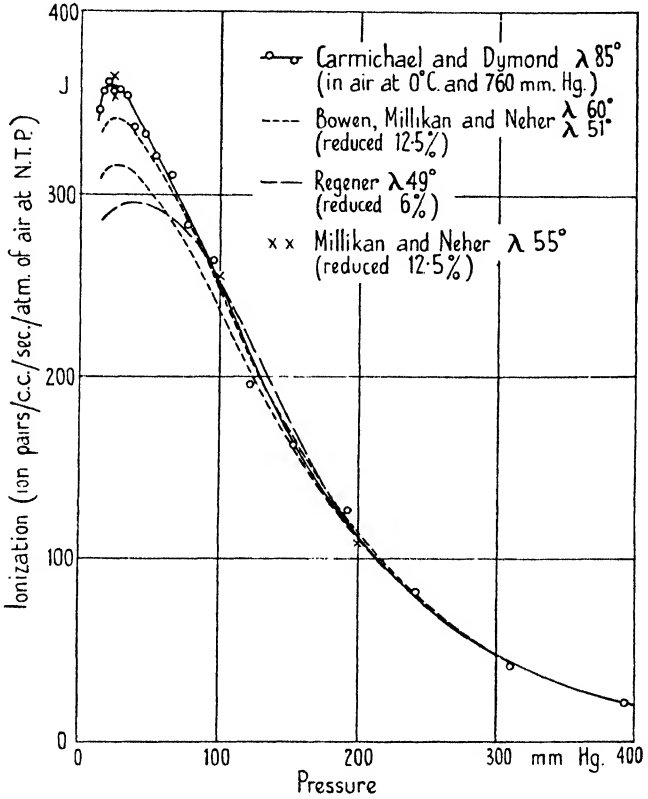

FIG. 96. Height-ionization curve near the geomagnetic pole. From Carmichael and Dymond, *Proc. Roy. Soc.* A, **171**, 341.

of a counter telescope inclined at 60° to the vertical. The balloon rotated freely round a vertical axis. By means of a photo-cell operated by the sun, records obtained in positions where the counters were inclined to the west were separated from the records obtained in positions where the counters were inclined to the east.

The records thus obtained did not show any difference between the intensities from the west and the east. Considering the statistical fluctuation of the readings, it may be concluded that if there is an asymmetry it is not likely to exceed about 7 per cent.

C. Interpretation of the Geomagnetic Effects

1. *Numerical Data*

In the following section it is shown that the effects described in section B can be interpreted by assuming that the primary cosmic rays are electrically charged particles, and that they are deflected by the magnetic field of the earth when approaching from outside.

512. The data relevant to the magnetic field of the earth which are needed for the interpretation of the geomagnetic effects are as follows.†

1. The magnetic field of the earth can, to a good approximation, be taken as that of an equivalent dipole with a moment

$$\mathrm{M} = 8{\cdot}1 \times 10^{25} \text{ gauss} \times \text{cm.}^3 \tag{73}$$

2. The centre of the equivalent dipole lies at a distance of 300 km. from the centre of the earth. The line connecting the centre of the earth to the dipole intersects the surface of the earth at a point 10° N. geographic latitude and 168° W. geographic longitude. The axis of the dipole intersects the surface of the earth in the northern hemisphere at a point 78° 32′ N. latitude and 69° W. longitude. This point is the geomagnetic south pole.

3. The geomagnetic coordinates Λ, Φ of a point with the geographic latitude λ and longitude ϕ can be obtained with the help of the following expressions:

$$\begin{aligned} \tan\phi &= \tan(\Phi-\Phi_1)\sin\kappa/\sin(\kappa-\theta_1), \\ \tan\lambda &= \cos\phi\cot(\kappa-\theta_1), \end{aligned} \tag{74}$$

with

$$\tan\kappa = \cot\Lambda\cos(\Phi-\Phi_1), \qquad \theta_1 = 11{\cdot}5°, \qquad \Phi_1 = 69° \text{ W.} \tag{74a}$$

4. Störmer's unit of momentum is

$$p_{\max} = \frac{300\mathrm{M}}{R_E^2} \text{ eV./}c = 59{,}000 \text{ MEV./}c. \tag{75}$$

R_E is the mean radius of the earth. The physical significance of this unit is that it is equal to the momentum required for a particle to circle round the geomagnetic equator.

2. *Interpretation of the Latitude Effect*

(*a*) *Latitude Effect*

513. The latitude effect can be clearly understood in terms of the allowed cones described in section A. Particles with momenta below $\sim$ 60,000 MEV./c can approach the equator only from certain directions.

† Compare e.g. Chapman and Bartels, *Geomagnetism*, Oxford, 1940.

The cone formed by the allowed directions opens gradually when the point of observation is moving away from the equator towards the pole. Due to the increase of the allowed cones the intensity of the incident particles increases with geomagnetic latitude.

Energy considerations

Latitude effect of energy flow

514. The analysis of the latitude effect will be carried out in two steps. In the present section we derive certain conclusions from the observed effects without introducing specific assumptions as to the type of the primaries. It will be assumed only that the primaries contain singly charged particles.

In the subsequent section certain aspects of the latitude effect will be discussed assuming that the primaries consist of electrons and protons.

515. Assuming that the whole of the energy of the primary cosmic rays is spent eventually in ionization, it is found that the energy flowing into the top of the atmosphere reappears in the form of ionization at various depths. Therefore the integral over the height-intensity curve of cosmic rays has a simple physical significance. This integral is proportional to the total flow of energy into the atmosphere at a given latitude. Taking the average energy required to produce an ion pair to be 32 eV. we find

$$\mathfrak{W} = 32 \text{ eV.} \int_0^\infty I(\theta, \lambda)\, d\theta. \tag{76}$$

Using the height-ionization curves Millikan and co-workers find the following numerical values:

TABLE 3

Flow of primary energy into the atmosphere at various latitudes

(*Millikan, Neher, and Pickering*, 1942)

Latitude	*Flow of energy MEV. per cm.² per min. integrated over all directions of incidence*	*Relative flow of energy*
58°	$1{\cdot}42 \times 10^5$	2·22
52°	$1{\cdot}35 \times 10^5$	2·12
38°	$1{\cdot}09 \times 10^5$	1·70
3°	$0{\cdot}564 \times 10^5$	1

516. Integrating the distribution of the vertical intensity, as given

in Fig. 94, the flow of energy in the vertical direction was obtained as follows:

TABLE 4

Vertical energy flow at various latitudes

(Millikan, Neher, and Pickering, 1943)

Latitude λ	*Energy flow (arbitrary units)*
45–51°	185
41°	162
25°	121
3–15°	100

517. The variation of the vertical energy flow with geomagnetic latitude can be interpreted easily. According to eq. (68) the primary spectrum is cut off for moments below

$$p_{\text{vert}}(\lambda) = p(0)\cos^4\lambda. \tag{77}$$

Therefore the energy flow in the vertical direction can be written as

$$\mathfrak{W}_{\text{vert}}(\lambda) = \int_{p_{\text{vert}}(\lambda)}^{\infty} p\mathfrak{S}(p)\,dp, \tag{78}$$

where $\mathfrak{S}(p)$ is the differential spectrum of the primaries.

Assuming
$$\mathfrak{S}(p) \sim p^{-2.5} \tag{79}$$

it is found that
$$\mathfrak{W}_{\text{vert}}(\lambda) \sim \frac{1}{\sqrt{\{p_{\text{vert}}(\lambda)\}}} \sim \frac{1}{\cos^2\lambda}. \tag{80}$$

The values of the energy flow as given in Table 4 together with the values obtained from (80) are plotted in Fig. 97. It is seen that the observations are in reasonable agreement with the values (80) calculated from the spectrum (79).

518. To interpret the variation of the total flow of energy with latitude it is necessary to average over all directions of incidence. The primary intensity due to particles of a given momentum p is the same for all allowed directions. Therefore the total intensity due to particles of given momentum p is proportional to the solid angle $\Omega_s(\lambda, p)$ subtended by the allowed cone. Taking the Störmer cone as the first approximation for the allowed cone, we have thus

$$\mathfrak{W}(\lambda) = \int_0^{\infty} \Omega_s(\lambda, p)\mathfrak{S}(p)\,dp, \tag{81}$$

where
$$\Omega_s(\lambda, p) = \begin{cases} 0 & \text{for } p < p_{\min}(\lambda), \\ \pi\left(1 + \dfrac{2}{\cos\lambda\sqrt{(p/p_{\text{vert}})}} - \dfrac{p_{\text{vert}}\cos\lambda}{p}\right), \\ 2\pi & \text{for } p > p_{\max}(\lambda). \end{cases} \tag{82}$$

Introducing the spectrum (79) it is found that

$$\mathfrak{W}(\lambda) = \pi\{\mathfrak{W}_{\text{vert}}(\lambda) + w(\lambda)\};$$

$w(\lambda)$ is found to be small compared with the first term. It is concluded therefore that the total intensity varies very nearly in the same way as the vertical intensity. The values of Tables 3 and 4 are plotted

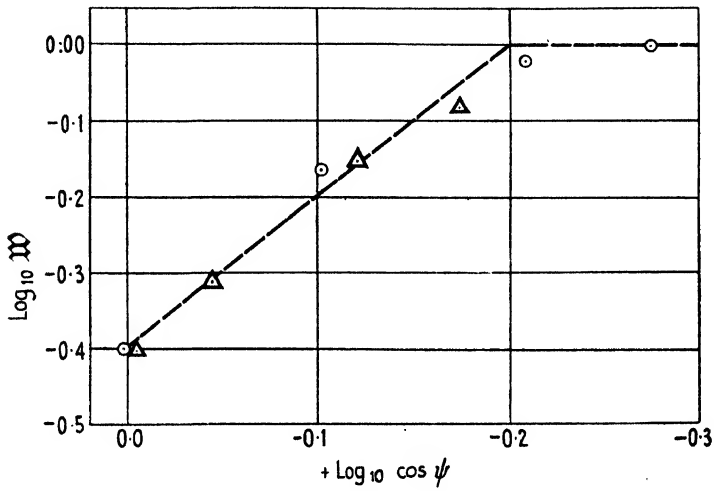

FIG. 97. Latitude effect of energy flow.

— — — Energy flow calculated from eq. (80), cut off at $\lambda = 50°$.
⊙ Energy flow observed by Millikan, Neher, and Pickering (1942).
△ Vertical energy flow, Millikan, Neher, and Pickering (1943).
Values for $\lambda = 0$ have been equalized.

in Fig. 97. It is seen that the values fit fairly well to the curve calculated for the vertical intensity. It is therefore concluded that both the integrated height-ionization curve and the integrated vertical-intensity curve can be understood in terms of the spectrum (79).

The latitude cut-off

519. The latitude effect extends only to latitudes up to about 50°, whereas for higher latitudes the intensity remains constant.

The latitude cut-off shows that the primary spectrum must have a sharp lower limit; this limit must be due to causes other than the magnetic field of the earth.

Indeed, particles of given momentum p are blocked by the magnetic field of the earth in certain directions only up to a geomagnetic latitude $\lambda(p)$ (see eq. (65), Fig. 87). Therefore the intensity distributions arising from primaries of a fixed momentum $p < p_{\max}$ increase when going

from the equator to higher latitudes up to the latitude $\lambda(p)$. For higher latitudes all directions are allowed and therefore the intensity remains constant.

The actual latitude effect arises from a primary spectrum containing various energies. The intensity above 50° remains, however, constant, and it must be concluded therefore that the primary spectrum contains no particles which are latitude sensitive above 50°. Putting $\mathfrak{g}_c = 1$ we obtain from (58)

$$p(50°) = 3{,}000 \text{ MEV./}c. \tag{83}$$

It must be assumed therefore that the primary spectrum contains no particles with momentum below 3,000 MEV./c.

520. The low-energy cut-off of the primary spectrum was postulated by Jánossy (1937) and it was proposed that the cut-off is due to the permanent magnetic field of the sun.

It was suggested by Hale and his co-workers (1918) that the sun might have a permanent magnetic dipole field with a moment of the order of

$$\mathrm{M}_\odot = 1{\cdot}7 \,.\, 10^{34} \text{ e.s.u.} \tag{84}$$

The dipole may be assumed to be perpendicular to the ecliptic. It can be assumed therefore that particles with momentum less than

$$p_\odot = \frac{\mathrm{M}_\odot e}{R_{S-E}^2} \tag{85}$$

are forbidden by the magnetic field of the sun in the neighbourhood of the earth, R_{S-E} being the distance between earth and sun. It is seen from (83), (84), and (85) that the sun's magnetic field can be taken to account for the latitude cut-off. The above suggestion was taken up by Vallarta (1937*b*) and by Epstein (1938). Compare also Vallarta and Godart (1939).

It may be pointed out that the direct evidence for the existence of a solar magnetic field is scanty.† According to Chapman (1928) even if a solar magnetic field exists near the surface of the sun this field would be cut off from outside by ionic currents. Cowling (1929, 32), however, concludes that the field of the sun should be expected to extend into outside space.

Whether or not the sun possesses a permanent field extending into space the primary spectrum of cosmic rays must be expected to be cut off below the value given by (84).

† Recently strong evidence for such a field has been obtained. Compare, for literature, Blackett, *Proc. Roy. Soc.* A (in the press).

The latitude effect of the soft component

521. In the following we discuss how far the latitude effect can be accounted for in terms of incident primary electrons. It will be seen in the course of this discussion that only the latitude effect at high altitudes can be accounted for in terms of incident electrons.

Assuming an incident electron spectrum of the type given in (79) the height-intensity curve observed at high latitudes can be accounted for satisfactorily (*vide* § 416, Fig. 73 (*a*)).

It was shown in § 416 that the incident spectrum must be assumed to be cut off below 2,000 MEV. in order to account for the observed position of the maximum of the height-intensity curve. It is particularly satisfactory that a cut-off at nearly the same value is implied from the observation of the geomagnetic effect (§ 519). Thus both the same cut-off and the same exponent z can be derived from two independent arguments.

522. According to the observation of Carmichael and Dymond (1939) the atmospheric-transition curve above the pole has a maximum at the same height as the transition curve observed above 50° (see Fig. 96, § 511). If the transition curve is to be interpreted in terms of primary electrons producing cascades one concludes therefore that the energy spectrum incident over the pole must be cut off at the same energy as the spectrum at 50°, thus near 2,000 MEV./c.

Primaries of any energy can approach the earth near the magnetic poles. Therefore the cut-off of the spectrum inferred from the shape of the transition curves found by Carmichael and Dymond cannot be due to the blocking effect of the earth field. This consideration further supports the conclusions arrived at in § 520.

523. The actual shape of the height-intensity curve at various latitudes can be accounted for in terms of an incident electron spectrum cut-off according to latitude by the magnetic field of the earth. This was shown by Heitler (1937 *b*) and also by Nordheim (1938).

Calculated and observed distributions are shown in Fig. 98.

524. A more sensitive test of the cascade theory is obtained when considering the difference of the vertical intensities measured at two latitudes. The difference curve is due to primary electrons with energies between the corresponding cut-off energies.

In Fig. 99 the difference between the curves obtained for $\lambda = 3°$ and $\lambda = 25°$ is plotted. The cut-off energies at these latitudes are

$$15{,}000 \text{ MEV.} \quad \text{and} \quad 11{,}000 \text{ MEV.} \tag{86}$$

Therefore the difference curve is expected to represent the transition curve of a cascade due to primaries in the interval (86). This interval is narrow and therefore the actual spectral distribution inside this interval must be of little importance.

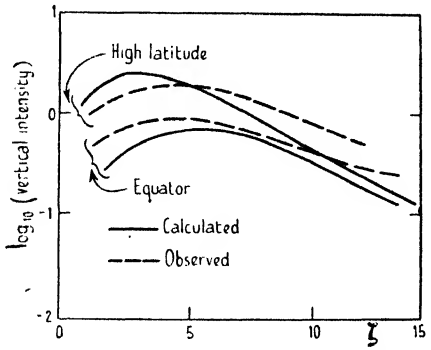

FIG. 98. Vertical intensities at high altitudes. Observed and calculated for $z = 1{\cdot}5$.

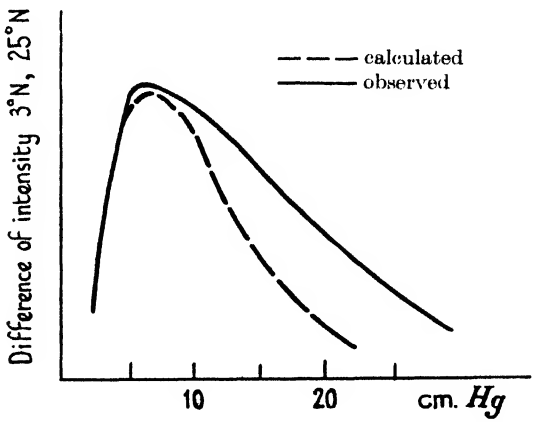

FIG. 99. Calculated and observed difference curves for the intensity between 3° N. and 25° N. (Chakrabarty).

The transition effect of a cascade due to primaries in the interval (86) has been evaluated by Chakrabarty (1942*b*). The result of this calculation is also shown in Fig. 99.

It is seen that the transition curve obtained from the cascade theory gives a maximum at the right depth. After the maximum, the intensity calculated from the cascade theory falls off more rapidly than the observed intensity.

The discrepancy between calculated and observed intensity is by no means surprising. We note that the meson component starts to build

up at very high altitudes and that because of the very low air density many of the mesons are expected to decay soon after their formation. Thus the intensity at high altitudes is probably a mixture of (1) primary soft component, (2) hard component, (3) decay electrons.

As there is no precise information available about the intensities of

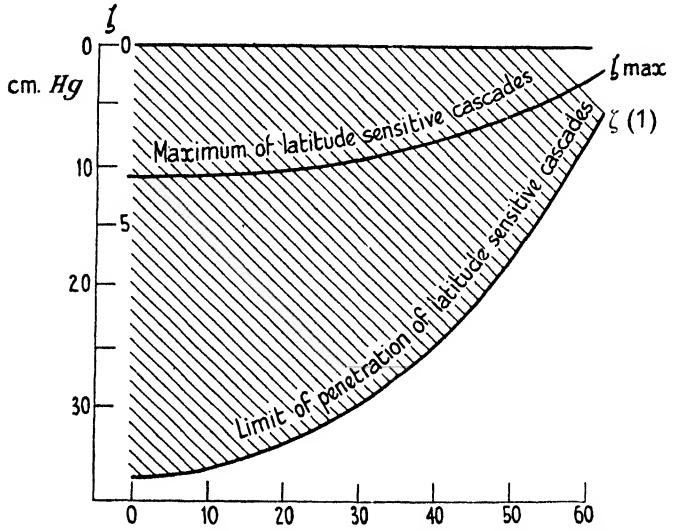

FIG. 100. Limits of latitude effect of primary cascades.

the contributions of (2) and (3) no strict comparison between the calculated intensity of the soft component and the observed intensity can be carried out.

Latitude effect at low altitudes

Cascades

525. Electron cascades produced by primary electrons cannot contribute to the latitude effect near sea-level, for to produce a cascade which contains on the average one electron near sea-level a primary energy of

$$10{,}000 w_c = 10^6 \text{ MEV}. \qquad (86\,a)$$

is required. An electron of this energy can approach the earth from any direction and at any point. Therefore primary electrons capable of penetrating the atmosphere are necessarily latitude insensitive.

526. Let us estimate the depths inside the atmosphere to which latitude-sensitive electrons can penetrate. In Fig. 100 $\zeta(1)$ has been plotted against latitude, where $\zeta(1)$ is the depth at which a primary electron of energy $cp_{\text{vert}}(\lambda)$ produces on the average one electron.

Note from Fig. 100 that latitude-sensitive cascades penetrate at the equator down to about 35 cm. Hg pressure, that is down to about 6,000 m. altitude.

It is concluded from Fig. 100 that the soft component contributes to the latitude effect only at heights above 6,000 m.

Latitude effect of hard component

527. The latitude effect at sea-level and at low altitudes must be regarded as being due to latitude-sensitive primaries giving rise to mesons.

The flow of energy through the surface of the solid earth can be evaluated either from the energy spectrum (§ 310, Ch. IV) or by integrating the depth ionization curve. Both methods give roughly the same value, namely,

$$6{,}000 \text{ MEV. per cm.}^2 \text{ per min.} \tag{87}$$

at high latitudes. The latitude effect at sea-level is about 10 per cent. and therefore the difference in energy is about

$$600 \text{ MEV. per cm.}^2 \text{ per min.} \tag{88}$$

The latter value is calculated assuming tentatively that the spectral distribution of the radiation does not change with latitude. (There is unfortunately no observational evidence as to the spectral distribution or to the depth ionization curve for low latitudes.)

The values for the flow at sea-level given in (87) and (88) are small compared with the total flow into the top of the atmosphere. From Table 3, § 515, it is found that about 5 per cent. of the energy incident on the earth at high latitudes reaches sea-level while only 1 per cent. of the latitude-sensitive primaries can reach sea-level.

Conclusions

528. An interesting conclusion can be drawn from the comparison of the average energy of the mesons at sea-level with the energies of the primaries as deduced from the latitude effect.

The average energy of the mesons at sea-level is about 3,000 MEV. Assuming that these mesons have been created high up in the atmosphere they may be assumed to have lost 2,000 MEV. through ionization in passing through the atmosphere. Thus the mesons must have been created with an average energy of about 5,000 MEV. (N.B.: Disregard mesons which do not reach sea-level.)

From the latitude effect it is concluded, however, that only 10 per cent. of the mesons have been produced by latitude-sensitive primaries,

i.e. by primaries between 3,000 and 15,000 MEV., and that 90 per cent. of the mesons have been produced by primaries with energies above 15,000 MEV.

It is seen therefore that most of the primaries must be assumed to give rise mainly to mesons with energies much smaller than their own energy. The average fraction which a primary transfers to a meson may be $\frac{1}{3}$. The above argument was taken as evidence that the penetrating component is of secondary nature at a time when the instability of the meson was not known (Nordheim (1938), Bowen, Millikan, and Neher (1937)).

529. While in most cases a primary produces mesons with energies rather smaller than the energy of the primary itself, it can be shown that occasionally a primary transfers most of its energy to one meson. The latitude effect extends up to 50° even at sea-level. It must be concluded, therefore, that some of the primaries with 2,500 MEV.† can give rise to secondaries reaching sea-level. If a primary of 2,500 MEV. splits its energy between several mesons, none of the mesons can reach sea-level. Therefore the extension of the latitude effect at sea-level up to 50° can only be understood if it is assumed that occasionally a primary of 2,500 MEV. transfers most of its energy to a single meson.

530. It is interesting to note that originally it was thought that the cut-off of the latitude effect at 50° is caused by the absorption of the atmosphere. It was argued that ionizing primaries with energies below about 2,000 MEV. cannot penetrate to sea-level, neither can they give rise to ionizing secondaries penetrating to sea-level, thus the primary spectrum below 2,000 MEV. must be assumed to be ineffective at sea-level.

The atmospheric absorption thus accounts for the cut-off at sea-level; it cannot, however, account for the cut-off at the same latitude for higher altitudes.

(*b*) *The Longitude Effect*

531. The variation of cosmic-ray intensity with geomagnetic longitude can be accounted for in terms of the eccentricity of the equivalent dipole inside the earth (Chapman and Bartels, *Geomagnetism*, Oxford, 1940, p. 651). The magnetic centre of the earth is found to lie at a point about

$$\epsilon \simeq 300 \text{ km}. \tag{89}$$

from the geometrical centre of the earth. The distance of an observer

† 2,500 MEV. is the limiting energy for vertical incidence for $\lambda = 50°$.

from the geomagnetic centre at the geomagnetic longitude Φ on the geomagnetic equator is given by

$$R^2(\Phi) = R_E^2 + \epsilon^2 - 2R\epsilon\cos(\Phi - \Phi_0), \tag{90}$$

where R_E is the mean radius of the earth and Φ_0 is the geomagnetic longitude of the point of nearest approach to the geomagnetic centre.

As the distance of the equivalent centre from the dipole varies with longitude the value of the limiting momentum also varies with longitude. The limiting momentum in the vertical direction at the equator is thus given by

$$p_{\text{vert}}(\lambda = 0, \Phi) = \frac{15{,}000 \text{ MEV.}/c}{1 + (\epsilon/R_E)^2 - 2(\epsilon/R_E)\cos(\Phi - \Phi_0)}. \tag{91}$$

Introducing numerical values it is found that p_{vert} varies along the geomagnetic equator between the following limits:

$$p'_{\text{vert}} = 13{,}700 \text{ MEV.}/c < p < 16{,}500 \text{ MEV.}/c = p''_{\text{vert}}. \tag{92}$$

532. The longitude effect of the total flow of energy can be obtained from (80) and (91). We have

$$\mathfrak{W}(\lambda = 0, \Phi) \sim \frac{1}{\sqrt{\{p_{\text{vert}}(\lambda = 0, \Phi)\}}}. \tag{93}$$

Introducing the value (89) the magnitude of the longitude effect becomes

$$200 \times \frac{\mathfrak{W}(\Phi_0) - \mathfrak{W}(\Phi_0 + \pi)}{\mathfrak{W}(\Phi_0) + \mathfrak{W}(\Phi_0 + \pi)} = 10 \text{ per cent.} \tag{94}$$

The actual height-intensity curves measured over Mexico and over the Philippines did not show a difference larger than the error of measurement. An effect of the order of 10 per cent., as predicted above, does not seem, however, to be incompatible with the observations.

533. The longitude effect at sea-level has been found to be about 7 per cent. of the total intensity. Thus the difference between equator and high latitudes is about 7 per cent. in America and about 14 per cent. in the Far East. This difference may be attributed to mesons produced by primaries in the interval given by (92).

To discuss the longitude effect in more detail it would be necessary to make detailed assumptions about the nature of the primaries giving rise to the mesons. A curious feature of the latitude and longitude effects near sea-level may, however, be noted.

The intensity is found to be constant between equator and $\pm 20°$ latitude when observing along constant longitude.

Thus the latitude effect seems to arise from primaries in the following interval

$$p < p'_{\text{vert}} \cos^4 20^\circ = 10{,}700 \text{ MEV./}c,$$

while the contribution from the interval

$$10{,}700 < p < 13{,}700 \text{ MEV./}c \tag{95}$$

appears to be small. The whole of the longitude variation has to be attributed to the interval (92), which is of the same order as (95) but lies in a slightly higher region.

It seems therefore that primaries in the interval (95) are either missing altogether, or that the primaries in this interval are particularly ineffective for producing mesons.

The experimental evidence leading to this conclusion is not very firm. It would be therefore most desirable if more observations in the equatorial belt were carried out.

(*c*) *Asymmetries*

East–west asymmetry at low altitudes

534. The east–west asymmetry of the radiation intensity at low geomagnetic latitudes can be accounted for on the assumption that the primary cosmic rays contain an excess of particles of one sign.

Considering, for instance, positive primaries, the forbidden cones point towards the east and therefore an excess of the intensity from the west is expected. Similarly the forbidden cones for negative particles point towards the west and therefore negative primaries are expected to give rise to an excess from the east.

The total east–west asymmetry is thus determined by the difference of the intensities of the positive and the negative primaries. The latitude effect and also the north–south asymmetry are determined by the sum of the intensities of the positively and negatively charged primaries. Therefore the comparison of the east–west effect with either the north–south effect or the latitude effect should give evidence as to the numbers of positively and negatively charged primaries.

535. Such a comparison was carried out by Johnson (1938*d*). In a number of publications Johnson elaborated the view that the primaries of the penetrating component are all positively charged and he suggested that these primaries are protons (compare also Blackett, 1941).

We now show that the east–west effect at moderate heights can be best understood by assuming that the primaries are all positively charged. These conclusions refer only to the primaries responsible for

the geomagnetic effects of the penetrating component. The effects at high altitudes have to be considered separately.

536. The asymmetry in a direction inclined at ϑ to the vertical can be characterized by the ratio

$$a(\vartheta) = 2\frac{I_W(\vartheta)-I_E(\vartheta)}{I_W(\vartheta)+I_E(\vartheta)}, \tag{96}$$

where $I_W(\vartheta)$ is the intensity in a direction inclined at an angle ϑ to the vertical towards the west, while $I_E(\vartheta)$ is the corresponding intensity in a direction inclined by ϑ to the east. If the observation is carried out at a geomagnetic latitude λ, then the limiting energies in the two directions are for positively charged primaries given approximately by

$$\begin{aligned} p_W(\lambda,\vartheta) &= p_{\text{vert}}\frac{4\cos^4\lambda}{\{\sqrt{(1+\sin\vartheta\cos^3\lambda)}+1\}^2}, \\ p_E(\lambda,\vartheta) &= p_{\text{vert}}\frac{4\cos^4\lambda}{\{\sqrt{(1-\sin\vartheta\cos^3\lambda)}+1\}^2}. \end{aligned} \tag{97}$$

Introducing

$$\cos\lambda' = \frac{\sqrt{2}\cos\lambda}{\sqrt{\{\sqrt{(1+\sin\vartheta\cos^3\lambda)}+1\}}}, \qquad \cos\lambda'' = \frac{\sqrt{2}\cos\lambda}{\sqrt{\{\sqrt{(1-\sin\vartheta\cos^3\lambda)}+1\}}}, \tag{98}$$

it is found that the limiting momenta in the two inclined directions are equal to the limiting momenta values for vertical incidence at the latitudes λ' and λ''. Thus the latitude effect between the latitudes λ' and λ'' can be compared with the east–west asymmetry at the intermediate latitude λ between the directions inclined by ϑ to the east and the west.

To make this comparison as close as possible let us compare the latitude effect of the vertical intensity at sea-level with the asymmetry at an elevation above sea-level, so that

$$\theta = \theta_0\cos\vartheta, \tag{99}$$

where θ_0 is the mass equivalent of the atmosphere above sea-level, while θ is the mass equivalent of the atmosphere above the observer of the east–west effect.

Except for effects caused by the instability of the meson the following identities should exist:

$$p_{\text{vert}}(\lambda';\theta_0) = p_W(\lambda,\vartheta;\theta), \qquad p_{\text{vert}}(\lambda'';\theta_0) = p_E(\lambda,\vartheta;\theta_0). \tag{100}$$

Because of the instability of the meson the intensities observed in the inclined directions must be expected to be smaller than the corresponding

intensities in the vertical directions. We are, however, probably not far wrong in assuming

$$\frac{p_{\text{vert}}(\lambda';\theta_0)}{p_W(\lambda,\vartheta;\theta)} = \frac{p_{\text{vert}}(\lambda'';\theta_0)}{p_E(\lambda,\vartheta;\theta)}. \tag{101}$$

537. We introduce the numerical values. The latitude effect of the vertical intensity was observed by Millikan, Neher, and Pickering (1943)

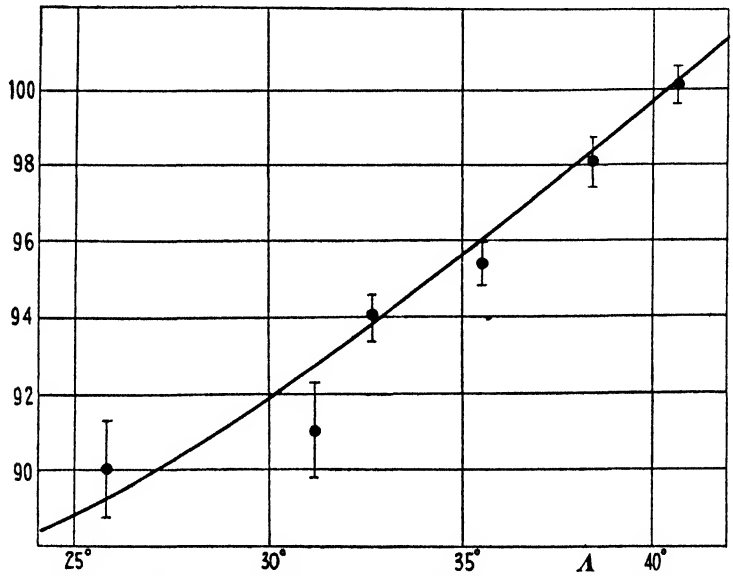

FIG. 101. Latitude effect of vertical intensity (Millikan, Neher, and Pickering, 1943).

and the results are shown in Fig. 101. A smooth curve has been laid through the observed points for the purpose of interpolation and extrapolation.

In the following table we reproduce some of Johnson's (1935*b*) observations of the east–west effect.

TABLE 5

Latitude λ	*Height*		*Angle*	*Asymmetry (%)*		*Equivalent latitudes*	
	Metres	*Water-equivalent*		*Obs.*	*Calc.*	λ'	λ''
29°	4,300	6·25	51·5	11	6·7	34·0°	17·5°
	3,300	6·80	49	8	7·3	33·8°	19·0°
	2,200	7·50	43·6	8	7·9	33·5°	20·5°
36°	1,730	8·45	35	5·5	7·6	38·3°	32·5°

The angles are chosen to satisfy (99). The values of the asymmetry for these angles are found by interpolation. The calculated values for the

asymmetry are obtained from (96), (101). The numerical values of the vertical intensities are taken from Fig. 101.

It is seen that the calculated and observed asymmetries agree as well as can be expected in view of the great inaccuracies involved.

Observations were also carried out at the geomagnetic equator. The observations were made in Peru, near to the maximum of the intensity on the equator (see § 505).

The observations were carried out at a height of 4,300 m. above sea-level with $\theta = 6{\cdot}24$ m. H_2O equivalent. For comparison with the vertical intensity consider the inclination defined by

$$\cos\vartheta = \frac{6{\cdot}24}{10{\cdot}3}, \qquad \vartheta = 53°.$$

The cut-off energies towards the west and east are found to be

$$p_W = 10{,}000 \text{ MEV.}/c, \qquad p_E = 25{,}400 \text{ MEV.}/c, \tag{102}$$

where we have assumed $p_{\text{vert}} = 13{,}700$ MEV./c in accordance with (92).

It follows from (92), (95) that the spectrum between

$$10{,}000 \text{ MEV.}/c \quad \text{and} \quad 16{,}500 \text{ MEV.}/c$$

contributes about 7 per cent. to the total intensity at sea-level. The observed asymmetry of 14 per cent. must be attributed to the considerably larger interval p_W to p_E (102). This is quite reasonable and thus the large east–west asymmetry observed in Peru fits in with the observed latitude and longitude effects.

538. It is clear, therefore, that the observations of the east–west effect appear to be compatible with the observed magnitude of the latitude and longitude effects provided it is assumed that *all* primaries are positively charged. The latter assumption is essential. If, for example, one-third of the primaries are assumed to have negative charges then the calculated values in Table 5 would have to be reduced by a factor three. The reduced values would be too small to be compatible with the observed data. It is concluded therefore that the larger part of the primaries of the hard component are positively charged.

The east–west asymmetry at high altitudes

539. The magnitude of the east–west asymmetry at high altitudes can also be estimated from the latitude effect on the assumption that all primaries are positively charged. Such an estimation, as we show presently, leads to a value for the asymmetry which is too large. It is

concluded therefore that the primaries of the soft component contain both positively and negatively charged primaries. The most likely assumption is that the soft component is due to positive and negative electrons.

540. The only measurements of the east–west asymmetry at high altitudes are those of Johnson and Barry (1939). The observations did not show an asymmetry at a height corresponding to 1·4 m. water equivalent. An effect exceeding 7 per cent. was regarded as incompatible with the observations.

The observations were carried out with a counter telescope inclined at an angle of 60° to the vertical and rotating freely round a vertical axis. We have to compare the intensities averaged separately over the positions where the direction of the telescope had a component towards the west and the positions where the direction of the telescope had a component to the east.

541. The angle ω between the direction of the telescope and the east–west direction is given by

$$\cos\omega = \sin 60^\circ \cos\phi, \tag{103}$$

where ϕ is the azimuth, counted from the east–west direction. The limiting momentum in the direction of the telescope is therefore

$$p(\phi) = p_{\text{vert}} \frac{4\cos^4\lambda}{\{\sqrt{(1+\sin 60^\circ \cos^3\lambda \cos\phi)}+1\}^2}. \tag{104}$$

Because of the inclination of the telescope the observed intensities may be compared with the vertical intensities at a depth

$$\theta = 1{\cdot}4/\cos 60^\circ = 2{\cdot}8 \text{ m. water equivalent.}$$

The vertical intensity at such a depth as a function of the cut-off momentum $p(\phi)$ can be obtained from Fig. 94. In this way the intensity $I(\phi)$ is obtained as a function of the azimuth ϕ of the arrangement. Integrating numerically it is found that

$$a = 2\frac{I_W - I_E}{I_W + I_E} = 0{\cdot}4, \qquad I_W = \int_{-\frac{1}{2}\pi}^{+\frac{1}{2}\pi} I(\phi)\, d\phi, \qquad I_E = \int_{\frac{1}{2}\pi}^{3\pi/2} I(\phi)\, d\phi.$$

The asymmetry thus obtained is too large to be compatible with the observed asymmetry $a_{\text{obs}} < 0{\cdot}07$. Therefore we conclude that the primaries of the soft component must contain both positively and negatively charged particles. The simplest assumption is that positively and negatively charged primaries are equally frequent.

North–south asymmetry

542. The north–south asymmetry is due to the peculiar shape of the allowed cone. It was seen in § 488 that the Störmer cone gives only a rough approximation of the actual allowed cone. Theory and observations of the north–south asymmetry have been discussed by Lemaître and Vallarta (1936*a*) and also Lemaître, Vallarta, and Bouckaert (1935) (compare also Johnson (1935*a*)).

3. *The Nature of the Primary Cosmic Rays*

543. The question of the nature of the primaries which are responsible for the geomagnetic effects will now be discussed.

The most important question is whether the primaries of the soft component and those of the penetrating component are identical.

It is our opinion that the primaries actually contain two different types of particle, probably electrons and protons. A similar view is taken by Ferretti (1942). In the following section the consequences of the assumption of a single primary and the consequences of the assumption of two primary components, are discussed.

544. An argument in favour of one kind of primary may be deduced from the latitude cut-off. From the latitude effects of both the soft component and the penetrating component we are led to conclude that the spectrum of the primaries does not contain particles with momenta below 3,000 MEV./*c*. If two types of primaries are assumed it is necessary to assume both primary spectra to be cut off near the same momentum. If, on the other hand, only one spectrum is assumed it is immediately clear that both components derived from the same primaries must show the same latitude cut-off.

On the assumption of two types of primaries the two cut-offs have to be assumed to coincide by accident or have to be assumed to be caused by the same agency, e.g. the magnetic field of the sun.

545. The main difficulty encountered with the assumption of one type of primary only, is that of accounting for the east–west asymmetry. While the hard component shows a marked east–west asymmetry no such asymmetry was observed for the soft component at high altitudes.

It appears from the evidence that the soft component is due to a mixture of positively and negatively charged primaries while the hard component is due to positively charged primaries only.

The above argument has to be taken very seriously. The only weakness is that there is only one observation of the east–west asymmetry at high altitudes available. Though there is no reason to doubt the

accuracy of these measurements it would be very desirable to confirm such a crucial experiment by independent observations.

Discussion of east–west effect at high altitude

546. Attempts have been made to uphold the hypothesis of one type of primary and to 'explain' the negative result of the east–west experiment of Johnson and Barry (1939) in terms of scattering. It is argued that the soft component may be due to positive primaries only, but that the east–west asymmetry is smoothed out by scattering.

It can be shown that the asymmetry which would arise if the primaries were all positively charged could hardly be smoothed out in this way (see Johnson (1939*c*)).

547. Assuming that the primaries are positive electrons only, the scattering reduces to the scattering of the particles in a cascade. This process is investigated in Chapter VIII, from which it is seen that the order of magnitude of the projected mean square angle of scattering is given by $14/w_c$, where w_c is the critical energy. Since for air $w_c = 100$ MEV. the mean square scattering is of the order of 10°. Such a scattering is clearly insufficient to smooth out the large asymmetry expected.

548. The particles are also deflected by the magnetic field of the earth. It is clear that the deflexion of the primaries throughout the atmosphere is negligibly small. Most of the radiation consists, however, of secondaries of small energies and it is necessary to estimate the deflexion suffered by these secondaries.

The radius of curvature of an electron of energy w is given by

$$R(w) = \frac{R_c}{w_c} w.$$

At the equator $R_c = 10$ km.

and therefore the deflexion along a path ds is

$$d\alpha = ds/R_c . (w_c/w). \tag{105}$$

Assuming for the moment that most of the energy loss is due to ionization, we may put

$$ds = \Delta dw/w_c, \tag{106}$$

where Δ is the cascade unit in air (see § 371). Introducing (106) into (105) we find after integration

$$\alpha = \frac{\Delta}{R_c} \log(w_1/w_2).$$

α is the deflexion suffered by a particle while its energy decreases from w_1 to w_2.

The above expression is of course only valid if w_1 is not much larger than w_c.

For higher energies the rate of loss exceeds very much the loss through ionization and therefore energies $w > w_c$ contribute only very little to the total deflexion. On the whole it is reasonable to assume that for slow particles the effective value of $\log(w_1/w_2)$ is of the order of one and that the angle of deflexion is of the order of

$$\alpha \sim \Delta/R_c;$$

the cascade unit is

0·342 km. for air at N.T.P.,

and at the height where the observations of the east–west were carried out

$$\Delta \sim 3{\cdot}5 \text{ km. (7 cm. Hg pressure).}$$

Thus the order of deflexion of slow particles is about

$$3{\cdot}5/10 \text{ radians} = 20°.$$

Such a deflexion is more serious than the deflexion through scattering but is still insufficient to smooth out a pronounced east–west asymmetry.

It must be concluded therefore that if the soft component is due to primary electrons it is necessary to assume both positive and negative electrons. The mesons which are produced by positive primaries only cannot be produced by an electron component which contains both signs of charge.

549. It remains to discuss the possibility that both mesons and electrons are the secondaries of a common primary. It has been suggested, for instance, that all primaries are protons which give rise to mesons which in their turn giving rise to electrons by decay. In this process the electrons appear as the *tertiaries* of the positive primaries and it is argued that they may lose their original directions to a greater extent than in the case of an ordinary cascade.

The actual amount of scattering involved depends on the details of the process and cannot be estimated without specific assumptions.

4. *Conclusions*

550. We summarize now the main conclusions which can be made from the analysis of the geomagnetic effects.

1. From the analysis of the height-intensity curves at various latitudes it can be concluded that the primary spectrum is of the form

$$\mathfrak{S}(p) \sim p^{-2{\cdot}5} \qquad (107)$$

for momenta greater than about 3,000 MEV./c. For momenta exceeding

$$p_{\text{vert}} = 15{,}000 \text{ MEV.}/c$$

no conclusions can be drawn about the shape of the spectrum, though the total momentum carried by the particles above p_{vert} is given correctly by (107).

The above conclusion is independent of any assumption as to the nature of the particles except that all particles have single charge and that all of the incident energy appears eventually in the form of ionization. The actual flow of energy at high latitudes is estimated to be

$$1{\cdot}4 \times 10^5 \text{ MEV. per cm.}^2 \text{ per min.}$$

and about $0{\cdot}7 \times 10^5$ MEV. per cm.^{2} per min.

above the equator.

The flow refers to the energy crossing a sphere with cross-section 1 cm.^{2} The flow through a horizontal area of 1 cm.^{2} is equal to half of the former.

About half of the total energy is carried by latitude-sensitive primaries. The flow through the top of the atmosphere near the equator is only half of the flow at high latitudes.

2. Only a small fraction of the primary energy penetrates down to sea-level. The total flow of energy near sea-level is about

$$6{,}000 \text{ MEV. per cm.}^2 \text{ per min.},$$

that is about 5 per cent. of the primary flow. Only 10 per cent. of this energy is carried by latitude-sensitive primaries. Thus 1 per cent. of the energy of latitude-sensitive primaries reaches sea-level and 8 per cent. of the energy of primaries above 15,000 MEV. reaches sea-level.

3. The above conclusions refer to the spectrum of all primaries taken together. There are arguments to the effect that the primaries consist of two different types of primaries: (1) positive and negative electrons producing the soft component; (2) positive primaries, probably protons, giving rise to the penetrating component. The main argument in favour of the two primary components is derived from the east–west asymmetry. The penetrating component at sea-level and at moderate heights above sea-level shows a marked east–west asymmetry. The magnitude of this asymmetry when compared with the latitude effect at sea-level suggests that the whole of the penetrating component is produced by positive primaries. The soft component at high altitudes does not show any east–west asymmetry, according to the measurements of Johnson and

Barry; therefore the soft component must be assumed to be due to positive and negative primaries.

4. The average energy of the penetrating particles near sea-level is 3,000 MEV. These particles must be assumed to have been produced near the top of the atmosphere and therefore they must have started with energies not greater than

$$3{,}000+2{,}000 = 5{,}000 \text{ MEV.},$$

2,000 MEV. being the loss of energy by collision suffered through the whole of the atmosphere. The primaries giving rise to the penetrating component must have average energies much higher than 5,000 MEV. and therefore it is concluded that most mesons receive only a fraction of the energy of their primary. Therefore each primary gives rise to several mesons.

The above conclusion refers to the average energy transfer. From the fact that the latitude effect of the hard component extends up to 50° it must be concluded that instances occur where most of the energy of a primary is transferred to one meson.

VIII

EXTENSIVE AIR SHOWERS

551. AUGER, Maze, and Grivet-Meyer (1938) observed large showers extending over areas several metres in diameter; similar observations were also reported by Kolhörster, Matthes, and Weber (1938). It was suggested that these showers might be large cascades started by energetic electrons in the atmosphere. The question as to the nature of these showers has not yet been settled satisfactorily, though it is likely that most of them are in fact cascades as assumed originally.

We shall develop in the following the theory of large cascade showers in order to compare them with the observed showers.

A. THEORY OF LARGE CASCADES IN AIR

552. In Chapter VI the numbers of electrons and photons produced by a primary were determined. The cascade problem was treated as a one-dimensional problem. In the following we show how the theory can be extended so as to include the lateral spread of the showers. The lateral spread of showers was dealt with first by Euler and Wergeland (1940). The theory was further elaborated by many authors. We mention Bethe (quoted from Rossi and Greisen (1941)), Nordheim (1941), Landau (1940), Roberg (1942), Belenky (1942, 4), Skobelzyn (1944 *a*, *b*). The following treatment follows the ideas of these authors.

1. *Elastic Scattering*

553. The most important cause of the spreading of a shower is the elastic scattering of the electrons (Euler). According to §§ 243, 370, the mean square angle of scattering of an electron of energy w in a layer $d\zeta$ (cascade units) is given by

$$d\vartheta^2 = \left(\frac{w_s}{w}\right)^2 d\zeta \tag{1}$$

with $w_s = 21$ MEV.

Other causes of spread are:

(i) The angular spread of quanta.

(ii) The angular spread of electron pairs.

(iii) Compton scattering of the photons.

The angles involved in processes (i) and (ii) are of the order of

$$m_e c^2/w. \tag{2}$$

The mean distances between radiative collisions are of the order of one cascade unit. Thus the change of direction due to processes (i) and (ii) is small compared with the change due to scattering.

The mean square angle of Compton scattering per cascade unit is also of the order of (ii) and therefore this scattering produces a much smaller spread than the elastic scattering of the electrons.

554. We shall therefore consider the lateral spread of cascade showers due to elastic scattering only.

Consider an electron with initial energy w_0 passing through a homogeneous absorber of thickness ζ. Assume that the electron loses energy continuously; let the energy at a depth $\zeta-\zeta'$ be $w(\zeta')$.

The mean square displacement of such an electron at the depth ζ is found with help of (1) as

$$x^2 = w_s^2 \int_0^\zeta \frac{d\zeta'}{w(\zeta')^2}\zeta'^2. \tag{3}$$

The mean square angular displacement is found similarly as

$$\vartheta^2 = w_s^2 \int_0^\zeta \frac{d\zeta'}{w(\zeta')^2}. \tag{4}$$

555. We have to consider how the scattering affects the distribution of the electrons in a cascade. Note that each electron at a depth ζ in a cascade can be traced back to the primary in a unique way (see Fig. 102). The mean square displacement of an electron of energy w can thus be written as

$$x^2 = w_s^2 \int_0^\zeta \frac{a(\zeta')\zeta'^2 d\zeta'}{w(\zeta')^2}, \tag{5}$$

where the energy $w(\zeta')$ refers to the energy of the electron at the depth ζ' in the trail of the electron under consideration.

$$a(\zeta') = \begin{cases} 0 & \text{if the parent at } \zeta' \text{ is a photon,} \\ 1 & \text{if the parent at } \zeta' \text{ is an electron.} \end{cases}$$

The factor $a(\zeta')$ in (5) takes care of the fact that the scattering of photons is small compared with the scattering of electrons.

In order to obtain the mean square deviations of the electrons with a final energy w, it is necessary to average over all possible histories of the electron.

Denote the number of electrons in an interval w, dw at the depth ζ by

$$q(w_0, w; \zeta)\, dw, \tag{6}$$

where w_0 refers to the primary energy. At any depth the parents of the electrons given in (6) have energies w' with

$$w \leqslant w' \leqslant w_0.$$

Denote the number of parents in an interval w', dw' by

$$P(w', w; \zeta')\, dw' dw, \tag{7}$$

where each parent is counted several times if it gives rise to several

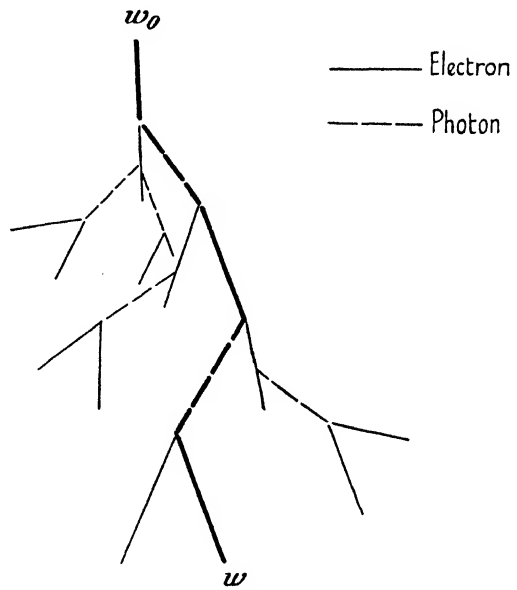

FIG. 102. The history of a particle in a cascade.

electrons, while photons are not counted at all. The average scattering is obtained by averaging over all possible energies of the parents. Thus

$$\langle x^2 \rangle = w_s^2 \int_0^{\zeta} \zeta'^2\, d\zeta' \int_w^{w_0} \frac{P(w', w; \zeta')\, dw'}{w'^2} \Big/ \mathrm{q}(w_0, w; \zeta). \tag{8}$$

The number of electrons with energies in the interval w', dw' is given by

$$\mathrm{q}(w_0, w'; \zeta - \zeta')\, dw'. \tag{9}$$

Each of these electrons gives rise to

$$\mathrm{q}(w', w; \zeta')\, dw \tag{10}$$

electrons with energies in the interval w, dw at ζ. Therefore the number of parents defined in (7) is given by

$$P(w', w; \zeta') = \mathrm{q}(w_0, w'; \zeta - \zeta')\mathrm{q}(w', w; \zeta'). \tag{11}$$

The mean square deviation of electrons with energies w at the depth ζ is therefore given by

$$\langle x^2\rangle_{w,\zeta} = w_s^2 \int_0^{\zeta} \zeta'^2\, d\zeta' \int_w^{w_0} \mathfrak{q}(w_0, w'; \zeta-\zeta')\mathfrak{q}(w', w; \zeta')\frac{dw'}{w'^2}\Big/\mathfrak{q}(w_0, w; \zeta). \tag{12}$$

Similarly the mean square angular spread is given by

$$\langle \vartheta^2\rangle_{w,\zeta} = w_s^2 \int_0^{\zeta} d\zeta' \int_w^{w_0} \mathfrak{q}(w_0, w'; \zeta-\zeta')\mathfrak{q}(w', w; \zeta')\frac{dw'}{w'^2}\Big/\mathfrak{q}(w_0, w; \zeta). \tag{13}$$

Equations (12) and (13) are due to Bethe and to Nordheim, quoted from Rossi and Greisen (1941).

(*a*) *High Energies*

556. Numerical values for the spread of showers can be obtained by introducing the values for the functions $\mathfrak{q}$ from Chapter VI. Note, however, that expression (12) refers to the spread of a shower in a homogeneous medium. The atmosphere cannot be regarded as homogeneous because of the decrease in density with height. The inhomogeneity of the medium can be taken care of by replacing ζ' under the first integral by

$$x(\zeta-\zeta', \zeta'), \tag{14}$$

where $x(\zeta_1, \zeta_2)$ is the distance between the depth corresponding to ζ_1 cascade units and the depth corresponding to ζ_2 cascade units.

557. The integrals (12) and (13) can be evaluated easily using the approximate expression (38, Ch. VI) valid for $w \gg w_c$. Since the spread of a shower does not depend largely on the depth ζ, the spread averaged over all depths will be determined. We put

$$\langle x^2\rangle_w = \int_0^{\infty} \langle x^2\rangle_{w,\zeta}\, \mathfrak{q}_0(w_0, w; \zeta)\, d\zeta \Big/ \int_0^{\infty} \mathfrak{q}_0(w_0, w; \zeta)\, d\zeta \quad \text{for} \quad w \gg w_c. \tag{15}$$

With help of (12) and (15) it is found that

$$\langle x^2\rangle_w = w_s^2 \int_w^{w_0} \frac{dw'}{w'^2} \int_0^{\infty} \mathfrak{q}_0(w_0, w', \zeta'')\, d\zeta'' \int_0^{\infty} \mathfrak{q}_0(w', w; \zeta')\zeta'^2\, d\zeta' \Big/ \int_0^{\infty} \mathfrak{q}_0(w_0, w; \zeta)\, d\zeta. \tag{16}$$

With help of Table 3, Ch. VI, § 385, we have further

$$\int_0^{\infty} \mathfrak{q}_0(w_0, w; \zeta)\, d\zeta = 0{\cdot}437\frac{w_0}{w^2}, \tag{17}$$

and therefore

$$\langle x^2\rangle_w = w_s^2 w^2 \int_w^{w_0} \frac{dw'}{w'^4} \int_0^{\infty} \mathfrak{q}(w', w; \zeta')\zeta'^2 \, d\zeta'. \tag{18}$$

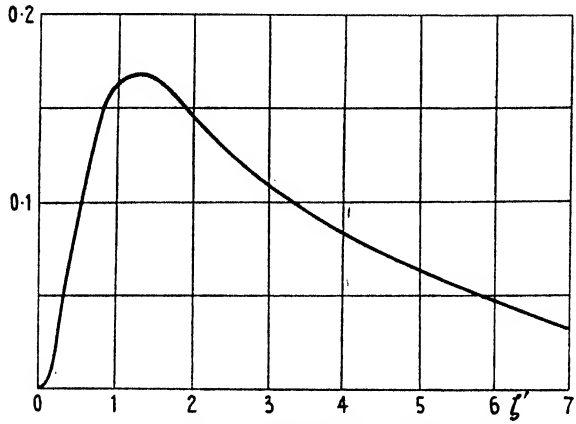

FIG. 103. The function $\{\mathfrak{M}(4)e^{-a_1\zeta}+\mathfrak{N}(4)e^{-a_2\zeta}\}\zeta^2$.

The first integration can be extended to infinity without introducing a large error. It is found from (56, Ch. VI, § 384) that

$$\int_w^{\infty} \frac{dw'}{w'^4} \mathfrak{q}(w', w; \zeta')\zeta'^2 = \frac{\zeta'^2}{w^4}\{\mathfrak{M}(4)e^{-a_1(4)\zeta'}+\mathfrak{N}(4)e^{-a_2(4)\zeta'}\}. \tag{19}$$

Finally, introducing (19) into (18) and with numerical values from Table 3, Appendix II, we have

$$\langle x^2\rangle_w = 2\left\{\frac{\mathfrak{M}(4)}{a_1(4)^3}+\frac{\mathfrak{N}(4)}{a_2(4)^3}\right\}(w_s/w)^2 = 0{\cdot}724(w_s/w)^2 \text{ (cascade units)}^2. \tag{20}$$

Similarly the angular spread is given by

$$\langle \vartheta^2\rangle_w = 0{\cdot}570(w_s/w)^2 \text{ (radians)}^2. \tag{21}$$

558. It is now necessary to justify the assumption that the spread of a shower does not depend to a great deal on ζ and that therefore it is legitimate to average over ζ.

The energy $w(\zeta')$ of the various parents of any electron increases rapidly with ζ'. Therefore for the actual amount of scattering the last few steps are most important.

It can be easily verified that the expression (19) is a measure of the importance of the spread of the parents at a height $\zeta-\zeta'$ for the spread of the electrons at the depth ζ.

Equation (19) has been plotted in Fig. 103, from which it is seen that

the most important contribution arises from the layer about one cascade unit above the observer.

The contribution from layers more than five cascade units above the observer is comparatively small. It is concluded that a large shower spreads out in about five cascade units and that for larger thicknesses the lateral spread remains stationary.

Similarly from Fig. 103 it is seen that no great error arises from the fact that the variation of the cascade unit with air density has been neglected. The variation of the cascade unit with height can be corrected roughly by assuming that most of the scattering takes place in a layer about one cascade unit above the observer; thus the cascade unit at the depth $\zeta-1$ can be used for the level ζ.

(*b*) *Low Energies*

559. There remains the question of the spread of particles of low energy.

Assuming that electrons with energy less than w_c lose energy only by ionization it follows that

$$w(\zeta') = \zeta' w_c \quad (\zeta' < 1), \tag{22}$$

where $w(\zeta')$ is the energy of an electron at the depth $\zeta-\zeta'$ which stops at the depth ζ (compare (4), Ch. VI, § 371).

With the help of (3) the mean-square displacement suffered by an electron while its energy decreased from w_c to 0 becomes

$$x^2_{w_c\to 0} = \int_0^1 \frac{w_s^2 \zeta'^2}{w(\zeta')^2} d\zeta' = (w_s/w_c)^2 \text{ (cascade units)}^2. \tag{23}$$

This scattering is a little larger than that obtained from (20) for particles of the final energy w_c. For final energies w_c the scattering as derived from (20) is, however, expected to be too large. Comparing (20) and (23) it is therefore plausible to assume that the total scattering for any energy w is given approximately by

$$\langle x^2\rangle_w = 0{\cdot}724\{w_s/(w+\alpha w_c)\}^2,$$

where α is a constant of the order of unity. In the following it will be assumed that $\alpha = 1$, as such an assumption facilitates calculation. The new equation (24) will be assumed valid for all energies

$$\langle x\rangle^2_w = 0{\cdot}724\{w_s/(w+w_c)\}^2. \tag{24}$$

2. *Distribution of Particles in a Shower*

560. Denote by $L(r,w)$ the distribution of particles with a final energy w. Thus assume that the number of particles with energy in the interval w, dw at a distance between r and $r+dr$ from the shower axis is

$$2\pi r\,dr\,\mathfrak{q}(w_0,w;\zeta)L(r,w)\,dw. \tag{25}$$

The density due to all particles at the distance r is

$$E(r)=\int_0^\infty \mathfrak{q}(w_0,w;\zeta)L(r,w)\,dw. \tag{26}$$

561. The function $L(r,w)$ differs greatly from a Gaussian. It has been investigated by Landau (1940), Mollière (1942), Belenky (1944). In the following we attempt only to obtain a rough approximation of the properties of large showers and therefore we replace schematically the distribution L by a step function. Thus we shall put approximately

$$L(r,w)=\begin{cases} 1/\pi\langle x^2\rangle_w & (r<\sqrt{\langle x^2\rangle_w}),\\ 0 & (r>\sqrt{\langle x^2\rangle_w}). \end{cases} \tag{27}$$

From (24) we obtain $$\sqrt{\langle x^2\rangle_w}=R\frac{w_c}{w+w_c} \tag{28}$$

with $$R=\begin{cases} 6{,}100 \text{ cm.} & \text{(sea-level)},\\ 147{,}000/\zeta & \text{(at depth } \zeta) \end{cases} \quad \text{(see § 371).} \tag{28a}$$

562. We have according to § 393, Ch. VI,

$$\mathfrak{q}(w_0,w;\zeta)\approx \mathfrak{q}_0(w_0,w+w_c;\zeta),$$

where $\mathfrak{q}_0$ is the solution of the cascade problem without ionization loss. Introducing the above approximation into (26), we find with help of (27), (28), and (28a)

$$E(r)=\begin{cases} \simeq \dfrac{(w_0/w_c)^2}{\pi R^2}\left\{F\left(\dfrac{r}{R}\dfrac{w_0}{w_c}\right)-F\left(\dfrac{w_0}{w_c}\right)\right\} & (r<R),\\ \simeq 0 \quad (r>R), \end{cases} \tag{29}$$

where $$F(x)=\int_0^{w_0/x}\left(\frac{w}{w_0}\right)^2\mathfrak{q}_0(w_0,w;\zeta)\,dw. \tag{30}$$

With help of (37, Ch. VI) and (56, Ch. VI) it follows that

$$F(x)=\begin{cases} \dfrac{1}{2\pi i}\displaystyle\int_{\mathfrak{y}_0-i\infty}^{\mathfrak{y}_0+i\infty}\frac{x^{\mathfrak{y}-z}}{z-\mathfrak{y}}\{\mathfrak{M}(\mathfrak{y})e^{-a_1\zeta}+\mathfrak{N}(\mathfrak{y})e^{-a_2\zeta}\}\,d\mathfrak{y} & \text{for } x>1,\\ F(1)=\mathfrak{M}(z)e^{-a_1(z)\zeta}+\mathfrak{N}(z)e^{-a_2(z)\zeta} & \text{for } x\leqslant 1. \end{cases} \tag{31}$$

The expression (31) can be evaluated by the saddle-point method as shown in § 383 and numerical values of $F(x)$ are given in Fig. 104.

In Fig. 105 we have plotted the density distribution of a shower at sea-level ($\zeta = 24$) due to primaries of 10^9, 10^{10}, and 10^{11} MEV. The

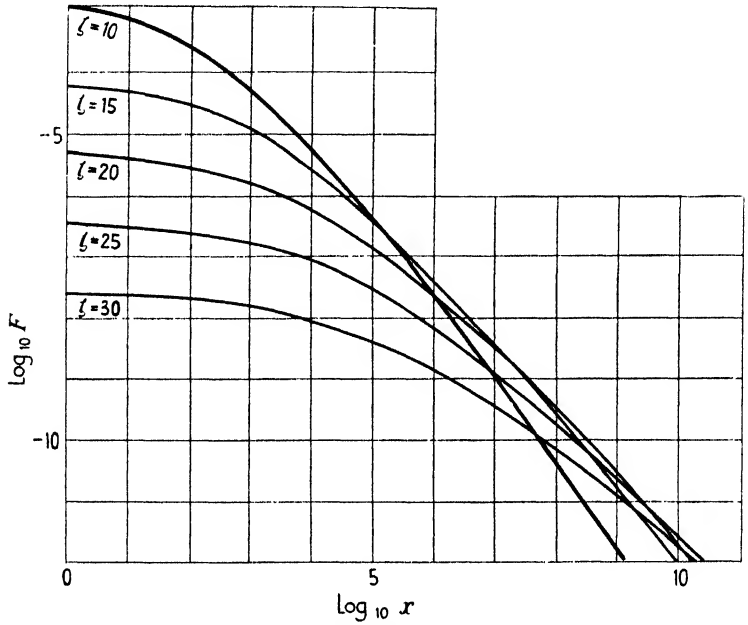

FIG. 104. The function $F(x)$.

abrupt cut-off at 61 m. is of course due to the approximation introduced by (27). A more accurate calculation would lead to an extended tail.

Examination of Fig. 105 shows that the density of particles at the fringe of a shower is roughly proportional to the primary energy.

563. The function $F(x)$ can be written

$$F(x) = a(x)x^{-\gamma(x)}, \tag{32}$$

where $a(x)$ and $\gamma(x)$ vary only slowly with x. For a small interval of x, $a(x)$ and $\gamma(x)$ can be treated as constants.

Evaluating $F(x)$ by the saddle-point method the following relation between γ and x is found:

$$\log_e x = \{a'\zeta - (\log \mathfrak{M})'\}_{v=z-\gamma} - \frac{1}{\gamma}. \tag{33}$$

And further

$$\log a = \log F + \gamma \log x. \tag{34}$$

ζ is the depth under which the cascade is observed. In Fig. 106 $\log_{10} x$ and $\log_{10} a$ have been plotted, regarding γ as an independent parameter.

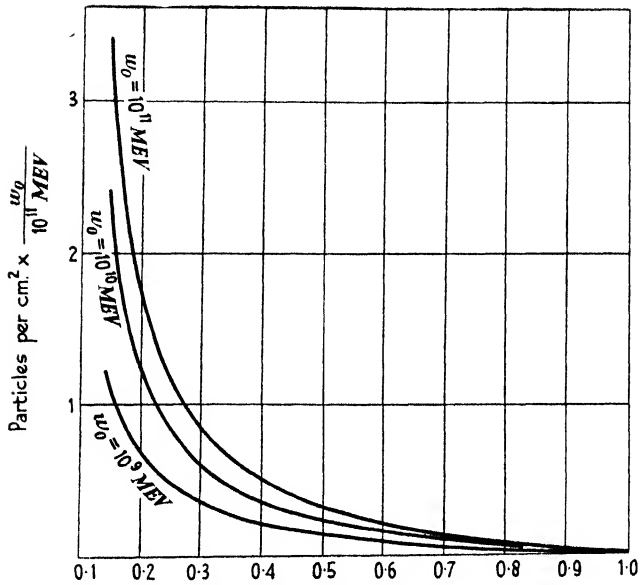

FIG. 105. Theoretical density distribution in a cascade shower.

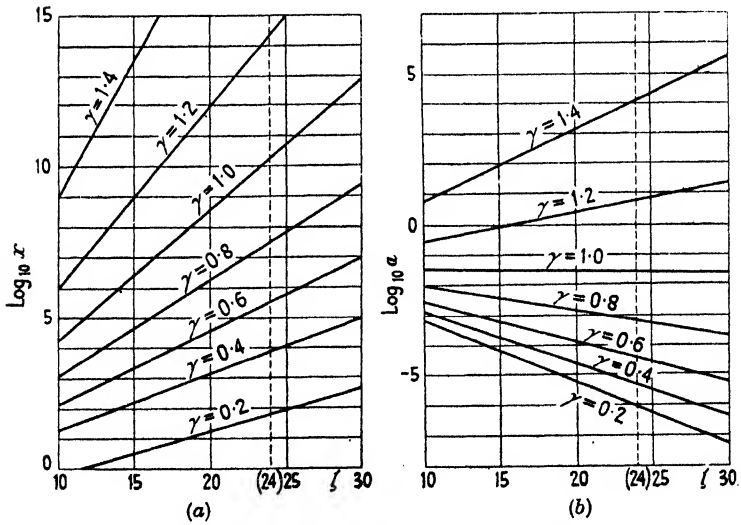

FIG. 106. (*a*) $\log_{10} x(\gamma)$, (*b*) $\log_{10} a(\gamma)$.

B. EXPERIMENTAL OBSERVATIONS OF EXTENSIVE AIR SHOWERS

1. *Spread of Extensive Air Showers*

564. The first experiments on extensive air showers were carried out with counter arrangements.

Coincidences were recorded between a number of counters placed several metres apart. A few results are collected in the tables below.

TABLE 1

Measurements of Auger, Maze, and Robley (1938) *at the Pic du Midi 2,870 m. above sea-level*

Distance between counters in metres	0·05	0·10	0·25	0·5	1·0	1·5	2·5	4·0	20	50	75	150	300
Rate of twofold coincidences per hour	580	320	230	190	120	90	81	60	30	15	10	4	1·5

TABLE 2

Measurements of Kohlhörster (1938) *and his co-workers at sea-level*

Distance between counters in metres	1·25	5·00	10·0	20·0
Rate per hour	38	22	10	$2{\cdot}5 \pm 1{\cdot}5$

It is seen from the above tables that the spread of the extensive air showers is much less at sea-level than at the Pic du Midi.

It is also of interest to note that Kohlhörster has carried out observations indoors (presumably under a thin roof) and there the rate was found to be much smaller than the values given in the table.

2. *Penetrating Power of Extensive Air Showers*

565. The rate of coincidences observed with an extensive shower arrangement is strongly affected by absorbers placed above one or more of the counters. Some of the results of Auger and Maze (1938) are reproduced below, and the arrangement is shown in Fig. 107. A variable lead absorber S was placed above the counter 1.

TABLE 3

Distance of extreme counters in metres	2	5	20
Absorber S in cm. Pb	Rate of fourfold coincidences per hour		
0·0	0·8	—	0·45
0·2	1·7	1·4	0·9
5·0	0·86	0·7	0·4
10·0	0·2	—	0·1
15·0	$< 0{\cdot}1$	—	$< 0{\cdot}1$

Thus extensive air showers show a small transition effect. The rate of showers is seen to increase at first and then it decreases strongly. Some extensive air showers do, however, penetrate 10 cm. of lead. In Chapter IX experiments will be reported which show that some of the extensive air showers penetrate 50 cm. of lead.

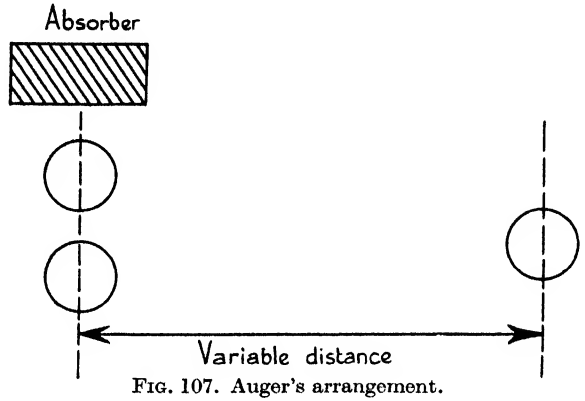

FIG. 107. Auger's arrangement.

3. *Density of Extensive Air Showers*

566. Samples of extensive air showers can be obtained by controlling a cloud chamber by a set of separated counters. The numbers of tracks obtained on individual photographs give an indication of the actual particle densities. It should be pointed out, however, that such a procedure gives some bias towards high particle densities, as dense showers have a greater probability of being recorded by the counter arrangement than less dense showers.

Photographs of this kind were taken by Auger (1938) on the Pic du Midi and some of his results are given in Table 4.

TABLE 4

No. of tracks	0	1	2	3	4	5	6–10	11–20	21–50	50
No. of photographs										
I . . .	45	25	19	22	11	10	37	24	12	2
II . . .	16	5	3	2	5	1	8	3	2	3

I and II refer to two slightly different arrangements. The average number of particles per photograph and the average densities per square metre assuming an effective area of 400 cm.^{2} are as follows:

TABLE 5

		$\langle n \rangle$	*Density*
Arrangement	I	4·3	110
	II	5·0	125

Cloud-chamber photographs of extensive air showers at sea-level were also taken by Daudin (1942); by Lovell and Wilson (1939) and others. The average particle density was estimated as 700 particles per sq. m. The distribution of shower densities approximately followed a power law.

The figures in Table 4 can be roughly represented by the following expression:

$$R(>N) \sim (N_0+N)^{-z}, \tag{35}$$

with $N_0 = 3$, $z \sim 1{\cdot}7$.

The distribution of densities near sea-level is of the same type, though the numerical values of both N_0 and z may differ between sea-level and the Pic du Midi.

Two cloud chambers controlled by the same counter system were used by Lovell and Wilson (1939) and a remarkable pair of photographs thus obtained is shown in Plate III *h*. From the geometry of the arrangement it was estimated that the shower seen in the two chambers must have contained at least 40,000 particles. If the shower is to be interpreted as a cascade it must be due to a primary of not less than 10^8 MEV.

567. The rate of coincident bursts as a function of the distance of separation of the two ionization chambers was investigated by Lewis (1945). It was found that the rate of coincident bursts decreases rapidly with increasing separation of the chambers.

An arrangement consisting of an ionization chamber and a set of counters separated by several metres was used by Lapp (1943). Observations were carried out both with the chamber unshielded and shielded by 10 cm. lead.

With the unshielded chamber most coincidences were accompanied by bursts, but only a small fraction of the counter coincidences were accompanied by bursts in the shielded chamber.

568. The density distribution of extensive air showers was measured with a counter arrangement by Daudin (1942) and by Cocconi and co-workers (1943). Four sets of counters were used; three sets placed on the corners of an equilateral triangle while the fourth was placed at the centre. The effective collecting area S of each set was varied by connecting counters in parallel. In Fig. 108 the rates of both threefold coincidences and fourfold coincidences as functions of S are plotted. The measurements were carried out 2,200 m. above sea-level corresponding to a depth $\zeta = 18{\cdot}5$ under the top of the atmosphere. There

are also plotted points obtained from the cascade theory; the details of the calculation are found in §§ 574–80.

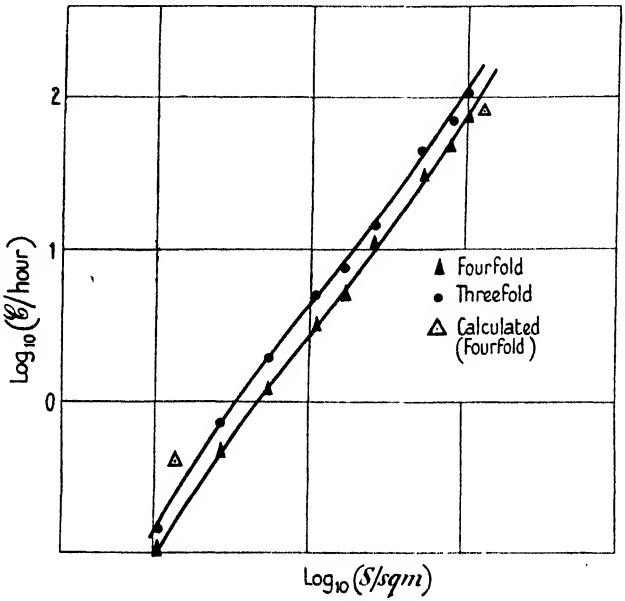

FIG. 108. Cocconi's results. *Nuovo. Cim.* **1**, 314 (1943) (△ calculated by us).

4. *Nature of Shower Particles*

569. In order to investigate the nature of shower particles photographs have been taken with a cloud chamber containing a horizontal lead plate. Particles passing through the plate without producing secondaries are likely to be penetrating particles, i.e. mesons or protons. Electrons are expected to give rise to cascades inside the plate.

Photographs taken in this way show that the majority of particles in the air showers are electrons. Whether or not the dense parts of showers contain also mesons cannot be decided from such photographs.

Cloud-chamber photographs taken with an arrangement selective for penetrating extensive air showers show cases of penetrating particles traversing a lead plate. Such cases are, however, very rare, and it seems probable that showers observed with unshielded apparatus consist largely of electrons.

5. *Height-intensity Distribution of Extensive Air Showers*

570. The height-intensity distribution of air showers was studied by Hilberry (1941, 3). Hilberry observed coincidences with the counter

arrangement shown schematically in Fig. 109. The arrangement was mounted rigidly inside a van and the rate of coincidences was determined at various heights between Chicago and the top of Mount Evans.

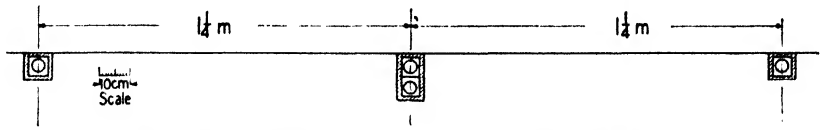

FIG. 109. Hilberry's arrangement, from *Phys. Rev.* **60**, 2.

The results, averaged over several ascents, are reproduced in the following table.

TABLE 5

Station	*Height (metres)*	*Cascade units below top of atmosphere*	*Rate per hour*
Mt. Evans . .	4,320	14·2	24·1 ±0·3
Summit Lake .	3,900	14·9	20·5 ±0·5
Echo Lake . .	3,100	16·6	14·0 ±0·5
Idaho Springs .	2,190	18·0	7·3 ±0·8
Denver . .	1,610	19·3	5·0 ±0·4
Chicago . .	91	23·2	1·47±0·15

The height-intensity distribution thus obtained is shown in a semi-log

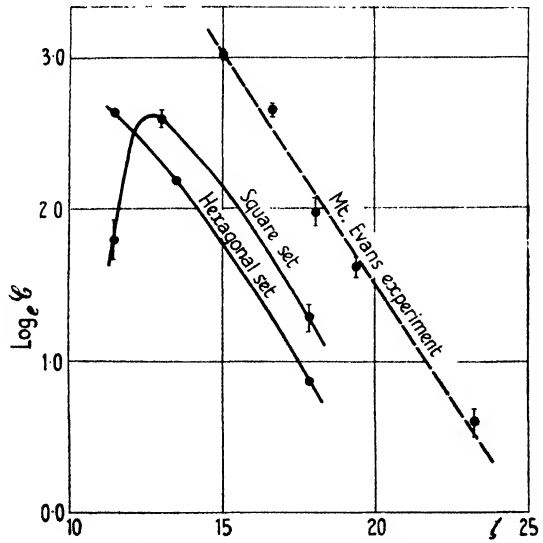

FIG. 110. Hilberry's results.

plot in Fig. 110. It is seen that all points, except the one for 16·6 cascade units lie inside the error of measurement on a straight line. Therefore

the intensity distribution can be roughly represented by an exponential function

$$\mathscr{C}(\zeta) \sim \exp[-0{\cdot}3\zeta]. \tag{36}$$

571. Hilberry (1943) measured the intensity of extensive air showers in Peru up to 6,000 m. above sea-level (1943) with two different arrangements. One arrangement consisted of four counters placed on the sides of a square of side 1·25 m. and the second, twelve counters placed on the sides of a (horizontal) hexagon. Symmetric groups of three counters were connected in parallel and fourfold coincidences were observed. The results are collected below.

TABLE 6

Height (metres)	*Cascade units below top of atmosphere*	*Counts per hour:*	
		Hexagon	*Square*
5,850	11·6	369±7	10·0±1·4
4,750	13·5	240±3	22·3±1·1
2,320	17·8	52±1·6	5·7±0·5

The variation of intensity from 2,320 to 4,750 can also be represented by (36). For larger heights, when observing with the square set, the intensity passes through a maximum (see Fig. 110).

Barometer Effect

572. Closely connected with the height-intensity distribution of extensive air showers is the barometer effect of these showers. A change of barometric pressure is equivalent to a change of the height of the point of observations.

The percentage change of intensity due to a change of pressure of 1 cm. Hg is thus expected to be given by

$$100 \times 0{\cdot}31 \times \frac{d \log \mathscr{C}}{d\zeta} \tag{37}$$

(note that 1 cm. Hg is equal to 0·31 cascade units). Thus, with help of (36),

$$B_{\mathscr{C},p} = 9{\cdot}3 \text{ per cent. per cm. Hg.} \tag{38}$$

The barometer effect of extensive air showers was measured by Auger and Daudin (1942) and by Cosyns (1940). These authors find values varying between 10 and 20 per cent. per cm. Hg, the coefficient being larger the greater the separation of the counters. As equation (36) refers to showers observed with comparatively closely placed counters (2·5 m.), the agreement between (38) and the observed values must be regarded as satisfactory.

Temperature Effect

573. A change of temperature not accompanied by any pressure change should still affect the counting rate. The temperature change affects the air density and therefore alters both the spread and density of the showers. This effect was first pointed out by Euler (1940), but no observational evidence has yet been reported.

C. INTERPRETATION OF EXPERIMENTAL OBSERVATIONS

574. The comparison between observation and cascade theory is rendered difficult by the fact that experimental arrangements recording extensive air showers are always selective for certain types of showers. No comparison between theory and observation can be carried out without taking care of the particular geometry of the recording arrangement.

It follows from § 562 that showers are spread over an area with a diameter of approximately $2R$ (see (29)), where R depends on height but not on the primary energy.

From the numerical values given in (28) it is found that at sea-level the spread ($2R$) is 120 m. while in the Pic du Midi it is 240 m.

These values agree qualitatively with observation.

1. *Application of the Theory of Large Cascades*

575. Two factors must be distinguished in the consideration of the density distribution obtained from cloud-chamber photographs, namely:

1. The distribution resulting from the spatial density distribution in any one shower.
2. The distribution resulting from showers of different sizes.

The two effects will be dealt with separately.

(a) Spatial Distribution in Individual Showers

576. Consider showers arising from primaries of a given energy w_0. The particle density in the shower varies with the distance r from the centre of the shower in a manner discussed in § 562.

Write for the density at a distance $r < R$ from the centre

$$E(r) = \frac{a}{\pi R^2}\left(\frac{w_0}{w_c}\right)^{2-\gamma}\left\{\left(\frac{R}{r}\right)^{\gamma} - 1\right\}, \tag{39}$$

where a and γ are functions of

$$x = \frac{w_0 r}{w_c R} \tag{40}$$

(see (29), (30), (32)).

The probability of observing a region with a density exceeding an arbitrarily given density D is proportional to

$$P(>D) = (r_D/R)^2 \tag{41}$$

with $$E(r_D) = D, \tag{42}$$

provided $r_D \gg$ dimensions of the cloud chamber. (43)

From (39) and (41) the relative probability of observing a region of density exceeding D becomes

$$P(>D) = \left(\frac{\pi R^2 D}{a(w_0/w_c)^{2-\gamma}} + 1\right)^{-2/\gamma}. \tag{44}$$

(*b*) *Energy Distribution of Showers*

577. The observed densities are due to showers created by primaries of different energies. The probability (44) has therefore to be averaged over the primary spectrum.

Assume for the integral spectrum

$$\mathfrak{T}(w_0) = A\left(\frac{w_c}{w_0}\right)^z \quad (w_0 > w_1), \tag{45}$$

and assume further that (45) represents the intensity for all directions. Then, according to §§ 416, 521, we may put

$$w_1 = 2{,}000 \text{ MEV. and } A \sim 2{,}000(w_1/w_c)^z \text{ electrons per cm.}^2 \text{ per hour} \quad (z \sim 1{\cdot}5). \tag{46}$$

The differential spectrum referred to the intensity per unit solid angle is therefore given by

$$\mathfrak{S}(w_0)\,dw_0 = \frac{zA}{2\pi}\left(\frac{w_c}{w_0}\right)^{z+1}\frac{dw_0}{w_c}. \tag{47}$$

Taking into account both factors 1 and 2, the rate of events when a cloud chamber is covered by a region of density exceeding D is therefore

$$\mathscr{C}(>D) = \int_{w_1}^{\infty} \pi r_D^2 \mathfrak{S}(w_0)\,dw_0. \tag{48}$$

In this expression the shower is assumed to come from any direction within unit solid angle.

(*c*) *Numerical Evaluation of the Distribution*

Vertical incidence

578. The integral (48) may be evaluated by the saddle-point method. Putting

$$\log_e(w_0/w_c) = y \tag{49}$$

and
$$(R/r)^\gamma = \frac{\pi R^2 D e^{-(2-\gamma)y}}{a} + 1 = f \tag{50}$$

we obtain
$$\mathscr{C}(>D) = \frac{zR^2A}{2} \int_{\log w_1/w_c}^{\infty} \exp\left(-yz - \frac{2}{\gamma}\log f\right) dy. \tag{51}$$

Write
$$\Xi(y) = -zy - \frac{2}{\gamma}\log f(y). \tag{52}$$

The exponent has a maximum for $y = y_0$ with
$$\Xi'(y_0) = -z - \frac{2}{\gamma}\frac{f'(y_0)}{f(y_0)} = 0. \tag{53}$$

Hence the integrand of (48) has a maximum for
$$\left.\begin{aligned} w_0 = w(D) &\equiv w_c\left(\frac{\pi R^2 D}{a}\,\frac{4-\gamma(2+z)}{\gamma z}\right)^{1/2-\gamma} \\ \text{and} \qquad f = f_D &\equiv \frac{4-2\gamma}{4-\gamma(2+z)}. \end{aligned}\right\} \tag{54}$$

We find further that
$$-\tfrac{1}{2}\Xi''(y_0) = \tfrac{1}{4}z\{4-\gamma(2+z)\} \tag{55}$$

and finally,
$$\begin{aligned} \mathscr{C}(>D) &= \frac{zR^2A}{2}\,\frac{e^{\Xi(y_0)}\sqrt{\pi}}{\sqrt{\{-\tfrac{1}{2}\Xi''(y_0)\}}} \\ &= \pi r_D^2 A\left(\frac{w_c}{w(D)}\right)^z \frac{\sqrt{(\pi z)}}{\sqrt{\{4-\gamma(2+z)\}}}. \end{aligned} \tag{56}$$

The quantity $w(D)$ is the primary energy which gives the most important contribution to the cases having densities exceeding D.

In the above derivation the slight dependence of a and γ on w_0 and r has been neglected.

579. In numerical work on extensive showers it is usually better to treat γ as an independent parameter. For any fixed value of γ, the values of x and a can be obtained from (33) and (34). Further, f_D and r_D are obtained from (54) and (50), and finally D may be obtained from (39) and (42).

Intermediate D values can be obtained by interpolation. Some numerical values calculated for $z = 1{\cdot}5$ are collected in Table 7.

In Table 7 is given the rate (per hour and per unit solid angle). Note that R depends on ζ according to (26), hence the columns of the table below do not refer to the same absolute density D.

TABLE 7

$\log_{10}(w_D/w_c)$

$\log_{10}(\pi R^2 D)$ =	5	6	7	8	9
ζ = 16	6·45	7·40	8·85	—	—
20	6·85	7·50	8·22	9·15	—
24	7·5	8·0	8·7	9·4	10·2
30	8·52	9·03	9·63	10·30	10·92
		$-\log_{10}(r_D/R)^2$			
ζ = 16	0·96	1·14	1·23	—	—
20	0·80	0·90	1·04	1·23	—
24	0·72	0·78	0·86	0·96	1·10
30	0·66	0·70	0·74	0·80	0·86
		$\log_{10}[(\zeta/24)\mathscr{C}(> D)]$			
ζ = 16	2·50	0·97	−1·18	—	—
20	1·99	0·97	−0·20	−1·72	—
24	1·06	0·28	−0·81	−1·92	−3·21
30	−0·44	−1·23	−2·15	−3·18	−4·14

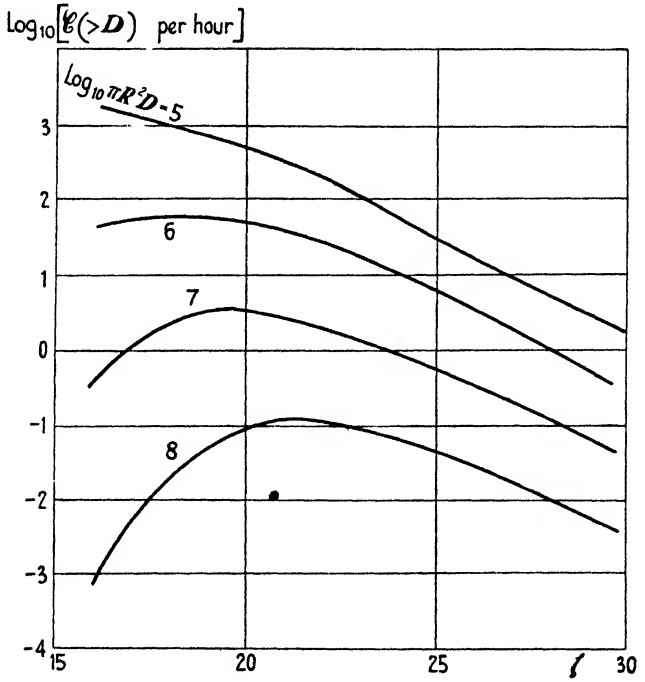

FIG. 111.

In Fig. 111 there has been plotted the rate $\mathscr{C}(> D)$ as a function of ζ for fixed values of $\pi R^2 D$. It is seen that $\mathscr{C}$ has a maximum, which is the lower in the atmosphere the larger the value of $\pi R^2 D$.

Inclined directions

580. In order to estimate the absolute rates of showers it is necessary to average over all directions of incidence. The intensity at an angle ϑ inclined to the vertical is obtained by replacing the depth ζ of observation by

$$\zeta(\vartheta) = \zeta/\cos\vartheta \tag{57}$$

but retaining the value of R.

The total rate is given by

$$\bar{\mathscr{C}} = 2\pi \int_0^1 \mathscr{C}(\vartheta)\, d(-\cos\vartheta). \tag{58}$$

For high altitudes the integral (58) has to be evaluated numerically; the maximum contribution does not necessarily arise from the showers incident near the vertical direction (see Fig. 111).

Near sea-level the rate $\mathscr{C}$ drops rapidly with increasing ζ and therefore the maximum contribution comes from the vertical direction.

The actual distribution near sea-level can be approximated by

$$\mathscr{C}(\vartheta) = \mathscr{C}(0)\exp[-\alpha(1-\cos\vartheta)], \tag{59}$$

where α has the following numerical values:

TABLE 8

$\log_{10}(\pi R^2 D)$ =	5	6	7	8	9
α =	17·3	17·4	15·4	14·5	10·7

Neglecting $e^{-\alpha}$, we obtain with help of (58) and (59)

$$\bar{\mathscr{C}} = \frac{2\pi}{\alpha}\mathscr{C}(0). \tag{60}$$

In Fig. 112 there has been plotted the absolute rate $\mathscr{C}(> D)$ against density for sea-level $\zeta = 24$, and for $\zeta = 20$.

2. *Comparison with Observations*

(*a*) *Cloud-chamber Observations at Sea-level*

581. Lovell and Wilson (1939) observed showers with densities ranging from 100 to 10,000 particles per m.^{2}

The observed and calculated frequencies are compared in Table 9.

TABLE 9

Density D in particles per m.^{2}	10	100	1,000	10,000
Rate per hour: (Calculated)	8	0·7	0·06	0·005
(Observed by Lovell and Wilson)	—	0·39	0·049	about 0·001†

† One shower of this density was observed in 600 hours.

The agreement between observed and calculated rates as shown in Table 9 is rather good considering the uncertainties of the calculation. The largest uncertainty is due to the choice of the exponent z. The value $z = 1{\cdot}5$, used in all our calculations, has been adjusted as to give

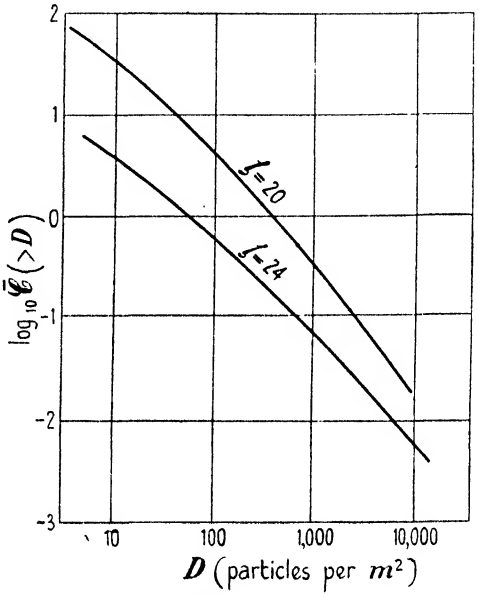

FIG. 112. The calculated density spectrum for $\zeta = 20$ and $\zeta = 24$.

the best possible agreement between cascade theory and extensive air showers. The same value for z was deduced independently from the analysis of the geomagnetic effects in Chapter VII.

(*b*) *The Results of Hilberry* (1941) *and of Cocconi* (1943)

582. In order to estimate the rates of coincidences due to large cascades it is necessary to calculate the probability of a shower discharging all the counters of a given coincidence arrangement. This probability has to be averaged over shower size, position of the shower, and inclination of the shower. Such a calculation was carried out by Hilberry (1941) in detail. The problem will be treated here in rough approximation only.

583. Consider a counter arrangement consisting of n counters in coincidence. Assume that the separation of the counters is small compared with R and that the particle density D due to any individual shower is constant over the area of the arrangement.

The average number of particles falling on any of the counters is therefore

$$S.D,$$

where S is the area of the counters and D the density of particles in the vicinity of the arrangement for a particular event.

The probability that each of the n counters is discharged is given by

$$P_n = (1-e^{-SD})^n. \tag{61}$$

This quantity P_n is small for small values of D and becomes nearly 1 for large values of D. For simplicity replace P_n by a step function, namely,

$$P_n = \begin{cases} 1 & \text{for} \quad D > D_n, \\ 0 & \text{for} \quad D < D_n. \end{cases} \tag{62}$$

The quantity D_n may be defined to satisfy the following equation:

$$(1-e^{-D_n S})^n = \tfrac{1}{2}; \tag{63}\dagger$$

and $D_n S$ has the values given by the following table:

TABLE 10

n =	1	2	3	4	5
$D_n S$ =	0·69	1·23	1·58	1·84	2·04

584. Hilberry (1941) used fourfold coincidences. Two of the counters were, however, placed close above each other, and therefore for sea-level, where most of the showers are expected from the vertical direction, n may be put equal to 3. For greater heights the effective value of n must be between 3 and 4.

The area of the counters was 196 cm.^{2} and therefore the effective value of D_n is between

$$1{\cdot}58/0{\cdot}0196 = 81 \text{ particles per m.}^2$$

and

$$1{\cdot}84/0{\cdot}0196 = 94 \text{ particles per m.}^2,$$

whence we obtain the following results:

TABLE 11

Height	*Calculated*	*Observed (Hilberry)*
$\zeta = 24$	0·7	1·5
16	16	14·0

The agreement between calculation and observation is reasonably good.

† As the density distribution obeys a power law, we could also use the methods of § 447; in this way we obtain instead of (63)

$$D_n S = a \quad \text{with} \quad \frac{a}{e^a - 1} = \frac{\gamma}{n}. \tag{63a}$$

585. The results of Cocconi (1943) can be interpreted in a similar way. The effective D as function of S can be found from eq. (63) (or (63 a)). The corresponding intensity can be evaluated with help of Table 7.

We have evaluated both the threefold and fourfold rates for the extreme values of S used by Cocconi. The results are shown in Fig. 108 together with the experimental results of Cocconi. (We have integrated numerically over the directions of incidence.)

The agreement between calculated and observed intensities is very satisfactory.

It is seen therefore that the spectrum (45) can give a good account of the observations.

Calculations of Hilberry (1941) and of Cocconi (1943) lead to a spectrum with an exponent larger than 1·5.

(c) *The Barometer Effect*

586. The barometer effect of extensive air showers can also be accounted for qualitatively in terms of cascade showers.

The regression coefficient of the effect is given by (37) as

$$B_{\mathscr{C},p} = 31 \frac{d \log \mathscr{C}}{d\zeta}. \tag{64}$$

Writing for the vertical intensity

$$\mathscr{C} \sim e^{-\alpha\zeta/24},$$

where α has the values given in Table 8, we find

$$B_{\mathscr{C},p} = 31 \times \tfrac{17}{24} = 20 \text{ per cent. per cm. Hg.} \tag{65}$$

Regression coefficients of this order were observed by Cosyns (1940) for very large showers. The value seems somewhat too large.

(d) *The Penetrating Power of Large Cascades*

587. A large cascade shower has its greatest penetrating power near the centre where the high-energy electrons and photons are concentrated. The fringe of the shower should, however, be very soft, as it should consist mainly of particles with energies of the order of the critical energy.

From Table 7 in § 579 it follows that for the most important region of cascades

$$(r_D/R)^2 \sim 0{\cdot}1$$

and therefore

$$r_D \sim R/3.$$

Thus particles with energies of the order of

$$3w_c \lesssim 300 \text{ MEV.}$$

should be expected to be predominant. Thus most of the showers should be very soft.

588. Large fluctuations are to be expected; occasionally we shall observe the region near the core which contains many energetic electrons.

The area containing particles with energies exceeding w is given roughly by

$$A_w = \pi R^2 (w_c/w)^2 = 10^8 (w_c/w)^2 \text{ cm.}^2$$

The density of particles of given energy w decreases with increasing w. In Table 12 we consider showers in which the density of particles with energies

$$w > 10w_c, 100w_c, \ldots$$

exceeds an arbitrary limit, namely 100 particles per m.^{2} The particles with energy w are assumed, according to (27) to be distributed uniformly inside a circular disc. The area A_w of this disc is given in Table 12.

Further we have collected in Table 12 the values of primary energy w_0 giving rise at sea-level to showers containing more than 100 particles of energy $> w$ per m.^{2}; finally, we have collected the rate of events in which such a shower falls on a given point at sea-level.

TABLE 12

Energy of observed particles	$(w/w_c) =$	10	100	1,000
	$A_w =$	10^6	10^4	10^2 cm.^{2}
Primary, giving rise to $A_w/100$ particles each exceeding w	$\log_{10}(w_0/w_c) =$	7·3	6·9	6·6
Rate of incidence per hour, per unit solid angle, upon A_w		2	0·08	0·002

From the above table it is seen that parts of showers containing electrons up to $100w_c = 10{,}000$ MEV. are comparatively frequent. The actual core of a shower should be very rare. At sea-level one should expect the core of a shower once in about 1,000 hours.

Electrons of 10,000 MEV. produce cascades penetrating up to 10 cm. of lead and therefore the numerical values given above are at least qualitatively in agreement with the observations reported in § 565.

It will be seen in the next chapter that extensive air showers penetrating much more than 10 cm. of lead have also been observed. These

penetrating extensive air showers cannot be accounted for in terms of ordinary cascades. They have to be interpreted with the assumption that electron cascades contain also particles more penetrating than electrons. Compare Cocconi (1943) and others.

(e) *Local Showers*

589. It remains to discuss the effects of cascade showers originating from secondary electrons or decay electrons.

An electron originating inside the atmosphere may be more effective in setting off a counter arrangement than a primary electron of the same energy because it is created close to the apparatus. A large shower, however, requires the greater part of the atmosphere for its full development. It was shown in § 579 that at a depth of 16 cascade units below the top of the atmosphere, the most important contributions come from inclined directions, since a thickness of 16 units is not sufficient for full development. Thus electrons originating inside the atmosphere are only slightly more effective in producing large extensive showers than electrons coming from outside.

Local electrons may, however, be responsible for showers of comparatively small extension. Take, for instance, the case of a shower containing 100 particles in the centre area of 10^4 cm.^{2} According to Table 12 a primary of 8.10^9 MEV. on the top of the atmosphere will produce such a shower near sea-level. Using the cascade figures given in Chapter VI it is found that such a shower can also be produced by a primary of 10^7 MEV. originating at a distance of about 5 cascade units from the arrangement.

Thus a shower covering only about 10^4 cm.^{2} can be produced by a local electron of much smaller energy than the energy required for a primary. Since the spectrum of the local electrons falls off much more rapidly than that of the primary electrons (see Ch. VI), the contributions of the local electrons may be comparable to the primaries.

590. Lewis (1945) observed that the number of coincident bursts increases strongly when the distance between two burst chambers is reduced. These observations are not in agreement with the density distribution as expected for large showers, as the density in large showers should change only slowly inside large areas.

The observations of Lewis may, possibly, be accounted for in terms of local cascades as discussed in the previous paragraph. No quantitative treatment of the problem of local showers is available.

3. *Conclusions*

591. From the above analysis it can be concluded that most of the extensive air-shower phenomena can be accounted for in terms of an incident electron spectrum obeying a power law. The exponent of the integral spectrum has to be assumed to be about 1·5; this is the same spectrum as deduced for low energies from the study of geomagnetic effects.

Similar conclusions have been reached by Skobelzyn (1942, 1944 *a*, *b*).

The effects which cannot be accounted for in a simple way are (1) dependence of burst coincidences upon distance for small distances, (2) the penetrating extensive air showers.

The first discrepancy may be explicable in terms of local showers, while the second discrepancy indicates either that cascade showers contain some mesons or the existence of non-cascade showers.

IX

THE ORIGIN OF THE MESON COMPONENT

592. It was shown in Chapter IV that near sea-level the main part of the penetrating component consists of mesons.

As mesons are unstable they must have originated inside the atmosphere of the earth. The question arises as to the process by which the mesons are created and to the nature of the primaries giving rise to the mesons.

A theory of the production of mesons has been put forward by Hamilton, Heitler, and Peng (1943) and continued by Heitler and Walsh (1945). It is assumed that the primaries giving rise to the meson component are protons. It was shown by Heitler and Peng (1944) that fast protons colliding with nucleons inside atomic nuclei give rise to the emission of mesons, the process being analogous to the emission of *bremsstrahlung* by fast electrons.

In the following section the experimental evidence relating to the process of meson production will be reviewed. In the later part of this chapter the experimental evidence will be compared with the theory of meson production.

A. Experimental Evidence

593. It was shown in Chapter VII that the secondary origin of the mesons can be deduced from simple energy considerations. Actually, even before the experimental discovery of the meson, it was concluded by Nordheim (1938) and also by Bowen, Millikan, and Neher (1937) that the hard component must be of secondary origin (compare § 550).

The argument of Chapter VII is based on the fact that the average energy of the primaries, as determined from the geomagnetic effects, greatly exceeds the average energy of the mesons observed near sea-level.

It is therefore concluded that primaries split up their energies in producing several mesons.

1. *The Height of Formation of Mesons*

(*a*) *Absorption Anomaly*

594. Evidence of the height of formation of the meson component may be derived from the temperature effect. The effect was discussed in

detail in § 354. According to Duperier (1944*b*) one can conclude from this effect that the bulk of the mesons are produced at a height exceeding 16 km., i.e. one-tenth of the mass of the atmosphere is above the average height of formation.

Experiments of Fréon (1944) suggest that the mesons are not produced at one layer but that some meson production continues down to moderate altitudes.

(*b*) *Experiments of Schein and co-workers*

595. Direct evidence for the production of mesons at high altitudes was obtained by Schein, and various co-workers (1940). Two different experimental arrangements were used.

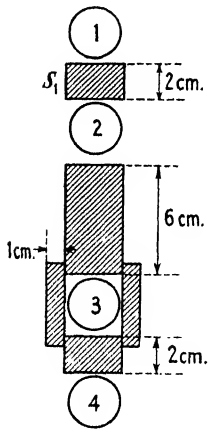

Fig. 113.

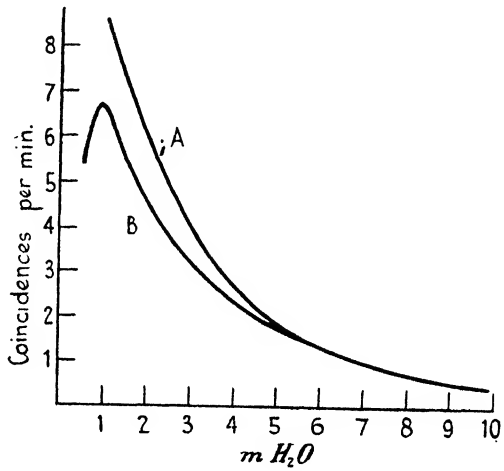

Fig. 114.

Fig. 113. Schein's arrangement.
Fig. 114. Results of Schein, Jesse, and Wollan.

Experiments were carried out with the object of observing the production of mesons by non-ionizing primaries. The experimental layout is shown in Fig. 113 and the experimental method is discussed in § 285.

Coincidences of the counters 1, 2, 3 and simultaneously the coincidences of the counters 2, 3, 4 were recorded. The rates $\mathscr{C}(123)$ and $\mathscr{C}(234)$ as function of height are shown in Fig. 114. It is seen that the two rates differ by about 25 per cent. for heights of the order of 16 km.

The difference between the two rates may be interpreted in terms of ionizing secondaries produced by non-ionizing primaries in the absorber S_1. Thus if a non-ionizing primary falls on S_1 and gives rise to an ionizing secondary, this secondary may give rise to a coincidence (234),

but it is incapable of giving rise to a coincidence (123). Therefore in the presence of non-ionizing primaries the difference

$$\Delta\mathscr{C} = \mathscr{C}(234) - \mathscr{C}(123) > 0. \qquad (1)$$

The difference actually observed is sufficiently large to justify its interpretation in terms of non-ionizing primaries. Note that a very small effect might be due to the slight difference in geometry (see § 294).

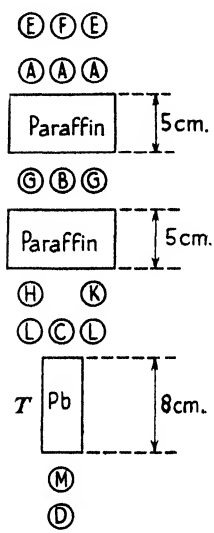

FIG. 115. Arrangement of Schein, Iona, and Tabin.

The secondaries observed with the arrangement Fig. 113 have a range of at least 8 cm. of lead. It is therefore likely that these secondaries are mesons. As an alternative interpretation it might be assumed that the coincidences $\Delta\mathscr{C}$ are due to cascades initiated by photons of about 10^4 MEV. and not to mesons. The interpretation of the effect in terms of meson production is, however, the more likely one. Photons of 10^4 MEV. are rare, and they can hardly exceed 1/1,000 of the total intensity (see Ch. VI).

596. Coincidences up to very great heights were observed by Schein, Iona, and Tabin (1943) with the arrangement as shown in Fig. 115. An absorber T consisting of 8 cm. Pb is placed between the counters C and D. Absorbers of 5 cm. paraffin each are placed between A and B, and B and C. The coincidences $ABCD$ were taken as a measure of the vertical intensity. The counters E, F, G, H, K, and L were used to detect various types of showers.

The following results were obtained.

(i) Less than 3 per cent. of the coincidences $ABCD$ (i.e. verticals) were accompanied by coincidences $EFACD$. Thus most of the incident particles were single.

(ii) At high altitudes a considerable fraction of the primaries discharged not only the counters $ABCD$ but also some of the side-counters G, H, K, L. Such coincidences indicate the production of showers in the paraffin. Some of the results are shown below.

The observations are interpreted in terms of the production of showers in paraffin by primaries. It is suggested that showers $ABCDG$, etc., are observed whenever a primary is absorbed in the paraffin and gives rise to a shower containing at least one meson.

TABLE 1

Shower coincidences as fraction of the rate ABCD

Pressure (*cm.* Hg)	*Accompanied by the discharge of:*	
	G (%)	*L* (%)
6	25	50
17	15	35

Schein concluded from his analysis that the cross-section for shower production was about 2.10^{-25} cm.^{2}, i.e. of the same order as the cross-section of a nucleus.

597. The data of Schein cannot be accounted for either by cascade showers or by knock-on showers. The probability for the production of a cascade in 5–10 cm. of paraffin is negligibly small; and even if a cascade was produced in the paraffin it could hardly penetrate the absorber T (8 cm. of lead).

The probability of a meson giving rise to a knock-on electron in 5 cm. of paraffin is also very small, and therefore only a small fraction of the mesons passing through the counters *ABCD* are expected to discharge any of the side-counters by giving rise to secondary electrons.

It is concluded that the most plausible interpretation of the results seems to be the production of mesons.

2. *Penetrating Showers*

598. The general argument mentioned in § 550 suggests that mesons are produced in small groups which should be observed as showers of penetrating particles. Many observers have succeeded in observing penetrating showers. It has usually been assumed that penetrating showers consist mainly of mesons and that the process of production of penetrating showers is the process responsible for the bulk of the meson component of cosmic radiation. The relevant experimental data will be discussed in the following paragraphs.

(*a*) *Cloud-chamber Evidence*

599. Groups of mesons were observed on cloud-chamber photographs. Showers containing penetrating particles were observed by Fussel (1938).

Photographs containing two mesons passing simultaneously through a lead plate were observed by Braddick and Hensby (1939). It is interesting to note that these observations were carried out underground with 60 m. water equivalent above the chamber.

A large number of photographs have since been obtained by various observers (see § 68, Ch. I). A few interesting cases of penetrating showers are reproduced in Plate 4, *a–d*. *a* shows three particles passing simultaneously through a lead plate. The three particles appear to have originated in one point inside a lead absorber above the chamber. In *b* a photograph obtained by Hazen (1944) is reproduced. The cloud chamber contains a number of horizontal lead plates. A penetrating particle which comes from above the chamber passes through two of the upper plates and gives rise to a shower in the third plate. The shower particles are partly penetrating themselves, but one heavily ionizing particle is also seen to emerge from the lead plate.

This process shows the complex nature of some of the penetrating particles.

In *c* we have reproduced a very complex shower obtained by Rochester. This shower is known to be penetrating because the chamber was controlled by a counter arrangement which only responded to penetrating showers (see § 597).

A photograph obtained by Auger and Daudin (unpublished) is shown in *d*.

Photographs showing penetrating showers were also obtained by many others; a bibliography is given by Rochester (1946).

600. Penetrating showers were observed by V. H. Regener (1943*a*, *b*) with an arrangement consisting of about 100 self-recording counters arranged in a number of trays separated by lead absorbers.

The neon lamps controlled by the counters gave pictures of showers setting off the arrangement.

(*b*) *Counter Experiments*

601. The experiments of Schein, Iona, and Tabin (1943), as described in § 596, give evidence that mesons are produced in showers. Detailed experiments near sea-level into the properties of penetrating showers were carried out by Wataghin (1940) and his co-workers and independently by Jánossy and Ingleby (1940), and Jánossy (1941, 3).

Wataghin's experiments

602. A typical arrangement used by Wataghin (1940) with four counters, 1, 2, 3, 4, placed at the corners of a rectangle is shown in Fig. 116. The lower counters 3, 4 are well surrounded by lead and the top counters 1, 2 are separated by 17 cm. of lead from the bottom

counters 3, 4. Fourfold coincidences 1234 are observed, and the rate is of the order of one coincidence in five hours.

We show in the following that Wataghin's observations cannot be accounted for by either cascade showers or knock-on showers.

The absorber separating the top counters 1, 2 from the lower counters 3, 4 is about 30 cascade units. From the cascade figures of Appendix II

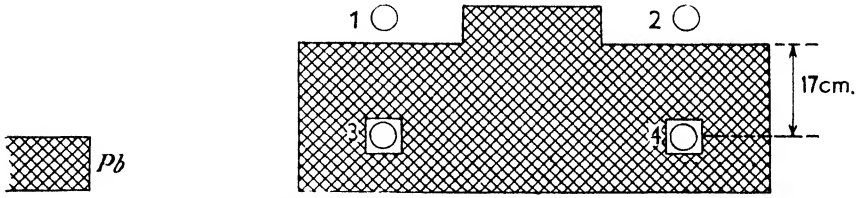

FIG. 116. Arrangement of Wataghin and co-workers.

it follows that a primary energy of about $3.10^4 w_c$ is needed to start a cascade with a range exceeding 30 cascade units. The critical energy in lead is about 7 MEV. therefore the primary energy required is approximately

$$w = 2.10^5 \text{ MEV.} \tag{2}$$

The above energy is not unreasonably high, and therefore occasionally electrons will penetrate 17 cm. of lead. Nevertheless the coincidences of Wataghin cannot be accounted for in terms of such electrons, in fact, to give rise to a fourfold coincidence at least two particles with ranges exceeding 17 cm. of lead are needed. Thus a coincidence 1234 could only be accounted for in terms of *two* electrons each having an energy greater than 2.10^5 MEV. and the two electrons have to be separated by a distance of the same order as the horizontal separation of the counters. The mean square separation of electrons of energy w in an air shower is according to § 557 of the order of

$$(21 \text{ MEV.}/w) \text{ cascade units.} \tag{3}$$

It follows from equation (2) that the separation is 2.10^{-4} cascade units, i.e. 7 cm. (note one cascade unit in air N.T.P. is 342 m.).

The horizontal separation of the counters in the various arrangements varied from 40 cm. to 1 m. The probability of finding electrons of energy w separated by 1 m. instead of 7 cm. is negligibly small.

603. Further, the coincidences cannot be accounted for in terms of knock-on showers.

A coincidence 1234 may result if one meson passes through two of the counters, say 1 and 3, and a knock-on shower which passes through the

remaining counters 2 and 4. Clearly the knock-on shower must have an energy of at least 2.10^5 MEV. A shower of this energy is, however, projected almost in the forward direction and therefore the shower cannot separate from the primary meson.

The meson itself has high energy and is not scattered appreciably. Hence the separation of knock-on shower and primary meson is of the same order as the separation of the electrons in a cascade. A knock-on shower is incapable of giving rise to a coincidence 1234.

604. Further, the lateral spread of a cascade shower in lead is of the order of one cascade unit of lead and therefore a shower in lead can be taken as a column of about 1 cm. diameter. Thus the shower, whether primary or secondary, cannot spread sufficiently to cover both of the lower counters.†

Properties of the showers observed by Wataghin

605. It was found by Wataghin (1940) that a fifth counter 5 placed in between the counters 3 and 4 is frequently discharged simultaneously with the fourfold coincidence 1234. It was therefore concluded that many of the penetrating showers contain more than two penetrating particles. The average density of penetrating particles in a shower was estimated at 30 particles per m.^{2}

An unshielded counter placed at a distance of 3 m. from the main set also showed coincident discharges with the main set. Thus at least part of the penetrating showers were extensive air showers.

As shown in the preceding paragraphs these extensive air showers could not have been ordinary cascade showers.

The experiments of Jánossy and his co-workers

606. The arrangement used by Jánossy and Ingleby (1940) (compare also Jánossy (1941)) is shown in Fig. 117. The eight counters, H, in the middle of the arrangement were made to control neon indicators; and records were taken showing which of the counters H was discharged simultaneously with any fivefold coincidence $123AB$. A fivefold coincidence accompanied by the discharge of n H-counters will be denoted $\mathscr{C}_5(n)$.

Fivefold coincidences $\mathscr{C}_5(n \geqslant 2)$, that is fivefold coincidences accompanied by the discharges of two or more of the counters H were recorded frequently. Such coincidences cannot be accounted for in terms of either cascade showers or knock-on showers, as we show presently.

† This argument was also put forward by Auger (unpublished).

607. The top and bottom trays were separated by 30 to 50 cm. of lead. Further, the bottom counters were shielded from the sides by lead more than 50 cm. thick. Hence a cascade shower reaching the bottom counters must have penetrated 30 cm. of lead or about 60 cascade units. A primary energy of the order of 10^{10} MEV. is required for such a cascade.

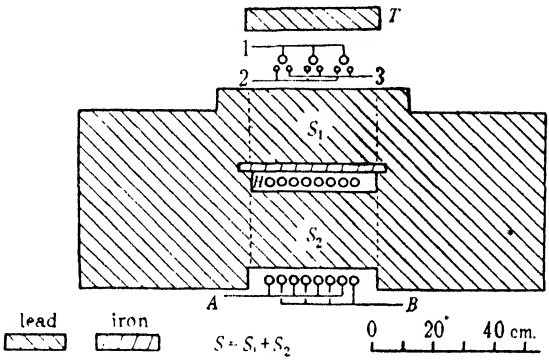

FIG. 117. Arrangement of Jánossy and Ingleby, from *Proc. Roy. Soc.* A, **179**, 362.

The number of electrons with energies exceeding 10^{10} MEV. is much too small to account for the observed coincidence rate of one in five hours. Indeed, the area covered by the lower counters is about 1,000 cm.^{2}, and if each coincidence was due to an electron of more than 10^{10} MEV. energy falling on the system the rate of such electrons would have to be

$$\frac{0{\cdot}2 \text{ per hour}}{1{,}000 \text{ cm.}^2} = 3\times10^{-6} \text{ per min. per cm.}^2$$

The resulting flow of energy would be

$$3\times10^{-6}\times10^{10} \text{ MEV.} = 3\times10^{4} \text{ MEV. per cm.}^2 \text{ per min.}$$

The observed energy flow is

$$\mathfrak{B} = 6\times10^{3} \text{ MEV. per cm.}^2 \text{ per min.}$$

and the larger part of this flow is due to mesons and slow electrons. It is therefore seen that the energy flow which would accompany cascades penetrating sufficiently frequently 30 cm. of lead is far larger than the total flow of electron energy observed at sea-level.

The discrepancy becomes very much larger for the experiments using 50 cm. of lead. It is found that the number of coincidences is only slightly affected when the absorber S is increased from 30 to 50 cm. of lead. Since the cascade energy required to penetrate 50 cm. of lead is of the order of 10^{13} MEV., a flow of energy about 10,000 times the observed flow would be necessary in order to account for the coincidence

in terms of cascades. It is concluded that the coincidences $\mathscr{C}_5$ are not due to cascades.

608. Further, fivefold coincidences $\mathscr{C}_5(n \geqslant 2)$ cannot be due to knock-on showers:

A meson passing through the arrangement Fig. 117 can discharge at most one counter out of each of the three trays. In order to produce a coincidence $\mathscr{C}_5(n \geqslant 2)$ at least two counters in each of the three trays have to be discharged. The additional three counters can be discharged by means of three independent secondaries of the meson. Such a shower may be called a 'triple knock-on'. The rate of triple knock-ons can be estimated accurately, and their rate is small compared with the observed rate of coincidences $\mathscr{C}_5(n \geqslant 2)$.

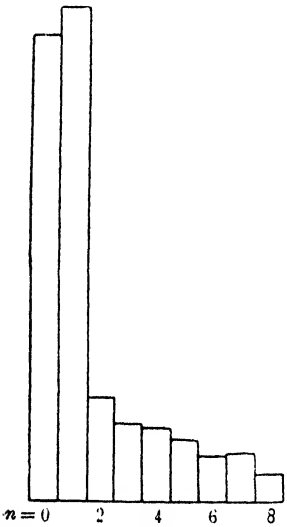

FIG. 118. Size distribution of penetrating showers. From *Proc. Roy. Soc.* A, 179, 366.

The number of mesons passing through the arrangement can be determined by counting coincidences of any counter of the top tray with any counter of the bottom tray. Write for this rate $\mathscr{C}_2$. A certain fraction of the coincidences $\mathscr{C}_2$ is found to be accompanied by the discharge of an additional counter in the bottom tray. Write for the rate of such coincidences $\mathscr{C}_3$. Thus the probability (p_b) of a counter of the bottom tray being discharged by a knock-on shower is

$$p_b = \mathscr{C}_3/\mathscr{C}_2.$$

Similarly the probabilities of knock-ons in the other trays can be determined.

The knock-on probabilities are thus found to be of the order of

1–2 per cent.

An examination of the records shows that most of the coincidences $\mathscr{C}_5(n = 2)$ are due to double knock-on showers, but that the rate of triple knock-on showers is much smaller than the rate of coincidences $\mathscr{C}_5(n \geqslant 2)$.

Thus these coincidences cannot be caused by triple knock-on showers.

609. The multiplicities of discharges observed with the counters H is shown in Fig. 118. Note that the rates $n = 0$ and $n = 1$ are comparatively high because of the contribution of knock-on showers. The rates $n \geqslant 2$ decrease only moderately with increasing n, the rate for

$n = 8$ being only about half of the rate for $n = 2$. The shower sizes seem therefore to be distributed fairly uniformly.

The distribution shown in Fig. 118 is additional evidence that the discharges $n \geqslant 2$ are not due to knock-ons. Most of the knock-on secondaries have low energies and therefore the knock-on shower should

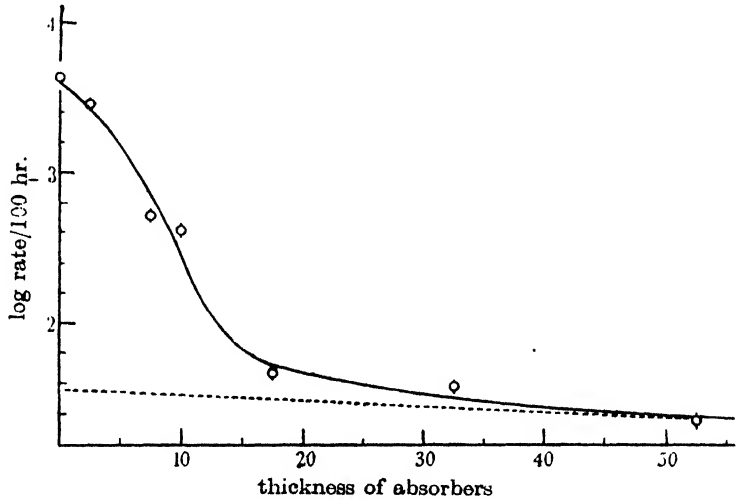

FIG. 119. Absorption curve of penetrating showers. From *Proc. Roy. Soc.* A, **179**, 365.

as a rule discharge only few of the counters H. The observations show no strong predominance of small multiplicities.

610. In Fig. 119 there is plotted the absorption curve of the shower particles observed with the arrangement of Fig. 119. It is seen that for small thicknesses of the absorber S the rate of coincidences is large. The absorption curve up to about 12 cm. of lead resembles strongly the absorption curves of cascade showers shown in Fig. 69, Ch. VI. For larger thicknesses the rate of absorption becomes small. The absorption between 30 and 50 cm. of lead is only of the order of 30 per cent.

It is clear from this curve that the coincidences for S $<$ 10 cm. of lead are mainly due to cascades, while for larger thicknesses of S the cascades are filtered out and only the penetrating showers remain.

3. *Local and Extensive Penetrating Showers*

(*a*) *Local Penetrating Showers*

Transition effect

611. The arrangement used by Jánossy (1941) is particularly suited for the observation of the transition effect of penetrating showers.

It is found that the rate of sevenfold coincidences increases

considerably when an absorber T is brought close above the top tray of counters. The lead transition effect found by Jánossy and Rochester (1944*a*) is shown in Fig. 120.

The transition effect is interpreted in terms of the production of penetrating showers in the lead absorber T by incident primaries.

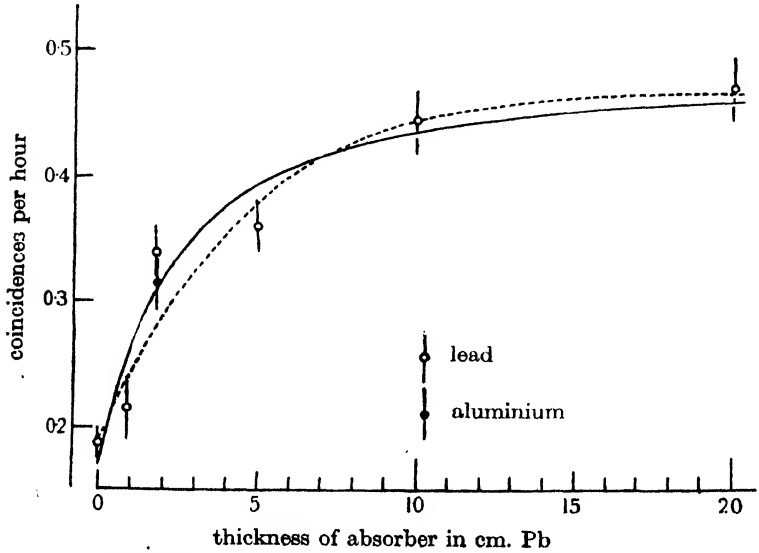

FIG. 120. Transition curve of penetrating showers. Jánossy and Rochester. From *Proc. Roy. Soc.* A, **183**, 183.

The transition effect up to 10 cm. Pb can be represented fairly accurately by the following analytic expression (full curve, Fig. 120)

$$\mathscr{C}_7 = 0{\cdot}19+0{\cdot}29\{1-\exp(-x/x_0)\}, \tag{4}$$

where x is the thickness of the absorber and

$$x_0 = 4{\cdot}5 \text{ cm. of lead}$$
$$= 51 \text{ gm. per cm.}^2 \tag{5}$$

612. The transition effect has been observed up to large thicknesses of absorber (Table 2, Jánossy and Rochester (1943*b*)).

TABLE 2

	Thickness of absorber T *in cm.* Pb			
	0	*10*	*15*	*45*
Rate of coincidences under T cm. of lead	0·53	0·82	0·85	0·69
Increase of rate above background rate	—	0·29	0·32	0·16

It is seen that the rate of coincidences decreases for large thicknesses of absorber.

The decrease shows clearly that the penetrating showers are produced in the top layer of the absorber T only.

The two terms in (4) have a simple significance. The constant term represents the background due to showers coming from the air and the second term represents the showers produced in the absorber above the counters. It will be seen in § 621 that the showers produced in T result from single particles and are not accompanied by air showers. The background coincidences on the other hand are always accompanied by extensive air showers. It seems that these two types of shower have rather different properties. (Jánossy and Broadbent, 1947.)

The showers produced in the absorber will be called 'local penetrating showers' or simply 'penetrating showers' while the term 'extensive penetrating showers' will be used for the showers contributing to the background.

Nature of the primaries of local penetrating showers

613. It is seen from equation (4) that the range of the primaries producing local penetrating showers is equal to x_0, i.e. 4·5 cm. of lead. Expressed in cascade units we have

$$x_0 = 8{\cdot}5 \text{ cascade units in lead.} \qquad (6)$$

Using the arrangement of counters shown in Fig. 121 Jánossy and Rochester (1943*b*) found that the primaries of the local penetrating showers consist of both ionizing and non-ionizing particles.

Sevenfold coincidences $\mathscr{C}_7$ and anticoincidences $\mathscr{C}_7 - A$ were recorded.

The absorber T was surrounded on five sides by the anticoincidence counters A. Anticoincidences $\mathscr{C}_7 - A$ were therefore caused mainly by non-ionizing primaries which were absorbed in T giving rise to penetrating showers.

614. The rate of anticoincidences did not decrease noticeably when a lead absorber 5 cm. thick was placed above the anticoincidence counters. This observation shows clearly that the penetrating showers are not due to photons. Photons would either be absorbed in a layer of 5 cm. of lead or else would give rise to ionizing particles. The probability of photons traversing 5 cm. of lead and arriving unaccompanied on the bottom is negligibly small. Therefore anticoincidences due to photon-produced showers would be completely cut out by 5 cm. of lead.

This observation, together with the observed value of the mean free path x_0 of the primaries giving rise to penetrating showers, shows clearly that the penetrating showers are not produced by the soft component.

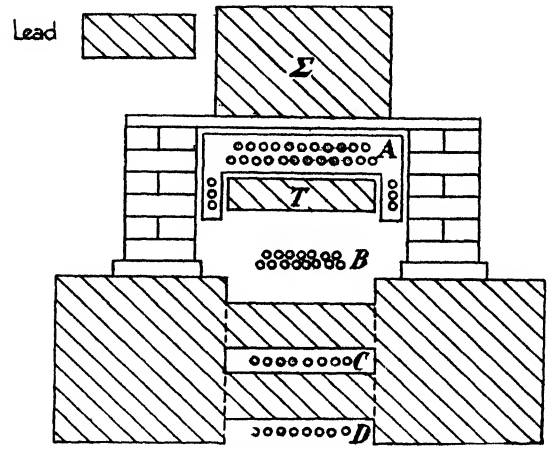

FIG. 121. Anticoincidence arrangement for the observation of penetrating showers. Jánossy and Rochester. From *Phys. Rev.* **64**, 348.

615. Assuming an absorption coefficient a for the non-ionizing primaries the rate of anticoincidences can be estimated as follows.

An anticoincidence $\mathscr{C}_7 - A$ is only recorded if the non-ionizing primary succeeds in traversing the absorber Σ placed above the anticoincidence counters A, without encounter. If the thickness of Σ is y, the probability that a primary is not absorbed in Σ is e^{-ay}.

In order to give rise to a penetrating shower in T the primary has to be absorbed in T. If the thickness of T is x, the probability that the primary is absorbed in T is $1-e^{-ax}$. The probability of observing an anticoincidence is therefore proportional to

$$\text{Probability } (\mathscr{C}_7 - A) \sim e^{-ay}(1-e^{-ax}). \tag{7}$$

616. It is found that the rate of anticoincidences $\mathscr{C}_7 - A$, although only slightly affected when increasing Σ from 0 to 5 cm. of lead, was considerably reduced when y was increased from 5 to 35 cm. of lead.

The observations can be interpreted by assuming that part of the local penetrating showers are due to non-ionizing primaries with ranges exceeding 5 cm. of lead.

It appears that the range of the non-ionizing primaries is somewhat larger than that of the ionizing primaries discussed in § 611. The difference between the two ranges is, however, inside the experimental uncertainty and may not be real.

It is therefore concluded that the local penetrating showers are produced by ionizing and non-ionizing primaries, both types of particles being more penetrating than electrons or photons.

617. From the geometry of the arrangement the absolute intensities of the primaries can be estimated. The following orders of magnitude are found: (1) The non-ionizing primaries represent about one-third of all primaries. (2) The intensity of all primaries is of the order of 1/10,000 of the total cosmic-ray intensity.

The barometer effect

618. Closely connected with the transition effect of penetrating showers is the barometer effect. Consider an increase db of the atmo-

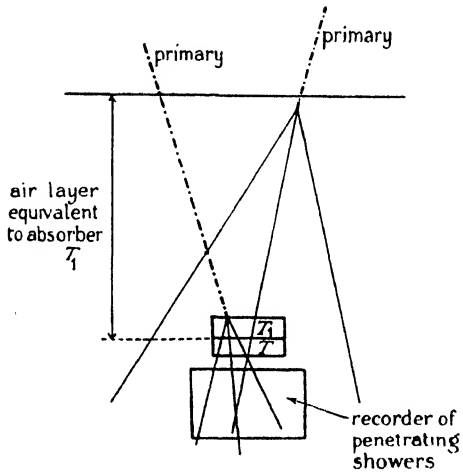

FIG. 122. Showers produced in equivalent layers of air and lead. From *Proc. Roy. Soc.* A, **183**, 191.

spheric pressure b, corresponding to an increase in the mass equivalent of the atmosphere of

$$d\theta = \frac{1{,}033 \text{ gm./cm.}^2}{76 \text{ cm. Hg}} db. \tag{8}$$

During the period of higher pressure, primaries which would have been normally absorbed in the top layer of the absorber (Fig. 122), are now absorbed somewhere in the atmosphere between the pressure levels b and $b+db$. Because of the low density of air the height difference between the two levels is rather large and the showers produced near the pressure level b will diffuse before reaching the apparatus at the level $b+db$ (see Fig. 122). Roughly speaking, only those primaries will be capable of discharging the recorder which can penetrate to the level

$b+db$. Thus the decrease of penetrating shower intensity due to increase of air pressure is equal to the rate of absorption of the *primaries* in air.

619. Jánossy and Rochester (1944*b*) found for the barometer coefficient of penetrating showers

$$B_{ps} = -12 \text{ per cent. per cm. Hg.} \tag{9}$$

Assuming that the primaries are absorbed exponentially with an absorption coefficient α, the intensity at a depth θ is proportional to

$$\mathscr{I}(\theta) \sim e^{-\alpha\theta} \tag{10}$$

and the barometer coefficient is

$$B_{ps} = -\frac{100}{\mathscr{I}} \frac{d\mathscr{I}(\theta)}{d\theta} \frac{d\theta}{db} = -1360\alpha. \tag{11}$$

Inserting (9) into (11) we find

$$1/\alpha = 113 \text{ gm. per cm.}^2 \tag{12}$$

Note that the mass absorption coefficient (12) calculated from the barometer effect is of the same order as (5) found from the transition effect of penetrating showers (§ 611).

Penetrating non-ionizing rays

620. Observations of penetrating non-ionizing rays have been reported in §§ 295–6, Ch. IV. The radiation investigated in those experiments appears to have a mean free path comparable with the primaries of penetrating showers. It is therefore plausible to assume that the two radiations have the same nature.

On comparing the absolute intensities it is found that the non-ionizing radiation discussed in Chapter IV has an intensity of about 1/700 of the sea-level intensity. The non-ionizing radiation giving rise to penetrating showers is estimated to have an intensity equal to about 1/30,000 of the sea-level intensity. Therefore the non-ionizing radiation reported in Chapter IV is about forty times more intense than the radiation discussed here.

In spite of the discrepancy of intensities the two radiations may have the same nature.

Only primaries with energies sufficient to produce penetrating showers containing several particles are recorded in the experiments described in §§ 613–15. The arrangement of Chapter IV was sensitive to those non-ionizing primaries with secondaries of more than 5 cm. Pb range.

It is clear that the latter arrangement was sensitive to a considerably larger part of the spectrum of non-ionizing particles.

The difference in the two intensities can thus possibly be accounted for by the different sensitivities of the two arrangements.

(*b*) *Extensive Penetrating Showers*

621. Extensive penetrating showers were reported in § 605 and § 612.

The spread of extensive penetrating showers was investigated by Jánossy, Rochester, and Broadbent (1945). A penetrating shower arrangement similar to that shown in Fig. 117 was connected in coincidence with a tray of counters covering about 2,000 cm.^{2} Eightfold coincidences between the tray E and the main set P were recorded as a function of the distance between E and P. The results are given in the following table.

TABLE 3†

	$\mathscr{C}_7$ ($T = 0$)	$\mathscr{C}_8$ (*distance PE*)		
		0·5 m.	3 m.	10 m.
Rate per hour	0·15±0·01	0·11±0·01	0·10±0·01	0·08±0·01

† Broadbent and Jánossy (1947 *b*).

It is seen from the above table that the rate of coincidences (P, E) does not decrease to a noticeable extent when the distance is increased up to 10 m., in fact the rate of sevenfold coincidences is substantially the same as the rate of eightfold coincidences. It follows that practically every sevenfold coincidence recorded without absorber above the arrangement is part of an eightfold coincidence. Thus most sevenfold coincidences recorded without lead over the top tray of counters must be regarded as parts of extensive penetrating showers.

622. If an absorber T is placed above the top tray of counters of the set P then the rate of sevenfold coincidences is increased as described in § 611, while the rate of eightfold coincidences is not affected by such an absorber. It follows that the penetrating showers produced in the absorber T are not extensive. The above experiment justifies the distinction between extensive showers and local showers.

623. The question arises whether the extensive penetrating showers are penetrating throughout or whether they contain a penetrating core surrounded by less penetrating particles.

To investigate this question the arrangement P was coupled with an extension E_1 consisting of a battery of counters covered by 15 cm. of lead. Coincidences were recorded when one or two of the counters E_1

were discharged simultaneously with a coincidence of the main set P. The rate of such events was very small, as can be seen from Table 4 (Jánossy, Rochester, and Broadbent, 1945).

TABLE 4

E placed above E_1, distance $PE = 3$ m.

	Rate of coincidences PE	*Number of counters discharged in* E_1		
		0	*1*	*2*
Per 1,000 hours	240	100 ± 8	24 ± 4	11 ± 3

It is seen that at least some of the extensive penetrating showers contain a fair density of penetrating particles throughout. The large decrease in the rate of coincidences observed when the extension is covered with 15 cm. of lead seems to suggest that the extensive penetrating showers consist mainly of electrons.

Such an assumption is in agreement with the complicated penetrating shower photographs obtained by Rochester (see Plate 3).

624. Penetrating particles in extensive air showers were also found by Rogozinsky (1944). The extension of penetrating showers was studied also by Cocconi (1943, 6). The latter author finds that the density of particles in these showers obeys a power law very similar to that expected for the ordinary extensive air showers.

The nature of extensive penetrating showers has been discussed in detail recently by Broadbent and Jánossy (1947 *c*).

The local penetrating showers however cannot be assumed to be cascades interspersed with mesons (see §§ 613–15).

B. Theory of Meson Production

1. *Theory of Hamilton, Heitler, and Peng (1944)*

625. The most far-reaching attempt of interpreting the production of mesons is due to Heitler and various co-workers. The theory is based on the form of the meson theory proposed by Möller and Rosenfeld (1940). The divergency difficulties are eliminated by introduction of radiation damping according to a method due to A. H. Wilson (1941) and Heitler (1941).

The theory is described briefly in Chapter III. It is assumed that both charged and neutral mesons occur; also it is assumed that two types of mesons exist: (1) the pseudo-scalar meson with spin 0, corresponding to the meson ordinarily observed, and (2) a vector meson with spin 1 and a short life. The various types of mesons are introduced on

purely theoretical grounds, as explained in Chapter III; experimental evidence has been obtained for a charged meson only. The spin of the observed meson is probably 0 (see Chapter VI), though a spin $\frac{1}{2}$ would also be compatible with observations.

While there is no evidence in favour of other types of mesons, no evidence against the occurrence of such particles exists either. Both the neutral meson and the transverse meson would be very elusive if they exist and no great weight can be put on the fact that they have not been found so far. (See, however, Appendix III.)

Heitler and Peng (1944) have worked out the cross-sections for the emission of mesons in the collision of fast nucleons. Hamilton and Peng (1944) have worked out the cross-section for the production of mesons by a number of other processes. It turns out that the collision of fast nucleons should be the most important source of the production of cosmic-ray mesons.

We show in the following section that the emission of mesons as predicted accounts at least qualitatively for many cosmic-ray features.

2. *Qualitative Description of Meson Production and Penetrating Showers*

626. A primary proton entering the atmosphere is assumed to collide with nucleons inside atomic nuclei and thus to give rise to the emission of mesons. According to the theory described above it is expected that both (ordinary) pseudo-scalar mesons and the (short-lived) transverse mesons are emitted. The transverse meson decays almost immediately and produces an electron component, while the pseudo-scalar mesons form the hard component of cosmic rays.

(*a*) *Spectrum*

Mesons

627. The mesons produced by the primary protons are likely to have a spectrum similar to the primary spectrum. Therefore it must be assumed that the primary spectrum is a power spectrum with an exponent of the same order as that of the spectrum deduced from the absorption curves and from the momentum measurements near sea-level.

A nucleon is, however, assumed to lose its energy in a number of successive collisions, therefore the average energy of the mesons is a fraction of the average primary energy. This result of the theory of

meson production is in agreement with the qualitative conclusions arrived at in § 528 from the analysis of the geomagnetic effects.

628. The fact that the meson spectrum near sea-level can be accounted for in terms of meson production cannot be regarded as evidence for the theory of meson production, as any meson spectrum could be accounted for assuming a suitable primary spectrum.

Independent evidence for the theory is, however, obtained by considering the latitude effect of the meson component. With decreasing latitude a correspondingly decreasing part of the primary spectrum remains effective (see Ch. VII). The change of meson intensity with latitude can thus be derived from the spectral distribution of the primaries. In a more detailed calculation it was shown by Heitler and Walsh (1945) that it is possible to account at the same time for both the latitude effect and the meson spectrum at sea-level.

Electrons

629. A considerable part of the soft component at high altitudes can be accounted for in terms of decay electrons of the transverse mesons. Whether or not such an interpretation of the soft component at high altitudes is compatible with the east–west asymmetry needs further investigation. The high-energy part of the electron spectrum which is thought to be responsible for the extensive air showers cannot be accounted for in terms of the decay electrons of the transverse mesons.

The mean range of a transverse meson increases with energy according to eq. (5) of Chapter V. Assuming for the half-life of a transverse meson in the rest-system of the meson the value given in (12), the half-range of a transverse meson of 10^5 MEV. is 3 km., and of a 10^6 MEV. meson is 30 km. Thus the decay of very energetic transverse mesons is by no means instantaneous, in fact only a fraction of the transverse mesons with energies exceeding 10^6 MEV. will decay while traversing the atmosphere. The spectrum of the decay electrons from such high-energy mesons will therefore decrease more rapidly than the meson spectrum.

It was shown in Chapter VIII that the exponent of the electron spectrum must be assumed to be of the order of 1·5 up to very high energies in order to account for the extensive air showers. The meson spectrum itself has an exponent which is somewhat larger than 1·5 (see Ch. IV, § 310). The exponent of the decay electrons above 10^6 MEV. must therefore be larger than 2·5. It is concluded therefore that *the extensive air showers cannot be due to the decay electrons of transverse mesons.*

(*b*) *Penetrating Showers*

630. Penetrating showers of the type shown in Plate 4, which contain a few penetrating particles coming from a common origin, can be accounted for in terms of collisions of a nucleon with a nucleus of the absorbing material above the chamber.

631. The cross-section for nucleon-nucleus collision is of the order of the geometrical cross-section of the nucleus involved.

The geometrical cross-section of a nucleus with weight number A is according to Heisenberg (1937*a*)

$$r_A \sim 0{\cdot}53(c^2/m_e c^2)A^{\frac{1}{3}}. \tag{13}$$

The cross-section of a lead nucleus is therefore approximately

$$\Phi_{\mathrm{Pb}} = \pi r_{\mathrm{Pb}}^2 = 6.10^{-25} \text{ cm.}^2 \tag{14}$$

Thus the mean free path of a fast nucleon in lead is

$$m_{\mathrm{Pb}} = \frac{A}{N\Phi_{\mathrm{Pb}}} = \begin{cases} 57 \text{ gm. per cm.}^2, \\ 5 \text{ cm. of lead.} \end{cases} \tag{15}$$

The mean free path (15) is of the same order as that observed for the primaries of penetrating showers (see eq. (5)). It is therefore reasonable to assume that the primaries of the penetrating showers are nucleons.

It was shown in §§ 613–15 that penetrating showers are due to both ionizing and non-ionizing primaries. It is therefore reasonable to assume that these primaries are protons and neutrons. The theory of meson production leads in fact to the result that at sea-level both neutrons and protons will be expected even if it is assumed that the primary beam consisted of protons only. Protons in the process of emitting mesons may change over into neutrons and vice versa. A beam of protons will therefore soon change into one containing both neutrons and protons.

(*c*) *The Origin of the Fast Nucleons near Sea-level*

632. It remains to discuss how fast nucleons are able to reach sea-level.

The rate of loss of the nucleons in air must be large, since the observed height of formation of the bulk of the meson component is so great. The theory of meson formation also predicts cross-sections so large that most of the primary nucleons must be absorbed in the upper part of the atmosphere.

Considering *average* energy loss, only the most energetic nucleons, if indeed any, can reach sea-level. The bulk of the observed penetrating

showers contain, however, only a few particles and it is therefore not likely that the nucleons near sea-level have very high energies.

633. The presence of nucleons of relatively low energy can be accounted for in terms of fluctuation of energy loss (Jánossy, 1944*b*).

Assume that the cross-section Φ_0 for the total absorption of a nucleon depends only slightly upon the energy of the nucleon. Then the probability of a nucleon reaching sea-level without collision is given by

$$\exp(-\theta_0/a), \tag{16}$$

where

$$a = A_{\text{air}}/N\Phi_0 \tag{17}$$

and θ_0 is the mass equivalent of the atmosphere. The total number of nucleons reaching sea-level is therefore

$$I_{\text{sea-level}} = 2\pi\bar{I}_0 \int_0^{\frac{1}{2}\pi} \exp(-\theta_0/a\cos\vartheta)\sin\vartheta\, d\vartheta \approx \bar{I}_0 \frac{\theta_0}{a}\exp(-\theta_0/a), \tag{18}$$

where $I_0 = 2\pi\bar{I}_0$ is the rate of nucleons per cm.^{2} and per min. on the top of the atmosphere.

The intensity of nucleons at sea-level can be estimated from the transition effects described in § 611. Using an arrangement with a collecting area of about 1,000 cm.^{2} the rate of penetrating showers produced in an absorber T was 0·2 per hour, or

$$\tfrac{1}{3}.10^{-5} \text{ per min. per cm.}^2 \tag{19}$$

Assuming $\bar{I}_0 = 30$ per cm.^{2} per min. (compare § 413) it follows from (18) and (19) that

$$\theta_0/a = 13{\cdot}5, \tag{20}$$

or with the help of (17)

$$\Phi_0 = 4{\cdot}1.10^{-25} \text{ cm.}^2 \tag{21}$$

The nucleons reaching sea-level can thus be assumed to be primary nucleons which, by chance, have escaped collisions with atomic nuclei.

We note that the experiments of Schein, Iona, and Tabin (1943) and those of Regener (1943*b*) also indicate that the mesons are produced by primaries with cross-sections of the same order as the size of atomic nuclei.

3. *Conclusions*

634. It can thus be concluded that the production of mesons both at high altitudes and at sea-level can be accounted for by assuming ionizing and non-ionizing primaries which are absorbed with a cross-section of the same order as the geometrical cross-sections.

This process can be interpreted in terms of the production of mesons in the collision between fast nucleons. The theory of this process as

developed by Heitler and Peng (1944) and others is in qualitative agreement with all relevant observations.

635. No theoretical interpretation of the extensive penetrating showers can be given. There is, however, the possibility that the extensive air showers are large cascades and that by some process a small number of penetrating particles are formed by the electrons or photons of the cascade. The bulk of the mesons cannot be assumed to be produced in large cascades.

It was shown in Chapter VII that the meson component cannot be assumed to be secondary to the soft component, and therefore if mesons are produced in large cascades they cannot form an important fraction of the total meson component.

APPENDIX I

STATISTICAL TREATMENT OF OBSERVATIONS

636. COSMIC-RAY research frequently involves a knowledge of statistics; it is often not easy to distinguish between the significant features of a set of results and those which are due to chance.

Consider as an example two sets of observations. In the first set n_1 coincidences are observed during an interval t_1, while in the second set n_2 coincidences are observed during an interval t_2. The observed quantities are the counting rates

$$R_1 = n_1/t_1 \quad \text{and} \quad R_2 = n_2/t_2. \tag{1}$$

We consider the question whether the difference

$$R_1 - R_2 = \Delta R \tag{2}$$

can be regarded as significant.

637. Whatever the numerical values of the rates R_1 and R_2, any difference *might* be due to fluctuation and therefore it can never be concluded with certainty that a difference is significant. It is only possible to give the probability that a difference is or is not due to fluctuation.

For practical purposes an arbitrary limit has to be chosen as to how improbable a thing will be accepted. Sometimes fluctuations with a probability less than 1/16 are excluded as unlikely. This is, however, a very dangerous practice as it leads to a wrong conclusion once in sixteen cases. It is safer to exclude fluctuations with probabilities less than 1/370, but it must be emphasized that even this limit is by no means generous. The number of cosmic-ray observations published goes into thousands and therefore even excluding fluctuations of 1/370 many wrong conclusions must have been arrived at.

A. DISTRIBUTION FUNCTIONS

A short mathematical survey is given in section A of the more important properties of some statistical distributions. In section B applications to experimental results will be discussed. The present section A is not essential for the understanding of the following section and it can be omitted by the reader.

1. *The Poisson Distribution*

638. Consider events which take place at random. To fix ideas consider cosmic-ray particles falling on a counter. Assume the average

number of events in a period t to be p. The probability P that during a particular period of observation n events take place will be determined. Subdivide the interval t into a large number N of sub-intervals

$$dt = t/N. \tag{3}$$

The probability that an event takes place in any given interval dt can be taken as

$$p\,dt/t; \tag{4}$$

while the probability that no event takes place during dt is given by

$$1-p\,dt/t. \tag{5}$$

The probability of more than one event taking place in the interval dt is of the order of dt^2 and will be neglected.

If n events occur during the total interval t, it can be assumed that one event takes place in each of n specified intervals dt, while no event takes place in any of the remaining $N-n$ intervals. The probability that the events happen in the n given intervals is

$$(p\,dt/t)^n(1-p\,dt/t)^{N-n}. \tag{6}$$

The total probability of n events taking place is obtained by summing (6) over all different combinations of n intervals which can be picked out from the total of N intervals. The number of these combinations is

$$N!/n!(N-n)! = N^n\left(1-\frac{1}{N}\right)\ldots\left(1-\frac{n-1}{N}\right)\Big/n! \tag{7}$$

With help of (3), (6), and (7) it follows that

$$P(p,n) = \frac{p^n}{n!}\left(1-\frac{p}{N}\right)^{N-n}\left(1-\frac{1}{N}\right)\ldots\left(1-\frac{n-1}{N}\right).$$

For the limiting case $N\to\infty$ and $n/N\to 0$,

$$P(p,n) = e^{-p}(p^n/n!). \tag{8}$$

The function $P(p,n)$ is the Poisson distribution.

639. With help of (8) we introduce as a generating function

$$X(x,p) \equiv \sum_{n=0}^{\infty} e^{nx}P(p,n) = \exp[(e^x-1)p]. \tag{9}$$

From (9) the following expressions are obtained

$$X(0,p) = \sum_{n=0}^{\infty} P(p,n) = 1; \tag{10}$$

further

$$\langle n\rangle = \sum_{n=0}^{\infty} nP(p,n) = \left(\frac{\partial}{\partial x}\log X\right)_{x=0} = p \tag{11}$$

and

$$\langle (n-\langle n\rangle)^2\rangle = \sum_{n=0}^{\infty}(n-\langle n\rangle)^2P(p,n) = \left(\frac{\partial^2\log X}{\partial x^2}\right)_{x=0} = p. \tag{12}$$

Expressions (11) and (12) give the mean value and the mean square deviation of n. Sometimes use will be made of the root mean square deviation, which is given by

$$\delta n = \sqrt{\langle (n - \langle n \rangle)^2 \rangle} = \sqrt{p}. \tag{13}$$

640. An important property of the Poisson distribution which might have been taken as an alternative definition will now be derived.

Consider two series of random events. The average number of the one type of event in a fixed interval is p_1, and the average number of the other type of event is p_2. It will be shown that the total number of events is on the average p_1+p_2, and the distribution is Poissonian.

As a physical example take the case of cosmic rays with an average rate of p_1 superimposed on to a background of p_2 radioactive particles. The total number of particles will obviously obey a Poisson distribution as the radioactive particles are just as independent of the cosmic-ray particles as they are independent of each other. The problem is then to determine mathematically the result of the superposition of two Poisson distributions. Thus we consider the probability that n' events of the one type are taking place and n'' events of the other type are taking place, with

$$n' + n'' = n. \tag{14}$$

The probability of a total number of n events is

$$P(p_1, p_2; n) = \sum_{n'+n''=n} P(p_1, n') P(p_2, n''). \tag{15}$$

With help of (9)

$$X(p_1, x) X(p_2, x) = \sum_{n=0}^{\infty} e^{nx} \sum_{n'+n''=n} P(p_1, n') P(p_2, n'') = \sum_{n=0}^{\infty} e^{nx} P(p_1, p_2; n). \tag{16}$$

Further

$$X(p_1, x) X(p_2, x) = X(p_1+p_2, x) \tag{17}$$

and thus the generating function of $P(p_1, p_2, n)$ is simply $X(p_1+p_2, x)$, i.e. the generating function of $P(p_1+p_2, n)$. Thus†

$$P(p_1, p_2; n) = P(p_1+p_2; n) \tag{18}$$

as was stated above.

641. For some applications the distribution of a difference is of importance. Consider now two series of random events, one having an average of p_1 and the other p_2. Let us find the probability that the one type of event occurs n' times while the second type occurs n'' times so that

$$n' - n'' = n. \tag{19}$$

† It is assumed that the generating function determines the distribution uniquely.

Write for the final probability

$$Q(p_1, p_2; n) = \sum_{n'-n''=n} P(p_1, n') P(p_2, n''). \tag{20}$$

Define the generating function of Q as

$$Y(p_1, p_2; x) = \sum_{-\infty}^{+\infty} e^{nx} Q(p_1, p_2; n). \tag{21}$$

Then, with help of (9), (20), and (21)

$$Y(p_1, p_2, n) = X(p_1, x) X(p_2, -x).$$

Note that
$$\frac{1}{2\pi i} \int_{-i\pi}^{+i\pi} e^{-mx} Y(p_1, p_2; x)\, dx = Q(p_1, p_2; m). \tag{22}$$

And therefore

$$Q(p_1, p_2; m) = \frac{e^{-(p_1+p_2)}}{2\pi i} \int_{-i\pi}^{+i\pi} e^{-mx + p_1 e^x + p_2 e^{-x}}\, dx.$$

The right-hand integral can be expressed in terms of Bessel functions with imaginary argument. We have

$$Q(p_1, p_2; m) = \left(\frac{p_1}{p_2}\right)^{\frac{1}{2}m} I_m\{2\sqrt{(p_1 p_2)}\} e^{-(p_1+p_2)} \tag{23}$$

(compare Watson, *Bessel Functions*).

The case $p_1 = p_2 = p$ is of interest. $Q(p, p, m)$ gives the probability that a difference of m counts arises between two equal rates p. We have

$$Q(p, p, m) = I_m(2p) e^{-2p}. \tag{24}$$

2. *The Gaussian Distribution*

(a) *Asymptotic Representation of the Poisson Distribution*

642. The Poisson distribution $P(p, n)$ has a strong maximum in the vicinity of $p \sim n$. If p is not an integer, then the most probable value of n is given by

$$p_0 = [p], \tag{25}$$

where $[p]$ stands for the largest integer less than p. If p is an integer, then p and $p+1$ are equally probable. It will now be shown that the Poisson distribution in the neighbourhood of p_0 can be represented in good approximation by a Gaussian distribution provided

$$\delta n = \sqrt{p} \gg 1. \tag{26}$$

Write
$$n = p_0 + h. \tag{27}$$

With help of (8) and (25)

$$P(p, p_0+h) = P(p, p_0) \frac{p^h}{(p_0+1)\ldots(p_0+h)}. \tag{28}$$

And therefore

$$\log\{P(p,p_0+h)\} = \log P(p,p_0)+h\log(p/p_0)- \\ -\log\left(1+\frac{1}{p_0}\right)-\ldots-\log\left(1+\frac{h}{p_0}\right). \qquad (29)$$

A similar expression can be obtained for $\log P(p,p_0-h)$.

Neglecting terms in $(h/p)^2$

$$\log\{P(p,p_0+h)\} \sim \log P(p,p_0)+\frac{h\epsilon}{p_0}-\frac{h(h+1)}{2p_0}, \qquad (30)$$

$$\epsilon = p-[p].$$

Introduce a new variable

$$z = h+\frac{1-2\epsilon}{2} = n-p-\tfrac{1}{2}$$

and we have $$P(p,n) \sim \text{const.}\ \exp(-z^2/2p_0). \qquad (31)$$

The right-hand side of (31) has the form of a Gaussian distribution. The constant can be most easily determined by the normalization condition. The probability of finding n inside an interval dz, where

$$1 \ll dz \lesssim p^{\frac{1}{2}}, \qquad (32)$$

is given approximately by

$$\sum_{n-\frac{1}{2}dz}^{n+\frac{1}{2}dz} P(p,n) \sim P(p,n)\,dz.$$

Therefore $$1 = \sum_{n=0}^{\infty} P(p,n) \sim \text{const.} \int_{-\infty}^{+\infty} e^{-z^2/2p_0}\,dz.$$

The error which arises from putting the lower limit $-\infty$ is negligibly small. Using the known value of the right-hand integral it follows that

$$\text{const.} = \frac{1}{\sqrt{(2\pi p_0)}}, \qquad (33)$$

and thus the following asymptotic representation is obtained:

$$P(p,p+\tfrac{1}{2}+z) \sim \frac{1}{\sqrt{(2\pi p_0)}} e^{-z^2/2p_0}. \qquad (34)$$

(*b*) *Error Integral*

643. Assume $$G(\kappa,z) = \frac{1}{\sqrt{(2\pi\kappa^2)}} e^{-z^2/2\kappa^2}, \qquad (35)$$

and further that $G(\kappa,z)\,dz$ is the probability of finding a deviation in the interval z, dz. For practical purposes it is important to find the probability that a deviation exceeding z takes place.

The probability of absolute deviation $> z$ is

$$\frac{2}{\sqrt{\pi}} \int_{z/\sqrt{(2\kappa^2)}}^{\infty} e^{-y^2}\, dy = E\{z/\sqrt{(2\kappa^2)}\}. \tag{36}$$

The last expression (36) is known as the error integral. A few numerical values are collected in the following table.

z/κ	$100E\{z/\sqrt{(2\kappa^2)}\}$	*Probability of deviation* $> z$
0·674	50	1/2
1	31·8	1/3·14
2	4·6	1/21·7
3	0·272	1/368
4	0·0063	1/16000
5	$5{\cdot}5.10^{-7}$	$1/(1{\cdot}8.10^8)$

κ is called the standard deviation. We see that deviations exceeding three times the standard deviation are rare.

We note that the probability of a deviation exceeding

$$\bar{\kappa} = 0{\cdot}674\kappa \tag{37}$$

is equal to $\frac{1}{2}$. This deviation is called the mean deviation. It is useful to express deviations in terms of either the standard deviation or the mean deviation $0{\cdot}674\kappa$. It is irrelevant whether deviations are expressed in terms of mean deviation or standard deviation. It is, however, important to state clearly which definition is being used. In this book *standard deviations* have always been used.

644. For the investigation of the properties of the Gaussian distribution it is useful to introduce the Laplace transform of the Gaussian. The Laplace transform plays the role of the 'generating function' introduced in § 639.

Introduce $$\mathscr{L}_G(\lambda, \kappa) = \int_{-\infty}^{+\infty} e^{\lambda z} \frac{e^{-z^2/2\kappa^2}}{\sqrt{(2\pi\kappa^2)}}\, dz = e^{\lambda^2\kappa^2/2}. \tag{38}$$

The mean square deviation becomes

$$\langle z^2 \rangle = \left(\frac{\partial^2 \log \mathscr{L}_G}{\partial\lambda^2}\right)_{\lambda=0} = \kappa^2$$

(compare § 639).

(c) *Superposition of Gaussian Distributions*

645. Consider a quantity which is subject to Gaussian fluctuations due to a number of different and independent causes. The probability that the quantity shows a deviation between z_1 and z_1+dz_1 due to the

first cause, a deviation between z_2 and z_2+dz_2 due to the second cause, and so on is given by the product of the probabilities of the individual deviations. The probability is thus

$$\frac{e^{-z_1^2/2\kappa_1^2}}{\sqrt{(2\pi\kappa_1^2)}}\frac{e^{-z_2^2/2\kappa_2^2}}{\sqrt{(2\pi\kappa_2^2)}}\ldots dz_1\,dz_2\ldots.$$

Let us determine the probability that a given linear combination of the deviations

$$Z = A_1 z_1+A_2 z_2+\ldots+A_n z_n$$

has a value between Z and $Z+dZ$.

The probability for this to happen is

$$G(Z)\,dZ = \int\ldots\int_{Z\leqslant A_1 z_1+\ldots A_n z_n\leqslant Z+dZ} \frac{e^{-z_1^2/2\kappa_1^2}}{\sqrt{(2\pi\kappa_1^2)}}\frac{e^{-z_2^2/2\kappa_2^2}}{\sqrt{(2\pi\kappa_2^2)}}\ldots dz_1\,dz_2\ldots. \tag{39}$$

Introducing the Laplace transform of (39), we find

$$\int_0^\infty e^{\lambda Z}G(Z)\,dZ = e^{\lambda^2(A_1^2\kappa_1^2+A_2^2\kappa_2^2+\ldots)/2}. \tag{40}$$

The right-hand expression is the Laplace transform of the Gaussian with the standard deviation (see (38))

$$\kappa = \sqrt{(A_1^2\kappa_1^2+A_2^2\kappa_2^2+\ldots)}. \tag{41}$$

Thus the distribution of Z is a Gaussian distribution with the standard deviation given in (41).

In particular the sum and the difference of two quantities both show Gaussian distributions, provided the quantities themselves have Gaussian distributions. The standard deviation of both sum and difference is given by

$$\kappa = \sqrt{(\kappa_1^2+\kappa_2^2)}. \tag{42}$$

3. *The* Γ*-distribution*

646. Let us determine the probability that the sum of the squares of N subsequent deviations $x_1, x_2, \ldots x_N$ of a quantity is between u^2 and u^2+du^2; that is the probability that n deviations $x_1, x_2, \ldots, x_n$ take place so that

$$u^2 \leqslant x_1^2+x_2^2\ldots+x_N^2 \leqslant u^2+du^2. \tag{43}$$

The probability for any N deviations x_i is given by

$$\frac{1}{(2\pi\kappa^2)^{\frac{1}{2}N}}e^{-(x_1^2+x_2^2+\ldots x_N^2)/2\kappa^2}\,dx_1\,dx_2\ldots dx_N.$$

Therefore the probability of such N deviations which satisfy the condition (43) is given by

$$\Gamma(u^2)\,du^2 = \frac{1}{(2\pi\kappa^2)^{\frac{1}{2}N}} \int\cdots\int_{u^2+du^2 \geqq x_1^2+x_2^2+\ldots x_N^2 \geqq u^2} e^{-(x_1^2+\ldots x_N^2)/2\kappa^2}\,dx_1\ldots dx_N. \quad (44)$$

To evaluate the probability (44) take the Laplace transform of $\Gamma/2u$ with respect to u^2

$$\mathscr{L}_{\Gamma/2u} = \int_0^\infty e^{\lambda u^2}\Gamma(u^2)\,du = \left\{\int_0^\infty \frac{e^{\{(\lambda-1)/(2\kappa^2)\}u}}{\sqrt{(2\pi\kappa^2)}}\,du\right\}^N = \frac{1}{(1-2\lambda\kappa^2)^{\frac{1}{2}N}}. \quad (45)$$

From a table of Laplace transforms we find thus

$$\Gamma(u^2) = \frac{u^{N-1}e^{-u^2/2\kappa^2}}{2\{(N-2)/2\}!\,(2\kappa^2)^{\frac{1}{2}N}}, \quad (46)$$

and therefore (46) gives the required distribution.

647. Note the following properties of the Γ-distribution.

1. The maximum of the distribution lies at

$$u^2 = (N-1)\kappa^2. \quad (47)$$

For $N = 1$ the maximum of the distribution lies at $u^2 = 0$.

2. The average value of u^2 can be obtained from (45) differentiating with respect to λ. We find

$$\langle u^2\rangle = \int_0^\infty u^2\Gamma(u^2)\,du = \left(\frac{\partial}{\partial x}\log\mathscr{L}_{\Gamma/2u}\right)_{\lambda=0} = N\kappa^2. \quad (48)$$

Finally, the mean square deviation of u^2 becomes

$$\langle(u^2-\langle u^2\rangle)^2\rangle = \left\{\frac{\partial^2}{\partial\lambda^2}(\log\Gamma/2u)\right\}_{\lambda=0} = 2N\kappa^4. \quad (49)$$

For large N the Γ-distribution in the vicinity of its maximum can be approximated by a Gaussian distribution.

4. *Bayes's Theorem*†

648. A distribution $D(p,n)$ defines the probability of observing a value n when the average value is p. In practice, however, p is unknown, and the value of p has to be estimated from the observed value n.

† Objections to the use of Bayes's theorem have been raised. Different treatments are given, for example, by A. V. Fisher.

According to a theorem due to Bayes the probability of p being found in an interval p, dp is given by

$$D(p,n)f(p)\,dp, \tag{50}$$

where $f(p)$ is a slowly varying function of p. The function $f(p)$ cannot be determined and therefore the statement has a certain ambiguity. In all practically important cases, however, $D(p,n)$ has a sharp maximum in the neighbourhood of $p = n$ and it is possible to assume that $f(p)$ does not change appreciably in this region. It is therefore usual to remove the ambiguity by assuming

$$f(p) \sim f(p_0) = \text{const.} \tag{51}$$

The ambiguity due to the function $f(p)$ seems to be an essential feature of the statistical method and, presumably, it cannot be removed at all.

649. The inverse distribution corresponding to the Poisson distribution is

$$P(p,n)\,dp = e^{-p}\frac{p^n}{n!}\,dp, \tag{52}$$

where p is regarded as the variable. The distribution (52) is normalized. It is interesting to calculate the average value of p for a given n. From (52) it follows that

$$\langle p\rangle = \int P(p,n)\,dp = n+1. \tag{53}$$

In particular for $n = 0$, $\langle p\rangle = 1$. No great weight can be attached to the actual numerical value $\langle p\rangle$ thus obtained, but it is significant that

$$\langle p\rangle > 0 \quad \text{for} \quad n = 0. \tag{54}$$

Physically this means that if no count is observed in a given period, it cannot be concluded that the average rate is zero; the only conclusion to be drawn is that the average rate is small. In fact, with an average rate of 1, the probability of having no count is appreciable.

(54) should be compared with the ordinary Poisson distribution. If the average rate is known to be zero, no value but zero can be observed. Therefore for the ordinary Poisson distribution

$$\langle n\rangle = 0 \quad \text{for} \quad p = 0. \tag{55}$$

650. Further, for the inverse Poisson distribution

$$\delta p = \sqrt{(n+1)}. \tag{56}$$

It can be seen easily that for large values of p and n the inverse Poisson distribution is very similar to the ordinary Poisson distribution. (Of course the one distribution is discrete while the other is continuous.)

B. The Analysis of Observational Data

1. *Single Observation*

651. If n counts are observed during a time t, then the observed rate is

$$R = n/t. \tag{57}$$

The standard error of n is

$$\delta n = \sqrt{n} \quad (n \gg 1). \tag{58}$$

Thus using the numerical values of the table on p. 371, and with help of the considerations of § 648, it follows that

(1) there is a probability of 68 per cent. that the average number p is inside the interval

$$n-\sqrt{n}, \quad n+\sqrt{n}; \tag{59}$$

(2) the probability of p being outside the interval

$$n-3\sqrt{n}, \quad n+3\sqrt{n}$$

is only $\frac{1}{3}$ of one per cent.

Therefore the average rate $\mathscr{C}$, which can be defined by

$$\mathscr{C} = p/t, \tag{60}$$

is likely to be inside the interval

$$R\left(1-\frac{1}{\sqrt{n}}\right) \quad \text{to} \quad R\left(1+\frac{1}{\sqrt{n}}\right).$$

But the rate $\mathscr{C}$ is unlikely to be outside the interval

$$R\left(1-\frac{3}{\sqrt{n}}\right) \quad \text{to} \quad R\left(1+\frac{3}{\sqrt{n}}\right).$$

2. *Observation of a Difference*

652. Consider two rates

$$R_1 = n_1/t_1 \quad \text{and} \quad R_2 = n_2/t_2. \tag{61}$$

Assume

$$R_1 - R_2 = r > 0. \tag{62}$$

If n_1 and n_2 are sufficiently large it can be assumed that they obey a Gaussian distribution. Further from (34) and (41) it is concluded that the standard error of r is given by

$$\delta r = \sqrt{\left(\frac{n_1}{t_1^2}+\frac{n_2}{t_2^2}\right)}. \tag{63}$$

If

$$r > 3\delta r, \tag{64}$$

then the probability of the correct value of r being zero or negative is less than 1/740. (Note that the values of the table on p. 371 refer to both

tails of the Gaussian: $740 = 2 \times 370$.) Thus if the condition (64) is satisfied it is safe to conclude that the rate

$$\mathscr{C}_1 = p_1/t_1$$

is significantly greater than the rate

$$\mathscr{C}_2 = p_2/t_2.$$

In planning experiments it is often of importance to estimate beforehand how long a period of recording will be required to establish a difference between two counting rates.

Assume that two rates R_1 and R_2 have a ratio

$$R_1/R_2 = 1+h.$$

To establish the difference $R_1 - R_2 = r$ we must have

$$\delta r/r \simeq \frac{1}{Rh}\sqrt{\frac{2R}{t}} < \tfrac{1}{3} \quad (R \sim R_1 \sim R_2),$$

and thus the estimated time of observation is

$$2t = 36/h^2R.$$

For instance, for $h = 0{\cdot}1$ $\quad 2t = 3600/R,$

thus 3600 counts are necessary to establish a difference of about 10 per cent.

653. If the condition (64) is just fulfilled then the difference between the rates can be assumed to be significant, but the actual magnitude of the difference remains very uncertain. In order to determine the magnitude of the difference r it is necessary to have

$$r \geqslant 3\delta r.$$

If it is desired to determine the difference between two very different counting rates, the question arises of how to divide the time of observation between observing the two rates. The best choice is obviously the one which makes (63) a minimum for $t_1 + t_2 = \text{const}$. We find δr attains a (flat) minimum for

$$t_1/t_2 = \sqrt{(R_1/R_2)}. \tag{65}$$

Thus more time should be spent in measuring the faster rate than in measuring the slower rate.

3. *Series of Observations*

(*a*) *Counting Rate*

654. When determining a counting rate $\mathscr{C}$, a number of independent readings may be taken. During a number of periods $t_1, t_2, \ldots, t_N$ the counts recorded are $n_1, n_2 \ldots, n_N$. The rates during these periods are $R_1 = n_1/t_1$, etc. The best value for the rate is an average of the rates

R_1, etc. It can be shown, however, that the most significant combination of the readings is obtained when they are taken together as one reading. Thus the most significant value for the rate during the whole period is given by

$$R = \frac{n_1+n_2+n_3+\ldots n_N}{t_1+t_2+t_3+\ldots t_N}. \tag{66}$$

It is seen from this result that no direct advantage is gained by subdividing a longer interval into a number of shorter intervals.

The subdivision of a long period of readings into a number of smaller periods has, however, the advantage that from an inspection of the individual rates R_1, R_2, etc., it can be established whether or not these readings are consistent. Large fluctuation of the single readings shows that the radiation intensity is subject to systematic fluctuations during observation.

(*b*) *Fluctuations of a Series of Observations*

655. The fluctuations of a number of readings

$$n_1, n_2, \ldots, n_N$$

will now be considered.

Assume that the readings n_1, etc., are the numbers of coincidences recorded with one arrangement in subsequent periods of equal duration. The results will be illustrated with help of the table at the end of this appendix containing observational results of Duperier.†

Normal fluctuation

656. If the radiation intensity remains constant during the time of observation, then the individual readings will fluctuate according to a Poisson distribution. If the values of n are sufficiently large, the Poisson distribution can be replaced by the corresponding Gaussian distribution.

Introduce the mean of the N readings, that is

$$\bar{n} = \frac{1}{N}\sum_{i=1}^{N} n_i. \tag{67}$$

Further, introduce the quantity

$$\kappa^2 = \frac{1}{N-1}\sum (n_i-\bar{n})^2, \tag{68}‡$$

which is a measure of the fluctuation of the values n_i. If the values n_i

† We are very much indebted to Prof. A. Duperier for communicating the records collected in Table 4.

‡ We divide by $N-1$, and not by N, as only $N-1$ of the N quantities n_i-n are independent.

show a *normal distribution*, that is if their fluctuation obeys the Poisson law, then

$$\kappa^2 \simeq \bar{n}. \tag{69}$$

More precisely, in determining the values of κ^2 from a large number of similar series, it is expected that the individual values of κ^2 will be distributed according to a Γ-distribution. The average value of κ^2 should be given by

$$\langle \kappa^2 \rangle = \bar{n} \quad \text{(condition for normal fluctuation)} \tag{70}$$

and the standard deviation of the κ^2's will be

$$\delta\kappa^2 = \langle \kappa^2 \rangle \sqrt{\left(\frac{2}{N-1}\right)}. \tag{71}$$

The equation (70) holds only if the distribution of the n_i's is normal, while (71) holds if the n_i's show any Gaussian distribution.

657. The quantity κ^2 can be determined numerically from (68) for any given series of N readings. The difference

$$\Delta\kappa^2 \equiv \kappa^2 - \bar{n} \tag{72}$$

has to be regarded as the fluctuation of κ^2 provided that the n_i's have a normal distribution. The probability of finding a deviation $\Delta\kappa^2$ depends on the ratio

$$r = \frac{\Delta\kappa^2}{\delta\kappa^2} = \left(1 - \frac{\bar{n}}{\kappa^2}\right)\sqrt{\left(\frac{N-1}{2}\right)}. \tag{73}$$

If the Γ-distribution is replaced by a Gaussian distribution the probability of a fluctuation equal or larger $\Delta\kappa^2$ is equal to

$$E(r/\sqrt{2}). \tag{74}$$

658. If the probability (74) is of the order of one, or at any rate not very small, then the hypothesis that the n_i values fluctuate according to the Poisson law is reasonable. If, however, the probability (74) becomes very small, then it must be concluded that the n_i's do not show a normal distribution. Usually the fluctuation of the n_i's, if not normal, is larger than normal.

659. The procedure is illustrated by investigating the fluctuations shown in the three series of observations of Table 4.

TABLE 1

	Series		
	I	II	III
eq. (67) $\bar{n}$ =	25827	27118	27847
eq. (68) κ^2 =	31827	59303	290933
eq. (73) r =	0·79	4·0	32
$E(r/\sqrt{2})$ =	0·43	1/16000	0

It is concluded from the above table that the series I shows normal fluctuation while the series II and III show fluctuation exceeding the normal.

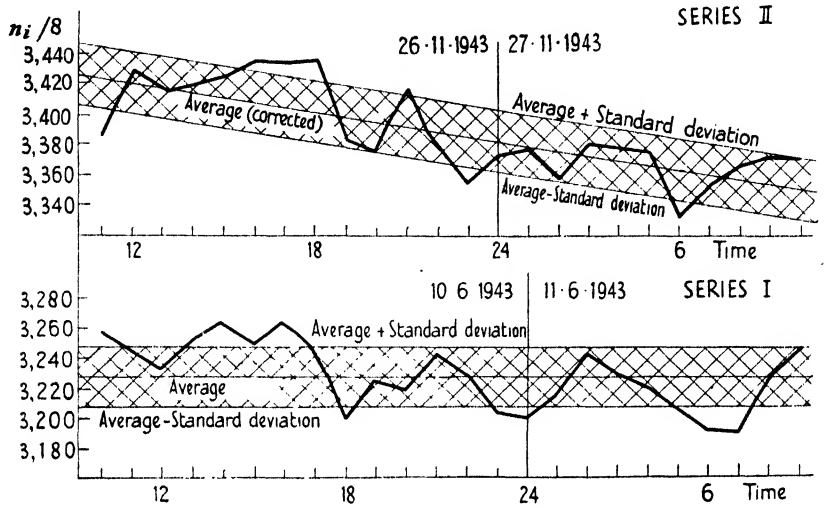

FIG. 123. Duperier's records.

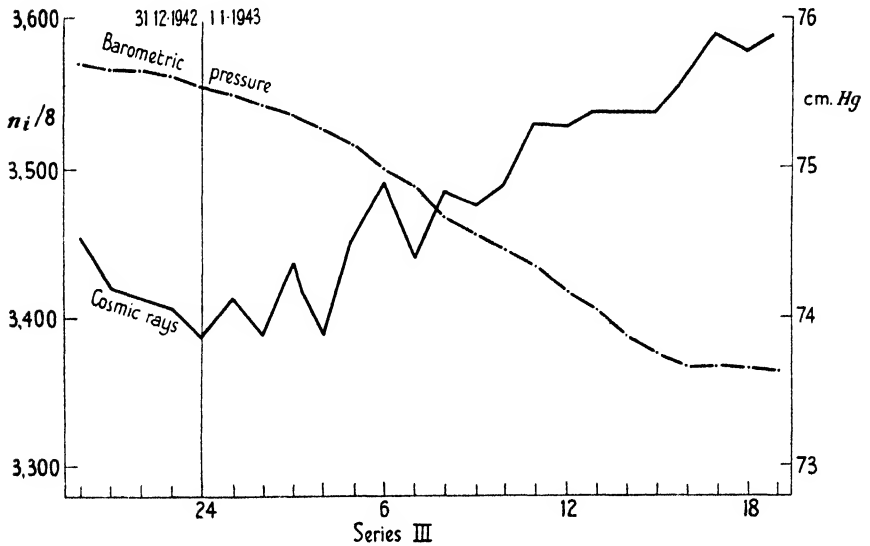

FIG. 124. Duperier's records.

The intensities given in Table 4 have been plotted in Figs. 123, 124, together with the barometric pressure. The large fluctuation of series III is obviously due to the change of pressure during the period of

observation. The large fluctuation of series II cannot be attributed to the pressure. We notice, however, from Fig. 123 that the intensity drops by about 2 per cent. in the course of the observation. It will be seen that the large fluctuation exhibited by this series is due to this systematic drop of intensity.

(c) *Systematic Variation*

Amplitude

660. Consider now a slow systematic change of the cosmic-ray intensity. Assume that the intensity at a time t is given by

$$n(t) = \bar{n}+a(t). \tag{75}$$

The slow change will be superposed, and partly masked, by the random fluctuation of the counting rate. The random deviation at the time t_i is

$$d_i = n_i-n(t_i). \tag{76}$$

If all systematic changes are taken care of by $a(t)$, then d_i should be the random deviation of the counting rate and

$$\frac{1}{N-1}\sum d_i^2 \simeq \bar{n}. \tag{77}$$

The d_i's are, however, not known; usually only the deviations $n_i-\bar{n}$ are known. The d_i's can be eliminated as follows:

$$\kappa^2 = \frac{1}{N-1}\sum (n_i-\bar{n})^2 = \frac{1}{N-1}\left\{\sum_{i=1}^{N} d_i^2+\sum_{i=1}^{N} a(t_i)^2+2\sum_{i=1}^{N} a(t_i)d_i\right\}. \tag{78}$$

Averaging (78) over a large number of similar cases we have, with the help of (77),

$$\langle\kappa^2\rangle = \bar{n}+\frac{1}{N-1}\sum_{i=1}^{N} a(t_i)^2. \tag{79}$$

Note that $$\left\langle\sum_{i=1}^{N} a(t_i)d_i\right\rangle = 0.$$

661. It is seen from (79) that in the presence of systematic changes the fluctuation expressed in terms of $n_i-\bar{n}$ appears larger than normal. Conversely, if it can be established for a series of observations that the fluctuation is larger than normal, then it can be concluded that a systematic fluctuation is superimposed on the random fluctuations. The root mean square amplitude κ_a of the systematic change is given by

$$\kappa_a = \sqrt{(\kappa^2-\bar{n})}. \tag{80}$$

For the three series of Table 4 it is found that the fluctuation of series I is normal, i.e. the difference between $\bar{n}$ and κ^2 cannot be

assumed to be significant. The series II and III, however, show a systematic change, their respective root mean square amplitudes as obtained from Table 4 being:

TABLE 2

	κ_a (*coincidences per hour*)	*Relative amplitude*
Series II	180	0·66 %
Series III	512	1·85 %

Fast and slow variations

662. The systematic variation can be either a fast fluctuation or a slow secular variation, and it is shown below how it is possible to distinguish between these two cases.

Consider the following sum:

$$f^2 = \frac{1}{2(N-2)} \sum_{i=1}^{N-1} (d_{i+1}-d_i)^2. \tag{81}$$

It can be shown easily that the average value of f^2 is given by

$$\langle f^2 \rangle = \langle d^2 \rangle = \bar{n}. \tag{82}$$

The last equation (82) holds only if the d_i's have normal fluctuation.

However, $$d_{i+1}-d_i = n_{i+1}-n_i-\{a(t_{i+1})-a(t_i)\}.$$

If the variation $a(t)$ is slow, the difference $a(t_{i+1})-a(t_i)$ can be neglected and approximately

$$f^2 \simeq \frac{1}{2(N-2)} \sum_{i=1}^{N-1} (n_{i+1}-n_i)^2. \tag{83}$$

The following practical use can be made of (83). For a given series of observation we can determine numerically a quantity g^2 defined by

$$g^2 = \frac{1}{2(N-2)} \sum_{i=1}^{N-1} (n_{i+1}-n_i)^2. \tag{84}$$

The value of g^2 should, according to (83), be of the same order as f^2. Thus g^2 is the mean square amplitude of the 'fast' fluctuation.

If there is no significant difference between g^2 and $\bar{n}$ for a series, then it can be concluded that the variations of the individual values are due to *normal fluctuation* superimposed on a *slow secular variation*. If, however, the difference

$$g^2-\bar{n}$$

is significantly greater than zero, then it must be assumed that a *fast*

systematic fluctuation is superimposed on the *normal fluctuation*. The difference

$$\kappa^2_{\text{slow}} = \kappa^2 - g^2$$

gives a measure of the mean square amplitude of the slow variation.

663. The quantity g^2, evaluated for the three series of Table 4, is given below.

TABLE 3

	Series		
	I	II	III
$\bar{n}$ =	25827	27118	27847
g^2 =	13593	22241	32433
DIFFERENCE	−12234	−4877	4586
with standard deviation	±8800	±9200	±9400

We see from the above table that none of the differences

$$g^2 - \bar{n}$$

can be regarded as significant. It is concluded therefore that all three series show *normal* fluctuation, but that the series II and series III

TABLE 4

Series I: 10–11.6.1943			*Series II:* 26–7.11.1943			*Series III:* 31.12.1942–1.1.1943		
Time	$n_i/8$	B_i	*Time*	$n_i/8$	B_i	*Time*	$n_i/8$	B_i
10	3257	762·4	11	3386	755·7	20	3454	757·0
11	245	2·4	12	430	5·6	21	420	56·6
12	232	2·3	13	417	5·5	22	412	56·5
13	251	2·3	14	421	5·4	23	407	56·2
14	263	2·1	15	426	5·4	24	387	55·5
15	248	2·0	16	436	5·6	01	414	54·9
16	263	2·0	17	436	5·8	02	388	54·2
17	243	2·0	18	436	6·0	03	438	53·5
18	197	2·0	19	384	6·2	04	388	52·5
19	224	2·0	20	375	6·2	05	455	51·6
20	219	2·2	21	419	6·3	06	491	50·0
21	241	2·4	22	379	6·4	07	439	48·8
22	229	2·7	23	356	6·5	08	486	46·9
23	203	2·7	24	375	6·4	09	476	45·6
24	200	2·8	01	379	6·4	10	490	44·5
01	214	2·8	02	359	6·4	11	530	43·5
02	242	2·6	03	382	6·3	12	530	41·7
03	229	2·5	04	379	6·3	13	538	40·5
04	220	2·4	05	377	6·1	14	538	38·7
05	205	2·5	06	334	6·0	15	539	37·7
06	192	2·6	07	355	5·9	16	564	36·8
07	190	2·7	08	366	5·9	17	590	36·8
08	227	2·7	09	394	6·0	18	578	36·7
09	246	2·4	10	353	5·7	19	590	36·5

show a slow secular variation superimposed on the random fluctuations of the individual values.

The root mean square amplitudes of these slow variations are given in Table 2.

TABLE 5

Derived quantities

Quantity	*Defined by equation*	*Series* I	II	III
$\bar{n}$	(67)	25827	27118	27847
κ^2	(68)	31827	59303	290933
g^2	(84)	13593	22241	32433

C. CORRELATION

664. It has been shown in the last section how the fluctuation of a set of readings is analysed. In particular it has been shown that a secular variation can be separated from the random fluctuation of the numbers of recorded coincidences.

Once the existence of a slow variation is established, as it is established e.g. for the series II and III, the question arises how to find the variation $a(t)$ itself.

1. *Barometer Effect*

665. Inspecting Fig. 124, where the series III is plotted, it is clear that the change of intensity is connected with the change of air pressure. It can be assumed as a first approximation that the change of intensity is proportional to the change of pressure,

$$a(t) = \alpha . b(t), \tag{85}$$

where α is a constant and $b(t)$ is the deviation of the pressure from the mean at the time t. Thus

$$b(t) = B(t) - \bar{B} \tag{86}$$

with

$$\bar{B} = \sum_{i=1}^{N} B(t_i)/N. \tag{87}$$

(*a*) *Regression Coefficient*

666. The counts when corrected for pressure are thus

$$m_i = n_i - \alpha . b(t_i); \tag{88}$$

if the whole of the slow variation is due to a pressure effect as defined by (85), then the m_i's should contain no systematic variation and

therefore they should have a normal fluctuation. If, on the other hand, (85) gives only part of the slow variation then the m_i's have still more than normal fluctuation, but in any case the fluctuation of the m_i's must be less than that of the n_i's.

Unless it is known from other observations what the value of α is, it can be determined from our series by postulating that the correct value of α makes the fluctuation of the m_i's a minimum.

Thus we postulate

$$\kappa_\alpha^2 \equiv \frac{1}{N-1}\sum_{i=1}^{N}\{n_i-\bar{n}-\alpha.b(t_i)\}^2 = \frac{1}{N-1}\sum_{i=1}^{N}(m_i-\bar{n})^2 = \text{minimum in } (\alpha). \quad (89)$$

From (78) the best value α_0 for α is

$$\alpha_0 = \frac{\sum b_i(n_i-\bar{n})}{\sum b_i^2}. \quad (90)$$

Further, from (68), (89), and (90)

$$\kappa_{\alpha_0}^2 = \kappa^2 - \frac{\alpha_0}{N-1}\sum_{i=1}^{N} b_i^2. \quad (91)$$

The correlation can be regarded as significant, provided the fluctuation of the corrected values m_i is significantly smaller than that of the uncorrected values n_i.

(*b*) *Mean Square Fluctuation*

667. It is interesting to plot the fluctuation of the m_i's as a function of α. We find

$$\kappa_\alpha^2 = \frac{1}{N-1}\sum_{i=1}^{N}(n_i-\alpha b_i-\bar{n})^2 = \kappa_{\alpha_0}^2+(\alpha-\alpha_0)^2\frac{\sum b_i^2}{N-1}. \quad (92)$$

Introducing the values of Table 4, series III,

$$\frac{1}{N-1}\sum_{i=1}^{N} b_i^2 = 0{\cdot}579 \text{ (cm. Hg)}^2$$

and

$$\frac{1}{N-1}\sum_{i=1}^{N} b_i(n_i-\bar{n}) = -381{\cdot}3 \text{ cm. Hg coincidences per hour}$$

and $\alpha_0 = -658{\cdot}5$ coincidences per hour per cm. Hg.

The relative regression coefficient of the pressure effect is therefore

$$\Gamma_{bn} = \frac{100\alpha_0}{\bar{n}} = -2{\cdot}36 \text{ per cent. per cm. Hg.}$$

(c) *Significance of Correlation*

668. The correlation appears to be significant because the barometer correction reduces significantly the fluctuation of the observed values.

From Table 5, $\kappa^2 = 290933$

and $\kappa_{\alpha_0}^2 = 39870.$

The average amplitude for the normal fluctuation is

$$\langle \kappa_{\text{normal}}^2 \rangle = \bar{n} = 27847.$$

Therefore the excess of the fluctuation of the m_i's over that of the average normal fluctuation is

$$\kappa_{\alpha_0}^2 - \bar{n} = 12020.$$

The standard deviation of the normal fluctuation is, according to (71),

$$\delta\langle \kappa_{\text{normal}}^2 \rangle = \bar{n}\sqrt{\frac{2}{N-1}} = 8200.$$

Therefore the fluctuation of the corrected values m_i deviates from that of the normal fluctuation by

$$\frac{12020}{8200} = 1{\cdot}5 \times \text{standard deviation of normal fluctuation.}$$

A deviation equal to 1·5 times the standard deviation occurs with a probability of 14 per cent. Such a deviation must be regarded as likely, and therefore it is concluded that the corrected fluctuation does not differ significantly from a normal fluctuation.

It is concluded that the excessive fluctuation of the series III can be fully accounted for in terms of the change of intensity with barometric pressure.

669. It remains to find the limits between which the actual value of α can reasonably be expected to lie.

The mean square amplitude of the fluctuation has been plotted as a function of α in Fig. 125. As can be inferred from (92) this fluctuation is represented by a parabola having its minimum at $\alpha = \alpha_0$.

The value of the average normal fluctuation ($\bar{n}$) has also been shown in Fig. 125 by a horizontal line and also this fluctuation plus single, double, and threefold standard deviations. The line representing average normal+three times standard deviation is the largest fluctuation which can be regarded as a chance deviation from normal. This line is intersected by the parabola at

$$\alpha = -805 \quad \text{and} \quad \alpha = -511. \tag{93}$$

Thus α values inside the interval (93) reduce the fluctuation to such a

degree that the reduced fluctuation cannot be regarded as significantly different from a normal fluctuation.

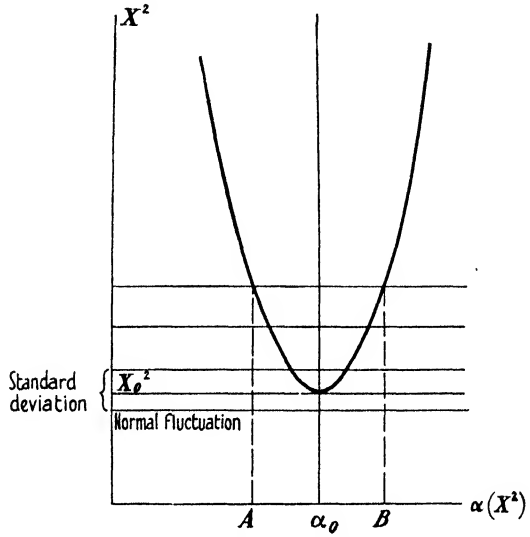

FIG. 125. Single correlation.

670. The actual experimental uncertainty of α is, however, not necessarily given by (93) if no hypothesis is made as to the fluctuation of the corrected values.† The uncertainty of α can be estimated in the latter case as follows. A value α_1 will give a significantly worse correlation than the optimum value α_0, provided the fluctuation $\kappa^2_{\alpha_1}$ obtained for $\alpha = \alpha_1$ is significantly greater than the minimum fluctuation α_0.

The difference between the two mean square fluctuations is

$$\kappa^2_{\alpha_1} - \kappa^2_{\alpha_0} = \Delta\kappa^2_{\alpha_0} = (\alpha_1 - \alpha_0)^2 \frac{\sum b_i^2}{N-1}, \tag{94}$$

and the standard deviation of a mean square fluctuation is

$$\delta\kappa^2_{\alpha_0} = \sqrt{\left(\frac{2}{N-1}\right)}\kappa^2_{\alpha_0},$$

The difference $\Delta\kappa^2_{\alpha_0}$ is significant if it exceeds three times the standard deviation $\delta\kappa^2_{\alpha_0}$ of $\kappa^2_{\alpha_0}$.

Therefore the difference between α_0 and α_1 has to be taken seriously, provided

$$\Delta\kappa^2_{\alpha_0} > 3\delta\kappa^2_{\alpha_0}.$$

† If we have reason to suppose that the fluctuation is normal apart from the barometer effect, then it must be concluded that α is not likely to lie outside the interval (93).

And therefore $$|\alpha_1-\alpha_0| > |\kappa_{\alpha_0}| \left\{\frac{18(N-1)}{(\sum b_i^2)^2}\right\}^{\frac{1}{4}}. \qquad (95)$$

Introducing numerical values from series III,

$$|\alpha_1-\alpha_0| > 250.$$

Thus the correlation deteriorates noticeably if α is taken *outside* the interval

$$\alpha_0 \pm 250.$$

Hence it is not likely that α lies outside the interval

$$-400 \quad \text{to} \quad -810.$$

The comparatively large margin of admissible α values is due to the fact that the period of observation is comparatively short.

2. *Secular Variation*

671. The fluctuation of series II cannot be reduced significantly by correcting the readings for changing pressure as is apparent from the inspection of Fig. 123.

It was shown, however, in § 663 that the large fluctuation of the readings of series II is due to a slow change of intensity. It is plausible therefore to assume that the intensity of cosmic rays was changing gradually during the period of observation due to some outside cause.

Assume therefore that

$$n(t) = \bar{n} + \beta\tau_i, \qquad (96)$$

with $$\tau_i = t_i - \bar{t} \quad \text{and} \quad \bar{t} = \sum t_i/N,$$

where β is a constant signifying the rate of change of the intensity.

The quantity β may be determined by the condition that

$$\kappa_\beta^2 = \frac{1}{N-1}\sum_{i=1}^{N}(n_i-\bar{n}-\beta\tau_i)^2 = \text{minimum for } \beta = \beta_0.$$

Thus $$\beta_0 = \frac{\sum (n_i-\bar{n})\tau_i}{\sum \tau_i^2}$$

and $$\kappa_\beta^2 = \kappa_{\beta_0}^2 + (\beta-\beta_0)^2 \frac{\sum \tau_i^2}{N-1}, \qquad \kappa_{\beta_0}^2 = \kappa^2 - \beta_0^2 \frac{\sum \tau_i^2}{N-1}.$$

Introducing numerical values from Table 4,

$$\beta_0 = -25{\cdot}0 \text{ coincidences per (hour)}^2$$

and $$\kappa_{\beta_0}^2 = 28153.$$

The latter fluctuation is almost exactly equal to the average normal fluctuation, namely

$$\bar{n} = 27118.$$

It is concluded therefore that the large fluctuation shown by the series II can be fully accounted for by assuming that the intensity of the radiation was decreasing in the course of observation at a constant rate, namely at a rate of 25 coincidences per hour, or

$$\frac{25\times 100\times 24}{27118} = 2{\cdot}2 \text{ per cent. per day.}$$

The actual value of β is likely to be inside the interval

$$25\pm 11{\cdot}8 = \begin{cases} 36{\cdot}8, \\ 13{\cdot}2. \end{cases}$$

The fluctuation κ_β^2 corresponding to such β-values differs by not more than the standard deviation from the average normal fluctuation. Further, it is unlikely that the value of β is outside the interval

$$25\pm 21{\cdot}5 = \begin{cases} 3{\cdot}5, \\ 46{\cdot}5, \end{cases}$$

because the fluctuation κ_β^2 corresponding to a β value outside the above limits would exceed the average normal fluctuation by more than three times the standard deviation.

3. *Multiple Correlation*

Regression Coefficients

672. The cosmic-ray intensity is known to depend on both the pressure and the average temperature of the atmosphere. The readings n_i obtained in a series of measurements have then to be correlated with both changes of pressure and changes of temperature.

In general it is necessary to assume

$$a(t) = \alpha b(t)+\gamma\Theta(t), \tag{97}$$

where α and γ are the regression coefficients for barometer and temperature correlations.

The best values for α and for γ can again be assumed to be those which make the fluctuation of the corrected values a minimum. Thus

$$\kappa_{\alpha\gamma}^2 \equiv \frac{1}{N-1}\sum \{n_i-\bar{n}-\alpha b(t_i)-\gamma\Theta(t_i)\}^2 = \text{minimum for } \alpha=\alpha_0,\ \gamma=\gamma_0. \tag{98}$$

The best values are therefore given as the solutions of the following system of linear equations.

$$\left.\begin{aligned} \alpha_0 \sum b_i^2 + \gamma_0 \sum b_i \Theta_i &= \sum (n_i - \bar{n}) b_i, \\ \alpha_0 \sum b_i \Theta_i + \gamma_0 \sum \Theta_i^2 &= \sum (n_i - \bar{n}) \Theta_i. \end{aligned}\right\} \tag{99}$$

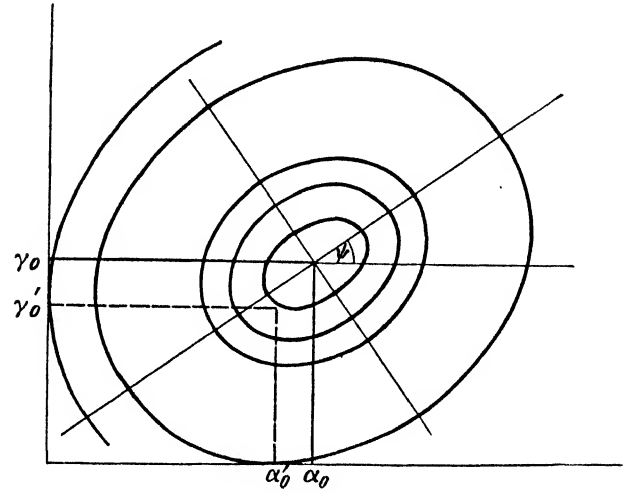

FIG. 126. Multiple correlation.

673. Introducing the values for α_0 and γ_0 from (99) into (98) it is found that

$$\kappa_{\alpha\gamma}^2 = \kappa_{\alpha_0\gamma_0}^2 + (\alpha-\alpha_0)^2 \sum b_i^2/(N-1) + (\gamma-\gamma_0)^2 \sum \Theta_i^2/(N-1) + \\ + \frac{2}{N-1} \sum b_i \Theta_i (\alpha-\alpha_0)(\gamma-\gamma_0), \tag{100}$$

$$\kappa_{\alpha_0\gamma_0}^2 = \frac{1}{N-1} \{\alpha_0 \sum (n_i - \bar{n}) b_i + \gamma_0 \sum (n_i - \bar{n}) \Theta_i\}.$$

The equation (100) can be regarded as the equation of a family of concentric ellipses as shown in Fig. 126.

Choosing pairs of values α and γ along the same ellipse the same value for the fluctuation $\kappa_{\alpha\gamma}^2$ is obtained.

The best pair of values for α and γ is represented by the centre of the family. In Fig. 126 there have been drawn (schematically) the ellipses which correspond to a fluctuation equal to the average normal fluctuation plus ν times standard deviation; $\nu = 1, 2, 3, \ldots$ for a hypothetical case.

The probabilities that the actual values of α and γ lie inside any of these ellipses are therefore given by

$$\sim E(\nu/\sqrt{2}) \quad .(\nu = 1, 2, 3, \ldots).$$

Correlation Coefficient

674. For the investigation of the system of ellipses Fig. 126, it is useful to introduce the correlation coefficient r between the b_i's and the Θ_i's. Define r by

$$r = \frac{\sum b_i \Theta_i}{(\sum b_i^2 \sum \Theta_i^2)^{\frac{1}{2}}}.$$

The following extreme cases are of interest.

(1) $r^2 = 1$. In this case the ellipses degenerate into a system of parallel lines.

The physical significance of this case is that the b_i and Θ_i are exactly proportional to each other and therefore the double correlation becomes

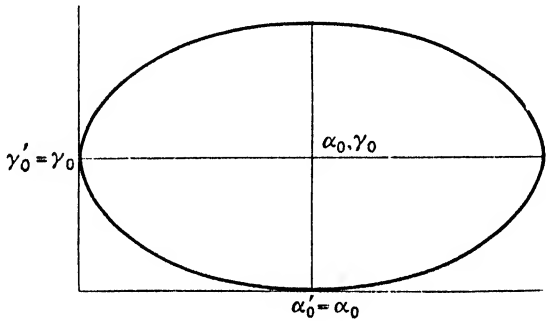

FIG. 127. Double correlation (independent causes).

meaningless. In this case a single correlation with one of the two quantities has to be used. The case $r^2 \sim 1$ is of course similar and in this case a family of very elongated ellipses is obtained.

(2) $r = 0$. In this case the ellipses have axes parallel to the α- and γ-axes. It can be seen easily (see Fig. 127) that in this case the result of the multiple correlation is exactly the same as that of two independent single correlations.

(3) If r is significantly different from both zero and 1, the ellipses are inclined at an angle of ψ to the axis. And, as the result of a single calculation, it follows that†

$$\tan 2\psi = \frac{2 \sum b_i \Theta_i^2}{\sum b_i^2 - \sum \Theta_i^2}.$$

In this case the result of the single correlation differs from that of the double correlation. It can be seen easily that single correlation for α would give a value α_0' instead of α_0, where α_0' is the point of contact of the α-axis with the ellipse touching this axis (see Fig. 126).

† For $\sum b_i^2 = \sum \Theta_i^2$ the family degenerates into a family of concentric circles.

APPENDIX II

AUXILIARY TABLES FOR CASCADE COMPUTATIONS

675. In § 375, Ch. VI, three functions $\mathfrak{A}(\mathfrak{y})$, $\mathfrak{B}(\mathfrak{y})$, $\mathfrak{C}(\mathfrak{y})$, and a constant $\mathfrak{D}$ were introduced. Numerical values for these quantities are collected in Table 1.

TABLE 1

$\mathfrak{y}$	$\mathfrak{A}(\mathfrak{y})$	$\mathfrak{B}(\mathfrak{y})$	$\mathfrak{C}(\mathfrak{y})$	$\mathfrak{y}$	$\mathfrak{A}(\mathfrak{y})$	$\mathfrak{B}(\mathfrak{y})$	$\mathfrak{C}(\mathfrak{y})$
1·0	0·00000	1·54735	—	3·0	1·54828	0·53088	0·47632
1·1	0·15204	1·40100	12·82106	3·1	1·59094	0·51528	0·45249
1·2	0·28621	1·28089	6·11261	3·2	1·63220	0·50065	0·43098
1·3	0·40625	1·18064	3·91667	3·3	1·67213	0·48689	0·41147
1·4	0·51487	1·09575	2·84155	3·4	1·71084	0·47393	0·39369
1·5	0·61406	1·02295	2·21058	3·5	1·74839	0·46170	0·37742
1·6	0·70538	0·95984	1·79913	3·6	1·78486	0·45013	0·36247
1·7	0·79000	0·90461	1·51149	3·7	1·82031	0·43917	0·34870
1·8	0·86888	0·85586	1·30015	3·8	1·85480	0·42876	0·33596
1·9	0·94278	0·81250	1·13894	3·9	1·88838	0·41888	0·32415
2·0	1·01230	0·77368	1·01230	4·0	1·92110	0·40947	0·31316
2·1	1·07797	0·73870	0·91043	4·1	1·95300	0·40051	0·30292
2·2	1·14020	0·70702	0·82687	4·2	1·98413	0·39195	0·29335
2·3	1·19936	0·67817	0·75719	4·3	2·01452	0·38378	0·28438
2·4	1·25574	0·65179	0·69827	4·4	2·04422	0·37596	0·27596
2·5	1·30962	0·62756	0·64783	4·5	2·07324	0·36848	0·26804
2·6	1·36120	0·60523	0·60421	4·6	2·10163	0·36130	0·26057
2·7	1·41071	0·58457	0·56612	4·7	2·12941	0·35442	0·25353
2·8	1·45829	0·56539	0·53259	4·8	2·15661	0·34781	0·24686
2·9	1·50410	0·54754	0·50286	4·9	2·18325	0·34145	0·24055
				5·0	2·20935	0·33534	0·23456
				5·5	2·33257	0·30793	0·20871
				6·0	2·44520	0·28484	0·18812

$\mathfrak{D} = 0{\cdot}77368$; $\alpha = 0{\cdot}02460$.

676. Neglecting ionization loss, the numbers of electrons or photons with energies exceeding w produced by a primary of energy w_0 under a layer of thickness ζ cascade units is given by the following complex integral:

$$\mathfrak{Q}_0(w_0, w; \zeta) = \frac{1}{2\pi i} \int_{\mathfrak{y}_0 - i\infty}^{\mathfrak{y}_0 + i\infty} \left(\frac{w_0}{w}\right)^{\mathfrak{y}-1} \frac{1}{\mathfrak{y}-1} \{\mathfrak{M}(\mathfrak{y}) e^{-a_1(\mathfrak{y})\zeta} + \mathfrak{N}(\mathfrak{y}) e^{-a_2\zeta}\}\, d\mathfrak{y}. \quad (1)$$

The above integral can be evaluated by the saddle-point method in the following way.

$\mathfrak{Q}_0$ and ζ can be represented as functions of an independent parameter η_0 using the following formulae:

$$\zeta = \left\{\log_e \frac{w_0}{w} + \frac{1}{\eta_0 - 1} + \frac{d}{d\eta}\log_e \mathfrak{M}(\eta)\right\} \Big/ \left(\frac{da_1}{d\eta}\right), \tag{2}$$

$$\log_{10} \mathfrak{Q}_0 = (\eta_0 - 1)\log_{10}\frac{w_0}{w} + \log_{10}\mathfrak{M}(\eta_0) - \log_{10}(\eta_0 - 1) - \\ - \bar{a}_1(\eta_0)\zeta - \tfrac{1}{2}\log(-\Xi'') - 0{\cdot}3991, \tag{3}$$

with

$$a_1(\eta) = \log_{10} e a_1(\eta), \tag{4}$$

$$-\Xi'' = -\frac{d^2 a_1}{d\eta^2}\zeta + \frac{1}{(\eta_0 - 1)^2} + \frac{d^2}{d\eta^2}(\log_e \mathfrak{M}), \tag{5}$$

$$0{\cdot}3991 = \log_{10}\sqrt{(2\pi)}.$$

The coefficients $\mathfrak{M}$ and $\mathfrak{N}$ have to be chosen according to whether the cascade is initiated by an electron or a photon and also according to whether one wants to calculate the number of photons or electrons. The choice of the $\mathfrak{M}$ and $\mathfrak{N}$ in the corresponding four cases is as follows:

	Cascade produced by			
	Electron		*Photon*	
$\mathfrak{Q}_0$ is to represent numbers of—	$\mathfrak{M}$	$\mathfrak{N}$	$\mathfrak{M}$	$\mathfrak{N}$
Electrons . .	$\dfrac{\mathfrak{D} - a_1}{a_2 - a_1}$	$\dfrac{a_2 - \mathfrak{D}}{a_2 - a_1}$	$\dfrac{\mathfrak{B}}{a_2 - a_1}$	$\dfrac{-\mathfrak{B}}{a_2 - a_1}$
Photons . .	$\dfrac{\mathfrak{C}}{a_2 - a_1}$	$\dfrac{-\mathfrak{C}}{a_2 - a_1}$	$\dfrac{a_2 - \mathfrak{D}}{a_2 - a_1}$	$\dfrac{\mathfrak{D} - a_1}{a_2 - a_1}$

The numerical values needed for the evaluation of (1) according to equations (2), (3), (4), (5), are collected in Tables 2–5.

Computation of $\mathfrak{Q}_0(w_0, w; \zeta)$

677. In order to compute a family of cascade curves it is convenient to introduce (2) into (5). In this way the following expression is obtained:

$$\log_{10} \mathfrak{Q}_0(w_0, w; \zeta) = A \log_{10}\left(\frac{w_0}{w}\right) + B - \tfrac{1}{2}\log_{10}\left(\frac{w_0}{w} + C\right), \tag{6}$$

$$\zeta = \frac{1}{a_1'}\left\{\log_{10}\left(\frac{w_0}{w}\right) + (\log_{10}\overline{\mathfrak{M}})'\right\}. \tag{7}$$

The coefficients A, B, C are functions of η. Numerical values of these

TABLE 2

$\mathfrak{y}$	$a_1(\mathfrak{y})$	$da_1/d\mathfrak{y}$	$d^2a_1/d\mathfrak{y}^2$	$a_2(\mathfrak{y})$	$\log\frac{\mathfrak{D}-a_2}{a_2-a_1}$	$\frac{d}{d\mathfrak{y}}\log\frac{\mathfrak{D}-a_1}{a_2-a_1}$	$\frac{d^2}{d\mathfrak{y}^2}\log\frac{\mathfrak{D}-a_2}{a_2-a_1}$
1·0	$-\infty$	$+\infty$	—	$+\infty$	−0·6932	—	—
1·1	−3·78671	24·9912	—	4·71243	−0·6226	0·233	—
1·2	−2·27879	9·4500	—	3·33868	−0·6099	0·043	—
1·3	−1·56826	5·4113	—	2·74819	−0·6114	−0·067	—
1·4	−1·12501	3·6526	−12·6	2·41356	−0·6226	−0·152	−0·77
1·5	−0·81201	2·6908	−7·4	2·19975	−0·6415	−0·226	−0·70
1·6	−0·57503	2·0909	−4·86	2·05408	−0·6675	−0·294	−0·66
1·7	−0·38751	1·6832	−3·42	1·95119	−0·7002	−0·359	−0·65
1·8	−0·23466	1·3884	−2·537	1·87722	−0·7393	−0·423	−0·64
1·9	−0·10745	1·1653	−1·961	1·82391	−0·7848	−0·487	−0·63
2·0	0·00000	0·9902	−1·562	1·78598	−0·8366	−0·549	−0·62
2·1	0·09175	0·8493	−1·274	1·75990	−0·8946	−0·610	−0·60
2·2	0·17069	0·7332	−1·064	1·74319	−0·9585	−0·669	−0·57
2·3	0·23899	0·6357	−0·894	1·73405	−1·0282	−0·725	−0·54
2·4	0·29832	0·5532	−0·762	1·73110	−1·1033	−0·776	−0·49
2·5	0·35001	0·4825	−0·654	1·73329	−1·1833	−0·822	−0·44
2·6	0·39515	0·4217	−0·564	1·73974	−1·2676	−0·863	−0·37
2·7	0·43463	0·3692	−0·488	1·74975	−1·3555	−0·896	−0·31
2·8	0·46923	0·3238	−0·423	1·76274	−1·4466	−0·924	−0·24
2·9	0·49958	0·2843	−0·367	1·77820	−1·5401	−0·944	−0·18
3·0	0·52626	0·2501	−0·319	1·79570	−1·6353	−0·959	−0·11
3·1	0·54974	0·2203	−0·277	1·81488	−1·7316	−0·967	−0·05
3·2	0·57046	0·1945	−0·241	1·83542	−1·8285	−0·970	−0·02
3·3	0·58876	0·1721	−0·209	1·85706	−1·9255	−0·969	0·04
3·4	0·60496	0·1525	−0·182	1·87956	−2·0222	−0·963	0·08
3·5	0·61934	0·1355	−0·158	1·90273	−2·1181	−0·955	0·09
3·6	0·63214	0·1207	−0·138	1·92640	−2·2131	−0·944	0·13
3·7	0·64355	0·1077	−0·121	1·95044	−2·3069	−0·931	0·16
3·8	0·65375	0·0965	−0·106	1·97473	−2·3992	−0·916	0·17
3·9	0·66288	0·0865	−0·093	1·99917	−2·4900	−0·899	0·17
4·0	0·67109	0·0767	−0·081	2·02368	−2·5791	−0·883	0·18

(Base e)

TABLE 3

$\mathfrak{y}$	$\bar{a}_1(\mathfrak{y})$	$d\bar{a}_1/d\mathfrak{y}$	$d^2\bar{a}_1/d\mathfrak{y}^2$	$\bar{a}_2(\mathfrak{y})$	$\log_{10}\frac{\mathfrak{D}-a_1}{a_2-a_1}$	$\frac{d}{d\mathfrak{y}}\log_{10}\frac{\mathfrak{D}-a_1}{a_2-a_1}$	$\frac{d^2}{d\mathfrak{y}^2}\log_{10}\frac{\mathfrak{D}-a_1}{a_2-a_1}$
1·0	$-\infty$	$+\infty$	—	$+\infty$	−0·3010	—	—
1·1	−1·64455	10·8536	—	2·04645	−0·2704	0·101	—
1·2	−0·98967	4·1041	−28·4	1·44997	−0·2649	0·019	—
1·3	−0·68109	2·3501	−10·7	1·19352	−0·2655	−0·029	—
1·4	−0·48859	1·5863	−5·4	1·04819	−0·2704	−0·066	−0·34
1·5	−0·35265	1·1686	−3·21	0·95534	−0·2786	−0·098	−0·31
1·6	−0·24973	0·9081	−2·11	0·89208	−0·2899	−0·128	−0·29
1·7	−0·16829	0·7310	−1·49	0·84739	−0·3041	−0·156	−0·28
1·8	−0·10191	0·6030	−1·102	0·81527	−0·3211	−0·184	−0·28
1·9	−0·04667	0·5061	−0·852	0·79211	−0·3408	−0·211	−0·27
2·0	0·00000	0·4300	−0·678	0·77564	−0·3633	−0·239	−0·27
2·1	0·03985	0·3689	−0·553	0·76431	−0·3885	−0·265	−0·26
2·2	0·07413	0·3184	−0·462	0·75706	−0·4163	−0·291	−0·25
2·3	0·10379	0·2761	−0·388	0·75309	−0·4466	−0·315	−0·23
2·4	0·12956	0·2402	−0·331	0·75181	−0·4792	−0·337	−0·21
2·5	0·15201	0·2096	−0·284	0·75276	−0·5138	−0·357	−0·19
2·6	0·17161	0·1832	−0·245	0·75556	−0·5505	−0·375	−0·16
2·7	0·18876	0·1604	−0·212	0·75991	−0·5887	−0·389	−0·13
2·8	0·20378	0·1406	−0·184	0·76555	−0·6283	−0·401	−0·10
2·9	0·21697	0·1235	−0·160	0·77226	−0·6688	−0·410	−0·08
3·0	0·22855	0·1086	−0·138	0·77986	−0·7101	−0·416	−0·05
3·1	0·23875	0·0957	−0·120	0·78819	−0·7520	−0·420	−0·02
3·2	0·24775	0·0845	−0·105	0·79711	−0·7941	−0·421	−0·01
3·3	0·25569	0·0747	−0·091	0·80651	−0·8362	−0·421	0·02
3·4	0·26273	0·0662	−0·079	0·81628	−0·8782	−0·418	0·03
3·5	0·26898	0·0589	−0·069	0·82634	−0·9199	−0·415	0·04
3·6	0·27453	0·0524	−0·060	0·83663	−0·9611	−0·410	0·06
3·7	0·27949	0·0468	−0·052	0·84707	−1·0019	−0·404	0·07
3·8	0·28392	0·0419	−0·046	0·85762	−1·0420	−0·398	0·07
3·9	0·28789	0·0376	−0·040	0·86823	−1·0814	−0·391	0·07
4·0	0·29145	0·0333	−0·035	0·87887	−1·1201	−0·383	0·08

(Base 10)

TABLE 4

$\mathfrak{y}$	$\log \frac{\mathfrak{B}}{a_2-a_1}$	$\frac{d}{d\mathfrak{y}} \log \frac{\mathfrak{B}}{a_2-a_1}$	$\frac{d^2}{d\mathfrak{y}^2} \log \frac{\mathfrak{B}}{a_2-a_1}$	$\log \frac{\mathfrak{C}}{a_2-a_1}$	$\frac{d}{d\mathfrak{y}} \log \frac{\mathfrak{C}}{a_2-a_1}$	$\frac{d^2}{d\mathfrak{y}^2} \log \frac{\mathfrak{C}}{a_2-a_1}$
1·0	—	—	—	—	—	—
1·1	−1·8028	4·771	—	0·4111	−4·808	—
1·2	−1·4783	2·286	—	0·0844	−2·294	—
1·3	−1·2964	1·465	—	−0·0972	−1·452	—
1·4	−1·1723	1·056	—	−0·2194	−1·032	—
1·5	−1·0798	0·810	−1·99	−0·3093	−0·785	1·95
1·6	−1·0076	0·643	−1·42	−0·3794	−0·627	1·27
1·7	−0·9498	0·518	−1·11	−0·4365	−0·523	0·85
1·8	−0·9032	0·417	−0·92	−0·4851	−0·454	0·55
1·9	−0·8659	0·332	−0·80	−0·5281	−0·410	0·34
2·0	−0·8366	0·256	−0·73	−0·5678	−0·385	0·18
2·1	−0·8146	0·185	−0·68	−0·6056	−0·363	0·06
2·2	−0·7994	0·120	−0·63	−0·6428	−0·372	−0·04
2·3	−0·7905	0·058	−0·60	−0·6803	−0·389	−0·10
2·4	−0·7877	0·000	−0·56	−0·7188	−0·392	−0·14
2·5	−0·7904	−0·054	−0·52	−0·7586	−0·406	−0·15
2·6	−0·7982	−0·103	−0·47	−0·7999	−0·421	−0·16
2·7	−0·8108	−0·148	−0·42	−0·8429	−0·437	−0·16
2·8	−0·8276	−0·187	−0·37	−0·8874	−0·452	−0·14
2·9	−0·8481	−0·222	−0·33	−0·9332	−0·465	−0·11
3·0	−0·8718	−0·252	−0·27	−0·9802	−0·475	−0·10
3·1	−0·8982	−0·282	−0·22	−1·0282	−0·483	−0·06
3·2	−0·9269	−0·296	−0·19	−1·0767	−0·488	−0·04
3·3	−0·9574	−0·308	−0·14	−1·1257	−0·491	−0·02
3·4	−0·9893	−0·325	−0·11	−1·1748	−0·491	0·01
3·5	−1·0224	−0·335	−0·08	−1·2239	−0·490	0·02
3·6	−1·0562	−0·341	−0·06	−1·2728	−0·487	0·04
3·7	−1·0905	−0·346	−0·03	−1·3212	−0·482	0·05
3·8	−1·1252	−0·348	−0·02	−1·3692	−0·476	0·06
3·9	−1·1601	−0·349	0·01	−1·4165	−0·469	0·07
4·0	−1·1949	−0·348	0·01	−1·4630	−0·462	0·08

(Base e)

TABLE 5

ϑ	$\log_{10}\frac{\mathfrak{B}}{a_2-a_1}$	$\frac{d}{d\vartheta}\log_{10}\frac{\mathfrak{B}}{a_2-a_1}$	$\frac{d^2}{d\vartheta^2}\log_{10}\frac{\mathfrak{B}}{a_2-a_1}$	$\log_{10}\frac{\mathfrak{C}}{a_2-a_1}$	$\frac{d}{d\vartheta}\log_{10}\frac{\mathfrak{C}}{a_2-a_1}$	$\frac{d^2}{d\vartheta^2}\log_{10}\frac{\mathfrak{C}}{a_2-a_1}$
1·0	—	—	—	—	—	—
1·1	−0·7829	2·072	—	0·1786	−2·088	—
1·2	−0·6420	0·993	—	0·0367	−0·996	—
1·3	−0·5630	0·636	—	−0·0422	−0·631	—
1·4	−0·5091	0·459	—	−0·0953	−0·448	—
1·5	−0·4690	0·352	−0·86	−0·1343	−0·341	0·85
1·6	−0·4376	0·279	−0·62	−0·1648	−0·272	0·55
1·7	−0·4125	0·225	−0·48	−0·1896	−0·227	0·37
1·8	−0·3923	0·181	−0·40	−0·2107	−0·197	0·24
1·9	−0·3760	0·144	−0·35	−0·2294	−0·178	0·15
2·0	−0·3633	0·111	−0·32	−0·2466	−0·167	0·08
2·1	−0·3538	0·080	−0·30	−0·2630	−0·158	0·03
2·2	−0·3472	0·052	−0·28	−0·2792	−0·161	−0·02
2·3	−0·3433	0·025	−0·26	−0·2955	−0·169	−0·04
2·4	−0·3421	0·000	−0·24	−0·3122	−0·170	−0·06
2·5	−0·3433	−0·023	−0·23	−0·3295	−0·176	−0·07
2·6	−0·3467	−0·045	−0·20	−0·3474	−0·183	−0·07
2·7	−0·3521	−0·064	−0·18	−0·3661	−0·190	−0·07
2·8	−0·3594	−0·081	−0·16	−0·3854	−0·196	−0·06
2·9	−0·3683	−0·096	−0·14	−0·4053	−0·202	−0·05
3·0	−0·3786	−0·109	−0·12	−0·4257	−0·206	−0·04
3·1	−0·3901	−0·122	−0·10	−0·4465	−0·210	−0·03
3·2	−0·4025	−0·129	−0·08	−0·4676	−0·212	−0·02
3·3	−0·4158	−0·134	−0·06	−0·4889	−0·213	−0·01
3·4	−0·4297	−0·141	−0·05	−0·5102	−0·213	0·00
3·5	−0·4440	−0·145	−0·03	−0·5315	−0·213	0·01
3·6	−0·4587	−0·148	−0·03	−0·5528	−0·212	0·02
3·7	−0·4736	−0·150	−0·01	−0·5738	−0·210	0·02
3·8	−0·4887	−0·151	−0·01	−0·5946	−0·207	0·03
3·9	−0·5038	−0·151	0·00	−0·6152	−0·204	0·03
4·0	−0·5189	−0·151	0·00	−0·6354	−0·201	0·03

(Base 10)

coefficients are found in Table 6. The cascade curves reproduced in Fig. 128 have been computed with the help of Table 6.

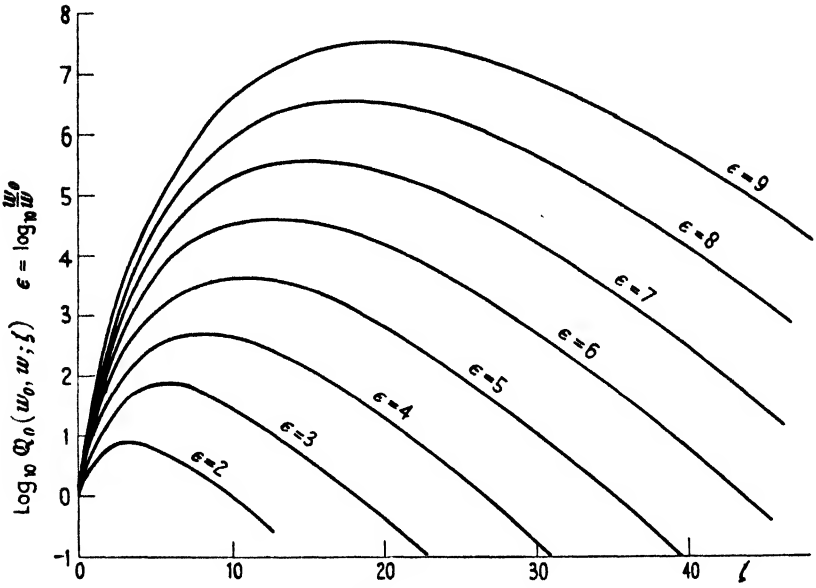

FIG. 128. Cascade figures.

TABLE 6

η	1·2	1·4	1·6	1·8	2·0	2·2	2·4	2·6	2·8	3·0
$A =$	0·441	0·708	0·875	0·969	1·000	0·967	0·861	0·662	0·350	−0·103
$-B =$	1·084	1·073	1·065	1·056	1·042	1·004	0·926	0·793	0·591	0·312
$C =$	0·676	0·452	0·456	0·508	0·571	0·619	0·640	0·639	0·619	0·586
$-(\log_{10}\overline{\mathfrak{M}})' =$	2·151	1·151	0·852	0·726	0·673	0·653	0·647	0·646	0·642	0·633
$a_1' \log_{10} e =$	4·104	1·586	0·908	0·603	0·430	0·318	0·240	0·183	0·141	0·109

Tables for Computation of Extensive Air Showers

678. In Chapter VIII we have introduced a function

$$F(x) = a(\gamma)x^{-\gamma}. \tag{8}$$

The function F is connected with the density distribution of an extensive air shower at the depth ζ, where

$$\zeta = \frac{1}{a_1'(\gamma+3)}\left\{\log x(\gamma) + \frac{1}{\gamma} + (\log \mathfrak{M})'_{\gamma+3}\right\}. \tag{9}$$

A few numerical values are collected in Table 7.

TABLE 7

$\log_{10} x(\gamma)$

$\gamma =$	1·4	1·2	1·0	0·8	0·6	0·4	0·2
$\zeta = 10$	8·90	5·85	4·11	2·93	2·02	1·12	—
15	13·44	8·87	6·26	4·52	3·22	2·04	0·34
20	—	11·88	8·41	6·12	4·42	2·95	1·04
25	—	—	10·56	7·71	5·62	3·87	1·75
30	—	—	12·71	9·30	6·82	4·79	2·45

$\log_{10} a(\gamma)$

$\zeta = 10$	0·82	−0·48	−1·36	−1·99	−2·45	−2·80	−3·10
15	1·98	−0·06	−1·45	−2·44	−3·17	−3·70	−4·13
20	—	0·39	−1·51	−2·88	−3·87	−4·60	−5·16
25	—	0·85	−1·56	−3·29	−4·56	−5·49	−6·20
30	—	—	−1·60	−3·70	−5·24	−6·38	−7·23

$-\log_{10} |F(x)|$

$\gamma =$	1·4	1·2	1·0	0·8	0·6	0·4	0·2	$x = 1$
$\zeta = 10$	11·64	7·50	5·47	4·33	3·66	3·25	..	2·03
15	16·84	10·70	7·71	6·06	5·10	4·53	4·20	4·17
20	—	13·87	9·92	7·78	6·52	5·78	5·38	5·31
25	—	—	12·12	9·46	7·93	7·04	6·55	6·45
30	—	—	14·31	11·14	9·33	8·30	7·72	7·59

The function $F(x)$ is plotted in Fig. 104 and Fig. 129.

Cascade Theory Including Ionization Loss

679. It was shown by Bhabha and Chakrabarty (1943) that the number of secondaries with energies exceeding w produced by an electron of energy w_0 is given to a first approximation by

$$\mathfrak{Q}(w_0, w; \zeta) \cong \mathfrak{Q}_0\{w_0, w + g(\zeta, \eta_0) w_c; \zeta\}, \tag{10}$$

where the function $g(\zeta, \eta_0)$ depends on the thickness ζ and on the

TABLE 8

Values of $g(\eta, \zeta)$†

η \ $\xi =$	1·0	1·3	1·5	2·0	4·0	10·0	∞
1·5	0·4892	0·5113	0·5174	0·5269	0·5353	0·5364	0·5364
2·0	0·6309	0·7071	0·7155	0·7705	0·8009	0·8186	0·8186
2·5	0·7264	0·8298	0·8759	0·9339	0·9564	0·9993	1·013
3·0	0·7738	0·9035	0·9659	1·048	1·037	1·083	1·141
3·5	0·8054	0·9545	1·029	1·129	1·066	1·094	1·226
4·0	0·8317	0·9949	1·079	1·189	1·064	1·067	1·292
4·5	0·8475	1·023	1·116	1·239	1·047	1·027	1·350
5·0	0·8630	1·050	1·149	1·287	1·027	0·9876	1·386

† The above table is taken from Bhabha and Chakrabarty (1943).

position of the saddle-point defined by η_0. Numerical values for the function g computed by Bhabha and Chakrabarty are reproduced in Table 8.

Fluctuation of Cascades

680. The distribution function giving the probability that an electron gives rise to exactly N electrons instead of the average number $\langle N \rangle$ has

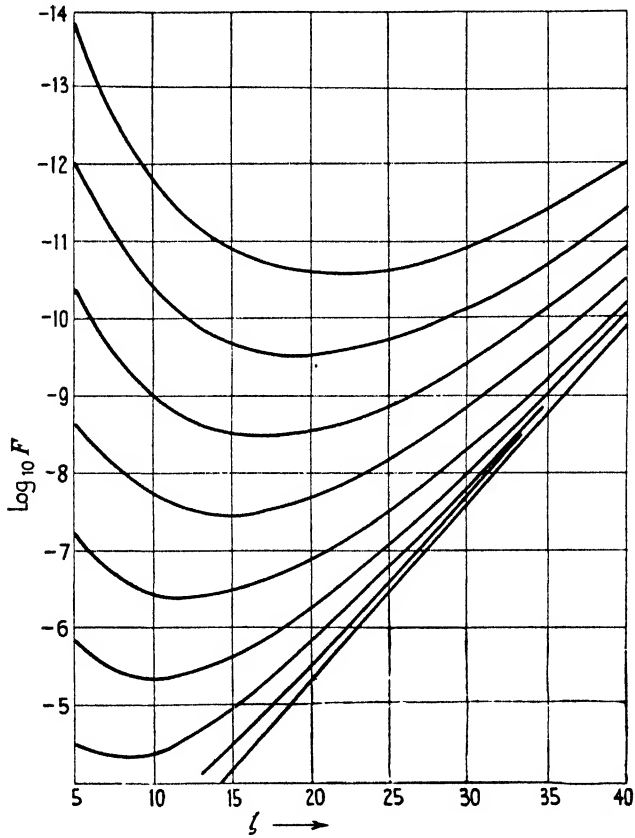

FIG. 129. The function $F(x)$. Compare also Fig. 104.

been computed by Arley (1943). The distribution function is represented by a Pólya distribution; this distribution differs appreciably from the Poisson distribution. Some data given by Arley are reproduced in Table 9.†

† Arley uses conventions for the critical energy and the cascade unit different from those used in this book (compare also Ch. VI, § 390). The units are explained on the top of Table 9.

TABLE 9

Probability Distribution

Probability $\mathscr{P}(y_c, \zeta', N)$ that a primary energy W_0 gives rise to exactly N electrons at the depth ζ'.

$$y_c = \log_e(W_0/W'_c).$$

$$\zeta' = \log_e 2 \times \zeta.$$

	$\zeta' = 0{\cdot}2$			$\zeta' = 0{\cdot}4$		
$y_c =$	2	4	6	2	4	6
$N = 0$	0·0126	0·0010	0·0001	0·0296	0·00255	0·00021
1	0·958	0·940	0·911	0·873	0·796	0·704
2	0·0288	0·0572	0·0847	0·0924	0·180	0·243
3	0·00043	0·00174	0·00394	0·00489	0·0203	0·0462
4	4×10^{-6}	$3{\cdot}5 \times 10^{-5}$	0·000122	2×10^{-4}	0·00153	0·00638
$\geqslant 5$	0	0	0	0	0	5×10^{-4}
	$\zeta' = 0{\cdot}6$			$\zeta' = 0{\cdot}8$		
$N = 0$	0·0483	0·00421	0·00043	0·0676	0·00616	0·00055
1	0·768	0·645	0·533	0·669	0·533	0·393
2	0·165	0·254	0·278	0·217	0·275	0·263
3	0·0178	0·0726	0·117	0·0400	0·115	0·154
4	0·00127	0·0181	0·0453	0·00545	0·0448	0·0868
$\geqslant 5$	7×10^{-5}	0·00530	0·0261	0·00060	0·0267	0·103
	$\zeta' = 1$			$\zeta' = 2$		
$N = 0$	0·0884	0·00793	0·00073	0·186	0·0208	0·00220
1	0·599	0·430	0·291	0·373	0·222	0·126
2	0·226	0·267	0·230	0·204	0·165	0·103
3	0·0651	0·145	0·163	0·110	0·127	0·0886
4	0·0169	0·0749	0·110	0·0591	0·0991	0·0771
$\geqslant 5$	0·00538	0·0746	0·206	0·0683	0·366	0·603
	$\zeta' = 3$			$\zeta' = 5$		
$N = 0$	0·279	0·0395	0·00476	0·0513	0·0905	0·0116
1	0·280	0·154	0·0758	0·201	0·112	0·0380
2	0·158	0·111	0·0611	0·102	0·0815	0·0305
3	0·0982	0·0900	0·0537	0·0615	0·0670	0·0271
4	0·0628	0·0754	0·0485	0·0392	0·0574	0·0250
$\geqslant 5$	0·121	0·530	0·756	0·0824	0·591	0·868
	$\zeta' = 7$			$\zeta' = 10$		
$N = 0$	0·704	0·149	0·0164	0·903	0·277	0·0315
1	0·147	0·106	0·0237	0·0594	0·136	0·0262
2	0·650	0·0773	0·0201	0·0202	0·0939	0·0223
3	0·0342	0·0631	0·0183	0·00868	0·0720	0·0201
4	0·0194	0·0536	0·0171	0·00414	0·0569	0·0200
$\geqslant 5$	0·0302	0·551	0·905	0·00447	0·365	0·880

TABLE 9 (*continued*)

	$\zeta' = 14$		
$y_c =$	2	4	6
$N = 0$	0·984	0·583	0·0727
1	0·0121	0·162	0·0505
2	0·00270	0·0855	0·0422
3	0·00079	0·0522	0·0372
4	0·00026	0·0340	0·0336
$\geqslant 5$	0·00015	0·0837	0·764

APPENDIX III

THE PHOTOGRAPHIC METHOD

681. SINCE the greater part of this book was written the photographic method, very briefly discussed in Chapter II, §§ 141–3, has come into prominence. Powell, Occhialini, and various co-workers (1947) have obtained lately remarkable results which are reported in the following.

682. The investigations were carried out using Ilford 'Nuclear Research' emulsions specially suitable for recording cosmic ray and nuclear phenomena. Only the tracks of comparatively slow particles can be thus recorded. Meson tracks, for instance, become visible only for energies below 10 MEV., while no tracks of electrons have been so far reported.

Particular attention was paid to the investigation of tracks of slow mesons. The track of a *meson* can be clearly distinguished from that of a heavier particle as the meson track shows frequent changes in direction due to the Coulomb scattering suffered by the meson; the track of a heavier particle is comparatively straight. Further, the rate of change of ionization near the end of a meson track is much greater than it is near the end of the track of a heavier particle.

683. Lattes, Occhialini, and Powell (1947) report observations of 400 meson tracks observed to end in photographic emulsions. The *grain density* along the tracks is a measure of the rate of ionization and therefore is a measure of velocity. The range of the particle is a measure of its energy. Thus, the observed grain density at a specified distance from the end of a track provides a means of determining simultaneously the velocity and energy of the particle; from these data the mass of the particle can be determined in a way discussed in § 274. Nevertheless, no reliable determination of the meson mass from observations of this kind has been obtained so far as the actual grain density is affected by the *fading* of the latent image, and, therefore, tracks of different age cannot be compared directly.

Disintegrations produced by Negative Mesons

684. Lattes, Muirhead, Occhialini, and Powell (1947) show that a considerable proportion of the slow mesons, after reaching the end of their range, produce disintegrations with the emission of heavy particles. It

Microphotograph of a meson (m) giving rise to a nuclear disintegration. At least three charged particles are omitted (Powell and Occhialini)

PLATE 6

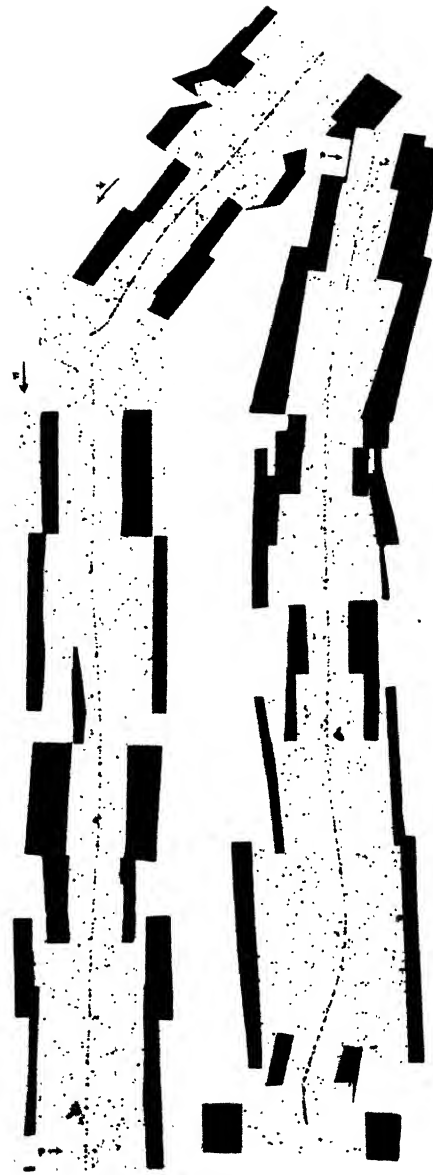

Microphotograph of μ-decay. A π-meson is brought to rest in the photographic emulsion. From the end of the π-track a μ-track emerges. For convenience of reproduction the μ-track is presented in two parts; the right-hand track shows the end of the range of the μ-meson. This should be joined at the point P to the left-hand part of the photograph (Powell and Occhialini)

is reasonable to assume that events of this type, of which an example is shown in Plate 5, correspond to the entry of a meson into a nucleus, the energy required for the disintegration being provided by the disappearance of the rest-mass of the particle. The Coulomb repulsion between a nucleus and a positive meson would tend to prevent the latter from approaching a nucleus at low speed; it is therefore assumed that such disintegrations are produced by negative mesons.

The frequency of arrival of slow mesons in photographic emulsions exposed at a height of 2,800 m. (at the Observatoire du Pic du Midi, Hautes Pyrénées) is about 2 per c.c. per diem. This value is in reasonable accord with the numbers of slow mesons observed in delayed coincidence experiments at sea-level—making appropriate estimates of the increase in the numbers of slow mesons to be expected at increasing altitudes. It can be concluded, therefore, that the mesons observed in these experiments do not constitute a rare component of the cosmic rays with special properties, but form at least an important part of the penetrating component.

Mesons of Different Mass

685. In a number of instances it has been observed by Powell and others that a slow meson comes to the end of its range and leads to the emission of a secondary slow meson. Photo-micrographs of such an event are given in Plate 6. In several cases the secondary particles come to rest in the emulsion so that their range can be determined. The evidence strongly suggests that, in processes of this type, the secondary mesons are always emitted with constant velocity, for the variation in the length of the track of the secondary meson in the different events is small and can be attributed to straggling.

686. These observations show clearly that mesons of a heavier mass come to rest in the emulsion and emit somewhat lighter mesons after having come to rest. The heavier meson may be termed a π-meson while the lighter secondary meson may be termed a μ-meson. The process may be conveniently referred to as the μ-decay. Evidence in support of this view is provided by grain counts. We have seen that the fugitive nature of the latent image prevents a successful application of the method of grain-counting for the determination of the mass of individual mesons. It may be assumed, however, that the two mesons in the process of μ-decay are formed in quick succession. It is, therefore, legitimate to compare the grain density along the tracks of the π- and μ-mesons and

thus to compare their masses, for the two tracks of a particular event will be subject to the same degree of fading. The ratio of the masses of the two particles is thus found to be about 2; $m_\pi/m_\mu \sim 2$. The authors state that the actual value of the ratio must be accepted with reserve until it can be confirmed by further measurements, but that the difference in mass can be regarded as definitely established.

Identification of π and μ mesons

687. The two types of mesons reported above may have to be identified with the vector and pseudo-scalar mesons of the Møller–Rosenfeld theory described in § 220. An even better agreement is found with the modification of this theory by Schwinger (1942). In the latter theory the two mesons are assumed to be of different mass.

Though such an identification appears natural it must be taken with great reserve, and more experimental material has to be awaited.

Ejection of Mesons from Disintegrating Nuclei

688. In plates exposed at high altitudes, large numbers of examples of the 'explosive' disintegration of nuclei are to be observed, their rate of production at 3,000 m. being about 15 per c.c. per diem. In general it is not possible to identify the primary particles producing these disintegrations. In many cases the energy of the particles must be assumed to be of such a magnitude—to account for the observed release of energy in the disintegration—that even if they were charged they would leave no track in the emulsion. In some cases, however, an analysis of a particular disintegration is possible and it has been shown by Lattes and Occhialini (1947) and by Lattes (unpublished) that both fast neutrons and high-energy quanta contribute to such nuclear 'explosions'.

In a few cases particles of low mass have been observed to be emitted during the explosive disintegration of nuclei. It appears likely that the emission of mesons may be a common feature of such disintegrations, for it is only possible to recognize the ejected meson in the rare instances in which they are emitted with low energies and, by chance, in a direction nearly parallel to the surface of the photographic emulsion. In all the events of this type observed up to the present, in which the ejected meson comes to rest in the emulsion, no secondary particles have been observed to originate from the end of the range.

We are greatly indebted to Drs. Powell and Occhialini for permission to reproduce the photographs shown in Plates 5 and 6.

BIBLIOGRAPHY

AGENO, BERNARDINI, CACCIAPUOTI, FERRETTI, and WICK, *Phys. Rev.* **57,** 945 (1940).

ALICHANJAN, ALICHANOV, and NIKITIN, *Journ. Phys. USSR,* **6,** 230 (1942).

ALLEN, *Phys. Rev.* **61,** 692 (1942).

ALTMANN, WALKER, and HESS, ibid. **58,** 1011 (1940).

ANDERSON, *Science,* **76,** 238 (1932).

—— *Phys. Rev.* **43,** 491 (1933 *a*).

—— ibid. **44,** 406 (1933 *b*).

—— and NEDDERMEYER, *Int. Conf. Phys.,* London (1934).

—— —— *Phys. Rev.* **50,** 263 (1936).

—— —— ibid. **51,** 884 (1937).

ARLEY, *Proc. Roy. Soc.* A **168,** 519 (1938).

—— *Stochastic Processes,* Copenhagen (1943).

—— and HEITLER, *Nature,* Lond. **142,** 158 (1938).

AUGER, *Thèse,* Paris (1926).

—— *Compt. Rend.* **200,** 739 (1935 *a*).

—— *Journ. d. Phys.* **6,** 226 (1935 *b*).

—— *Compt. Rend.* **207,** 907 (1938).

—— and DAUDIN, *Phys. Rev.* **61,** 91 (1942).

—— —— *Journ. de Phys.* **6,** 17 (1945).

—— EHRENFEST, FRÉON, and FOURNIER, *Compt. Rend.* **204,** 257 (1937).

—— and MAZE, ibid. **207,** 228 (1938).

—— —— and CHARMINADE, *Phys. Rev.* **62,** 307 (1942).

—— —— and GRIVET-MAYER, *Compt. Rend.* **206,** 1721 (1938).

—— —— and ROBLEY, ibid. **208,** 1641 (1938).

—— and ROSENBERG, ibid. **201,** 1116 (1935 *a*).

—— —— ibid. **200,** 447 (1935 *b*).

—— —— *Journ. Phys.* **6,** 229 (1935 *c*).

BARNÓTHY and FORRÓ, *Z. Phys.* **100,** 742 (1936).

—— —— ibid. **104,** 744 (1937).

—— —— *Phys. Rev.* **55,** 870 (1939).

BEARDEN, *Rev. Sci. Inst.* **6,** 256 (1935).

BEARDSLEY, *Phys. Rev.* **57,** 336 (1940).

BEHOUNEK, *Phys. Z.* **27,** 8, 536 (1926).

BELENKY, *C.R. USSR,* **30,** 608 (1941).

—— ibid. **36,** no. 4 (1942).

—— *Journ. Phys. USSR,* **8,** 9, 347 (1944).

BERNARDINI, *Nature,* Lond. **129,** 578 (1932).

—— CACCIAPUOTI, FERRETTI, PICCIONI, and WICK, *Atti. Ac. It.* **9,** 471 (1940).

BETHE, *Z. Phys.* **76,** 239 (see also *Handb. d. Phys.*) (1932).

—— *Phys. Rev.* **57,** 260, 390 (1940).

—— and HEITLER, *Proc. Roy. Soc.* A **146,** 83 (1934).

——, KORFF, and PLACZEK, *Phys. Rev.* **57,** 573 (1940).

BHABHA, *Proc. Roy. Soc.* A **164,** 257 (1938 *a*).

—— ibid. A **166,** 501 (1938 *b*).

—— *Ind. Ac. Sci.* **11,** 247 (1940 *a*).

—— ibid. 347 (1940 *b*).

BHABHA, *Phys. Rev.* **59,** 100 (1941).
—— and CHAKRABARTY, *Proc. Roy. Soc.* A **181,** 267.
—— and HEITLER, ibid. A **159,** 432 (1937).
BLACKETT, *Journ. Sci. Inst.* **4,** 433 (1927).
—— *Proc. Roy. Soc.* A **146,** 281 (1934).
—— ibid. A **159,** 1 (1937 *a*).
—— ibid. 19 (1937 *b*).
—— ibid. A **165,** 11 (1938 *a*).
—— *Phys. Rev.* **54,** 973 (1938 *b*).
—— *Nature,* Lond. **144,** 30 (1939).
—— *Proc. Phys. Soc.* **53,** 203 (1941).
—— and BRODE, *Proc. Roy. Soc.* A **154,** 564 (1936).
—— and OCCHIALINI, *Nature,* Lond. **130,** 363 (1932).
—— —— *Proc. Roy. Soc.* A **139,** 699 (1933).
—— and WILSON, J. G., *Proc. Roy. Soc.* A **160,** 304 (1937).
—— —— ibid. A **165,** 209 (1938).
BLAU and WAMBACHER, *Nature,* Lond. **140,** 585 (1937 *a*).
—— —— *Proc. Ac. Vienna,* **146,** 623 (1937 *b*).
BLOCH, *Ann. d. Physik,* **16,** 285; *Z. Phys.* **81,** 363 (1933).
BØGGILD and KARKOV, *Naturw.* **25,** 158 (1937).
BOHR, *Phil. Mag.* **25,** 10 (1913).
—— ibid. **30,** 581 (1915).
BOOTH and WILSON, A. H., *Proc. Roy. Soc.* A **166,** 501 (1940).
BOSE and CHOUDHURI, *Nature,* Lond. **148,** 259 (1941).
—— —— ibid. **149,** 30 (1942).
—— —— and SINHA, *Phys. Rev.* **65,** 341 (1944).
BOSTICK, *Phys. Rev.* **61,** 557 (1942).
BOTHE and KOLHÖRSTER, *Z. Phys.* **56,** 751 (1929).
BOWEN, MILLIKAN, and NEHER, *Phys. Rev.* **46,** 641 (1934).
—— —— —— ibid. **52,** 80 (1937).
—— —— —— ibid. **53,** 217 (1938).
BRADDICK, *Proc. Roy. Soc.* A **171,** 314 (1939).
—— and HEMSBY, *Nature,* Lond. **144,** 1012 (1939).
BRANDT and SCHERRER, *Helv. Phys. Act.* (March) (1943).
BROADBENT and JÁNOSSY, *Proc. Roy. Soc.* in the press (1947 *a, b, c*).
BRODE, MCPHERSON, and STARR, *Phys. Rev.* **50,** 581 (1936).

CARLSON and OPPENHEIMER, ibid. **51,** 220 (1937).
CARMICHAEL and CHOU, *Nature,* Lond. **144,** 325 (1939).
—— and DYMOND, *Proc. Roy. Soc.* A **171,** 321 (1939).
CHADWICK, BLACKETT, and OCCHIALINI, *Nature,* Lond. **131,** 473 (1933).
CHAKRABARTY, *Ind. Journ. Phys.* **16,** 377 (1942 *a*).
—— *Phys. Nat. Sc. Ind.* **8,** 331 (1942 *b*).
—— and MAJUMDAR, *Phys. Rev.* **65,** 206 (1944).
CHAPMAN, *Month. Not. Roy. A. Soc.* **89,** 59 (1928).
CHARMINADE, FRÉON, and MAZE, *Compt. Rend.* **218,** 402 (1944).
CHOU, *Papers College Sci. and Eng. Univ. Amoy* (China), **1** (1943).
CHRISTY and KUSAKA, *Phys. Rev.* **59,** 405 (1941 *a*).
—— —— ibid. 414 (1941 *b*).
CLAY, *Proc. Ac. Amst.* **33,** 711 (1930).
—— *Physica,* **1,** 363 (1934).
—— ibid. **2,** 861 (1935 *a*).

CLAY, *Physica*, **2**, 867 (1935 *b*).
—— ibid. **3**, 352 (1936).
—— ALPHEN, and HOOFT, ibid. **1**, 829 (1934).
—— and BRUINS, ibid. **6**, 638 (1939).
—— and CLAY, ibid, **2**, 1042 (1935).
—— and GEMERT, *Proc. Ac. Amst.* **42**, 672 (1939).
—— —— and CLAY, ibid. **41**, 694 (1938).
—— —— —— *Physica*, **6**, 184, 497 (1939).
—— HOOFT and CLAY, ibid. **2**, 1033 (1935).
COCCONI, LOVERDO, and TONGIORGI, *Nuovo Cim.* **1**, 314 (1943).
—— —— —— ibid. **2**, 214 (1944).
—— —— —— *Phys. Rev.* **70**, 840, 846 (1946).
CODE, ibid. **59**, 229 (1941).
COMPTON, ibid. **43**, 387 (1933).
—— and GETTING, ibid. **47**, 817 (1935).
—— and TURNER, ibid. **52**, 799 (1937).
—— WOLLAN, and BENETT, *Rev. Sci. Inst.* **5**, 415 (1934).
CONVERSI and SEROCCO, *Nuovo Cim.* (August) (1943).
—— PANCINI, and PICCIANI, *Phys. Rev.* **71**, 209 (1947).
COOPER, ibid. **58**, 288 (1940).
CORLIN, *Ann. Obs. Lund*, Nr. 4 (1934).
CORSON and BRODE, *Phys. Rev.* **53**, 773 (1938).
COSYNS, *Nature*, Lond. **137**, 616 (1936 *a*).
—— *Bull. Tech. Ass. Ing. Brussels*, p. 173 (1936 *b*).
—— *Roy. Belg. Ac.* **23**, 498, 960 (1937).
—— *Nature*, Lond. **145**, 668 (1940).
—— *Roy. Belg. Ac.* **28**, 574 (1942).
—— and BRUINS, *Bull. Ac. Belg.*, Nr. 4 (1934).
COWLING, *Month. Not. Roy. A. Soc.* **90**, 139 (1929).
—— ibid. **92**, 407 (1932).
CRUSSARD and LEPRINCE-RINGUET, *Compt. Rend.* **204**, 240 (1937 *a*).
—— —— —— *Journ. d. Phys.* **8**, 213 (1937 *b*).
CURIE and JOLIOT, *Compt. Rend.* **196**, 1105, 1581, 1885 (1933 *a*).
CURRAN and PETRŽILKA, *Proc. Camb. Soc.* **35**, 309 (1939).

DANFORTH and RAMSAY, *Phys. Rev.* **49**, 854 (1936).
DAUDIN, *Thèse*, Paris (1942).
—— *Compt. Rend.* **216**, 483 (1943).
—— ibid. **218**, 275 (1944).
—— *Ann. d. Physique*, **20**, 563 (1945).
DRIGO, *Ric. Sci.* **1**, 11 (1935).
DUPERIER, *Proc. Roy. Soc.* A **177**, 204 (1940).
—— *Nature*, Lond. **153**, 529 (1944 *a*).
—— *Terr. Magn. Atm. El.* **49**, 1 (1944 *b*).
ECKART, *Phys. Rev.* **45**, 451 (1934).
—— and SHONKA, ibid. **53**, 752 (1938).
EHMERT, *Z. Phys.* **106**, 751 (1937).
EHRENBERG, *Proc. Roy. Soc.* A **155**, 532.
EHRENFEST, *Compt. Rend.* **206**, 428 (1938 *a*).
—— ibid. **207**, 573 (1938 *b*).
—— and AUGER, *Journ. Phys.* **7**, 65 (1936).
ELSTER and GEITEL, *Phys. Z.* **2**, 560 (1900, 1).

EPSTEIN, *Phys. Rev.* **53,** 862 (1938).
EULER, *Z. Phys.* **116,** 73 (1940).
—— and HEISENBERG, *Erg. d. exakt. Naturwiss.*, vol. 17, Springer (1938).
—— and WERGELAND, *Astr. Norw.* **3,** 165 (1940).

FERMI, *Phys. Rev.* **56,** 1242 (1939).
—— and ROSSI, *Acc. Linc. Att.* **17,** 346 (1933).
FLOOD, *Z. Phys. Chem.* **170,** 286 (1934).
FOLLET and CRAWSHAW, *Proc. Roy. Soc.* A **155,** 546 (1936).
FORBUSH, *Rev. Mod. Phys.* **11,** 168 (1939).
FRÉON, *Thèse,* Paris (1942).
—— *Compt. Rend.* **218,** 277 (1944).
FRÖHLICH, HEITLER, and KEMMER, *Proc. Roy. Soc.* A **166,** 154 (1938).
FROMAN and STEARNS, *Phys. Rev.* **50,** 787 (1936).
FÜNFER, *Z. Phys.* **83,** 92 (1933).
—— ibid. **111,** 351 (1938).
FURRY, *Phys. Rev.* **52,** 569 (1937).
FUSSEL (quoted from EULER and HEISENBERG (1938)).

GEIGER, *Z. Phys.* **27,** 7 (1924).
—— and KLEMPERER, ibid. **49,** 753 (1928).
—— and MÜLLER, *Phys. Z.* **29,** 839 (1928).
—— —— ibid. **30,** 489 (1929).
GEORGE, JÁNOSSY, and MCCAIG, *Proc. Roy. Soc.* A **180,** 219 (1942).
GETTING, *Rev. Sci. Inst.* **8,** 412 (1937).
—— *Phys. Rev.* **53,** 103 (1938).
GILBERT, *Proc. Roy. Soc.* A **144,** 559 (1934).
GOCKEL, *Phys. Z.* **10,** 845 (1909).
—— ibid. **11,** 280 (1910).
—— ibid. **12,** 595 (1911).
—— ibid. **16,** 345 (1915).
GODART, *Ann. Soc. Sci. Brussels,* **58,** 27 (1938).
GORDON, *Z. Phys.* **48,** 180 (1928).
GORODETZKY, *Thèse,* Paris (1942).
—— *Compt. Rend.* **217,** 479 (1943).
GROSS, *Z. Phys.* **83,** 214 (1933).

HALE, SEARRES, MAANEN, ELLERMAN, *Astr. Journ.* **47,** 1 (1918).
HALPERN and CRANE, *Phys. Rev.* **56,** 232 (1939).
HAMILTON, HEITLER, and PENG, ibid. **64,** 78 (1943).
—— and PENG, *Proc. Ir. Ac.* **49,** 197 (1944).
HAZEN, *Phys. Rev.* **63,** 213 (1943).
—— ibid. **65,** 67 (1944 *a*).
—— ibid. 259 (1944 *b*).
HEISENBERG, *Ak. Wiss. Lpz.* **89,** 369 (1937 *a*).
—— *Naturw.* **25,** 749 (1937 *b*).
HEITLER, *Proc. Roy. Soc.* A **161,** 261 (1937).
—— ibid. A **166,** 529 (1938).
—— *Proc. Camb. Soc.* **37,** 291 (1941).
—— *Proc. Ir. Ac.* **50** (1945).
—— and MA. *Proc. Roy. Soc.* A **176,** 368 (1940).

HEITLER, and PENG, *Phys. Rev.* **62,** 81 (1942).
—— —— *Proc. Ir. Ac.* **49,** 101 (1944).
—— POWELL, F. C., and FERTEL, *Nature*, Lond. **144,** 283 (1939).
—— and WALSH, *Rev. Mod. Phys.* **17,** 252 (1945).
HERZOG and BOSTICK, *Phys. Rev.* **58,** 218 (1940).
—— and SCHERRER, *Journ. Phys.* **6,** 489 (1935).
HESS, *Phys. Z.* **13,** 1084 (1912).
—— ibid. **14,** 610 (1913).
—— ibid. **27,** 159 (1926).
—— GRAZIADEI, and STEIMAURER, *Proc. Vien. Ac.* **143,** 313 (1934).
—— —— —— ibid. **144,** 53 (1935).
—— and LAWSON, ibid. **125,** 285 (1916).
HILBERRY, *Phys. Rev.* **60,** 1 (1941).
—— *Simposium*, Rio de Janeiro, p. 85 (1943).
HOFFMANN, *Phys. Z.* **26,** 669 (1925).
—— *Ann. Physik*, **80,** 779 (1926).
—— ibid. **82,** 413 (1927 *a*).
—— *Z. Phys.* **42,** 565 (1927 *b*).
—— and LINDHOLM, *Beitr. Geophys.* **20,** 12 (1928).
—— and PFORTE, *Phys. Z.* **31,** 347 (1930).
HU CHIEN SHAN, *Proc. Roy. Soc.* A **158,** 581 (1937).
—— KISELBASH, and KETILADGE, *Proc. Roy. Soc.* A **161,** 95 (1937).
HUGHES, *Phys. Rev.* **57,** 592 (1940).
—— ibid. **60,** 414 (1941).
HUNTER, ibid. **55,** 15, 614 (1939).

IWANENKO and SOKOLOW, ibid. **53,** 910 (1918).

JÁNOSSY, *Z. Phys.* **101,** 129 (1936).
—— ibid. **104,** 430 (1937).
—— *Proc. Roy. Soc.* A **167,** 499 (1938 *a*).
—— *Proc. Camb. Soc.* **34,** 614 (1938 *b*).
—— *Proc. Roy. Soc.* A **179,** 361 (1941).
—— *Phys. Rev.* **64,** 345 (1943).
—— *Nature*, Lond. **153,** 165, 592 (1944 *a*).
—— *Proc. Roy. Soc.* A **183,** 190 (1944 *b*).
—— and INGLEBY, *Nature*, Lond. **145,** 511 (1940).
—— —— *Journ. Sci. Inst.* **19,** 30 (1942).
—— and LOVELL, *Nature*, Lond. **142,** 716 (1938).
—— and ROCHESTER, *Proc. Roy. Soc.* A **181,** 399 (1943 *a*).
—— —— ibid. A **182,** 180 (1943 *b*).
—— —— ibid. A **183,** 181 (1944 *a*).
—— —— ibid. 186 (1944 *b*).
—— —— and BROADBENT, *Nature*, Lond. **155,** 142 (1945).
—— —— and MCCUSKER, ibid. **148,** 660 (1941).
—— and ROSSI, *Proc. Roy. Soc.* A **175,** 88 (1940).
—— and TZU, *Nature*, Lond. **157,** 62 (1946).
JOHNSON, *Phys. Rev.* **43,** 703 (1933 *a*).
—— *Journ. Frankl. Inst.* **215,** 749 (1933 *b*).
—— *Phys. Rev.* **45,** 569 (1934).
—— ibid. **47,** 91 (1935 *a*).
—— ibid. **48,** 287 (1935 *b*).

JOHNSON, ibid. **54,** 385 (1938 *a*).
—— *Rev. Mod. Phys.* **10,** 193 (1938 *b*).
—— ibid. **11,** 208 (1939 *a*).
—— *Journ. Frankl. Inst.* **227,** 37 (1939 *b*).
—— *Phys. Rev.* **56,** 226 (1939 *c*).
—— BENEDETTI, and SHUTT, *Rev. Sci. Inst.* **14,** 265 (1943).
—— and BARRY, *Phys. Rev.* **56,** 219 (1939).
—— and SHUTT, ibid. **61,** 380 (1942).
—— and STEVENSON, *Journ. Frankl. Inst.* **216,** 329 (1933).
—— and STREET, *Phys. Rev.* **43,** 381 (1933).
JONES, *Rev. Mod. Phys.* **11,** 235 (1939).
JÜTTNER, *Z. Math. Phys.* **62,** 410 (1914).

KELLOG, RABI, RAMSAY, and ZACHARIAS, *Phys. Rev.* **57,** 677 (1940).
KEMMER, *Proc. Roy. Soc.* A **166,** 127 (1938 *a*).
—— *Proc. Camb. Soc.* **34,** 354 (1938 *b*).
KLEIN and NISHINA, *Z. Phys.* **52,** 853 (1929).
KOLHÖRSTER, *Ber. deutsch. Phys. Ges.* **16,** 719 (1914–19).
—— *Proc. Berlin Ac.*, p. 366 (1923).
—— *Phys. Z.* **27,** 62 (1926).
—— *Z. Phys.* **88,** 536 (1934).
—— MATTHES, and WEBER, *Naturwiss.* **26,** 576 (1938).
KORFF, *Phys. Rev.* **56,** 210 (1939).
—— and PRESENT, *Phys. Rev.* **65,** 274 (1944).
KULENKAMPFF, *Verh. d. Phys. Ges.* (1938).
KUNZE, *Z. Phys.* **79,** 203 (1932).
—— ibid. **80,** 559 (1933 *a*).
—— ibid. **83,** 1 (1933 *b*).

LABY, *Phil. Trans. Roy. Soc.* (1908).
LANDAU, *Journ. Phys. USSR,* **3,** 237 (1940).
—— ibid. **4,** 201 (1944).
—— and RUMER, *Proc. Roy. Soc.* A **166,** 213 (1938).
LAPP, *Phys. Rev.* **63,** 60; **64,** 255 (1943).
—— ibid. **65,** 347 (1944).
LATTES, MUIRHEAD, OCCHIALINI, and POWELL, *Nature,* Lond. **159,** 694 (1947).
—— and OCCHIALINI, ibid. **159** (1947).
—— —— and POWELL, ibid. **159** (1947).
LEMAÎTRE, *Ann. Soc. Sci. Belg.* A **54,** 194 (1934).
—— and VALLARTA, *Phys. Rev.* **43,** 87 (1933).
—— —— ibid. **49,** 719 (1936 *a*).
—— —— ibid. **50,** 493 (1936 *b*).
—— —— and BOUCKAERT, *Phys. Rev.* **47,** 434 (1935).
LEPRINCE-RINGUET and CRUSSARD, *Compt. Rend.* **204,** 112 (1937); also *Journ. Phys.* **8,** 207 (1937).
—— and GORODETZKY, *Compt. Rend.* **213,** 765 (1941).
—— and L'HÉRITIER, ibid. **219,** 618 (1944).
—— NAGEOTTE, and L'HÉRITIER, ibid. **214,** 545 (1941).
LEWIS, B., *Proc. Camb. Phil. Soc.* **30,** 543 (1934).
LEWIS, L. G., *Phys. Rev.* **67,** 230 (1945).
LOVELL, *Proc. Roy. Soc.* A **172,** 568 (1939).
—— and WILSON, *Nature,* Lond. **144,** 863 (1939).

MA, *Phys. Rev.* **62,** 403 (1942).
MAASS, *Ann. Physik,* **27,** 507 (1936).
MASSEY and CORBEN, *Proc. Camb. Soc.* **35,** 84 (1939 *a*).
—— —— ibid. **35,** 463 (1939 *b*).
MAZE, *Thèse,* Paris (1941).
MCLENNAN and BURTON, *Phys. Z.* **4,** 533 (1902–3).
MEDICUS, *Z. Phys.* **74,** 350, 847 (1932).
MIEHLNICKEL, *Höhenstrahlung,* Steinkopff, Dresden and Leipzig (1938).
MILLIKAN and BOWEN, *Phys. Rev.* **22,** 198 (1923).
—— and CAMERON, ibid. **31,** 921 (1928).
—— —— ibid. **37,** 235 (1931).
—— and NEHER, ibid. **47,** 434 (1935).
—— —— ibid. **50,** 15 (1936).
—— —— and PICKERING, ibid. **61,** 397 (1942).
—— —— —— —— ibid. **63,** 234 (1943).
—— and OTIS, ibid. **23,** 778 (1924).
MOLIÈRE, *Naturwiss.* **30,** 87 (1942).
MØLLER, *Ann. Physik,* **14,** 531 (1932).
—— and ROSENFELD, *Kgl. Dansk. Vid. Sel.* **17** (1940).
MONTGOMERY and MONTGOMERY, *Phys. Rev.* **47,** 429 (1935 *a*).
—— —— ibid. **48,** 786 (1935 *b*).
—— —— ibid. **56,** 10 (1939).
—— —— ibid. **57,** 1030 (1940).
—— —— RAMSEY, and SWANN, ibid. **50,** 403 (1936).
—— —— and COWIE, ibid. **56,** 635 (1939).
MORGAN and NIELSEN, ibid. **50,** 882 (1936).
—— —— ibid. **52,** 564 (1937).
MOTT, *Proc. Roy. Soc.* **A 124,** 425 (1929).
—— ibid. **A 135,** 429 (1932).
MYSSOWSKY and TUWIM, *Z. Phys.* **35,** 299 (1925).
—— —— ibid. **36,** 615 (1926).
—— —— ibid. **50,** 273 (1928).

NEDDERMEYER and ANDERSON, *Phys. Rev.* **54,** 88 (1938).
NEHER, *Rev. Sci. Inst.* **10,** 29 (1939).
—— and HARPER, *Phys. Rev.* **49,** 940 (1936).
—— and PICKERING, ibid. **61,** 407 (1942).
—— and STEVER, ibid. **58,** 766 (1940).
NERESON, ibid. **61,** 111 (1942).
NIE, *Z. Phys.* **99,** 453 (1936).
NIELSEN, *Journ. Frankl. Inst.* **226,** 601 (1938).
—— and MORGAN, *Phys. Rev.* **52,** 568 (1937).
—— and POWELL, W. M., ibid. **63,** 384 (1943).
NISHINA and ISHII, *Nature,* Lond. **140,** 774 (1937).
—— TAKEUCHI, ICHINIYA, *Phys. Rev.* **55,** 585 (1939).
NORDHEIM, ibid. **53,** 694 (1938).
—— ibid. **55,** 506 (1939 *a*).
—— ibid. **59,** 929 (1941).
—— and HEBB, *Phys. Rev.* **56,** 494 (1939).
NORDSIECK, LAMB, and UHLENBECK, *Physica,* **7,** 344 (1940).

OCCHIALINI and POWELL, *Nature,* Lond. **159,** 186 (1947).
OPPENHEIMER, SNYDER, and SERBER, *Phys. Rev.* **57,** 75 (1940).

PACINI, *Nuovo Cim.* **3**, 93 (1912).
PFOTZER, *Z. Phys.* **102**, 23, 41 (1936).
PICKERING, *Rev. Sci. Inst.* **9**, 180 (1938).
POWELL, W. M., *Phys. Rev.* **58**, 474 (1940).
—— ibid. **60**, 413 (1941).

RAMSEY, ibid. **57**, 1022 (1940).
—— ibid. **61**, 96 (1942).
RASETTI, ibid. **60**, 198 (1941).
REGENER, E., *Phys. Z.* **31**, 1018 (1930).
—— *Nature*, Lond. **131**, 130 (1933).
—— and EHMERT, *Z. Phys.* **111**, 501 (1939).
REGENER, V. H., *Phys. Rev.* **64**, 250 (1943 *a*).
—— ibid. **64**, 252 (1943 *b*).
RIBNER, ibid. **56**, 1069 (1939).
RICHARDSON, *Nature*, Lond. **73**, 607 (1906).
ROCHESTER, ibid. **154**, 399 (1944).
—— *Proc. Roy. Soc.* **A 178**, 464 (1946).
ROGOZINSKY, *Phys. Rev.* **65**, 207, 291, 300 (1944).
ROSE and RAMSEY, ibid. **59**, 616 (1941).
ROSSI, *Linc. Rend.* **11**, 831, also *Nature*, Lond. **125**, 636 (1930).
—— *Z. Phys.* **68**, 64, also *Nuovo Cim.* **8**, 49 (1931 *a*).
—— ibid. 3 (1931 *b*).
—— *Z. Phys.* **82**, 151 (1933).
—— *Ric. Sci.* **5**, 583 (1934 *a*).
—— ibid. 569 (1934 *b*).
—— *Int. Conf. Physics*, London, p. 233 (1934 *c*).
—— *Rev. Mod. Phys.* **11**, 291 (1939).
—— and ALOCCO, *Acc. Linc. Att.* **21**, 167 (1935).
—— and BENEDETTI, *Ric. Sci.* **5**, 379 (1934).
—— and GREISEN, *Rev. Mod. Phys.* **13**, 240 (1941).
—— —— *Phys. Rev.* **61**, 121 (1942).
—— —— STEARNS, FROMAN, and KOONTZ, ibid. **61**, 675 (1942).
—— and HALL, ibid. **59**, 223 (1941).
—— HILBERRY and HOAG, ibid. **57**, 461 (1940).
—— JÁNOSSY, ROCHESTER, and BOUND, ibid. **58**, 761 (1940).
—— and KLAPMANN, ibid. **61**, 414 (1942).
—— and NERESON, ibid. **62**, 417 (1942).
—— —— ibid. **64**, 199 (1943).
—— and REGENER, V. H., ibid. **58**, 837 (1940).
RUMBAUGH and LOCHER, ibid. **49**, 855 (1936).
RUTHERFORD and COOK, ibid. **16**, 183 (1903).

SAWYER, ibid. **44**, 241 (1933).
—— ibid. **47**, 515 (1935).
SCHEIN and GILL, *Rev. Mod. Phys.* **11**, 267 (1939).
—— IONA, and TABIN, *Phys. Rev.* **64**, 253 (1943).
—— JESSE, and WOLLAN ibid. **59**, 615 (1941).
—— WOLLAN, and GROETZINGER, ibid. **58**, 1027 (1940).
SCHINDLER, *Z. Phys.* **72**, 625 (1931).
SCHMEISER and BOTHE, *Ann. Physik*, **32**, 161 (1938).
SCHÖNBERG, *An. Ac.*, Brazil, **12**, 281 (1940).

SCHOPPER and SCHOPPER, *Phys. Z.* **40,** 22 (1939).
SCHREMP, *Phys. Rev.* **54,** 153, 158 (1938).
SCHROEDINGER, *Nature,* Lond. **153,** 592 (1944).
SCHWEGLER, *Z. Phys.* **96,** 62 (1935).
SCHWINGER, *Phys. Rev.* **61,** 387 (1942).
SCOTT and UHLENBECK, *Phys. Rev.* **62,** 497 (1942).
SEN GUPTA, *Nature,* Lond. **146,** 65 (1940).
—— *Proc. Nat. Inst. Ind.* **9,** 295 (1943).
SERBER, *Phys. Rev.* **54,** 317 (1938).
SEREN, ibid. **62,** 204 (1942).
SHUTT, ibid. **61,** 6 (1942).
—— BENEDETTI, and JOHNSON, ibid. **62,** 552 (1942).
SIMPSON, J. A., ibid. **66,** 39 (1944).
SIMPSON, G. C. and WRIGHT, *Proc. Roy. Soc.* **85,** 175 (1911).
SKOBELZYN, *Z. Phys.* **43,** 354 (1927).
—— ibid. **54,** 686 (1929).
—— *C.R. USSR,* **37,** 141 (1942).
—— ibid. **42,** 388 (1944 *a*).
—— ibid. **44,** 142 (1944 *b*).
SMOWOLINSKY, *C.R. USSR,* **3,** no. 2 (1940).
SNYDER, *Phys. Rev.* **53,** 960 (1938).
STEARNS, ibid. **49,** 473 (1936).
STEINKE, *Z. Phys.* **42,** 570 (1927).
—— ibid. **48,** 647 (1928).
—— ibid. **30,** 767 (1929).
—— and STREET, *Phys. Rev.* **49,** 425 (1936).
—— and TIELSCH, *Z. Phys.* **84,** 425 (1933).
STEVER, *Phys. Rev.* **61,** 38 (1942).
STÖRMER, *Z. Astr. Phys.* **1,** 237.
—— *Obs. Oslo,* no. 10, also *Astr. Norv.* **1,** 1 (1934).
STREET, WOODWARD, and STEVENSON, *Phys. Rev.* **47,** 891 (1935).
SWANN, ibid. **44,** 224 (1933).

TAM and BELENKY, *Journ. Phys. USSR,* **1,** 177 (1939).
—— —— *Phys. Rev.* **70,** 660 (1946).
THIBAUD, *Compt. Rend.* **197,** 237 (1933 *a*).
—— ibid. **197,** 915 (1933 *b*).
TROST, *Z. techn. Phys.* **16,** 407 (1935).
—— *Z. Phys.* **105,** 319 (1937).
TRUMPY, *Det Dansk. Vid. Sel.* **20,** no. 6 (1943).

VALLARTA, *Phys. Rev.* **47,** 647 (1935).
—— *Nature,* Lond. **139,** 24 (1937 *a*).
—— ibid. **139,** 839 (1937 *b*).
—— *On the allowed cone of cosmic radiation,* Toronto University Press (1938).
—— and GODART, *Rev. Mod. Phys.* **11,** 180 (1939).

WATAGHIN, SANTOS, and POMPEIA, *Phys. Rev.* **57,** 61, 339 (1940).
WEBB, *Phil. Mag.* **19,** 927 (1935).
WEISCHEDEL, *Z. Phys.* **101,** 732 (1936).
WEIZSÄCKER, ibid. **88,** 612 (1934).
WENTZEL, ibid. **40,** 590 (1927).

WERNER, *Z. Phys.* **90,** 384 (1934).
WHEELER and LADENBURG, *Phys. Rev.* **60,** 754 (1941).
WILKENING and KANE, ibid. **62,** 534 (1942).
WILLIAMS, E. J., *Proc. Roy. Soc.* A **135,** 108 (1932 *a*).
—— *Phys. Rev.* **42,** 881 (1932 *b*).
—— *Proc. Roy. Soc.* A **139,** 163 (1933 *a*).
—— *Nature,* Lond. **131,** 511 (1933 *b*).
—— *Int. Conf. Physics.,* London (1934 *a*).
—— *Phys. Rev.* **45,** 729 (1934 *b*).
—— *Sci. Prog.* **121,** 14 (1936).
—— *Nature,* Lond. **142,** 431 (1938).
—— *Proc. Camb. Soc.* **35,** 512 (1939 *a*).
—— *Proc. Roy. Soc.* A **172,** 194 (1939 *b*).
—— ibid. A **169,** 531 (1939 *c*).
—— *Phys. Rev.* **58,** 292 (1940 *a*).
—— *Proc. Camb. Soc.* **36,** 183 (1940 *b*).
—— and EVANS, *Nature,* Lond. **145,** 818 (1940).
—— and PICKUP, ibid. **141,** 684 (1938).
—— and ROBERTS, ibid. **145,** 102 (1940).
WILSON, A. H., *Proc. Camb. Soc.* **36,** 363 (1940).
—— ibid. **37,** 301 (1941).
WILSON, C. T. R., *Proc. Camb. Soc.* **11,** 32 (1900).
—— *Proc. Roy. Soc.* A **68,** 151; A **69,** 277 (1901).
—— ibid. A **85,** 285 (1911).
—— *Proc. Camb. Soc.* **15,** 534 (1925).
—— *Proc. Roy. Soc.* A **142,** 88 (1933).
WILSON, J. G., ibid. A **166,** 482 (1938).
—— *Nature,* Lond. **142,** 73 (1938 *a*).
—— *Proc. Roy. Soc.* A **172,** 517 (1939).
—— ibid. A **174,** 73 (1940).
—— *Nature,* Lond. **158,** 414 (1946).
WILSON, V. C., *Phys. Rev.* **52,** 559 (1937).
—— ibid. **53,** 337 (1938).
—— ibid. **55,** 6 (1939).
—— and HUGHES, ibid. **63,** 161 (1943).
WOLLAN, ibid. **60,** 532 (1941).
WOODWARD, ibid. **49,** 711 (1936).
WULF, *Phys. Z.* **10,** 152 (1909).
—— ibid. **11,** 811 (1910).
WYNN-WILLIAMS, *Proc. Roy. Soc.* A **132,** 295 (1931).

YOUNG and STREET, *Phys. Rev.* **46,** 823 (1934).
—— —— ibid. **52,** 559 (1937).
YUKAWA, *Proc. Phys. Math. Soc. Jap.* **17,** 48 (1935).
—— KOBAYASHI, and TAKETANI, ibid. **20,** 720 (1938).
—— and SAKATA, ibid. **19,** 1084 (1937).

AUTHOR INDEX

SUBJECT INDEX